



An introduction to Inverse Problems

Ge193

Malcolm Sambridge
Research School of Earth Sciences
Australian National University
Malcolm.Sambridge@anu.edu.au

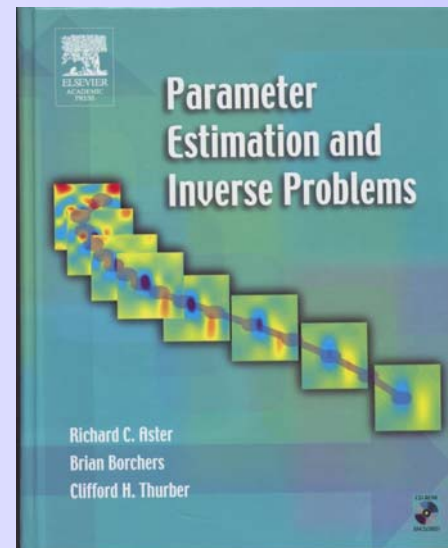
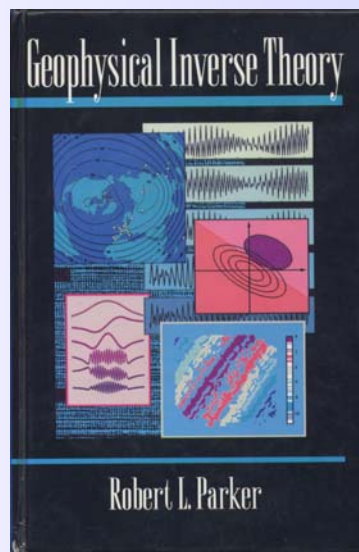
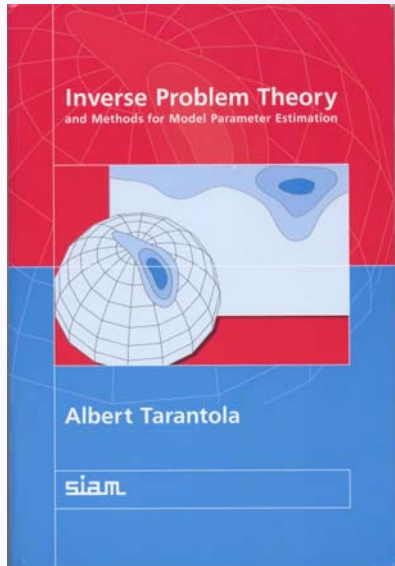
Visiting Caltech (GPS) until mid December
Room 252F malcolms@gps.caltech.edu



Course Contents

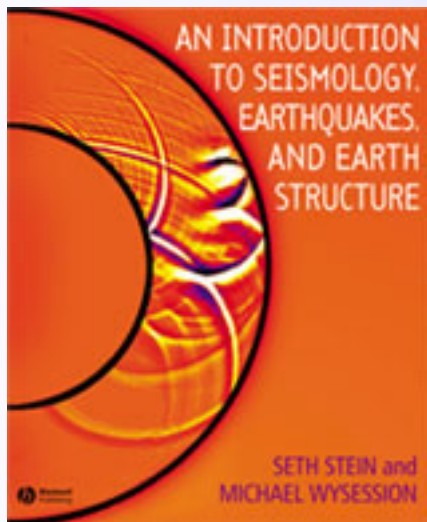
- Characterizing inverse problems
- Linear, discrete inverse problems
- Linearizing nonlinear problems
- Discrete ill-posed inverse problems
- Regularization
- Fully nonlinear inversion and parameter search
- Probabilistic inference

Books

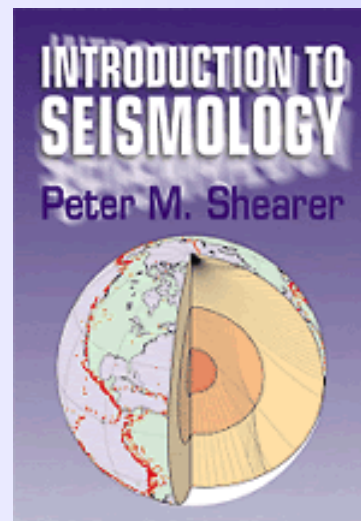


See also Menke '*Geophysical data analysis: discrete inverse theory*'
(Academic Press, 1989)

Books

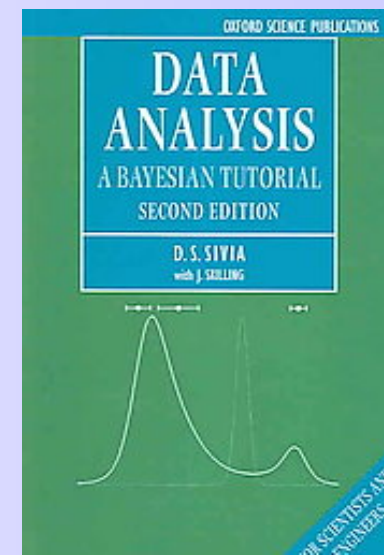


Chapter 7 on inverse problems



Introductory Chapter on
inverse problems

Useful Bayesian tutorial
(First 5 chapters)





Reference works

Some papers:

- Understanding inverse theory
Ann. Rev. Earth Planet. Sci., **5**, 35-64, Parker (1977).
- Interpretation of inaccurate, insufficient and inconsistent data
Geophys. J. Roy. astr. Soc., **28**, 97-109, Jackson (1972).
- Monte Carlo sampling of solutions to inverse problems
J. Geophys. Res., **100**, 12,431–12,447,
Mosegaard and Tarantola, (1995)
- *Monte Carlo methods in geophysical inverse problems,*
Rev. of Geophys., **40**, 3.1-3.29,
Sambridge and Mosegaard (2002)

There are also several manuscripts on inverse problems available on the Internet. I can not vouch for any of them.

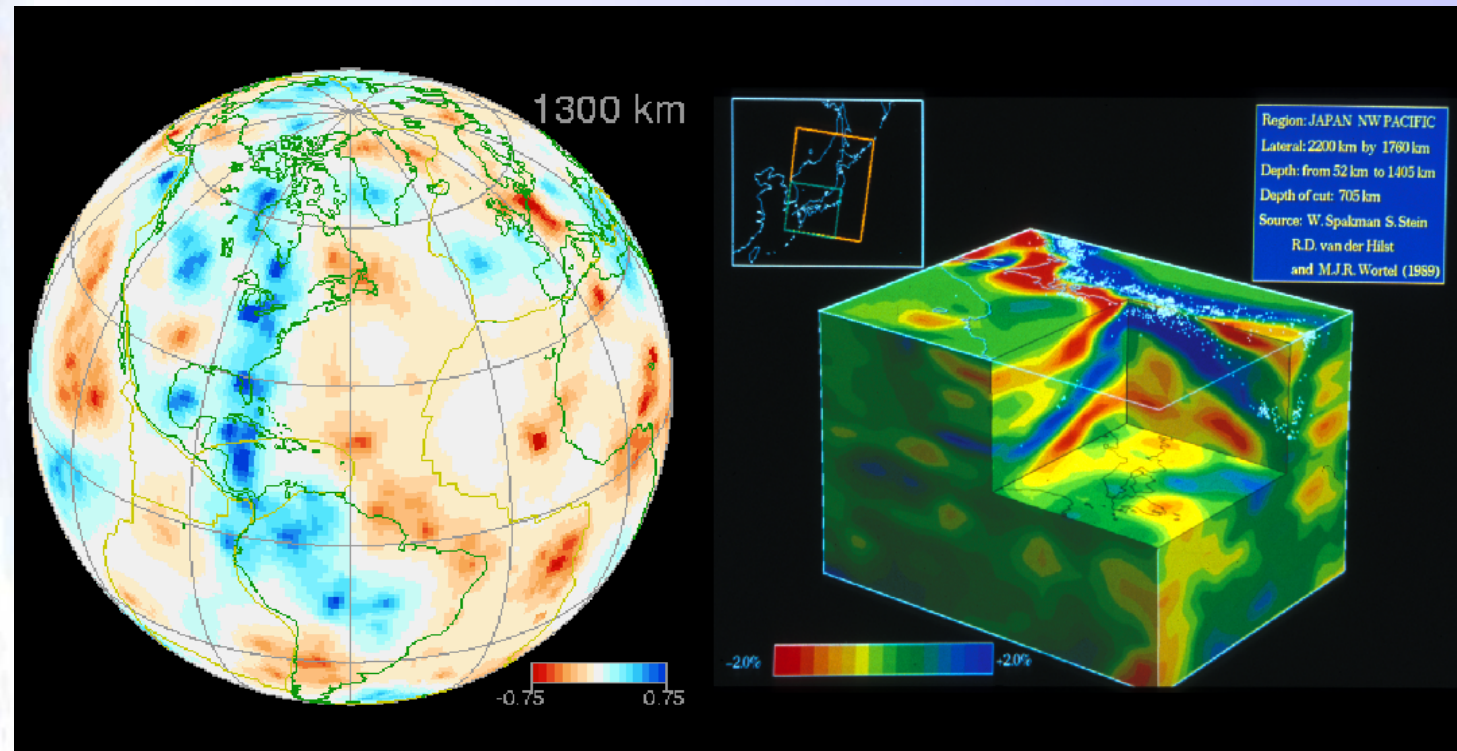
See http://www.ees.nmt.edu/Geop/Classes/GEOP529_book.html



Lecture 1: Introduction

What are inverse problems and why do we care...

Geophysical inverse problems



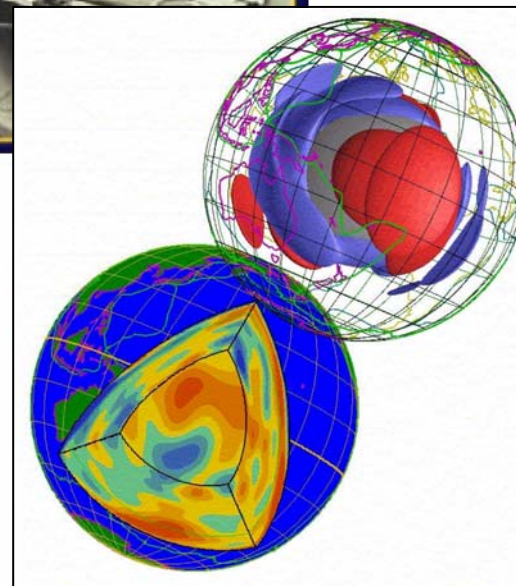
Inferring seismic properties of the Earth's interior
from surface observations



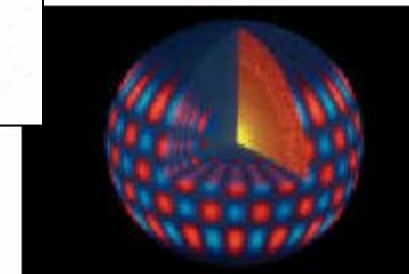
Inverse problems are everywhere



Medical tomography
1970s



Seismic
tomography
1980s



Helioseismology
1990s

When data only indirectly constrain quantities of interest



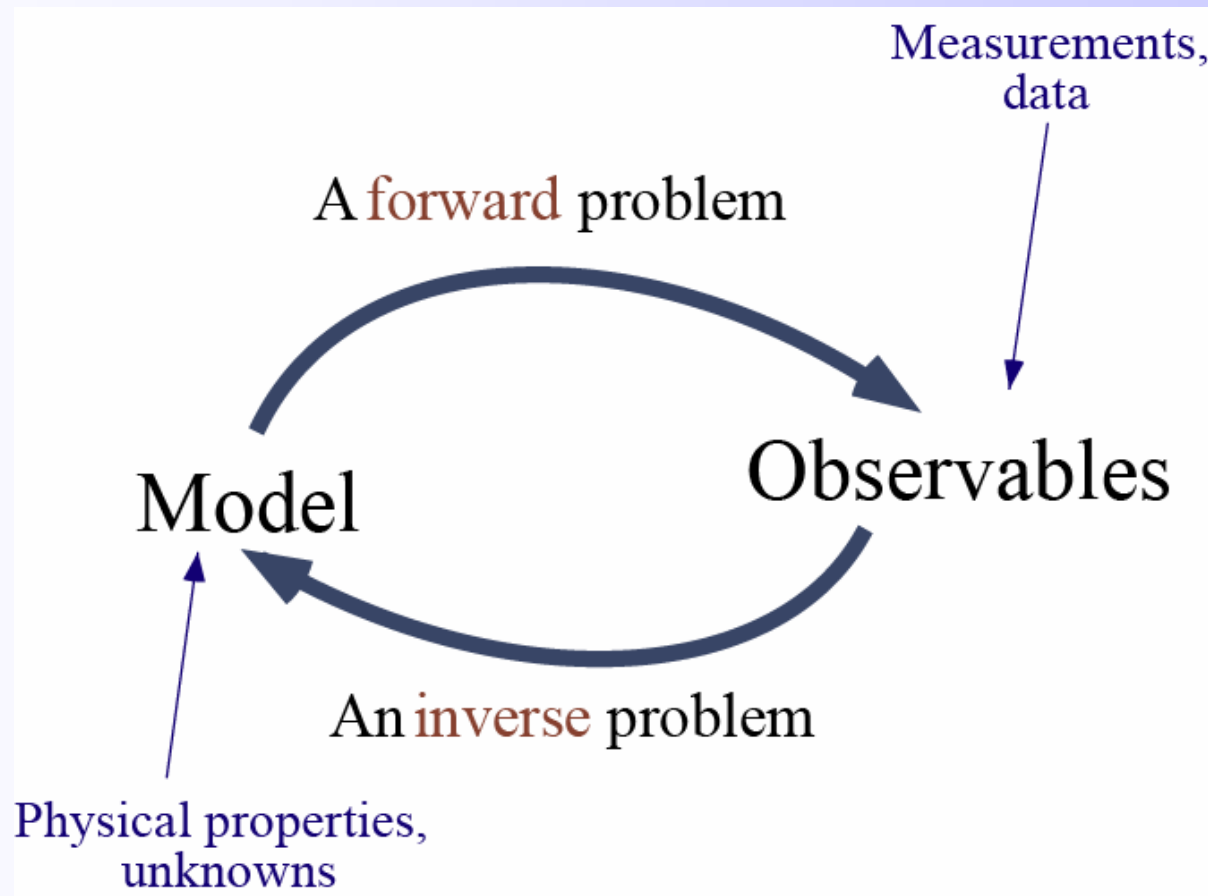
Thinking backwards

Most people, if you describe a train of events to them will tell you what the result will be. There are few people, however that if you told them a result, would be able to evolve from their own inner consciousness what the steps were that led to that result. This power is what I mean when I talk of reasoning backward.

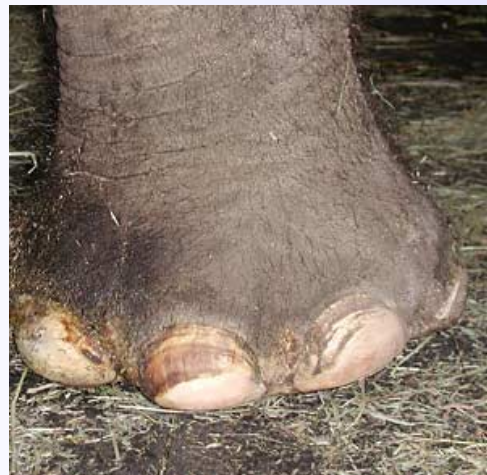
Sherlock Holmes,
A Study in Scarlet,
Sir Arthur Conan Doyle (1887)



Reversing a forward problem



Inverse problems=quest for information



What is that ?

What can we tell about
Who/whatever made it ?

Collect data:

- ➊ Measure size, depth properties of the ground

Can we expect to reconstruct the
whatever made it from the evidence ?

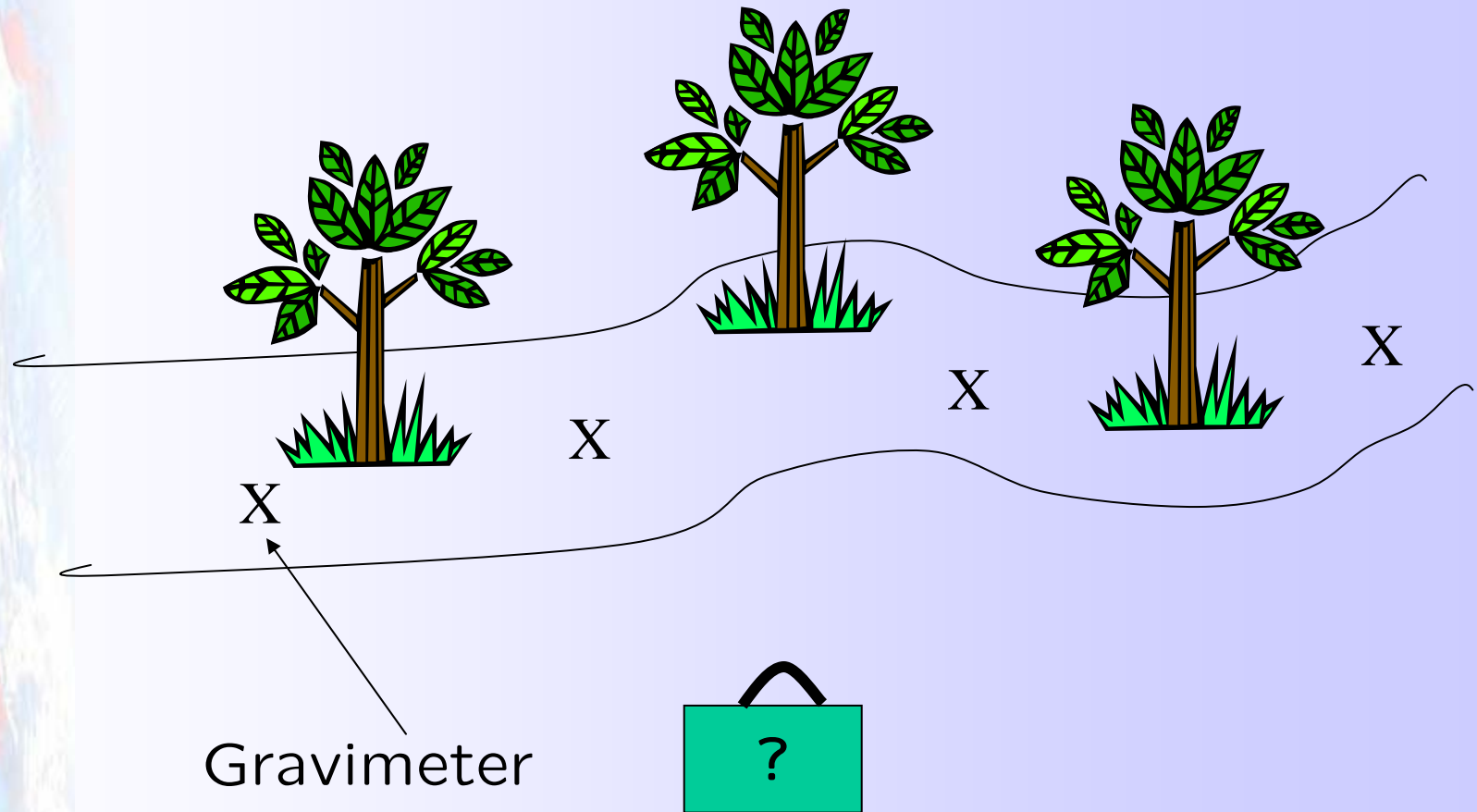
Use our prior knowledge:

- ➋ Who lives around here ?

Make guesses ?

Anatomy of an inverse problem

Hunting for gold at the beach with a gravimeter



Courtesy Heiner Igel

Forward modelling example: Treasure Hunt

We have observed some values:

10, 23, 35, 45, 56 μ gals

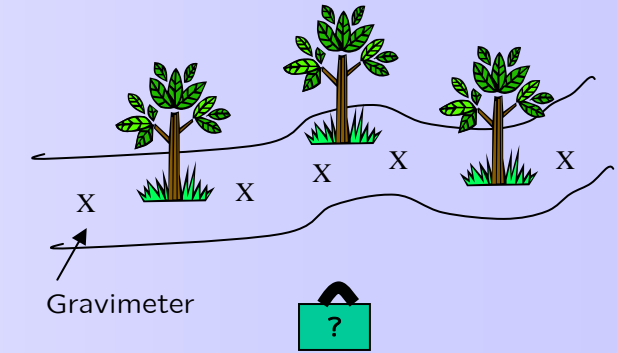
How can we relate the observed gravity values to the subsurface properties?

We know how to do the *forward* problem:

$$\Phi(r) = \int \frac{G\rho(r')}{|r - r'|} dV'$$

This equation relates the (observed) gravitational potential to the subsurface density.

-> given a density model we can predict the gravity field at the surface!



Treasure Hunt: Trial and error

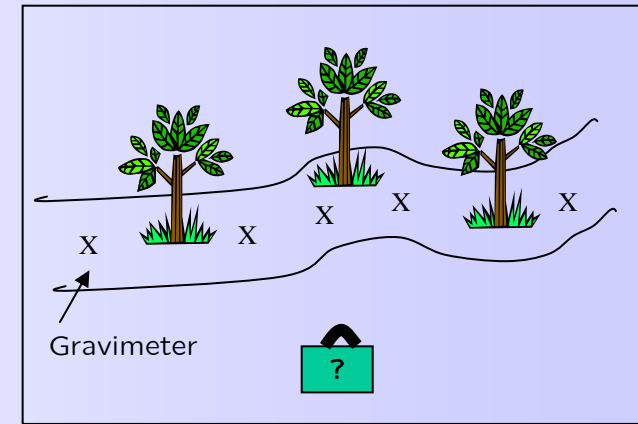
What else do we know?

Density sand: 2.2 g/cm^3

Density gold: 19.3 g/cm^3

Do we know these values *exactly*?

Where is the box with gold?



One approach is trial and (t)error forward modelling

Use the *forward* solution to calculate many models for a rectangular box situated somewhere in the ground and compare the *theoretical (synthetic)* data to the observations.

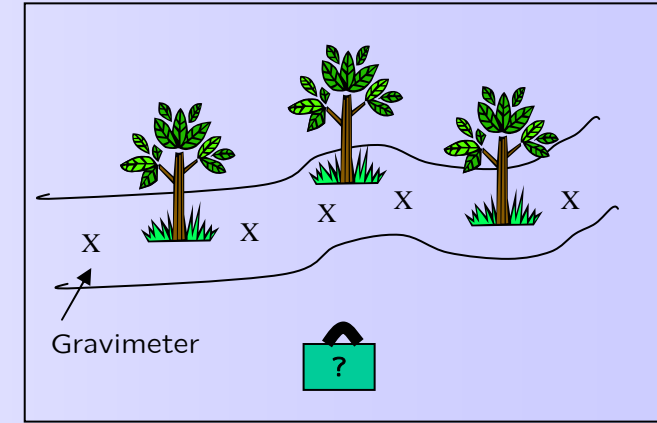
Treasure Hunt: model space

But ...

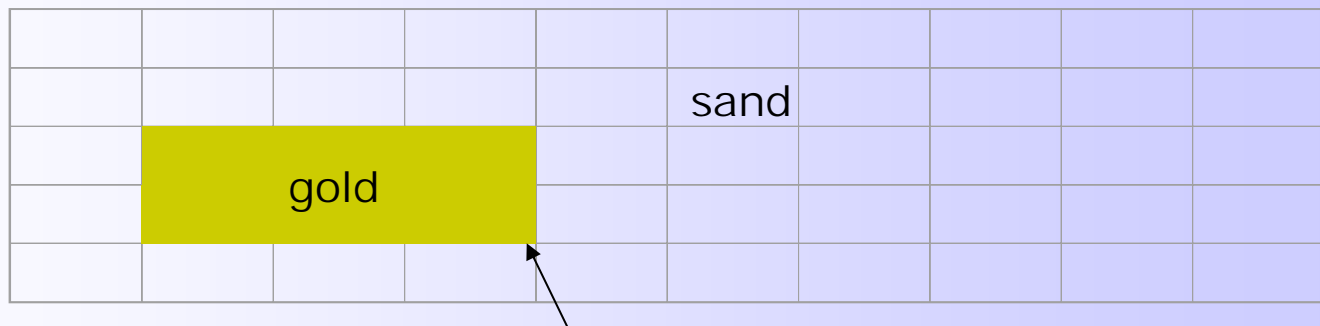
... we have to define *plausible* models for the beach. We have to somehow describe the model geometrically.

We introduce simplifying approximations

- divide the subsurface into rectangles with variable density
- Let us assume a flat surface



X X X surface X X



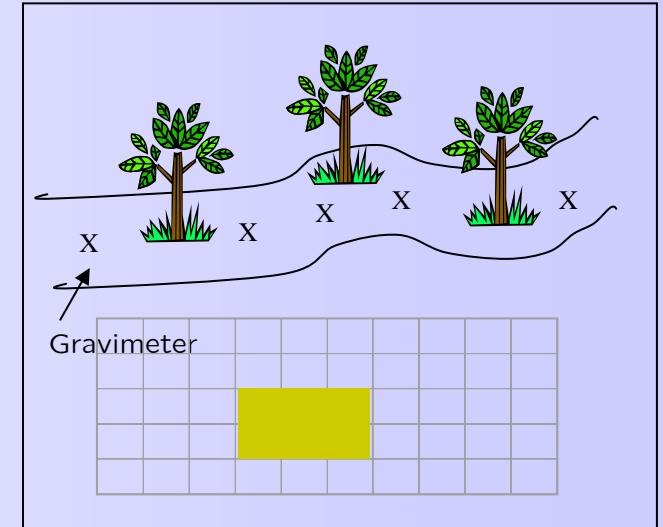
Treasure Hunt: Non-uniqueness

Could we compute all possible models and compare the synthetic data with the observations?

- at every rectangle two possibilities (sand or gold)
- $2^{50} \sim 10^{15}$ possible models

(Age of universe $\sim 10^{17}$ s)

Too many models!



- We have 10^{15} possible models but only 5 observations!
- It is likely that two or more models will fit the data (maybe exactly)

Non-uniqueness is likely

Treasure hunt: a priori information

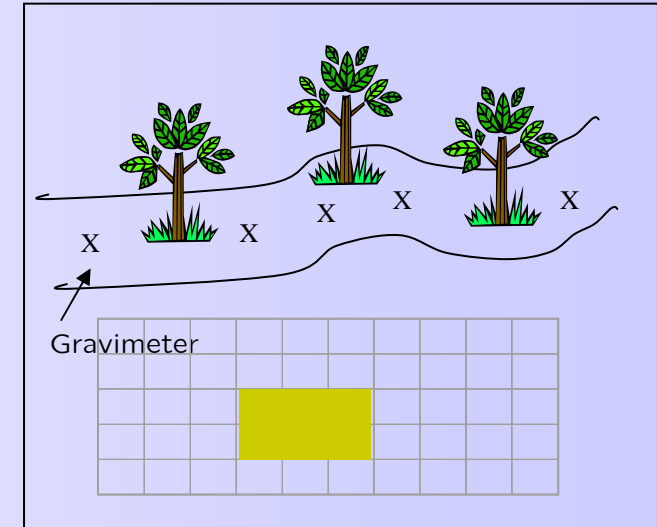
Is there anything we know about the treasure?

How large is the box?

Is it still intact?

Has it possibly disintegrated?

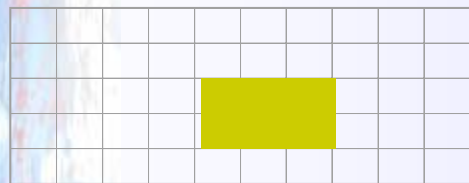
What was the shape of the box?



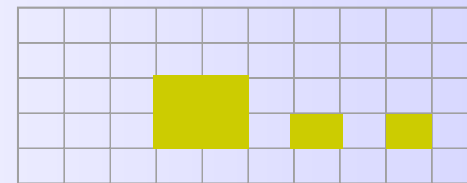
This is called *a priori* (or prior) information.

It will allow us to define plausible, possible, and unlikely models:

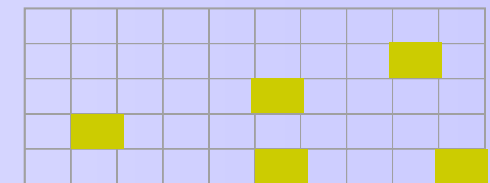
plausible



possible



unlikely

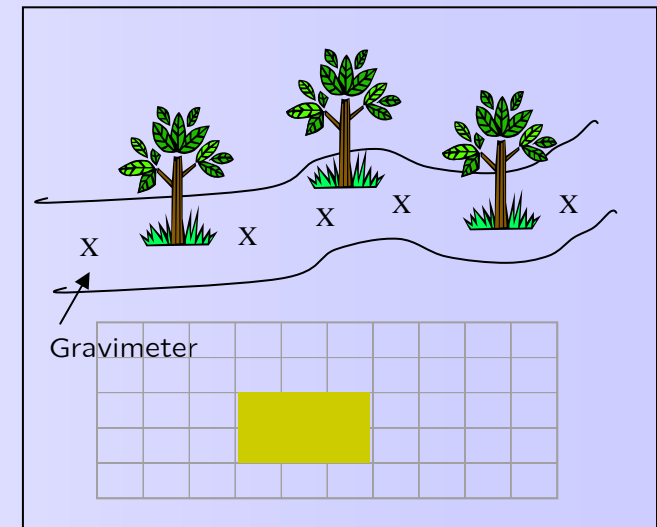


Treasure hunt: data uncertainties

Things to consider in formulating the inverse problem

- Do we have errors in the data ?
 - Did the instruments work correctly ?
 - Do we have to correct for anything?
(e.g. topography, tides, ...)

- Are we using the right theory ?
 - Is a 2-D approximation adequate ?
 - Are there other materials present other than gold and sand ?
 - Are there adjacent masses which could influence observations ?

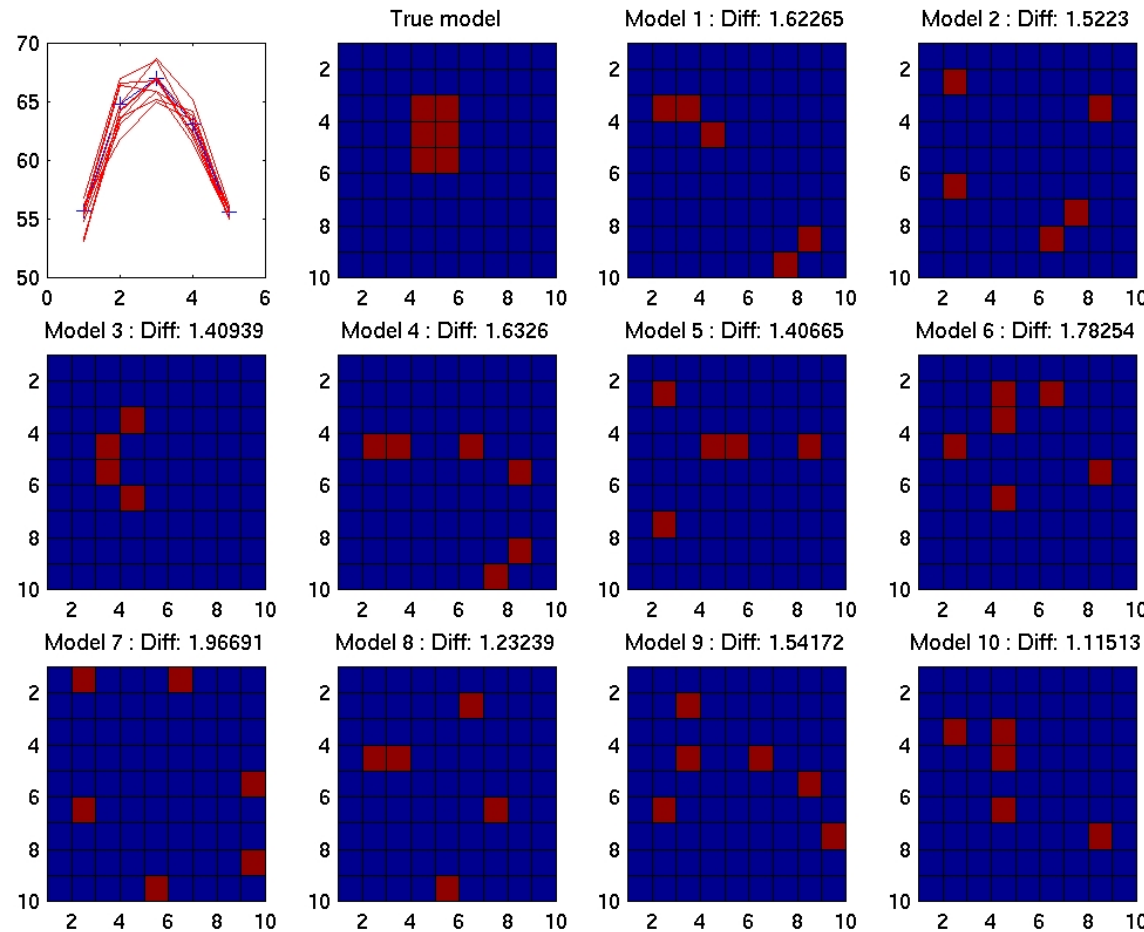


Answering these questions often requires introducing more simplifying assumptions and guesses.

All inferences are dependent on these assumptions. (GIGO)

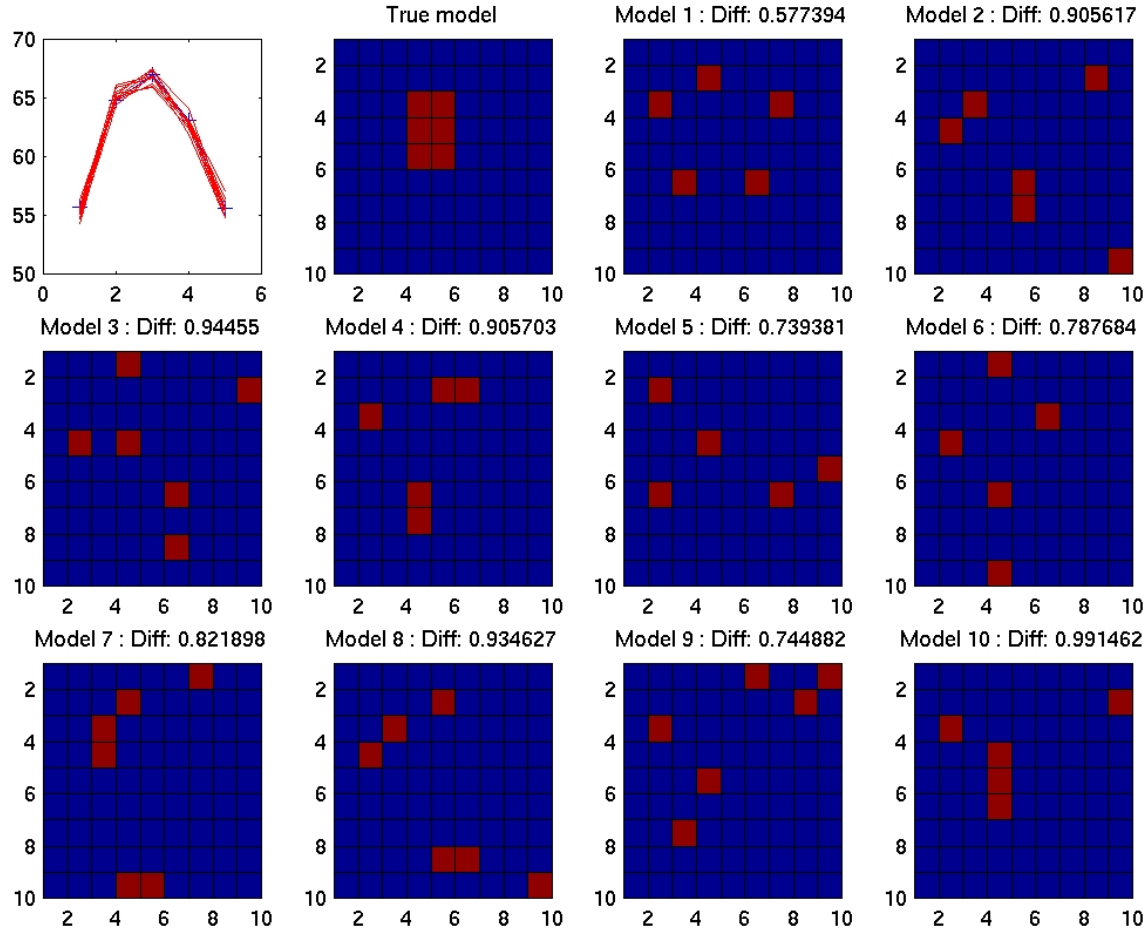
Treasure Hunt: solutions

Models with less than 2% error.



Treasure Hunt: solutions

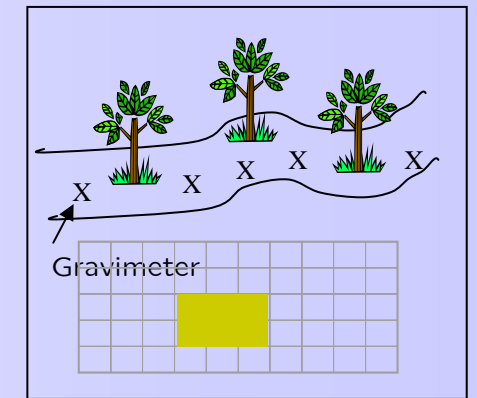
Models with less than 1% error.



What we have learned from one example

Inverse problems = inference about physical systems from data

- Data usually contain errors (data uncertainties)
- Physical theories require approximations
- Infinitely many models will fit the data (non-uniqueness)
- Our physical theory may be inaccurate (theoretical uncertainties)
- Our forward problem may be highly nonlinear
- We always have a finite amount of data



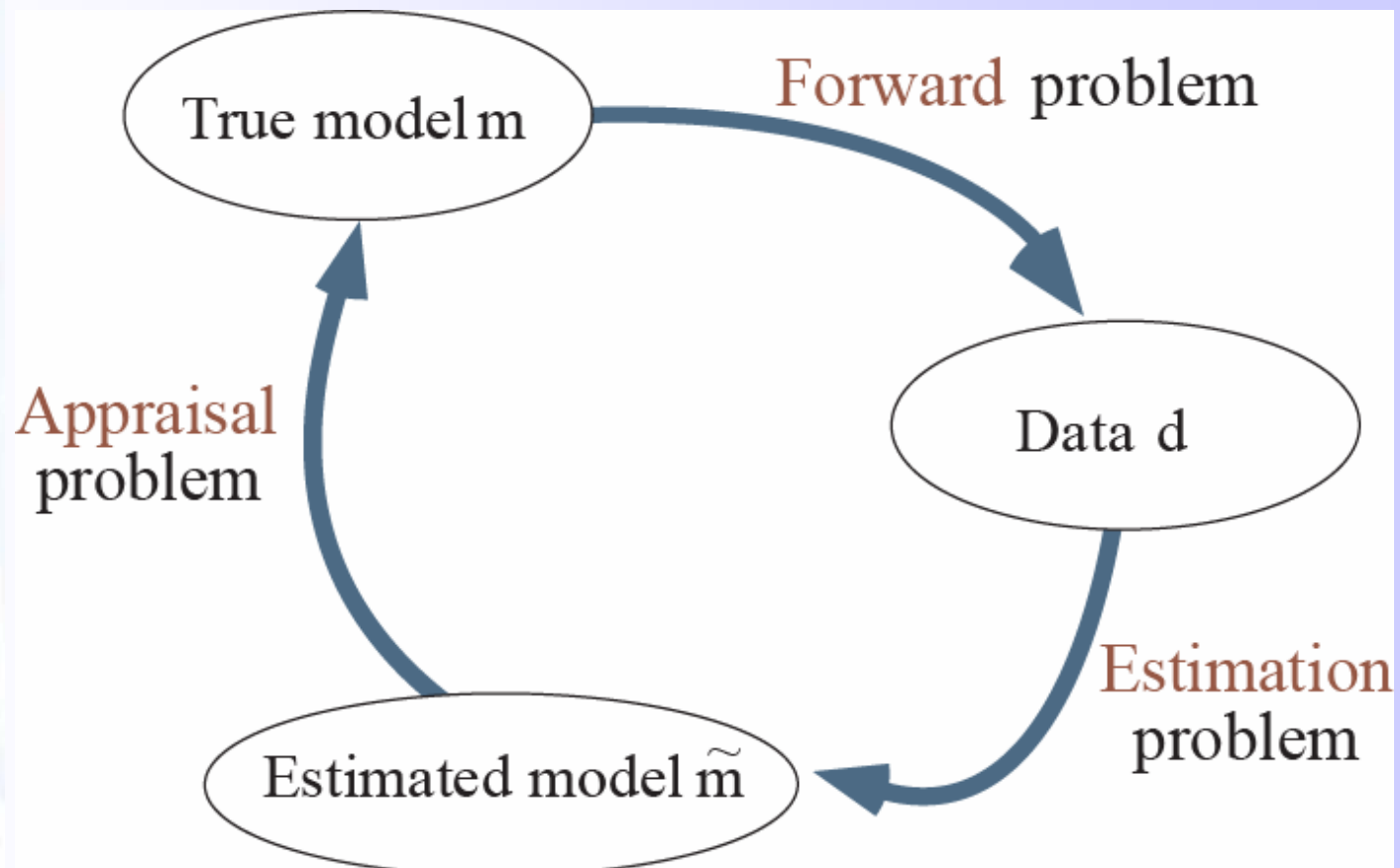
Detailed questions are:

How accurate are our data?

How well can we solve the forward problem?

What independent information do we have on the model space (a priori information) ?

Estimation and Appraisal





Let's be a bit more formal...



What is a model ?

A simplified way of representing physical reality:

- A seismic model of the Lithosphere might consist of a set of layers with P-wavespeed of rocks as a constant in each layer. This is an approximation. The real Earth is more complex.
- A model of density structure that explains a local gravity anomaly might consist of a spherical body of density $\rho + \Delta\rho$ and radius R , embedded in a uniform half-space.
- A model may consist of:
 - A finite set of unknowns representing parameters to be solved for,

$$\mathbf{m} = [m_1, m_2, \dots, m_j, \dots, m_M]$$

e.g. the intercept and gradient in linear regression.

- A continuous function,

$$m(\mathbf{x})$$

e.g. the seismic velocity as a function of depth.



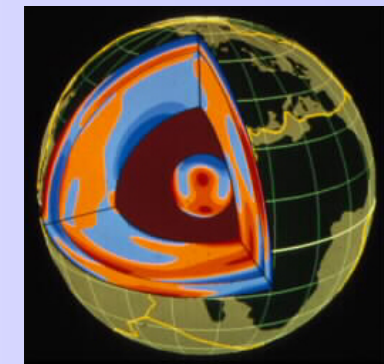
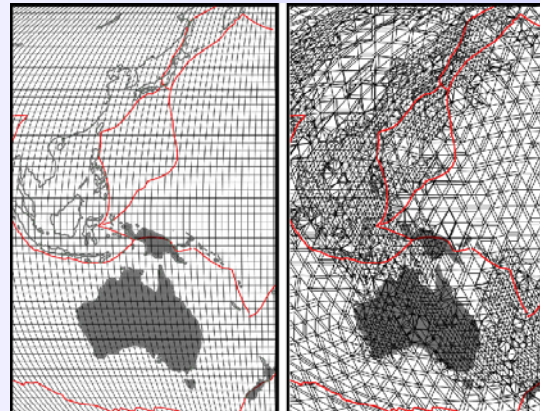
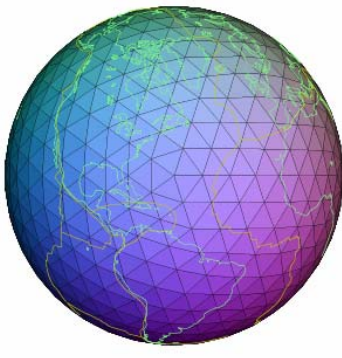
Discretizing a continuous model

Often continuous functions are discretized to produce a finite set of unknowns. This requires use of *Basis functions*

$$m(\mathbf{x}) = \sum_{j=1}^M m_j \phi_j(\mathbf{x})$$

m_j become the unknowns ($j = 1, \dots, M$)

$\phi_j(\mathbf{x})$ are the *chosen* basis functions



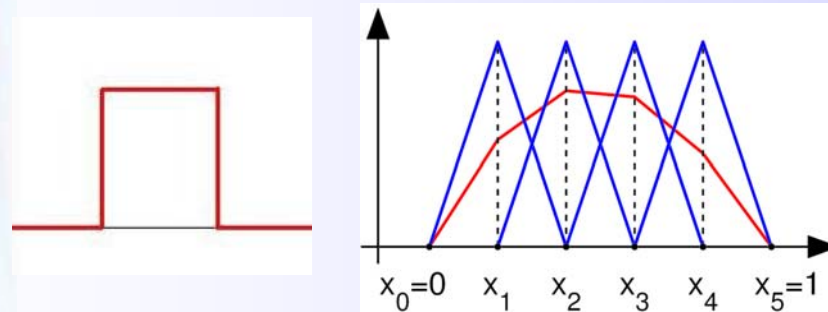
All inferences we can make about the continuous function will be influenced by the choice of basis functions. They must *suit the physics* of the forward problem. They *bound the resolution* of any model one gets out.



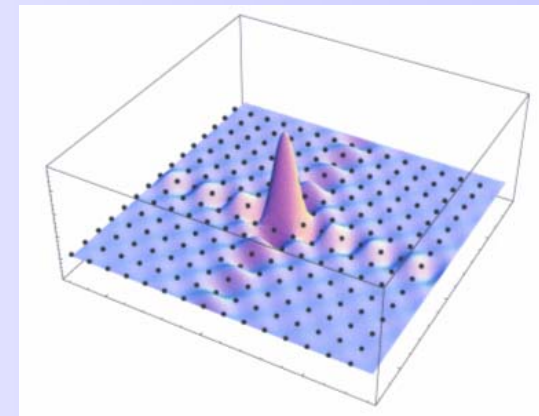
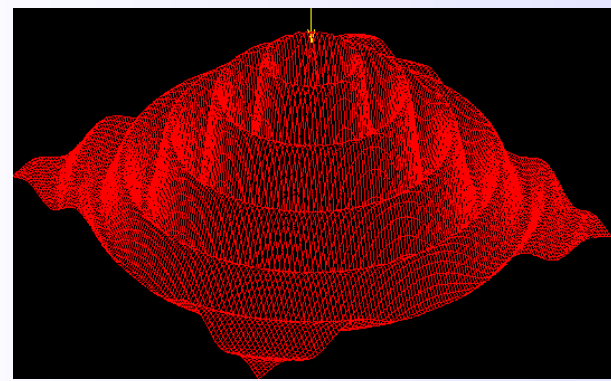
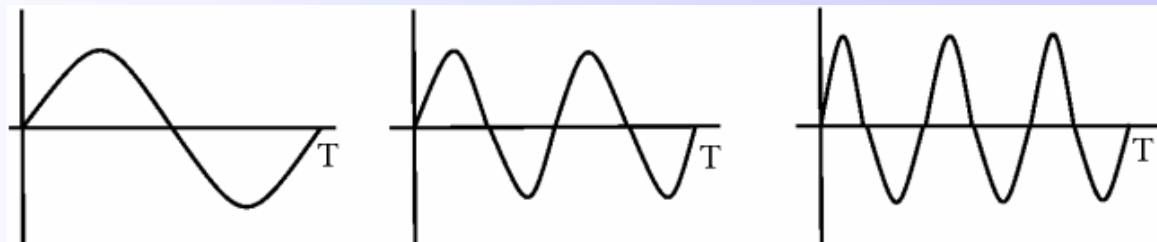
Discretizing a continuous model

Example of *Basis functions*

Local support



Global support





Forward and inverse problems

- Given a model \mathbf{m} the *forward problem* is to predict the data that it would produce \mathbf{d}

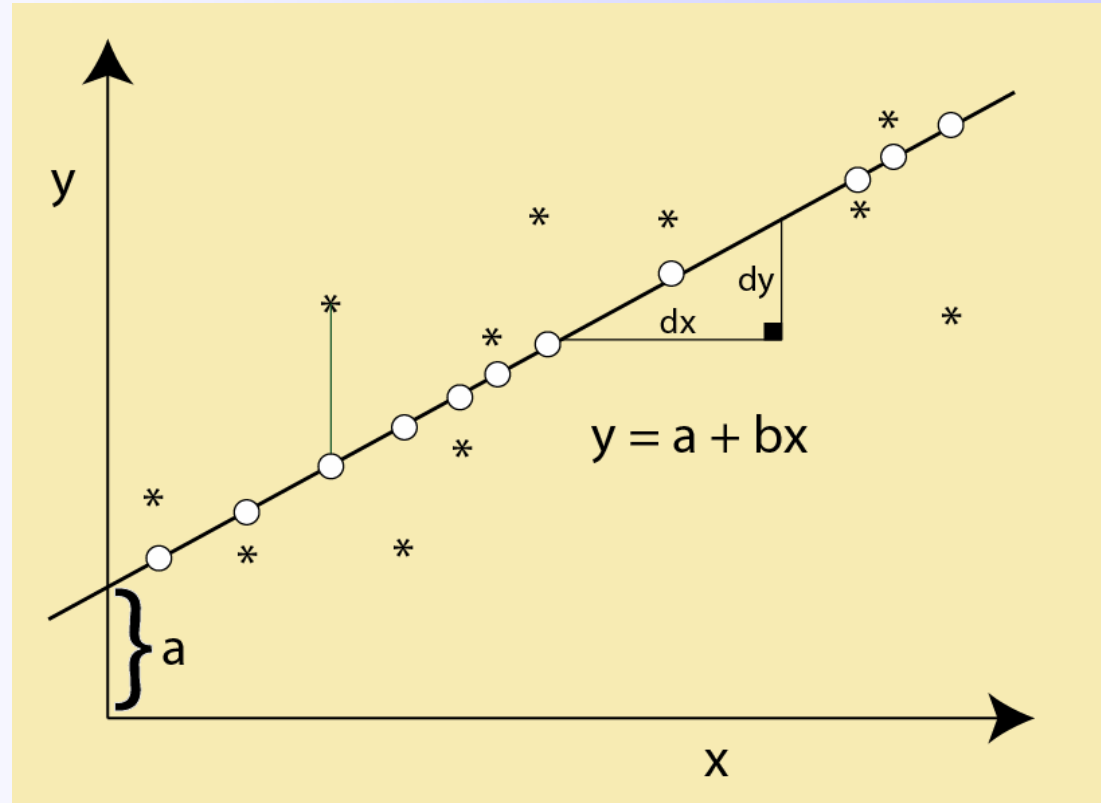
$$\mathbf{d} = g(\mathbf{m})$$

- Given data \mathbf{d} the *inverse problem* is to find the model \mathbf{m} that produced it.

Terminology can be a problem. Applied mathematicians often call the equation above a *mathematical model* and \mathbf{m} as its parameters, while other scientists call G the *forward operator* and \mathbf{m} the model.

Consider the example of linear regression...

Linear Regression



What is the forward problem ?

What is the inverse problem ?



Characterizing inverse Problems

They come in all shapes and sizes...

Types of inverse problem

- Nonlinear and discrete

$$\mathbf{d} = g(\mathbf{m})$$

\mathbf{m} and \mathbf{d} are vectors of finite length and G is a function

Can you think
of examples in
each category ?

- Linear and discrete

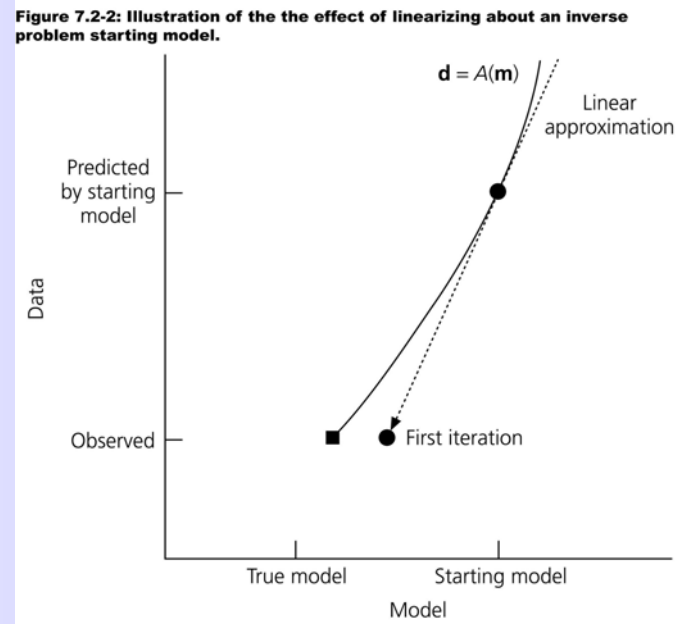
$$\mathbf{d} = \mathbf{G}\mathbf{m}$$

\mathbf{m} is a vector of M unknowns

\mathbf{d} is a vector of N data
and \mathbf{G} is an $M \times N$ matrix.

- Linearized

$$\delta\mathbf{d} = \mathbf{G}\delta\mathbf{m}$$



Perturbations in model parameters from a reference model related linearly to differences between observations and predictions from the reference model.



Types of inverse problem

- Linear and continuous

$$\int_a^b g(s, x)m(x)dx = d(s)$$

$G(x)$ is called an operator and $g(s, x)$ is a kernel.

Fredholm integral equation of the first kind
(these are typically ill-posed)

- Non-Linear and continuous

Can you think
of examples in
each category ?

$$\int_a^b g(s, x, m(x))dx = d(s)$$

$g(s, x, m(x))$ is a nonlinear function of the unknown
function $m(x)$



Linear functions

- A linear function or operator obey the following rules

Superposition $G(m_1 + m_2) = G(m_1) + G(m_2)$

Scaling $G(\lambda m) = \lambda G(m)$

Are the following linear or nonlinear inverse problems

1. We want to predict rock density ρ in the Earth at a given radius r from its center from the known mass M and moment of inertia I of the Earth. We use the following relation:

$$d_i = \int_0^a g_i(r) \rho(r) dr$$

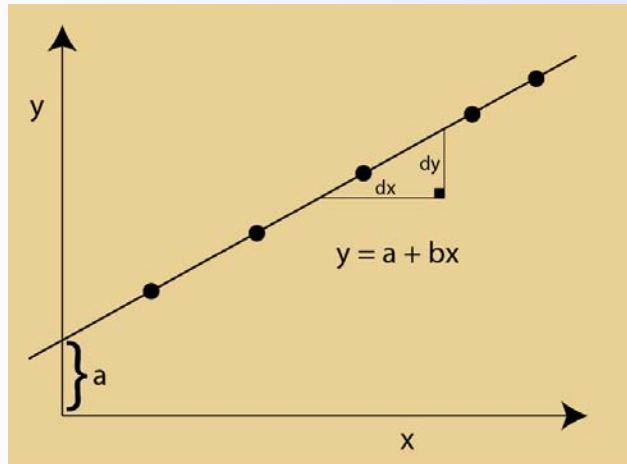
where $d_1 = M$ and $d_2 = I$ and $g_i(r)$ are the corresponding Frechet kernels: $g_1(r) = 4 \pi r^2$ and $g_2(r) = 8/3 \pi r^4$.

2. We want to determine $v(r)$ of the medium from measuring travel time, t for many wave paths.

$$t_i = \int_{R_i} \frac{1}{V(r)} ds$$

Formulating inverse problems

Regression



- Discrete or continuous ?
- Linear or nonlinear ? Why ?
- What are the data ?
- What are the model parameters ?
- Unique or non-unique solution ?

$$\mathbf{d} = \mathbf{Gm}$$

$$\mathbf{d} = [y_1, y_2, \dots, y_N]^T$$

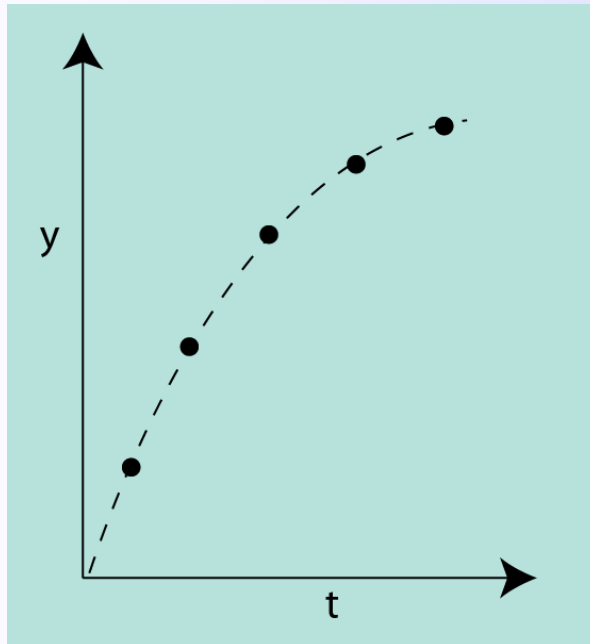
$$\mathbf{m} = [a, b]^T$$

$$G = \begin{pmatrix} 1 & x_1 \\ 1 & x_2 \\ \vdots & \vdots \\ 1 & x_N \end{pmatrix}$$

$$y = a + bx$$

Formulating inverse problems

Ballistic trajectory



- Discrete or continuous ?
- Linear or nonlinear ? Why ?
- What are the data ?
- What are the model parameters ?
- Unique or non-unique solution ?

$$\mathbf{d} = \mathbf{G}\mathbf{m}$$

$$\mathbf{d} = [y_1, y_2, \dots, y_N]^T$$

$$\mathbf{m} = [m_1, m_2, m_3]^T$$

$$G = \begin{pmatrix} 1 & t_1 & -1/2t_1^2 \\ 1 & t_2 & -1/2t_2^2 \\ \vdots & \vdots & \vdots \\ 1 & t_M & -1/2t_M^2 \end{pmatrix}$$

$$y = m_1 + m_2 t - \frac{1}{2} m_3 t^2$$



Recap: Characterising inverse problems

- Inverse problems can be continuous or discrete
- Continuous problems are often discretized by choosing a set of basis functions and projecting the continuous function on them.
- The forward problem is to take a model and predict observables that are compared to actual data. Contains the Physics of the problem. This often involves a mathematical model which is an approximation to the real physics.
- The inverse problem is to take the data and constrain the model in some way.
- We may want to build a model or we may wish to ask a less precise question of the data !



Three classical questions (from Backus and Gilbert, 1968)

The problem with constructing a solution

- The existence problem

Does any model fit the data ?

- The uniqueness problem

Is there a unique model that fits the data ?

- The stability problem

Can small changes in the data produce large changes in the solution ?

(III-posedness)

*Backus and Gilbert (1970)
Uniqueness in the inversion of inaccurate gross earth data.
Phil. Trans. Royal Soc. A, 266, 123-192, 1970.*



Linear discrete inverse Problems

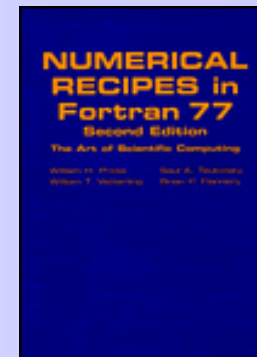
(parameter estimation)

Least squares and all that....

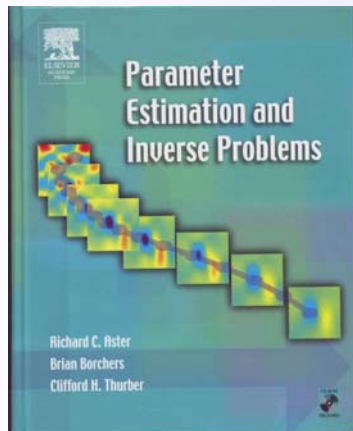
Least squares problems

Least squares is the basis of many parameter estimation and data fitting procedures.

A concise tutorial can be found in Chapter 15 of the book *Numerical Recipes* Press et al. (1992) Cambridge Univ. Press.



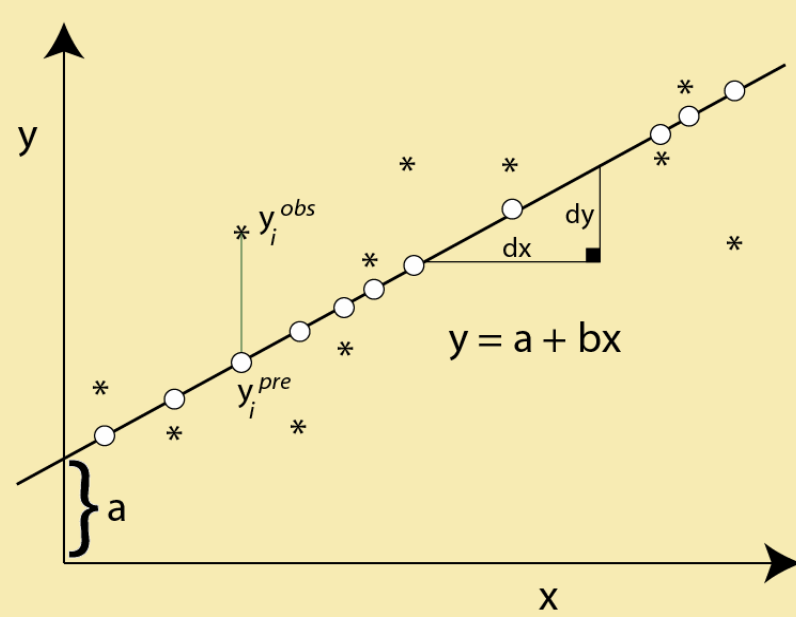
Available for free online at <http://www.nrbook.com>



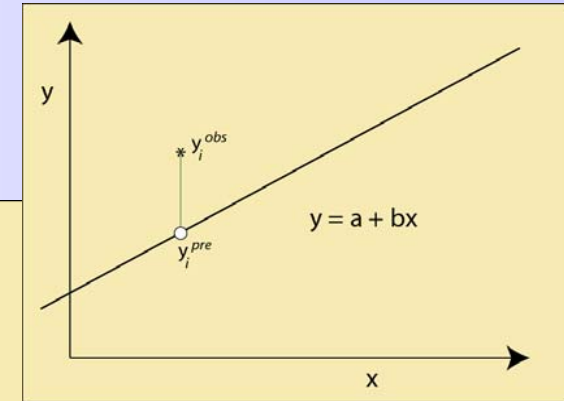
Good explanation of essentials in Aster et al. (2005).

Linear discrete inverse problems

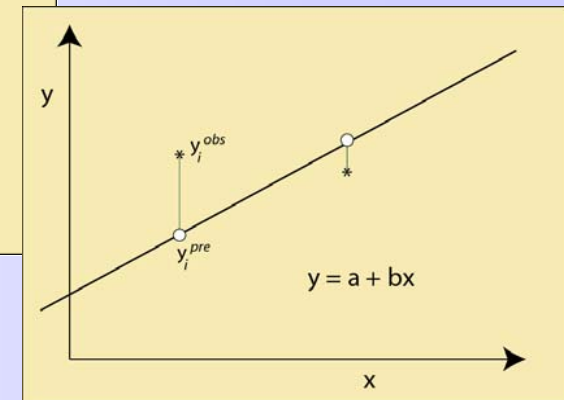
Can a and b be resolved ?



Over-determined



Under-determined



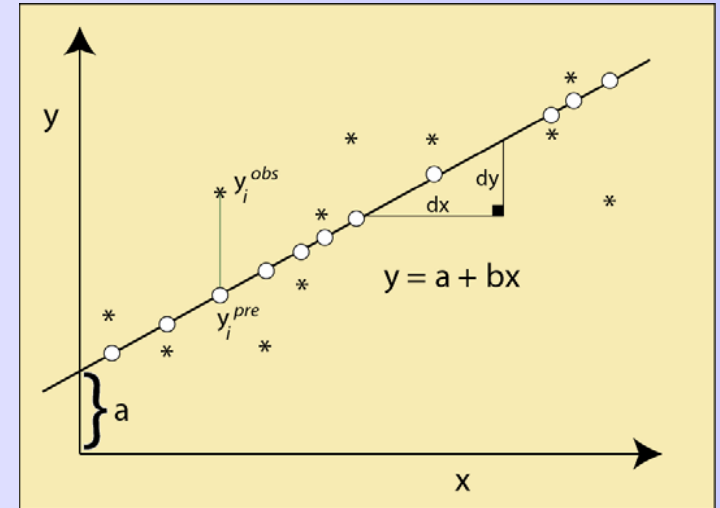
Even-determined

Over-determined: Linear discrete inverse problem

To find the best fit model we can minimize the *prediction error* of the solution

$$r_i(\mathbf{m}) = y_i^{obs} - y_i^{pre}(\mathbf{m})$$

$$\mathbf{r} = \mathbf{d} - \mathbf{G}\mathbf{m}$$



But the data contain errors. Let's assume these are *independent* and *normally* distributed, then we weight each residual inversely by the standard deviation of the corresponding (known) error distribution.

We can obtain a least squares solution by minimizing the *weighted prediction error* of the solution.

$$\phi(\mathbf{m}) = \sum_{i=1}^N \left(\frac{y_i^{obs} - y_i^{pre}(\mathbf{m})}{\sigma_i} \right)^2 = \mathbf{r}^T C_d^{-1} \mathbf{r}$$

$$C_d = \text{diag} [\sigma_1^2, \sigma_2^2, \dots, \sigma_N^2]$$

Over-determined: Linear discrete inverse problem

We seek the model vector \mathbf{m} which minimizes

$$\phi(\mathbf{m}) = \frac{1}{2} \mathbf{r}^T C_d^{-1} \mathbf{r} = \frac{1}{2} (\mathbf{d} - G\mathbf{m})^T C_d^{-1} (\mathbf{d} - G\mathbf{m})$$

Compare with maximum likelihood

Note that this is a quadratic function of the model vector.

Solution: Differentiate with respect to \mathbf{m} and solve for the model vector which gives a zero gradient in $\phi(\mathbf{m})$

This gives...

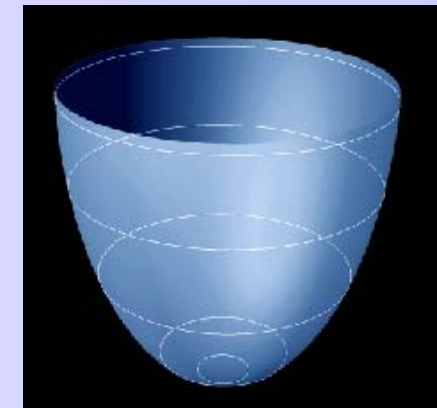
$$\nabla \phi(\mathbf{m}) = -G^T C_d^{-1} (\mathbf{d} - G\mathbf{m}) = 0$$

$$\Rightarrow \mathbf{m} = (G^T C_d^{-1} G)^{-1} G^T C_d^{-1} \mathbf{d}$$

This is the **least-squares** solution.

A solution to the normal equations:

$$G^T G \mathbf{m} = G^T \mathbf{d}$$



Over-determined: Linear discrete inverse problem

How does the Least-squares solution compare to the standard equations of linear regression ?

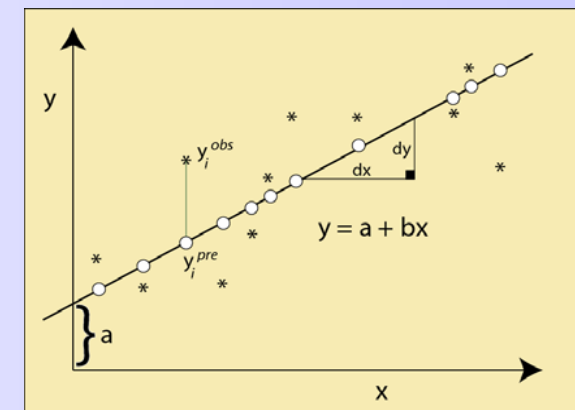
$$\mathbf{m} = (G^T C_d^{-1} G)^{-1} G^T C_d^{-1} \mathbf{d}$$

Given N data y_i with independent normally distributed errors and standard deviations σ_i what are the expressions for the model parameters $\mathbf{m} = [a,b]^\top$?

$$G\mathbf{m} = \begin{bmatrix} 1 & x_1 \\ 1 & x_2 \\ \vdots & \vdots \\ 1 & x_{N_d} \end{bmatrix} \begin{bmatrix} m_1 \\ m_2 \\ \vdots \\ m_N \end{bmatrix} = \begin{bmatrix} d_1 \\ d_2 \\ \vdots \\ d_N \end{bmatrix} = \mathbf{d}$$

$$\mathbf{m} = \begin{bmatrix} N & \sum_{i=1}^N x_i \\ \sum_{i=1}^N x_i & \sum_{i=1}^N x_i^2 \end{bmatrix}^{-1} \begin{bmatrix} \sum_{i=1}^N y_i \\ \sum_{i=1}^N x_i y_i \end{bmatrix}$$

$$\mathbf{m} = \frac{1}{N \sum_{i=1}^N x_i^2 - (\sum_{i=1}^N x_i)^2} \begin{bmatrix} \sum_{i=1}^N x_i^2 & -\sum_{i=1}^N x_i \\ -\sum_{i=1}^N x_i & N \end{bmatrix} \begin{bmatrix} \sum_{i=1}^N y_i \\ \sum_{i=1}^N x_i y_i \end{bmatrix}$$



Linear discrete inverse problem: Least squares

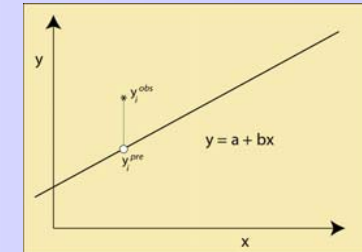
$$\mathbf{m}_{LS} = (G^T C_d^{-1} G)^{-1} G^T C_d^{-1} \mathbf{d} = G^{-g} \mathbf{d}$$

What happens in the under and even-determined cases ?

$$\mathbf{m} = \frac{1}{N \sum_{i=1}^N x_i^2 - (\sum_{i=1}^N x_i)^2} \begin{bmatrix} \sum_{i=1}^N x_i^2 & -\sum_{i=1}^N x_i \\ -\sum_{i=1}^N x_i & N \end{bmatrix} \begin{bmatrix} \sum_{i=1}^N y_i \\ \sum_{i=1}^N x_i y_i \end{bmatrix}$$

- Under-determined, $N=1$:

Matrix has a zero determinant
and a zero eigenvalue
an infinite number of solutions exist

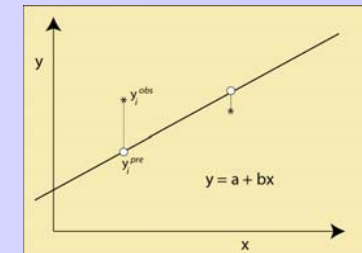


- Even-determined, $N=2$:

$$\mathbf{m} = [m_1, m_2]^T, \quad m_2 = \left[\frac{y_1 - y_2}{x_1 - x_2} \right], \quad m_1 = y_1 - m_2 x_1.$$

$$r = d - Gm = 0$$

Prediction error is zero !



Example: Over-determined, Linear discrete inverse problem

The Ballistics example

Given data and noise

t	y
1	109.3827
2	187.5385
3	267.5319
4	331.8753
5	386.0535
6	428.4271
7	452.1644
8	498.1461
9	512.3499
10	512.9753

$$y_i = m_1 + m_2 t_i - \frac{1}{2} m_3 t_i^2$$

Calculate G

$$C_d^{-1} = \frac{1}{\sigma^2} I \quad G = \begin{pmatrix} 1 & t_1 & -1/2t_1^2 \\ 1 & t_2 & -1/2t_2^2 \\ \vdots & \vdots & \vdots \\ 1 & t_M & -1/2t_M^2 \end{pmatrix}$$
$$\sigma = 8m$$

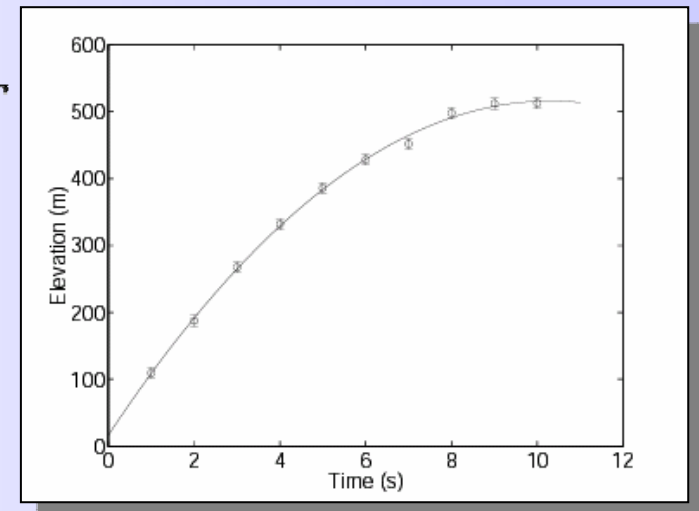
$$\mathbf{m}_{LS} = (G^T C_d^{-1} G)^{-1} G^T C_d^{-1} \mathbf{d}$$

$$\mathbf{m}_{LS} = [16.4m, 97.0m/s, 9.4m/s^2]^T$$

$$\mathbf{m}_{true} = [10m, 100m/s, 9.8m/s^2]^T$$

Is the data fit good enough ?

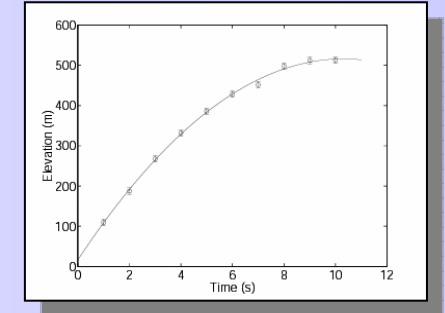
And how to errors in data propagate into the solution ?



The two questions in parameter estimation

We have our fitted model parameters

...but we are far from finished !



We need to:

- Assess the quality of the data fit.

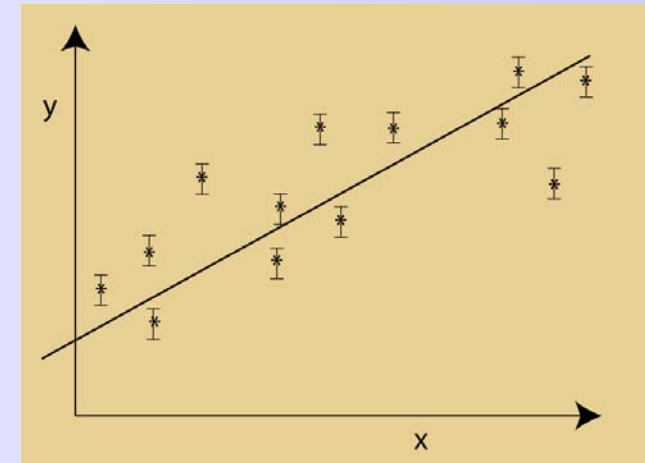
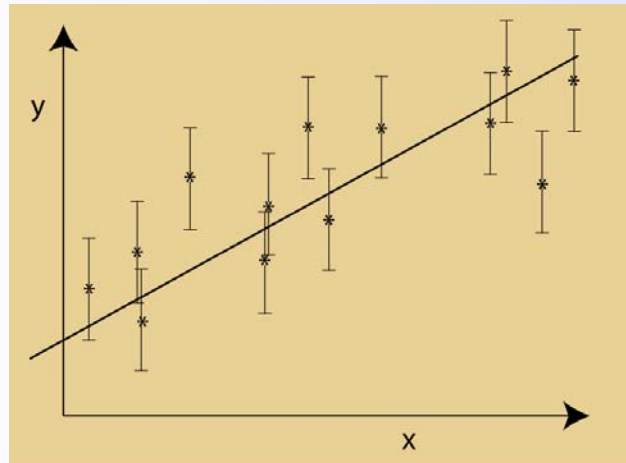
Goodness of fit: Does the model fit the data to within the statistical uncertainty of the noise ?

- Estimate how errors in the data propagate into the model

What are the errors on the model parameters ?

Goodness of fit

Once we have our least squares solution \mathbf{m}_{LS} how do we know whether the fit is good enough given the errors in the data ?



Use the prediction error at the least squares solution !

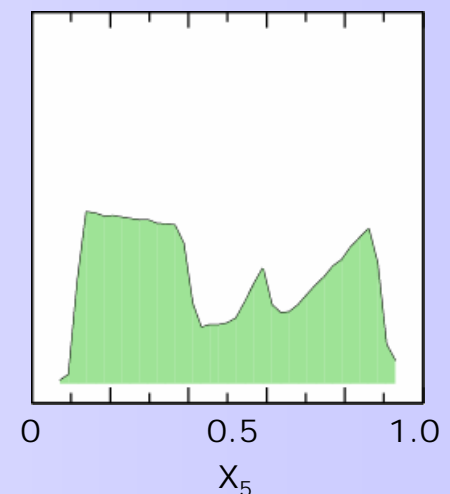
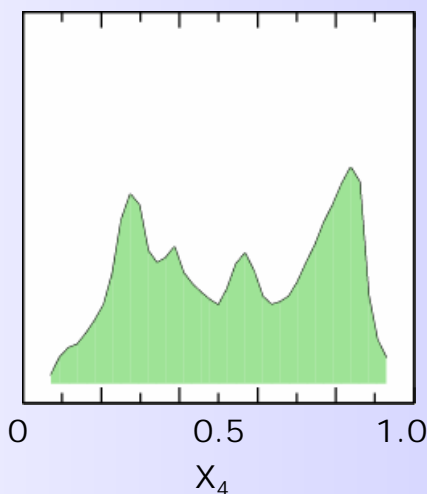
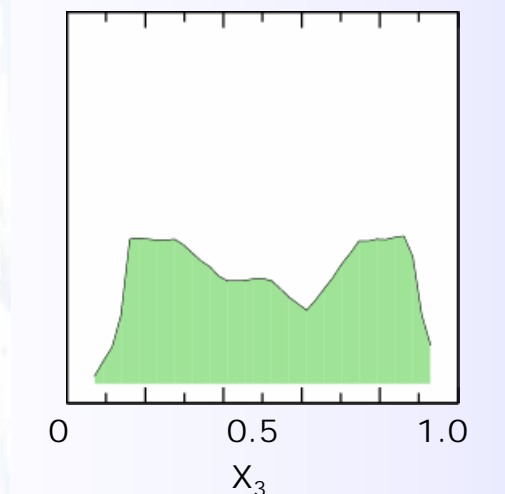
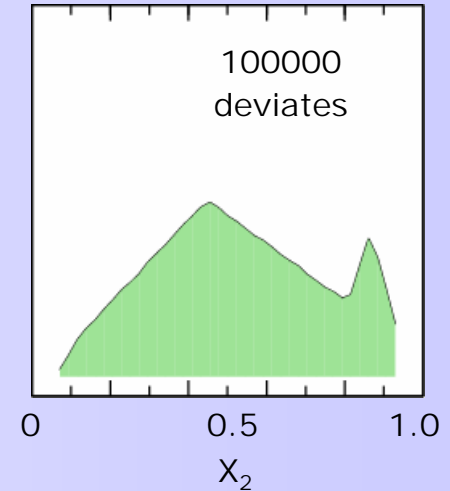
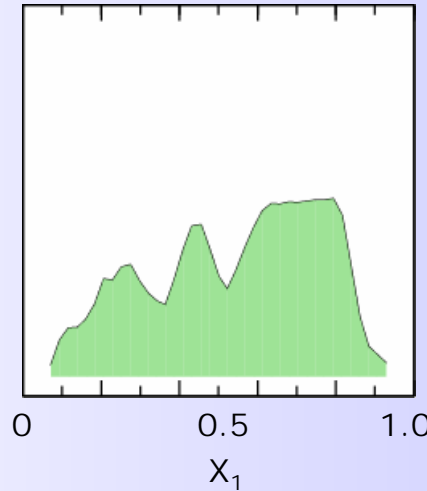
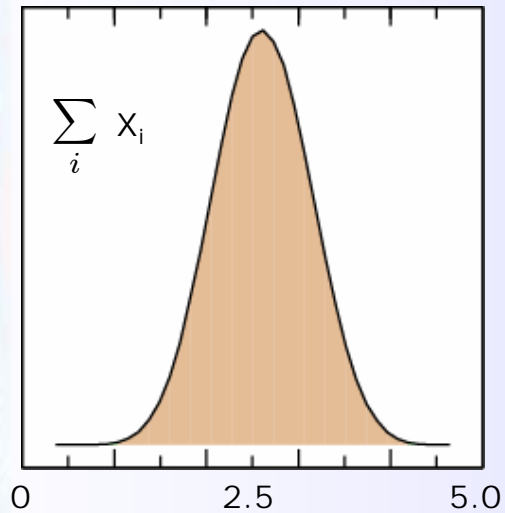
$$\phi(\mathbf{m}_{LS}) = \frac{1}{2} (\mathbf{d} - \mathbf{G}\mathbf{m}_{LS})^T \mathbf{C}_d^{-1} (\mathbf{d} - \mathbf{G}\mathbf{m}_{LS}) = \sum_{i=1}^N \left(\frac{d_i - \sum_{j=1}^M G_{i,j} m_j}{\sigma_i} \right)^2$$

If data errors are Gaussian this as a chi-square statistic χ^2_{obs}



Why do we always assume errors are Gaussian ?

Probability density functions of 5 random variables

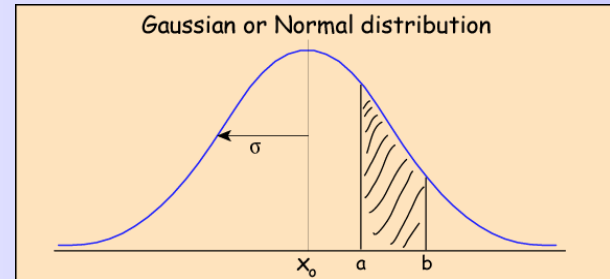


Mathematical Background: Probability distributions

- A random variable x follows a *Normal* or *Gaussian* probability density function if

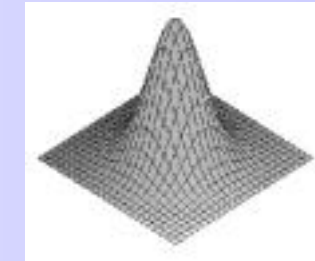
$$p(x) = \frac{1}{\sigma\sqrt{2\pi}} \exp\left\{-\frac{(x - x_o)^2}{2\sigma^2}\right\}$$

$$\Pr(x : a \leq x \leq b) = \int_a^b p(x) dx$$



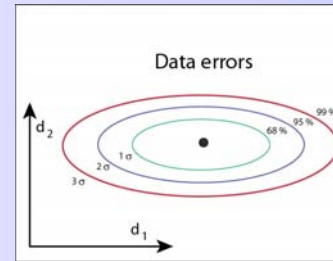
- Multivariate case

$$p(\mathbf{x}) = \frac{1}{\sigma^N (2\pi)^{N/2}} \exp\left\{\sum_{i=1}^N \frac{-(x_i - x_{o,i})^2}{2\sigma^2}\right\}$$



$$p(\mathbf{x}) = \frac{1}{(2\pi)^{N/2} |C_d|^{N/2}} \exp\left\{-1/2(\mathbf{x} - \mathbf{x}_o)^T C_d^{-1} (\mathbf{x} - \mathbf{x}_o)\right\}$$

If data covariance matrix is diagonal then data errors are independent.

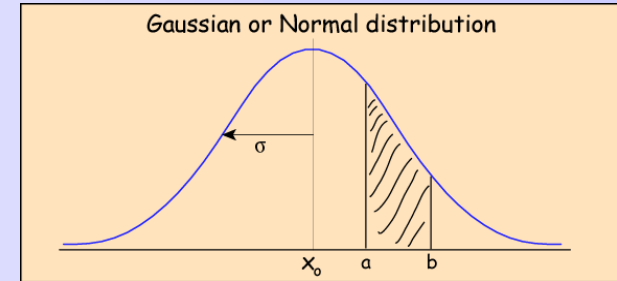


Mathematical Background: Probability distributions

Expectation operator

$$E\{X\} = \int_{-\infty}^{\infty} xp(x)dx$$

$$E\{g(X)\} = \int_{-\infty}^{\infty} g(x)p(x)dx$$



Expectation of a Gaussian random variable

$$E\{X\} = \frac{1}{\sigma\sqrt{2\pi}} \int_{-\infty}^{\infty} xe^{\frac{-(x-\mu)^2}{2\sigma^2}} dx = \mu$$

Variance

$$\text{Var}(X) = E\{(X - E\{X\})^2\} = E\{X^2\} - (E\{X\})^2 = \sigma^2$$

Covariance

$$\text{Cov}(X, Y) = E\{(X - E\{X\})(Y - E\{Y\})\} = E\{XY\} - E\{X\}E\{Y\}$$

If X and Y are independent then

$$E\{XY\} = E\{X\}E\{Y\} \Rightarrow \text{Cov}(X, Y) = 0$$

Mathematical Background: Probability distributions

Multi-dimensional Gaussian

$$p(\mathbf{x}) = k \exp \left\{ -1/2(\mathbf{x} - \mathbf{x}_o)^T C_d^{-1} (\mathbf{x} - \mathbf{x}_o) \right\}$$

Expectation of a Gaussian random vector

$$E\{\mathbf{X}\} = \int \mathbf{x} p(\mathbf{x}) d\mathbf{x} = \mathbf{x}_o$$

Covariance matrix

$$E\{(\mathbf{X} - E\{\mathbf{X}\})(\mathbf{Y} - E\{\mathbf{Y}\})\} = E\{\mathbf{XY}\} - E\{\mathbf{X}\}E\{\mathbf{Y}\}$$

Correlation matrix

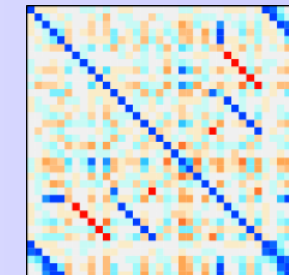
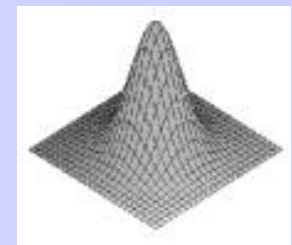
$$\rho(X, Y) = \frac{Cov(X, Y)}{\sqrt{Var(X)Var(Y)}}$$

$$= C_d \quad \begin{bmatrix} \sigma_{1,1} & \sigma_{1,2} & \sigma_{1,3} & \sigma_{1,4} \\ \sigma_{2,1} & \sigma_{2,2} & \sigma_{2,3} & \sigma_{2,4} \\ \sigma_{3,1} & \sigma_{3,2} & \sigma_{3,3} & \sigma_{3,4} \\ \sigma_{4,1} & \sigma_{4,2} & \sigma_{4,3} & \sigma_{4,4} \end{bmatrix}$$

Independence between X and Y $\rho(X, Y) = 0$

Positive or negative correlation

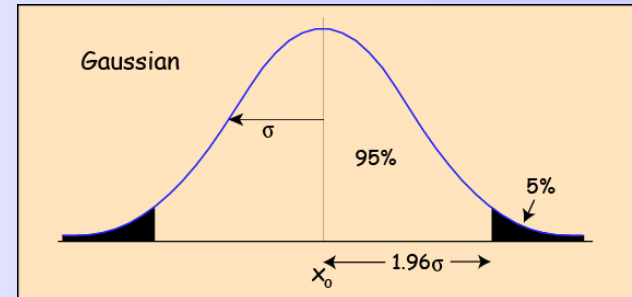
$$-1 \leq \rho(X, Y) \leq 1$$



Background: Chi-square distribution

If x follows a Normal distribution

$$p(x) = \frac{1}{\sigma\sqrt{2\pi}} \exp\left\{-\frac{x^2}{2\sigma^2}\right\}$$

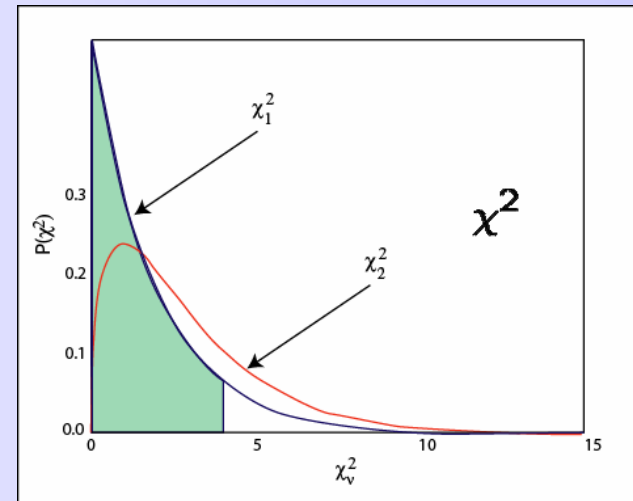


What distribution does the square of x follow ?

Answer: A chi-square distribution with
1 degree of freedom

$$\chi_1^2(95\%) = 3.84$$

$$\Rightarrow x = 1.96$$



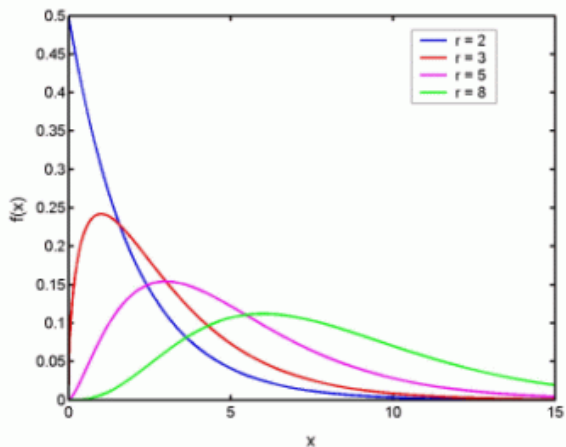
If x_1 and x_2 are Normal, what distribution does $y=x_1^2 + x_2^2$ follow ?

Answer: A chi-square distribution with
2 degrees of freedom

Goodness of fit

For Gaussian data errors the data prediction error is the square of a Gaussian random variable hence it has a chi-square probability density function with $N-M$ degrees of freedom.

$$\chi^2_{obs} = \sum_{i=1}^N \left(\frac{d_i - \sum_{j=1}^M G_{i,j} m_j}{\sigma_i} \right)^2$$



ndf	$\chi^2(5\%)$	$\chi^2(50\%)$	$\chi^2(95\%)$
5	1.15	4.35	11.07
10	3.94	9.34	18.31
20	10.85	19.34	31.41
50	34.76	49.33	67.50
100	77.93	99.33	124.34

$$p = Pr(\chi^2 \geq \chi^2_{obs})$$

$$f_{\chi^2}(x) = \frac{1}{2^{\nu/2}\Gamma(\nu/2)} x^{\nu/2-1} e^{-x/2}$$

$$p = \int_{\chi^2_{obs}}^{\infty} f_{\chi^2}(x) dx$$

The χ^2 test provides a means to testing the assumptions that went into producing the least squares solution. It gives the likelihood that the fit actually achieved is reasonable.

Example: Goodness of fit

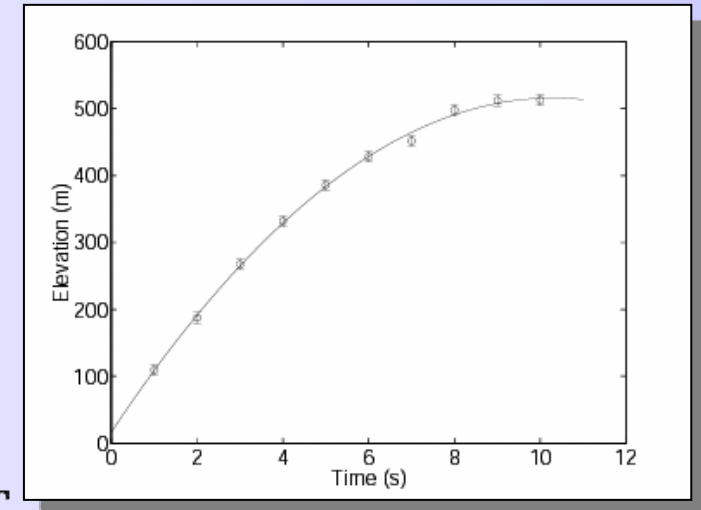
The Ballistics problem

Given data and noise

t	y
1	109:3827
2	187:5385
3	267:5319
4	331:8753
5	386:0535
6	428:4271
7	452:1644
8	498:1461
9	512:3499
10	512:9753

$$C_D^{-1} = \frac{1}{\sigma^2} I$$
$$\sigma = 8m$$

$$\mathbf{m}_{LS} = [16.4m, 97.0m/s, 9.4m/s^2]^T$$



$$\chi_{obs}^2 = \sum_{i=1}^N \left(\frac{d_i - \sum_{j=1}^M G_{i,j} m_j}{\sigma_i} \right)^2 = 4.2$$

How many degrees of freedom ? $v = N - M = 10 - 3 = 7$

$$p = Pr(\chi^2 \geq \chi_{obs}^2) = 0.76$$

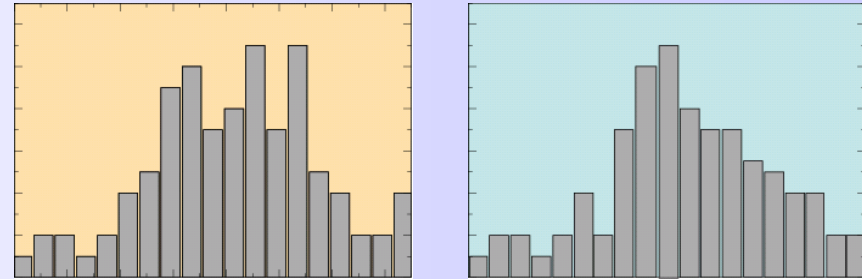
In practice values between 0.1 and 0.9 are plausible

Variance ratio

Another way of looking at the chi-square statistic is as the variance ratio of two distributions.

Given two sets of random samples

$$\begin{aligned}\{x_1, x_2, \dots, x_N\} \\ \{y_1, y_2, \dots, y_N\}\end{aligned}$$



Question: Did they come from the same distribution or not ?

The ratio of the variances of the two distributions follows a chi-square distribution.

$$\chi^2 = \frac{\sum_{i=1}^N (x_i - \bar{x})^2}{\sum_{j=1}^N (y_j - \bar{y})^2}$$

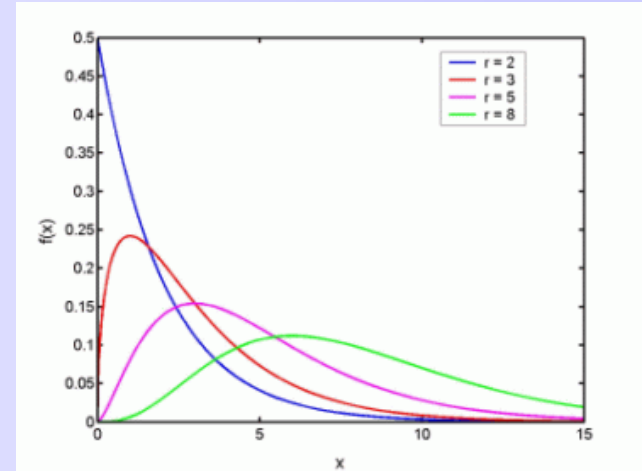
$$\left[\chi^2_{obs} = \sum_{i=1}^N \frac{(d_i - \sum_{j=1}^M G_{i,j} m_j)^2}{\sigma_i^2} \right]$$

Chi-square tables tell us the likelihood that the two sets of observables come from the same distribution.

Goodness of fit

For Gaussian data errors the chi-square statistic has a chi-square distribution with $v = N-M$ degrees of freedom.

<i>ndf</i>	$\chi^2(5\%)$	$\chi^2(50\%)$	$\chi^2(95\%)$
5	1.15	4.35	11.07
10	3.94	9.34	18.31
20	10.85	19.34	31.41
50	34.76	49.33	67.50
100	77.93	99.33	124.34



Exercise:

- If I fit 7 data points with a straight line and get $\chi^2 = 10^{-2}$ what would you conclude ?
- If I fit 102 data points with a straight line and get $\chi^2 = 1034.15$ what would you conclude ?
- If I fit 52 data points with a straight line and get $\chi^2 = 50$ what would you conclude ?

Goodness of fit

For Gaussian data errors the chi-square statistic has a chi-square distribution with $v = N-M$ degrees of freedom.

ndf	$\chi^2(5\%)$	$\chi^2(50\%)$	$\chi^2(95\%)$
5	1.15	4.35	11.07
10	3.94	9.34	18.31
20	10.85	19.34	31.41
50	34.76	49.33	67.50
100	77.93	99.33	124.34

What could be the cause if:

- the prediction error is much too large ? (poor data fit)

 Truly unlikely data errors

 Errors in forward theory

 Under-estimated data errors

- the prediction error is too small ? (too good data fit)

 Truly unlikely data errors

 Over-estimated the data errors

 Fraud !

Solution error

Once we have our least squares solution \mathbf{m}_{LS} and we know that the data fit is acceptable, how do we find the likely errors in the model parameters arising from errors in the data ?

$$\mathbf{m}_{LS} = G^{-g} \mathbf{d}$$

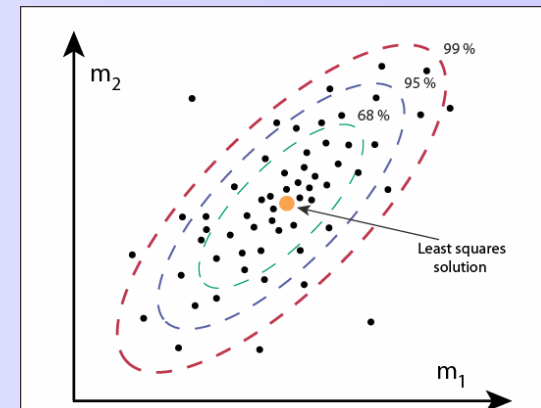
The data set we actually observed is only one realization of the many that could have been observed

$$\mathbf{d}' \rightarrow \mathbf{d} + \boldsymbol{\epsilon}$$

$$\mathbf{m}'_{LS} \rightarrow \mathbf{m}_{LS} + \boldsymbol{\epsilon}_m$$

$$\mathbf{m}'_{LS} = G^{-g} \mathbf{d}'$$

$$\mathbf{m}_{LS} + \boldsymbol{\epsilon}_m = G^{-g}(\mathbf{d} + \boldsymbol{\epsilon})$$



The effect of adding noise to the data is to add noise to the solution

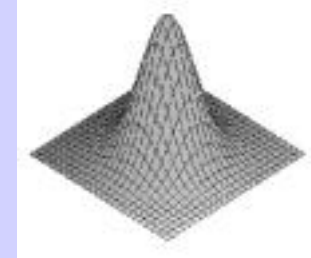
$$\boldsymbol{\epsilon}_m = G^{-g} \boldsymbol{\epsilon}$$

The model noise is a linear combination of the data noise !

Solution error: Model Covariance

Multivariate Gaussian data error distribution

$$p(\epsilon) = \frac{1}{(2\pi)^{N_d/2} |C_d|^{N_d/2}} \exp \left\{ -\frac{1}{2} \epsilon^T C_d^{-1} \epsilon \right\}$$



How to turn this into a probability distribution for the model errors ?

We know that the **solution error** is a linear combination of the **data error**

$$\epsilon_m = G^{-g} \epsilon$$

The covariance of any linear combination $A\mathbf{d}$ of Gaussian distributed random variables \mathbf{d} is

$$\text{Cov}(A\mathbf{d}) = A \text{Cov}(\mathbf{d}) A^T$$

So we have the covariance of the model parameters

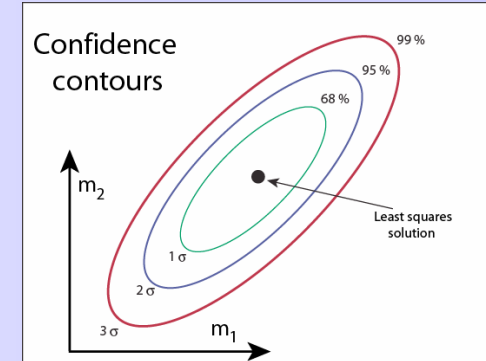
$$C_M = (G^{-g}) C_d (G^{-g})^T$$

Solution error: Model Covariance

$$C_M = (G^{-g}) C_d (G^{-g})^T$$

$$G^{-g} = (G^T C_d^{-1} G)^{-1} G^T C_d^{-1}$$

$$\Rightarrow \boxed{C_M = (G^T C_d^{-1} G)^{-1}}$$

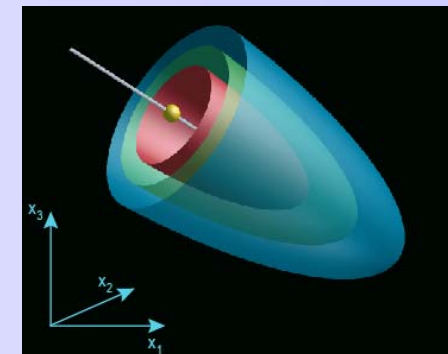


The model covariance for a least squares problem depends on data errors and not the data itself ! G is controlled by the design of the experiment.

$$p(\epsilon_m) = k' \exp \left\{ -\frac{1}{2} (\mathbf{m} - \mathbf{m}_{LS})^T C_M^{-1} (\mathbf{m} - \mathbf{m}_{LS}) \right\}$$

\mathbf{m}_{LS} is the least squares solution

The data error distribution gives a model error distribution !

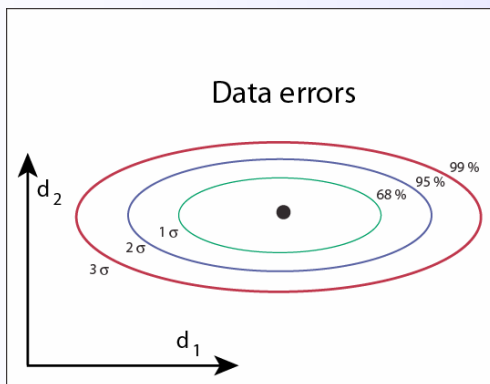


Solution error: Model Covariance

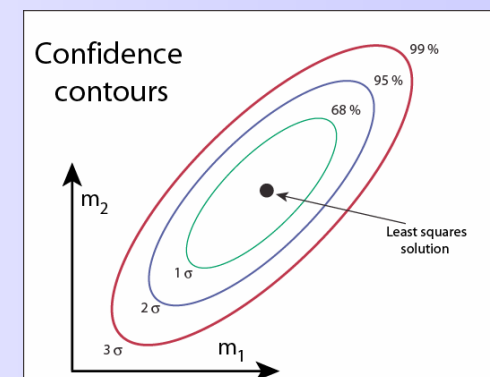
$$C_M = (G^T C_d^{-1} G)^{-1}$$

For the special case of independent data errors $C_d = \sigma^2 I$

$$C_M = \sigma^2 (G^T G)^{-1}$$



Independent data errors



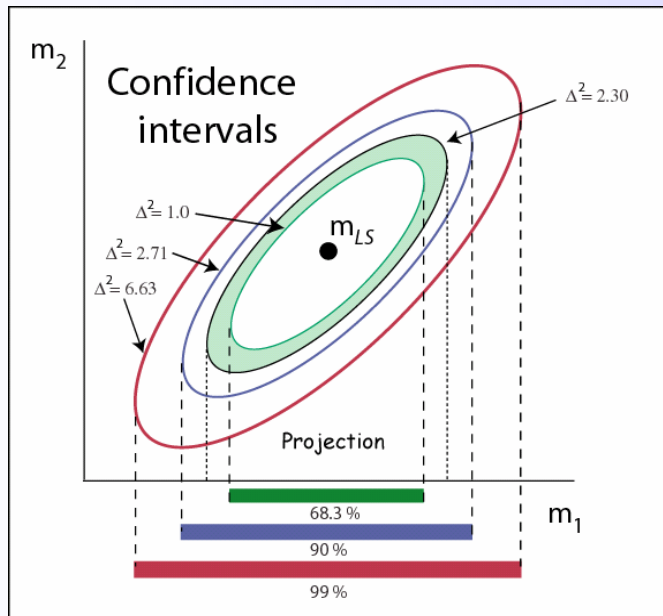
Correlated model errors

For linear regression problem

$$C_M = \frac{\sigma^2}{N \sum_{i=1}^N x_i^2 - (\sum_{i=1}^N x_i)^2} \begin{bmatrix} \sum_{i=1}^N x_i^2 & -\sum_{i=1}^N x_i \\ -\sum_{i=1}^N x_i & N \end{bmatrix}$$

Confidence intervals by projection (1-D)

The model covariance is a symmetric $M \times M$ matrix



$$C_M = \begin{bmatrix} \sigma_{1,1}^2 & \sigma_{1,2}^2 & \dots & \sigma_{1,M}^2 \\ \sigma_{1,2}^2 & \sigma_{2,2}^2 & \dots & \sigma_{2,M}^2 \\ \vdots & \vdots & \ddots & \vdots \\ \sigma_{1,M}^2 & \dots & \dots & \sigma_{M,M}^2 \end{bmatrix}$$

$$(\mathbf{m} - \mathbf{m}_{LS})^T C_M^{-1} (\mathbf{m} - \mathbf{m}_{LS}) < \Delta^2$$

In the multi-dimensional model space the value of Δ^2 follows a χ_M^2 distribution with M degrees of freedom.

Projecting onto the m_i axis the 1-D confidence interval becomes

$$\chi_{\nu}^2$$

$(\mathbf{m}_{LS})_i \pm \Delta \times \sigma_{i,i}$ Where Δ^2 follows a χ_1^2 distribution

e.g. for 90% interval on m_1 $(\mathbf{m}_{LS})_1 \pm \sqrt{(2.71) \times \sigma_{1,1}} = 1.65 \times \sigma_{1,1}$

Note this is 90% the confidence interval on m_1 alone.

The joint (m_1, m_2) 90% confidence ellipse is wider than this.

Example: Model Covariance and confidence intervals

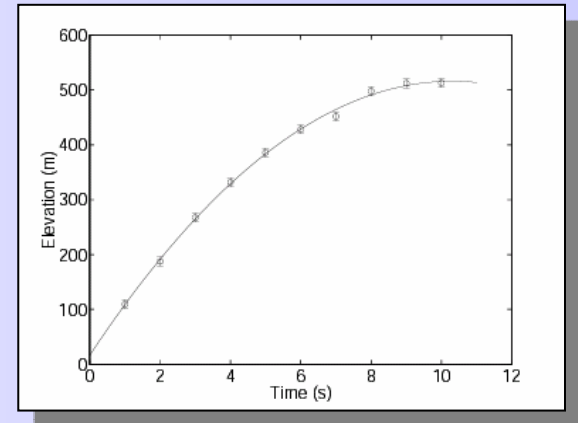
For Ballistics problem

$$y_i = m_1 + m_2 t_i - \frac{1}{2} m_3 t_i^2$$

$$C_M = (G^T C_d^{-1} G)^{-1}$$

$$C_d^{-1} = \frac{1}{\sigma^2} I$$

$$C_M = \begin{bmatrix} 88.53 & -33.60 & -5.33 \\ -33.60 & 15.44 & 2.67 \\ -5.33 & 2.67 & 0.48 \end{bmatrix}$$

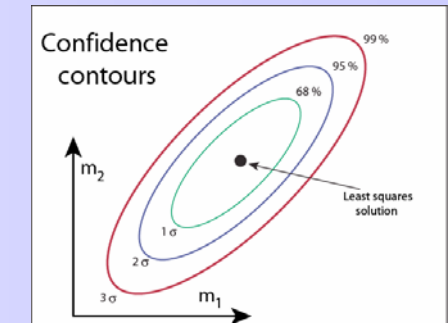


95% confidence interval for parameter i

$$= 1.96 \times (C_M)_{i,i}^{1/2}$$

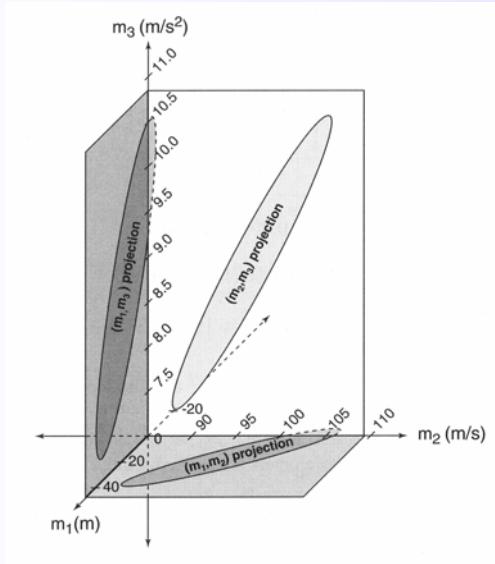
$$\mathbf{m}_{true} = [10m, 100m/s, 9.8m/s^2]^T$$

$$\mathbf{m}_{LS} = [16.4 \pm 18.4m, 97.0 \pm 7.7m/s, 9.4 \pm 1.4m/s^2]^T$$



Confidence intervals by projection

The M-dimensional confidence ellipsoid can be projected onto any subset (or combination) of Δ parameters to obtain the corresponding confidence ellipsoid.



To find the 90% confidence ellipse for (x,y) from a 3-D (x,y,z) ellipsoid

$$\Delta^2 = 4.61 \quad [= \chi^2_2(90\%)]$$

$$C_{M,proj} = \begin{bmatrix} \sigma_{1,1}^2 & \sigma_{1,2}^2 \\ \sigma_{1,2}^2 & \sigma_{2,2}^2 \end{bmatrix}$$

$$\delta m' = [m_1 - m_{LS,1}, m_2 - m_{LS,2}]^T$$

Full M-dimensional ellipsoid

$$\Delta^2 = (\mathbf{m} - \mathbf{m}_{LS})^T C_M^{-1} (\mathbf{m} - \mathbf{m}_{LS})$$

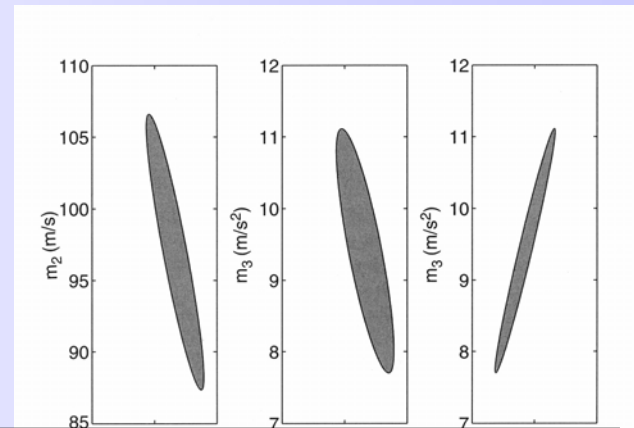
Projected v dimension ellipsoid

$$\Delta^2 = \delta m'^T [C_{M,proj}]^{-1} \delta m'$$

$\delta m'$ = Projected model vector

$C_{M,proj}$ = Projected covariance matrix

Δ^2 = Chosen percentage point of the χ^2_v distribution



Can you see that this procedure gives the same formula for the 1-D case obtained previously ?

Recap: Goodness of fit and model covariance

- Once a best fit solution has been obtained we test goodness of fit with a chi-square test (assuming Gaussian statistics)

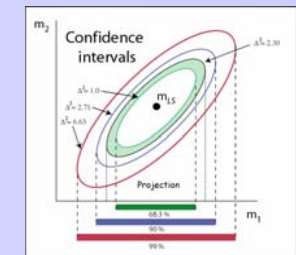
$$\chi^2_{obs} = \sum_{i=1}^N \frac{(d_i - \sum_{j=1}^M G_{i,j} m_j)^2}{\sigma_i^2}$$

- If the model passes the goodness of fit test we may proceed to evaluating model covariance (if not then your data errors are probably too small)
- Evaluate model covariance matrix

$$C_M = (G^T C_d^{-1} G)^{-1}$$

- Plot model or projections of it onto chosen subsets of parameters

$$\Delta'^2 = (\mathbf{m} - \mathbf{m}_{LS})'^T C_M^{-1} (\mathbf{m} - \mathbf{m}_{LS})'$$



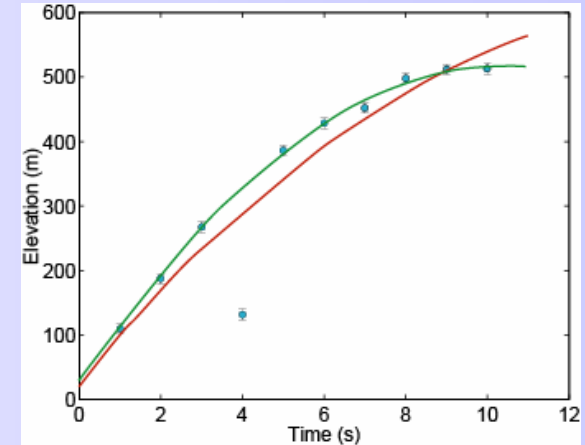
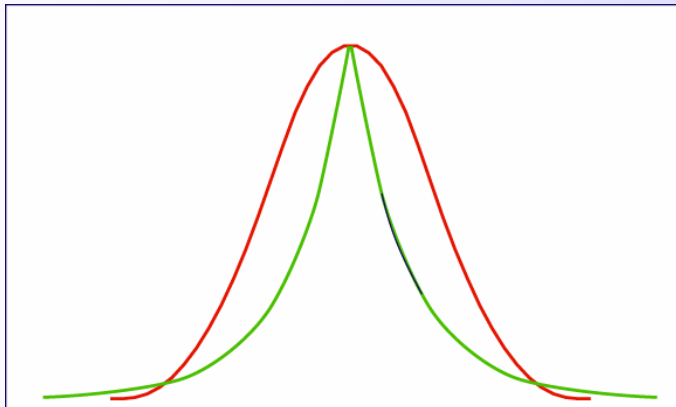
- Calculate confidence intervals using projected equation

$$\sigma_{M,i} = \Delta \times \sigma_{i,i}$$

Where Δ^2 follows a χ^2_1 distribution

Robust data fitting with the L₁ norm

Least squares solutions are not robust



Minimize

$$\phi(\mathbf{m}) = |\mathbf{d} - \mathbf{G}\mathbf{m}|_1 = \sum_i |r_i|$$

We can calculate an L₁ solution with the IRLS algorithm

$$\mathbf{m}_{L_1} = (\mathbf{G}^T \mathbf{R} \mathbf{G})^{-1} \mathbf{G}^T \mathbf{R} \mathbf{d}$$

\mathbf{R} is a diagonal weighting matrix that depends on the model

$$R_{i,i} = \frac{1}{|\mathbf{d}_i - \sum_j \mathbf{G}_{i,j} m_j|}$$

See section 2.4 of Aster (2005)

Monte Carlo error propagation

It's possible to define an approximate p statistic for the L₁ solution and hence test goodness of fit of the solution. However there is no analytical solution to error propagation.

...but Monte Carlo error propagation can be used.

1. Calculate data prediction from solution

$$\mathbf{d}_b = \mathbf{Gm}_{L_1}$$

2. Add random realization of noise to data and repeat IRLS algorithm

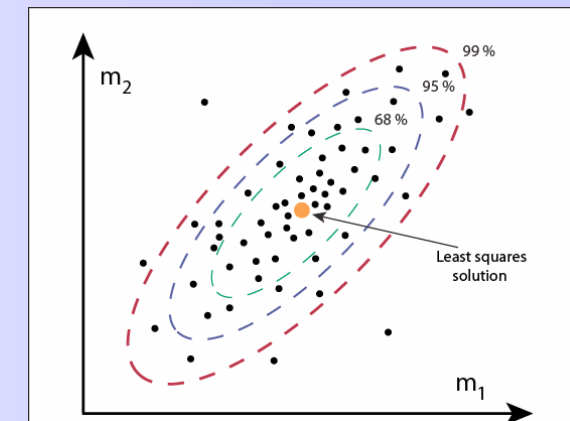
$$\mathbf{d}_b \rightarrow \mathbf{d}_b + \epsilon_i$$

$$\mathbf{m}_{L_1} \rightarrow \mathbf{m}_{L_1}^i$$

3. Repeat Q times and generate difference vectors

$$\mathbf{a}_i = \mathbf{m}_{L_1} - \mathbf{m}_{L_1}^i$$

$$C_M = \frac{1}{Q} \mathbf{aa}^T$$



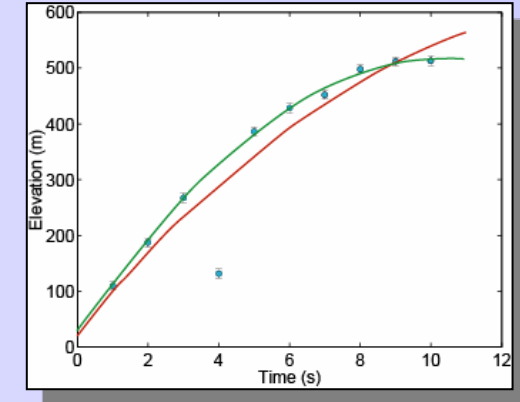
Monte Carlo error propagation

For the ballistics problem we get

$$C_M = \frac{1}{Q} \mathbf{a} \mathbf{a}^T$$

$$C_{M_{L_1}} = \begin{bmatrix} 122.52 & -46.50 & -7.37 \\ -46.50 & 21.49 & 3.72 \\ -7.37 & 3.72 & 0.68 \end{bmatrix}$$

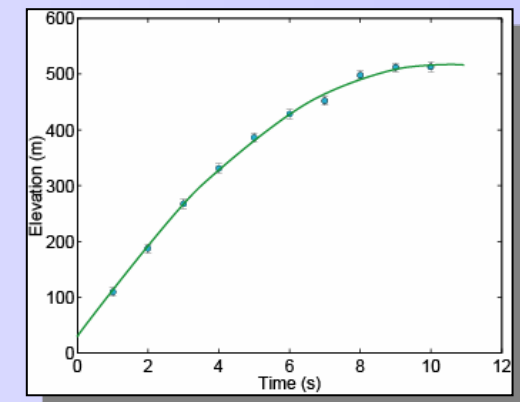
$$\mathbf{m}_{L_1} = [17.6 \pm 21.8 \text{m}, 96.4 \pm 7.7 \text{m/s}, 9.4 \pm 1.4 \text{m/s}^2]^T$$



Compare to LS solution without outlier

$$C_M = \begin{bmatrix} 88.53 & -33.60 & -5.33 \\ -33.60 & 15.44 & 2.67 \\ -5.33 & 2.67 & 0.48 \end{bmatrix}$$

$$\mathbf{m}_{LS} = [16.4 \pm 18.4 \text{m}, 97.0 \pm 7.7 \text{m/s}, 9.4 \pm 1.4 \text{m/s}^2]^T$$



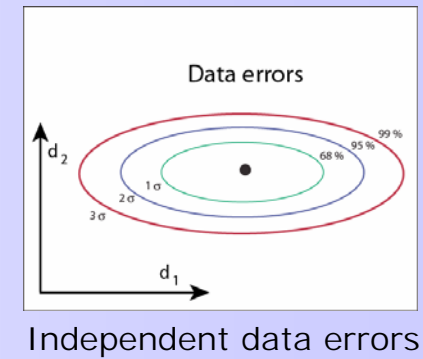
What if we do not know the errors on the data ?

Both Chi-square goodness of fit tests and model covariance Calculations require knowledge of the variance of the data.

What can we do if we do not know σ ?

Consider the case of

$$C_D = \sigma^2 I$$



$$\chi^2_{N-M} = \frac{1}{\sigma^2} \sum_{i=1}^N \left(d_i - \sum_{j=1}^M G_{i,j} m_j \right)^2 \Rightarrow \sigma^2 = \frac{1}{(N-M)} \sum_{i=1}^N \left(d_i - \sum_{j=1}^M G_{i,j} m_j \right)^2$$

$$C_M = \sigma^2 (G^T G)^{-1}$$

Calculated from least squares solution

So we can still estimate model errors using the calculated data errors but we can no long claim anything about goodness of fit.

Example: Over-determined, Linear discrete inverse problem

MATLAB exercise

Generate data with Gaussian noise for a linear regression problem and invert for the best fitting gradient and intercept

1. Generate x_i points randomly between 0 and 10

$$x_i (i = 1, 2, \dots, 10)$$

2. Calculate data y_i

$$d_i = ax_i + b$$

3. Add $N[0, \sigma]$ noise to data y_i

$$d_i \rightarrow d_i + \epsilon_i$$

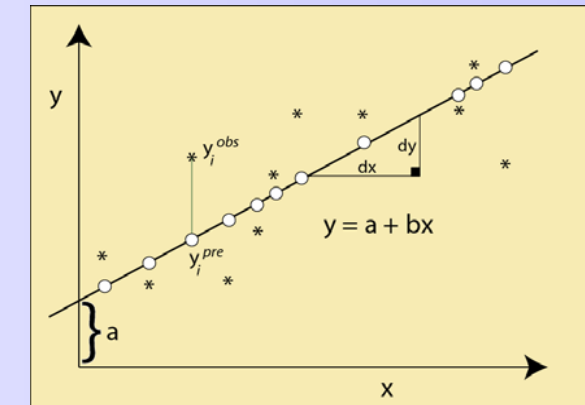
4. Calculate G matrix

$$G = \begin{bmatrix} 1 & x_1 \\ 1 & x_2 \\ \vdots & \vdots \\ 1 & x_{N_d} \end{bmatrix}$$

5. Use MATLAB matrix routines to solve the normal equations

$$\mathbf{m} = (G^T C_d^{-1} G)^{-1} G^T C_d^{-1} \mathbf{d}$$

6. Plot the data, plot the data errors and plot the least squares solution





Model Resolution matrix

If we obtain a solution to an inverse problem we can ask what its relationship is to the true solution

$$\mathbf{m}_{est} = G^{-g} \mathbf{d}$$

But we know

$$\mathbf{d} = G\mathbf{m}_{true}$$

and hence

$$\mathbf{m}_{est} = G^{-g}G\mathbf{m}_{true} = R\mathbf{m}_{true}$$

The matrix R measures how `good an inverse' G^{-g} is.

The matrix R shows how the elements of \mathbf{m}_{est} are built from linear combination of the true model, \mathbf{m}_{true} . Hence matrix R measures the amount of **blurring** produced by the inverse operator.

For the least squares solution we have

$$G^{-g} = (G^T C_D^{-1} G)^{-1} G^T C_D^{-1} \quad \Rightarrow R = I$$



Example: Model resolution in a tomographic experiment

$$\mathbf{m} = R\mathbf{m}_{true}$$

If the calculated model resolution matrix looked like this

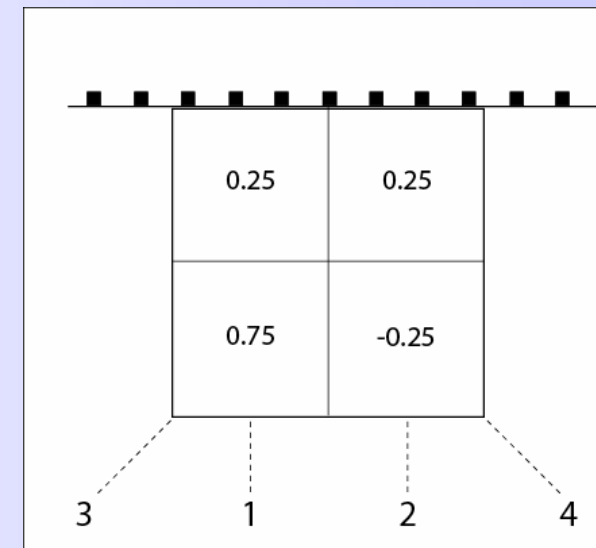
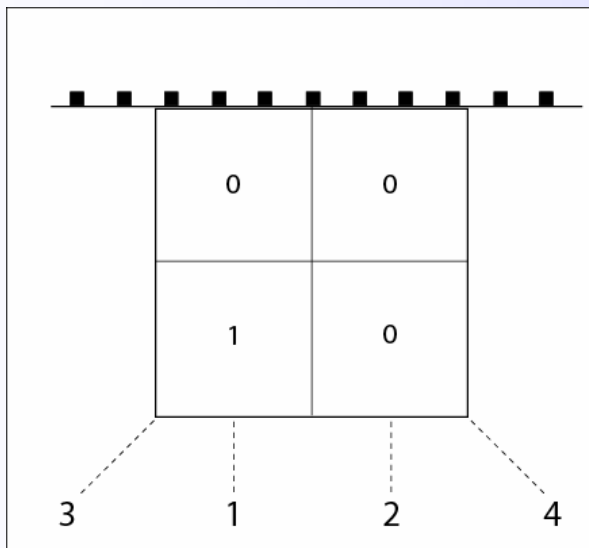
$$R = \begin{bmatrix} 0.75 & -0.25 & 0.25 & 0.25 \\ -0.25 & 0.75 & 0.25 & 0.25 \\ 0.25 & 0.25 & 0.75 & -0.25 \\ 0.25 & 0.25 & -0.25 & 0.75 \end{bmatrix}$$

What units do the elements of R have ?

Spike test

True model

Recovered model





Data Resolution matrix

If we obtain a solution to an inverse problem we can ask what how it compares to the data

$$\mathbf{d}_{pre} = G\mathbf{m}_{est}$$

But we know

$$\mathbf{m}_{est} = G^{-g}\mathbf{d}_{obs}$$

and hence

$$\mathbf{d}_{pre} = GG^{-g}\mathbf{d}_{obs} = D\mathbf{d}_{obs}$$

The matrix D is analogous to the model resolution matrix R but measures how independently the model produced by G^{-g} can reproduce the data. If $D = I$ then the data is fit exactly and the prediction error $\mathbf{d}-G\mathbf{m}$ is zero.



Recap: Linear discrete inverse problems

- The Least squares solution minimizes the prediction error.

$$\phi(\mathbf{m}_{LS}) = (\mathbf{d} - \mathbf{G}\mathbf{m}_{LS})^T \mathbf{C}_d^{-1} (\mathbf{d} - \mathbf{G}\mathbf{m}_{LS})$$

$$\mathbf{m}_{LS} = (\mathbf{G}^T \mathbf{C}_d^{-1} \mathbf{G})^{-1} \mathbf{G}^T \mathbf{C}_d^{-1} \mathbf{d} = \mathbf{G}^{-g} \mathbf{d}$$

- Goodness of fit criteria tells us whether the least squares model adequately fits the data, given the level of noise.

$$\phi(\mathbf{m}_{LS}) \rightarrow \chi_{N-M}^2 \quad \text{Chi-square with } N-M \text{ degrees of freedom}$$

- The covariance matrix describes how noise propagates from the data to the estimated model

$$\mathbf{C}_M = (\mathbf{G}^T \mathbf{C}_d^{-1} \mathbf{G})^{-1}$$

$$\Delta^2 \rightarrow \chi_M^2$$

Chi-square with M degrees of freedom

$$(\mathbf{m} - \mathbf{m}_{LS})^T \mathbf{C}_M^{-1} (\mathbf{m} - \mathbf{m}_{LS}) < \Delta^2$$

Gives confidence intervals

- The resolution matrix describes how the estimated model relates to the true model



Linearized inverse Problems

(Weakly nonlinear problems)

Using a Taylor expansion then away we go...

Linearized inverse problems

Nonlinear inverse problem

$$d_{obs,i} = g_i(\mathbf{m})$$

Choose a reference model \mathbf{m}_o and perform a Taylor expansion of $g(\mathbf{m})$

$$\mathbf{m} = \mathbf{m}_o + \delta\mathbf{m}$$

$$g_i(\mathbf{m}_o + \delta\mathbf{m}) = g_i(\mathbf{m}_o) + \nabla g_i \delta\mathbf{m} + \dots$$

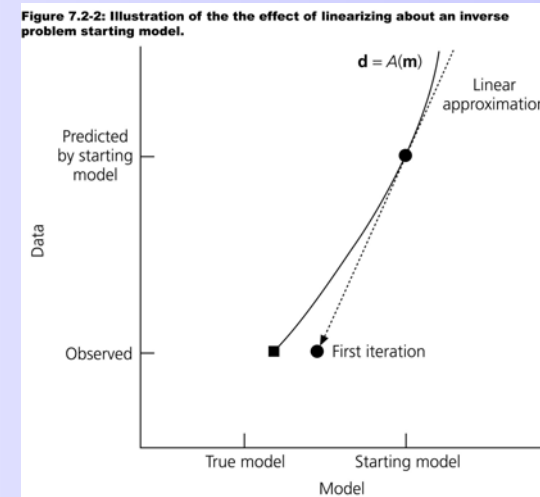
$$\nabla g_i = \left[\frac{\partial g_i}{\partial m_1}, \frac{\partial g_i}{\partial m_2}, \dots \right]^T$$

Linearized inverse problem

$$\delta d = d_{obs} - g(\mathbf{m}_o)$$

$$\delta d = G\delta\mathbf{m}$$

$$G_{i,j} = \frac{\partial g_i}{\partial m_j}$$



Linearized inverse problems

Data prediction error

$$\phi(\mathbf{m}) = (\mathbf{d} - g(\mathbf{m}))^T C_d^{-1} (\mathbf{d} - g(\mathbf{m}))$$

Linearized problem

$$\delta \mathbf{d} = G \delta \mathbf{m}$$

Least squares solution

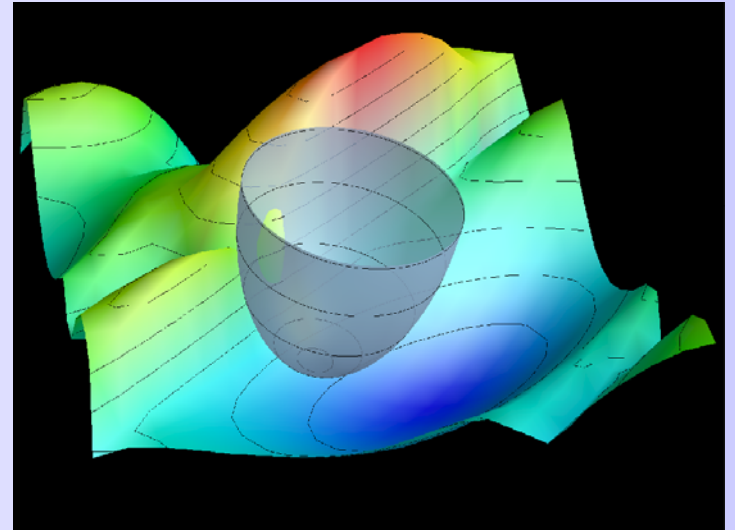
$$\phi'(\delta \mathbf{m}) = (\delta \mathbf{d} - G \delta \mathbf{m})^T C_d^{-1} (\delta \mathbf{d} - G \delta \mathbf{m})$$

It can be shown that $\phi'(\mathbf{m})$ is a quadratic approximation to $\phi(\mathbf{m})$ about the reference model \mathbf{m}_o .

Linearized problems need to be solved **iteratively**

$$\delta \mathbf{m} = (G^T C_d^{-1} G)^{-1} G^T C_d^{-1} \delta \mathbf{d}$$

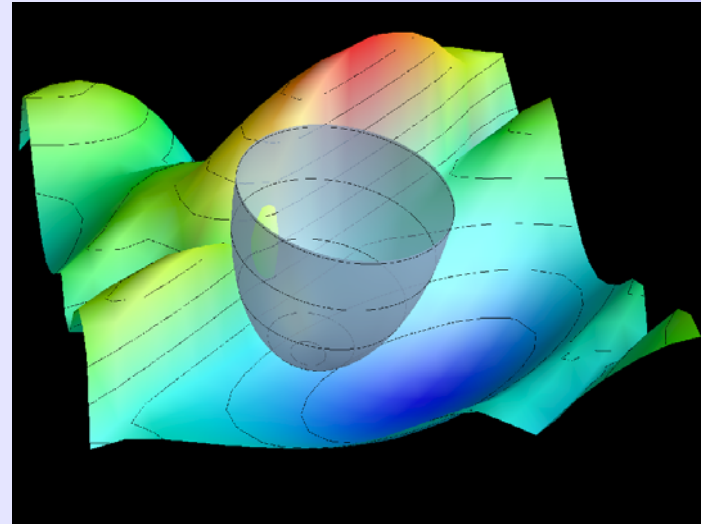
$$\delta \mathbf{m}_{n+1} = (G_n^T C_d^{-1} G_n)^{-1} G_n^T C_d^{-1} \delta \mathbf{d}_n$$



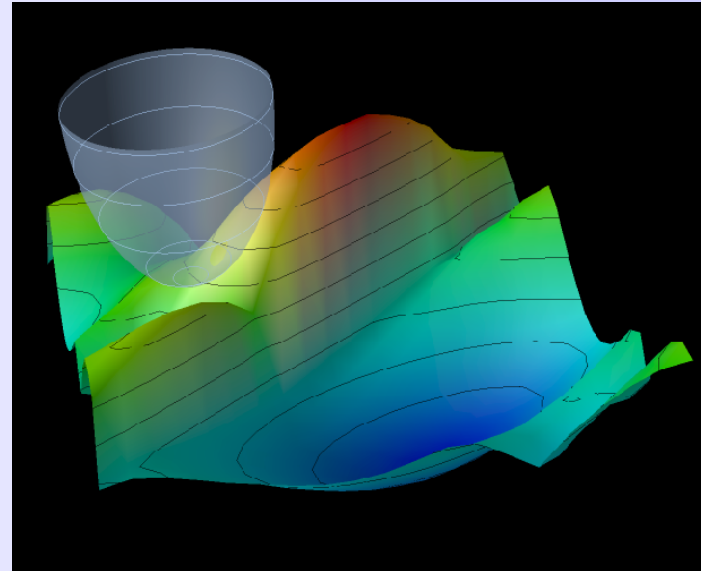


Linearized inverse problems

Linearization can succeed...



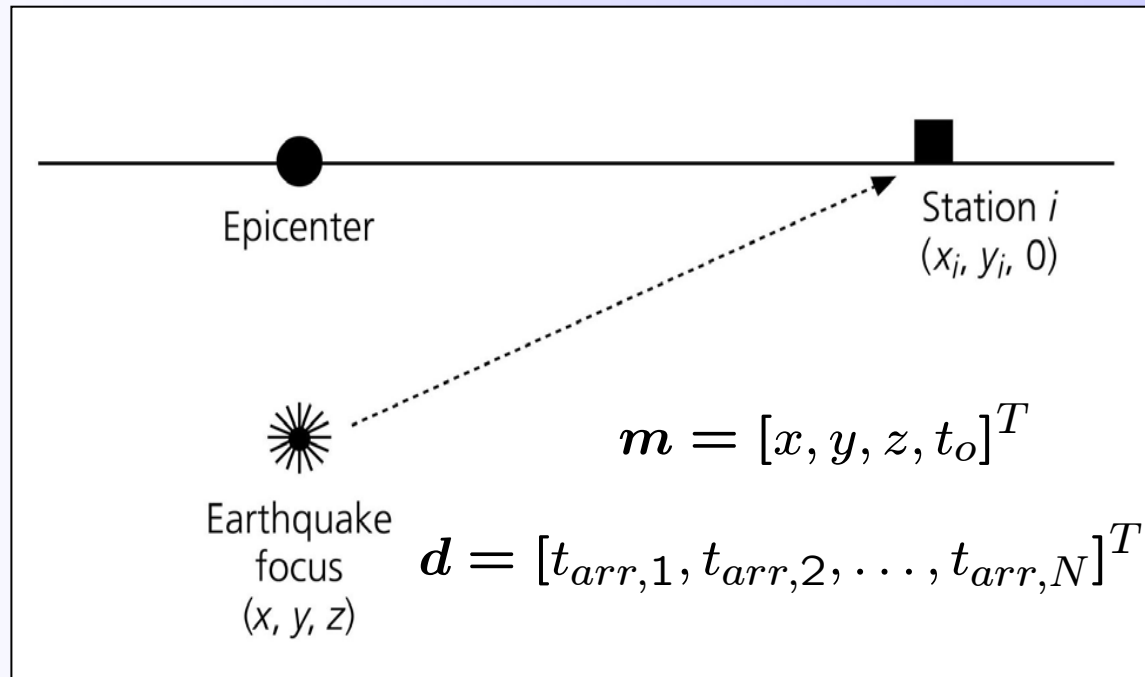
... and linearization can fail.



The starting point for an iterative procedure can be all important.

Example: Earthquake location

$$\delta \mathbf{m}_{n+1} = (G_n^T C_d^{-1} G_n)^{-1} G_n^T C_d^{-1} \delta \mathbf{d}_n$$



$$t_{arr,i} = t_o + \int_{R_i} \frac{1}{v(\mathbf{x})} dl$$

$$G_{i,j} = \frac{\partial g_i}{\partial m_j}$$

Derivative of the i th arrival time with respect to the j th hypocentral co-ordinate

Example: Earthquake location

$$t_r = \int_R \frac{1}{v(\mathbf{x})} dl$$

$$\mathbf{m} = [x, y, z, t_o]^T$$

$$\mathbf{d} = [t_1, t_2, \dots, t_N]^T$$

What is the data model parameter relationship ?

Assume homogeneous 3-D Earth model

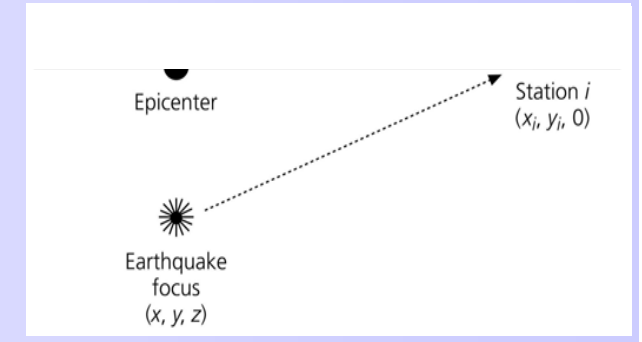
$$t_r = \frac{D(\mathbf{m})}{v}$$

$$t_i = t_o + \frac{D_i(x, y, z)}{v}$$

What are the Frechet derivatives ?

$$G_{i,j} = \frac{\partial d_i}{\partial m_j} \quad ?$$

$$\delta \mathbf{m}_{n+1} = (G_n^T C_d^{-1} G_n)^{-1} G_n^T C_d^{-1} \delta \mathbf{d}_n$$



Example: Linearized inversion

Inversion for earthquake location and origin time (error free)

Parameter	True value	Solution at each iteration		
		0	1	2
X	0.0	3.0	-0.5	0.0
Y	0.0	4.0	-0.6	0.0
Z	10.0	20.0	10.1	10.0
T ₀	0.0	2.0	0.2	0.0

Station	Arrival time residual		
1	-2.1	-0.4	0.0
2	-3.0	-0.2	0.0
3	-3.8	-0.1	0.0
4	-3.0	-0.2	0.0
5	-2.6	-0.3	0.0
6	-2.0	-0.3	0.0
7	-2.9	-0.2	0.0
8	-3.7	-0.2	0.0
9	-4.1	-0.2	0.0
10	-2.4	-0.4	0.0
Misfit	92.4	0.6	0.0

$$\delta \mathbf{m}_{n+1} = (G_n^T C_d^{-1} G_n)^{-1} G_n^T C_d^{-1} \delta \mathbf{d}_n$$

Example: Earthquake location

Inversion for earthquake location and origin time ($\sigma = 0.1$ s)

Parameter	True value	Solution at each iteration			
		0	1	2	3
X	0.0	3.0	-0.2	0.2	0.2
Y	0.0	4.0	-0.9	-0.4	-0.4
Z	10.0	20.0	12.2	12.2	12.2
T ₀	0.0	2.0	0.0	-0.2	-0.2

X	Y	Z	T _o	Station	Arrival time residual			
1.00	.144	.038	0.00	1	-2.0	-0.1	0.1	0.1
.144	1.00	-.427	.350	2	-3.0	-0.1	0.0	0.0
.038	-.427	1.00	-.743	3	-3.8	0.0	0.1	0.1
0.00	.350	-.743	1.00	4	-3.2	-0.1	0.0	0.0
Correlation				5	-2.8	-0.2	-0.1	-0.1
				6	-2.1	-0.3	-0.1	-0.1
				7	-2.9	-0.1	0.0	0.0
				8	-3.7	-0.1	0.0	0.0
				9	-4.0	-0.1	0.0	0.0
				10	-2.5	-0.3	0.0	0.0
				Misfit	93.74	0.33	0.04	0.04

$$C_M = (G^T C_d^{-1} G)^{-1} \quad C_d = \sigma^2 I$$

Where do significant the trade offs occur ?



Discrete non-unique inverse problems

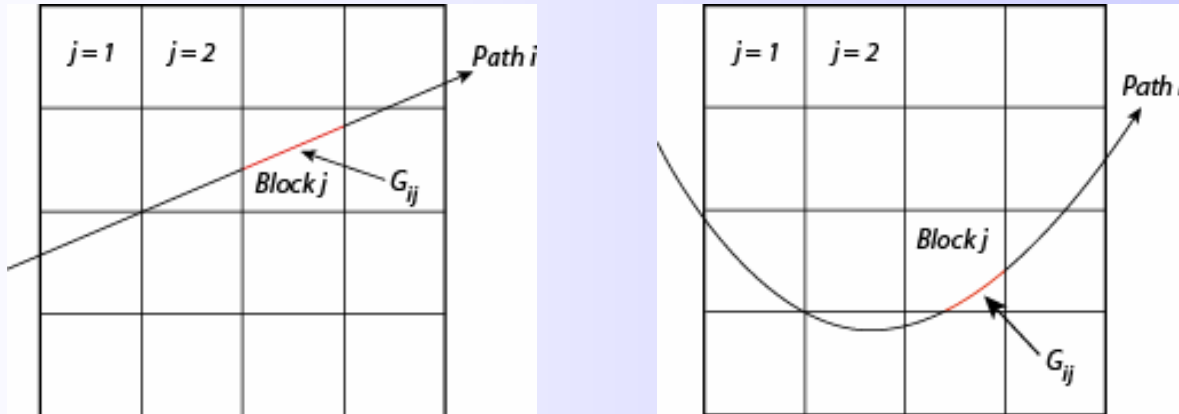
Non-uniqueness: When there is no one answer to the question...

Example: Travel time tomography

Seismic travel times are observed at the surface, and we want to learn about the Earth's structure at depth. Travel times are related to the wave speeds of rocks through the expression

$$t = \int_R \frac{1}{v(\mathbf{x})} dl = \int_R s(\mathbf{x}) dl$$

The raypath, R also depends on the velocity structure, v(\mathbf{x}). R can be found using ray tracing methods.



Is this a continuous or discrete inverse problem ?

Is it linear or nonlinear ?

Travel time tomography example

We can linearize the problem about a reference model $s_o(\mathbf{x})$ or $v_o(\mathbf{x})$. We get either...

$$\delta t = \int_{R_o} \delta s(\mathbf{x}) dl \quad \text{or} \quad \delta t = \int_{R_o} -\frac{1}{v_o^2} \delta v(\mathbf{x}) dl$$

$$\delta m(\mathbf{x}) = \sum_{j=1}^M \delta m_j \phi_j(\mathbf{x})$$

$$\phi_j(\mathbf{x}) = \begin{cases} 1 & \text{If } \mathbf{x} \text{ in block } j \\ 0 & \text{otherwise} \end{cases}$$

0	0	0	0
0	0	1	0
0	0	0	0
0	0	0	0

$$\delta t_i = \sum_{j=1}^M \delta m_j \int_{R_{o,i}} \phi_j(\mathbf{x}) dl = \sum_{j=1}^M \delta m_j G_{i,j}$$

How do elements of the matrix $G_{i,j}$ relate to the rays ?

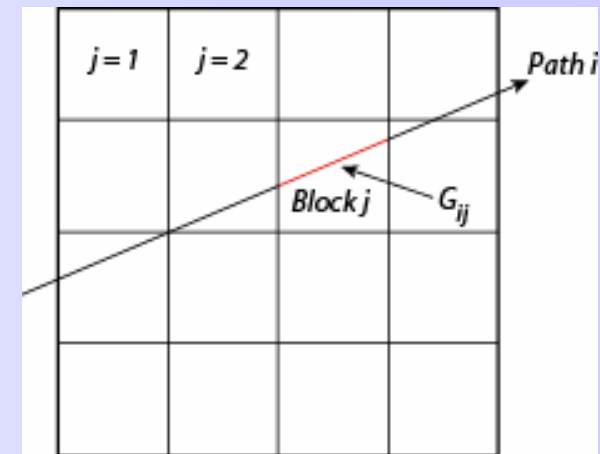
Travel time tomography example

The element of the matrix $G_{i,j}$ is the integral of the j-th basis function along the i-th ray. Hence for our chosen basis functions it is the length of the i-th ray in the j-th block.

$$\delta t_i = G_{i,j} \delta m_j$$

$$\delta d = G \delta m$$

$$G = \begin{bmatrix} l_{1,1} & l_{1,2} & \cdots & , l_{1,M} \\ l_{2,1} & l_{2,2} & \cdots & , l_{2,M} \\ \vdots & \vdots & \ddots & \vdots \\ l_{N,2} & l_{N,2} & \cdots & , l_{N,M} \end{bmatrix}$$



$$\delta d_j = t_i^o - t_i^c(s_o) \quad \text{Travel time residual for i-th path}$$

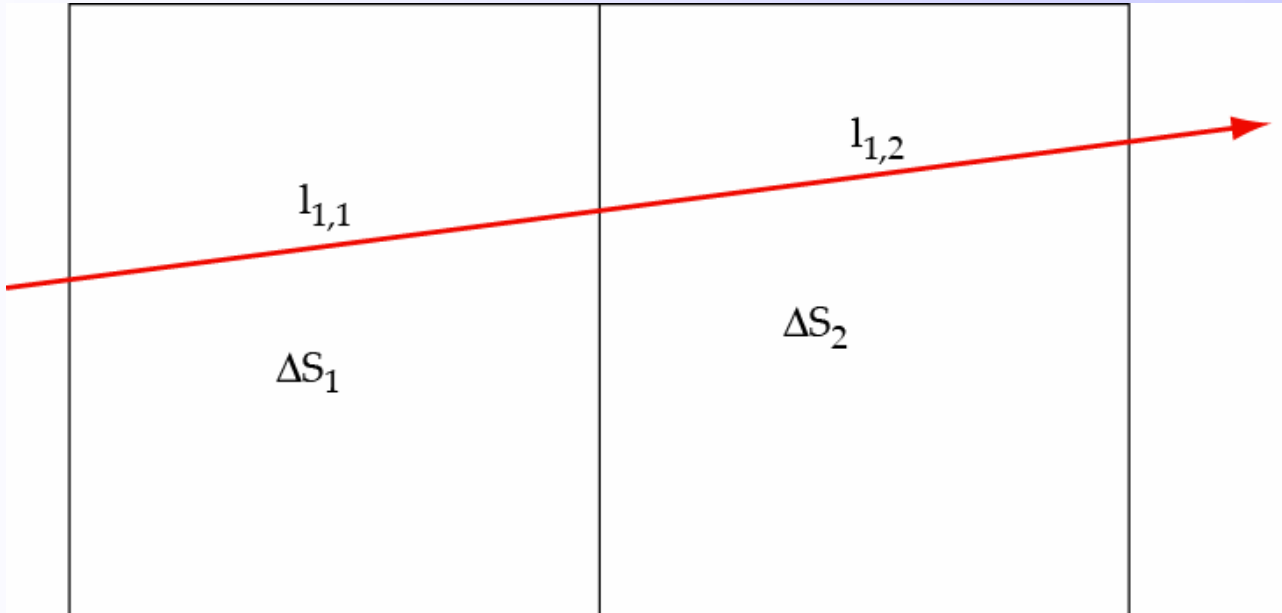
$$\delta m_j = s_j - s_{o,j} \quad \text{Slowness perturbation in j-th cell}$$

$$l_{i,j} = \text{Length of i-th ray in j-th cell}$$

Travel time tomography example

One ray and two blocks

$$\delta t_i = G_{i,j} \delta m_j$$



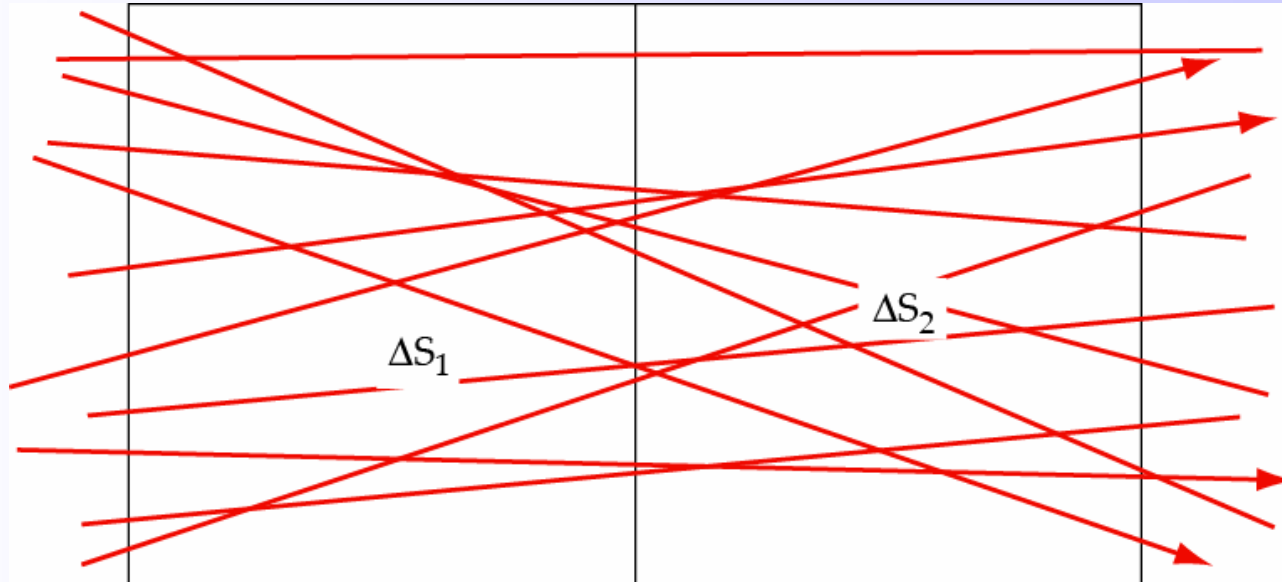
Non-uniqueness

$$\delta t_1 = l_{1,1} * \delta s_1 + l_{1,2} * \delta s_2$$

Travel time tomography example

Many rays and two blocks

$$\delta t_i = G_{i,j} \delta m_j$$



Uniqueness ?

NO !

$$\delta t_i = l_{i,1} * \delta s_1 + l_{i,2} * \delta s_2 \quad (i = 1, N)$$

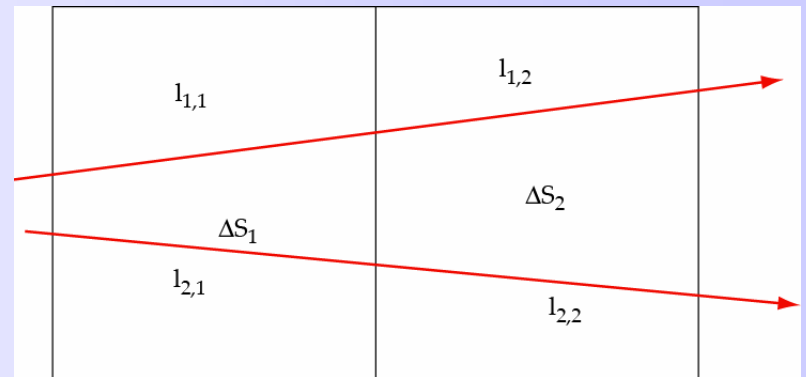
Travel time tomography example

Can we resolve both slowness perturbations ?

$$\delta t_1 = l_{1,1} * \delta s_1 + l_{1,2} * \delta s_2$$

$$\delta t_2 = l_{2,1} * \delta s_1 + l_{2,2} * \delta s_2$$

$$\delta \mathbf{d} = G \delta \mathbf{m}$$



$$\frac{l_{1,1}}{l_{1,2}} = \frac{l_{2,1}}{l_{2,2}} \quad \Rightarrow |G| = 0$$

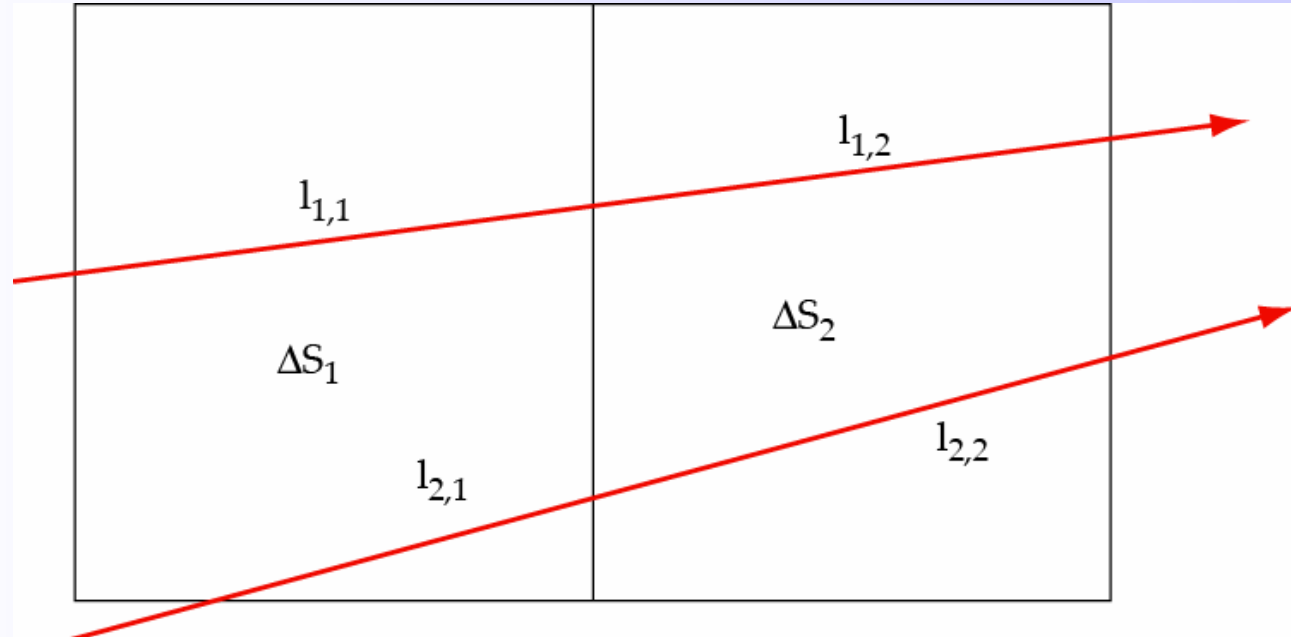
- G has a **zero determinant** and hence problem is under-determined
- Zero eigenvalues => Linear dependence between equations => **no unique solution**. An infinite number of solutions exist !

Same argument applies to all rays that enter and exit through the same pair of sides.

Travel time tomography example

Two rays and two blocks

$$\delta t_i = G_{i,j} \delta m_j$$



Uniqueness ?

YES

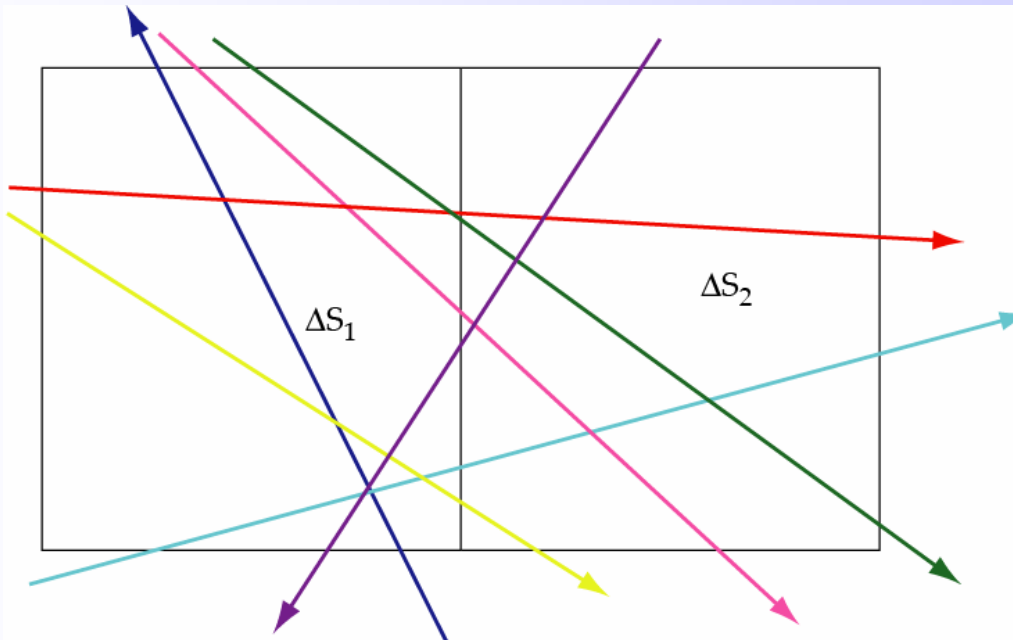
$$\delta t_i = l_{i,1} * \delta s_1 + l_{i,2} * \delta s_2 \quad (i = 1, 2)$$

Travel time tomography example

Two rays and two blocks

$$\delta t_i = G_{i,j} \delta m_j$$

$$C_M = (G^T C_d^{-1} G)^{-1}$$



Model variance
is low but cell
size is large

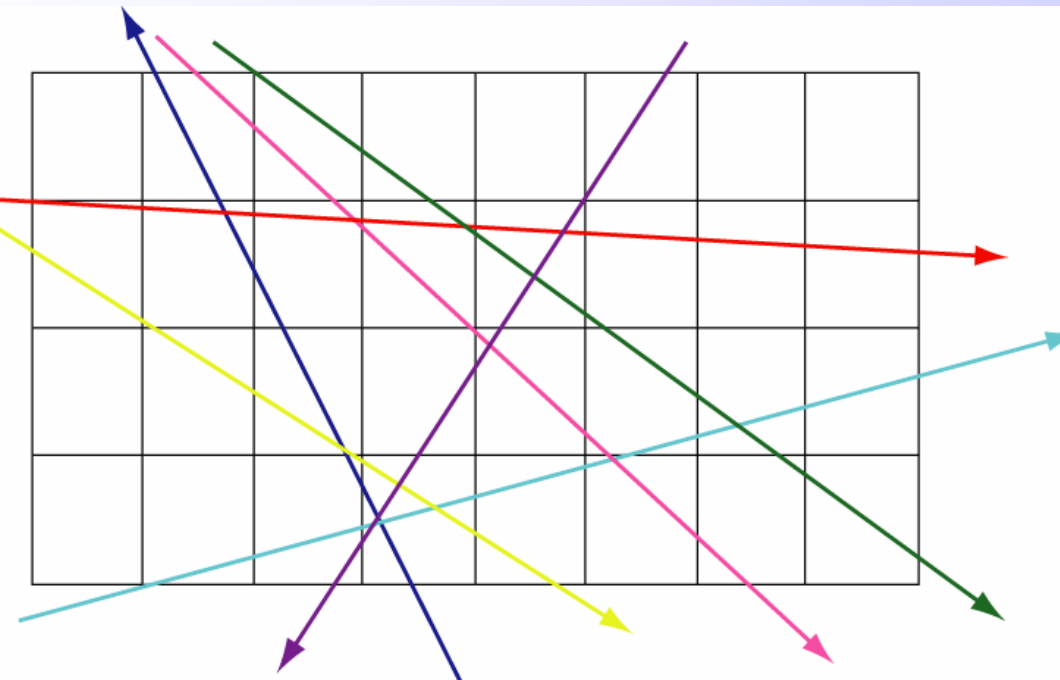
Over-determined Linear Least squares problem

$$\delta t_i = l_{i,1} * \delta s_1 + l_{i,2} * \delta s_2 \quad (i = 1, N)$$

Travel time tomography example

Many rays and many blocks

$$\delta t_i = G_{i,j} \delta m_j$$



Model variance is higher but cell size is smaller

Model variance and resolution trade off

Simultaneously over and under-determined
Linear Least squares problem

Mix-determined problem



Recap:

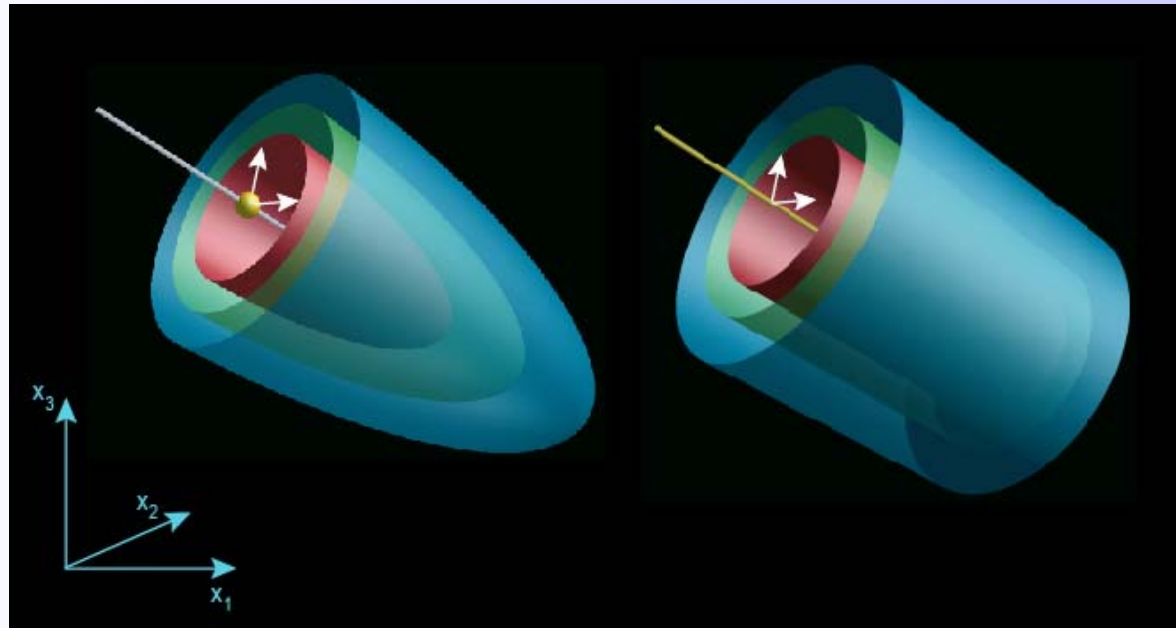
- In a linear problem, if the number of data is **less** than the number of unknowns then the problem will be **under-determined**.
- If the number of data is **more** than the number of unknowns the system **may not be over-determined**. The number of **linearly independent data** is what matters. This is the true number of pieces of information.
- Linear discrete problems can be simultaneously over and under-determined. This is a **mix-determined problem**.
- There is a trade-off between the **variance** (of the solution) and the **resolution** (of the parametrization).



Discrete ill-posed problems

What does the data misfit function look like in a non-unique problem ?

$$\psi(\mathbf{m}) = \frac{1}{2}(\mathbf{d} - \mathbf{G}\mathbf{m})^T \mathbf{C}_d^{-1} (\mathbf{d} - \mathbf{G}\mathbf{m})$$



$$\mathbf{G}\mathbf{m}_1 = 0$$

$$\mathbf{d} = \mathbf{G}(\mathbf{m}_o + \mathbf{m}_1) = \mathbf{G}\mathbf{m}_o$$

Discrete non-unique problems

What happens if the normal equations have no solution ?

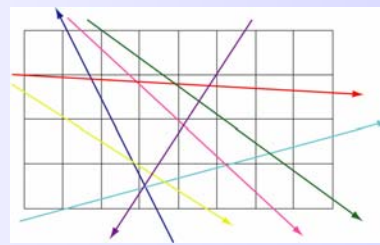
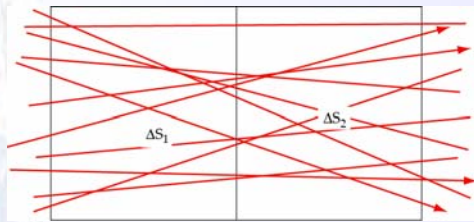
$$\mathbf{m}_{LS} = (G^T C_d^{-1} G)^{-1} G^T C_d^{-1} \mathbf{d} = G^{-g} \mathbf{d}$$

Recall that the inverse of a matrix is proportional to the reciprocal of the determinant

$$G = \begin{bmatrix} a & b \\ c & d \end{bmatrix} \quad |G| = ad - cb \quad G^{-1} = \frac{1}{|G|} \begin{bmatrix} d & -b \\ -c & a \end{bmatrix}$$

The determinant is the product of the eigenvalues. Hence the inverse does not exist if any of the eigenvalues of $G^T C_d^{-1} G$ are zero

We have seen examples of this in the tomography problem



This is an **ill-posed** or
under-determined problem
with **no unique** solution

The Minimum Length solution

If the problem is completely under-determined we can minimize the length of the solution subject to it fitting the data.

$$\text{Min} \quad L(\mathbf{m}) = \mathbf{m}^T \mathbf{m} : \mathbf{d} = G\mathbf{m}$$

Lagrange multipliers says minimize $\phi(\mathbf{m}, \lambda)$

$$\phi(\mathbf{m}, \lambda) = \mathbf{m}^T \mathbf{m} + \lambda^T (\mathbf{d} - G\mathbf{m})$$

...and we get

$$\mathbf{m}_{ML} = G^T (G G^T)^{-1} \mathbf{d} \quad G = [l_1 \ l_2]$$

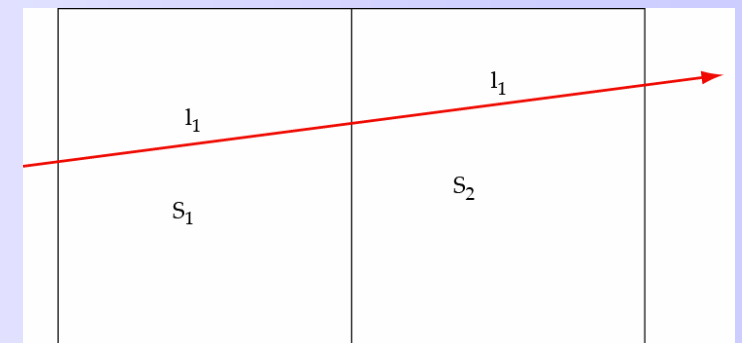
Example

$$T = l_1 s_1 + l_2 s_2$$

$$\phi = s_1^2 + s_2^2 + \lambda(T - l_1 s_1 - l_2 s_2)$$

$$\Rightarrow \frac{s_1}{s_2} = \frac{l_1}{l_2}$$

$$s_1 = \frac{l_1 T}{(l_2^2 + l_1^2)} \quad s_2 = \frac{l_2 T}{(l_2^2 + l_1^2)}$$



Minimum Length and least squares solutions

$$\mathbf{m}_{LS} = (G^T G)^{-1} G^T \mathbf{d} \quad \mathbf{m}_{ML} = G^T (G G^T)^{-1} G \mathbf{d}$$

$$\mathbf{m}_{est} = G^{-g} \mathbf{d}$$

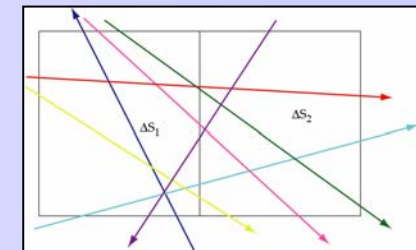
Model resolution matrix

$$\mathbf{m}_{est} = R \mathbf{m}_{true}$$

$$R = G^{-g} G$$

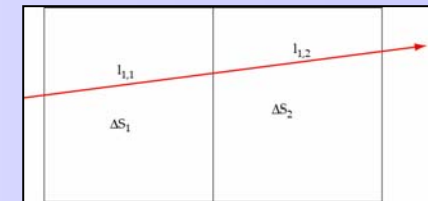
Least squares

$$R = (G^T G)^{-1} G^T G = I$$



Minimum length

$$R = G^T (G G^T)^{-1} G$$

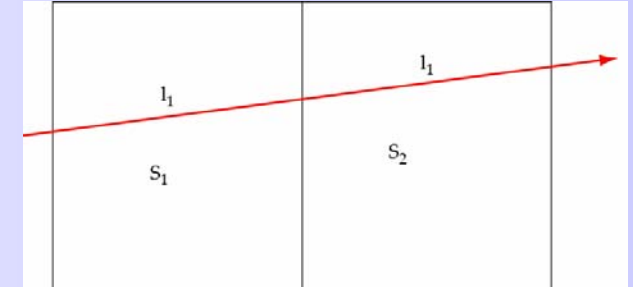


Example: Minimum Length resolution matrix

Model resolution matrix

$$\mathbf{m}_{ML} = G^T(GG^T)^{-1}\mathbf{d}$$

$$\mathbf{m}_{est} = G^{-g}\mathbf{d} = G^{-g}G\mathbf{m}_{true}$$



$$\mathbf{m}_{est} = R\mathbf{m}_{true}$$

$$R = G^{-g}G$$

$$R = G^T(GG^T)^{-1}G$$

$$R = \begin{pmatrix} l_1 \\ l_2 \end{pmatrix} = \left[\begin{pmatrix} l_1 & l_2 \end{pmatrix} \begin{pmatrix} l_1 \\ l_2 \end{pmatrix} \right]^{-1} \begin{pmatrix} l_1 & l_2 \end{pmatrix}$$

$$R = \frac{1}{(l_1^2 + l_2^2)} \begin{pmatrix} l_1^2 & l_1 l_2 \\ l_2 l_1 & l_2^2 \end{pmatrix}$$

Unlike the least squares case the model resolution matrix is not the identity

$$\text{If } l_1 = l_2 \Rightarrow R = \frac{1}{2} \begin{pmatrix} 1 & 1 \\ 1 & 1 \end{pmatrix}$$



Minimum Length and least squares solutions

$$\mathbf{m}_{LS} = (G^T G)^{-1} G^T \mathbf{d} \quad \mathbf{m}_{ML} = G^T (GG^T)^{-1} \mathbf{d}$$

$$\mathbf{m}_{est} = G^{-g} \mathbf{d}$$

Data resolution matrix

$$\mathbf{d}_{pre} = D \mathbf{d}_{obs}$$

$$D = GG^{-g}$$

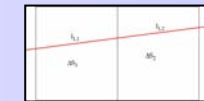
Least squares

$$D = G(G^T G)^{-1} G^T$$



Minimum length

$$D = GG^T (GG^T)^{-1} = I$$



There is symmetry between the least squares and minimum length solutions. Least squares completely solves the over-determined problem and has perfect model resolution, while the minimum length solves the completely under-determined problem and has perfect data resolution. For mix-determined problems all solutions will be between these two extremes.

Proof: Minimum Length solution

Constrained minimization

$$\text{Min} \quad L(\mathbf{m}) = \mathbf{m}^T \mathbf{m} : \mathbf{d} = G\mathbf{m}$$

Lagrange multipliers leads to unconstrained minimization of

$$\phi(\mathbf{m}, \boldsymbol{\lambda}) = \mathbf{m}^T \mathbf{m} + \boldsymbol{\lambda}^T (\mathbf{d} - G\mathbf{m}) = \sum_{j=1}^M m_j^2 + \sum_{i=1}^N \lambda_i (d_i - G_{i,j} m_j)$$

$$\frac{\partial \phi}{\partial \boldsymbol{\lambda}} = \mathbf{d} - G\mathbf{m} = \mathbf{0} \quad \longrightarrow \quad \frac{\partial \phi}{\partial \lambda_i} = \sum_{i=1}^N (d_i - G_{i,j} m_j)$$

$$\frac{\partial \phi}{\partial \mathbf{m}} = 2\mathbf{m} - G^T \boldsymbol{\lambda} = \mathbf{0} \quad \longrightarrow \quad \frac{\partial \phi}{\partial m_j} = 2m_j - \sum_{i=1}^N \lambda_i G_{i,j}$$

$$\Rightarrow \mathbf{m} = \frac{1}{2} G^T \boldsymbol{\lambda}$$

$$\Rightarrow \mathbf{d} = G\mathbf{m} = \frac{1}{2} GG^T \boldsymbol{\lambda}$$

$$\Rightarrow \boldsymbol{\lambda} = 2 (GG^T)^{-1} \mathbf{d}$$

$$\Rightarrow \mathbf{m} = G^T (GG^T)^{-1} \mathbf{d}$$



Minimum Length and least squares solutions

$$\mathbf{m}_{ML} = G^T(GG^T)^{-1}\mathbf{d} \quad \mathbf{m}_{LS} = (G^T G)^{-1}G^T\mathbf{d}$$

$$\mathbf{m}_{est} = G^{-g}\mathbf{d}$$

Data resolution matrix

$$\mathbf{d}_{pre} = D\mathbf{d}_{obs}$$

$$D = GG^{-g}$$

Minimum length

$$D = GG^T(GG^T)^{-1} = I$$

$$R = G^T(GG^T)^{-1}G \neq I$$

Least squares

$$D = G(G^T G)^{-1}G^T \neq I$$

$$R = (G^T G)^{-1}G^T G = I$$

There is symmetry between the least squares and minimum length solutions. Least squares complete solves the over-determined problem and has perfect model resolution, while the minimum length solves the completely under-determined problem and has perfect data resolution. For mix-determined problems all solutions will be between these two extremes.

Singular value decomposition

SVD is a method of analyzing and solving linear discrete ill-posed problems.

At its heart is the *Lanczos decomposition* of the matrix G

$$\boxed{\mathbf{d} = G\mathbf{m}}$$

$$G = USV^T$$

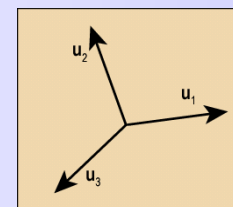
$$G = \underset{N \times M}{[\mathbf{u}_1, \mathbf{u}_2, \dots, \mathbf{u}_N]} \underset{N \times N}{S} \underset{M \times M}{[\mathbf{v}_1, \mathbf{v}_2, \dots, \mathbf{v}_M]}^T$$

U is an $N \times N$ ortho-normal matrix with columns that span the **data space**

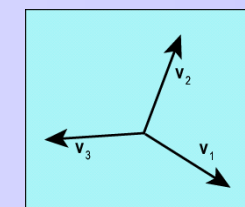
V is an $M \times M$ ortho-normal matrix with columns that span the **model space**

S is an $N \times M$ diagonal matrix with non-negative elements \rightarrow singular values

$$UU^T = U^T U = I_N$$



$$VV^T = V^T V = I_M$$



III-posed problems arise when some of the singular values are zero



Singular value decomposition

Given G , how do we calculate the matrices U , V and S ?

$$G = USV^T$$

$$U = [\mathbf{u}_1 | \mathbf{u}_2 | \dots | \mathbf{u}_N]$$

$$V = [\mathbf{v}_1 | \mathbf{v}_2 | \dots | \mathbf{v}_M]$$

It can be shown that the columns of U are the eigenvectors of the matrix GG^T

$$GG^T \mathbf{u}_i = s_i^2 \mathbf{u}_i$$

Try and prove this !

It can be shown that the columns of V are the eigenvectors of the matrix G^TG

$$G^T G \mathbf{v}_i = s_i^2 \mathbf{v}_i$$

Try and prove this !

The eigenvalues, s_i^2 , are the square of the elements in diagonal of the $N \times M$ matrix S .

If $N > M$

$$S = \begin{bmatrix} s_1 & 0 & \cdots & 0 \\ 0 & s_2 & 0 & 0 \\ \vdots & \ddots & \ddots & 0 \\ 0 & 0 & 0 & s_M \\ \hline 0 & 0 & 0 & 0 \\ \vdots & \vdots & \vdots & \vdots \\ 0 & 0 & 0 & 0 \end{bmatrix}$$

If $M > N$

$$S = \begin{bmatrix} s_1 & 0 & \cdots & 0 & 0 & \cdots & 0 \\ 0 & s_2 & 0 & 0 & 0 & \cdots & 0 \\ \vdots & \ddots & \ddots & 0 & 0 & \cdots & 0 \\ 0 & 0 & 0 & s_N & 0 & \cdots & 0 \end{bmatrix}$$

Singular value decomposition

$$S = \begin{bmatrix} s_1 & 0 & \cdots & 0 \\ 0 & s_2 & 0 & 0 \\ \vdots & \ddots & \ddots & 0 \\ 0 & 0 & 0 & s_M \\ \hline 0 & 0 & 0 & 0 \\ \vdots & \vdots & \vdots & \vdots \\ 0 & 0 & 0 & 0 \end{bmatrix} \quad S = \begin{bmatrix} s_1 & 0 & \cdots & 0 & 0 & \cdots & 0 \\ 0 & s_2 & 0 & 0 & 0 & \cdots & 0 \\ \vdots & \ddots & \ddots & 0 & 0 & \cdots & 0 \\ 0 & 0 & 0 & s_N & 0 & \cdots & 0 \end{bmatrix}$$

Suppose the first p are non-zero, then N x M non square matrix S can be written in a partitioned form

$$S = \begin{bmatrix} S_p & \mathbf{0} \\ \mathbf{0} & \mathbf{0} \end{bmatrix}^{\text{M}}_{\text{N}}$$

By convention we order the singular values

$$s_1 \geq s_2 \geq \cdots \geq s_p$$

$$S_p = \begin{bmatrix} s_1 & 0 & \cdots & 0 \\ 0 & s_2 & 0 & 0 \\ \vdots & \ddots & \ddots & 0 \\ 0 & 0 & 0 & s_p \end{bmatrix}^{\text{p}} \quad U = [\mathbf{u}_1 | \mathbf{u}_2 | \dots | \mathbf{u}_N] \\ V = [\mathbf{v}_1 | \mathbf{v}_2 | \dots | \mathbf{v}_M]$$

where the submatrix s_p is a p x p diagonal matrix contains the non-zero singular values

$$p_{max} = \min(N, M)$$



Singular value decomposition

If only the first p singular values are nonzero we write

$$G = [U_p \mid U_o] \begin{bmatrix} S_p & \mathbf{0} \\ \mathbf{0} & \mathbf{0} \end{bmatrix} [V_p \mid V_o]^T$$

U_p represents the first p columns of U

U_o represents the last N-p columns of U → A data null space is created

V_p represents the first p columns of V

V_o represents the last M-p columns of V → A model null space is created

Properties

$$U_p^T U_o = 0 \quad U_o^T U_p = 0 \quad V_p^T V_o = 0 \quad V_o^T V_p = 0$$

$$U_p^T U_p = I \quad U_o^T U_o = I \quad V_o^T V_o = I \quad V_p^T V_p = I$$

Since the columns of V_o and U_o multiply by zeros we get the *compact* form for G

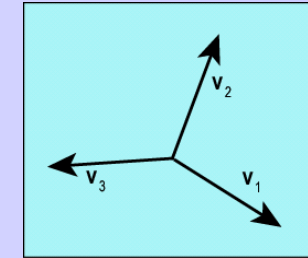
$$G = U_p S_p V_p^T$$

Model null space

Consider a vector made up of a linear combination of the columns of V_o

$$\mathbf{m}_v = \sum_{i=p+1}^M \lambda_i \mathbf{v}_i$$

The model \mathbf{m} lies in the space spanned by columns of V_o



$$G\mathbf{m}_v = \sum_{i=p+1}^M \lambda_i U_p S_p V_p^T \mathbf{v}_i = \mathbf{0}$$

So any model of this type has no affect on the data. It lies in the
model null space !

Where have we seen this before ?

Consequence: If any solution exists to the inverse problem then an infinite number will

Assume the model \mathbf{m}_{ls} fits the data $G\mathbf{m}_{ls} = \mathbf{d}_{obs}$

$$\begin{aligned} G(\mathbf{m}_{ls} + \mathbf{m}_v) &= G\mathbf{m}_{ls} + G\mathbf{m}_v \\ &= \mathbf{d}_{obs} + \mathbf{0} \end{aligned}$$

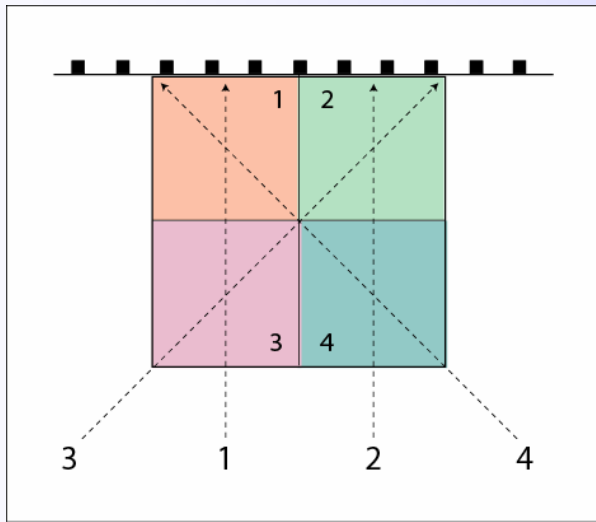
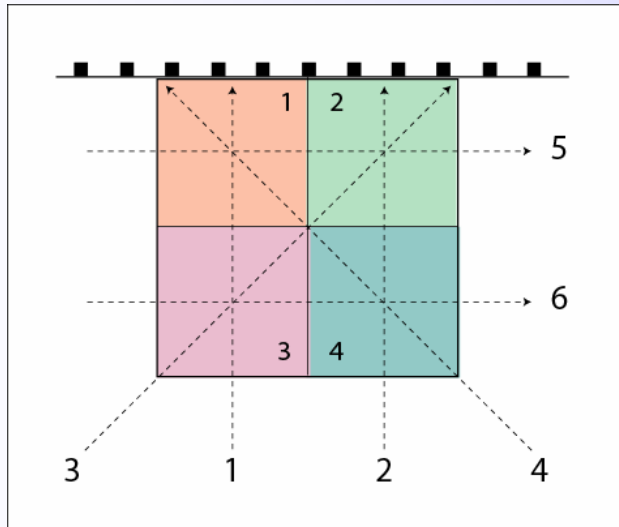


Uniqueness question
of Backus and Gilbert

The data can not constrain models in the model null space

Example: tomography

Idealized tomographic experiment



$$\delta d = G \delta m$$

$$G = \begin{bmatrix} G_{1,1} & G_{1,2} & G_{1,3} & G_{1,4} \\ \vdots & \vdots & \vdots & \vdots \\ \vdots & \vdots & \vdots & \vdots \\ \vdots & \vdots & \vdots & \vdots \end{bmatrix}$$

What are the entries of G ?

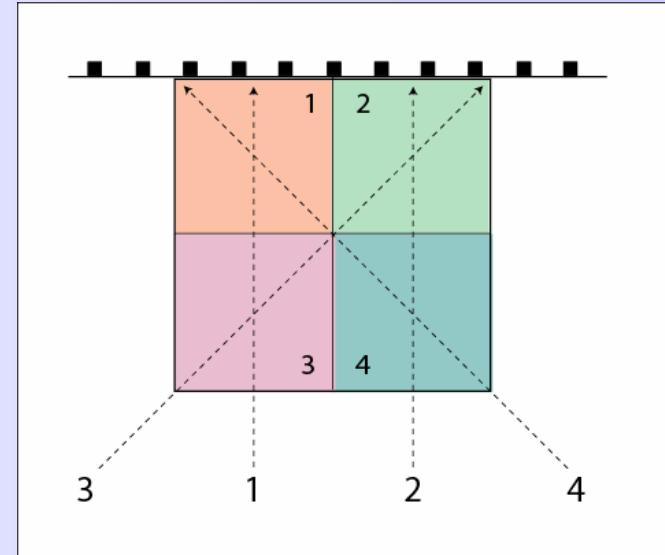
Example: tomography

Using rays 1-4

$$G = \begin{bmatrix} 1 & 0 & 1 & 0 \\ 0 & 1 & 0 & 1 \\ 0 & \sqrt{2} & \sqrt{2} & 0 \\ \sqrt{2} & 0 & 0 & \sqrt{2} \end{bmatrix}$$

$$G^T G = \begin{bmatrix} 3 & 0 & 1 & 2 \\ 0 & 3 & 2 & 1 \\ 1 & 2 & 3 & 0 \\ 2 & 1 & 0 & 3 \end{bmatrix}$$

$$\delta d = G\delta m$$



This has eigenvalues 6,4,2,0.

$$V_p = \begin{bmatrix} 0.5 & -0.5 & -0.5 \\ 0.5 & 0.5 & 0.5 \\ 0.5 & 0.5 & -0.5 \\ 0.5 & -0.5 & 0.5 \end{bmatrix}$$

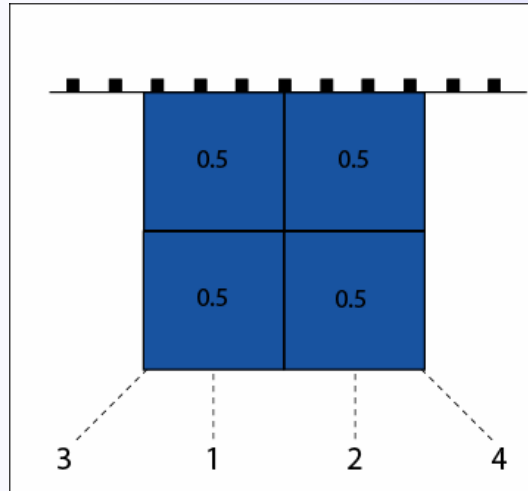
$$V_o = \begin{bmatrix} 0.5 \\ 0.5 \\ -0.5 \\ -0.5 \end{bmatrix}$$

$$Gv_o = 0$$

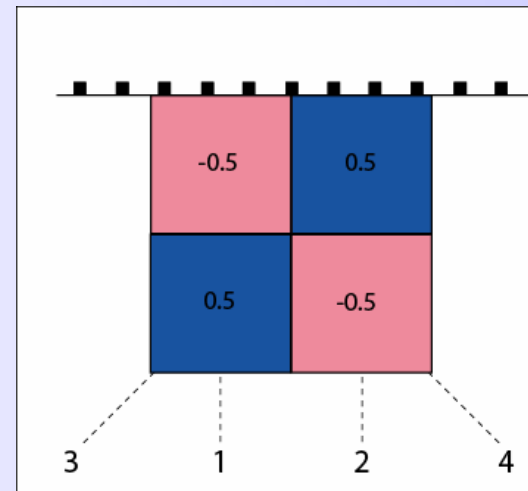
What type of change does the null space vector correspond to ?

Worked example: Eigenvectors

$$S_1^2=6$$

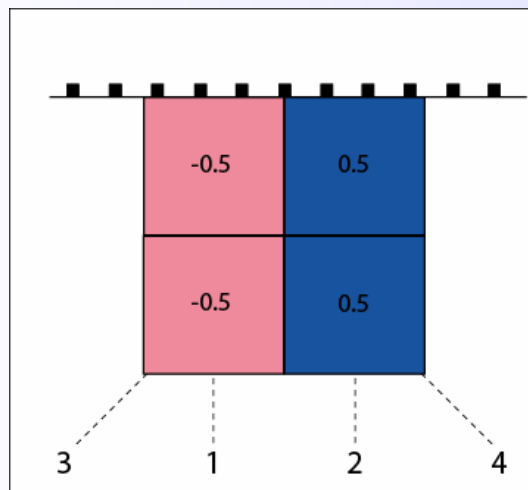


$$S_2^2=4$$

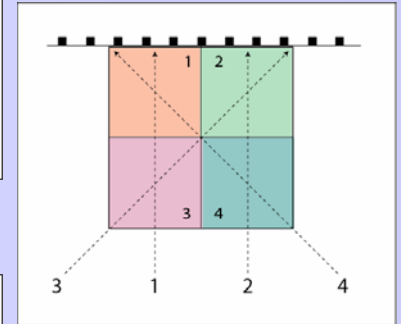
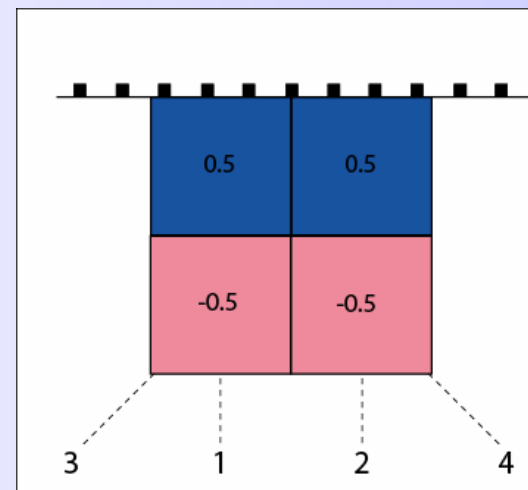


$$V_p = \begin{bmatrix} 0.5 & -0.5 & -0.5 \\ 0.5 & 0.5 & 0.5 \\ 0.5 & 0.5 & -0.5 \\ 0.5 & -0.5 & 0.5 \end{bmatrix}$$

$$S_3^2=2$$



$$S_4^2=0$$



$$V_o = \begin{bmatrix} 0.5 \\ 0.5 \\ -0.5 \\ -0.5 \end{bmatrix}$$

Data null space

Consider a data vector with at least one component in U_o

$$d_{obs} = d_o + \lambda_i u_i \quad (i > p)$$

For any model space vector m we have

$$\begin{aligned} d_{pre} &= Gm = U_p S_p V_p^T m \\ &= U_p a \end{aligned}$$

For the model to fit the data we must have

$$d_{obs} = d_{pre}$$

$$d_o + \lambda_i u_i = \sum_{j=1}^p a_j u_j$$

Where have we seen this before ?

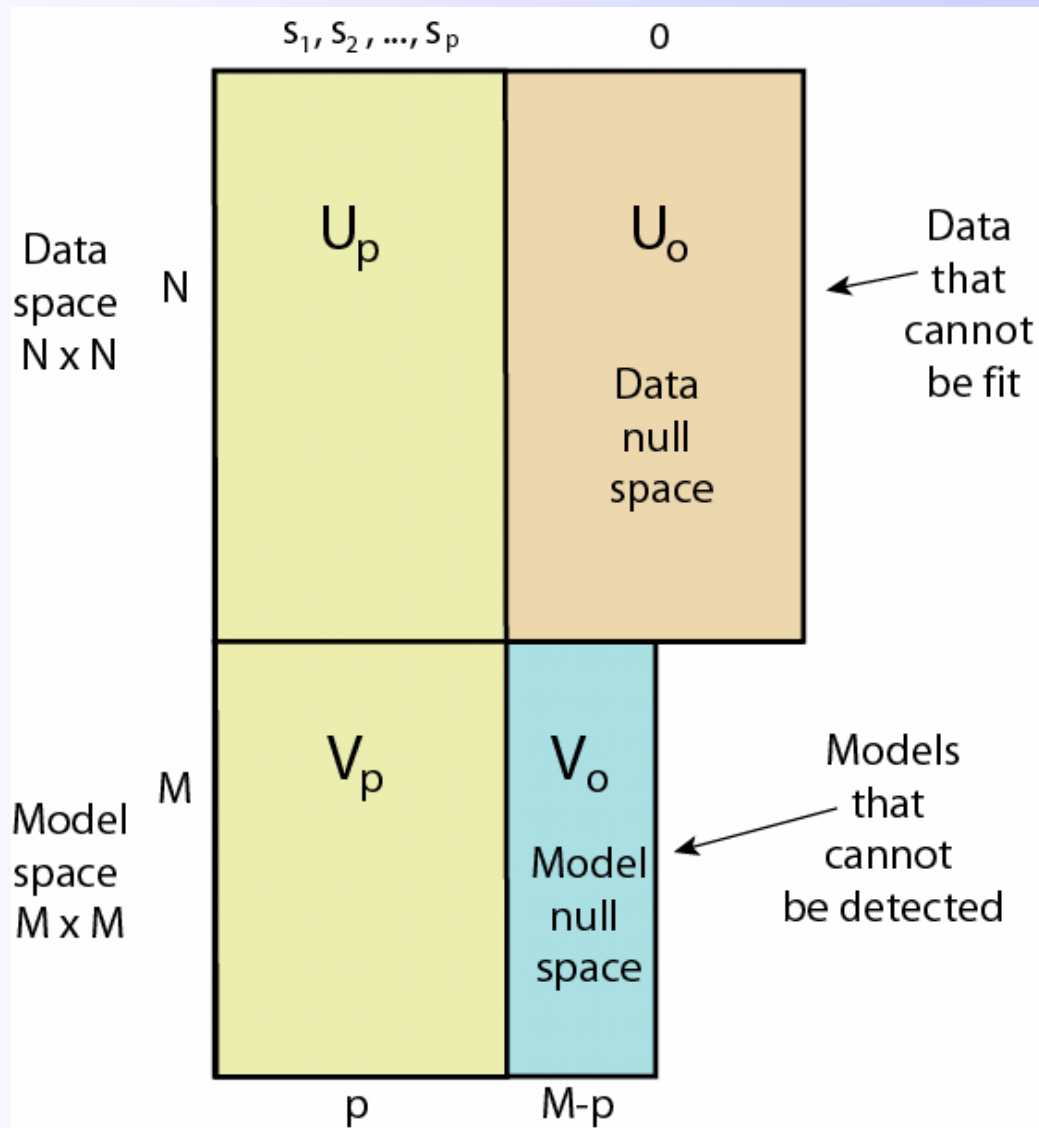
So data of this type can not be fit by any model. The data has a component in the **data null space** !

Consequence: No model exists that can fit the data

Existence question
of Backus and Gilbert

All this depends on the structure of the kernel matrix G !

Data and model null spaces





Moore-Penrose inverse and data null space

$$\mathbf{d} = G\mathbf{m} \quad G = U_p S_p V_p^T$$

The Moore-Penrose pseudo or **generalized inverse** of G is written

It is the unique matrix that satisfies four special properties

$$G^\dagger = V_p S_p^{-1} U_p^T$$

$$GG^\dagger G = G \quad (GG^\dagger)^T = GG^\dagger$$

$$G^\dagger GG^\dagger = G^\dagger \quad (G^\dagger G)^T = G^\dagger G$$

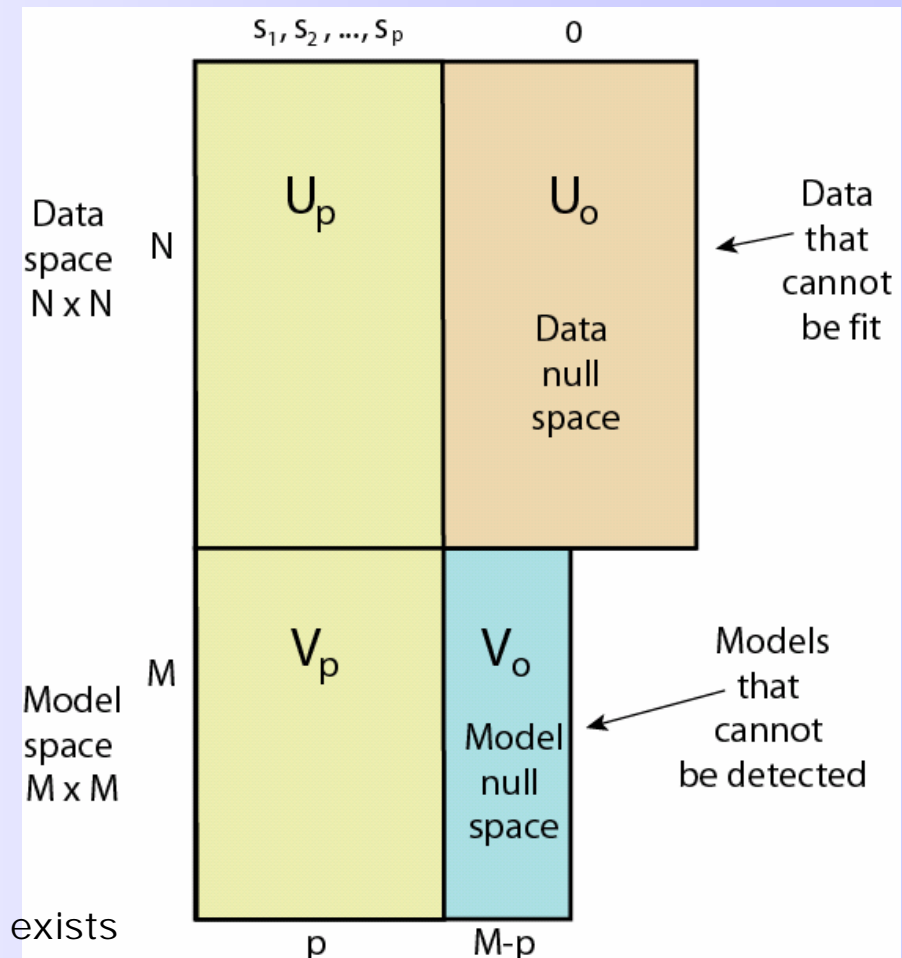
Even when G has zero eigenvalues the Moore-Penrose inverse **always exists** and has desirable properties

$$\mathbf{m}^\dagger = G^\dagger \mathbf{d}_{obs} = V_p S_p^{-1} U_p^T \mathbf{d}_{obs}$$

Properties of the Moore-Penrose inverse

U_p and V_p always exist and there are FOUR possible situations to consider

- Case 1:
No model or data null space
 U_o and V_o do not exist
- Case 2:
Only a model null space exists
 U_o does not exist, V_o exists
- Case 3:
Only a data null space exists
 U_o exists, V_o does not exist
- Case 4:
Both data and model null space exists
 U_o and V_o exists



Properties of the generalized inverse: case 1

There are FOUR possible situations

- Both model and data spaces have 'trivial' null spaces.
 $U_p = U$ and $V_p = V$ are square and orthogonal

$$U_p^T = U_p^{-1} \quad V_p^T = V_p^{-1}$$

Moore-Penrose inverse becomes

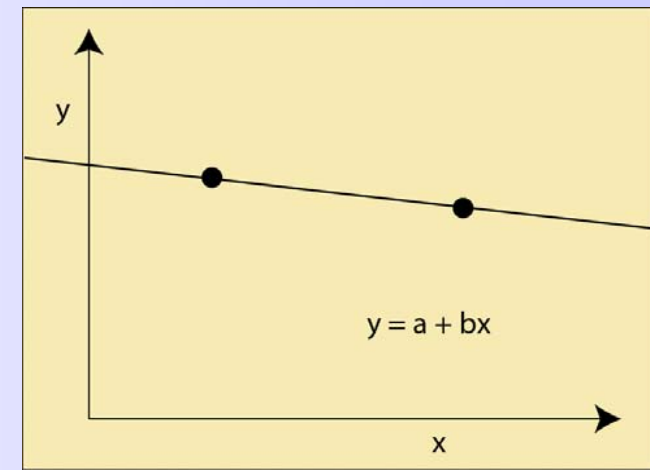
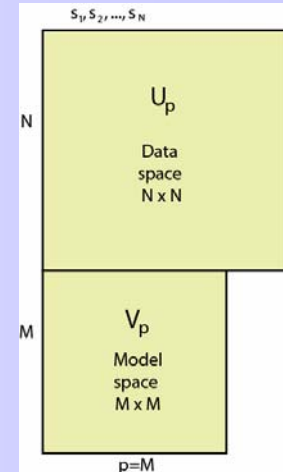
$$G^\dagger = V_p S_p^{-1} U_p^T$$

$$= (U_p S_p V_p^T)^{-1}$$

$$= G^{-1}$$

$$Gm^\dagger = GG^\dagger d$$

$$= d$$



The solution is unique and the data are fit exactly.

Properties of the generalized inverse: case 2

- Data null space is trivial, model null space is non-trivial.
 $U_p = U$ is square V_p is non-square

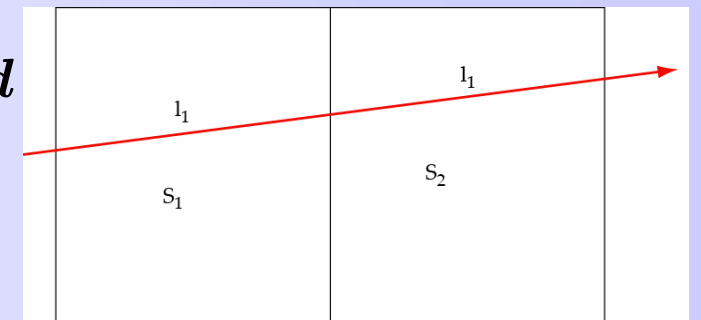
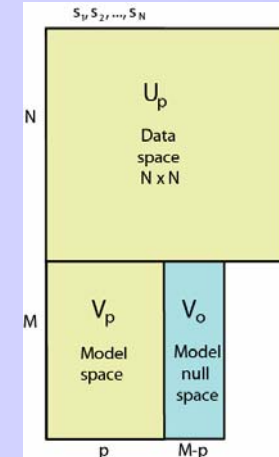
• The solution is non-unique $U_p^T = U_p^{-1}$

• The data are fit exactly $V_p^T V_p = I_p$

$$Gm^\dagger = GG^\dagger d = d$$

- But which of the infinite number of solutions do we get ?

$$\begin{aligned} m^\dagger &= V_p S_p^{-1} U_p^T d \\ &= (V_p S_p U_p^T) (U_p S_p^{-2} U_p^T) d \\ &= G^T (U_p S_p^{-2} U_p^T) d \\ &= G^T (GG^T)^{-1} d \end{aligned}$$



This is the minimum length solution !

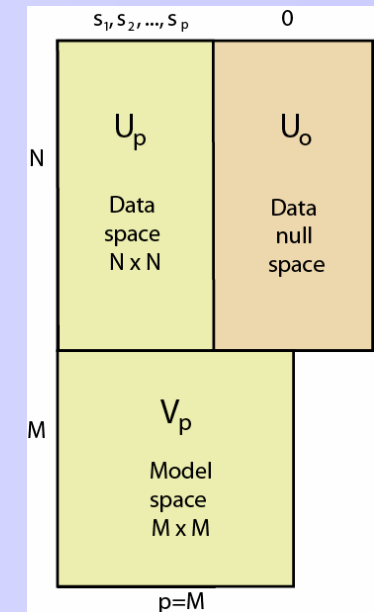
Properties of the generalized inverse: case 3

- Data null space is non-trivial, model null space is trivial.
 $V_p^T = V_p^{-1}$ and U_p is non-square

What happens when a data vector \mathbf{d}_o only lies in the space spanned by U_o ?

$$\mathbf{d}_o = \sum_{i=p+1}^N \beta_i \mathbf{u}_i$$

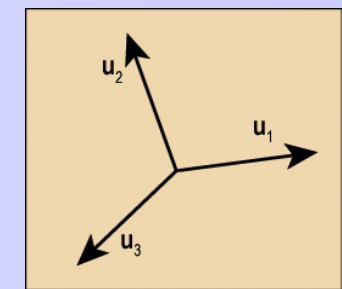
$$\mathbf{m}^\dagger = G^\dagger \mathbf{d}_o = \sum_{i=p+1}^N \beta_i V_p S_p^{-1} U_p^T \mathbf{u}_i = \mathbf{0}$$



Models can not satisfy data in the data null space

- The data are not fit exactly

$$\begin{aligned} G\mathbf{m}^\dagger &= GG^\dagger \mathbf{d} \\ &= (U_p S_p V_p^T)(V_p S_p^{-1} U_p^T) \mathbf{d} \\ &= U_p U_p^T \mathbf{d} \end{aligned}$$



Properties of the generalized inverse: case 3

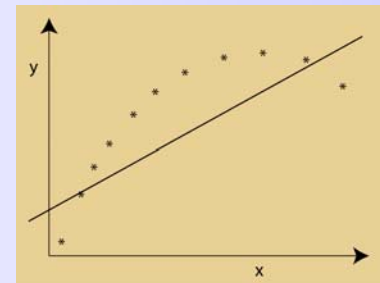
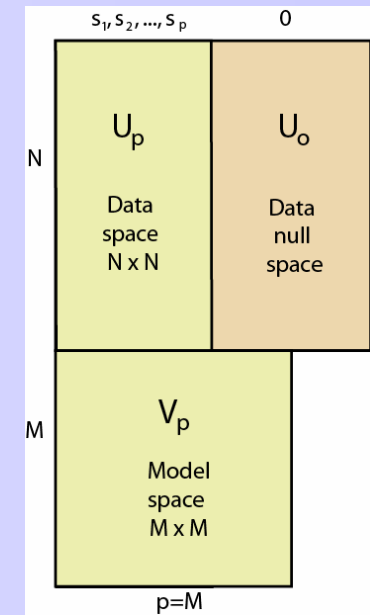
- Data null space is non-trivial, model null space is trivial.

$$V_p^T = V_p^{-1} \text{ and } U_p \text{ is non-square}$$

- The solution is unique

- We get a least squares solution

$$\begin{aligned} \mathbf{m} &= (G^T G)^{-1} G^T \mathbf{d} \\ &= (V_p S_p U_p^T U_p S_p V_p^T)^{-1} V_p S_p U_p^T \mathbf{d} \\ &= V_p S_p^{-1} U_p^T \mathbf{d} \\ &= G^\dagger \mathbf{d} \end{aligned}$$



We get the least squares solution which minimizes the prediction error!

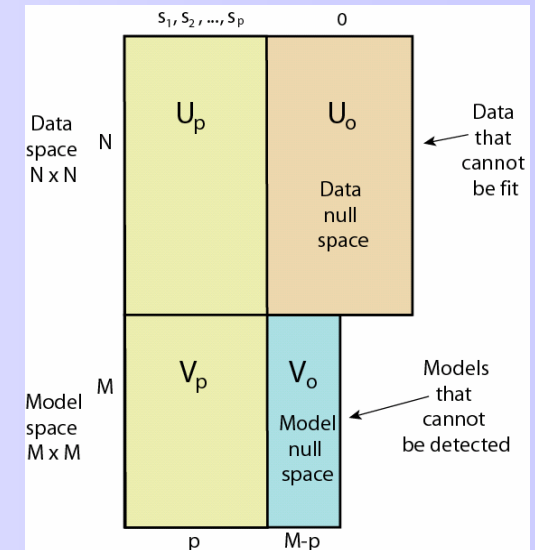
Properties of the generalized inverse: case 4

- Data and model space are non-trivial
 $p < N, M$
- Both case 2 and case 3 arguments apply
 - It minimizes the model length (case 2)
 - It minimizes data prediction error

$$L(\mathbf{m}^\dagger) = \mathbf{m}^{\dagger T} \mathbf{m}^\dagger$$

- It minimizes data prediction error

$$\phi(\mathbf{m}^\dagger) = (\mathbf{d} - G\mathbf{m}^\dagger)^T (\mathbf{d} - G\mathbf{m}^\dagger)$$



The generalized inverse combines the **best features** of both solutions.
In our linearized tomographic problem it gives the **best fit** to the data while also **minimizing the length** of the solution.



Covariance and Resolution of the pseudo inverse

How does data noise propagate into the model ?

What is the model covariance matrix for the generalized inverse ?

$$C_M = G^\dagger C_d (G^\dagger)^T$$

For the case $C_d = \sigma^2 I$

$$G^\dagger = V_p S_p^{-1} U_p^T$$

$$C_M = \sigma^2 G^\dagger (G^\dagger)^T$$

$$= \sigma^2 V_p S_p^{-2} V_p^T$$

Recall that S_p is a diagonal matrix of singular ordered values

$$S_p = \text{diag}[s_1, s_2, \dots, s_p]$$

$$\Rightarrow C_M = \sigma^2 \sum_{i=1}^p \frac{\mathbf{v}_i \mathbf{v}_i^T}{s_i^2}$$

As the number of singular values, p , increases the variance of the model parameters increases !

Covariance and Resolution of the pseudo inverse

How is the estimated model related to the true model ?

Model resolution matrix

$$R = G^\dagger G$$

$$\begin{aligned} &= V_p S_p^{-1} U_p^T U_p S_p V_p^T \\ &= V_p V_p^T \end{aligned}$$

$$\mathbf{m}^\dagger = R \mathbf{m}_{true}$$

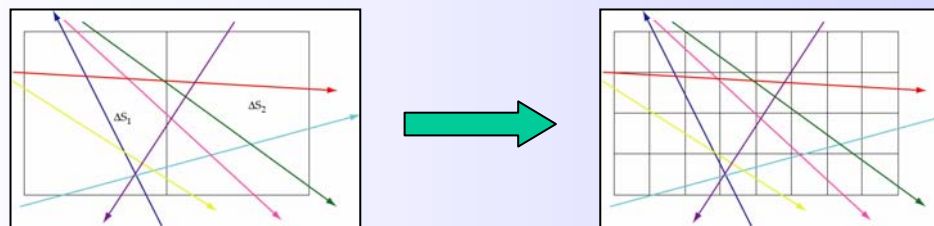
$$G^\dagger = V_p S_p^{-1} U_p^T$$

As p increases the model null space decreases

$$p \rightarrow M : \quad V_p^T \rightarrow V_p^{-1}, \quad R \rightarrow I$$

As the number of singular values, p, increases the resolution of the model parameters increases !

We see the trade-off between variance and resolution



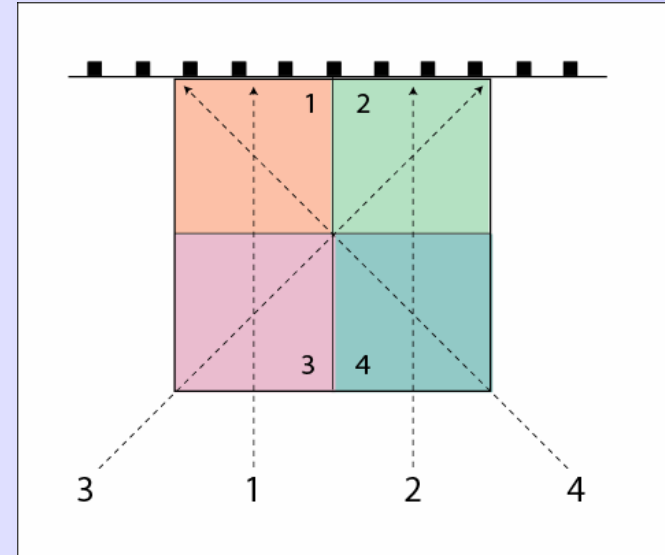
Worked example: tomography

Using rays 1- 4

$$G = \begin{bmatrix} 1 & 0 & 1 & 0 \\ 0 & 1 & 0 & 1 \\ 0 & \sqrt{2} & \sqrt{2} & 0 \\ \sqrt{2} & 0 & 0 & \sqrt{2} \end{bmatrix}$$

$$G^T G = \begin{bmatrix} 3 & 0 & 1 & 2 \\ 0 & 3 & 2 & 1 \\ 1 & 2 & 3 & 0 \\ 2 & 1 & 0 & 3 \end{bmatrix}$$

$$\delta d = G\delta m$$



This has eigenvalues 0, 2, 4, 6.

$$V_p = \begin{bmatrix} 0.5 & -0.5 & -0.5 \\ 0.5 & 0.5 & 0.5 \\ 0.5 & 0.5 & -0.5 \\ 0.5 & -0.5 & 0.5 \end{bmatrix}$$

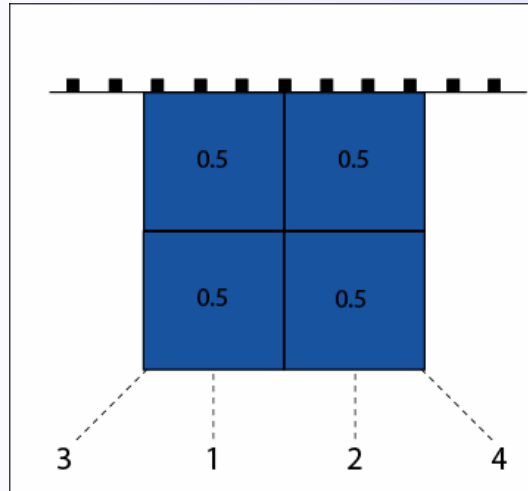
$s_1^2 = 6$ $s_2^2 = 4$ $s_3^2 = 2$

$$V_o = \begin{bmatrix} 0.5 \\ 0.5 \\ -0.5 \\ -0.5 \end{bmatrix} \quad Gv_o = 0$$

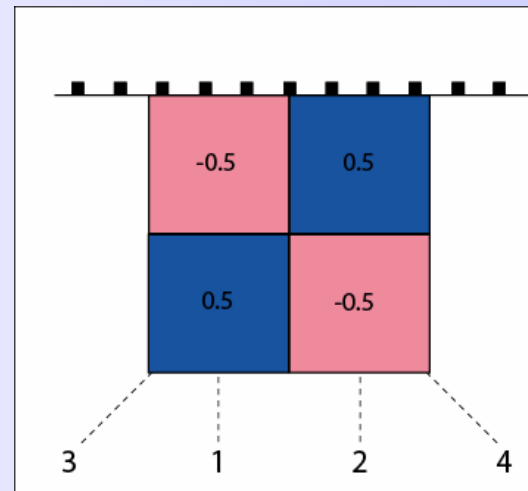
$s_4^2 = 0$

Worked example: Eigenvectors

$$S_1^2=6$$

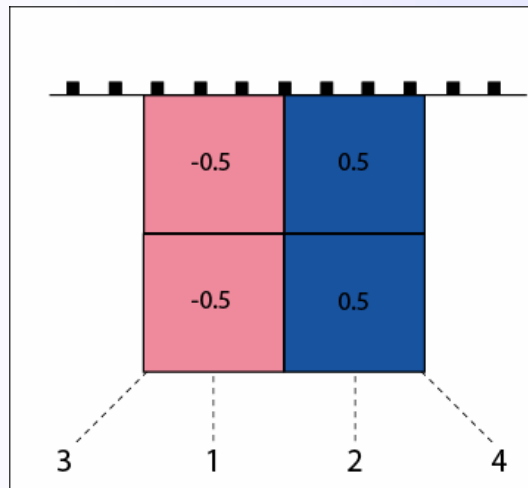


$$S_2^2=4$$



$$V_p = \begin{bmatrix} 0.5 & -0.5 & -0.5 \\ 0.5 & 0.5 & 0.5 \\ 0.5 & 0.5 & -0.5 \\ 0.5 & -0.5 & 0.5 \end{bmatrix}$$

$$S_3^2=2$$



$$V_o = \begin{bmatrix} 0.5 \\ 0.5 \\ -0.5 \\ -0.5 \end{bmatrix}$$

Worked example: tomography

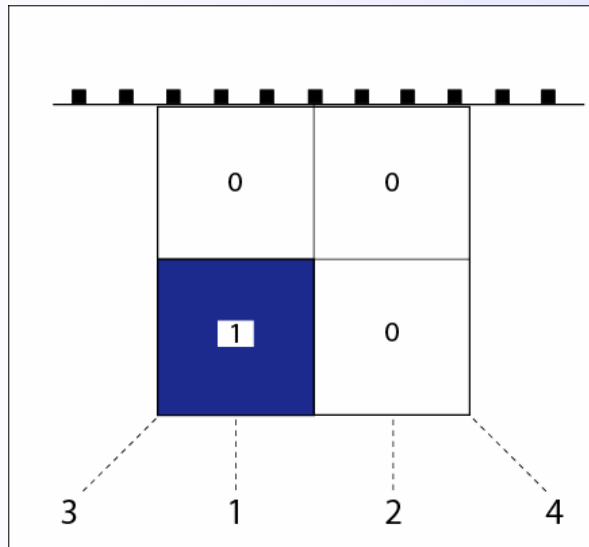
Using eigenvalues all non zero eigenvalues s_1 , s_2 and s_3 the resolution matrix becomes

$$\delta\mathbf{m} = R\delta\mathbf{m}_{true} = V_p V_p^T \delta\mathbf{m}_{true}$$

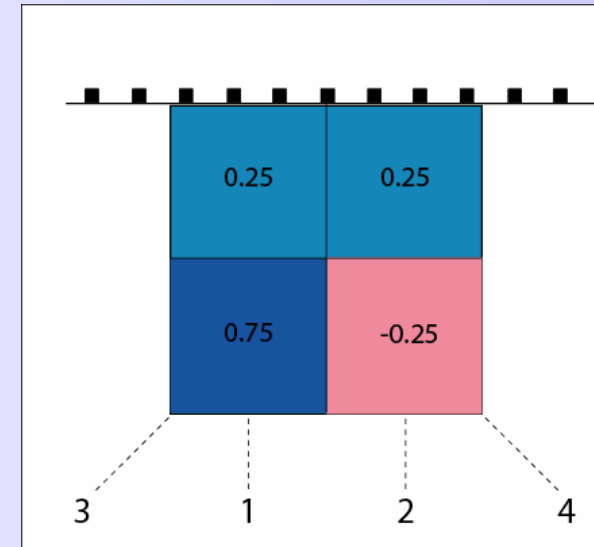
$$R = \begin{bmatrix} 0.75 & -0.25 & 0.25 & 0.25 \\ -0.25 & 0.75 & 0.25 & 0.25 \\ 0.25 & 0.25 & 0.75 & -0.25 \\ 0.25 & 0.25 & -0.25 & 0.75 \end{bmatrix}$$

$$V_p = \begin{bmatrix} 0.5 & -0.5 & -0.5 \\ 0.5 & 0.5 & 0.5 \\ 0.5 & 0.5 & -0.5 \\ 0.5 & -0.5 & 0.5 \end{bmatrix}$$

Input model



Recovered model



Worked example: tomography

Using eigenvalues s_1 , s_2 and s_3 the model covariance becomes

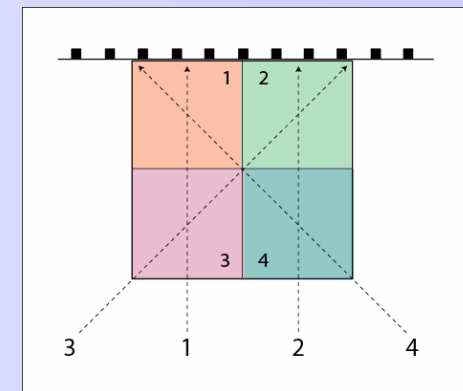
$$\Rightarrow C_M = \sigma^2 \sum_{i=1}^p \frac{\mathbf{v}_i \mathbf{v}_i^T}{s_i^2}$$

$$\mathbf{v}_p = \begin{bmatrix} -0.5 & -0.5 & 0.5 \\ 0.5 & 0.5 & 0.5 \\ -0.5 & 0.5 & 0.5 \\ 0.5 & -0.5 & 0.5 \end{bmatrix}$$

$\uparrow \quad \uparrow \quad \uparrow$
 $s_1^2 = 2 \quad s_2^2 = 4 \quad s_3^2 = 6$

$$C_M = \frac{\sigma^2}{4} \left\{ \frac{1}{2} \begin{pmatrix} 1 & -1 & 1 & -1 \\ -1 & 1 & -1 & 1 \\ 1 & -1 & 1 & -1 \\ -1 & 1 & -1 & 1 \end{pmatrix} + \frac{1}{4} \begin{pmatrix} 1 & -1 & -1 & 1 \\ -1 & 1 & 1 & -1 \\ -1 & -1 & 1 & -1 \\ 1 & -1 & -1 & 1 \end{pmatrix} + \frac{1}{6} \begin{pmatrix} 1 & 1 & 1 & 1 \\ 1 & 1 & 1 & 1 \\ 1 & 1 & 1 & 1 \\ 1 & 1 & 1 & 1 \end{pmatrix} \right\}$$

$$C_M = \frac{\sigma^2}{48} \begin{bmatrix} 11 & -7 & 5 & -1 \\ -7 & 11 & -1 & 5 \\ 5 & -1 & 11 & -7 \\ -1 & 5 & -7 & 11 \end{bmatrix}$$

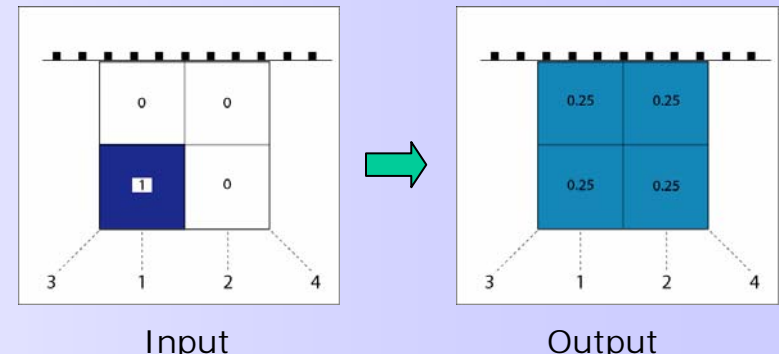


Worked example: tomography

Repeat using only one singular value $s_3 = 6$

Model resolution matrix

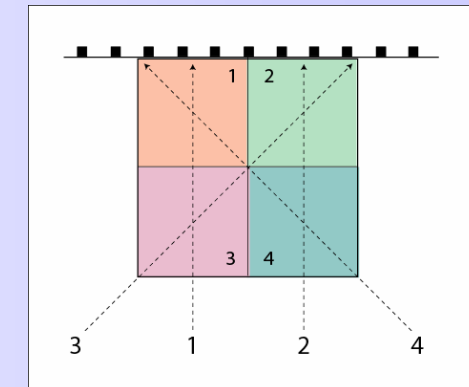
$$R = V_p V_p^T = \frac{1}{4} \begin{bmatrix} 1 & 1 & 1 & 1 \\ 1 & 1 & 1 & 1 \\ 1 & 1 & 1 & 1 \\ 1 & 1 & 1 & 1 \end{bmatrix}$$



Model covariance matrix

$$C_M = \sigma^2 \sum_{i=1}^p \frac{\mathbf{v}_i \mathbf{v}_i^T}{s_i^2}$$

$$= \frac{\sigma^2}{24} \begin{bmatrix} 1 & 1 & 1 & 1 \\ 1 & 1 & 1 & 1 \\ 1 & 1 & 1 & 1 \\ 1 & 1 & 1 & 1 \end{bmatrix}$$





Recap: Singular value decomposition

- There may exist a model null space -> models that can not be constrained by the data.
- There may exist a data null space -> data that can not be fit by any model.
- The general linear discrete inverse problem may be simultaneously under and over determined (mix-determined).
- Singular value decomposition is a framework for dealing with ill-posed problems.
- The Pseudo inverse is constructed using SVD and provides a unique model with desirable properties.
 - Fits the data in a least squares sense
 - Gives a minimum length model (no component in the null space)
- Model Resolution and Covariance can be traded off by choosing the number of eigenvalues to use in reconstruction.



Singular value decomposition

If only the first p singular values are nonzero we write

$$G = [U_p \mid U_o] \begin{bmatrix} S_p & \mathbf{0} \\ \mathbf{0} & \mathbf{0} \end{bmatrix} [V_p \mid V_o]^T$$

U_p represents the first p columns of U

U_o represents the last N-p columns of U → A data null space is created

V_p represents the first p columns of V

V_o represents the last M-p columns of V → A model null space is created

Properties

$$U_p^T U_o = 0 \quad U_o^T U_p = 0 \quad V_p^T V_o = 0 \quad V_o^T V_p = 0$$

$$U_p^T U_p = I \quad U_o^T U_o = I \quad V_o^T V_o = I \quad V_p^T V_p = I$$

Since the columns of V_o and U_o multiply by zeros we get the *compact* form for G

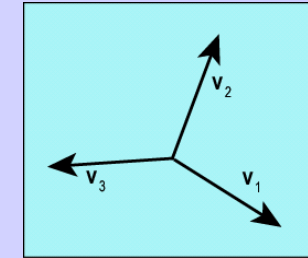
$$G = U_p S_p V_p^T$$

Model null space

Consider a vector made up of a linear combination of the columns of V_o

$$\mathbf{m}_v = \sum_{i=p+1}^M \lambda_i \mathbf{v}_i$$

The model \mathbf{m} lies in the space spanned by columns of V_o



$$G\mathbf{m}_v = \sum_{i=p+1}^M \lambda_i U_p S_p V_p^T \mathbf{v}_i = \mathbf{0}$$

So any model of this type has no affect on the data. It lies in the
model null space !

Where have we seen this before ?

Consequence: If any solution exists to the inverse problem then an infinite number will

Assume the model \mathbf{m}_{ls} fits the data $G\mathbf{m}_{ls} = \mathbf{d}_{obs}$

$$\begin{aligned} G(\mathbf{m}_{ls} + \mathbf{m}_v) &= G\mathbf{m}_{ls} + G\mathbf{m}_v \\ &= \mathbf{d}_{obs} + \mathbf{0} \end{aligned}$$



Uniqueness question
of Backus and Gilbert

The data can not constrain models in the model null space

Data null space

Consider a data vector with at least one component in U_o

$$d_{obs} = d_o + \lambda_i u_i \quad (i > p)$$

For any model space vector m we have

$$\begin{aligned} d_{pre} &= Gm = U_p S_p V_p^T m \\ &= U_p a \end{aligned}$$

For the model to fit the data we must have

$$d_{obs} = d_{pre}$$

$$d_o + \lambda_i u_i = \sum_{j=1}^p a_j u_j$$

Where have we seen this before ?

So data of this type can not be fit by any model. The data has a component in the **data null space** !

Consequence: No model exists that can fit the data

Existence question
of Backus and Gilbert

All this depends on the structure of the kernel matrix G !

Moore Penrose Generalized inverse

$$G^\dagger = V_p S_p^{-1} U_p^T$$

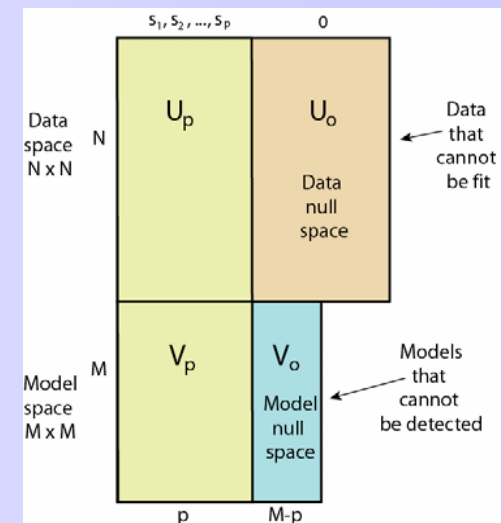
The generalized inverse combines the **features** of the least squares and minimum length solutions.

Purely over-determined problem it is equivalent to the least squares solution

$$m^\dagger = G^\dagger d = (G^T G)^{-1} G^T d$$

In a purely under-determined problem it is equivalent to the minimum length solution

$$m^\dagger = G^\dagger d = G^T (G G^T)^{-1} d$$



In general problems it minimizes the data **prediction error** while also producing a **minimizing the length** solution.

$$L(m^\dagger) = m^{\dagger T} m^\dagger \quad \phi(m^\dagger) = (d - Gm^\dagger)^T (d - Gm^\dagger)$$



Covariance and Resolution of the pseudo inverse

How does data noise propagate into the model ?

What is the model covariance matrix for the generalized inverse ?

$$C_M = G^\dagger C_d (G^\dagger)^T$$

For the case $C_d = \sigma^2 I$

$$G^\dagger = V_p S_p^{-1} U_p^T$$

$$C_M = \sigma^2 G^\dagger (G^\dagger)^T$$

Prove this

$$= \sigma^2 V_p S_p^{-2} V_p^T$$

Recall that S_p is a diagonal matrix of singular ordered values

$$S_p = \text{diag}[s_1, s_2, \dots, s_p]$$

$$\Rightarrow C_M = \sigma^2 \sum_{i=1}^p \frac{\mathbf{v}_i \mathbf{v}_i^T}{s_i^2}$$

Prove this

As the number of singular values, p , increases the variance of the model parameters increases !

Covariance and Resolution of the pseudo inverse

How is the estimated model related to the true model ?

Model resolution matrix

$$R = G^\dagger G$$

$$\begin{aligned} &= V_p S_p^{-1} U_p^T U_p S_p V_p^T \\ &= V_p V_p^T \end{aligned}$$

$$\mathbf{m}^\dagger = R \mathbf{m}_{true}$$

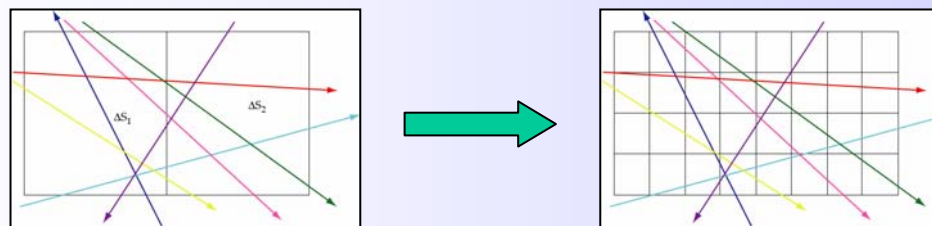
$$G^\dagger = V_p S_p^{-1} U_p^T$$

As p increases the model null space decreases

$$p \rightarrow M : \quad V_p^T \rightarrow V_p^{-1}, \quad R \rightarrow I$$

As the number of singular values, p, increases the resolution of the model parameters increases !

We see the trade-off between variance and resolution



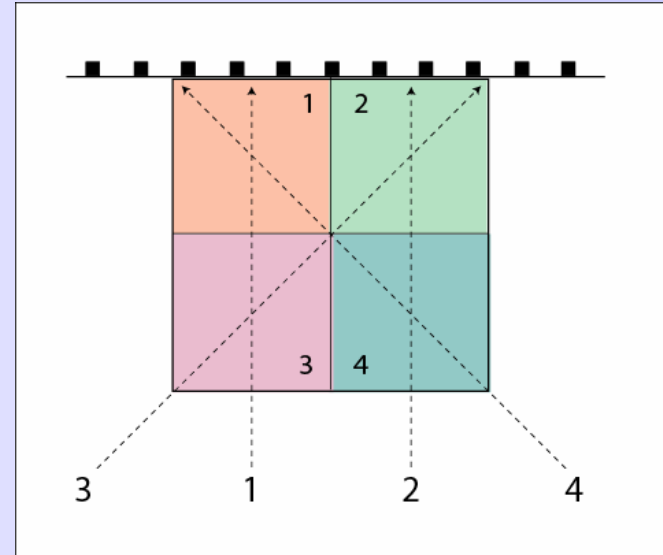
Worked example: tomography

Using rays 1- 4

$$G = \begin{bmatrix} 1 & 0 & 1 & 0 \\ 0 & 1 & 0 & 1 \\ 0 & \sqrt{2} & \sqrt{2} & 0 \\ \sqrt{2} & 0 & 0 & \sqrt{2} \end{bmatrix}$$

$$G^T G = \begin{bmatrix} 3 & 0 & 1 & 2 \\ 0 & 3 & 2 & 1 \\ 1 & 2 & 3 & 0 \\ 2 & 1 & 0 & 3 \end{bmatrix}$$

$$\delta d = G\delta m$$



This has eigenvalues 0, 2, 4, 6.

$$V_p = \begin{bmatrix} 0.5 & -0.5 & -0.5 \\ 0.5 & 0.5 & 0.5 \\ 0.5 & 0.5 & -0.5 \\ 0.5 & -0.5 & 0.5 \end{bmatrix}$$

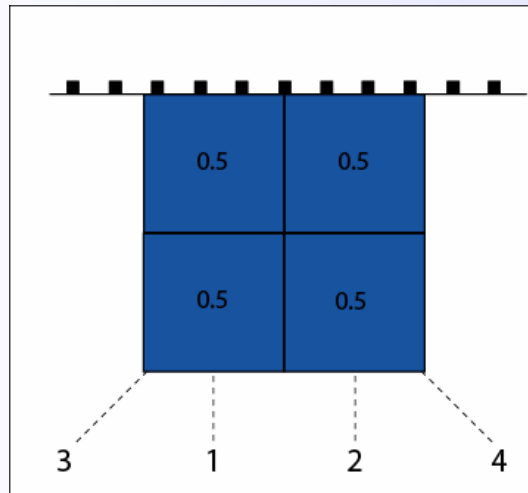
$s_1^2 = 6$ $s_2^2 = 4$ $s_3^2 = 2$

$$V_o = \begin{bmatrix} 0.5 \\ 0.5 \\ -0.5 \\ -0.5 \end{bmatrix} \quad Gv_o = 0$$

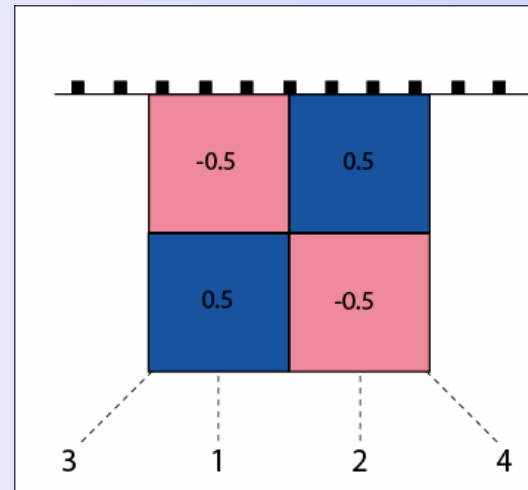
$s_4^2 = 0$

Worked example: Eigenvectors

$$S_1^2=6$$

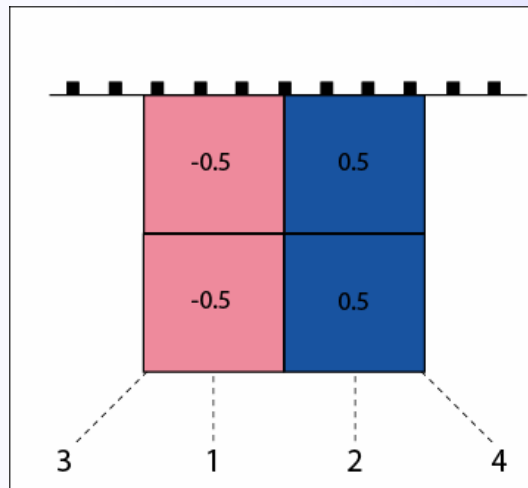


$$S_2^2=4$$



$$V_p = \begin{bmatrix} 0.5 & -0.5 & -0.5 \\ 0.5 & 0.5 & 0.5 \\ 0.5 & 0.5 & -0.5 \\ 0.5 & -0.5 & 0.5 \end{bmatrix}$$

$$S_3^2=2$$



$$V_o = \begin{bmatrix} 0.5 \\ 0.5 \\ -0.5 \\ -0.5 \end{bmatrix}$$

Worked example: tomography

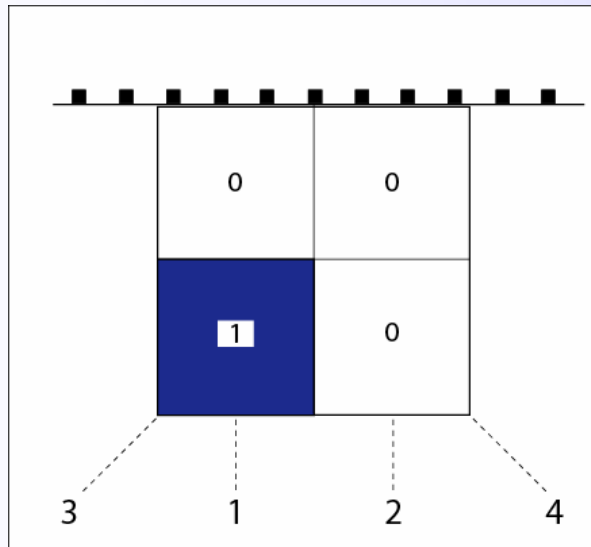
Using all non zero eigenvalues s_1 , s_2 and s_3 the resolution matrix becomes

$$\delta\mathbf{m} = R\delta\mathbf{m}_{true} = V_p V_p^T \delta\mathbf{m}_{true}$$

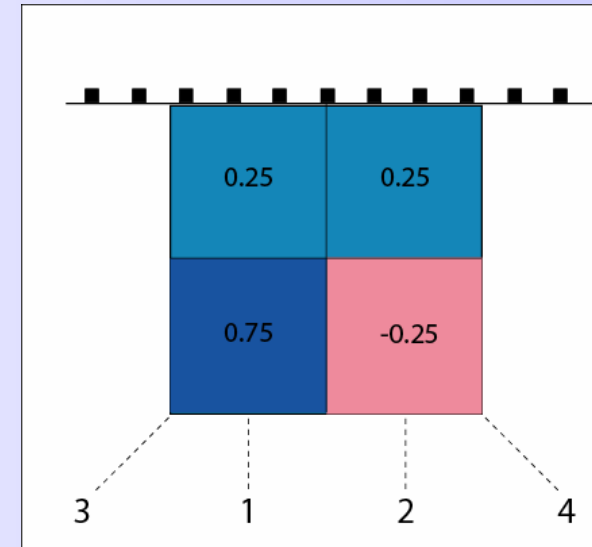
$$R = \begin{bmatrix} 0.75 & -0.25 & 0.25 & 0.25 \\ -0.25 & 0.75 & 0.25 & 0.25 \\ 0.25 & 0.25 & 0.75 & -0.25 \\ 0.25 & 0.25 & -0.25 & 0.75 \end{bmatrix}$$

$$V_p = \begin{bmatrix} 0.5 & -0.5 & -0.5 \\ 0.5 & 0.5 & 0.5 \\ 0.5 & 0.5 & -0.5 \\ 0.5 & -0.5 & 0.5 \end{bmatrix}$$

Input model



Recovered model



Worked example: tomography

Using eigenvalues s_1 , s_2 and s_3 the model covariance becomes

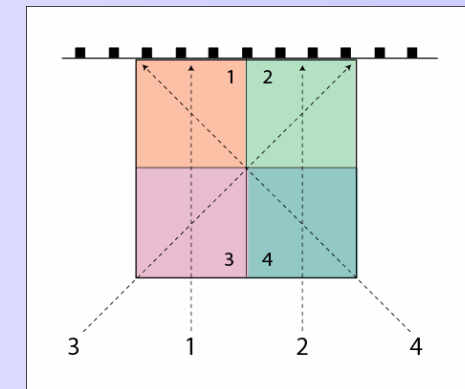
$$\Rightarrow C_M = \sigma^2 \sum_{i=1}^p \frac{\mathbf{v}_i \mathbf{v}_i^T}{s_i^2}$$

$$\mathbf{v}_p = \begin{bmatrix} -0.5 & -0.5 & 0.5 \\ 0.5 & 0.5 & 0.5 \\ -0.5 & 0.5 & 0.5 \\ 0.5 & -0.5 & 0.5 \end{bmatrix}$$

$\uparrow \quad \uparrow \quad \uparrow$
 $s_1^2 = 2 \quad s_2^2 = 4 \quad s_3^2 = 6$

$$C_M = \frac{\sigma^2}{4} \left\{ \frac{1}{2} \begin{pmatrix} 1 & -1 & 1 & -1 \\ -1 & 1 & -1 & 1 \\ 1 & -1 & 1 & -1 \\ -1 & 1 & -1 & 1 \end{pmatrix} + \frac{1}{4} \begin{pmatrix} 1 & -1 & -1 & 1 \\ -1 & 1 & 1 & -1 \\ -1 & -1 & 1 & -1 \\ 1 & -1 & -1 & 1 \end{pmatrix} + \frac{1}{6} \begin{pmatrix} 1 & 1 & 1 & 1 \\ 1 & 1 & 1 & 1 \\ 1 & 1 & 1 & 1 \\ 1 & 1 & 1 & 1 \end{pmatrix} \right\}$$

$$C_M = \frac{\sigma^2}{48} \begin{bmatrix} 11 & -7 & 5 & -1 \\ -7 & 11 & -1 & 5 \\ 5 & -1 & 11 & -7 \\ -1 & 5 & -7 & 11 \end{bmatrix}$$

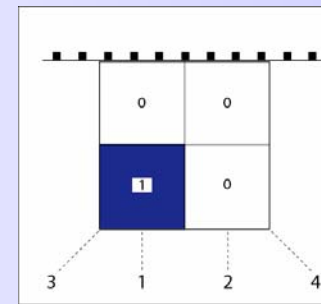


Worked example: tomography

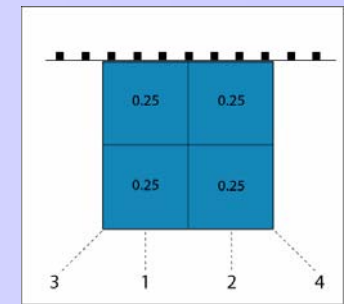
Repeat using only one singular value $s_3 = 6$

Model resolution matrix

$$R = V_p V_p^T = \frac{1}{4} \begin{bmatrix} 1 & 1 & 1 & 1 \\ 1 & 1 & 1 & 1 \\ 1 & 1 & 1 & 1 \\ 1 & 1 & 1 & 1 \end{bmatrix}$$



Input

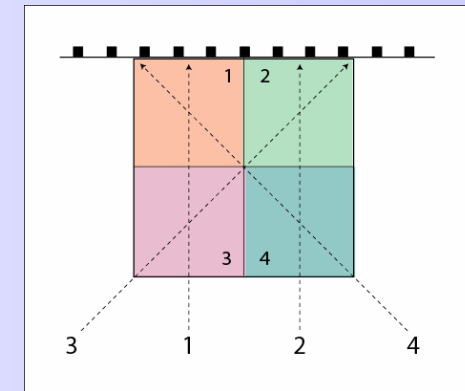


Output

Model covariance matrix

$$C_M = \sigma^2 \sum_{i=1}^p \frac{\mathbf{v}_i \mathbf{v}_i^T}{s_i^2}$$

$$= \frac{\sigma^2}{24} \begin{bmatrix} 1 & 1 & 1 & 1 \\ 1 & 1 & 1 & 1 \\ 1 & 1 & 1 & 1 \\ 1 & 1 & 1 & 1 \end{bmatrix}$$





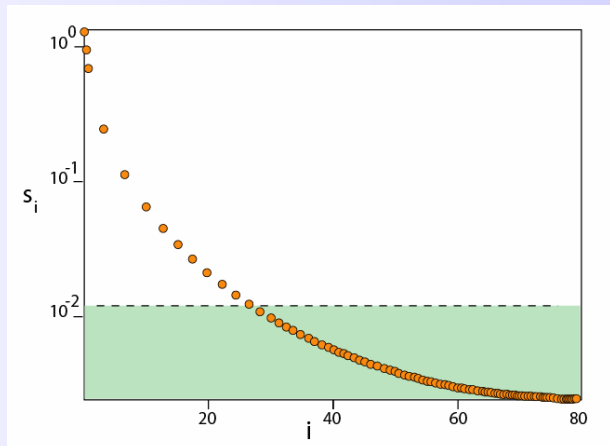
Recap: Singular value decomposition

- There may exist a model null space -> models that can not be constrained by the data.
- There may exist a data null space -> data that can not be fit by any model.
- The general linear discrete inverse problem may be simultaneously under and over determined (mix-determined).
- Singular value decomposition is a framework for dealing with ill-posed problems.
- The Pseudo inverse is constructed using SVD and provides a unique model with desirable properties.
 - Fits the data in a least squares sense
 - Gives a minimum length model (no component in the null space)
- Model Resolution and Covariance can be traded off by choosing the number of eigenvalues to use in reconstruction.

III-posedness = sensitivity to noise

- Look what happens when the eigenvalues are small and positive

Truncated SVD



$$\mathbf{m}^\dagger = V_p S_p^{-1} U_p^T \mathbf{d} = \sum_{i=1}^p \left(\frac{\mathbf{u}_i \cdot \mathbf{d}}{s_i} \right) \mathbf{v}_i$$

Discrete Picard condition

Stability question of Backus and Gilbert

Noise in the data is amplified in the model if $s_i \ll 1$. The eigenvalue spectrum needs to be truncated by reducing p .

TSVD: Choose the smallest p such
that data fit is acceptable

$$\|G\mathbf{m} - \mathbf{d}\|_2 \leq \delta$$

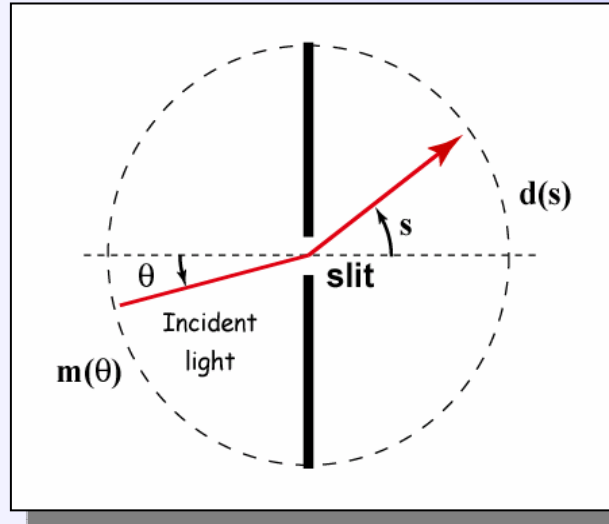
- As N or M increase the computational cost increases significantly !

(See example 4.3 of Aster et al., 2005)

SVD Example: The Shaw problem

$m(\theta)$ = intensity of light incident on a slit at angle θ $-\frac{\pi}{2} \leq m(\theta) \leq \frac{\pi}{2}$

$d(s)$ = measurements of diffracted light intensity at angle s $-\frac{\pi}{2} \leq s \leq \frac{\pi}{2}$



Shaw Problem
Given $d(s)$ find $m(s)$?

$$d(s) = \int_{-\pi/2}^{\pi/2} (\cos(s) + \cos(\theta))^2 \left(\frac{\sin(\pi(\sin(s) + \sin(\theta)))}{\pi(\sin(s) + \sin(\theta))} \right)^2 m(\theta) d\theta$$

Is this a continuous or discrete inverse problem ?

Is this a linear or nonlinear inverse problem ?

SVD Example: The Shaw problem

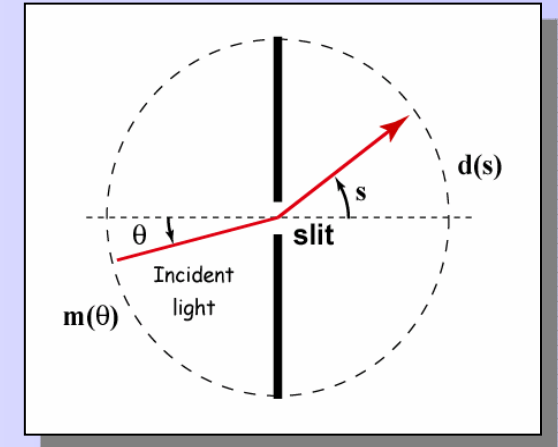
Let's discretize the inverse problem

Data $d(s)$ and model $m(\theta)$ at N equal angles

$$s_i = \theta_i = \frac{(i - 0.5)\pi}{n} - \frac{\pi}{2}, \quad (i = 1, 2, \dots, n)$$

$$d_i = d(s_i) \quad (i = 1, \dots, n)$$

$$m_j = m(\theta_j) \quad (j = 1, \dots, n)$$



This gives a system of $N \times N$ linear equations

$$\mathbf{d} = \mathbf{G}\mathbf{m}$$

where

$$G_{i,j} = \Delta s (\cos(s_i) + \cos(\theta_j))^2 \left(\frac{\sin(\pi(\sin(s_i) + \sin(\theta_j))))}{\pi(\sin(s_i) + \sin(\theta_j))} \right)^2$$

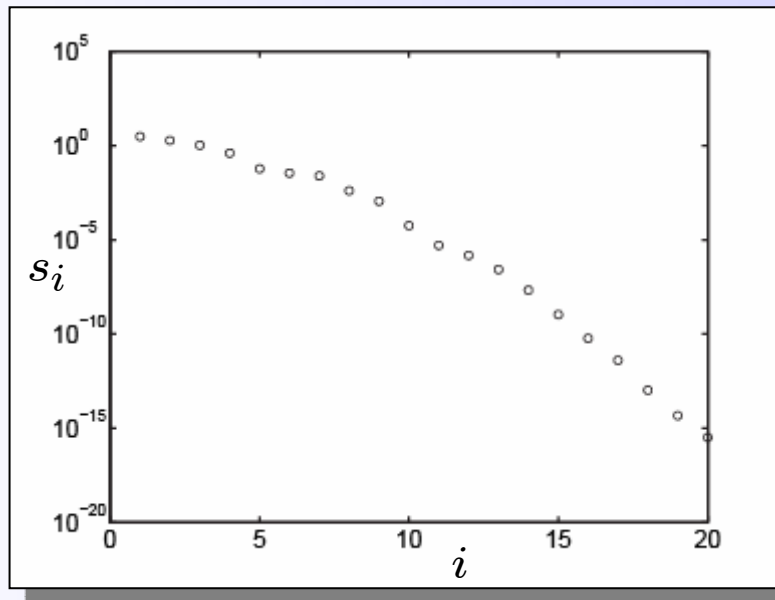
$$\Delta s = \frac{\pi}{n}$$

See MATLAB routine `shaw'

Example: Ill-posedness

- Ill-posedness means solution sensitivity to noise

$$\mathbf{m}^\dagger = V_p S_p^{-1} U_p^T \mathbf{d} = \sum_{i=1}^p \left(\frac{\mathbf{u}_i \cdot \mathbf{d}}{s_i} \right) \mathbf{v}_i$$



$$\mathbf{d} = G\mathbf{m}$$

20 data, 20 unknowns

$$N = M = 20$$

Eigenvalue spectrum for Shaw problem

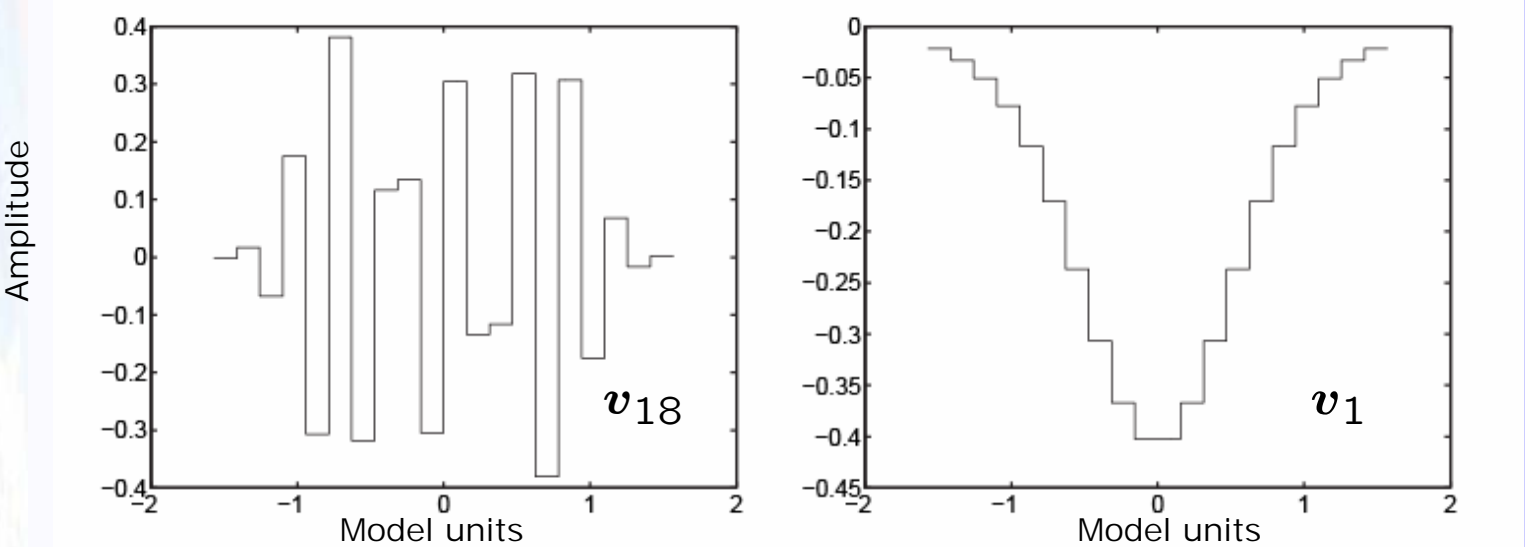
Condition number is the ratio of largest to smallest singular value = 10^{14}

Large condition number means severe ill-posedness

Example: Ill-posedness

Eigenvectors for different singular values: Shaw problem

$$\mathbf{m}^\dagger = V_p S_p^{-1} U_p^T \mathbf{d} = \sum_{i=1}^p \left(\frac{\mathbf{u}_i \cdot \mathbf{d}}{s_i} \right) \mathbf{v}_i$$



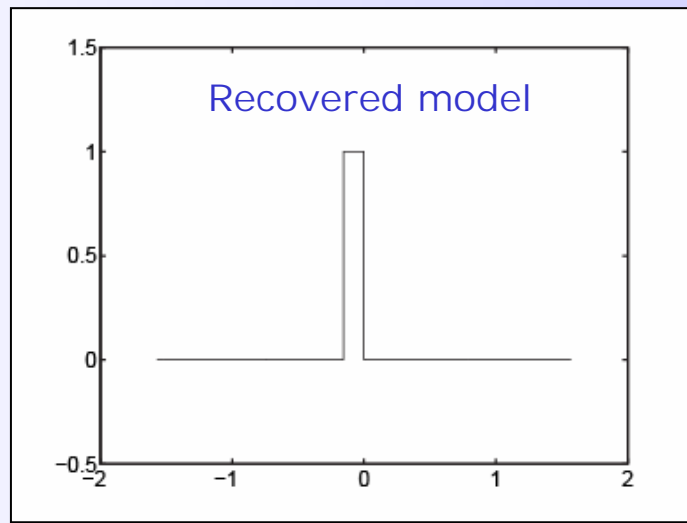
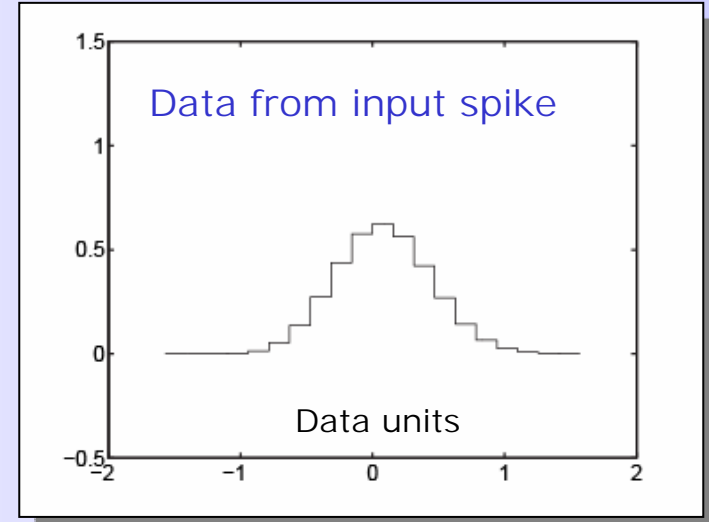
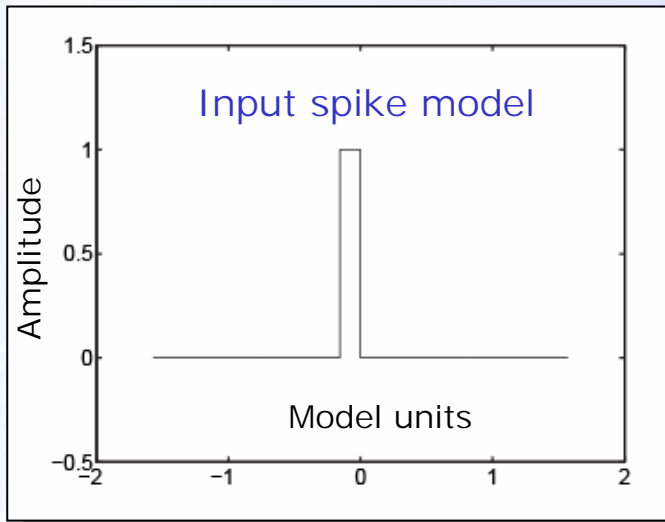
Eigenvector for smallest non-zero
singular value

Eigenvector for largest singular value

Test inversion without noise

$$\mathbf{d} = G\mathbf{m}$$

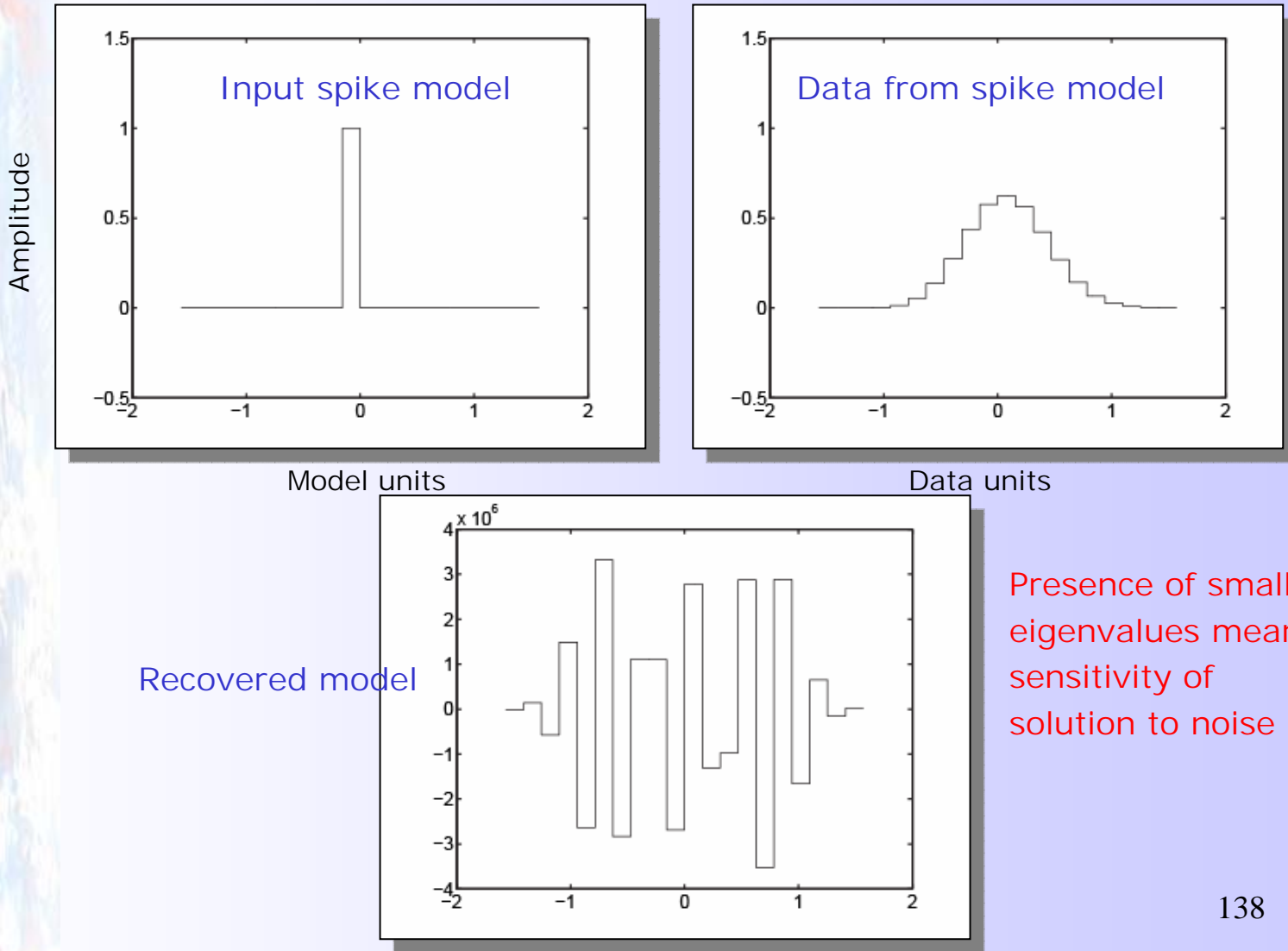
$$\mathbf{m}^\dagger = V_p S_p^{-1} U_p^T \mathbf{d} = \sum_{i=1}^p \left(\frac{\mathbf{u}_i \cdot \mathbf{d}}{s_i} \right) \mathbf{v}_i$$



Test inversion with noise

$$\mathbf{d} = G\mathbf{m}$$

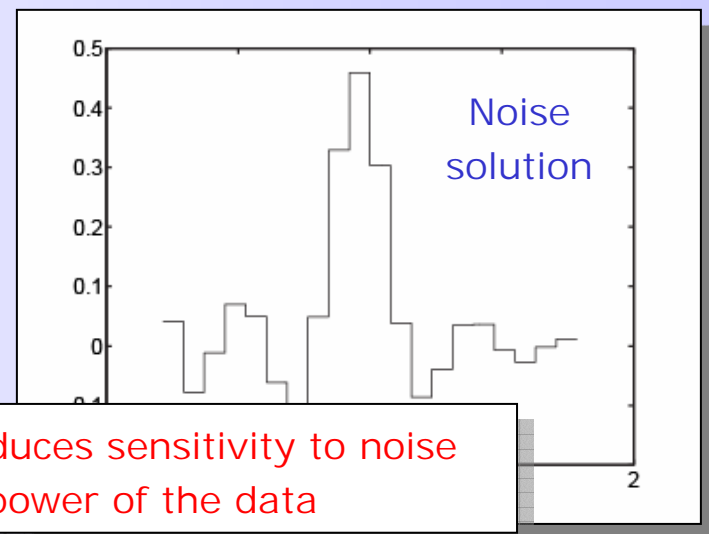
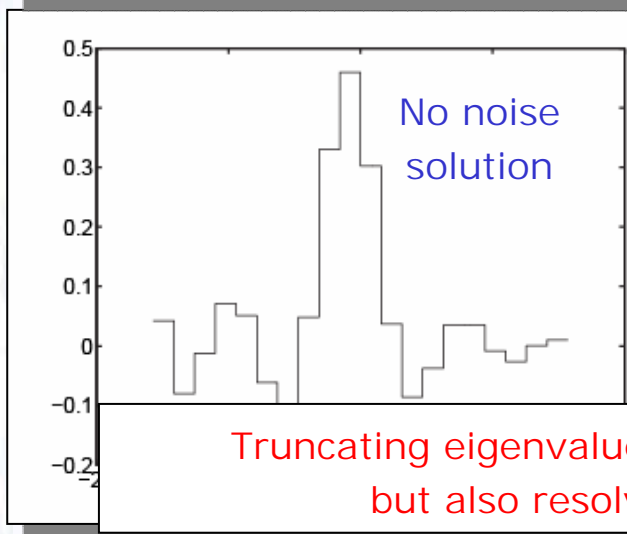
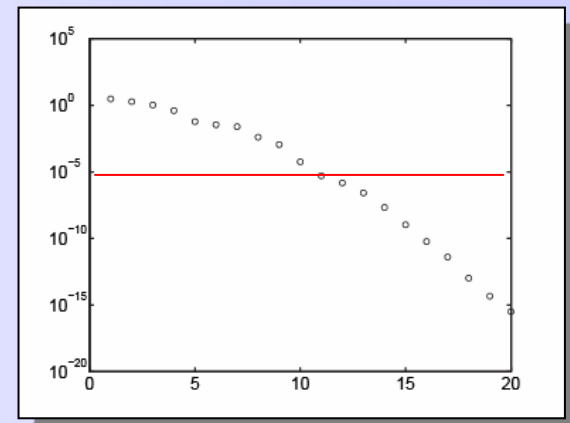
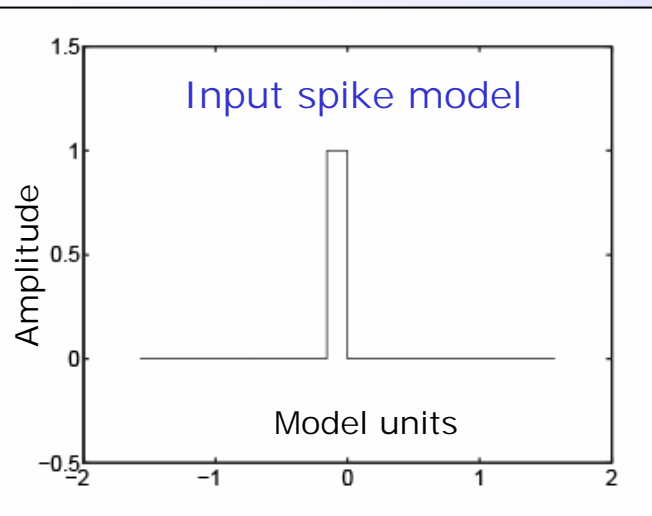
$$\mathbf{m}^\dagger = V_p S_p^{-1} U_p^T \mathbf{d} = \sum_{i=1}^p \left(\frac{\mathbf{u}_i \cdot \mathbf{d}}{s_i} \right) \mathbf{v}_i$$



Shaw problem with $p=10$

$$\mathbf{d} = G\mathbf{m}$$

$$\mathbf{m}^\dagger = V_p S_p^{-1} U_p^T \mathbf{d} = \sum_{i=1}^p \left(\frac{\mathbf{u}_i \cdot \mathbf{d}}{s_i} \right) \mathbf{v}_i$$

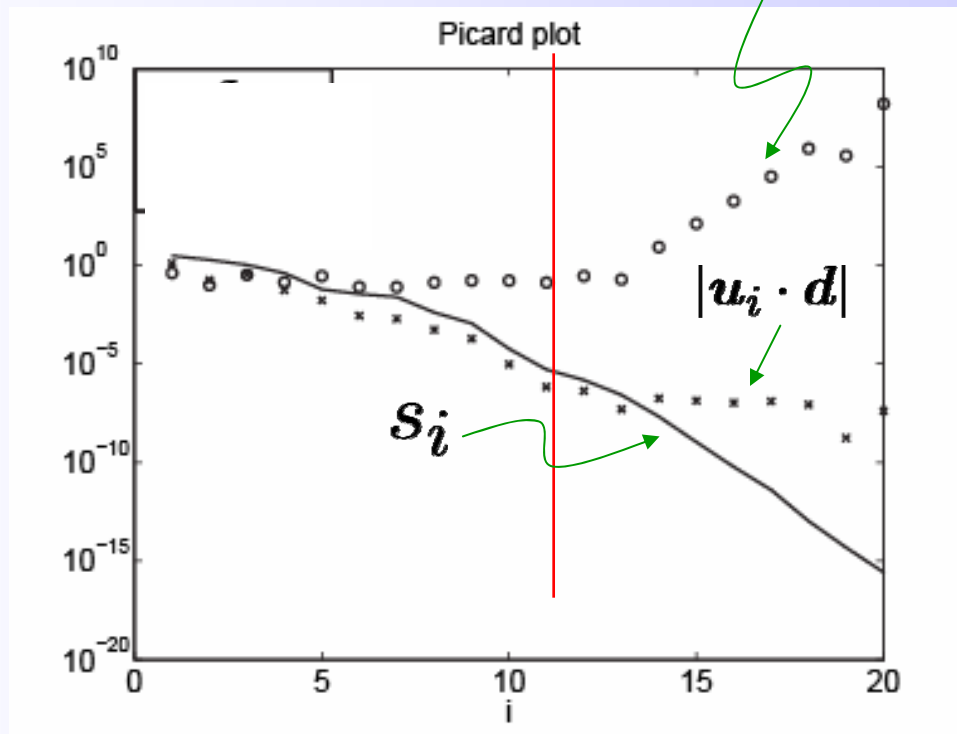


Truncating eigenvalues reduces sensitivity to noise
but also resolving power of the data

Shaw problem Picard plot

A guide to choosing the SVD truncation level p (=number of eigenvalues)

$$\mathbf{m}^\dagger = V_p S_p^{-1} U_p^T \mathbf{d} = \sum_{i=1}^p \left(\frac{\mathbf{u}_i \cdot \mathbf{d}}{s_i} \right) \mathbf{v}_i$$



The eigenvalue from the truncation level in SVD



Regularizing inverse problems

Damping and smoothing and choosing...

Regularization

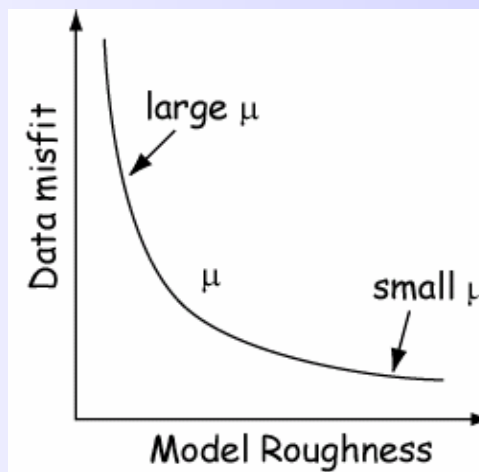
The idea behind SVD is to limit the degree of freedom in the model and fit the data to an acceptable level. Retain only those **features** necessary to fit the data.

A general framework for solving non-unique inverse problems is to introduce regularization. Regularization makes a **non-unique** problem become a **unique** problem. How does it do this ?

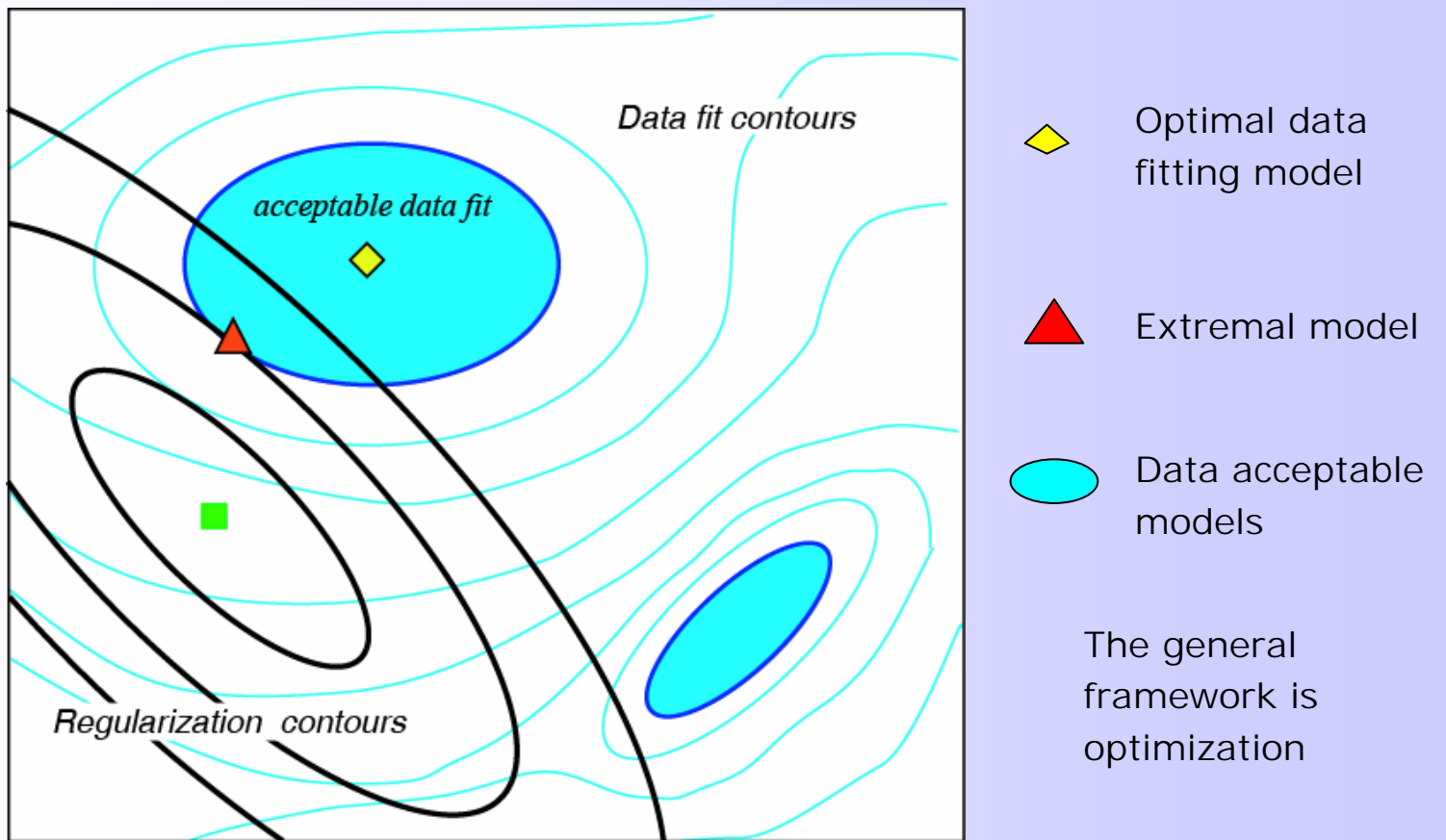
We want to minimize a combination of data misfit and some property of the model that measures extravagant behaviour, e.g.

$$\phi(\mathbf{m}) = (\mathbf{d} - \mathbf{g}(\mathbf{m}))^T C_d^{-1} (\mathbf{d} - \mathbf{g}(\mathbf{m})) + \mu (\mathbf{m} - \mathbf{m}_o)^T C_m^{-1} (\mathbf{m} - \mathbf{m}_o)$$

Inverse problem → nonlinear optimization problem



Solutions to inverse problems



$$\phi(\mathbf{m}) = (\mathbf{d} - \mathbf{g}(\mathbf{m}))^T \mathbf{C}_d^{-1} (\mathbf{d} - \mathbf{g}(\mathbf{m})) + \mu (\mathbf{m} - \mathbf{m}_o)^T \mathbf{C}_M^{-1} (\mathbf{m} - \mathbf{m}_o)$$



Damped least squares

We seek the model that minimizes

$$\phi(\mathbf{d}, \mathbf{m}) = (\mathbf{d} - G\mathbf{m})^T C_d^{-1} (\mathbf{d} - G\mathbf{m}) + \mu(\mathbf{m} - \mathbf{m}_o)^T C_M^{-1} (\mathbf{m} - \mathbf{m}_o)$$

After some algebra we get

$$\mathbf{m}_{DLS} = (G^T C_D^{-1} G + \mu C_M^{-1})^{-1} (G^T C_D^{-1} \mathbf{d} + \mu C_M^{-1} \mathbf{m}_o)$$

This is the **damped least squares** solution. A special case is to minimise a weighted sum of the data misfit and the model norm.

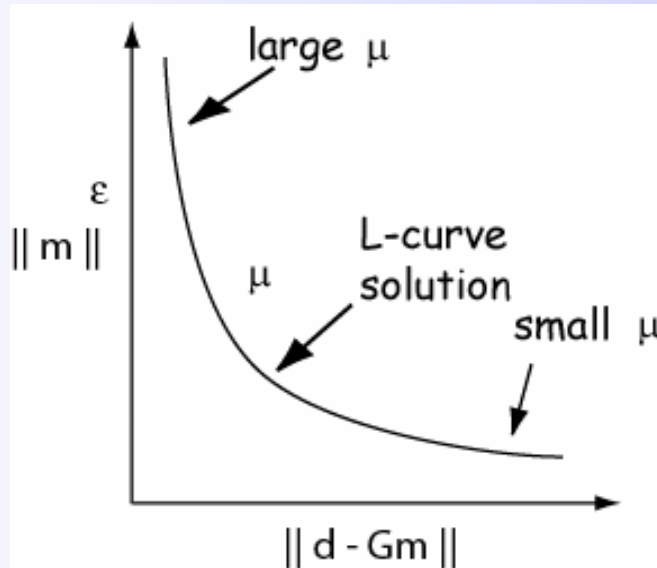
$$\min \quad \|(\mathbf{d} - G\mathbf{m})\|_2^2 + \mu \|\mathbf{m}\|_2^2$$

Normal equations become

$$(G^T G + \mu I) \mathbf{m} = G^T \mathbf{d}$$

this system of linear equations will have a unique solution which is called the **Tikhonov** solution

L-curve solution



Choose μ that is nearest the elbow of the curve

With this value of μ we can construct a particular Tikhonov solution

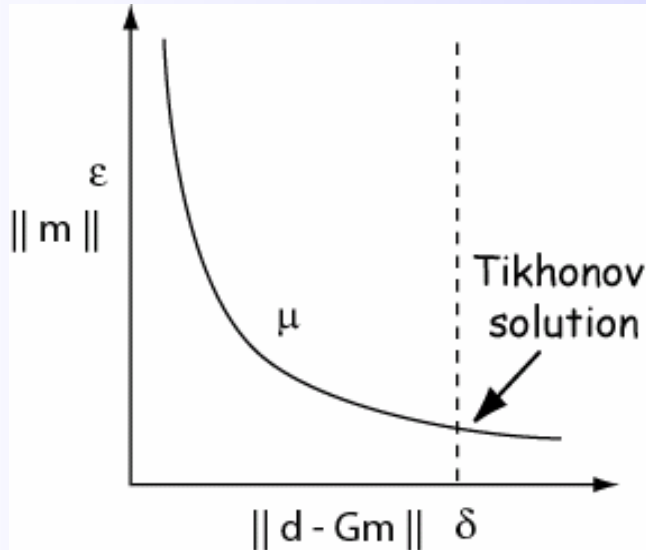
$$(G^T G + \mu I) \mathbf{m} = G^T \mathbf{d}$$

Perform repeat solutions of the normal equations for different μ and select the one which lies near the elbow of the trade-off curve

Elbow is estimated visually -> potentially subjective if elbow is not clear

See example 5.1 of Aster et al. (2005)

Tikhonov regularization



Choose μ that minimizes the length of the model while specifying a maximum value of the prediction

$$\min \|\mathbf{m}\|_2^2 \text{ s.t. } \|\mathbf{d} - \mathbf{Gm}\|_2^2 < \delta$$

Choice of μ depends on knowing the errors in the data

Discrepancy principle gives us a value of δ

Since each solution δ corresponds to a particular μ , we often refer to the Tikhonov solution as a function of μ on the curve

$$\min \|\mathbf{d} - \mathbf{Gm}\|_2^2 + \mu \|\mathbf{m}\|_2^2$$

$$(\mathbf{G}^T \mathbf{G} + \mu \mathbf{I}) \mathbf{m} = \mathbf{G}^T \mathbf{d}$$

See example 5.1 of Aster et al. (2005)

Tikhonov: Discrepancy principle

Discrepancy principle gives us a value of δ and consequently a value for μ

If the N data have Gaussian errors with known variance $N(0, \sigma^2)$ then we would expect that on average that each residual $(d_i - G_{i,j} m_j)$ would be approximately σ . Hence we have

$$\|d - Gm\|^2 = N\sigma^2$$

c.f. $\chi_N^2(50\%)$

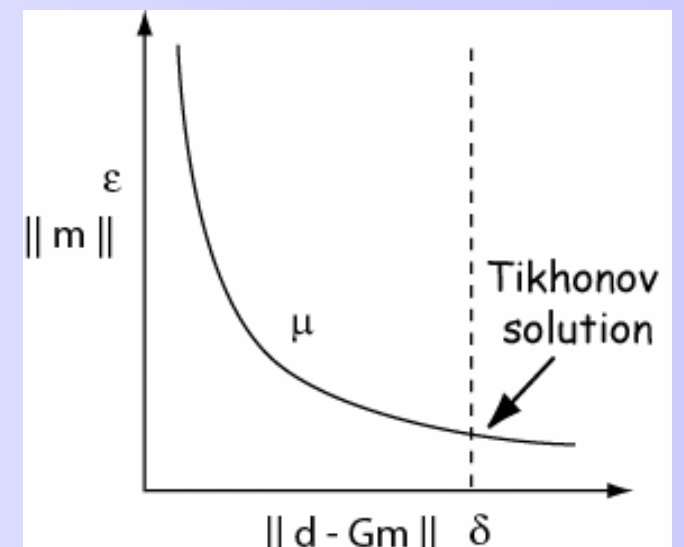
$$\Rightarrow \delta = \sigma\sqrt{N}$$

We get an expected value of the norm of the prediction error from the number of data and the standard deviation of the data

$$(G^T G + \mu I)m = G^T d$$

Perform repeated solutions until

$$\|d - Gm\| = \delta$$



Tikhonov Example: The Shaw problem

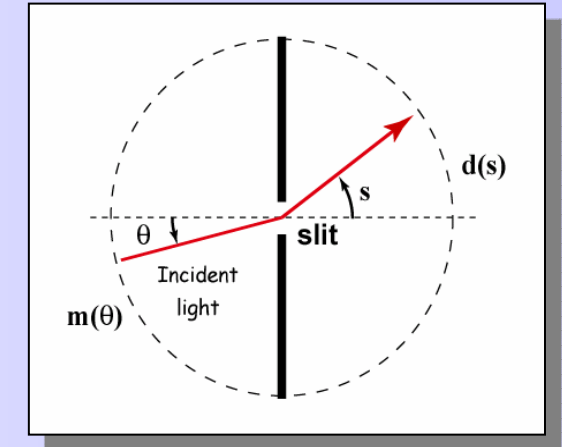
Recall the discretized Shaw problem

Data $d(s)$ and model $m(\theta)$ at N equal angles

$$s_i = \theta_i = \frac{(i - 0.5)\pi}{n} - \frac{\pi}{2}, \quad (i = 1, 2, \dots, n)$$

$$d_i = d(s_i) \quad (i = 1, \dots, n)$$

$$m_j = m(\theta_j) \quad (j = 1, \dots, n)$$



This gives a system of $N \times N$ linear equations

$$\mathbf{d} = G\mathbf{m}$$

where

$$G_{i,j} = \Delta s (\cos(s_i) + \cos(\theta_j))^2 \left(\frac{\sin(\pi(\sin(s_i) + \sin(\theta_j))))}{\pi(\sin(s_i) + \sin(\theta_j))} \right)^2$$

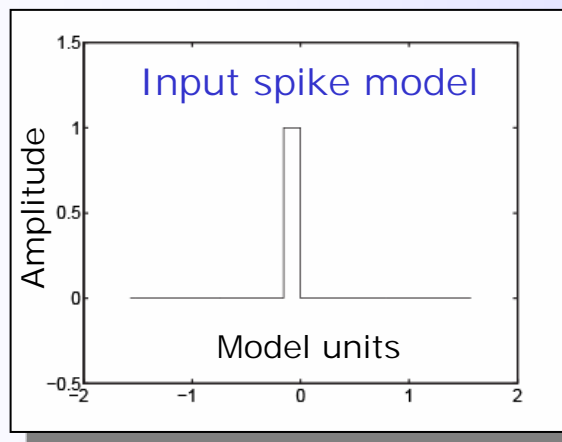
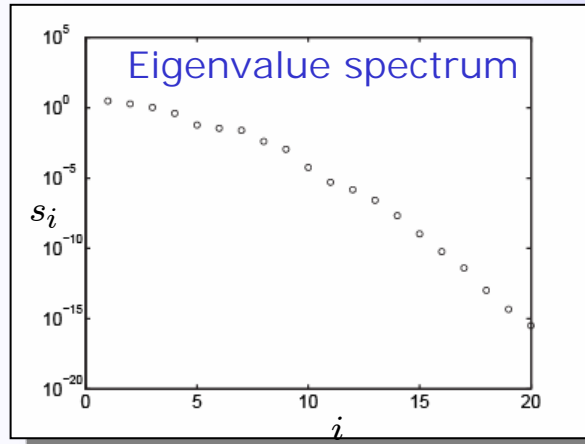
$$\Delta s = \frac{\pi}{n}$$

We know this problem was ill-posed and previously solved with truncated SVD.

Example: Shaw problem with Tikhonov regularization

Let's revisit the Shaw problem

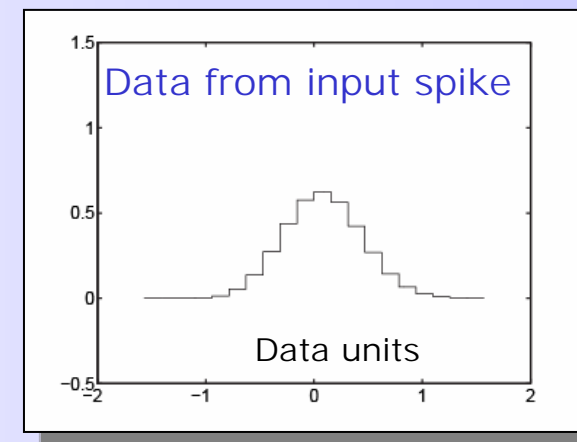
$$\mathbf{d} = \mathbf{G}\mathbf{m} \quad N = M = 20$$



An severely ill-posed inverse problem where \mathbf{G} has a condition number = 10^{14}

Extreme sensitivity to noise

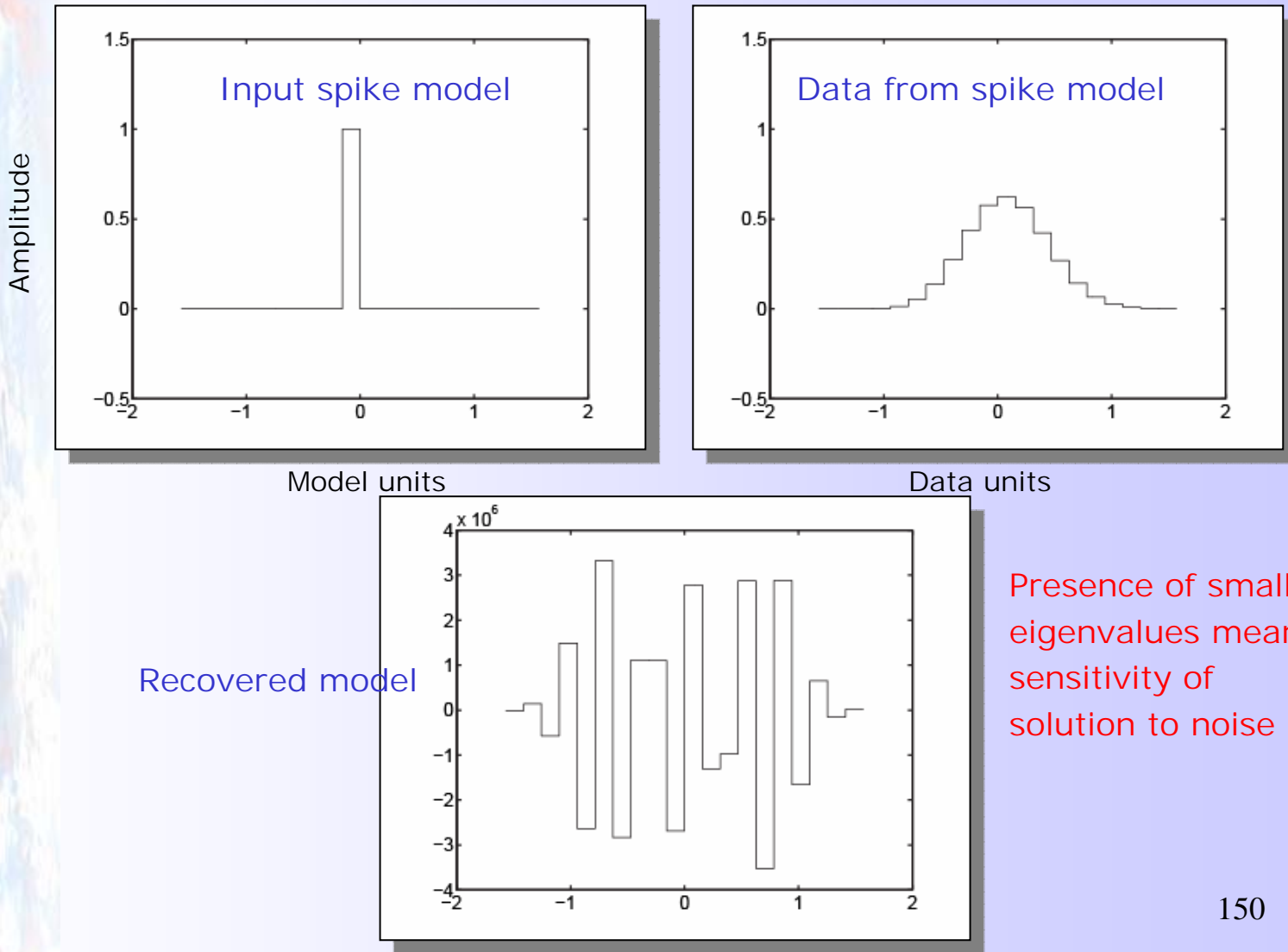
Resolution is sacrificed to achieve stability



Recall SVD applied to this problem (with noise)

$$\mathbf{d} = G\mathbf{m}$$

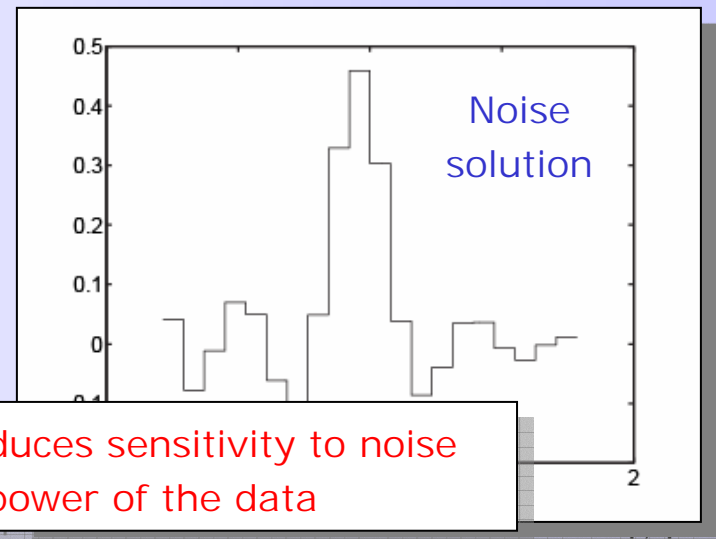
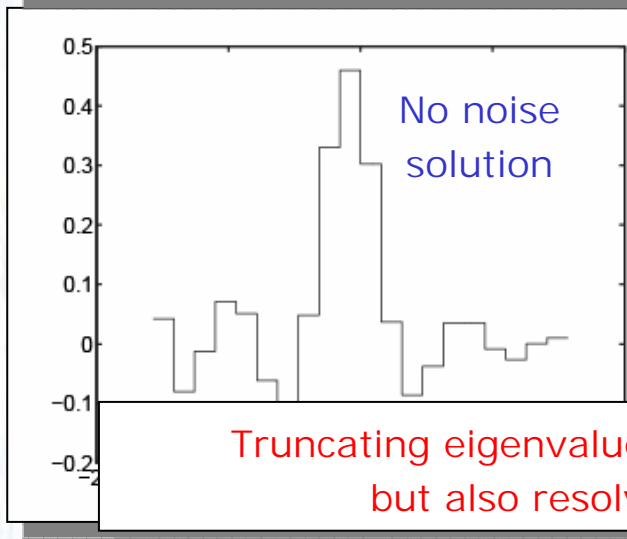
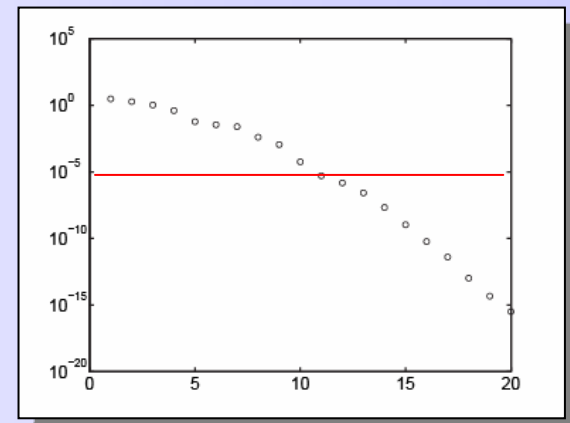
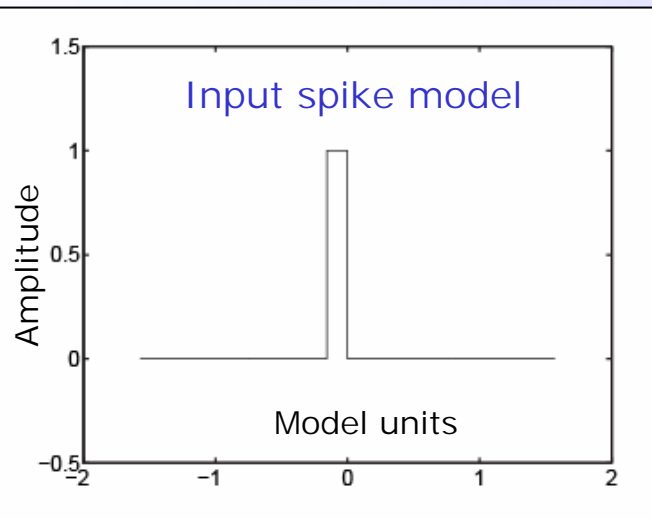
$$\mathbf{m}^\dagger = V_p S_p^{-1} U_p^T \mathbf{d} = \sum_{i=1}^p \left(\frac{\mathbf{u}_i \cdot \mathbf{d}}{s_i} \right) \mathbf{v}_i$$



SVD: Shaw problem with p=10

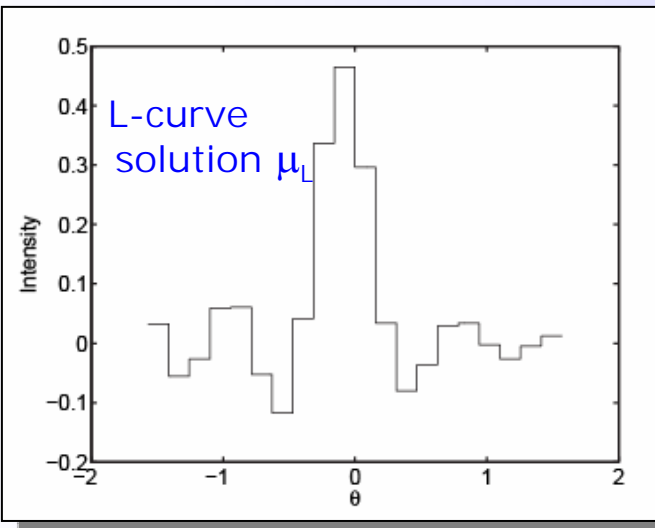
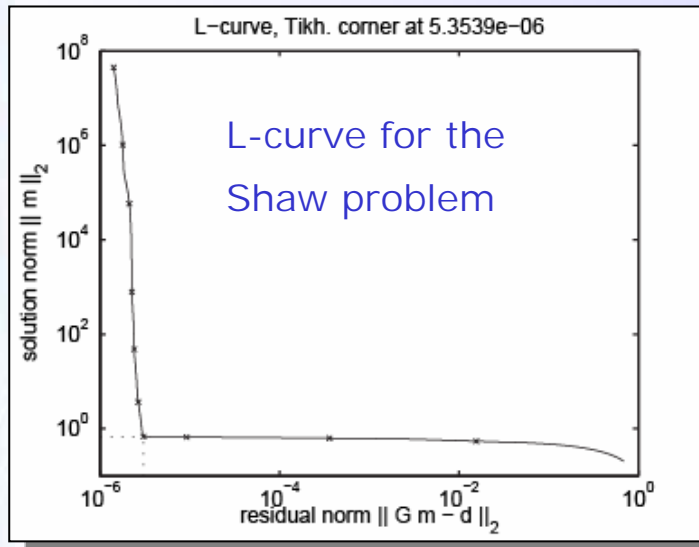
$$\mathbf{d} = G\mathbf{m}$$

$$\mathbf{m}^\dagger = V_p S_p^{-1} U_p^T \mathbf{d} = \sum_{i=1}^p \left(\frac{\mathbf{u}_i \cdot \mathbf{d}}{s_i} \right) \mathbf{v}_i$$

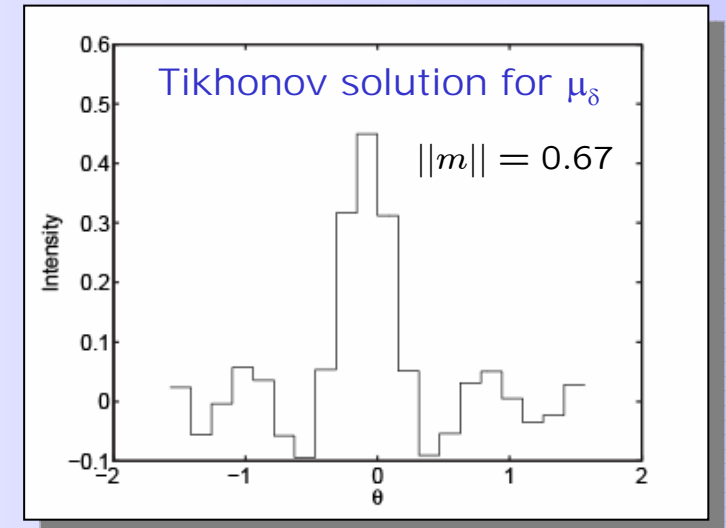


Tikhonov regularization: Shaw problem

$$(G^T G + \mu I) \mathbf{m} = G^T \mathbf{d}$$

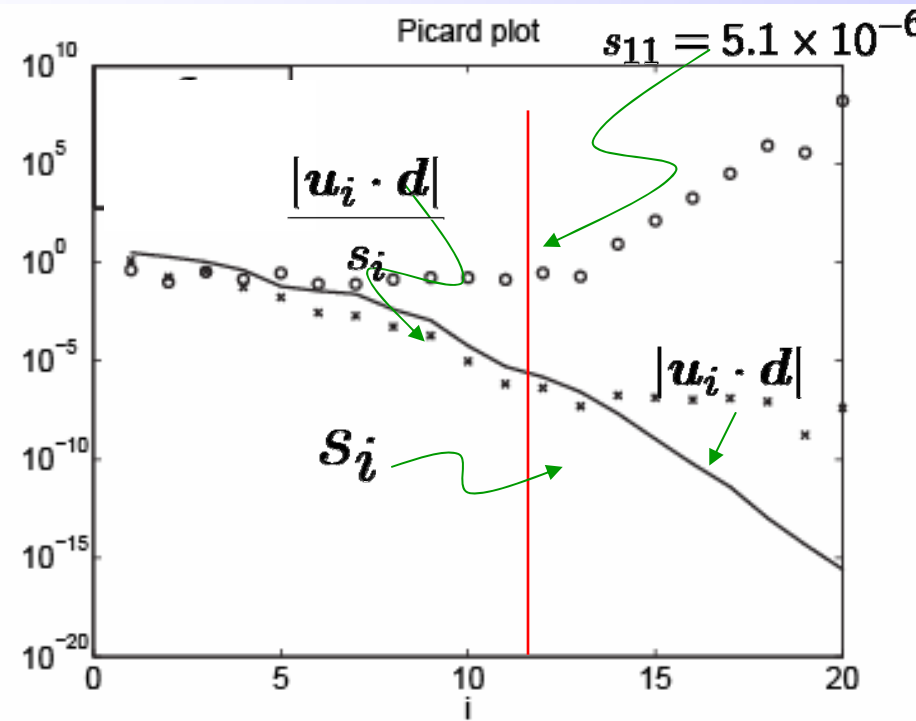


Fortunately a nice clear elbow is visible in this log-log plot, Trade off parameter μ is easily picked. $N[0, (10^{-6})^2]$

$$\sqrt{\mu_L} = 5.35 \times 10^{-6}$$
$$\delta = 20 \times 10^{-12} = 4.47 \times 10^{-6}$$
$$\sqrt{\mu_\delta} = 4.29 \times 10^{-6}$$


Example: Tikhonov regularization

How do these choices for μ relate to the SVD truncation level chosen earlier ?



$$\sqrt{\mu_L} = 5.35 \times 10^{-6}$$

$$\delta = \sigma \sqrt{N}$$

$$\delta = \sqrt{20} \times 10^{-12}$$

$$\sqrt{\mu_\delta} = 4.29 \times 10^{-6}$$

$$\mathbf{m}^\dagger = \sum_{i=1}^p \left(\frac{\mathbf{u}_i \cdot \mathbf{d}}{s_i} \right) \mathbf{v}_i$$

The eigenvalue from the truncation level in SVD is similar to the two choices of $\sqrt{\mu}$ in the Tikhonov scheme.

$$\mathbf{m}^\dagger = V_p S_p^{-1} U_p^T \mathbf{d} = \sum_{i=1}^p \left(\frac{\mathbf{u}_i \cdot \mathbf{d}}{s_i} \right) \mathbf{v}_i$$

$$(G^T G + \mu I) \mathbf{m} = G^T \mathbf{d}$$

SVD and Tikhonov regularization

Tikhonov solution

$$G = U_p S_p V_p^T$$

$$\mathbf{m} = (G^T G + \mu I)^{-1} G^T \mathbf{d}$$

It can be shown... that this can be written as

Page 91-93 of
Aster et al (2005)

Look ! 

$$\mathbf{m} = \sum_{i=1}^M \frac{s_i^2}{s_i^2 + \mu} \left(\frac{\mathbf{u}_i \cdot \mathbf{d}}{s_i} \right) \mathbf{v}_i$$

$$\mathbf{m}^\dagger = \sum_{i=1}^p \left(\frac{\mathbf{u}_i \cdot \mathbf{d}}{s_i} \right) \mathbf{v}_i$$

SVD

Now we get very different behaviour

Let

$$f_i = \frac{s_i^2}{s_i^2 + \mu} \quad \text{Filter factors}$$

As singular values $s_i \rightarrow 0$ the solution is not highly sensitive to noise

Because $f_i \rightarrow 0$ rather than ∞ .

If $s_i \gg \sqrt{\mu}$ then $f_i \rightarrow 1$

If $s_i \ll \sqrt{\mu}$ then $f_i \rightarrow 0$

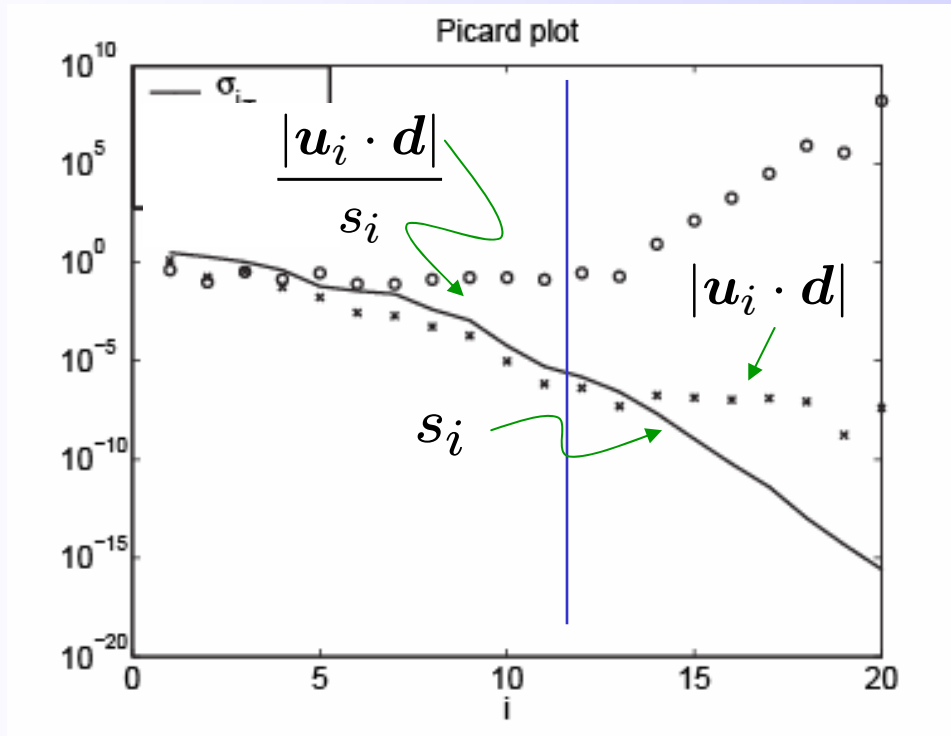
SVD

$$\begin{aligned} s_i > s_p & \quad f_i = 1 \\ s_i < s_p & \quad f_i = 0 \end{aligned}$$

μ filters out (damps) the unstable influence of the small eigenvalues

Filter factors

Filter factors control influence of singular values



Filter factors

$$f_i = \frac{s_i^2}{s_i^2 + \mu}$$

$$\mathbf{m} = \sum_{i=1}^M f_i \left(\frac{|u_i \cdot d|}{s_i} \right) \mathbf{v}_i$$

c.f. $f_i = 1$

As singular values $s_i \rightarrow 0$ the solution is not highly sensitive to noise

Because $f_i \rightarrow 0$ rather than ∞ .

If $s_i \gg \mu$ then $f_i \rightarrow 1$

If $s_i \ll \mu$ then $f_i \rightarrow 0$

μ filters out (damps) the unstable influence of the small eigenvalues

Model resolution for a Tikhonov solution

A Tikhonov solution has the form

$$\mathbf{m} = (G^T G + \mu I)^{-1} G^T \mathbf{d} = G^{-g} \mathbf{d}$$

Model resolution matrix

$$R_M = G^{-g} G = V F V^T$$

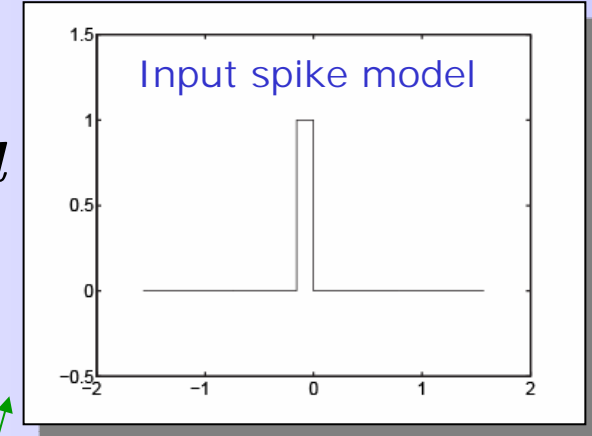
F is the $M \times M$ diagonal matrix of filter factors

$$\mathbf{m}_{est} = R_M \mathbf{m}_{true}$$

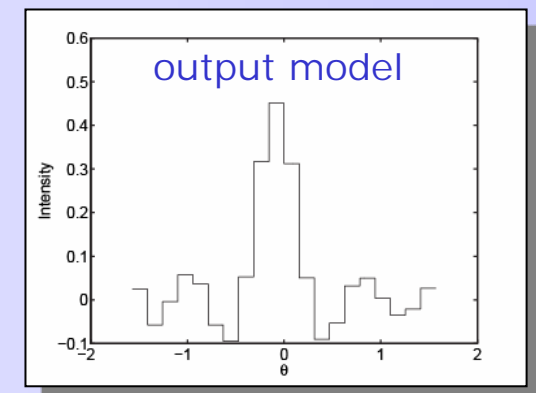
Each row of the resolution matrix can also be found using a spike test !

This is the row which corresponds to the parameter in the spike model.

Resolution tells us how the estimated model is a linear combination of the true model.



$$\mathbf{m} = (G^T G + \mu I)^{-1} G^T \mathbf{d}$$
$$\mathbf{m} = \sum_{i=1}^M \frac{s_i^2}{s_i^2 + \mu} \left(\frac{\mathbf{u}_i \cdot \mathbf{d}}{s_i} \right) \mathbf{v}_i$$



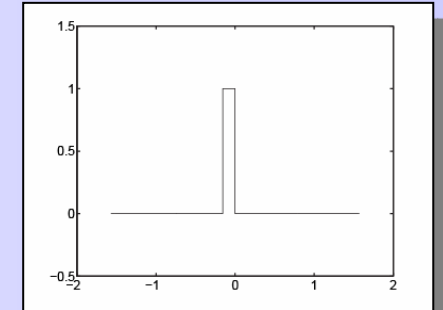
Relationship to true solution

Model covariance a Tikhonov solution

A Tikhonov solution has the form

$$\mathbf{m} = (G^T G + \mu I)^{-1} G^T \mathbf{d} = G^{-g} \mathbf{d}$$

Input spike model



$$\sqrt{\mu_\delta} = 4.29 \times 10^{-6}$$

Model covariance matrix

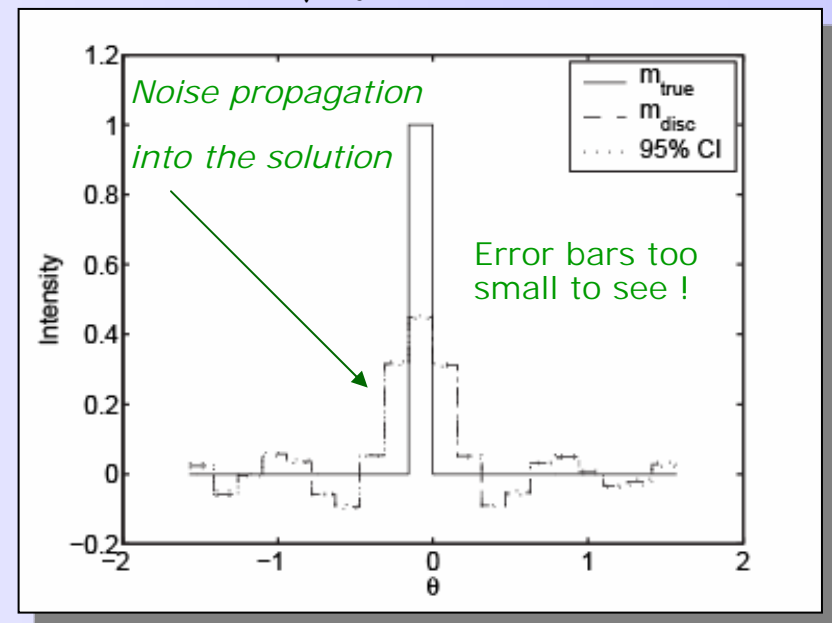
$$C_M = G^{-g} C_D^{-1} (G^{-g})^T$$

Confidence intervals calculated from the diagonal of the covariance matrix give unrealistically small errors

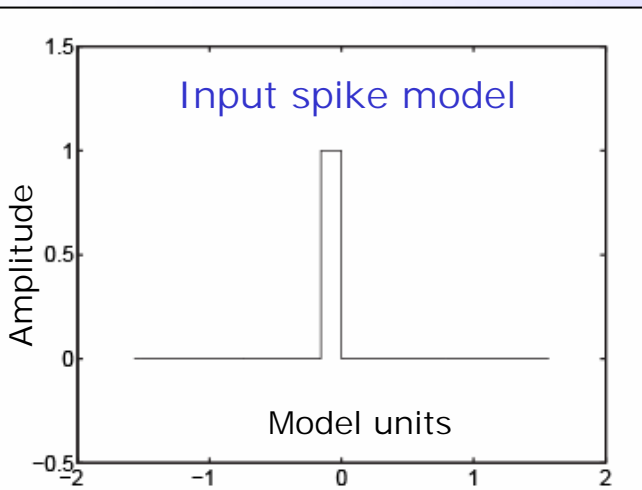
As regularization strength **increases** the size of confidence interval **decreases**

Confidence limits do not represent distance to the true solution

-> Regularized solutions are **ALWAYS BIASED !**



Effect of data noise on regularized solutions



Tikhonov

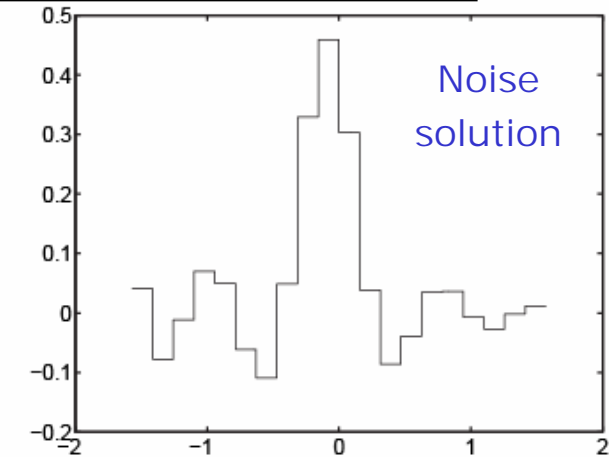
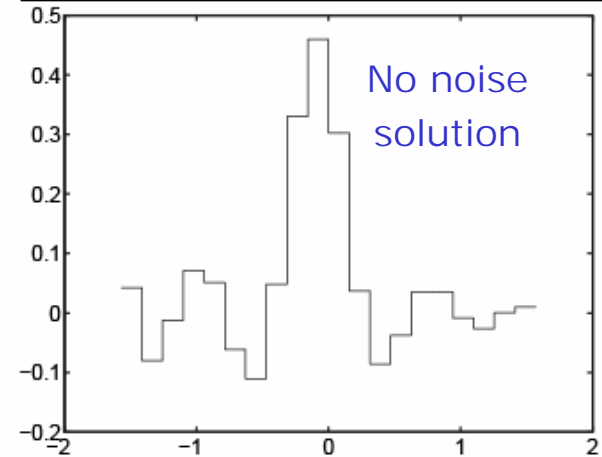
$$\mathbf{m} = (G^T G + \mu I)^{-1} G^T \mathbf{d}$$

$$\mathbf{m} = \sum_{i=1}^M \frac{s_i^2}{s_i^2 + \mu} \left(\frac{\mathbf{u}_i \cdot \mathbf{d}}{s_i} \right) \mathbf{v}_i$$

TSVD

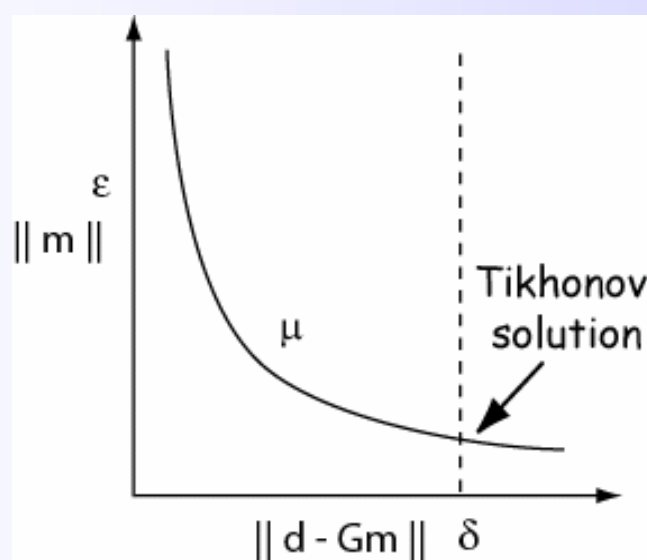
$$\mathbf{m} = \sum_{i=1}^p \left(\frac{\mathbf{u}_i \cdot \mathbf{d}}{s_i} \right) \mathbf{v}_i$$

Because regularized solutions are ALWAYS BIASED !



Choosing μ with Generalized cross validation

As we have seen the choice of trade-off parameter μ determines the level of fit to the data possible with a Tikhonov solution and vice versa



$$\delta = \sigma\sqrt{N}$$

What if I really don't have a good idea of how well I should fit my data ?

How can I choose δ or μ ?
Can I still get a robust solution ? Is all lost ?

(L-curve is one answer)

All is not lost. There is usually information in the variability of data itself about the likely level of fit needed.

We can use the data itself to estimate the regularization parameter !

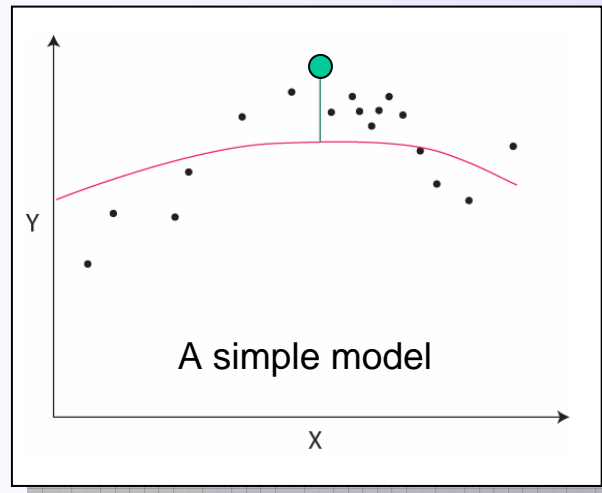
This approach is called Cross Validation.

Choosing μ by cross validation

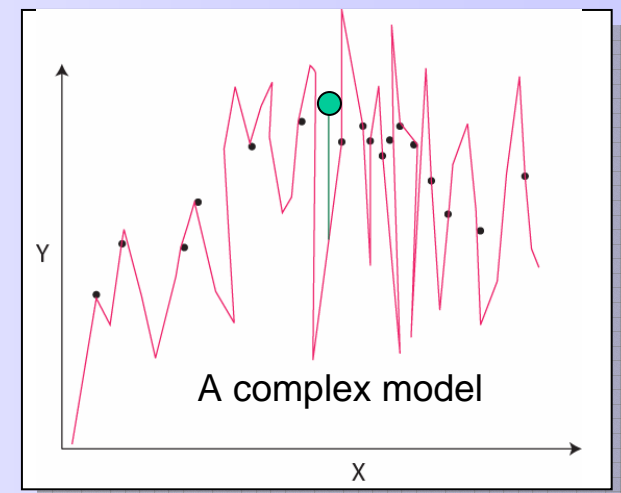
Cross validation is a way of assessing the **quality** of a solution based on the principle of measuring the fit to **missing data**

The Leave one out principle

Lets fit a curve (red) with one data point (green) left out



Large hyper-parameter μ_1



Small hyper-parameter μ_1

In both cases (on average) the missing data tend to be fit poorly !



Choosing μ with Cross validation

What does cross validation mean ?

For N data and a chosen value for μ ,

- Drop one data value, d_k and use your *favourite* algorithm to fit the remainder, d_i ($i=1..k-1, k+1..N$)

$$\mathbf{m}_k(\mu) = (G_k^T G_k + \mu I)^{-1} G_k^T \mathbf{d} = G_k^{-g} \mathbf{d}$$

- Compare prediction of recovered model with missing datum

$$r_k(\mu) = d_k - G \mathbf{m}_k(\mu)$$

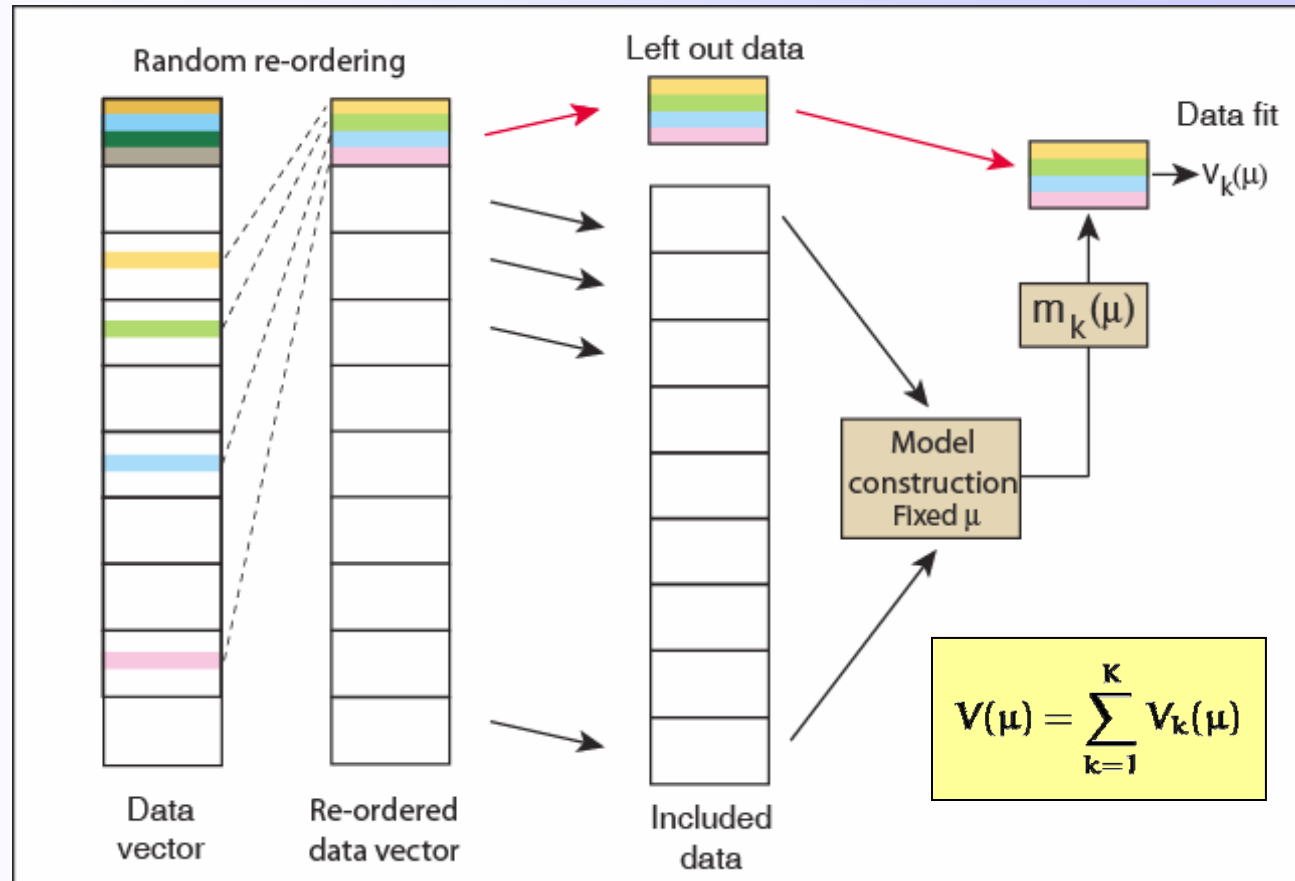
- Repeat for each datum ($k=1,\dots,N$) and sum the squares of the residuals to produce a fitness for μ

$$V(\mu) = \sum_{k=1}^N r_k^2$$

- Find the μ that minimizes of $V(\mu)$

Leave some out

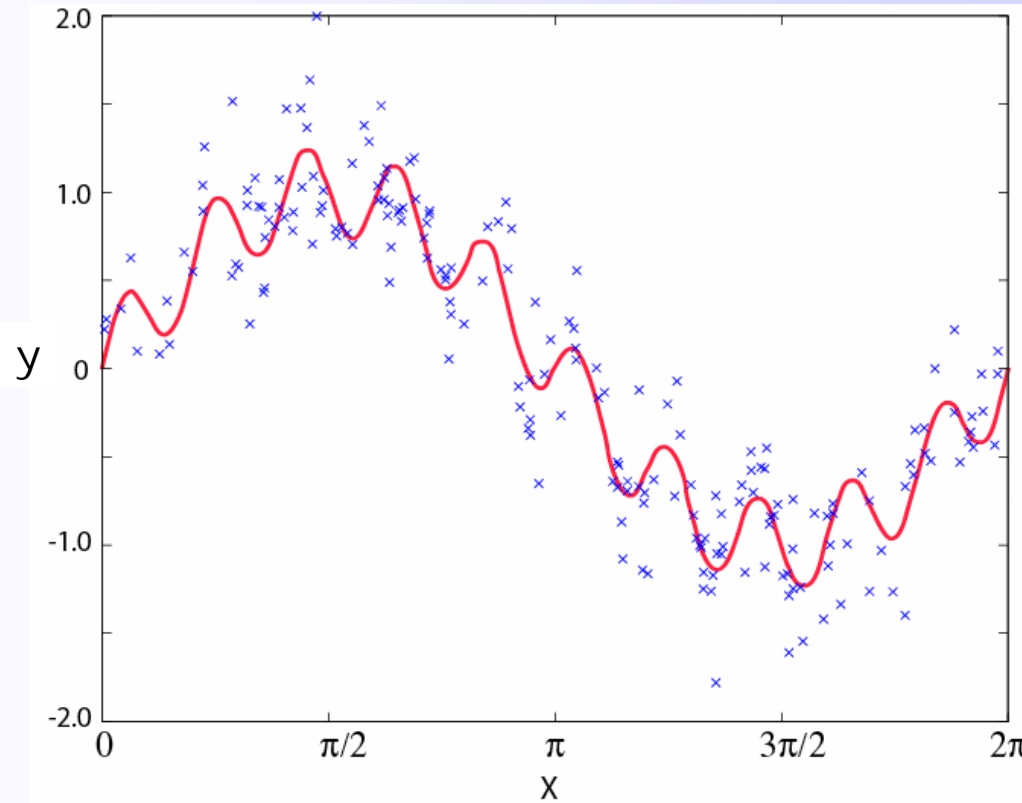
A general framework: *K-fold cross validation*



$V(\mu)$ is the cross validation measure for μ

Example: GCV in Curve fitting

Problem: Find the curve that generated this noisy data.



Data are the y_i values
for known x_i ($i=1,\dots,N$)
and each has
Gaussian random noise
 $N[0,0.25]$

What would you guess
is the solution ?

$$y = \sin x + 0.3 \sin \frac{x}{10}$$



Example: Curve fitting

Let $s(x, \mathbf{m})$ represent the **continuous** solution curve as a function of x , and let its shape be determined by some parameters \mathbf{m} .

Lets first choose to fit the data with the smoothest possible curve

i.e. minimize

$$\psi(\mathbf{d}, \mathbf{m}) = \sum_{i=1}^N (d_i - s(x_i, \mathbf{m}))^2$$

and also

$$J(s) = \int \left(\frac{\partial^2 s}{\partial x^2} \right)^2 dx$$

Duchon (1976) showed that its possible to fit the data d_i **exactly** and obtain a unique curve with minimum $J(s)$ using thin plate splines.

$$s(x, \mathbf{m}) = p(x) + \sum_{i=1}^N m_i \phi(x - x_i)$$

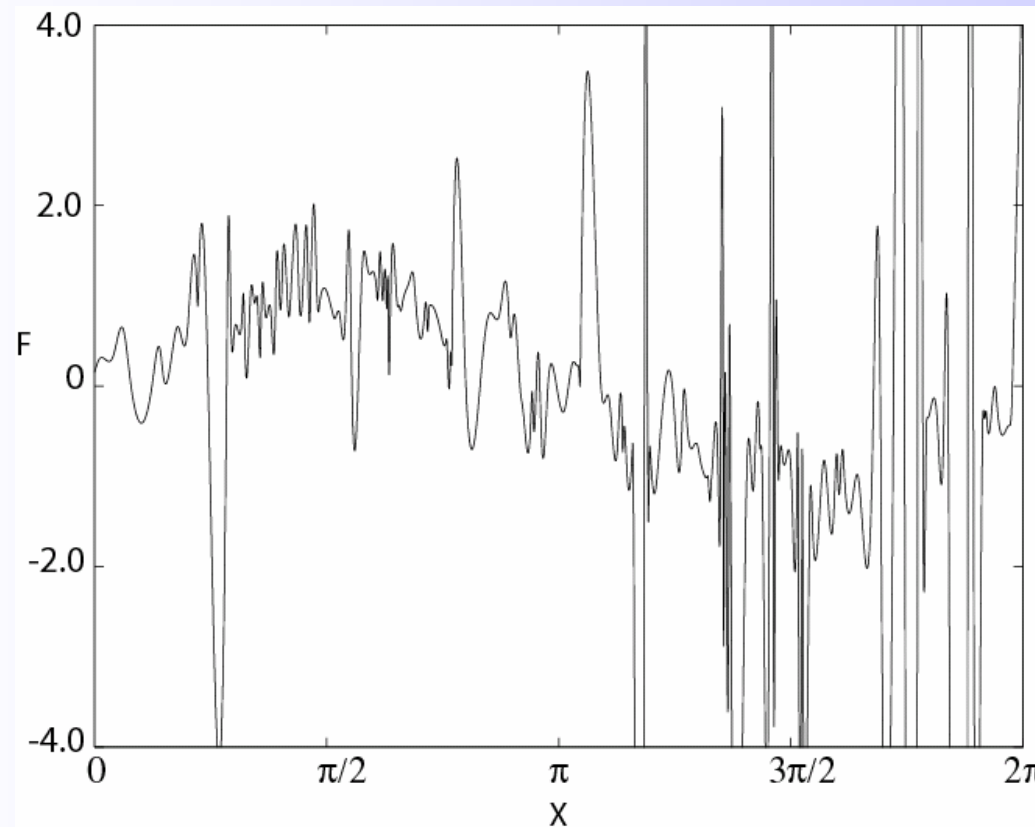
where $p(x)$ is a polynomial in x

$\phi(x - x_i)$ is a **Thin plate spline** basis function

The parameters m_i can be solved for using matrix inversion

The smoothest thin plate spline

The parameters \mathbf{m} in thin plate spline solution are given by the solution of a set of linear equations



Does this extremal solution look smooth ?

What has gone wrong ?

Answer:
Data is over fit



Choosing the trade-off parameter with GCV

We should not try to fit noisy data exactly but only to an acceptable level. To relax data fit we want to minimize

$$\phi(\mathbf{d}, \mathbf{m}) = \sum_{i=1}^N (d_i - s(x_i, \mathbf{m}))^2 + \mu J(s)$$

How to choose the trade off parameter μ ?

Answer: there are many ways.

If we do not know what an acceptable fit to the data is we can use **Generalized Cross Validation**. In this approach we use the data to find a value for μ

$$V(\mu) = \sum_{i=1}^N (d_i - s_i(x_i, \mathbf{m}))^2 \quad \text{Leave each datum out in turn and compute the solution}$$

$s_i(x_i, \mathbf{m})$ = thin plate spline interpolant with i-th datum missing

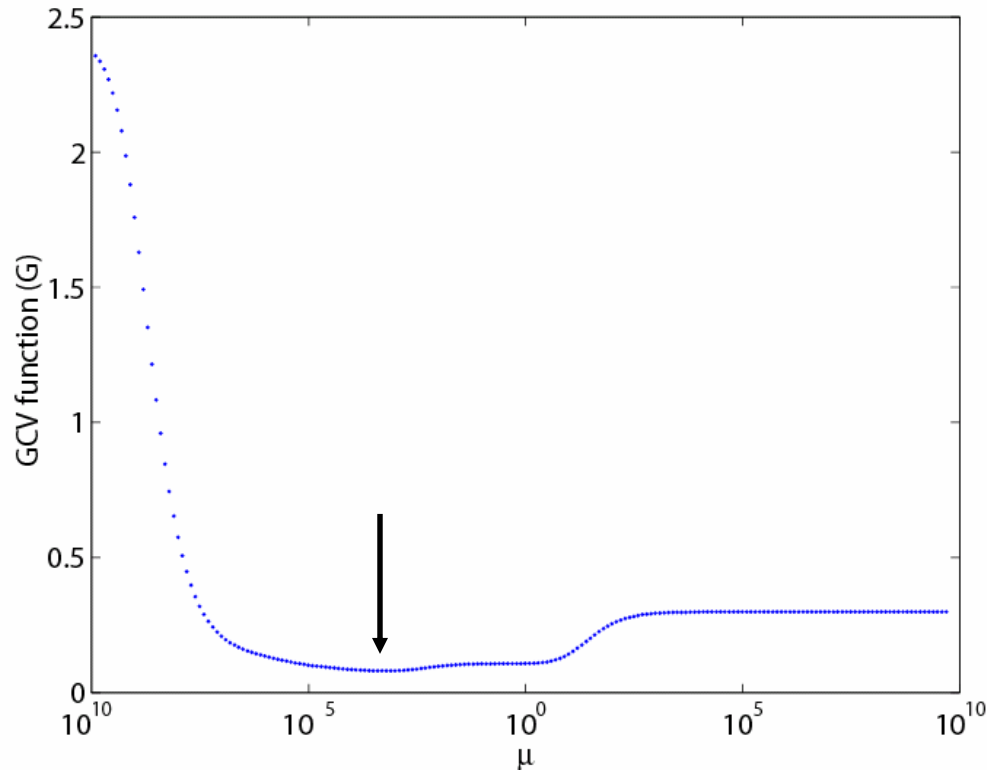
Look how $V(\mu)$ behaves as a function of μ

$\mu \rightarrow \infty \Rightarrow V(\mu) \uparrow$ The solution is very smooth

$\mu \rightarrow 0 \Rightarrow V(\mu) \uparrow$ The solution is very rough

Example: Curve fitting with GCV.

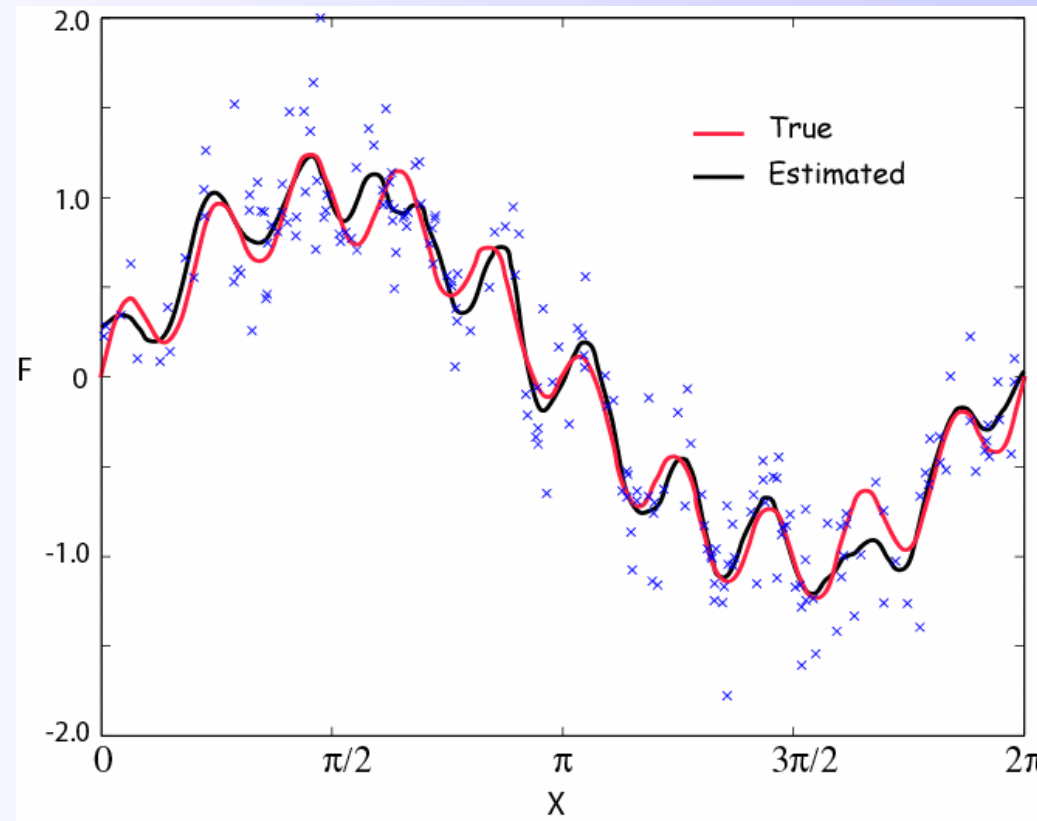
We find μ that minimizes $V(\mu)$ by repeated solutions of the TPS problem



We get a unique minimum in $V(\mu)$!

Example: Curve fitting with CV.

The TPS solution that corresponds to the minimum of μ



This is achieved **without** knowing in advance what a suitable acceptable data fit was. The GCV is in effect a way of estimating the error in the data and using it in model fitting.

Regularization by GCV in general

For a **general linear inverse problem** with the k-th datum left out a solution is obtained by minimizing

$$\phi_k(\mathbf{d}, \mathbf{m}) = \sum_{i \neq k}^N ((G\mathbf{m})_i - d_i)^2 + \mu \mathbf{m}^T L^T L \mathbf{m}$$

If $\mathbf{m}_k(\mu)$ is the solution model for given μ with k-th datum missing

$$\mathbf{m}_k(\mu) = (G_k^T G_k + \mu L^T L)^{-1} G_k^T \mathbf{d}_k = G_k^{-g} \mathbf{d}_k$$

then the cross validation function is the prediction error for all N solutions.

$$V(\mu) = \frac{1}{N} \sum_{k=1}^N (G_k \mathbf{m}_k - d_k)^2$$

We find μ that minimized $V(\mu)$. Evaluation of V for any μ would appear to require N solutions to the inverse problem...but its possible to show that

$$V(\mu) \approx N \frac{(\mathbf{d} - G\mathbf{m}(\mu))^T (\mathbf{d} - G\mathbf{m}(\mu))}{Tr(\mathbf{I} - GG_\mu^{-g})^2}$$

*See Aster et al.
(p108, 2005)*

Which requires only a single optimization solution to evaluate for any μ

Generalized cross validation

Note that calculation of a single value of the cross validation function $V(1_1)$ requires N-repeat inversion solutions. Where we choose N. This might become expensive.

Craven & Wahba (1979) devised *Generalized cross validation*, which removes the need to perform many repeat inversions. Hence its much more efficient and gives the same answer.

Minimize $\phi_k(\mathbf{d}, \mathbf{m}) = \sum_{i \neq k}^N ((G\mathbf{m})_i - d_i)^2 + \mu \mathbf{m}^T L^T L \mathbf{m}$

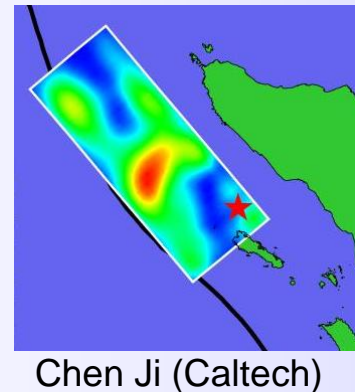
CV function $V(\mu) = \frac{1}{N} \sum_{k=1}^N (G_k \mathbf{m}_k - d_k)^2$ N solutions
for each μ

GCV function $V(\mu) \approx N \frac{(\mathbf{d} - G\mathbf{m}(\mu))^T (\mathbf{d} - G\mathbf{m}(\mu))}{Tr(\mathbf{I} - GG_\mu^{-g})^2}$ 1 solution
for each μ

Example: Cross validation in Finite Fault Slip inversions

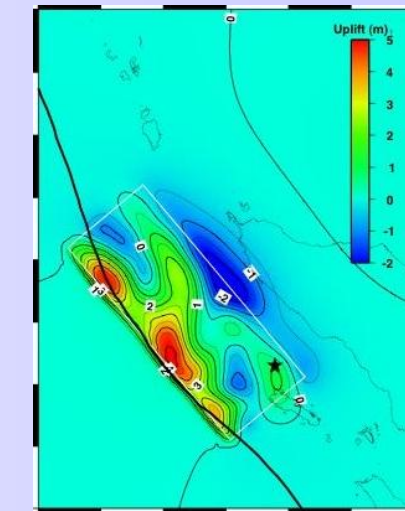
Fault slip model

2004 Sumatra-Andaman
earthquake



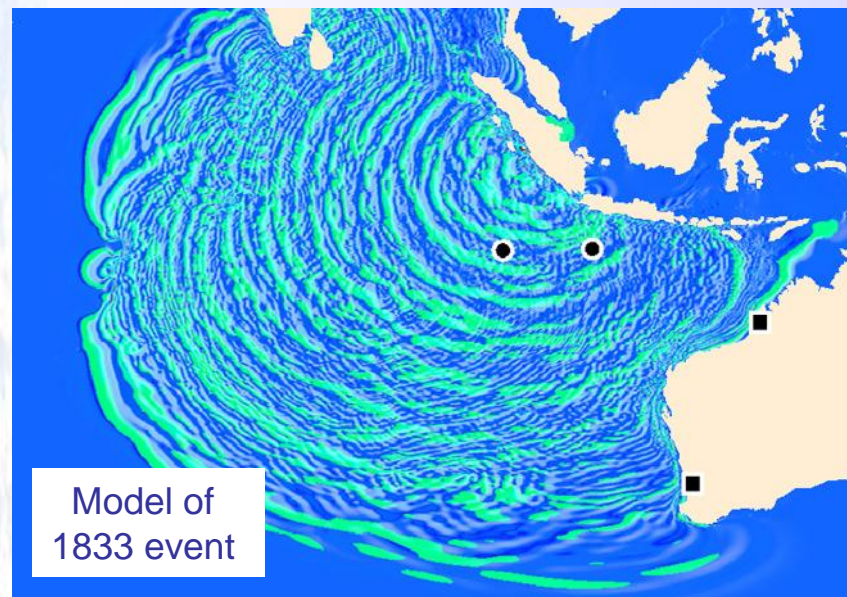
Chen Ji (Caltech)

Vertical Sea floor movement

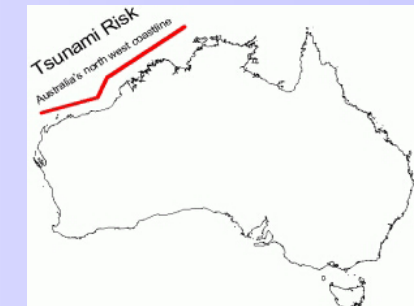


Australian Tsunami
Warning System

Model of
1833 event

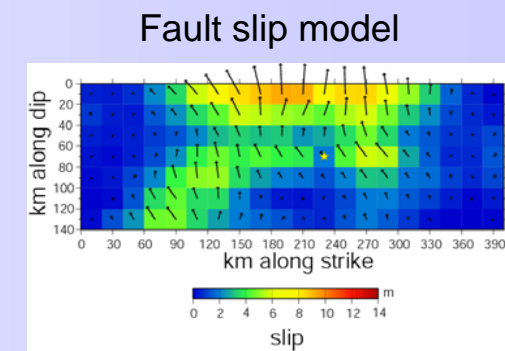
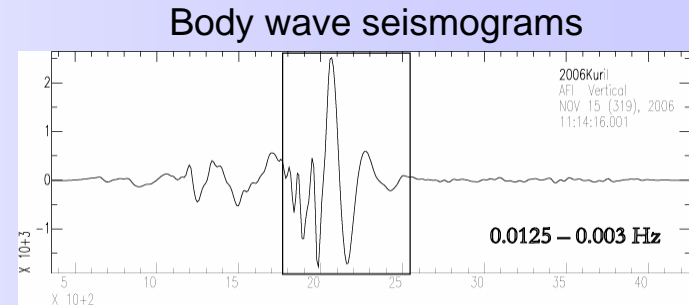


Courtesy Phil Cummins
(Geoscience Australia)



How does Finite Fault Slip inversion work ?

- Try to fit the data (body wave, surface wave seismograms, geodetic observations etc)
- Also try to seek the *least complex* model
 - Least complex may mean
 - Minimum length
 - flattest model
 - smoothest model
 - Most compact slip distribution (Lohman & Simons, 2004)



Posed as a *regularized linear inverse problem*: $d = Gm$

Minimize a combination of fit to data and control on the model

$$\phi = \{\text{Data misfit}\} + r \times \{\text{Model Roughness}\}$$



Solving for a finite fault slip model

$$\phi = \|\mathbf{d} - G\mathbf{m}\|^2 + \mu_1^2 \|\mathbf{L}_1\mathbf{m}\|^2 + \mu_2^2 \|\mathbf{L}_0\mathbf{m}\|^2$$

- For given values of the hyper-parameters (μ_1, μ_2) we find the
 - model \mathbf{m} which minimizes ϕ .
- Use non-negative least squares method (Lawson and Hansen 1972)
Solves the linear system

$$\begin{pmatrix} \mathbf{d} \\ 0 \\ 0 \end{pmatrix} = \begin{pmatrix} G \\ \mu_1 \mathbf{L}_1 \\ \mu_2 \mathbf{L}_0 \end{pmatrix} \mathbf{m}$$

A good stable,
reliable approach

$$\mathbf{d}' = G'\mathbf{m}$$

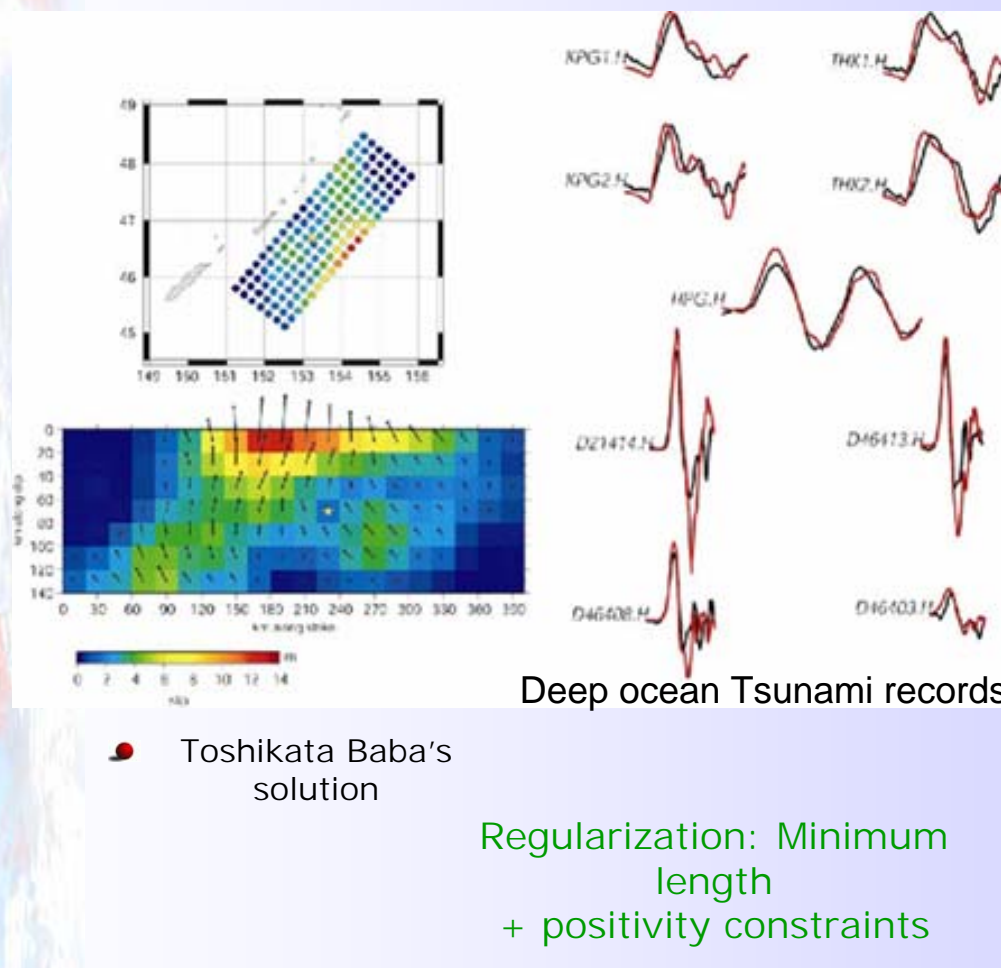
in a least squares sense subject to
positivity constraints on all variables

$$\mathbf{m} \geq 0$$

Existence of inequality constraints means GCV not applicable

2006 Kuril earthquake

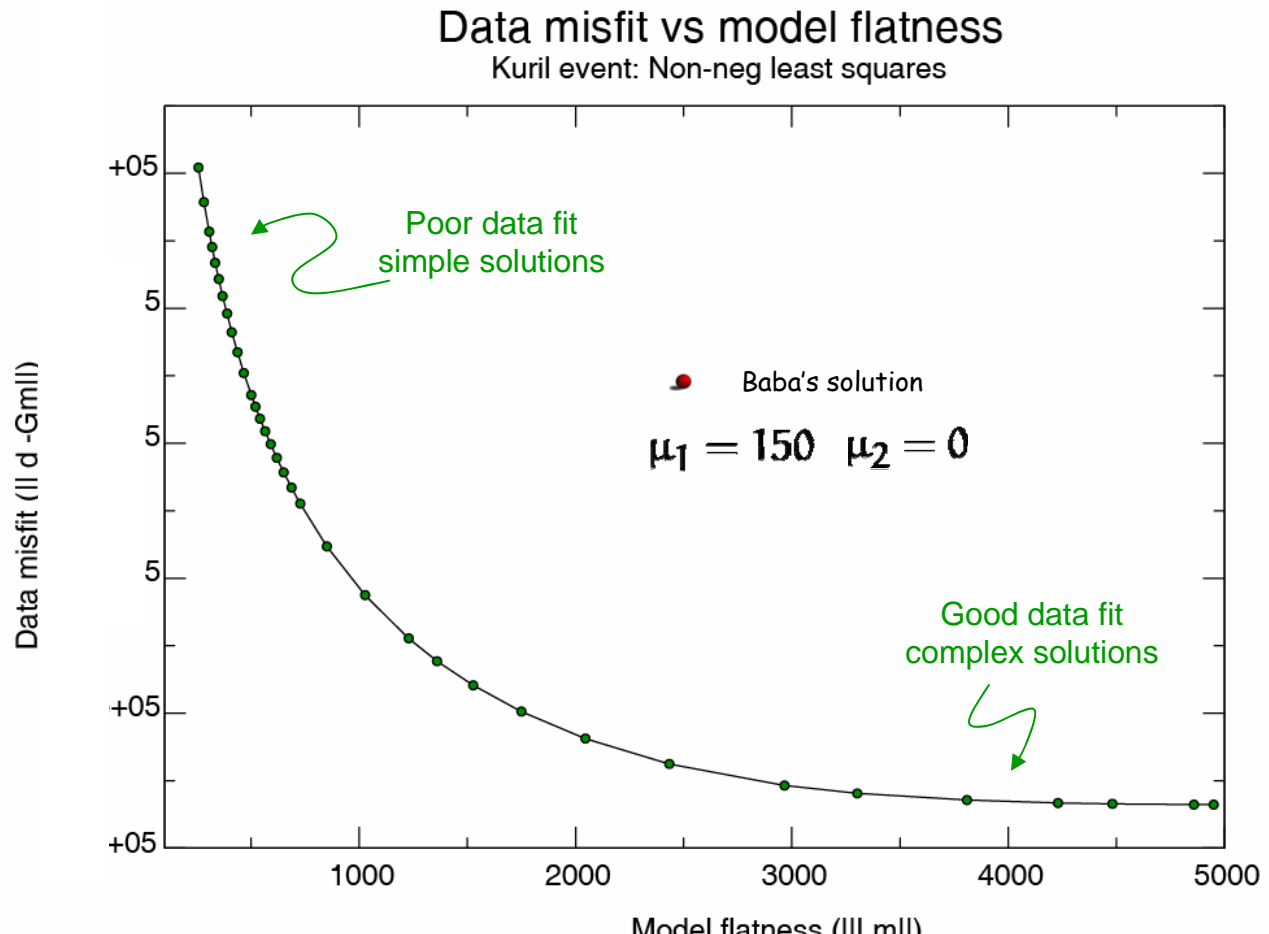
Fault plane solution obtained with interactively chosen hyper-parameter



40 waveforms to fit
4677 data equations
1676 model parameters

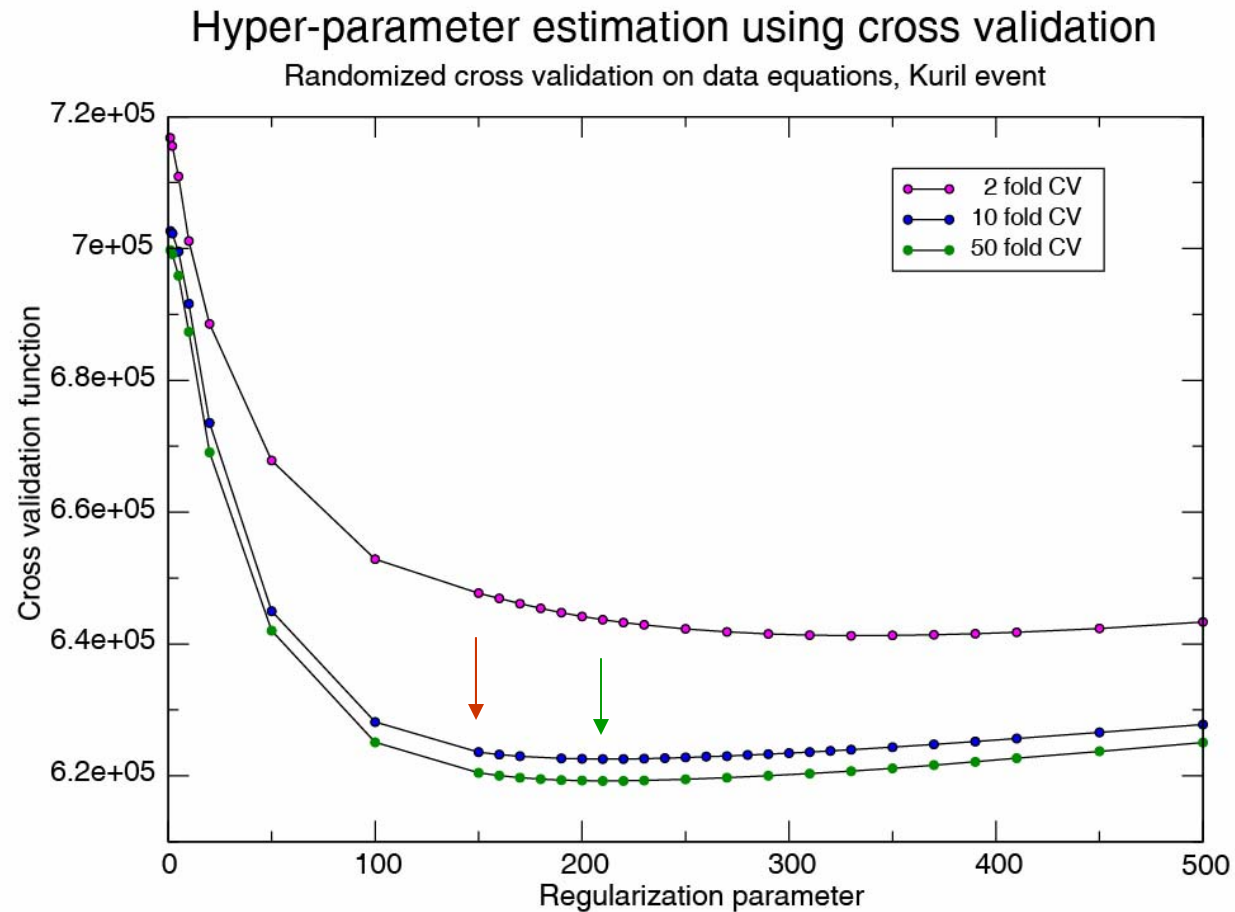


Interactive selection of hyper-parameters is not efficient enough !



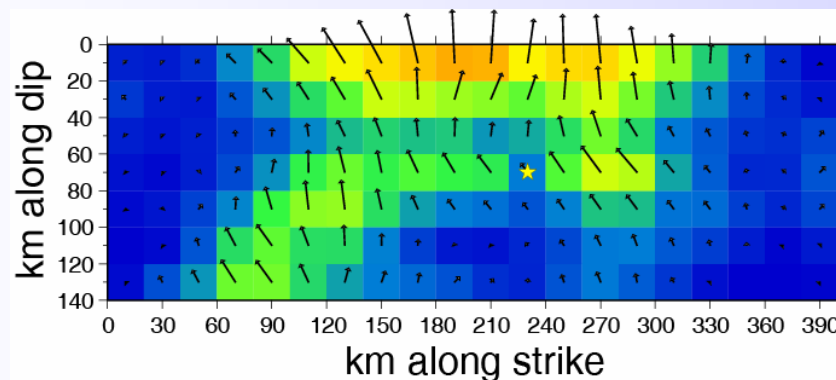
● Time consuming, subjective and difficult

2006 Kuril earthquake with CV

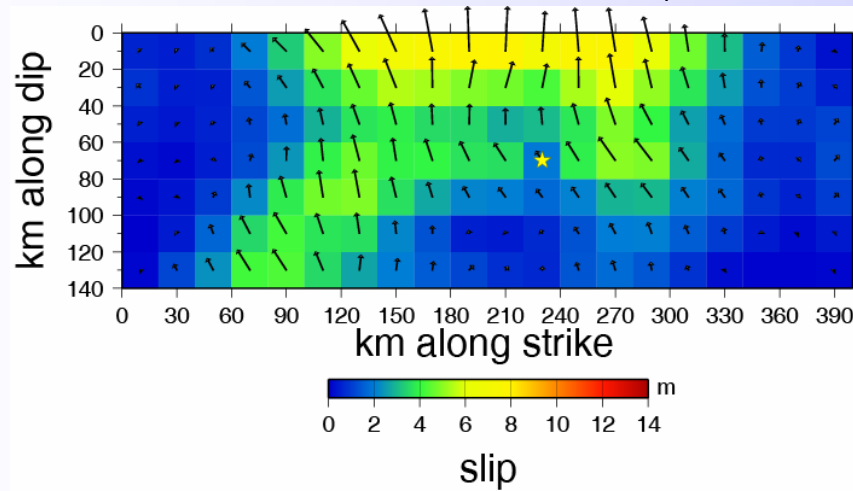


2006 Kuril earthquake: comparison between CV and interactive

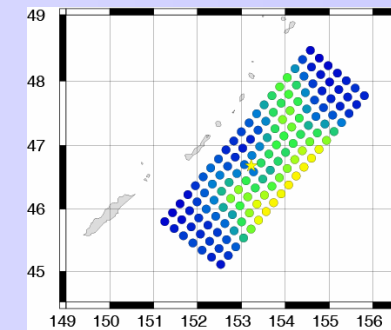
Interactive solution ($r_1 = 150$)



Cross validation solution ($r_1 = 210$)



Regularization: Minimum length + positivity constraints



40 waveforms to fit
4677 data equations
1676 model parameters

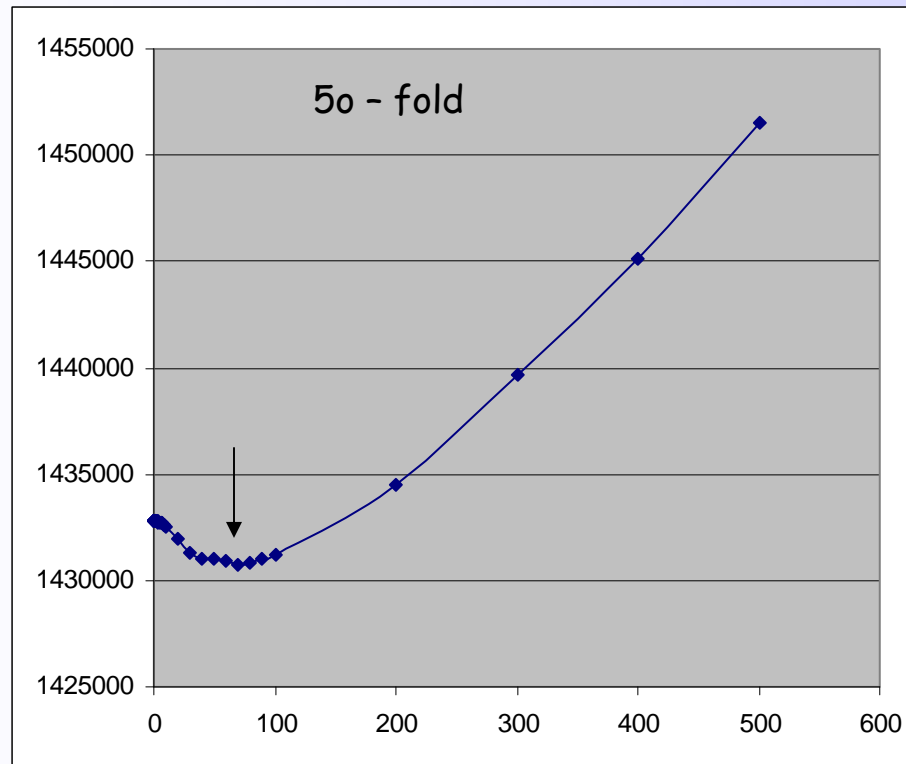




2007 Solomons earthquake with CV

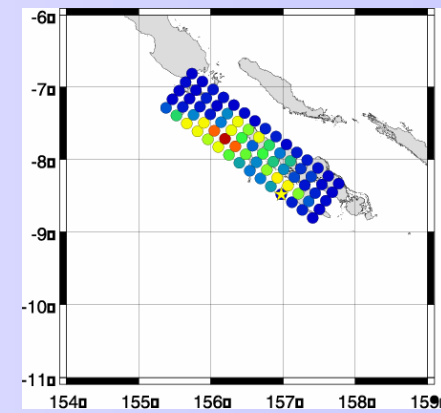
A clear minimum again !

Baba's Cross validation solution

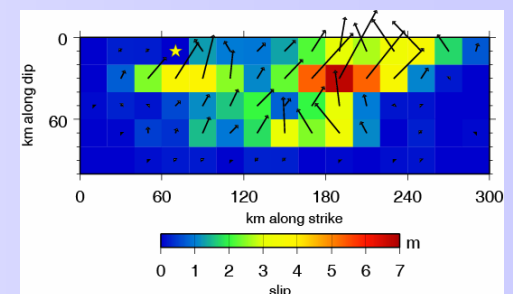


$$r_1 = 70, r_2 = 0$$

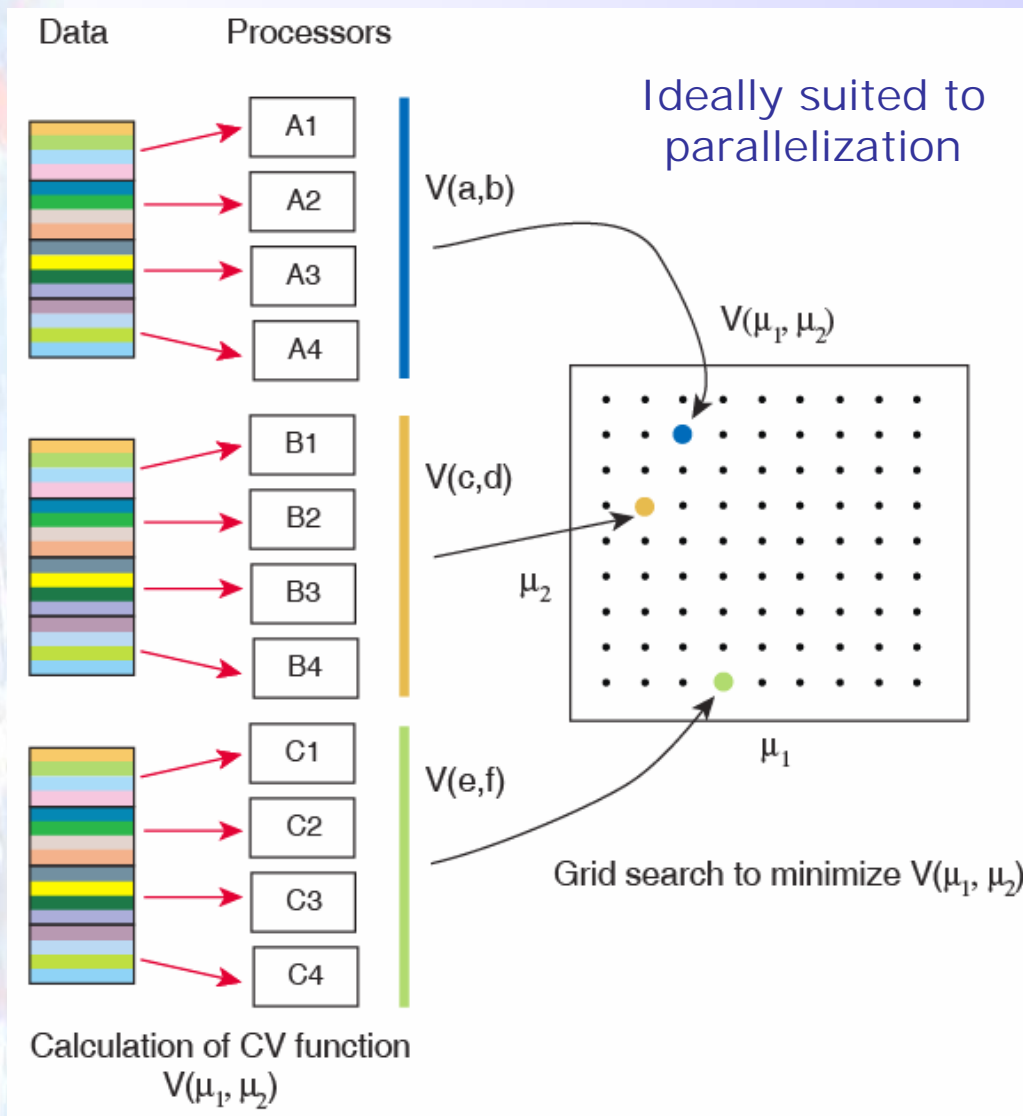
Regularization: Minimum length + positivity constraints



31 waveforms to fit
2562 data equations
896 model parameters



What about the computational cost of Cross validation ?



Parallelization possible
over **data space**
and
model space



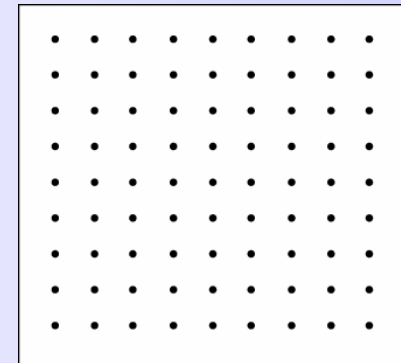
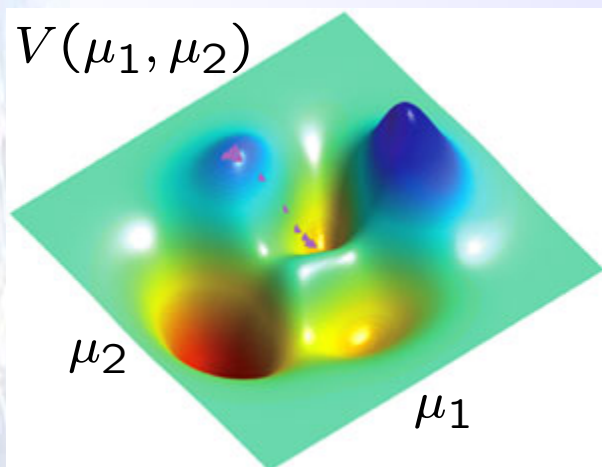
T. Baba parallelized
this calculation over
data space only and
was able to reduce
computation from 3
days to 2 hours.



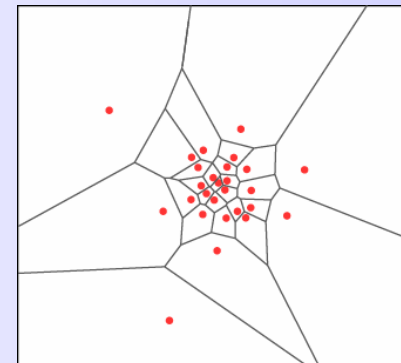
Grid search is not the only option

$$\phi = \|\mathbf{d} - G\mathbf{m}\|^2 + \mu_1^2 \|\mathbf{L}_1\mathbf{m}\|^2 + \mu_2^2 \|\mathbf{L}_o\mathbf{m}\|^2$$

More than one hyper-parameter requires
multi-dimensional direct search to minimize $V(\mu_1, \mu_2)$



Uniform grid search



Adaptive search
(NA, SA, GA)



Cross validation properties

Cross validation is a way of assessing the **quality** of a solution based on the principle of measuring the fit to **missing data**

On the plus side

- Cross validation can be used in cases where a suitable level of data misfit is not known in advance
(it is in effect a bootstrap measure of data variance)
- Provides an objective criterion for picking a preferred solution.
- Can be automated. (GCV for linear problems with no inequality constraints)

On the minus side

- Has been criticized for over-smoothing models.
- Computational burden has often seen it ignored
(e.g. by geophysicists !)



What we will be skipping over

Optimization and iterative solvers, Backus and Gilbert...

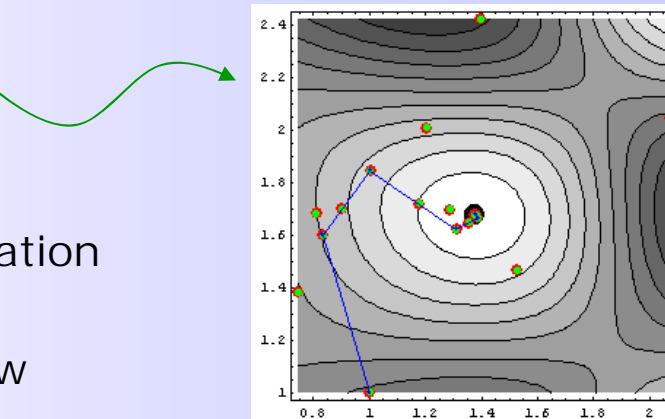
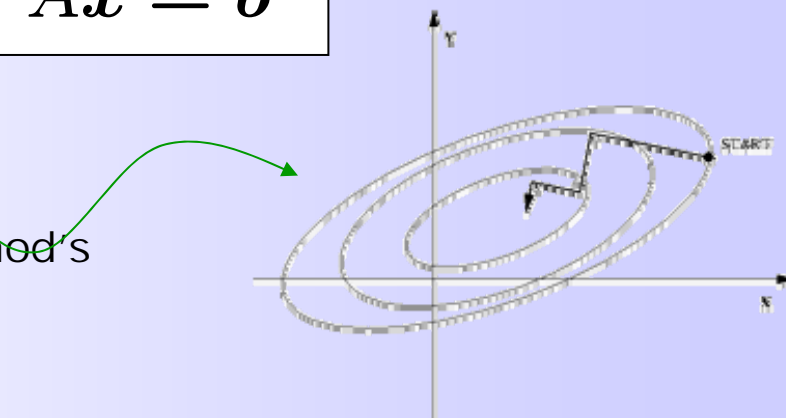


Iterative solvers and optimization

Iterative solution of large linear systems of equations and for nonlinear optimization

$$Ax = b$$

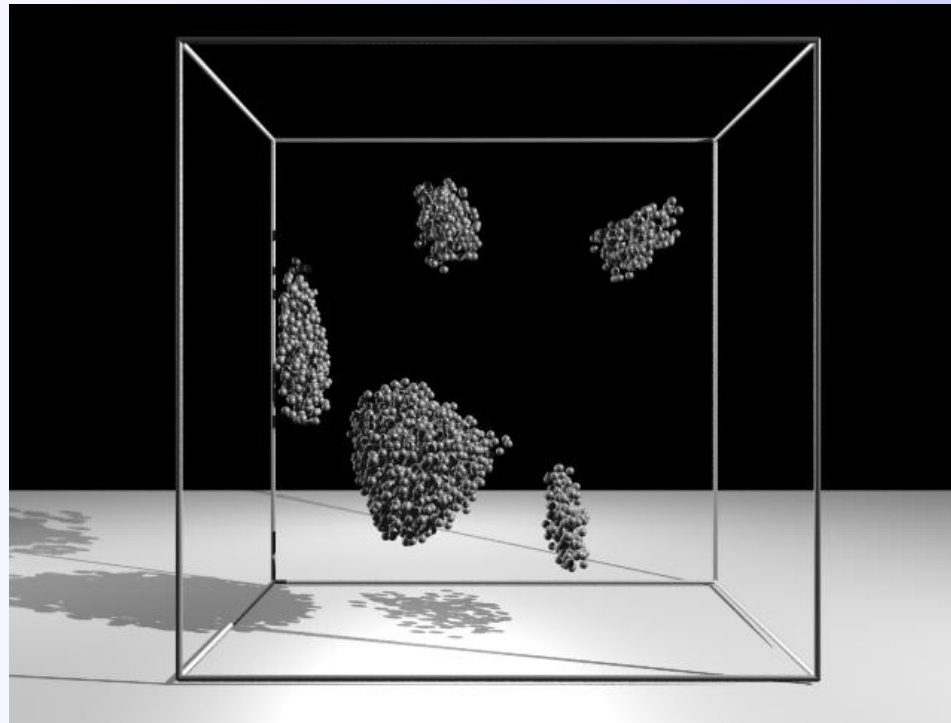
- Steepest descent
- (Quasi) Newton method's
- Conjugate gradients
- Preconditioning
- Gradient based optimization methods
- Parallelised libraries now available



Review material can be found in Ch. 6 of Aster et al. (2005) and Section 2.3 of Rawlinson and Sambridge (2003).



Fully nonlinear inversion and parameter search



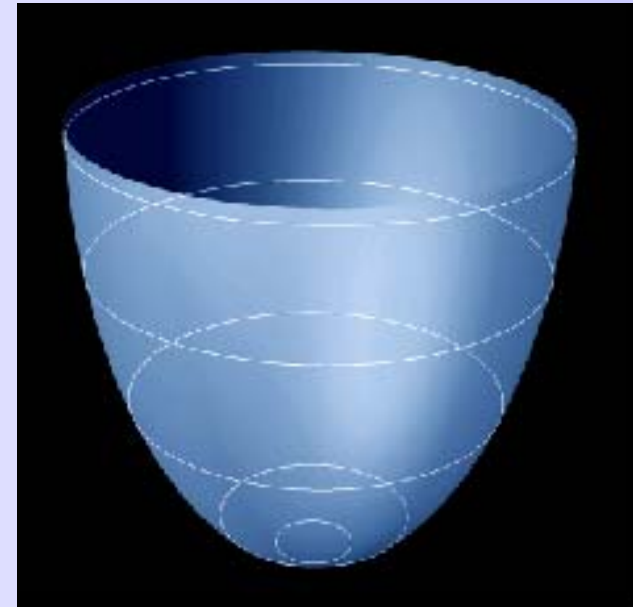


Recap: linear and nonlinear inverse problems

- Linear problems

- Single minima
- Gradient methods work
- Quadratic convergence
- Many unknowns

$$\mathbf{d} = \mathbf{Gm}$$



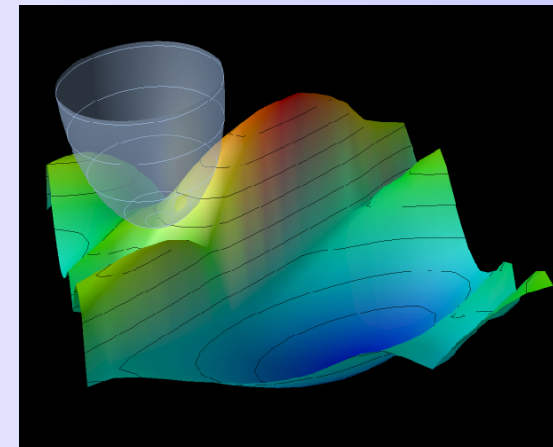
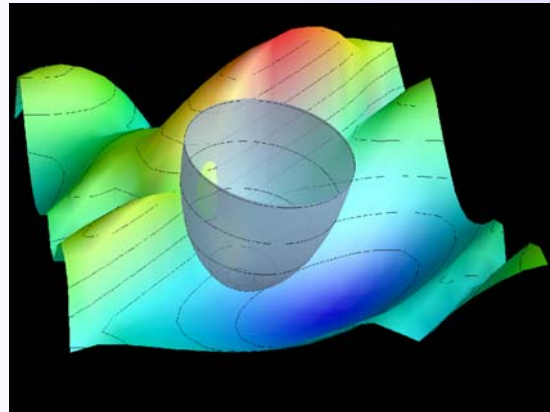
$$\phi(\mathbf{d}, \mathbf{m}) = (\mathbf{d} - \mathbf{Gm})^T \mathbf{C}_D^{-1} (\mathbf{d} - \mathbf{Gm}) + \mu (\mathbf{m} - \mathbf{m}_o)^T \mathbf{C}_M^{-1} (\mathbf{m} - \mathbf{m}_o)$$



Recap: linear and nonlinear inverse problems

- Weakly nonlinear problems $\delta\mathbf{d} = G\delta\mathbf{m}$
 - Single or multiple minima
 - Gradient methods might work if starting point good enough
 - Many unknowns

$$G_{i,j} = \frac{\partial d_i}{\partial m_j}$$



$$\begin{aligned}\phi(\mathbf{d}, \mathbf{m}) = & (\delta\mathbf{d} - G\delta\mathbf{m})^T C_D^{-1} (\delta\mathbf{d} - G\delta\mathbf{m}) + \\ & \mu(\mathbf{m} - \mathbf{m}_o)^T C_M^{-1} (\mathbf{m} - \mathbf{m}_o)\end{aligned}$$



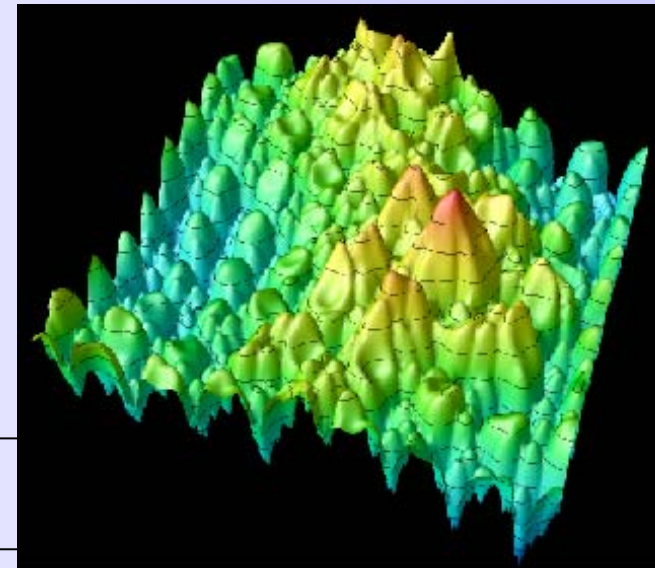
Recap: linear and nonlinear inverse problems

- Strongly nonlinear problems $\mathbf{d} = g(\mathbf{m})$
 - Multiple minima
 - Linearization and gradient methods fail
 - Tractable with relatively few unknowns 1-100 with direct search techniques

Derivatives of little use

$$\frac{\partial d_i}{\partial m_j}$$

Data misfit surface
in an infrasound array

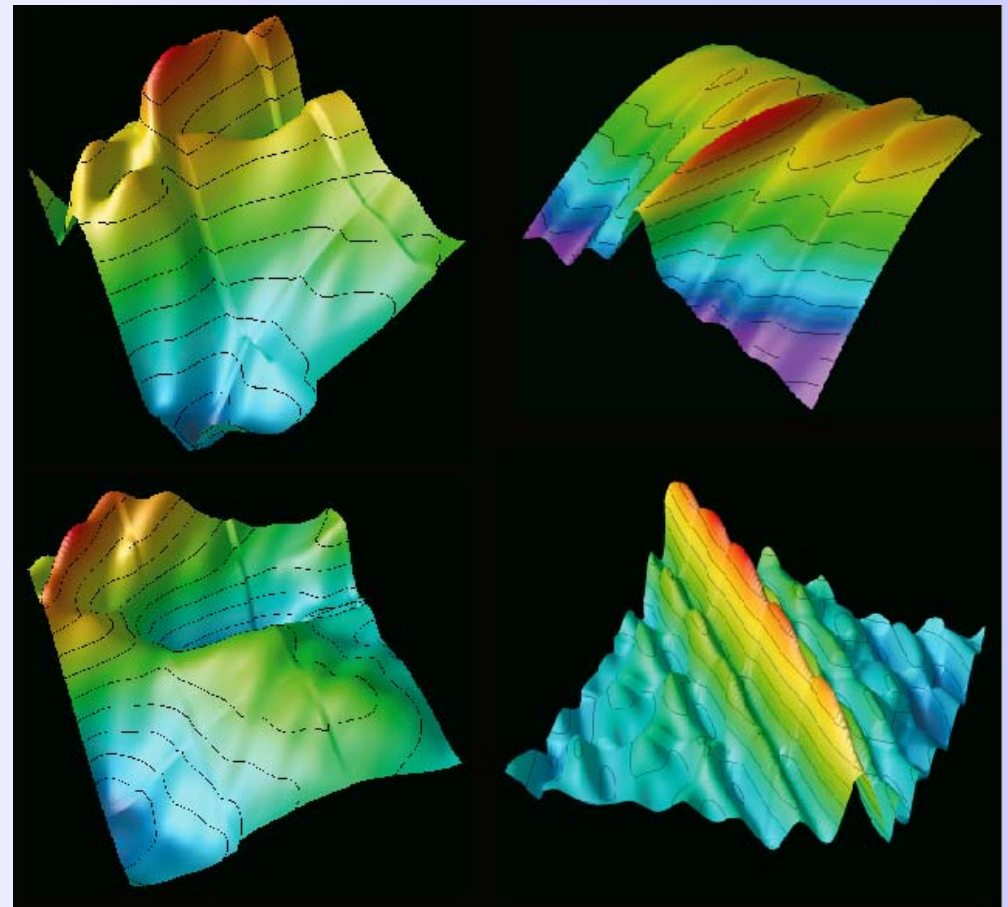
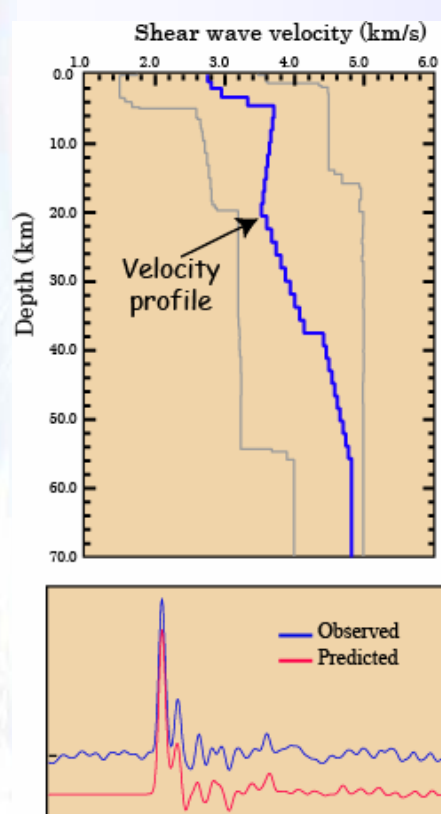


Kennett et al. (2003)

$$\begin{aligned}\phi(\mathbf{d}, \mathbf{m}) = & (\mathbf{d} - g(\mathbf{m}))^T C_D^{-1} (\mathbf{d} - g(\mathbf{m})) + \\ & \mu (\mathbf{m} - \mathbf{m}_o)^T C_M^{-1} (\mathbf{m} - \mathbf{m}_o)\end{aligned}$$

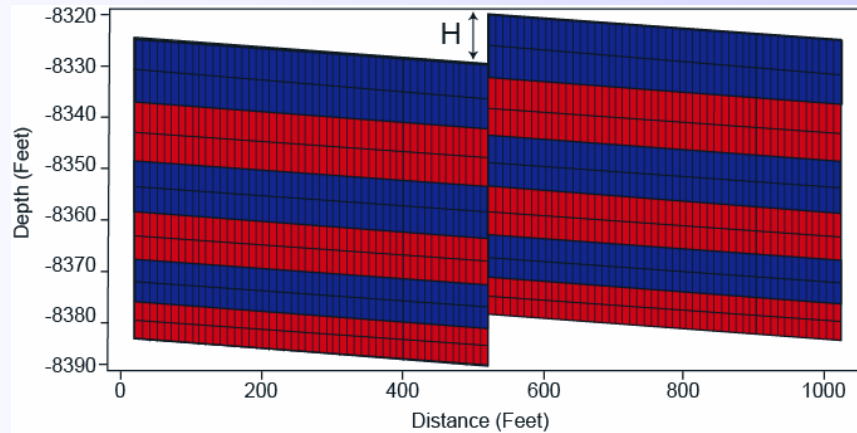
Example: nonlinear inverse problems

Seismic receiver function inversion

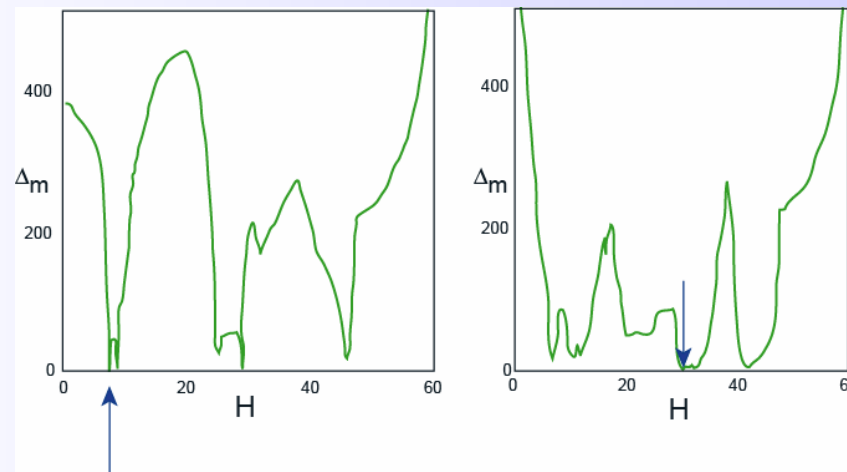


Example: nonlinear inverse problems

History matching in an oil reservoir



A one parameter data fitting problem



Courtesy P. King

Monte Carlo methods



"A branch of experimental mathematics that is concerned with experiments on random numbers"

Hammersley and Handscomb (1964)

Monte Carlo methods

‘Monte Carlo’ Phrase coined by *Metropolis and Ulam* (1949).

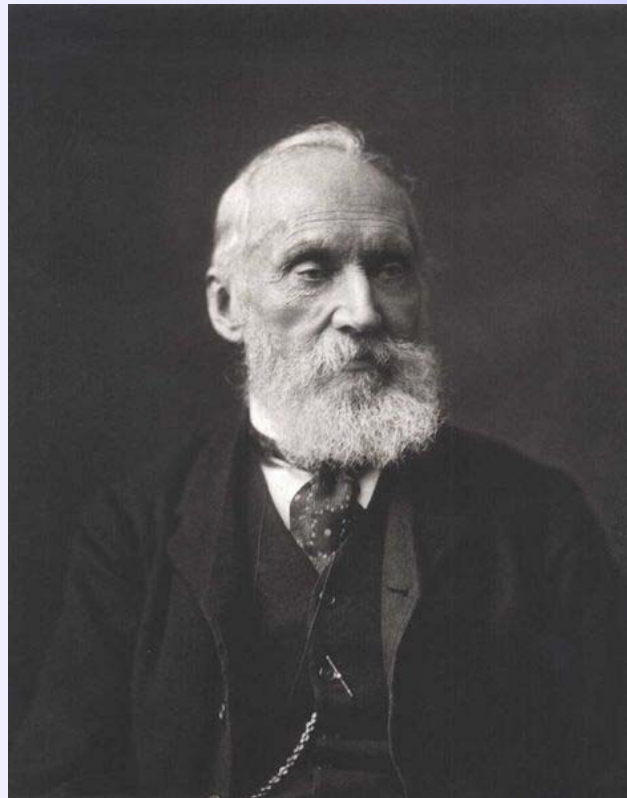
Originally developed by *Ulam, von Neumann, and Fermi* to simulate neutron diffusion in fissile materials development of the atomic bomb.





Monte Carlo methods

...but did someone think of it earlier ?



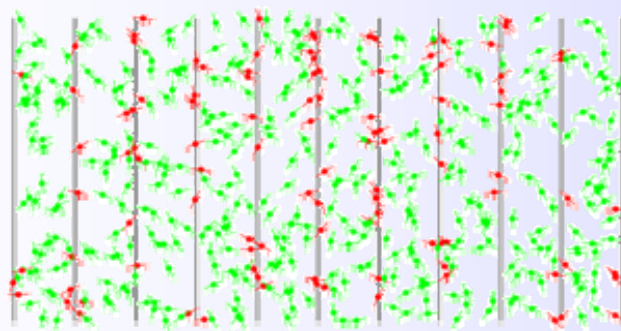
As noted by Hammersley and Handscomb (1964) Lord Kelvin (1901) described use of "ashtonishinglymodern Monte Carlo techniques" in a discussion of the Boltzmann equation.

$$S = k \ln W$$

Monte Carlo methods

...but Monte Carlo solutions had been around for even longer

Hall (1874) recounts numerical experiments to determine the value of π by injured officers during the [American Civil War](#)...



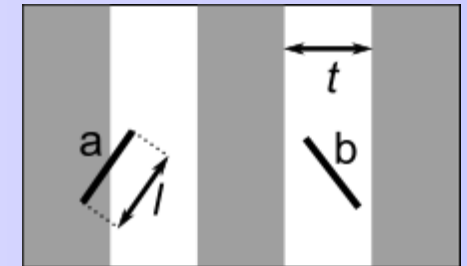
Throw a needle onto a board containing parallel straight lines.
The statistics of the number of times the needle intersected each line could be used to estimate π .

This is [Buffon's needle problem](#) (1733).

Buffon's needle problem

Posed by Buffon in 1733 (solved by Buffon in 1777)

Given a needle of length l dropped on a plane ruled with parallel lines a distance t apart, what is the probability that the needle will cross a line?

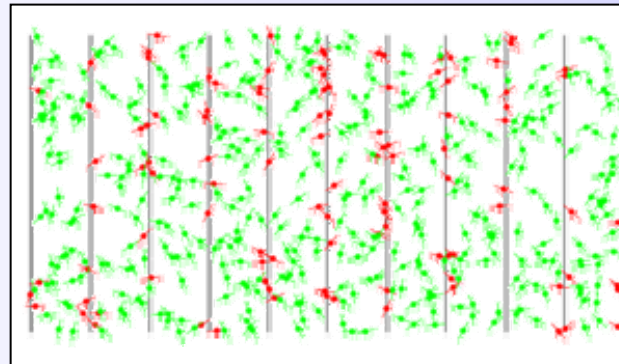


If h needles intersect the lines (red) out on n , the solution is

For $l \leq t$

$$\frac{h}{n} = \frac{2l}{t\pi}$$

For $l > t$



An experiment with 500 tosses of a needle ($l=t/3$). 107 needles cross a line, giving .

$$l = \frac{t}{3} \quad h = 107 \quad n = 500 \\ \Rightarrow \pi = 3.116 \pm 0.073$$

$$\frac{h}{n} = \frac{2}{t\pi} \left\{ l - \sqrt{l^2 - t^2} - t \sin^{-1} \left(\frac{t}{l} \right) \right\} + 1$$

Using a Monte Carlo trial of randomly throwing a needle on a board the statistics allow an estimate of π



Monte Carlo methods

Peacetime successes through operations research

Thomson (1957) describes a Monte Carlo simulation of fluctuations of traffic in the British Telephone system.

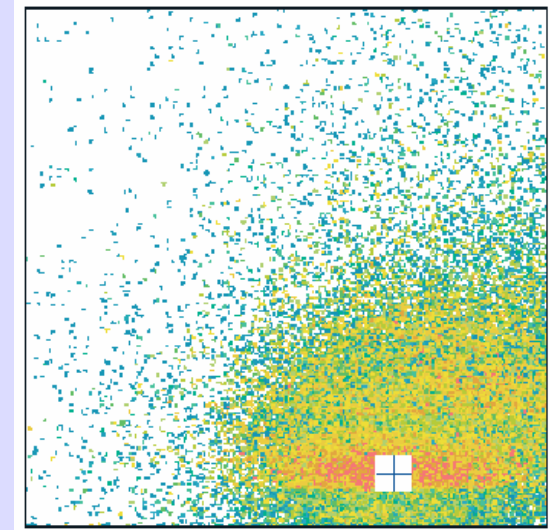
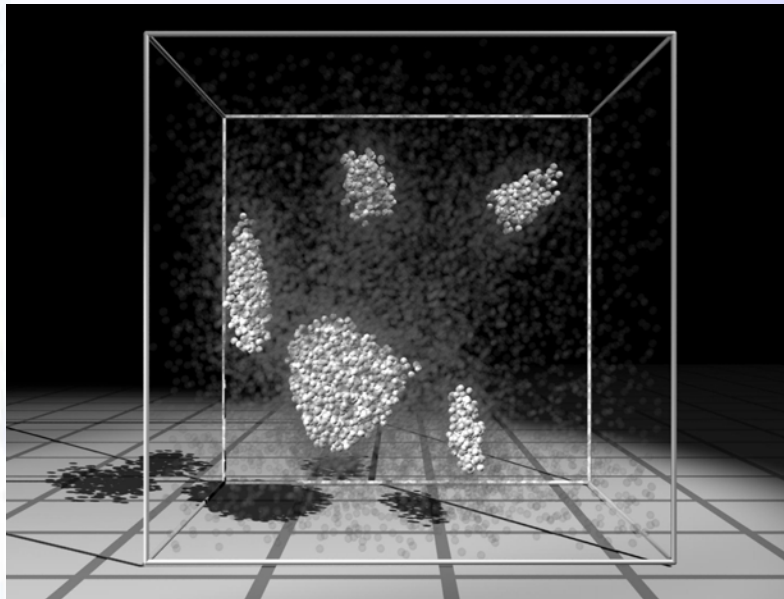


Direct search

Derivative free or ‘direct search’ techniques can be useful for weakly and strongly nonlinear problems.

Problem: Search a multi-dimensional parameter space to find models with satisfactory fit to data and other criteria.

As computational power has grown global optimization algorithms have become very popular.





Direct search methods

- Uniform random/nested search
- Simulated Annealing
(Thermodynamic analogy)
- Genetic/evolutionary algorithms
(Biological analogy)
- Neighbourhood algorithm

Uniform random search

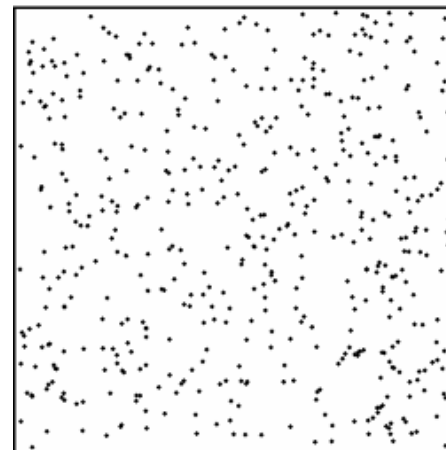
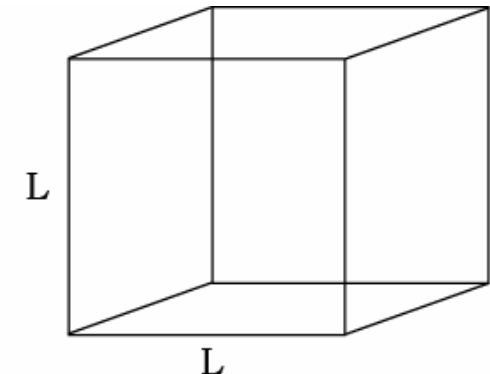
Uniform random search means uniform in volume

For M unknowns we have an M -dimensional parameter space. The volume of a cube with side L is

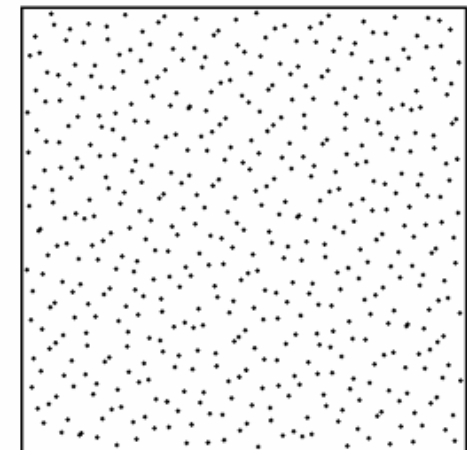
Data fit does not guide the search, although, we may wish to nest...

The curse of dimensionality always gets you in the end !

$$V = L^M$$



Pseudo - random



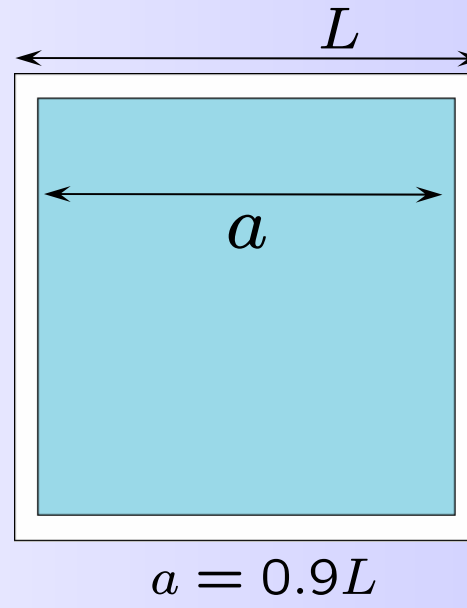
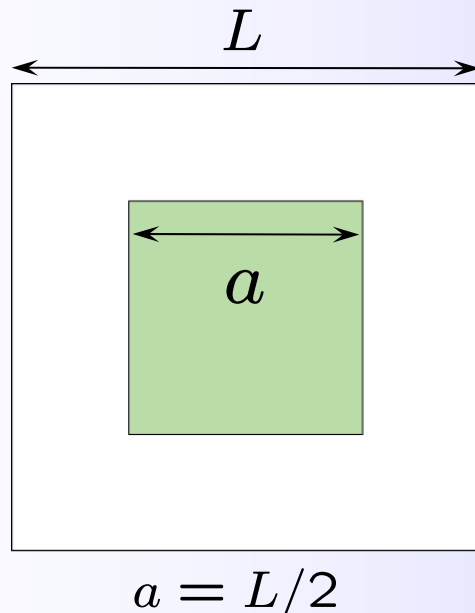
Quasi - random

What does random mean ?

The curse of dimensionality

Where is all the volume in a hyper-cube ?

A hyper-cube of volume V and side L of dimension M $V = L^M$



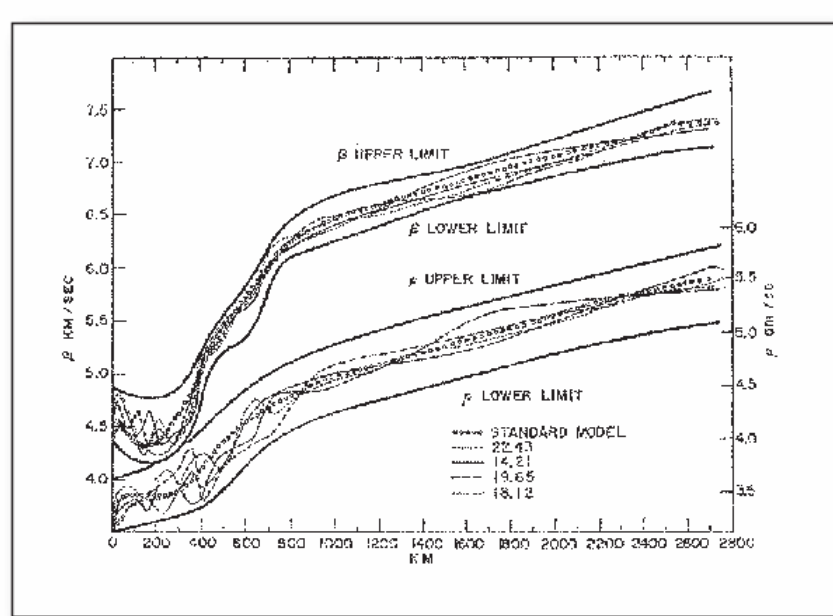
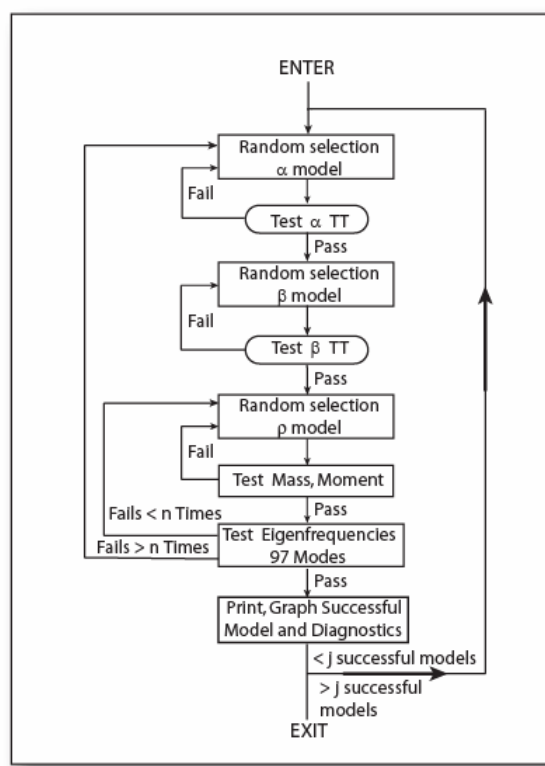
How many samples required to get one in the interior box ?

M		
1	50%	90%
2	25%	81%
5	3%	50%
10	0.1%	35%
20	$\frac{1}{10000}$ %	12%
50	10^{-15} %	0.5%

- ➊ Proportion of volume in the outside shell always dominates over the interior
- ➋ All volume tends to be in the exterior shell as $M \uparrow$

Example: Uniform random search

Uniform random search in seismology

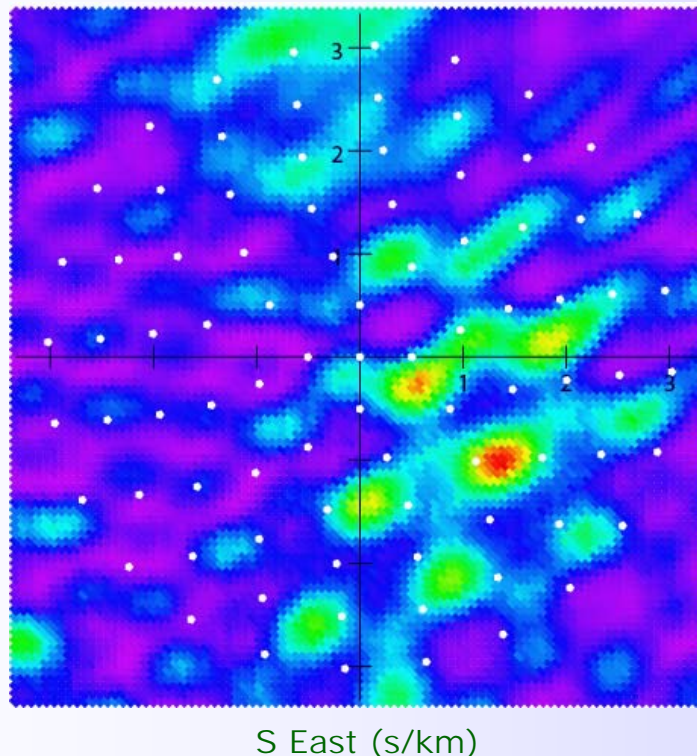


Press (1968)

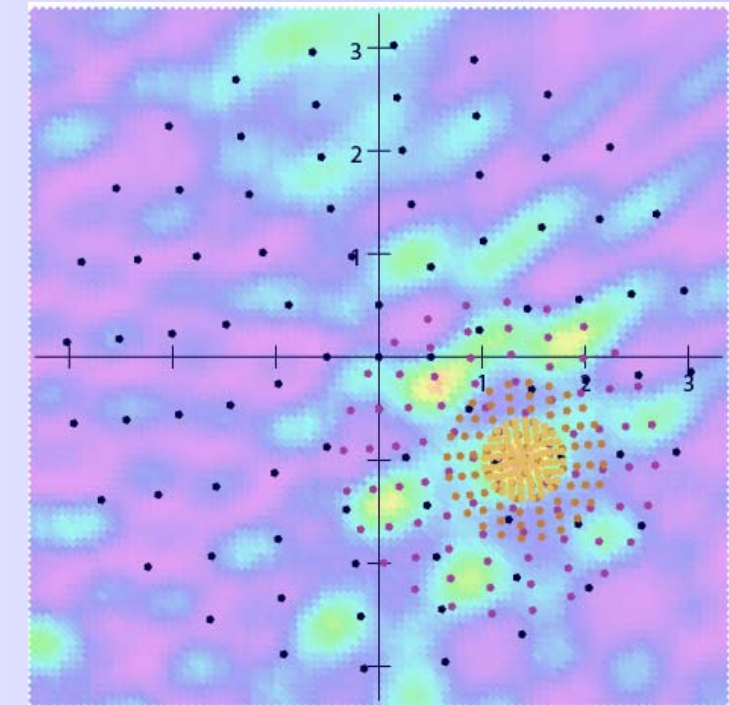
Nested uniform search

2-D global optimization

S North (s/km)



S East (s/km)



Maximizing beam power as a function of slowness

A simple but effective approach.

Issues are: Discretization level, number of samples, curse of dimensions

Global optimization: Simulated Annealing

A natural thermodynamic optimization process

Annealing is the process of heating a solid until thermal stresses are released. Then cooling it **very slowly**. The final state of the crystal depends on how fast the temperature is reduced. At each temperature it has a crystalline potential energy, which is lowest only for a perfect crystal.



Slow cooling produces a global minimum in potential energy

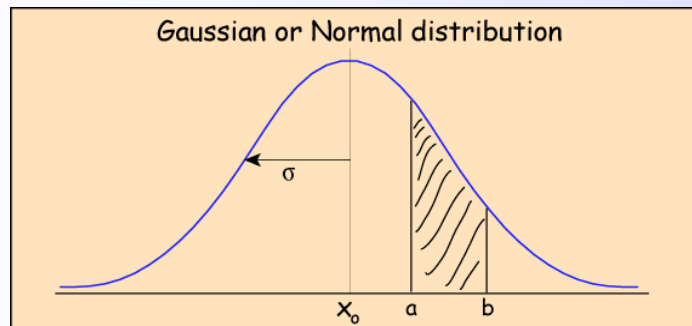


Fast cooling quenches the crystal into a local minimum in potential energy

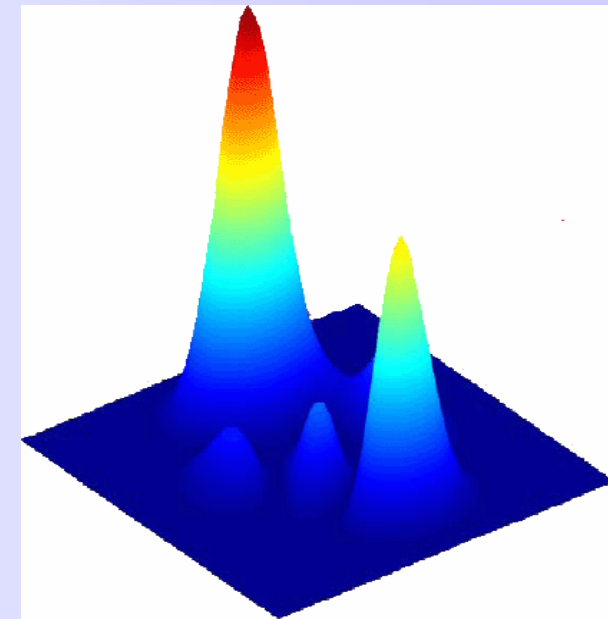
Multiple minima and multiple maxima

$$\phi(\mathbf{m}) = \frac{1}{2}(\mathbf{d} - g(\mathbf{m}))^T C_D^{-1}(\mathbf{d} - g(\mathbf{m})) + \frac{\mu}{2}(\mathbf{m} - \mathbf{m}_o)^T C_M^{-1}(\mathbf{m} - \mathbf{m}_o)$$

Single peaked Likelihood



Multi peaked Likelihood



Sampling according to a PDF means generating samples with density equal to its distribution

Global optimization: Simulated Annealing

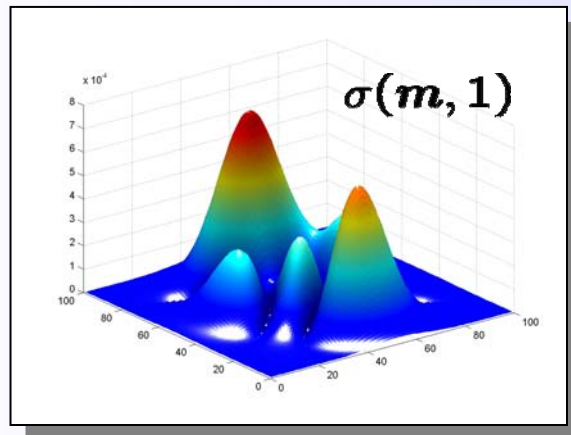
The **Gibbs-Boltzmann distribution**, $\sigma(m, T)$, describes the probability of a statistical system with state m having an energy $\phi(m)$ and temperature T .

$$\sigma(m, T) = e^{-\frac{\phi(m)}{T}} = e^{-\phi(m)/T}$$

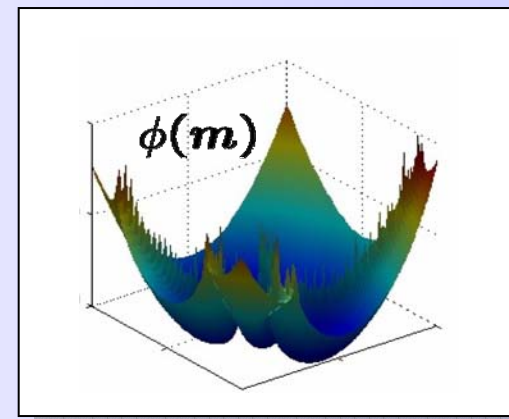
$\sigma(m, T)$ is a probability density function for m at temperature T . In **Simulated Annealing** we associate the energy $\sigma(m)$ with negative log likelihood, or the objective function in the inverse problem to be minimized e.g.

$$\phi(m) = \frac{1}{2}(d-g(m))^T C_D^{-1}(d-g(m)) + \frac{\mu}{2}(m-m_o)^T C_M^{-1}(m-m_o)$$

The minimum of $\phi(m)$ corresponds to the maximum of the PDF $\sigma(m, T)$.



Likelihood function



Misfit function

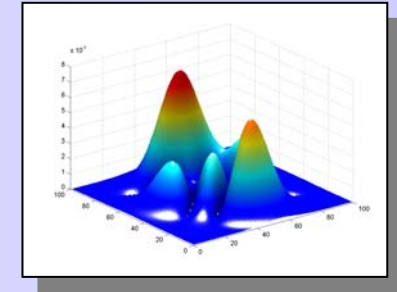
Recall the least squares case

A quadratic and a Gaussian

Global optimization: Simulated Annealing

The general structure of the algorithm is:

- Set T large (≈ 1000)
- Generate samples, m **probabilistically** with a density that follows the Gibbs-Boltzmann distribution for this T and energy $\phi(m)$



$$\sigma(\mathbf{m}, T) = e^{-\frac{\phi(\mathbf{m})}{T}}$$

- Cool the system by reducing T *slowly*. Use an **annealing schedule** e.g. $T = \alpha T$, then return to step 2

If the system is cooled too quickly then we get a local minimum. If it is cooled too slowly then we waste a lot of energy (forward) evaluation. The optimum annealing schedule will depend on the complexity of the energy function $\phi(m)$.

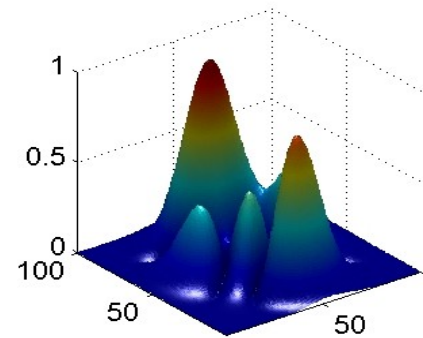
But what role does T play ?

Global optimization: Simulated Annealing

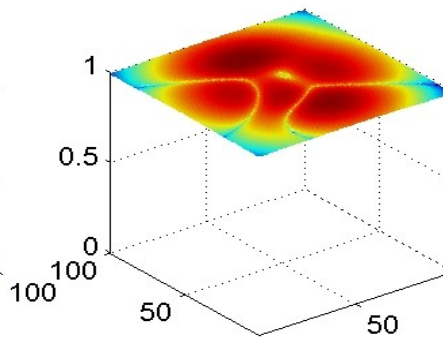
Global optimization using a heat bath

But what role does T play ?

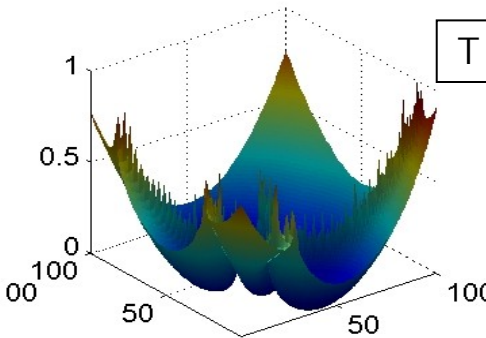
$\sigma(\mathbf{m}, 1)$



$\sigma(\mathbf{m}, T)$

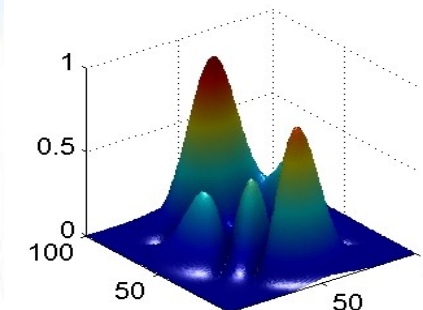


$\phi(\mathbf{m})$

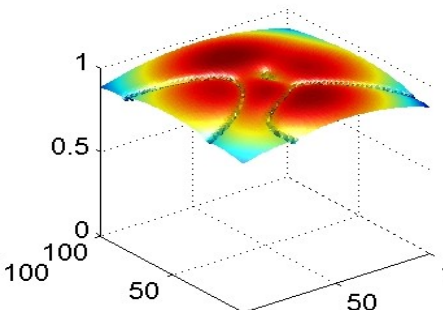


T = 1000

e.g. Likelihood



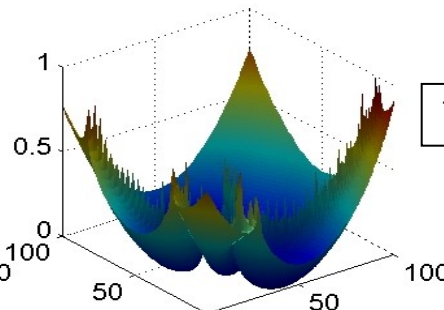
Gibbs-Boltzmann



PDF at temp T

$$\sigma(\mathbf{m}, T) = e^{-\frac{\phi(\mathbf{m})}{T}}$$

e.g. data misfit



T = 100



Global optimization: Simulated Annealing

$\sigma(\mathbf{m}, 1)$

$\sigma(\mathbf{m}, T)$

$\phi(\mathbf{m})$

$T = 10$

$T = 1$

$T = 0.1$

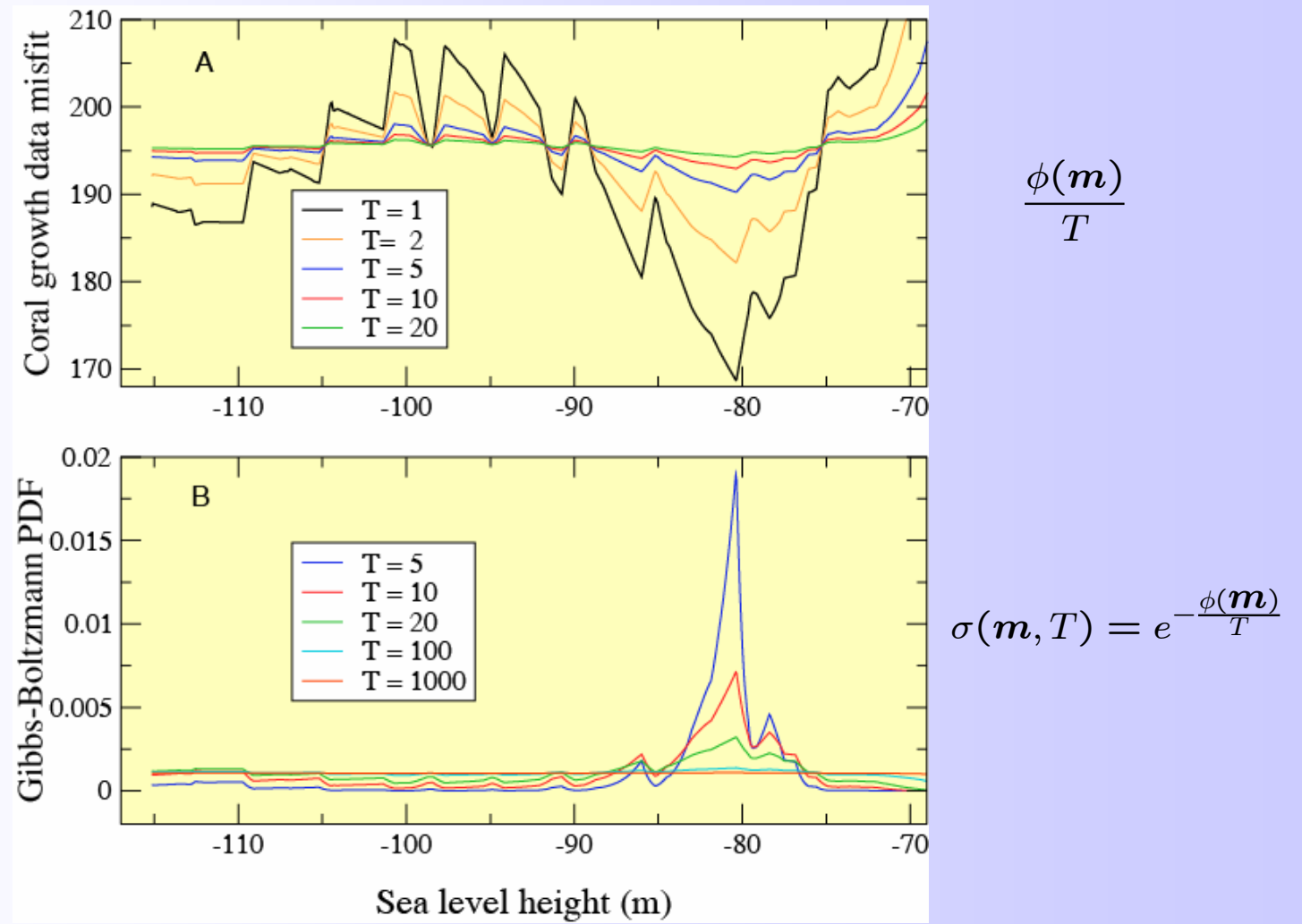
$T = 0.01$

e.g. Likelihood

Gibbs-Boltzmann
PDF at temp T

e.g. data misfit

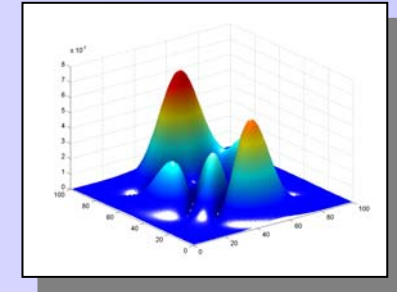
Example: Gibbs-Boltzmann distribution



Global optimization: Simulated Annealing

The general structure of the algorithm is:

- Set T large (≈ 1000)
- Generate samples, m **probabilistically** with a density that follows the Gibbs-Boltzmann distribution for this T and energy $\phi(m)$



$$\sigma(\mathbf{m}, T) = e^{-\frac{\phi(\mathbf{m})}{T}}$$

- Cool the system by reducing T *slowly*. Use an **annealing schedule** e.g. $T = \alpha T$, then return to step 2

If the system is cooled too quickly then we get a local minimum. If it is cooled too slowly then we waste a lot of energy (forward) evaluation. The optimum annealing schedule will depend on the complexity of the energy function $\phi(m)$.

But how to implement step 2 ?

Global optimization: Simulated Annealing

Implementing simulated annealing with the **Metropolis Algorithm**

- Set high **temperature**
- Define **annealing schedule**, e.g. $T_{i+1} = \alpha_i T_i$
- Define **starting model**, $m_o \leftarrow m_{\text{current}}$

Step 1

- Propose a new model $m_{new} = m_{cur} + \delta m$ where δm is some **local perturbation** of the old model, e.g. a Gaussian of fixed width
- Compared energy of new to old model

$$\Delta\phi = \phi(m_{new}) - \phi(m_{cur})$$

- Accept new model if fit improved

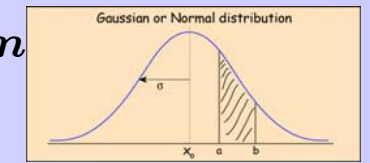
If $\Delta\phi < 0$, then $m_{cur} = m_{new}$

- Accept new model with probability p if fit worse $p = e^{\frac{-\Delta\phi}{T}}$

- If not enough samples for T_i go to **step 1**.

- **Stop** if **converged** else update $T_{i+1} = \alpha_i T_i$ go to **step 1**.

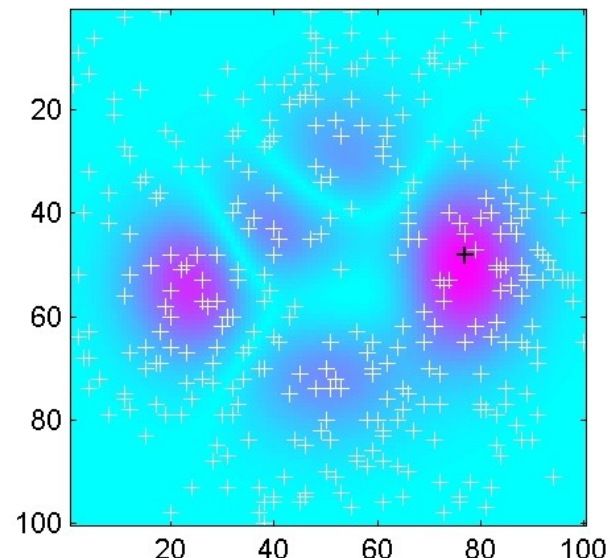
(Everything in **green** is a choice)



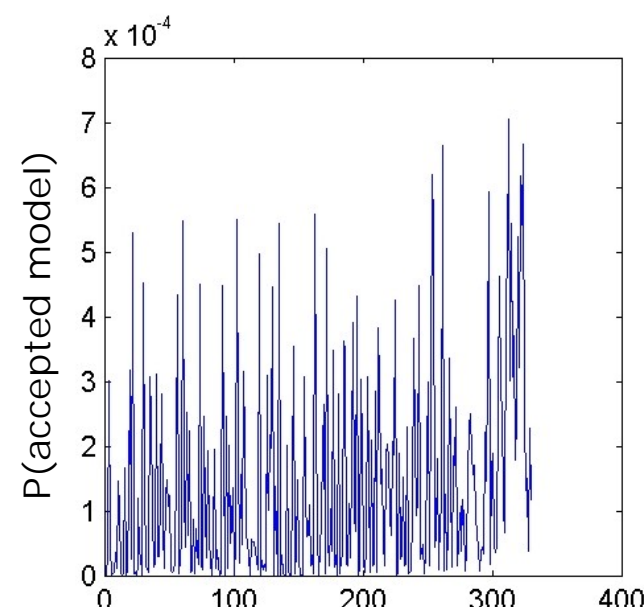
Moveclass

Example: Simulated Annealing

The Metropolis Algorithm produces a random walk in model space, initially T is high and the walk is random because all moves are accepted, As T decreases it slowly gets attracted to regions of high probability and toward the maximum in $\sigma(m, T)$.



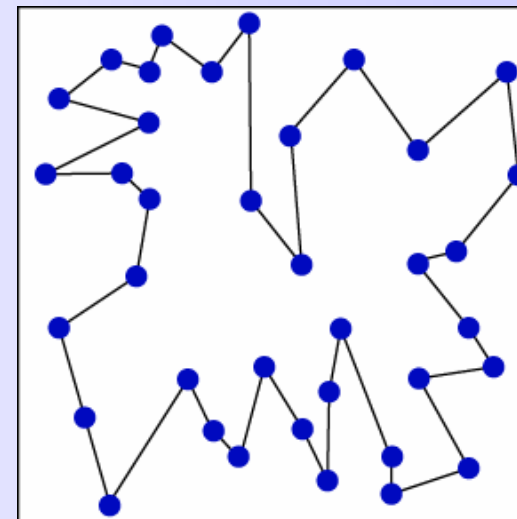
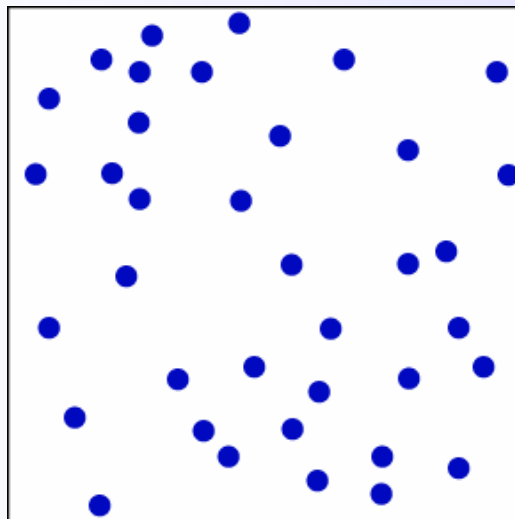
Gibbs-Boltzmann PDF



Number of accepted models

Simulated Annealing Example: TSP

In a famous paper Kirkpatrick et al. (1983) showed how simulated annealing could be used to solve a difficult combinatorial optimization problem known as the Travelling salesman problem.



Find the shortest closed path (tour) around the 37 cities.

This is known to be an NP-complete combinatorial optimization problem.



Recap: Simulated Annealing

- Simulated Annealing is a computational method for global optimization that uses an analogy to a physical (Thermodynamic) optimization process
- There are many variants of the method, each based on different **choices**. (Optimal annealing schedules are known in some cases.)
- Relatively simple to implement, for continuous and discrete optimization problems. Has been used in Geophysics since the 1999s.
- Can be inefficient if component **choices** are not made well.
- Although sequential in nature (random walk) can be run in parallel using independent random walks. *Ensemble annealing*.

Global optimization: Genetic algorithms

Genetic algorithms follow an analogy with another real world optimization technique, that of evolution, or natural selection.



Genetic algorithms are an attempt to exploit mimic the process of adaptation to systems to survive in a competitive environment. Their origin is attributed to the work of *Holland* (1975) devised original to study mathematical models of adaptation in artificial systems.

Genetic algorithms are closely related to **evolutionary computation**, an area independently devised by *Fogel & Fogel* (1961).

Applications are now widespread, especially as an optimization method.

First applications in geophysics were around 1991-1992.



Global optimization: Genetic algorithms

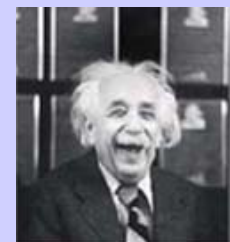
An analogy to natural selection

Human genotypes

Eye color	Hair color	Skin color	height	strength	Brain size	music ability	coordination	maths
-----------	------------	------------	--------	----------	------------	---------------	--------------	-------

Phenotypes of Albert

brown	black	bright	Avg.	Avg.	Avg.	high	low	medium
-------	-------	--------	------	------	------	------	-----	--------



Phenotypes of Sharon

green	blonde	fair	Avg.	Avg.	Avg	high	good	good
-------	--------	------	------	------	-----	------	------	------



Their offspring would depend on three processes

- Did Albert and Sharon select each other ?
- If so, what properties (phenotypes) were propagated ?
- What random mutations occurred ?

Selection

Crossover

Mutation

Genetic algorithms: bit encoding

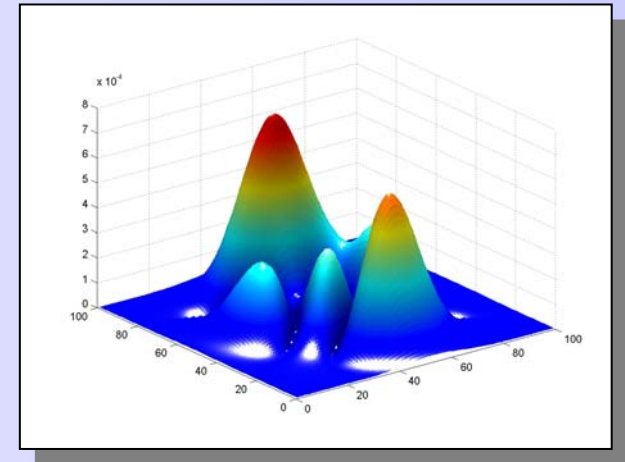
In GA an entire population of individuals is treated as a ensemble of chromosomes. The idea is to `evolve' the population toward optimal models.

Continuous variables (x_1, x_2, \dots) can be represented with a bit string

In the two parameter function opposite the model consists of a pair of variables (x, y). A fundamental (but absolutely necessary) is the coding of an individual into a bit string (*bit coding*)

	x	y
Model 1:	(3,25)	
Model 2:	(16,97)	
...		
Model N:	(23,45)	

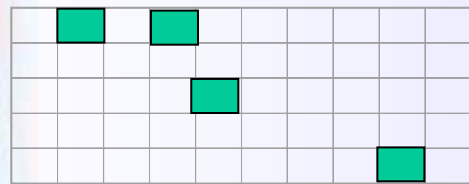
	x	y
->	001011	010101
->	100101	101010
->	001010	110111



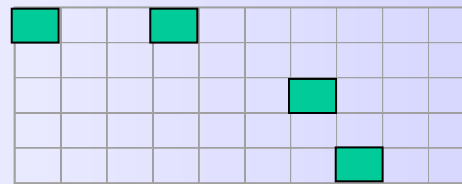
Generate an initial population randomly.

Genetic algorithms: bit encoding

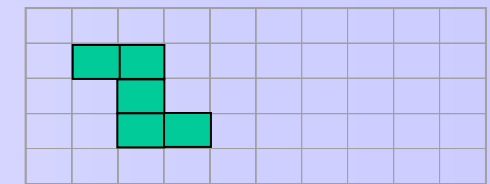
A natural example for a string representation for a geophysical inverse problem is the treasure hunt.



01010000010



100100000100



00000 0000

Here the actual binary coding would make sense: 0 would mean sand and 1 would represent gold. What if we want to describe a function taking on arbitrary values?

Example:

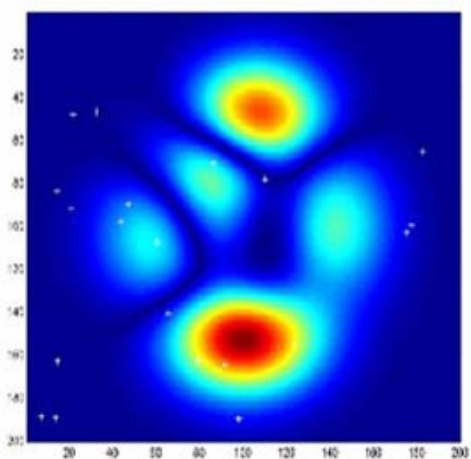
We want to invert for a depth dependent velocity model, described by layer thickness d and velocity c . Then a model vector m would look like:

$$m = (d_1, v_1, d_2, v_2, d_3, v_3, d_4, v_4, d_5, v_5, d_6, v_6, \dots, d_n, v_n)$$

... and could simply be described by a long bit-string. It is your choice how many bits you use for the possible range of values for each parameter.

Genetic algorithms: Selection

Rank	Model	x	y	Fitness
1	18	12	34	0.81
2	12	45	56	0.67
3	3	1	56	0.65
.				
.				
.				
N	7	24	98	0.01



Calculate the fit of each model to the data
-> survival fitness of model

Remove the half of the models with
the worst fits

Model rank determines survival

Rank	Model	x	y	Fitness
1	18	12	34	0.81
2	12	45	56	0.67
3	3	1	56	0.65
.				
N/2	5	11	44	0.58
.				
.				
N				

{ -> Siberia

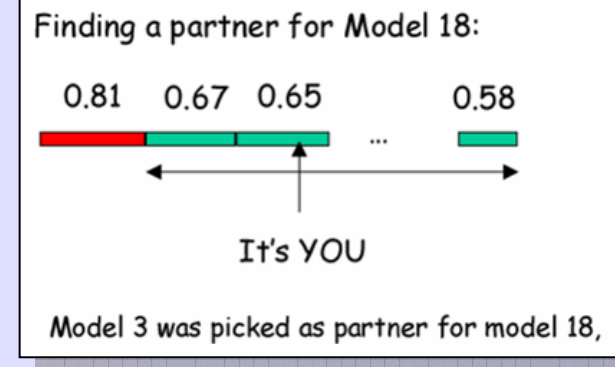
Genetic algorithms: Crossover

Randomly pair the remainders with probability of pairing depending on fitness

Rank	Model	x	y	Fitness
1	18	12	34	0.81
2	12	45	56	0.67
3	3	1	56	0.65
.				
N/2	5	11	44	0.58

Finding a partner for Model 18:

0.81 0.67 0.65 0.58
0.81 0.67 0.65 0.58
It's YOU



This requires a mapping between fitness and probability

Randomly choose a common point on the strings to cut and swap over

Before

Model 18 (12,34) -> 001010 101001

Model 3 (1,56) -> 101100 010110

After

1: 00101010 | 0110 -> (24, 56)

2: 10110001 | 1001 -> (76,87)

Total population then consists of N/2 of better models + N/2 offspring

Genetic algorithms: Mutation

Each of the offspring undergo a random mutation with a certain probability, P_m

Baby 1: 00101010 | 0110 → (24, 56)

Baby 2: 10110001 | 1001 → (76,87)



Baby 1: 001**1**1010 | 0110 → (**13**, 56)

Baby 2: 10110001 | 1001 → (76,87)

This adds a random component back in the population and encourages diversity.



Genetic algorithms: Iterations

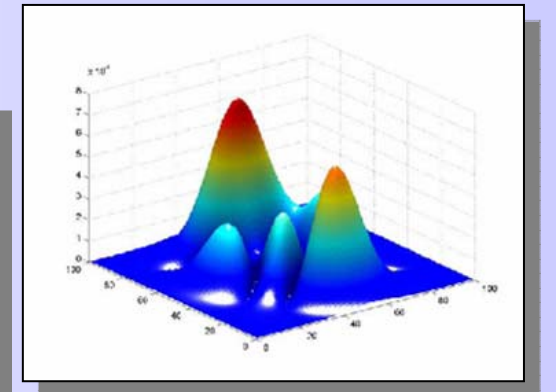
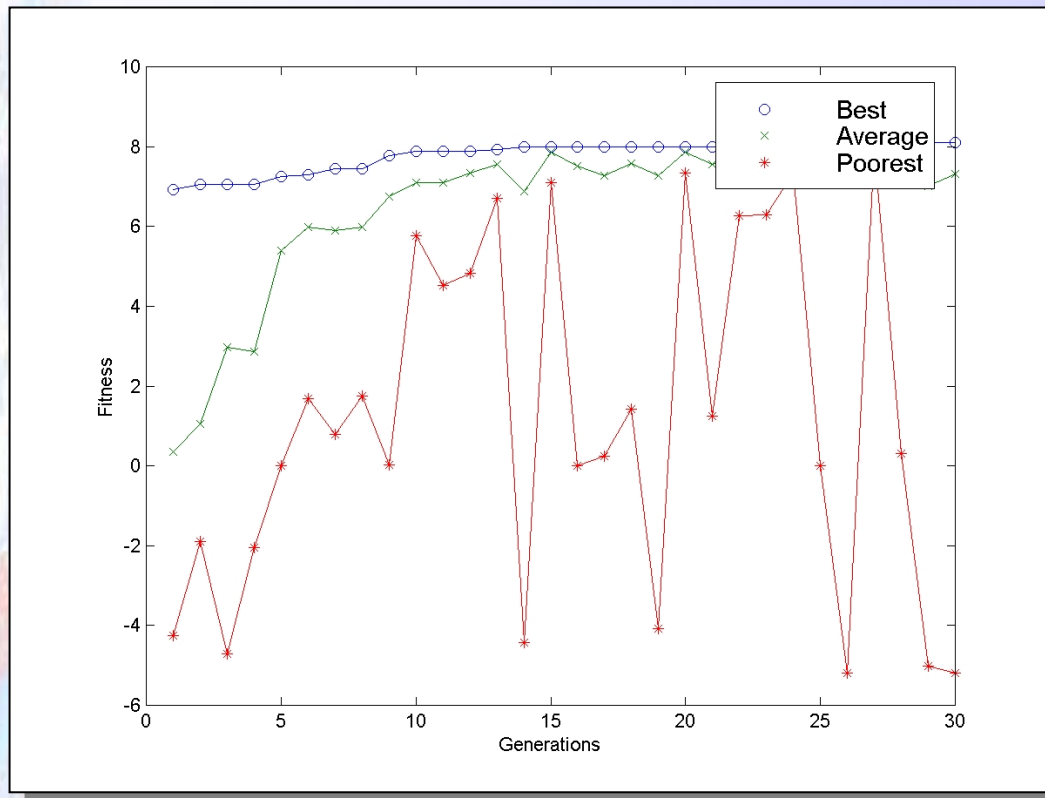
The three steps constitute one iteration



- At each iteration a **complete ensemble** of models are updated at once. No special treatment given to any one. Compare this to Simulated Annealing which repeatedly perturbs a **single model**.
- As iterations continue the average fitness of the population should increase.
- Iterations stop when the average fitness of the population, or the fitness of the best individual has reached an acceptable level.
- Overall the aim is for the three processes to combine to produce a self-adaptive search process.

Example: Genetic algorithms

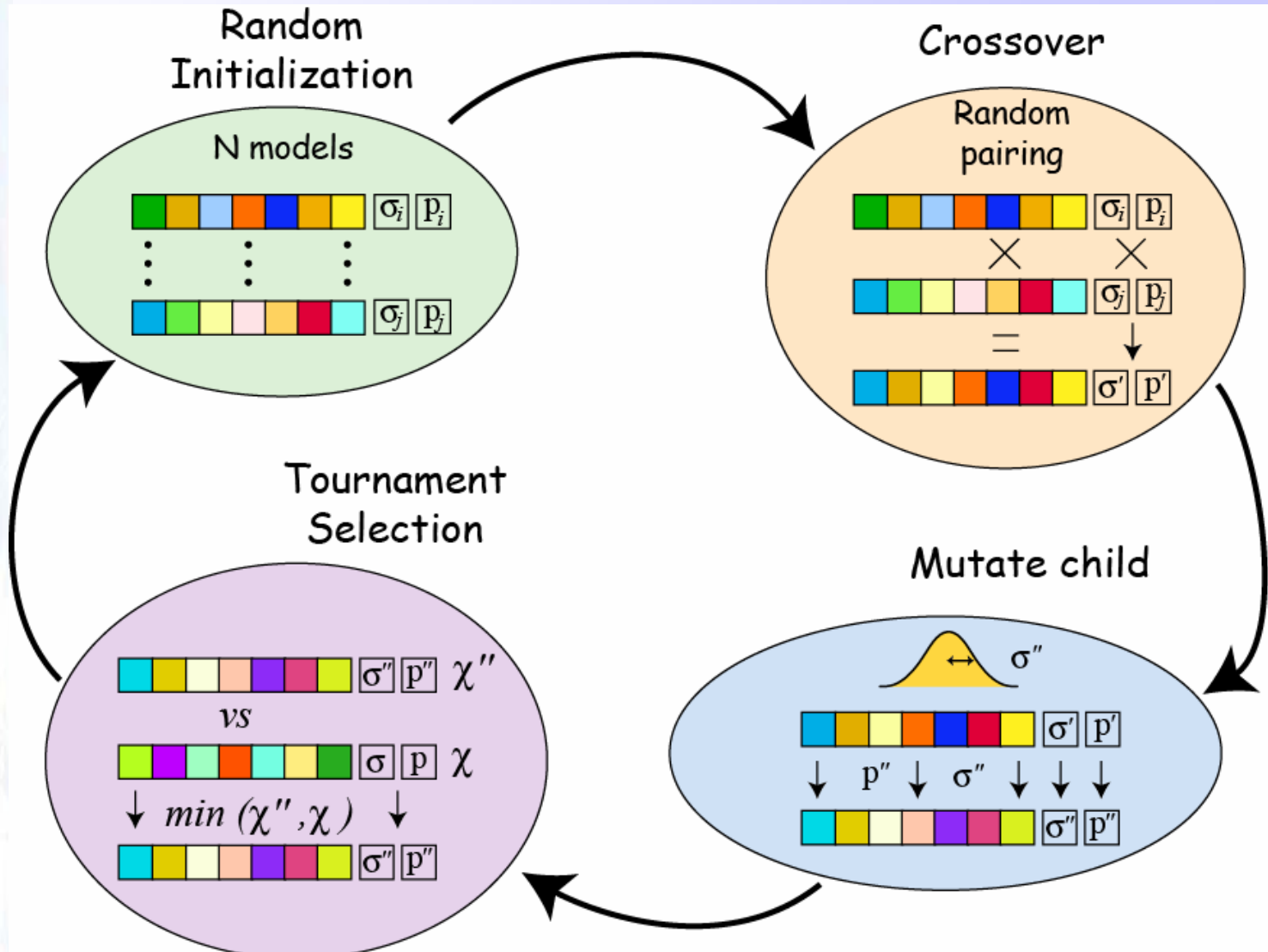
In a GA the average fitness should increase over time.



Example showing a GA operating on the peaks function above

In a GA the average fitness should increase over time.

Genetic algorithms: Ranking and Self-tuning





Genetic algorithms: features

- An ensemble based direct search method for optimization.
- Specific choices that need to be made:
 - How to encode the model parameters into a suitable (bit) string.
 - How to map data misfit into probability of survival (selection step)
 - How to choose the frequency/probability of Crossover and Mutation operators.
- There are many variants of the method each making different choices.
- Active area of research and many applications across a number of fields. Circuit board design, drug design...
- GA are related to the wider field of evolutionary computation → complex systems → emergent behaviour.

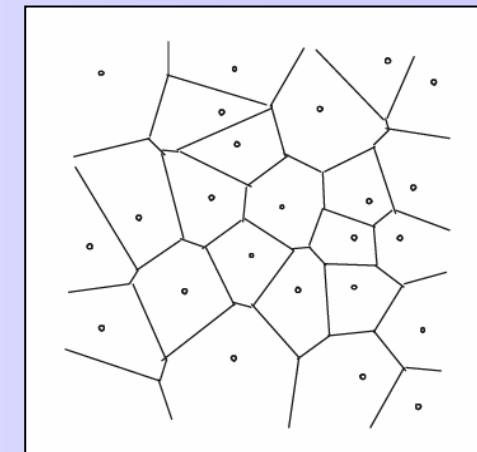
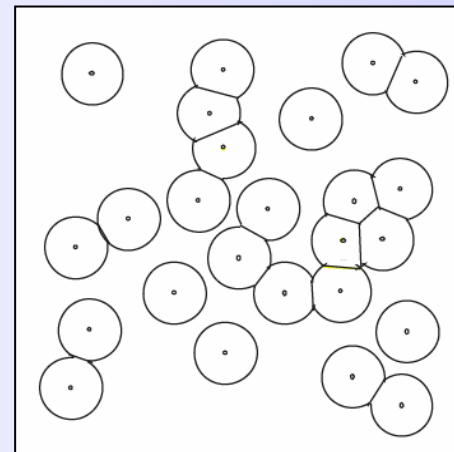
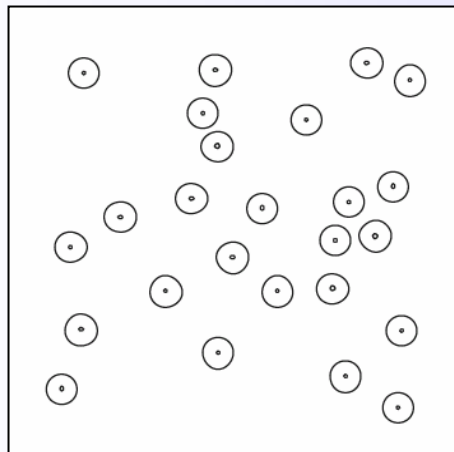
Neighbourhood Algorithm

The Neighbourhood Algorithm was designed as an ensemble based procedure to search multi-dimensional parameter spaces. The intent was to have as few parameters as needed to achieve a self adaptive search.

NA is motivated by simple **geometrical concepts**.

NA is based on a partition of the model space into neighbourhoods about any set of samples.

How do we define neighbourhoods ?

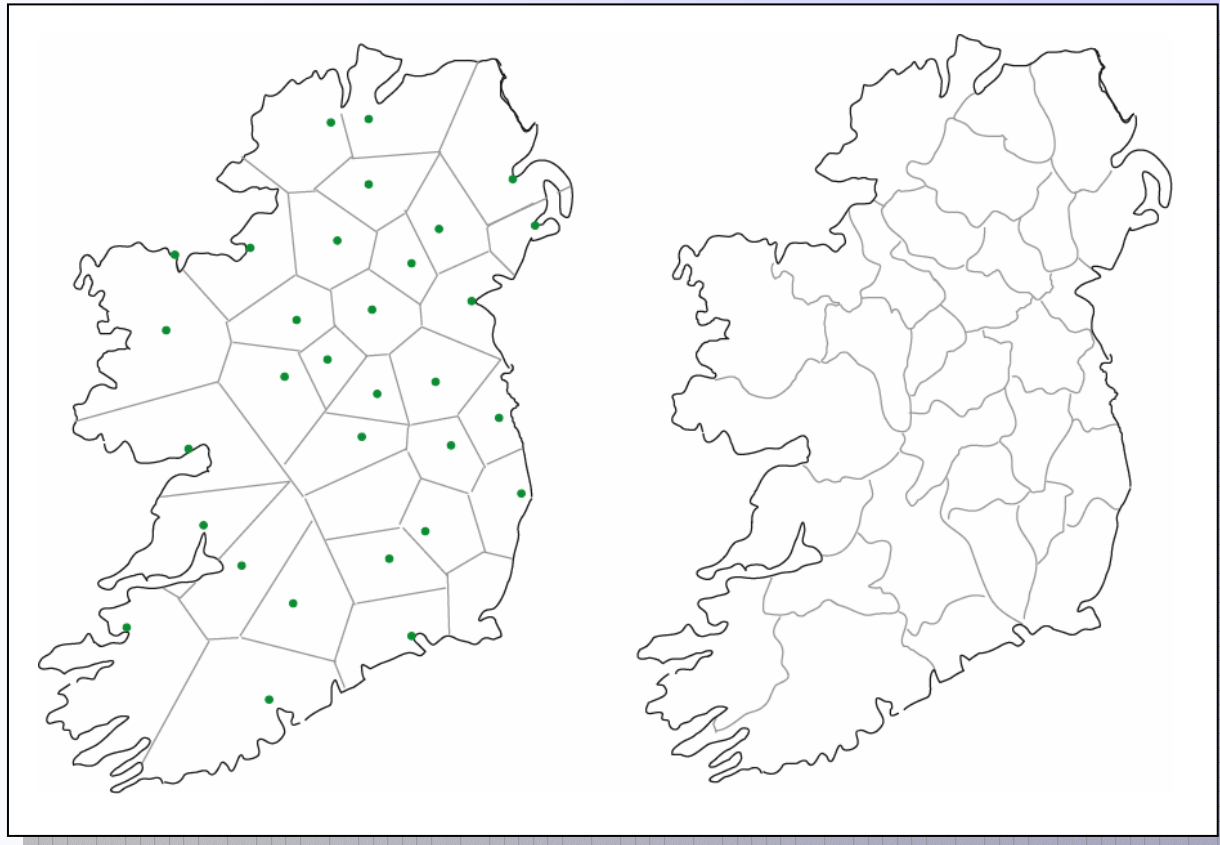


Growing Voronoi cells using Euclidean distance

Sambridge (1999)

Real world Voronoi cells

Voronoi cells appear in many parts of the natural world since they arise out of isotropic processes



From Okabe et al. (1995) after Cox and Agnew (1976)

Parameter search: Neighbourhood algorithm

The neighbourhood algorithm uses uniform random walks that adapt to the information contained in previous sampling.

NA explained using an illustration with three blind mice.

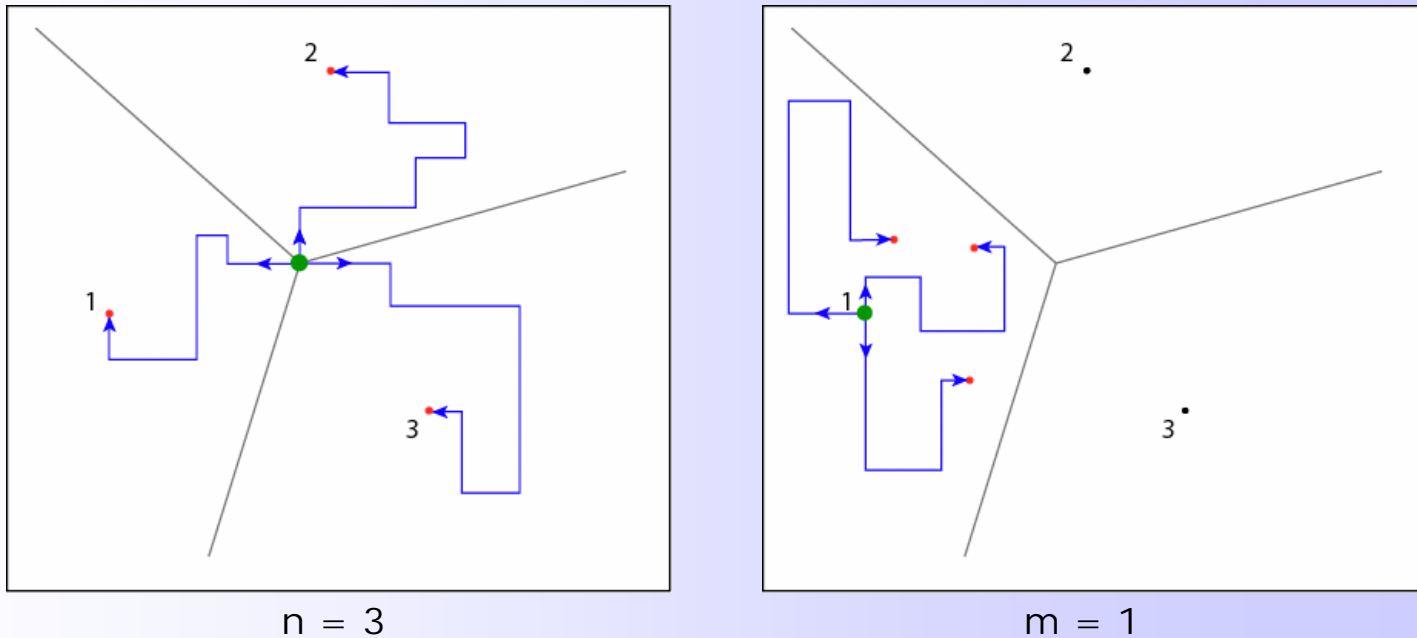


See how they run... (or walk randomly)



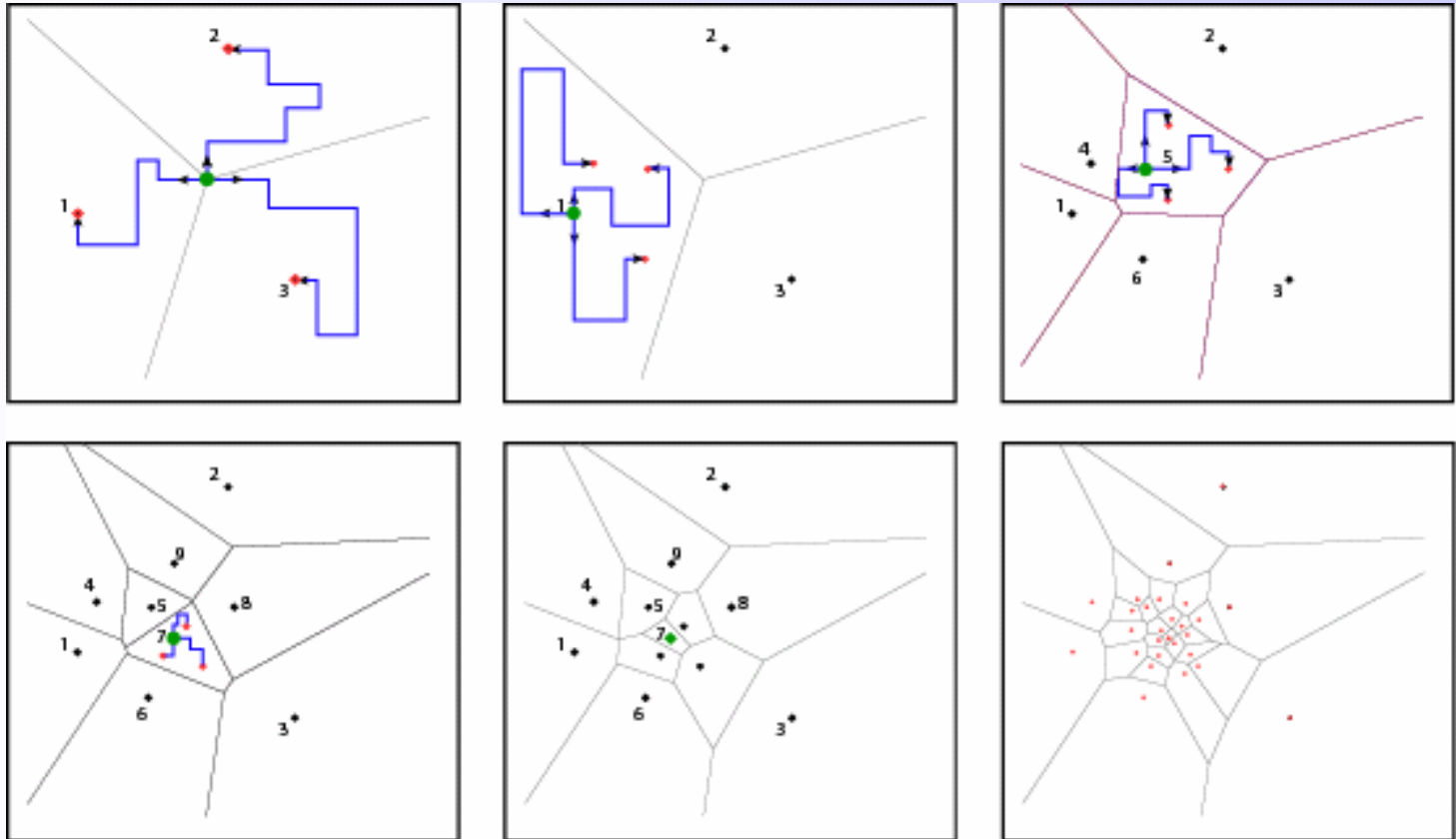
Parameter search: Neighbourhood algorithm

A conceptually simple methods for adaptive sampling of multi-dimensional parameter spaces.



1. Take n random walks to arrival at n new positions
2. Define Voronoi (nearest neighbour cells) between the n points
3. Resample the best m ranked neighbourhoods,
as determined by data misfit, $\phi(m)$

Parameter search: Neighbourhood algorithm



Repeat the process iteratively each time updating the Voronoi cells and generating n samples from a random walk inside m neighbourhoods.

Parameter search: Neighbourhood algorithm

How is it implemented ?

- Uniform random walk inside i-th cell starting at model m_i

$$\sigma(m) = \begin{cases} 1/V_i & : \text{if } m \text{ inside cell } i \\ 0 & : \text{otherwise} \end{cases}$$

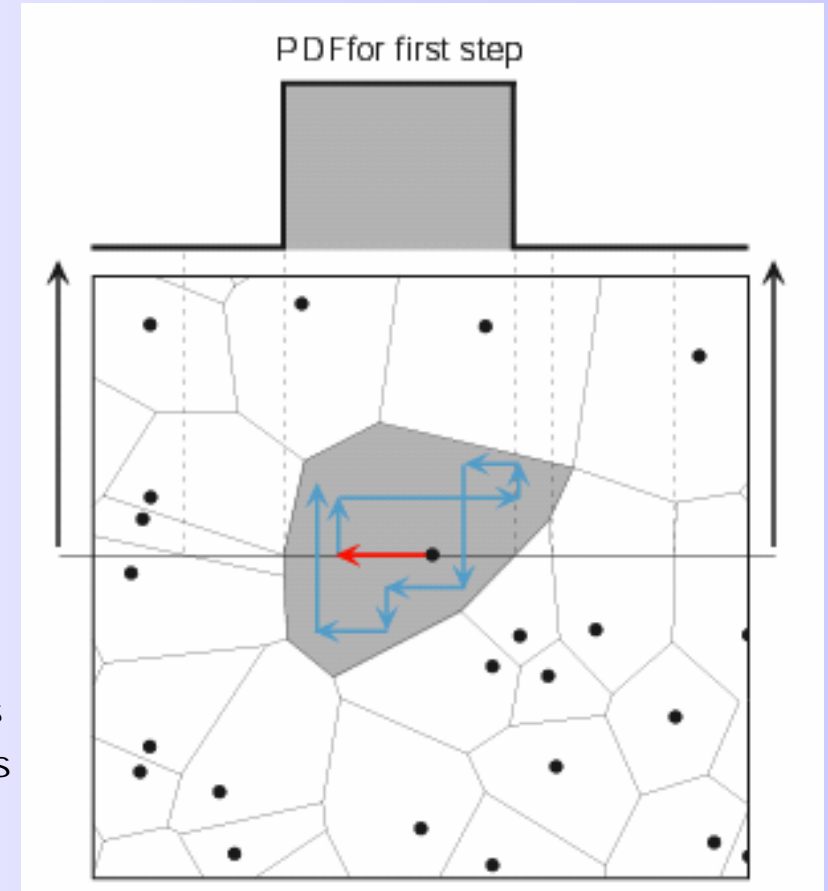
- First we sample from the conditional PDF along the x_1 axis

→ update the model along x_1

- The repeat for x_2 axis

→ update the model along x_2

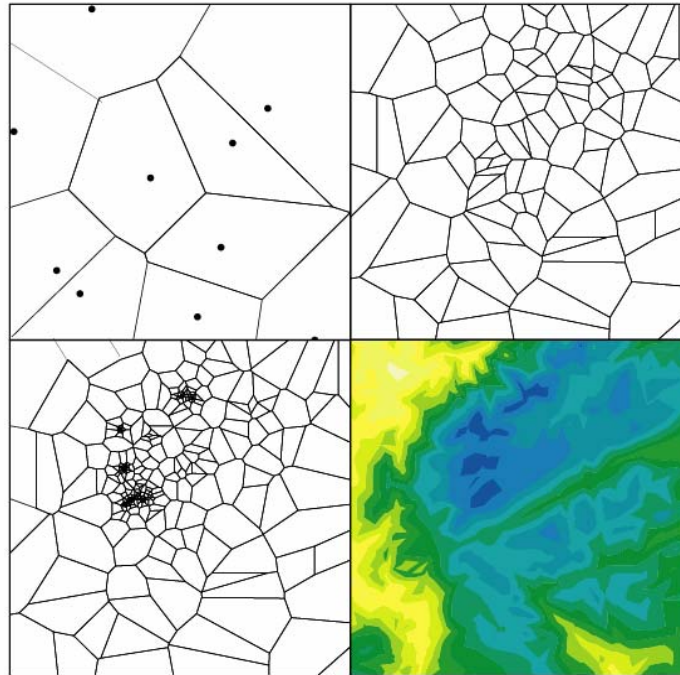
This process is repeated for each axis in rotation and the random walk maps out uniform samples inside the irregular polygon.



Must solve for the intersection points between the 1-D axis and the edge of each Voronoi cell.

Parameter search: Neighbourhood algorithm

This results in a self adapting search process



Behaviour

$$n \geq m$$

As n and m increase the search becomes more explorative

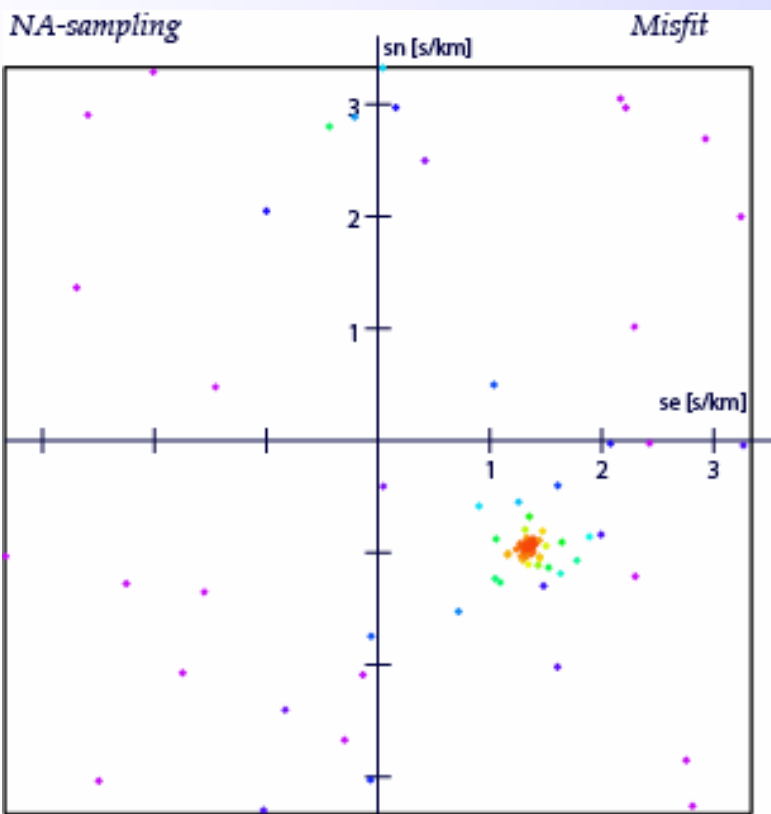
→ converge less quickly

As n and m decrease the search becomes more concentrated

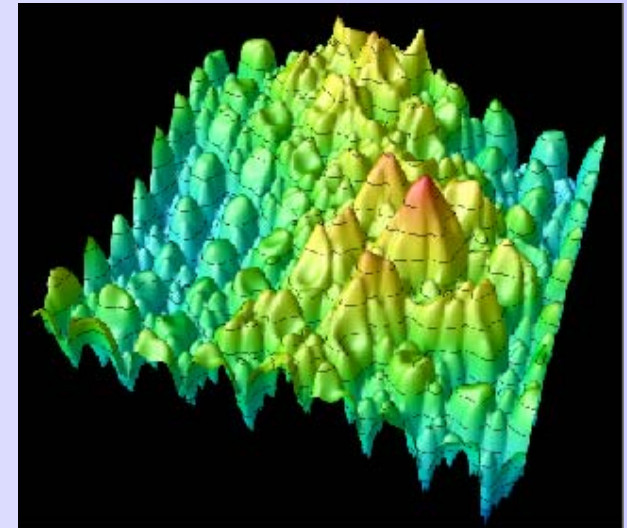
→ converge more quickly
but more likely to local minimum

Repeat the process iteratively each time generating n samples (*uniformly*) inside m previously generated neighbourhoods.

Example: Neighbourhood algorithm



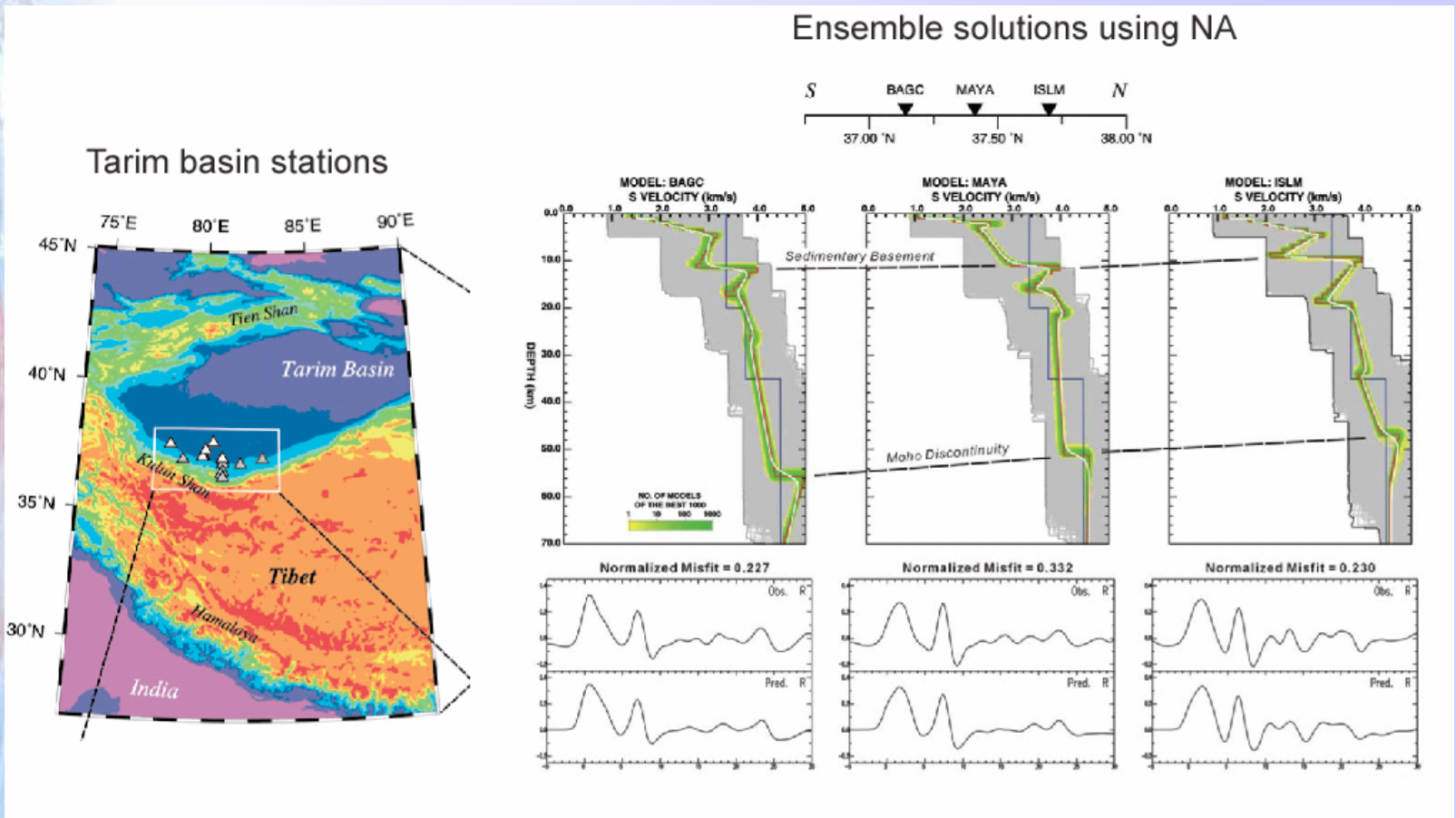
Samples from Neighbourhood algorithm



Infrasound misfit function

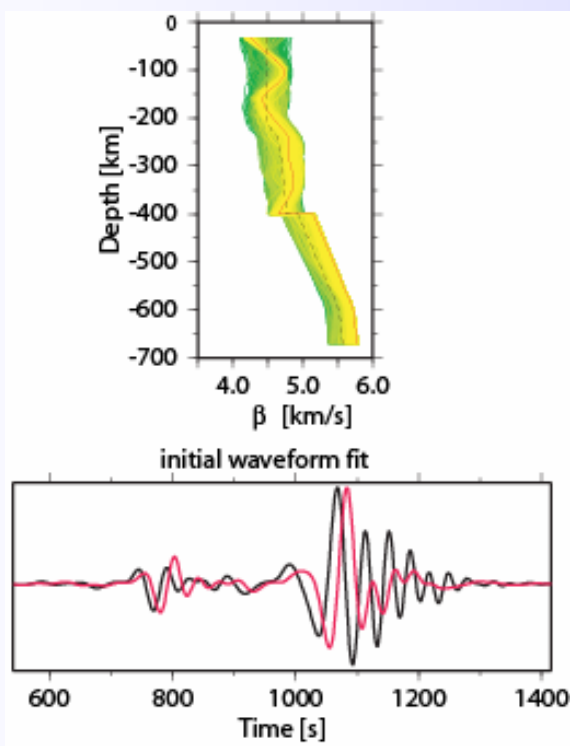
From Kennett et al. (2003)

Examples: Neighbourhood algorithm

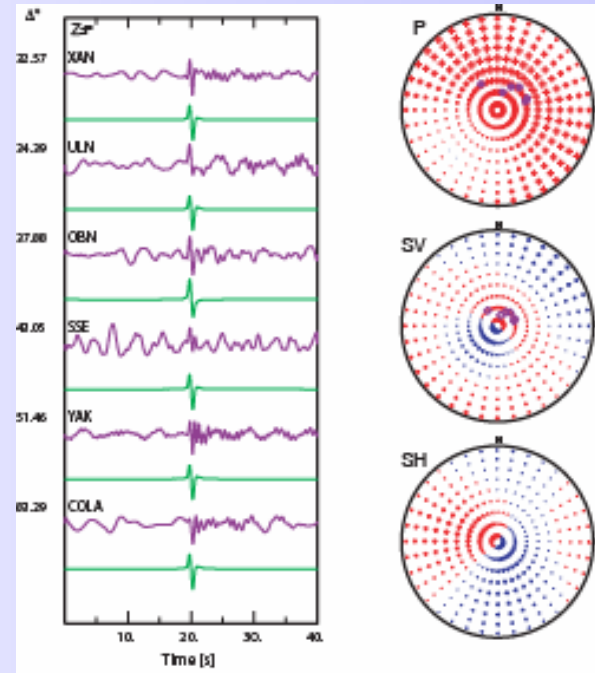


Receiver function waveform fitting for 1-D seismic earth models

Examples: direct search

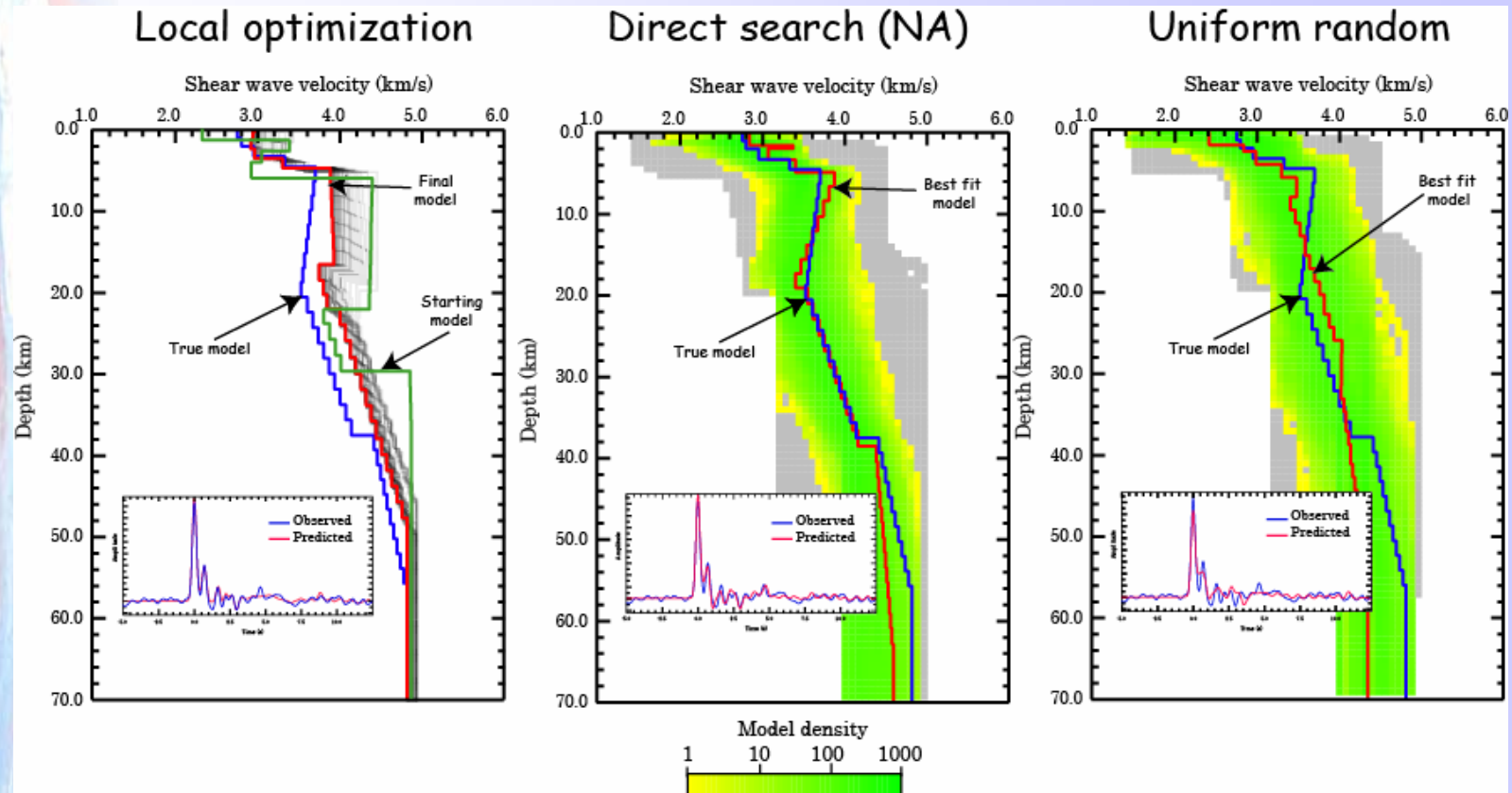


Seismic waveforms
Receiver functions &
Surface waves



Seismic sources
Coupled source moment
tensor & depth location

A comparison of techniques



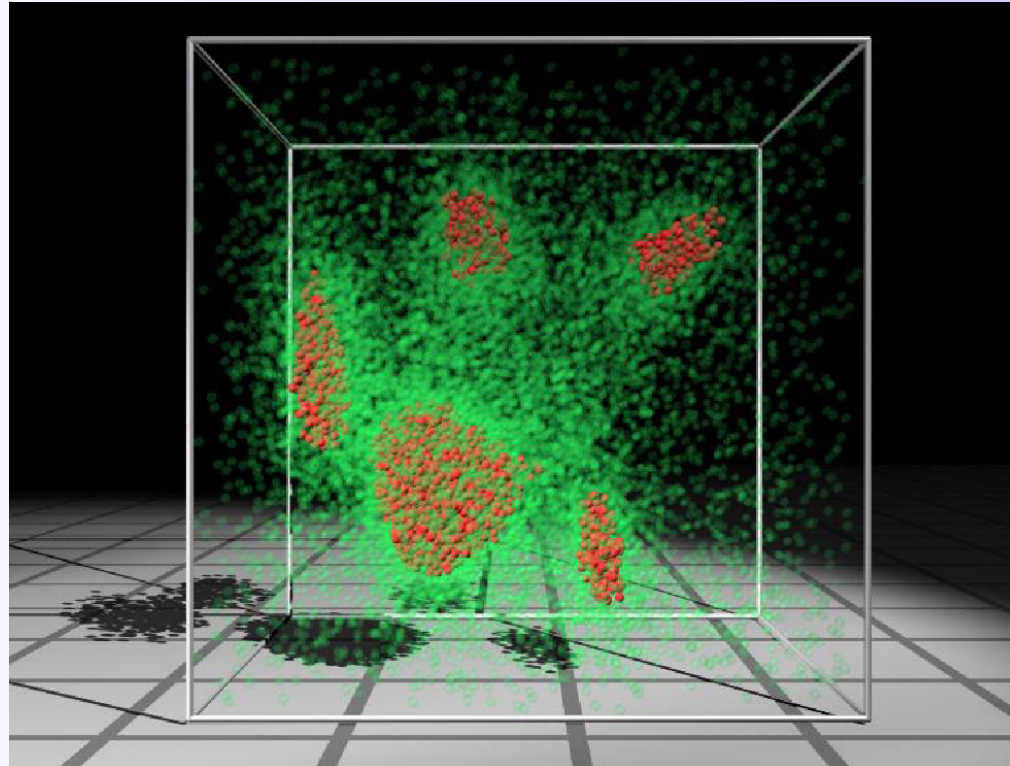


Neighbourhood algorithm

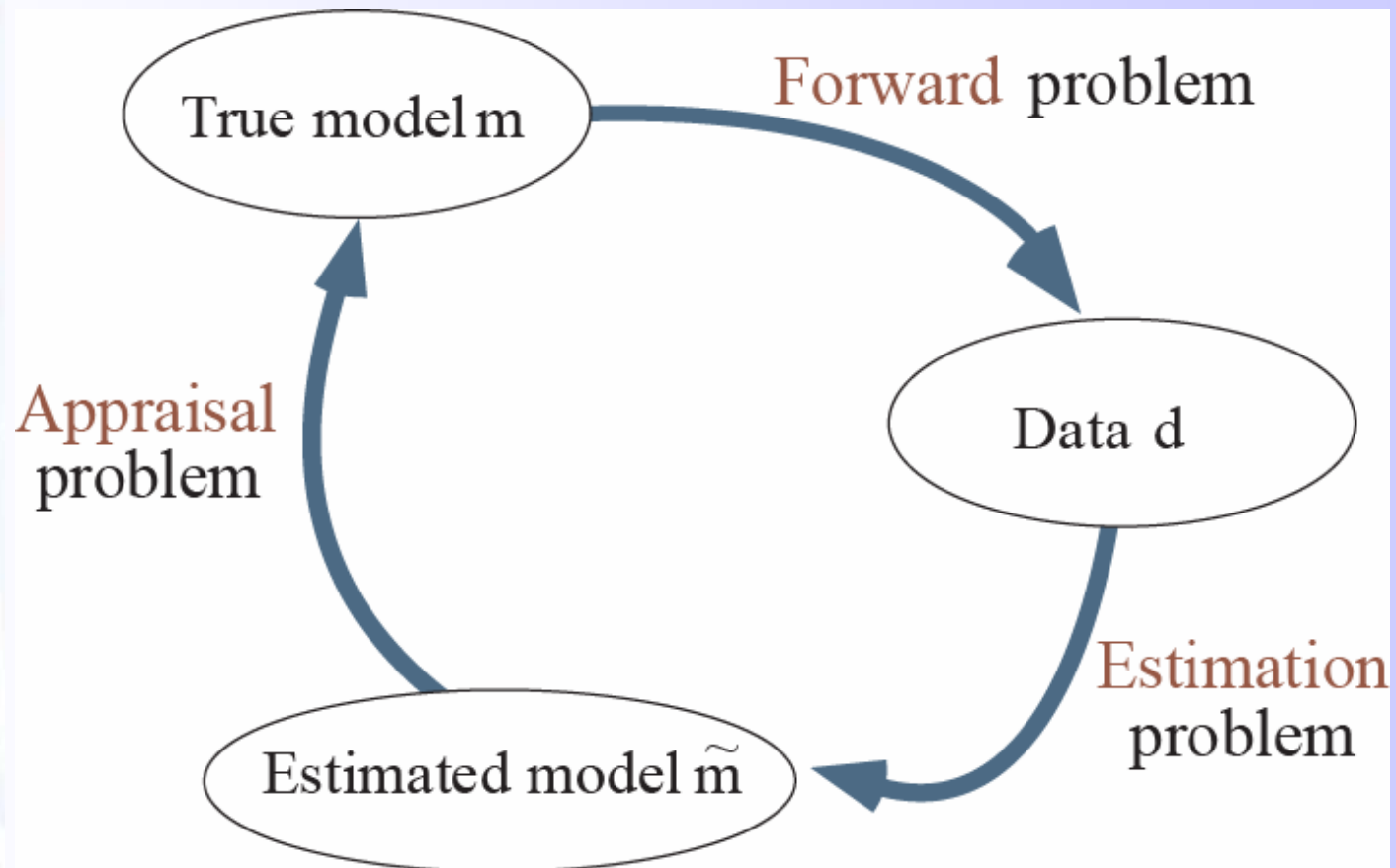
- Self adaptive search controlled by two variables.
- Ensemble based approach. At each stage random walks guided by all previous samples through Voronoi partition.
- Search driven by ranking of models rather than by a particular transformation of objective function.
- Behaviour as a function of variables predictable.



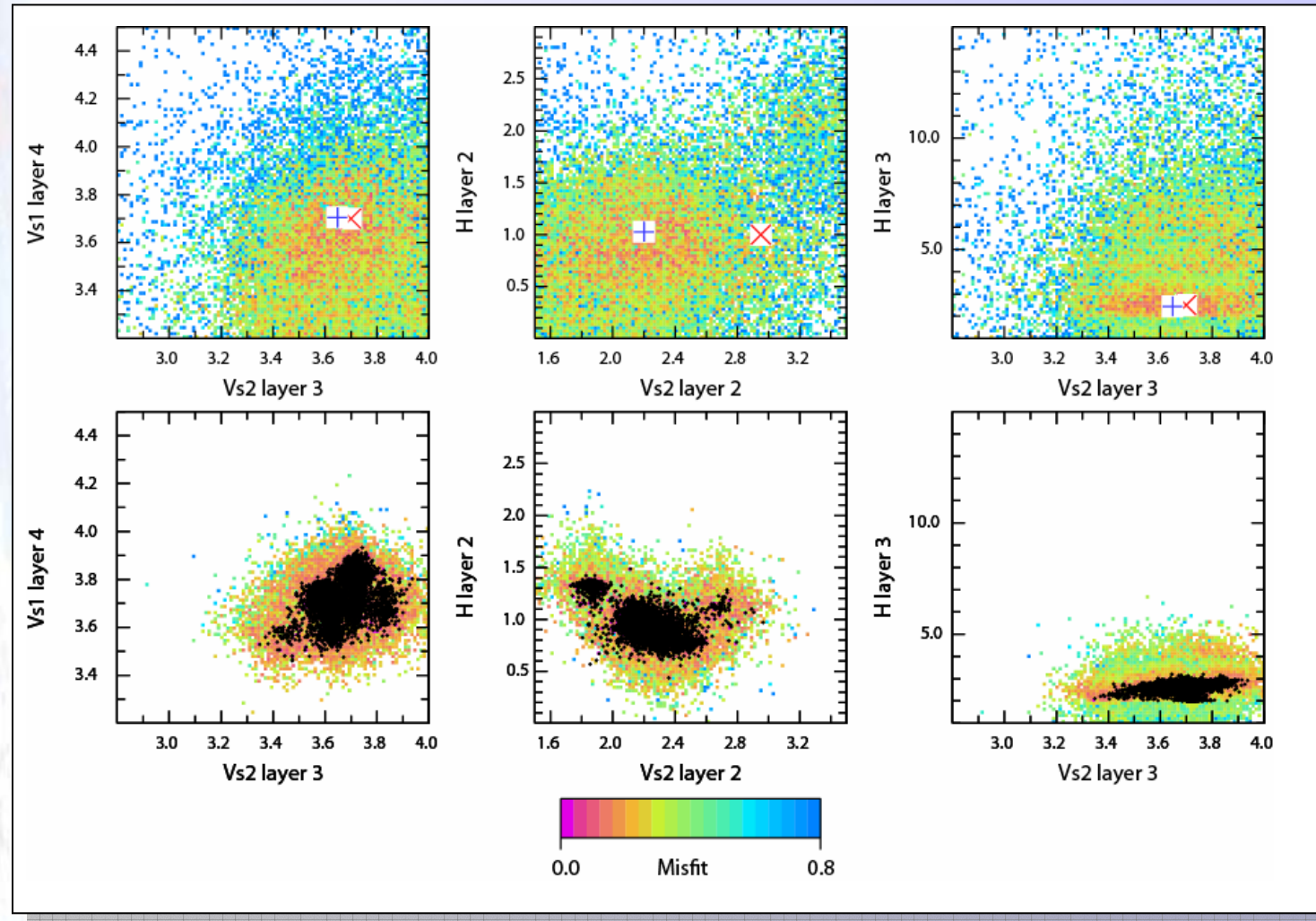
What to do with all the samples generated by a global search algorithm ?



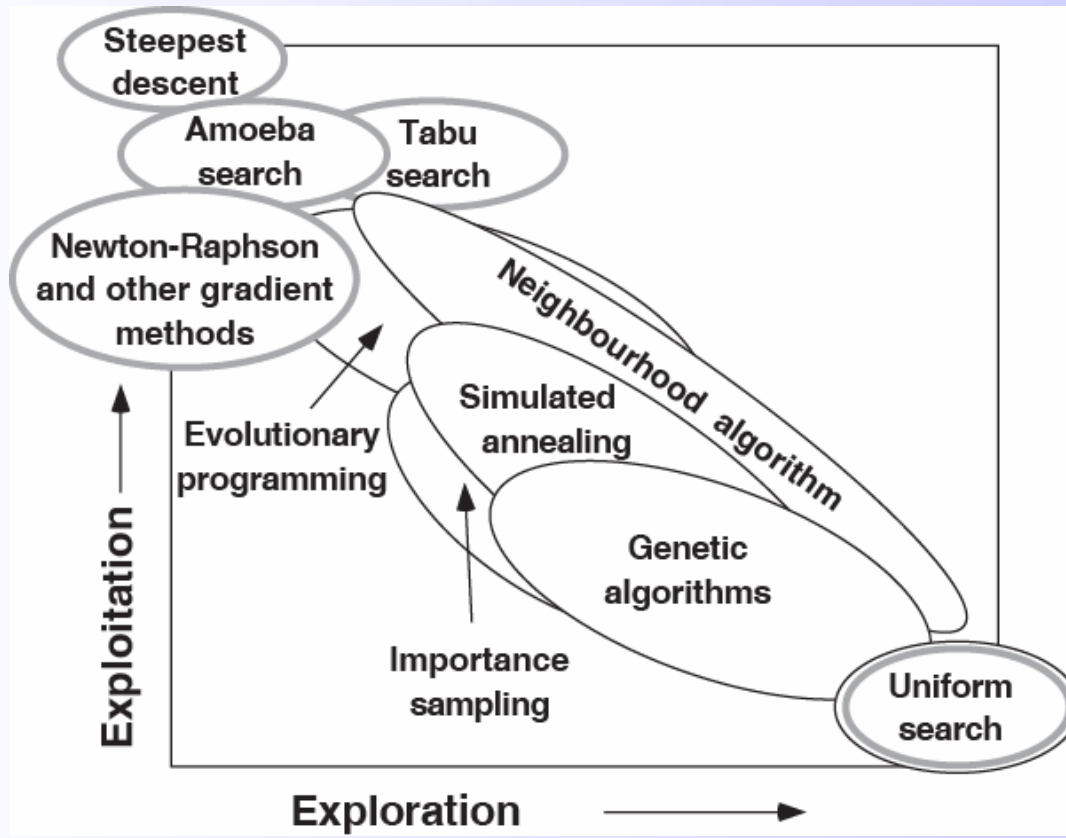
The appraisal problem



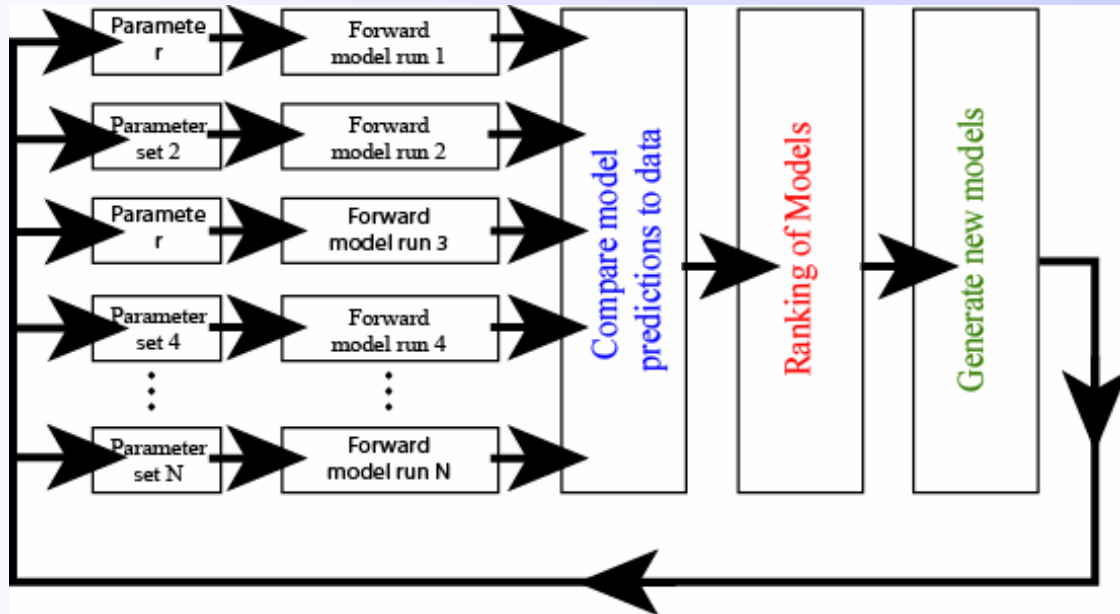
Mapping out the region of acceptable fit



Global search: exploration vs exploitation



Global search: Parallelisation



Ensemble based approaches are ideally suited to parallel computation



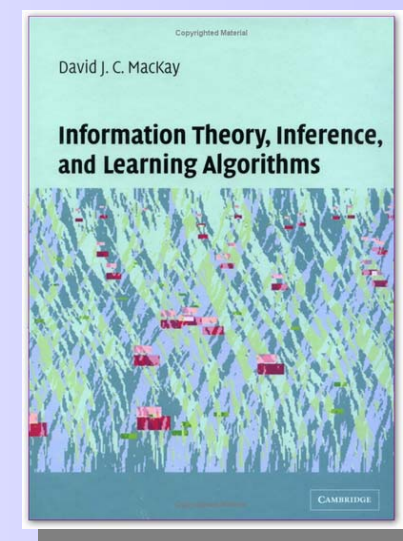
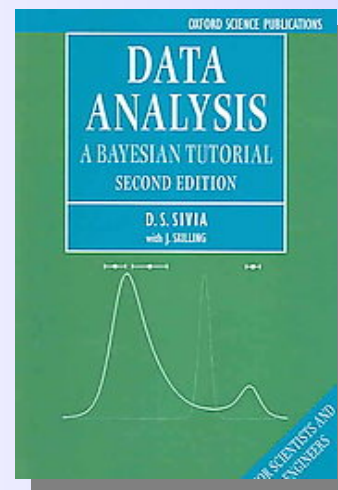
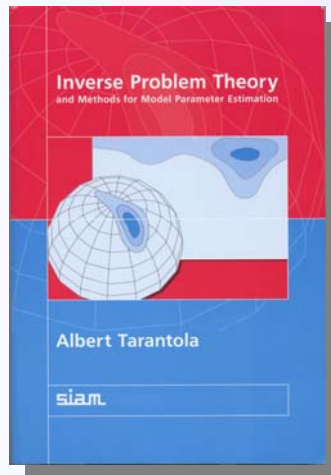


Probabilistic inference

Bayes theorem and all that....

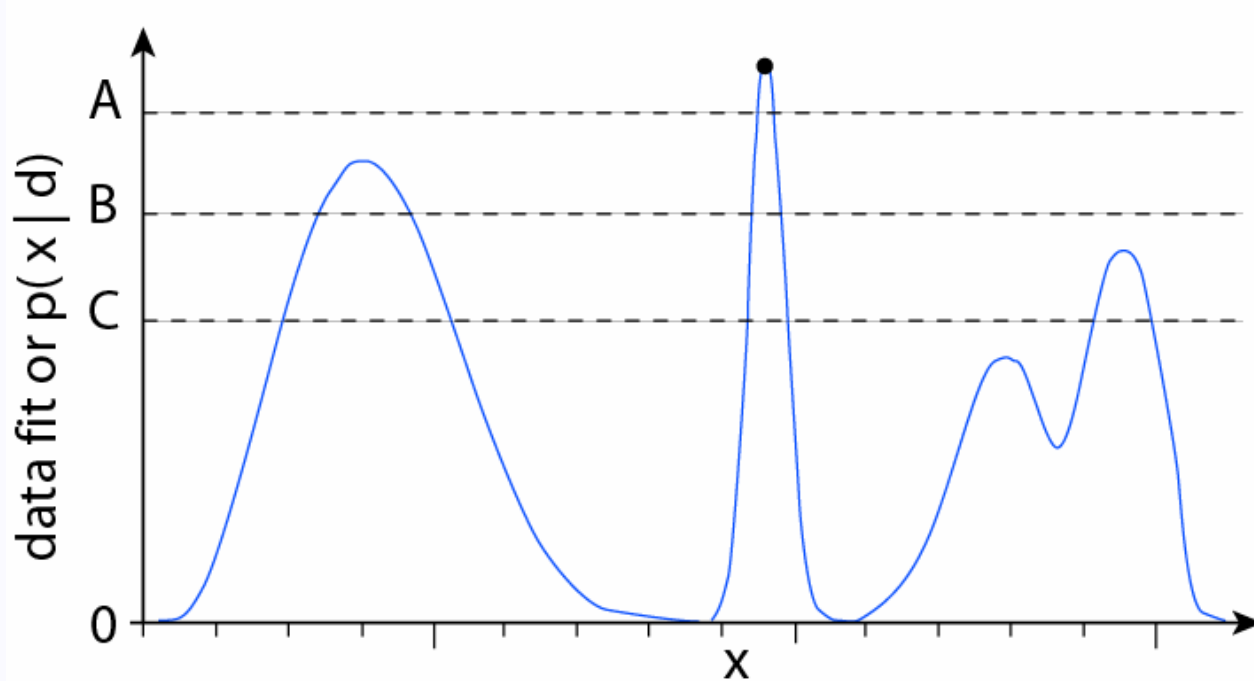


Books



Highly nonlinear inverse problems

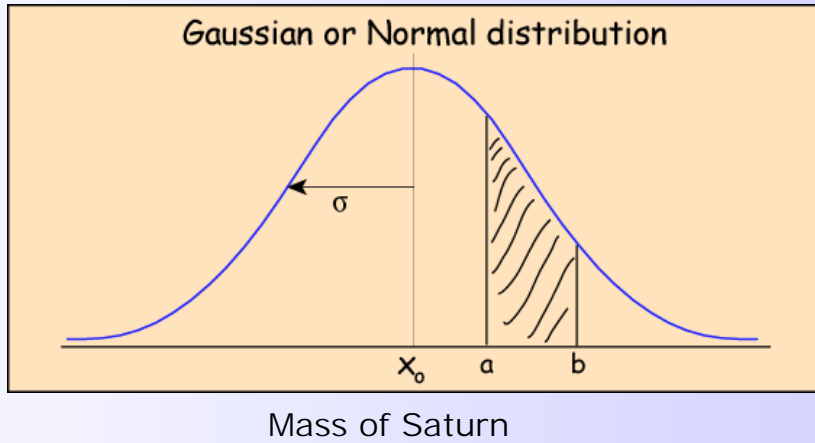
Multi-modal data misfit/objective function



What value is there in an optimal model ?

Probabilistic inference: History

$p(M|data, I)$



$$\int_{-\infty}^{\infty} p(x)dx = 1$$

(Laplace 1812)

$$Pr(x : a \leq x \leq b) = \int_a^b p(x)dx$$

We have already met the concept of using a probability density function $p(x)$ to describe the state of a **random variable**.

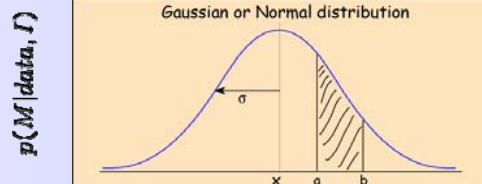
In the probabilistic (or *Bayesian*) approach, **probabilities** are also used to describe **inferences** (or *degrees of belief*) about x even if x itself is not a random variable.



Laplace (1812) rediscovered the work of Bayes (1763), and used it to constrain the mass of Saturn. In 150 years the estimate changed by only 0.63% !

But Laplace died in 1827 and then the arguments started...

Bayesian or Frequentist: the arguments



Mass of Saturn

Some thought that using probabilities to describe degrees of belief was too subjective and so they redefined probability as the *long run relative frequency* of a random event. This became the *Frequentist* approach.

To estimate the mass of Saturn the frequentist has to relate the mass to the data through a *statistic*. Since the data contain 'random' noise probability theory can be applied to the statistic (which becomes the random variable !). This gave birth to the field of statistics !

But how to choose the statistic ?

'.. a plethora of tests and procedures without any clear underlying rationale'
(D. S. Sivia)

'Bayesian is subjective and
requires too many guesses'

A. Frequentist

'Frequentist is subjective, but BI can
solve problems more completely'

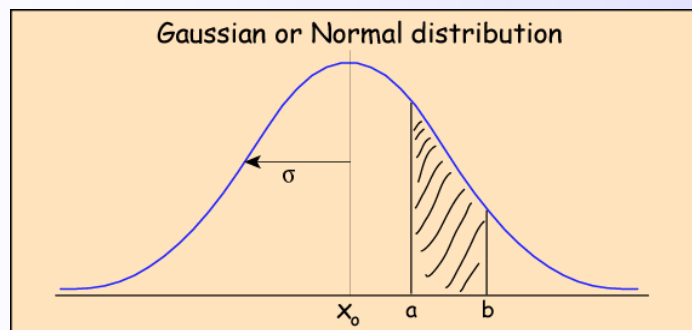
A. Bayesian

For a discussion see Sivia (2005, pp 8-11).

Probability theory: Joint probability density functions

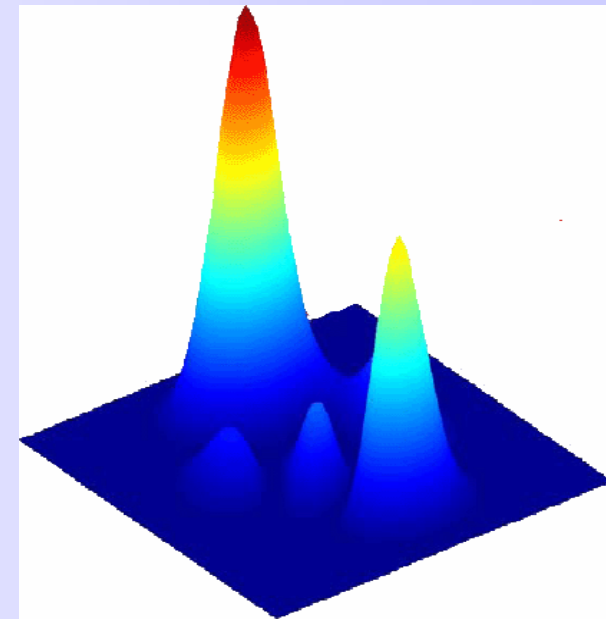
A PDF for variable x

$$p(x)$$



Joint PDF of x and y

$$p(x, y)$$



Probability is proportional to
area under the curve or surface

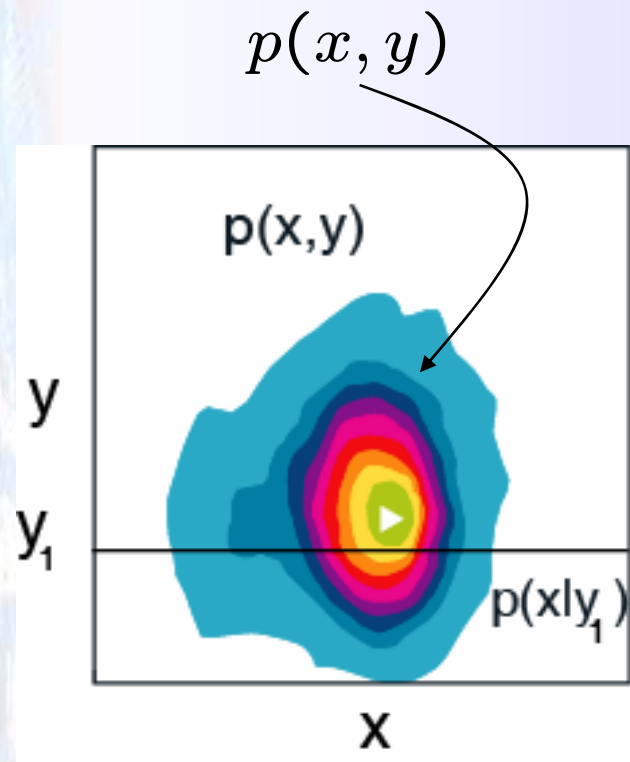
If x and y are independent their joint PDF is separable

$$p(x, y) = p(x) \times p(y)$$

Probability theory: Conditional probability density functions

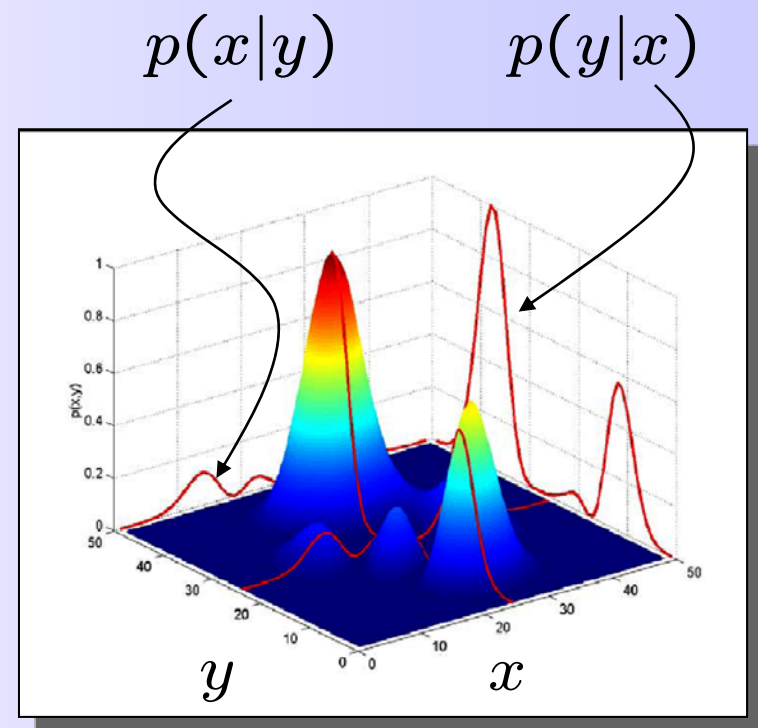
Joint PDF of x and y

"The PDF of x and y taken together"



Conditional PDFs

"The PDF of x given a value for y "

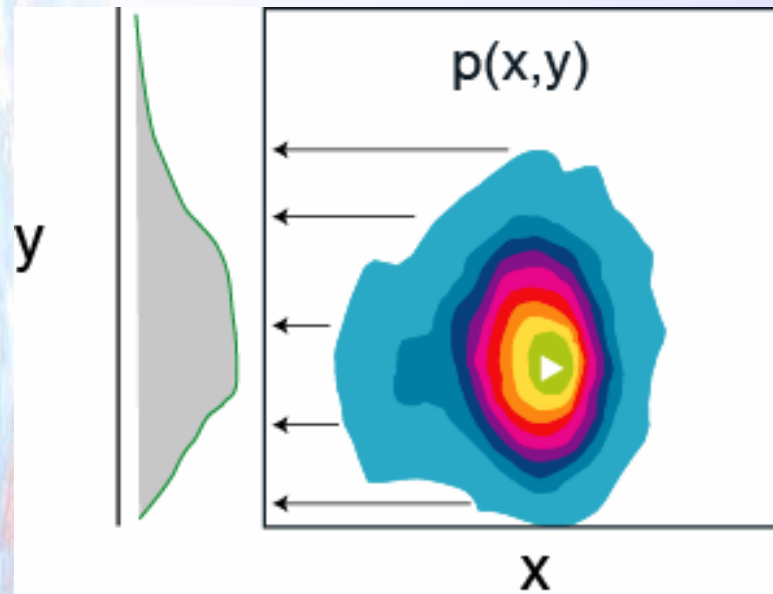


Relationship between joint and conditional PDFs

$$p(x, y) = p(x|y) \times p(y)$$

Probability theory: Marginal probability density functions

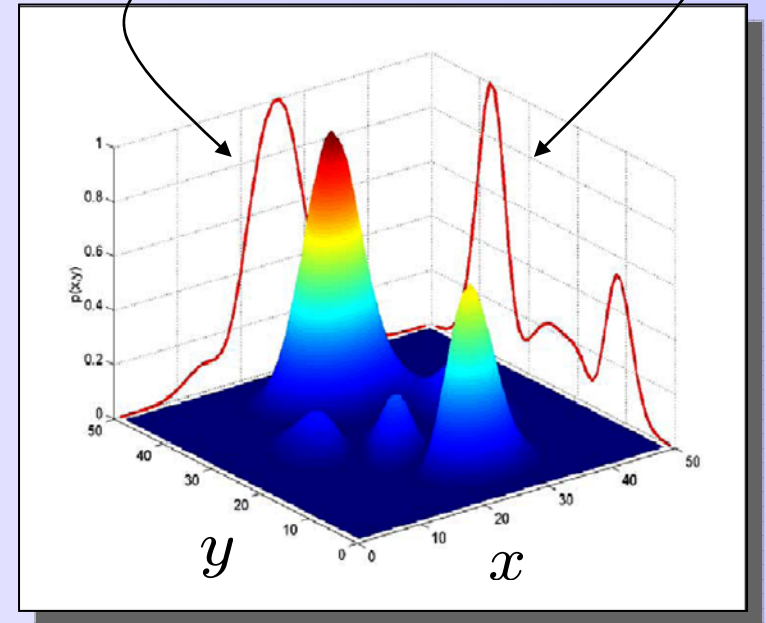
A marginal PDF is a summation of probabilities



Marginal PDFs

$$p(y) = \int p(x, y) dx$$

$$p(x) = \int p(x, y) dy$$

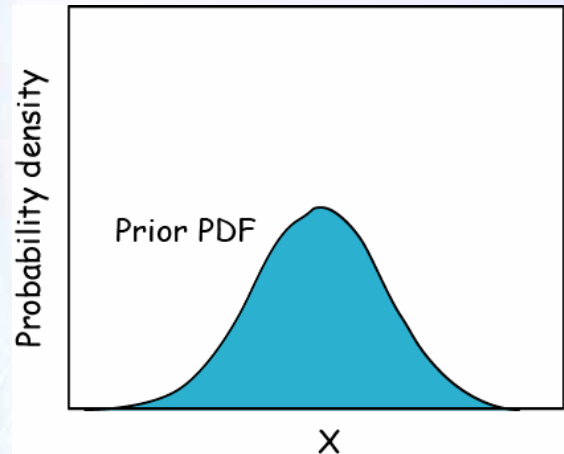


Relationship between joint, conditional and marginal PDFs

$$p(x, y) = p(x|y) \times p(y)$$

Prior probability density functions

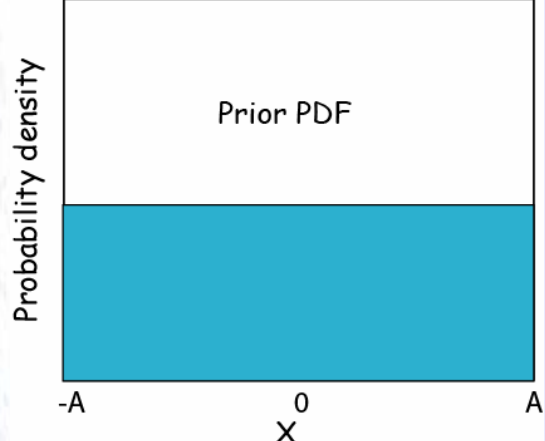
What we know from previous experiments, or what we guess...



$$p(x) = k \exp \left\{ -\frac{(x - x_o)^2}{2\sigma^2} \right\}$$

$$p(\mathbf{m}) = k \exp \left\{ -\frac{1}{2}(\mathbf{m} - \mathbf{m}_o)^T C_m^{-1} (\mathbf{m} - \mathbf{m}_o) \right\}$$

Beware: there is no such thing as a non-informative prior

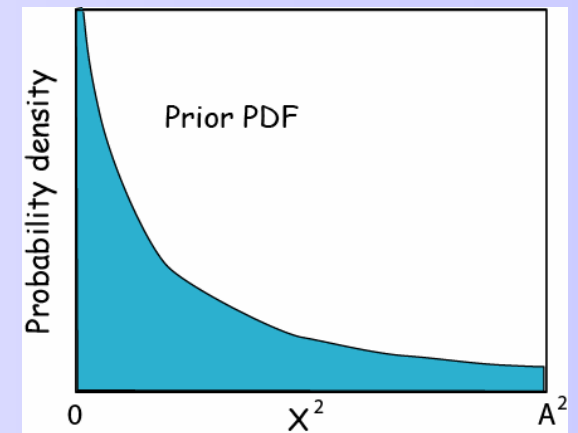


$$p(x)dx = p(y)dy$$

$$p(y) = p(x) \frac{dx}{dy}$$

$$p(x) = C$$

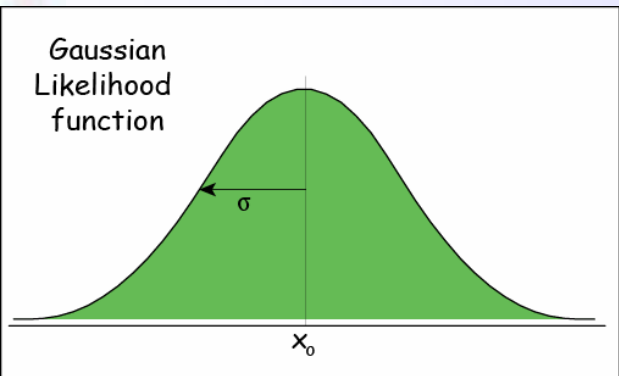
$$p(x^2) = \frac{C}{2x}$$



As $A \rightarrow \infty$ this is not proper !

Likelihood functions

The likelihood that the data would have occurred for a given model



$$p(d_i|x) = \exp \left\{ -\frac{(x - x_{o,i})^2}{2\sigma_i^2} \right\}$$

$$p(\mathbf{d}|\mathbf{m}) = \exp \left\{ -\frac{1}{2}(\mathbf{d} - G\mathbf{m})^T C_D^{-1}(\mathbf{d} - G\mathbf{m}) \right\}$$

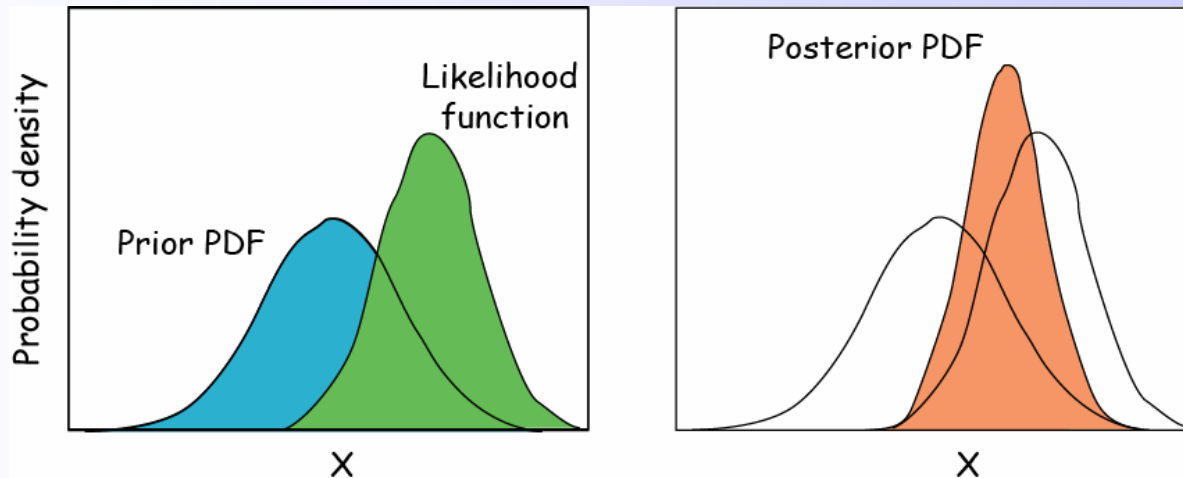
Maximizing likelihoods is what Frequentists do. It is what we did earlier.

$$\begin{aligned} \max_{\mathbf{m}} p(\mathbf{d}|\mathbf{m}) &= \min_{\mathbf{m}} -\ln(p(\mathbf{d}|\mathbf{m})) \\ &= \min_{\mathbf{m}} (\mathbf{d} - G\mathbf{m})^T C_D^{-1}(\mathbf{d} - G\mathbf{m}) \end{aligned}$$

Maximizing the likelihood = minimizing the data prediction error

Bayes' theorem

All information is expressed in terms of probability density functions



Bayes' rule (1763)

$$p(m|d, I) \propto p(d|m, I) \times p(m|I)$$

Conditional PDFs

Assumptions

data

model parameters

Posterior probability density \propto Likelihood \times Prior probability density



1702-1761

*What is known after
the data are collected*

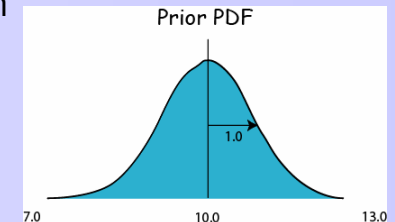
*Measuring fit
to data*

*What is known before
the data are collected*

Example: Measuring the mass of an object

If we have an object whose mass, m , we wish to determine. Before we collect any data we believe that its mass is approximately $10.0 \pm 1\mu\text{g}$. In probabilistic terms we could represent this as a Gaussian prior distribution

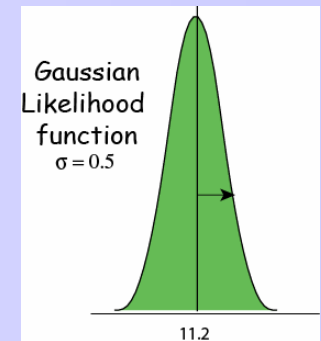
$$\text{prior} \curvearrowright p(m) = \frac{1}{\sqrt{2\pi}} e^{-\frac{1}{2}(m-10.0)^2}$$



Suppose a measurement is taken and a value $11.2 \mu\text{g}$ is obtained, and the measuring device is believed to give Gaussian errors with mean 0 and $\sigma = 0.5 \mu\text{g}$. Then the likelihood function can be written

$$p(d|m) = \frac{1}{0.5\sqrt{2\pi}} e^{-2(m-11.2)^2} \curvearrowleft \text{Likelihood}$$

$$p(m|d) = \frac{1}{\pi} e^{-\frac{1}{2}(m-10.0)^2 - 2(m-11.2)^2} \curvearrowleft \text{Posterior}$$

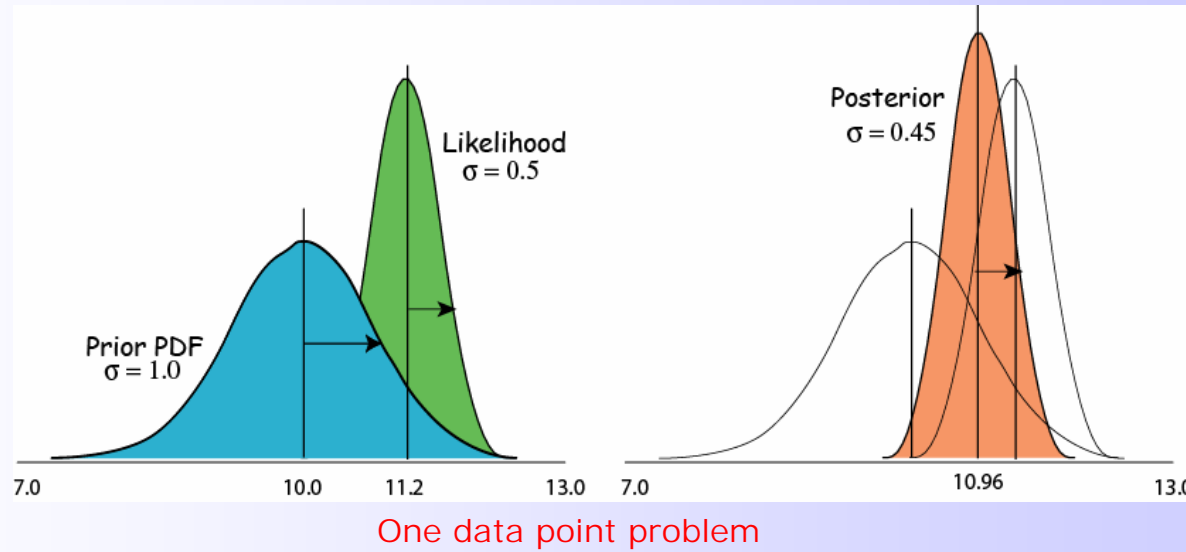


$$p(m|d) \propto e^{\frac{-\frac{1}{2}(m-10.96)^2}{1/5}}$$

The posterior PDF becomes a Gaussian centred at the value of $10.96 \mu\text{g}$ with standard deviation $\sigma = (1/5)^{1/2} \approx 0.45$.

Example: Measuring the mass of an object

The more accurate new data has changed the estimate of m and decreased its uncertainty



For the general linear inverse problem we would have

Prior:
$$p(\mathbf{m}) \propto \exp \left\{ -\frac{1}{2} (\mathbf{m} - \mathbf{m}_o)^T C_m^{-1} (\mathbf{m} - \mathbf{m}_o) \right\}$$

Likelihood:
$$p(\mathbf{d}|\mathbf{m}) \propto \exp \left\{ -\frac{1}{2} (\mathbf{d} - G\mathbf{m})^T C_d^{-1} (\mathbf{d} - G\mathbf{m}) \right\}$$

Posterior PDF

$$\propto \exp \left\{ -\frac{1}{2} [(\mathbf{d} - G\mathbf{m})^T C_d^{-1} (\mathbf{d} - G\mathbf{m}) + (\mathbf{m} - \mathbf{m}_o)^T C_m^{-1} (\mathbf{m} - \mathbf{m}_o)] \right\}$$

The biased coin problem



Suppose we have a suspicious coin and we want to know if it is biased or not ?

Let α be the probability that we get a head.

$$0 \leq \alpha \leq 1$$

$\alpha = 1$: means we always get a head.

$\alpha = 0$: means we always get a tail.

$\alpha = 0.5$: means equal likelihood of head or tail.

We can collect data by tossing the coin many times

$$\{H, T, T, H, \dots\}$$



We seek a probability density function for α given the data

$$p(\alpha | \mathbf{d}, I) \propto p(\mathbf{d} | \alpha, I) \times p(\alpha | I)$$

Posterior PDF \propto Likelihood x Prior PDF

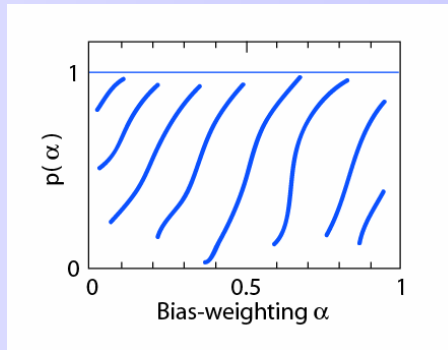


The biased coin problem

What is the **prior PDF** for α ?

Let us assume that it is uniform

$$p(\alpha|I) = 1, \quad 0 \leq \alpha \leq 1$$



What is the **Likelihood function** ?

The probability of observing R heads out of N coin tosses is

$$p(\mathbf{d}|\alpha, I) \propto \alpha^R (1 - \alpha)^{N-R}$$



$$p(\alpha|\mathbf{d}, I) \propto p(\mathbf{d}|\alpha, I) \times p(\alpha|I)$$

Posterior PDF \propto Likelihood \times Prior PDF

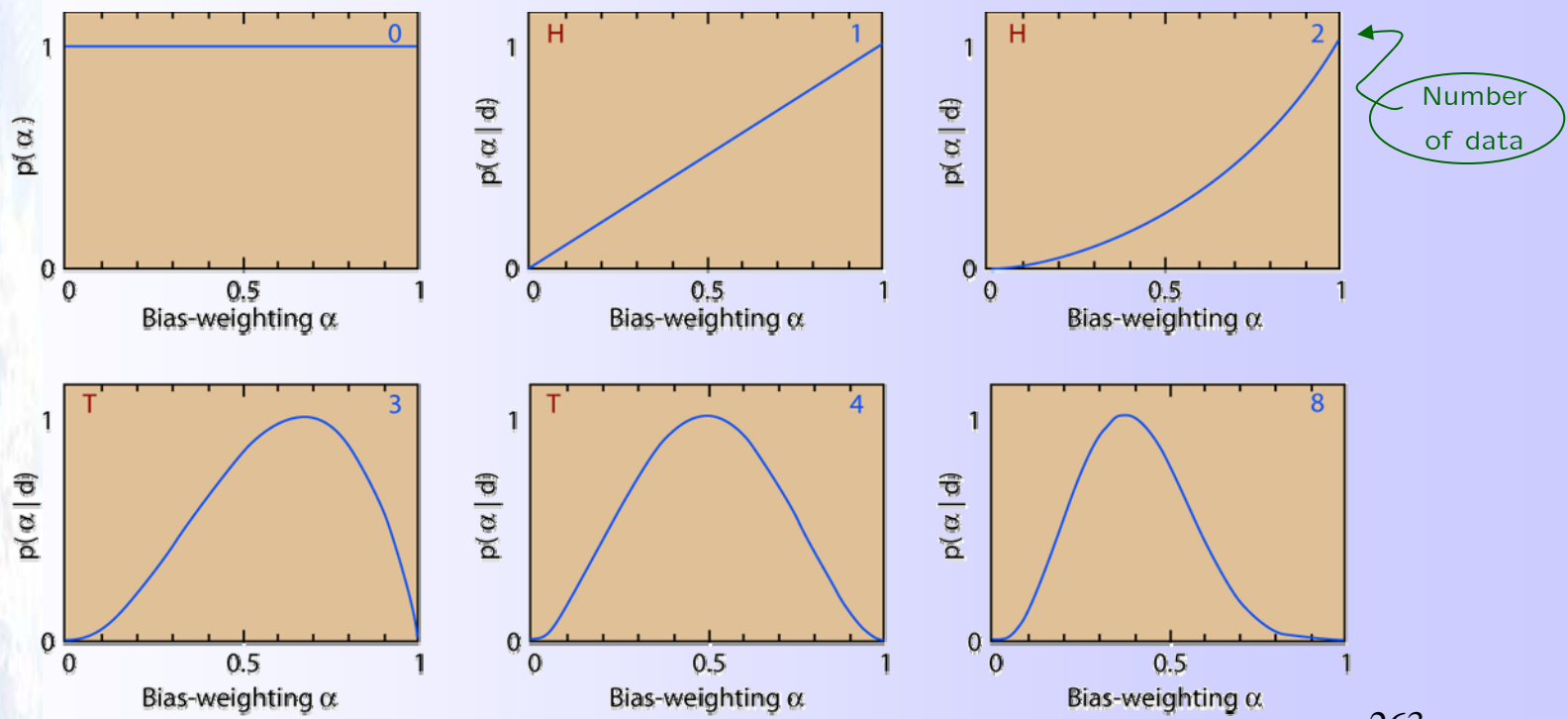


The biased coin problem

We have the posterior PDF for α given the data and our prior PDF

$$p(\alpha | \mathbf{d}, I) \propto \alpha^R (1 - \alpha)^{N-R}$$

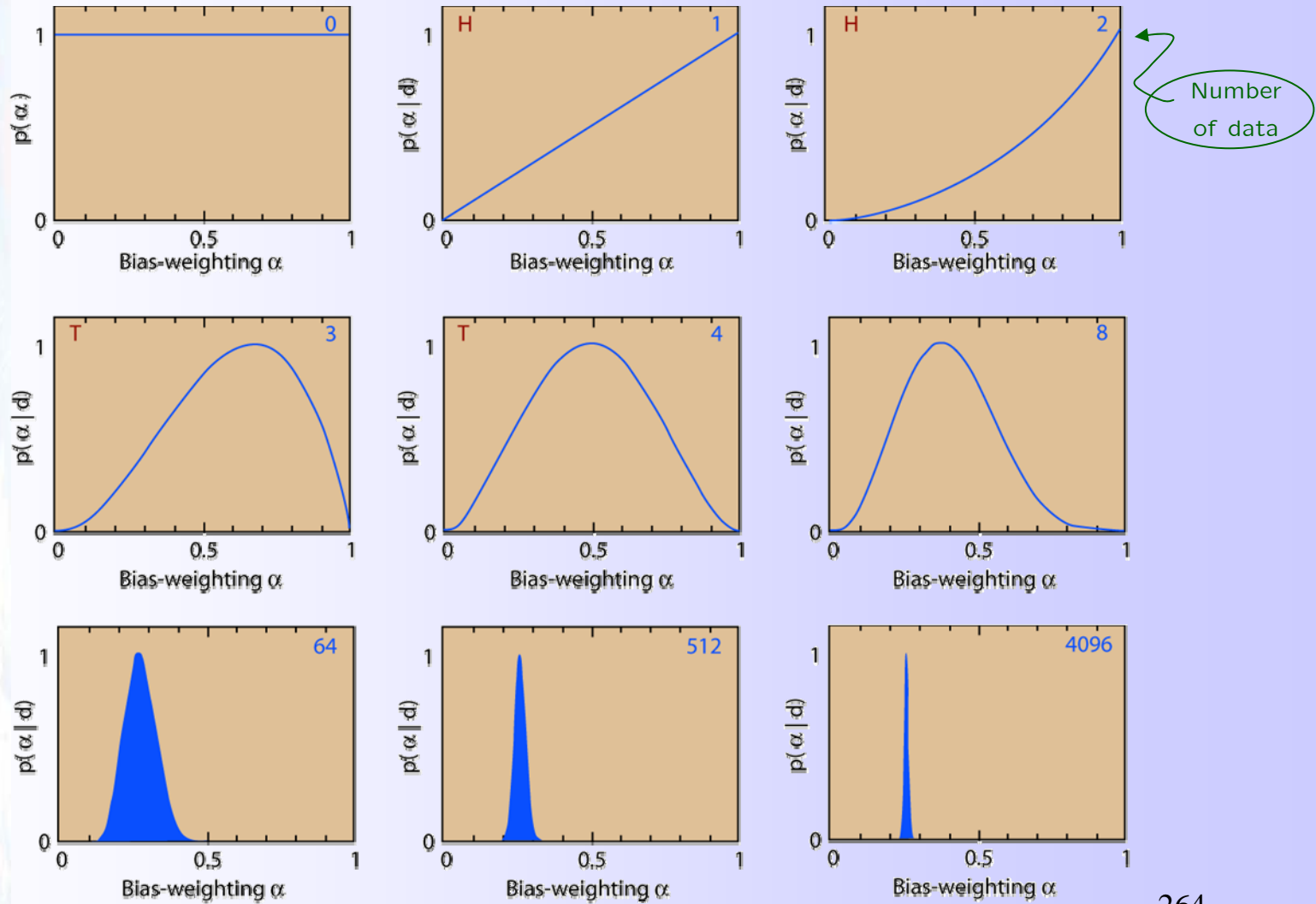
After N coin tosses let R = number of heads observed. Then we
Can plot the probability density for $p(\alpha | \mathbf{d})$ as data are collected





The biased coin problem

$$p(\alpha | d, I) \propto \alpha^R (1 - \alpha)^{N-R}$$



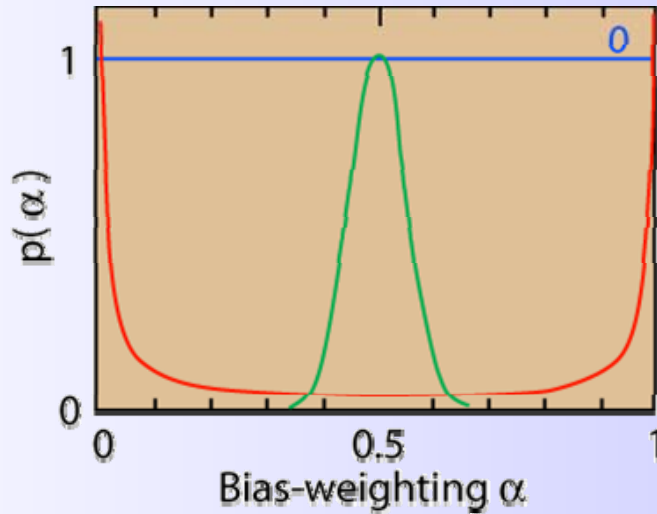
The biased coin problem

But what if three people had different opinions about the coin prior to collecting the data ?

Dr. **Blue** knows nothing about the coin.

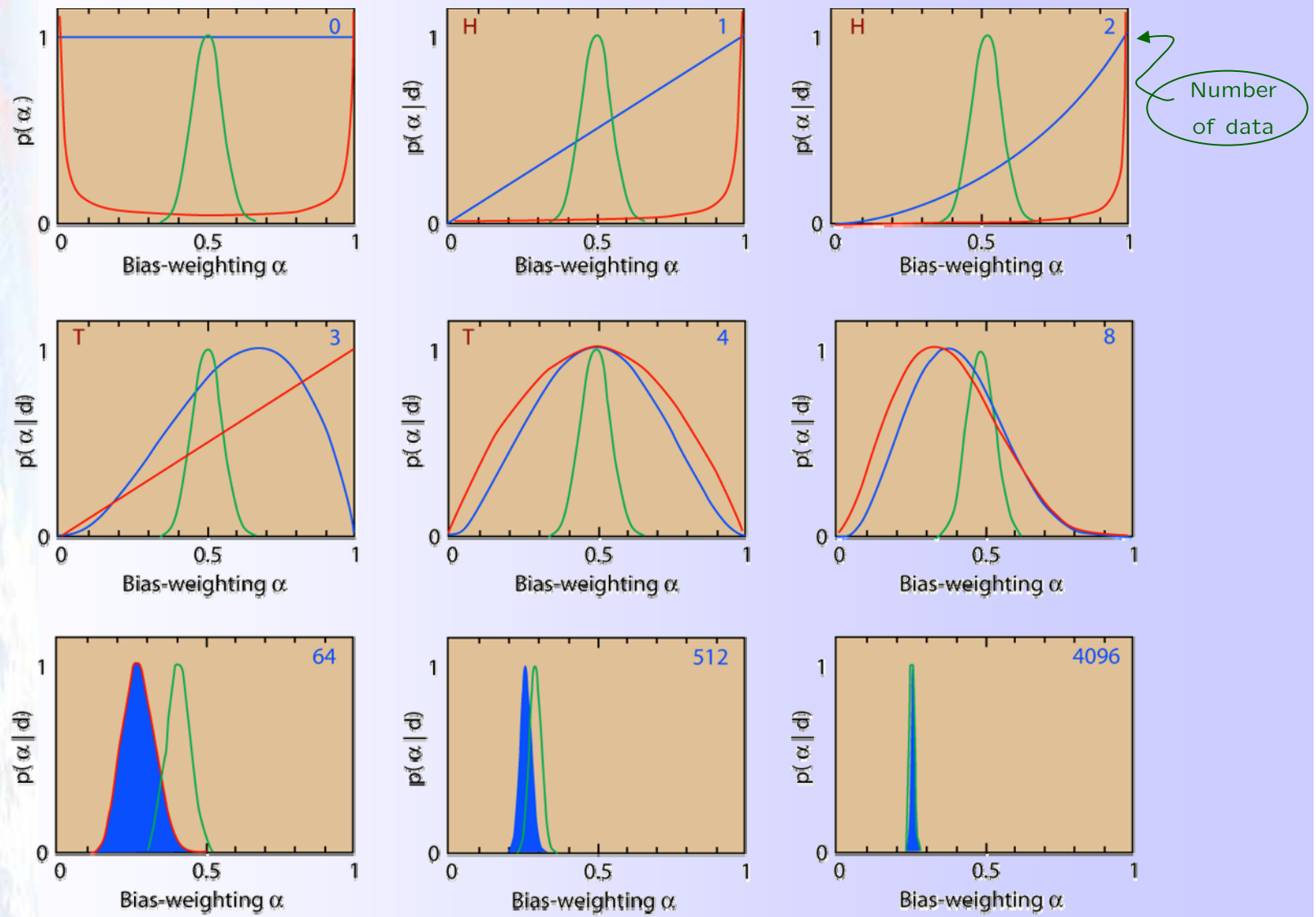
Dr. **Green** thinks the coin is likely to be almost fair.

Dr. **Red** thinks the coin is either highly biased to heads or tails.



$$p(d|\alpha, I) \propto \alpha^R (1 - \alpha)^{N-R}$$

The biased coin problem



The Lighthouse problem

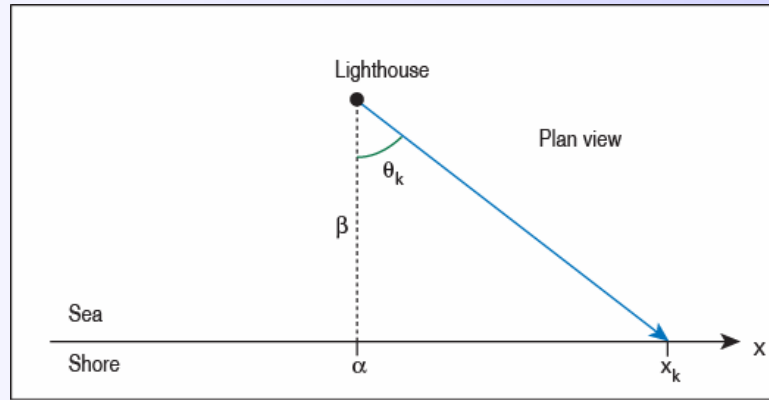


Photo-detectors along the shore record flashes from the light house but not the direction which the light came from.

Data: A total of N flashes have been recorded at positions x_k ($k=1, \dots, N$)

Question: Where is the lighthouse ?

After Gull (1988)



How to choose a prior ?

An often quoted weakness of Bayesian inversion is the subjectiveness of the prior.

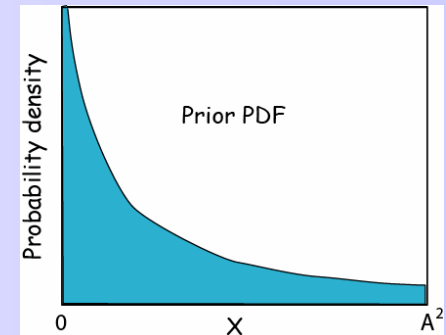
If we know that $x > 0$ and that $E\{x\} = \mu$.

What is an appropriate prior $p(x)$?

$$H(X) = \int_{-\infty}^{\infty} p(x) \ln p(x) dx \quad \text{Entropy}$$

A solution is to choose the prior $p(x)$ that maximizes entropy subject to satisfying the constraints. Using calculus of variations we get

$$p(x) = \frac{1}{\mu} e^{-x/\mu}, \quad x \geq 0$$



There is no such thing as a non-informative prior !

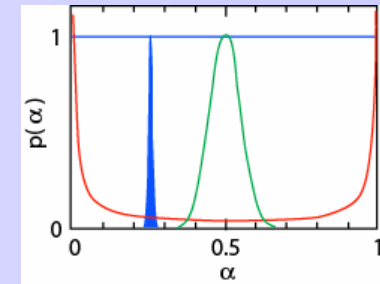


Recap: Probabilistic inference

- ➊ In the Bayesian treatment, all inferences are expressed in terms of probabilities.
- ➋ Bayes' theorem tells us how to combine a priori information with the information provided by the data, and all are expressed as PDFs.
- ➌ All Bayesian inference is relative. We always compare what we know after the data are collected to what we know before the data are collected. In practice this means comparing the a posteriori PDF with the a priori PDF.
- ➍ Bayesians argue that this is just a formalization of logical inference.
- ➎ Criticisms are that non-informative prior's do not exist, and hence we introduce information if prior's are assumed for convenience.
- ➏ The general framework is appealing but can not usually be applied when the number of unknowns is $\geq 10^3$.

What can we do with the posterior PDF ?

- We could map it out over all of model space
 - Only feasible when dimension of the model space is small.
- We seek the maximum of posterior PDF (MAP) and its covariance



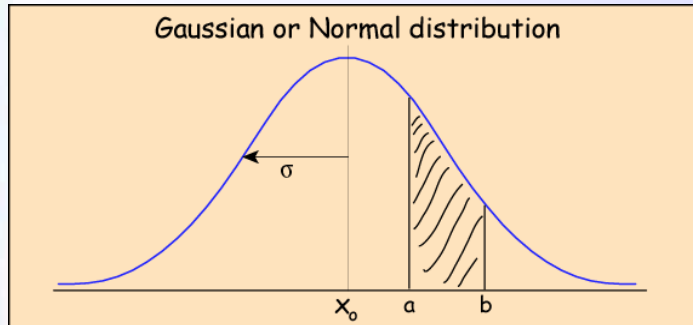
$$\phi(\mathbf{m}, \mathbf{d}) = (\mathbf{d} - G\mathbf{m})^T C_d^{-1} (\mathbf{d} - G\mathbf{m}) + (\mathbf{m} - \mathbf{m}_o)^T C_m^{-1} (\mathbf{m} - \mathbf{m}_o)$$

$$\max_{\mathbf{m}} \phi(\mathbf{m}, \mathbf{d}); \quad \text{calculate } C_M$$

- This is equivalent to the optimization approach earlier.
- Would not make sense when the problem is multi-modal or when the covariance is not representative of its shape.
- We generate model (samples) whose density follows the posterior PDF. Posterior simulation is the main technique used in computational statistics.

In a Bayesian approach the complete Posterior PDF is the answer to the inverse problem, and we always look at its properties.

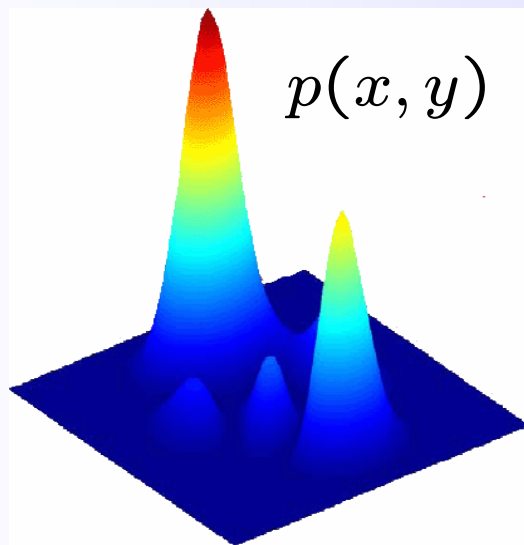
Sampling the posterior PDF



Histogram here

Probability is proportional to area under the curve or surface

Sample density is proportional to area under the curve or surface



$$p(\mathbf{m}|\mathbf{d}, \mathcal{I}) \propto p(\mathbf{d}|\mathbf{m}, \mathcal{I}) \times p(\mathbf{m}|\mathcal{I})$$

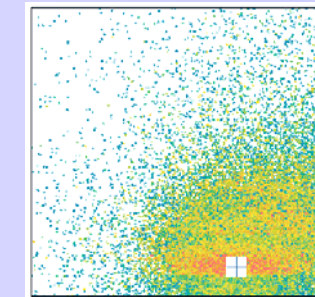
Generating samples from the posterior PDF

There are several techniques for generating samples that follow general probability density functions.

● The transform method

$$y = f(x)$$

1-D $p(y) = p(x) \left| \frac{dx}{dy} \right|$



2-D $p(y_1, y_2) = p(x_1, x_2) \left| \frac{\partial(x_1, x_2)}{\partial(y_1, y_2)} \right|$

$$\left| \frac{\partial(x_1, x_2)}{\partial(y_1, y_2)} \right| = \left| \begin{pmatrix} \frac{\partial x_1}{\partial y_1} & \frac{\partial x_2}{\partial y_1} \\ \frac{\partial x_1}{\partial y_2} & \frac{\partial x_2}{\partial y_2} \end{pmatrix} \right| = \left(\frac{\partial x_1}{\partial y_1} \right) \left(\frac{\partial x_2}{\partial y_2} \right) - \left(\frac{\partial x_2}{\partial y_1} \right) \left(\frac{\partial x_1}{\partial y_2} \right)$$

m-D $p(y_1, y_2, \dots, y_m) = p(x_1, x_2, \dots, x_m) \left| \frac{\partial(x_1, x_2, \dots, x_m)}{\partial(y_1, y_2, \dots, y_m)} \right|$

Example 1: a linear transform

Suppose we have a random variable x that is uniformly distributed between 0 and 1

$$p(x) = 1, \quad 0 \leq x \leq 1$$

Suppose we have the variable y where

$$y = (b - a)x + a$$

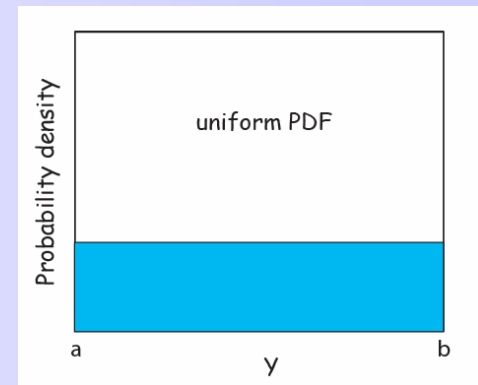
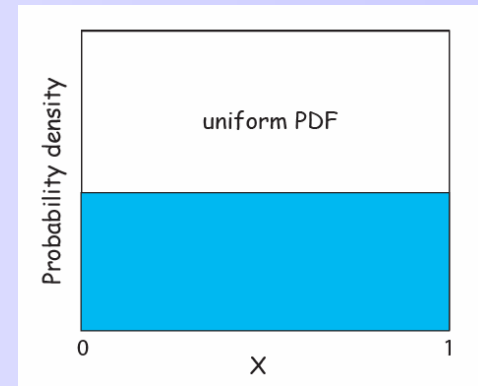
What is the PDF of y ?

$$x = \frac{y - a}{b - a}$$

Transformation rule gives

$$p(y) = p(x) \left| \frac{dx}{dy} \right|$$

$$\Rightarrow p(y) = \frac{1}{b - a}, \quad a \leq y \leq b$$



So y is a uniform random variable between a and b .

Example 2: a quadratic transform

Suppose we have x , such that

$$p(x) = \frac{1}{2A}, \quad -A \leq x \leq A$$

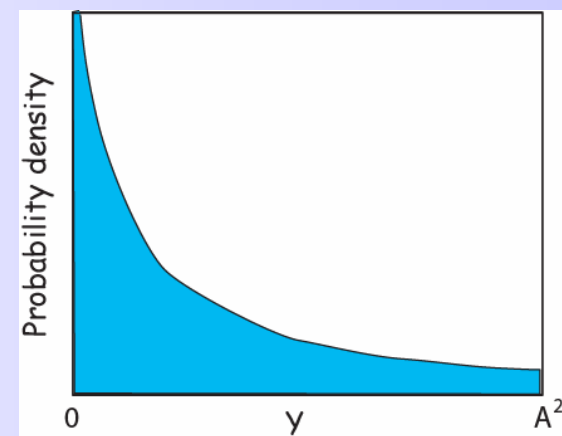
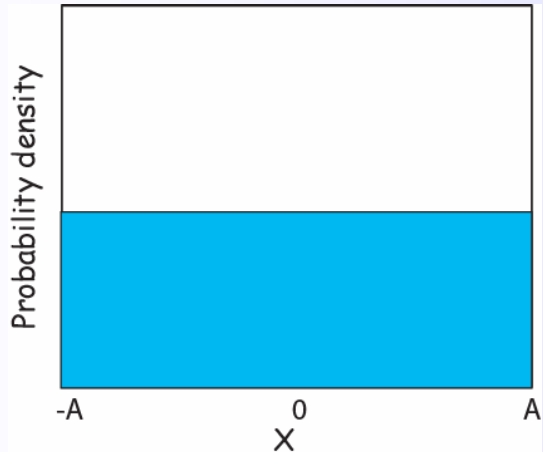
Suppose we have y such that

$$y = x^2$$

What is the PDF of y ?

$$p(y) = p(x) \left| \frac{dx}{dy} \right|$$

$$p(y) = \frac{1}{4Ay^{1/2}}$$





Example 3: Box-Muller transform

Suppose we have two independent uniform random variables, x_1 and x_2

$$p(x_1) = p(x_2) = 1, \quad 0 \leq x_1, x_2 \leq 1$$

Consider the transform to y_1 , y_2

$$y_1 = \sqrt{-2 \ln x_1} \cos 2\pi x_2, \quad y_2 = \sqrt{-2 \ln x_1} \sin 2\pi x_2$$

Inverting we get

$$x_1 = \exp \left[-\frac{1}{2}(y_1^2 + y_2^2) \right] \quad x_2 = \frac{1}{2\pi} \tan^{-1} \frac{y_2}{y_1}$$

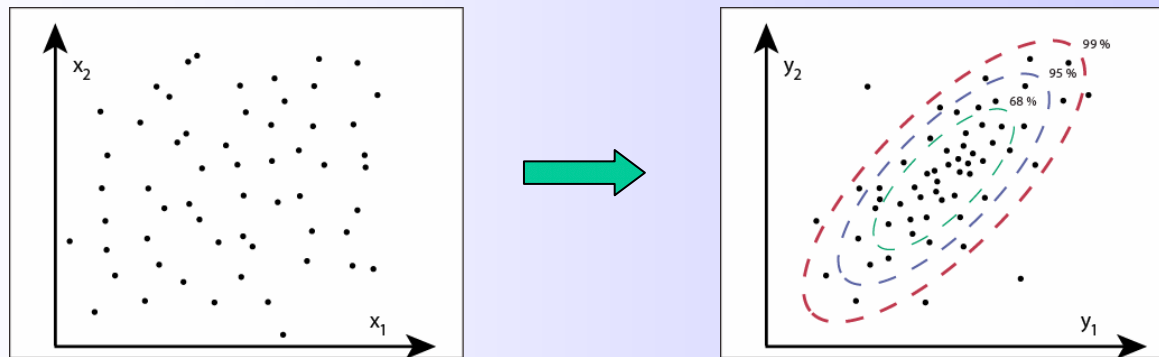
$$p(y_1, y_2) = p(x_1, x_2) \left| \frac{\partial(x_1, x_2)}{\partial(y_1, y_2)} \right|$$

$$\left| \frac{\partial(x_1, x_2)}{\partial(y_1, y_2)} \right| = - \left[\frac{1}{\sqrt{2\pi}} e^{-y_1^2/2} \right] \left[\frac{1}{\sqrt{2\pi}} e^{-y_2^2/2} \right]$$

Example 3: Box-Muller transform

So y_1 and y_2 have independent Gaussian distributions

$$p(y_1, y_2) = - \left[\frac{1}{\sqrt{2\pi}} e^{-y_1^2/2} \right] \left[\frac{1}{\sqrt{2\pi}} e^{-y_2^2/2} \right]$$

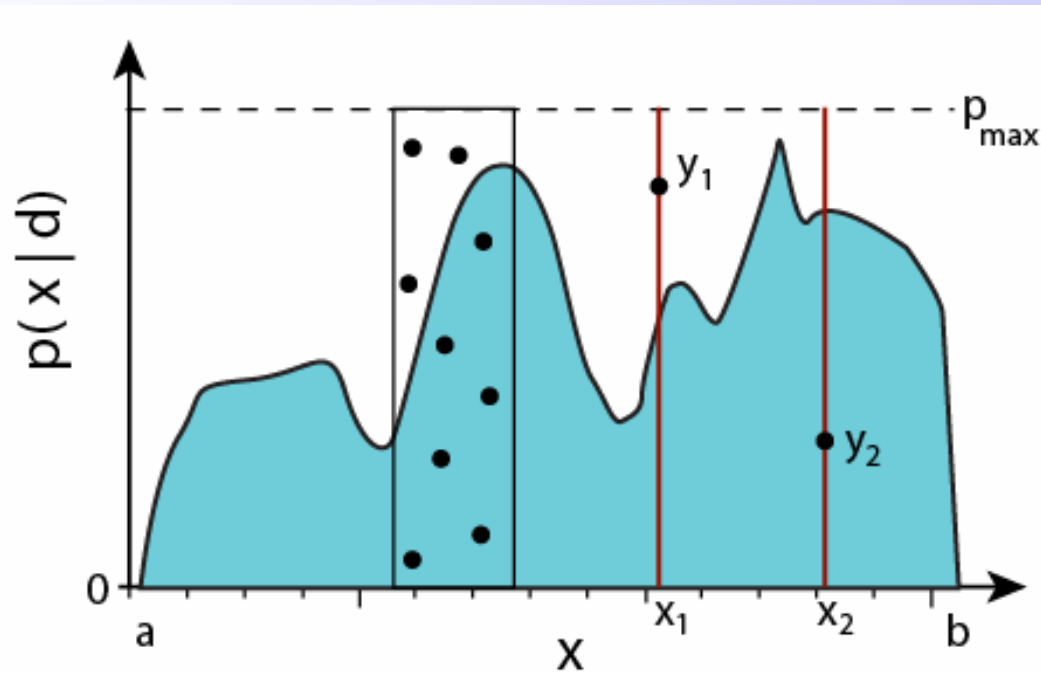


Transform methods are efficient because we get one set of output variables (y_1 and y_2) for each set of input, (x_1 , x_2) variables.

But transformations can not always be inverted. The transform method will be limited to those cases for which an invertible transform can be found. General PDFs $p(x_1, x_2, \dots)$ can not be handled.

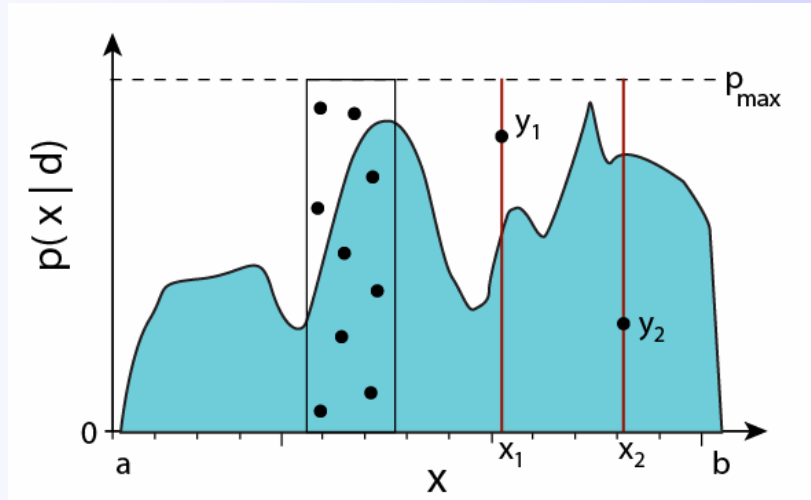
Generating samples from an arbitrary posterior PDF

- The rejection method



Generating samples from the posterior PDF

- Rejection method



But this requires
us to know P_{max}

Step 1: generate a uniform random variable, x_i between a and b

$$p(x_i) = \frac{1}{(b-a)}, \quad a \leq x_i \leq b$$

Step 2: generate a second uniform random variable, y_i

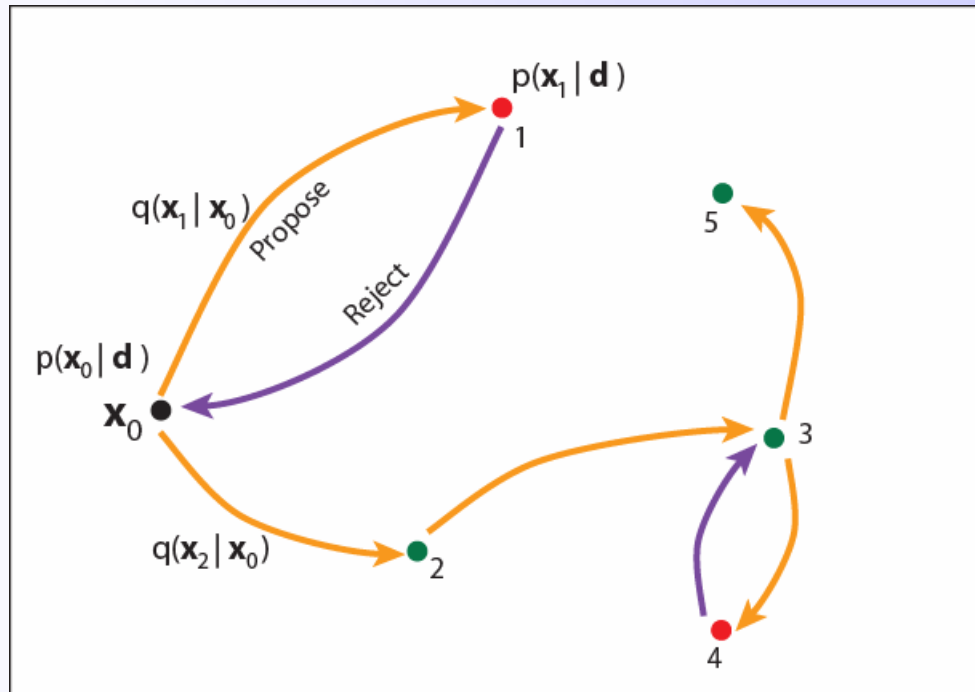
$$p(y_i) = \frac{1}{p_{max}}, \quad 0 \leq y_i \leq p_{max}$$

Step 3: accept x_i if $y_i \leq p(x_i|d)$ otherwise reject

Step 4: go to step 1

Generating samples from the posterior PDF

- Markov chain Monte Carlo (MCMC)



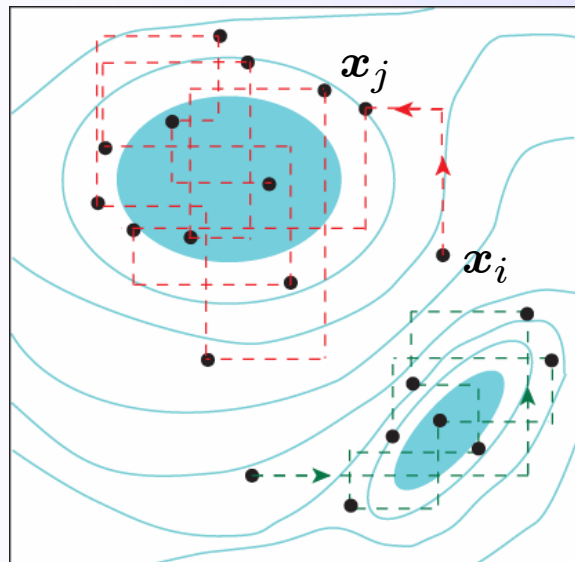
Metropolis algorithm random walk

Step 1: From point x_i generate a candidate model x_j , using a probabilistic *proposal density*

Step 2: Accept the new point with a probability dependent on the posterior PDF at that the new point.

Generating samples from the posterior PDF

- Markov chain Monte Carlo (MCMC)



Importance sampling

Metropolis algorithm
random walk

$$x_i \rightarrow x_j$$

Step 1: From point x_i generate a candidate model x_j , using a *proposal density*

$$q(x_j|x_i) = q(x_i|x_j)$$

Probabilistic
model generation

Step 2: Accept the new point randomly with probability p_a

Probabilistic
acceptance
criterion

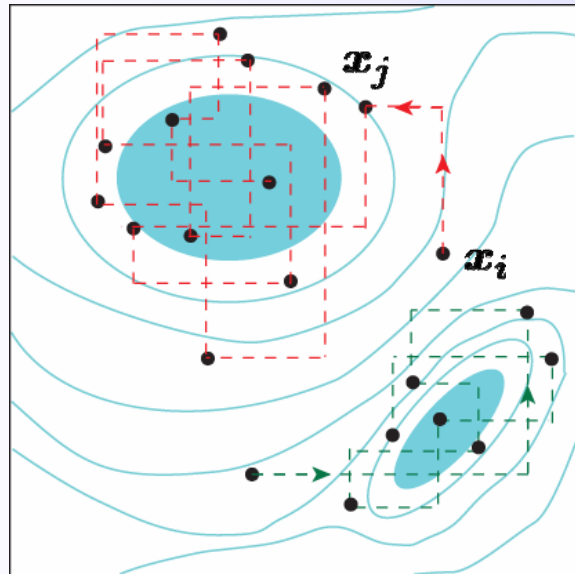
$$p = \min \left[1, \frac{q(x_i|x_j) \times p(x_i|d)}{q(x_j|x_i) \times p(x_j|d)} \right] = \min \left[1, \frac{p(x_i|d)}{p(x_j|d)} \right]$$

$$\Rightarrow p = \begin{cases} \frac{p(x_i|d)}{p(x_j|d)} & : p(x_j|d) \geq p(x_i|d) \\ 1 & : \text{otherwise} \end{cases}$$

If the step is rejected then we stay at x_i and return to step 1

Generating samples from the posterior PDF

Markov chain Monte Carlo (MCMC)



Importance sampling

- This works for general distributions and only requires evaluation of the posterior PDF for any input model, x .
- Efficiency depends on the choice of proposal distribution $q(\mathbf{x}_j|\mathbf{x}_i)$ and the chain may require 'thinning' to remove dependence between samples.

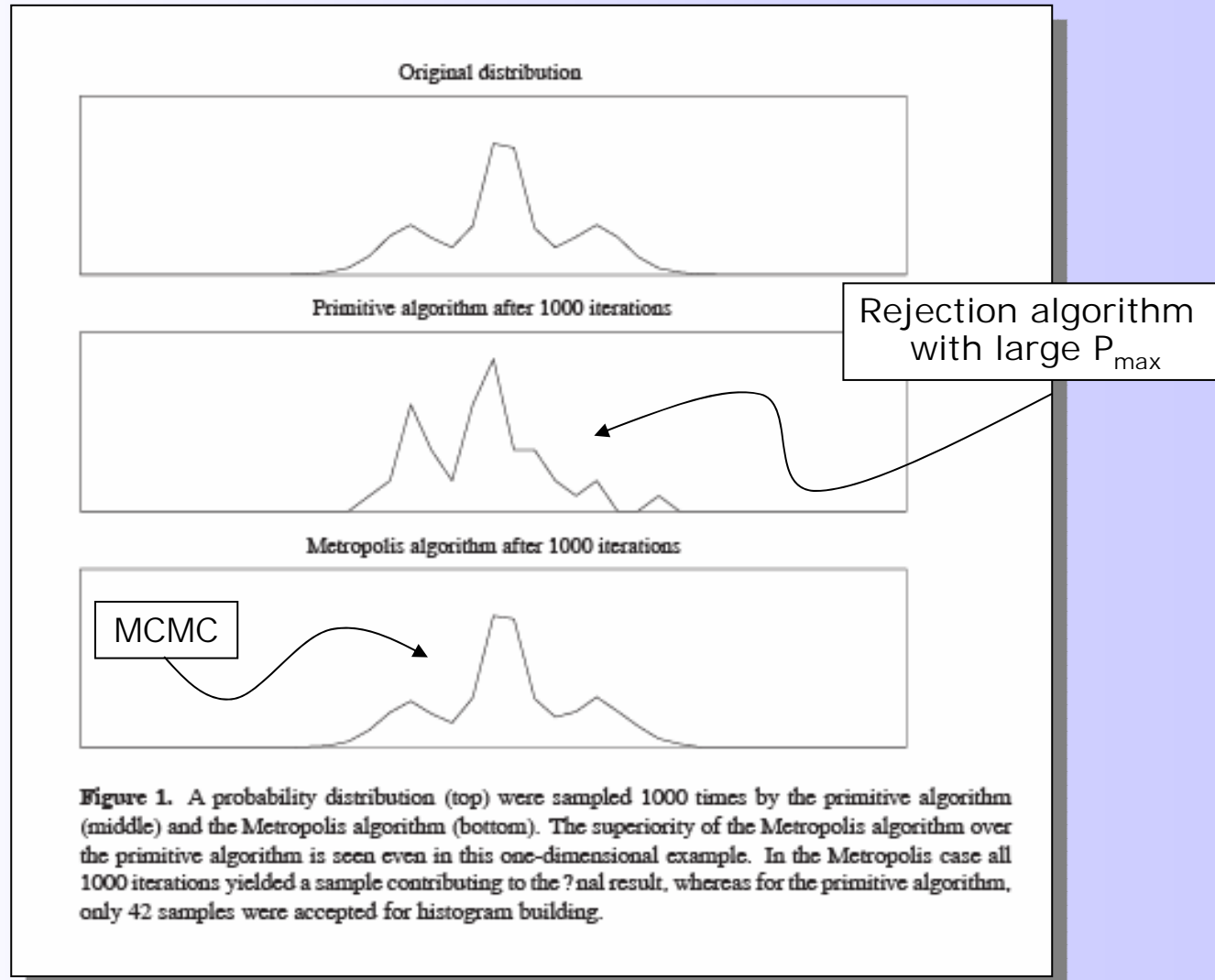
Acceptance probability

$$p = \left[1, \frac{p(\mathbf{x}_i|\mathbf{d})}{p(\mathbf{x}_j|\mathbf{d})} \right]$$

Under general conditions it can be proven that this algorithm converges to the desired posterior distribution $p(\mathbf{x}|\mathbf{d})$ asymptotically.

This is the workhorse technique in Bayesian statistics

Example: MCMC on a 1-D PDF

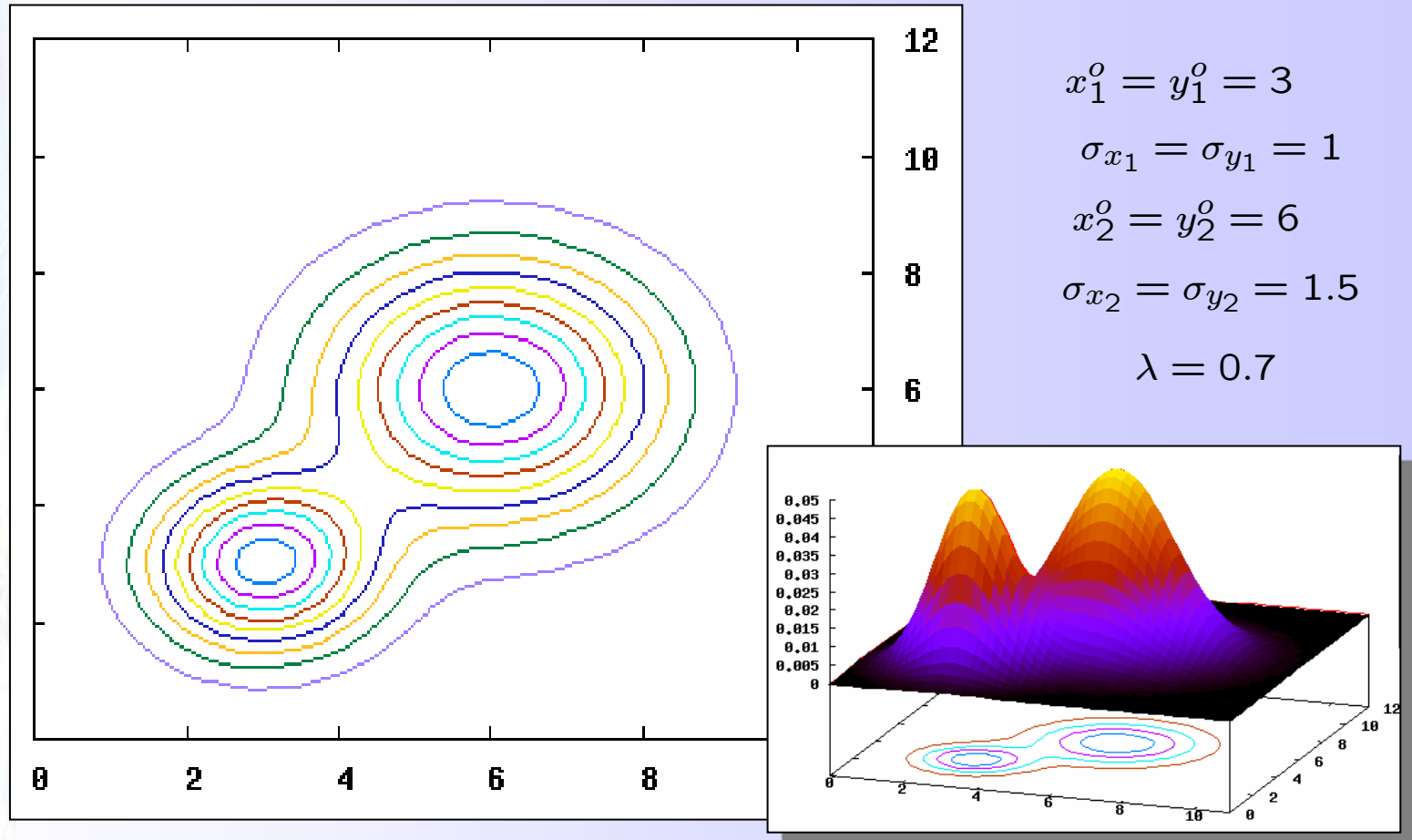


From Mosegaard and Sambrdge 2002

Example: MCMC on a multi-modal PDF

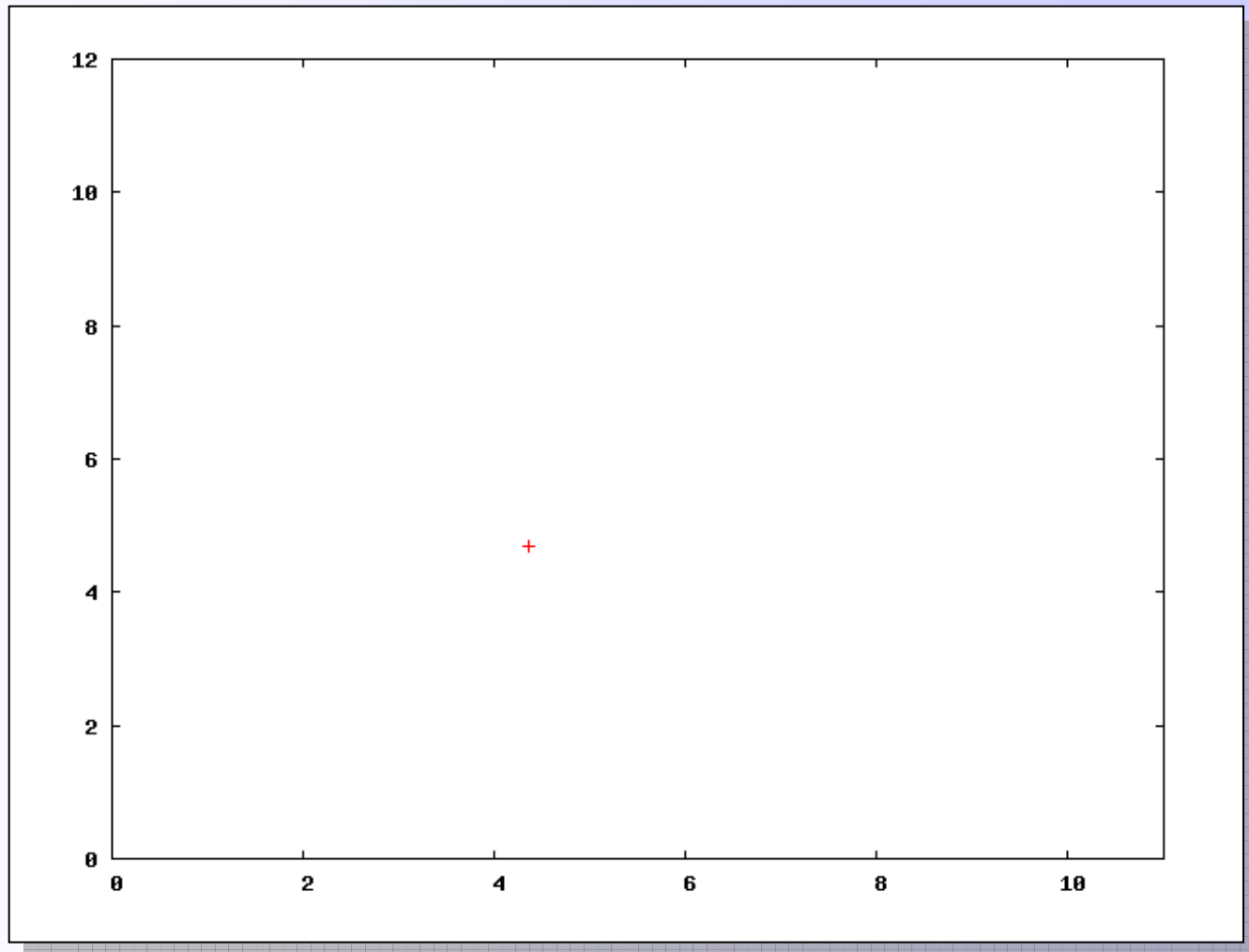
A sum of two 2-D Gaussian distributions

$$p(x, y) = \frac{1 - \lambda}{2\pi\sigma_{x_1}\sigma_{y_1}} \exp - \left\{ \frac{(x - x_1^o)^2}{2\sigma_{x_1}^2} + \frac{(y - y_1^o)^2}{2\sigma_{y_1}^2} \right\} + \frac{\lambda}{2\pi\sigma_{x_2}\sigma_{y_2}} \exp - \left\{ \frac{(x - x_2^o)^2}{2\sigma_{x_2}^2} + \frac{(y - y_2^o)^2}{2\sigma_{y_2}^2} \right\}$$

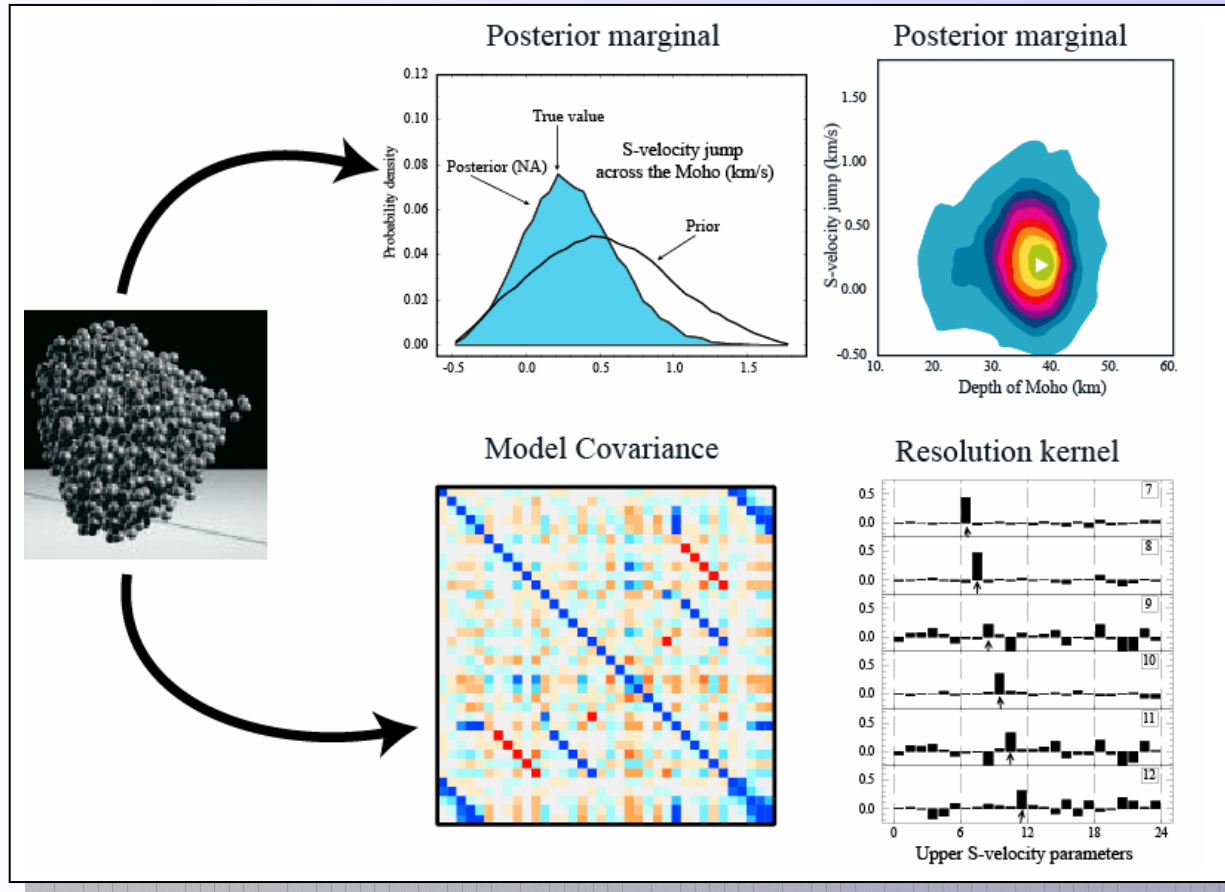


Example: MCMC on a multi-modal PDF

A sum of two Gaussian distributions



What can we do with samples from the Posterior PDF ?



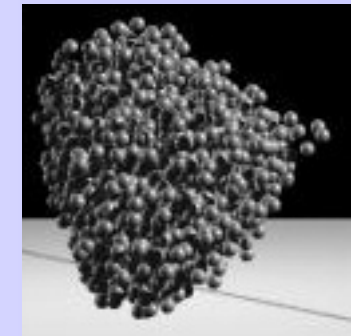
We are usually interested in things like the model covariance matrix, resolution kernels and marginal probability distributions, and each of these can be represented by an integral (sum over the posterior samples)

$$I = \int_{\mathcal{M}} f(\mathbf{m}) p(\mathbf{m}|d) d\mathbf{m}$$

Monte Carlo integration

Consider any integral of the form

$$I = \int_{\mathcal{M}} f(\mathbf{m}) p(\mathbf{m}|d) d\mathbf{m}$$



Given a set of samples \mathbf{m}_i ($i=1, \dots, N_s$) with sampling density $h(\mathbf{m}_i)$, the Monte Carlo approximation to I is given by

$$I \approx \sum_{i=1}^{N_s} \frac{f(\mathbf{m}_i)p(\mathbf{m}_i|d)}{h(\mathbf{m}_i)}$$

Only need to know
 $p(\mathbf{m} | d)$ to a
multiplicative constant

If the sampling density is proportional to $p(\mathbf{m}_i | d)$ then,

$$h(\mathbf{m}) = N_s \times p(\mathbf{m}|d)$$

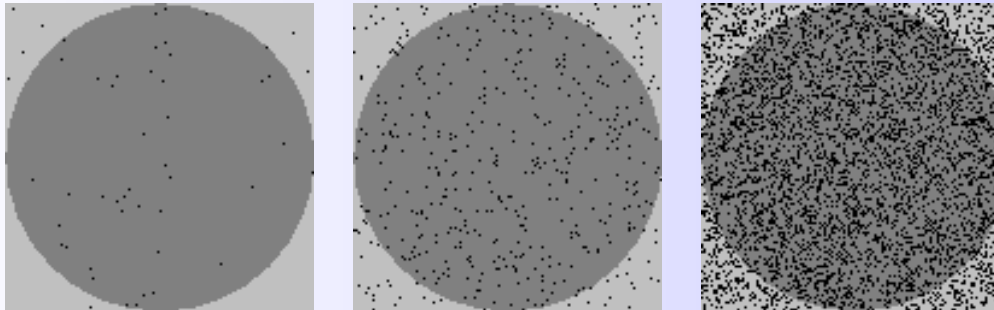
$$\Rightarrow I \approx \frac{1}{N_s} \sum_{i=1}^{N_s} f(\mathbf{m}_i)$$

The variance of the $f(\mathbf{m}_i)$ values gives the numerical integration error in I

Example: Monte Carlo integration

Finding the area of a circle by throwing darts

$$I = \int_A f(\mathbf{m}) d\mathbf{m}$$



$$f(\mathbf{m}) = \begin{cases} 1 & \mathbf{m} \text{ inside circle} \\ 0 & \text{otherwise} \end{cases}$$

$$h(\mathbf{m}) = \frac{N_s}{A}$$

$$I \approx \frac{1}{N_s} \sum_{i=1}^{N_s} f(\mathbf{m}_i)$$

$$\approx \frac{\text{Number of points inside the circle}}{\text{Total number of points}}$$



Monte Carlo integration

We have

$$I = \int_{\mathcal{M}} f(\mathbf{m}) p(\mathbf{m}|d) d\mathbf{m} \approx \sum_{i=1}^{N_s} \frac{f(\mathbf{m}_i)p(\mathbf{m}_i|d)}{h(\mathbf{m}_i)} \approx \frac{1}{N_s} \sum_{i=1}^{N_s} f(\mathbf{m}_i)$$

The variance in this estimate is given by

$$\sigma_I^2 = \frac{1}{N_s} \left\{ \frac{1}{N_s^2} \sum_{i=1}^{N_s} f^2(\mathbf{m}_i) - \left(\frac{1}{N_s} \sum_{i=1}^{N_s} f(\mathbf{m}_i) \right)^2 \right\}$$

- To carry out MC integration of the posterior we ONLY NEED to be able to evaluate the integrand **up to a multiplicative constant**.
- As the number of samples, N_s , grows the error in the numerical estimate will decrease with the square root of N_s .
- In principle any sampling density $h(\mathbf{m})$ can be used but the convergence rate will be fastest when $h(\mathbf{m}) \propto p(\mathbf{m} | d)$.

What useful integrals should one calculate using samples distributed according to the posterior $p(\mathbf{m} | d)$?

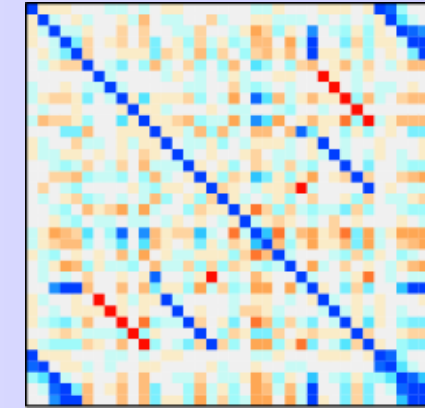
Model covariances from MC integration

The general definition of the Covariance matrix is in terms of a multi-dimensional integral.

First we define the expected value of the i -th parameter

$$E\{m_i\} = \int_{\mathcal{M}} m_i p(\mathbf{m}|\mathbf{d}) d\mathbf{m}$$

$$\approx \frac{1}{N_s} \sum_{k=1}^{N_s} m_i^{(k)}$$



$$C_{i,j} = \int_{\mathcal{M}} (m_i - E\{m_i\})(m_j - E\{m_j\}) p(\mathbf{m}|\mathbf{d}) d\mathbf{m}$$

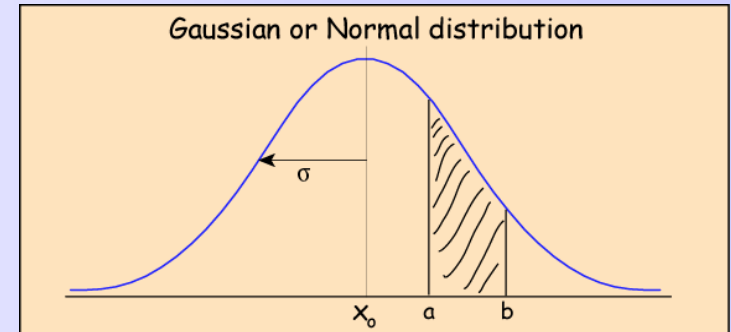
$$C_{i,j} = \int_{\mathcal{M}} m_i m_j p(\mathbf{m}|\mathbf{d}) d\mathbf{m} - E\{m_i\} E\{m_j\}$$

$$\approx \frac{1}{N_s^2} \sum_k m_i^{(k)} m_j^{(k)} - E\{m_i\} E\{m_j\}$$

Example: Model covariances from MC integration

Generate samples whose density is distributed according to a 1-D Gaussian

$$p(x) = \frac{1}{\sigma\sqrt{2\pi}} \exp\left\{-\frac{(x - x_o)^2}{2\sigma^2}\right\}$$



Calculate the expected value for x from the samples (x^1, x^2, \dots, X^{N_s})

$$E\{x\} = \frac{1}{N_s} \sum_{k=1}^{N_s} x^{(k)}$$

What value will
we get as $N_s \rightarrow \infty$?

Calculate the variance of the samples

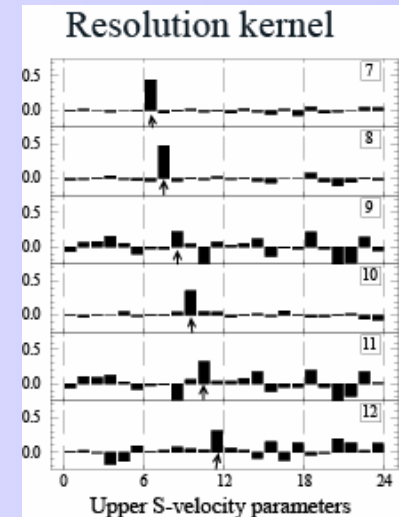
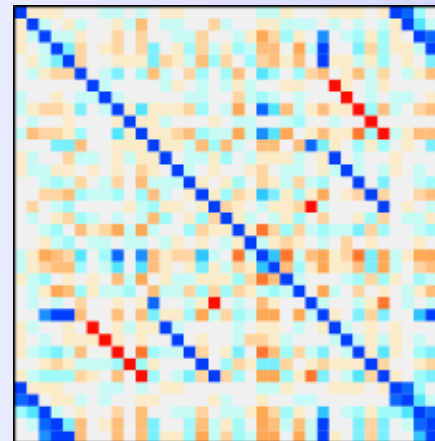
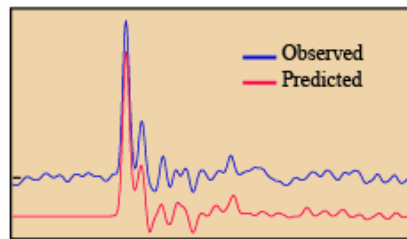
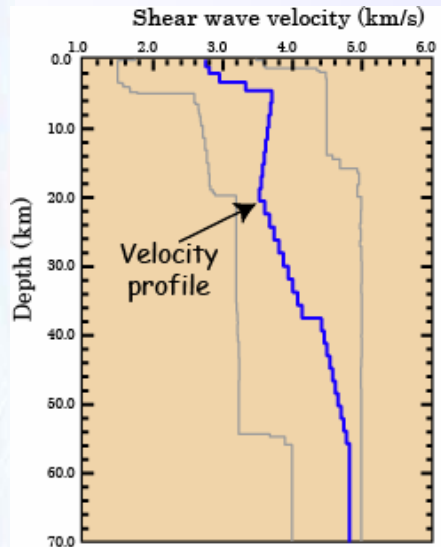
$$C_{1,1} = \frac{1}{N_s} \sum_k (x^{(k)} - E\{x\})^2$$

What value will
we get as $N_s \rightarrow \infty$?

$$C_{1,1} = \frac{1}{N_s^2} \sum_k x^{(k)} x^{(k)} - E\{x\}^2$$

Example: Model covariances from MC integration

Generate samples whose density is distributed according to a 1-D Gaussian



$$R = I - C_{prior}^{-1} C_M$$

MCMC from 10^5 samples

$$C_{1,1} = \frac{1}{N_s^2} \sum_k x^{(k)} x^{(k)} - E\{x\}^2$$

$$E\{x\} = \frac{1}{N_s} \sum_{k=1}^{N_s} x^{(k)}$$

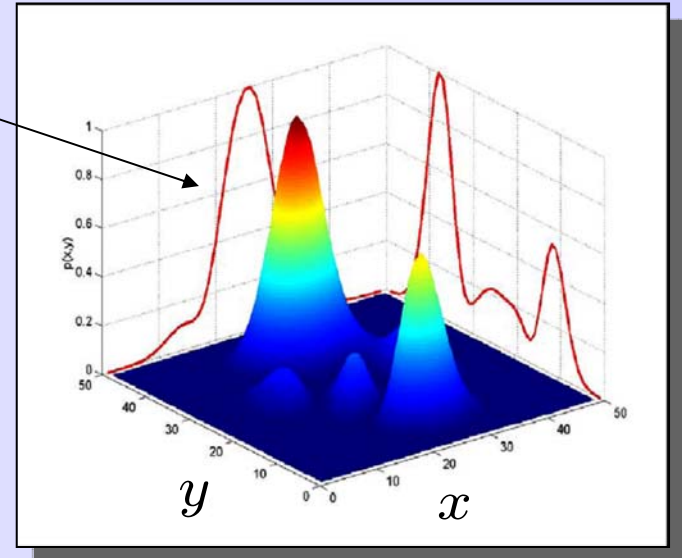
Marginal probability density functions

$$p(x|\mathbf{d}) = \int p(x, y|\mathbf{d}) dy$$

$$p(x, y|\mathbf{d}) = \int p(x, y, z|\mathbf{d}) dz$$

In general

$$p(m_i|\mathbf{d}) = \int \dots \int p(\mathbf{m}|\mathbf{d}) \prod_{\substack{k=1 \\ k \neq i}}^{N_s} dm_k$$



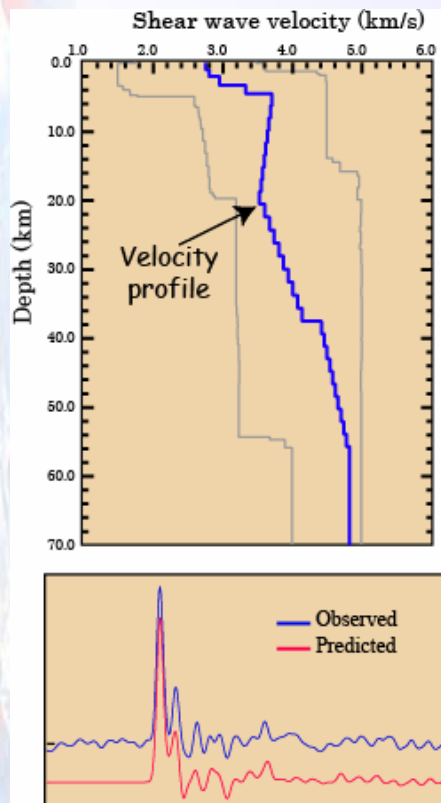
If we have a set of models x_i ($i=1, \dots, N_p$) distributed according to the posterior PDF, then we calculate the marginal of x by simply making a histogram of the models as a function of the x co-ordinate only.

Marginals give information about a variable while taking into account likely variations of all other parameters

In the same way from any set of M -dimensional model space vectors we can calculate marginals for a subset of the parameters by simply projecting the vectors onto the lower dimensional space.

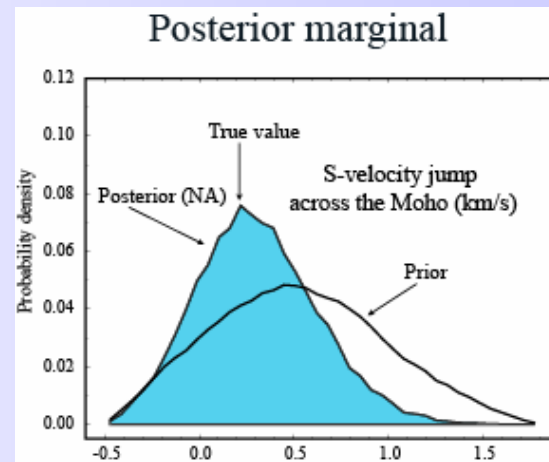
Example: Marginal probability density functions

Receiver function inversion

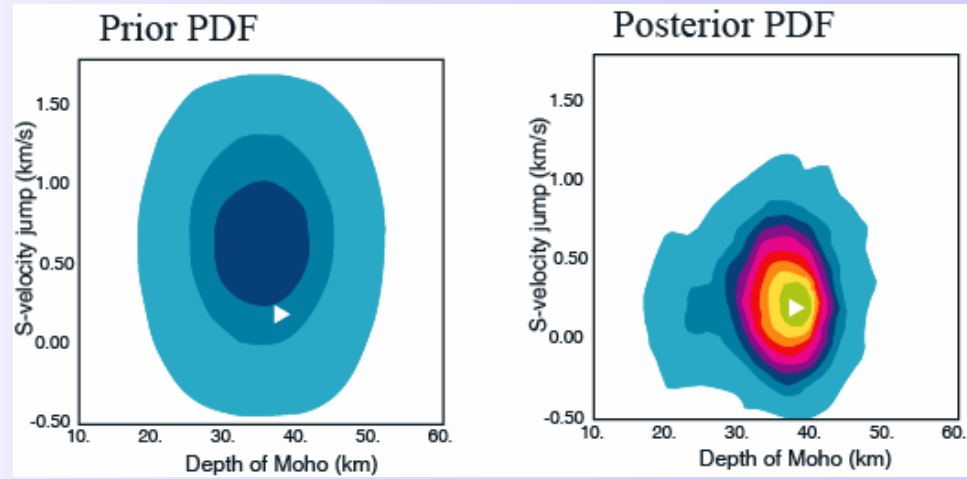


MCMC from 10^5 samples

1-D Marginal



2-D Marginals



From Sambridge (1999)

293

Example: Marginal probability density functions

Inversion of lunar seismograms from Apollo project 1969-1977

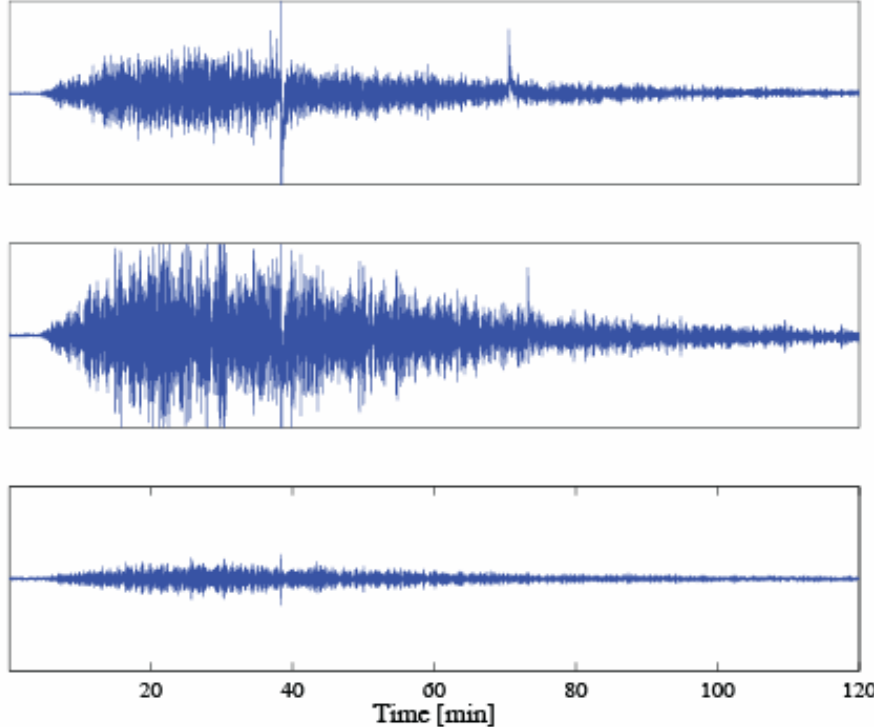


Figure 2. This figure shows a Lunar three-component seismic record from a meteoroid impact recorded at station 16 on day 310, 1970. The seismogram at the top is the N-S component (S positive), the middle is E-W (W positive) and the seismogram at the bottom is the vertical component (up positive). The seismograms commence at 23 h 16 min 50 s.

Moonquake from 2/02/1977

From Khan (2000)

Example: Marginal probability density functions

Marginals of P-wave velocity as a function of depth

Prior on velocity parameters

$$\log p(v(z)) = C, \quad a < v(z) < b$$

Likelihood,

$$\propto e^{-|d_i^{obs} - g_i(\mathbf{m})|}$$

MCMC details:

- ➊ 1.37 million iterations
- ➋ 40-50% acceptance ratio

Marginals were calculated for all velocity parameters and plotted as a function of depth.

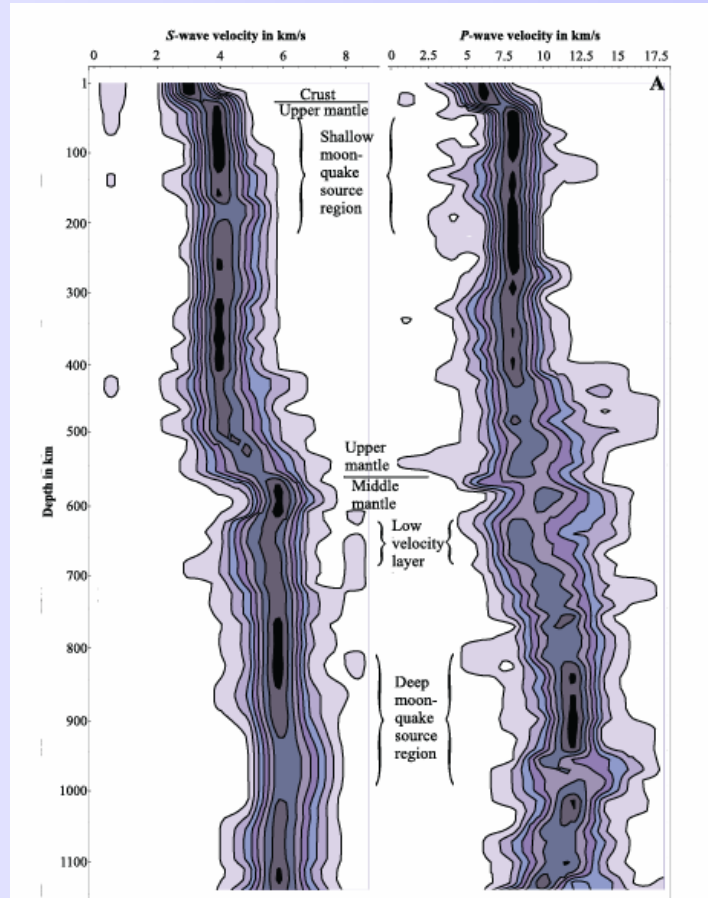


Figure 3. Marginal posterior velocity distributions for the velocity structure of the Moon. 50 000 models were used in constructing the two results. For each kilometre in depth, a histogram reflecting the marginal *a posteriori* probability distribution of sampled velocities has been computed. These marginals are lined up, and contour lines define nine equal-sized probability density intervals for the distributions.

From Khan (2000)



The End

Introduction to inverse problems

Homework sheet 1

Due end of class Thursday 1st November 2007

Question 1

Following are examples of inverse problems. Until now we have been interested in linear inverse problems. In discrete form linear inverse problems can be written in matrix notation and formal expressions exist for their solutions, such as for the least squares solution. Which of the following problems presents a linear inverse problem? Explain your answer.

- (i) The travel time t_i of a sound wave following path i through a medium can be described by

$$t_i = \int_{\text{path}} \frac{1}{v(\mathbf{r})} ds$$

where $v(\mathbf{r})$ is the sound velocity of the medium at location \mathbf{r} and s is the distance along the wave path. We want to determine $v(\mathbf{r})$ of the medium from measuring t for many ray paths.

- (ii) We want to find a straight line that predicts temperature increase with depth at the site of a planned tunnel. For this purpose we measure temperature T_i at n depths z_i in a borehole, where $1 < i < n$. We use the following relation:

$$T(z) = m_1 + m_2 z$$

- (iii) We want to predict rock density ρ in the Earth at a given radius r from its center from the known mass M and moment of inertia I of the Earth. We use the following relation:

$$g(r) = \int_0^a g_i(r) \rho(r) dr$$

where $d_1 = M$ and $d_2 = I$ and $g_i(r)$ are the corresponding Frechet kernels: $g_1(r) = 4\pi r^2$ and $g_2(r) = \frac{8}{3}\pi r^4$.

- (iv) We want to predict how much of a given rock mass, fraction X , in the Earth melts at a given value for dimensionless temperature T' , where T' depends on the temperature T as well as on the solidus and liquidus of the rock. The solidus and liquidus of a rock depend on the pressure. For this purpose we measure melt fraction at various combinations of temperature and pressure. We use the following relation:

$$X(T') = \frac{1}{2} + T' + \left(T'^2 - \frac{1}{4} \right) (m_o + m_1 T' + m_2 T'^2)$$

Question 2 Consider a mathematical relationship of the form $G(\mathbf{m}) = \mathbf{d}$, where \mathbf{m} is the model vector of length M , and \mathbf{d} is the data vector of length N . Suppose that the model obeys the superposition and scaling laws and is thus linear. Show that $G(\mathbf{m})$ can be written in the form

$$G(\mathbf{m}) = \Gamma \mathbf{m}$$

where Γ is an $N \times M$ matrix. What are the elements of Γ ? Hint: Consider the standard basis, and write \mathbf{m} as a linear combination of the vectors in the standard basis. Then apply superposition and scaling laws.

Question 3 Suppose you have a linear inverse problem with n observations and a model with m parameters. If you believe that the data errors follow a Gaussian distribution. Suppose that you had fit a model to the data using least squares.

- (i) What distribution would you use for testing the goodness of fit to data and why?
- (ii) How would you test whether the fit of the model to the data is satisfactory given the expected errors in the data?
- (iii) If $N = 55$ and $M = 5$, how many degrees of freedom are there and what would you say about the model if you obtained a χ^2 value of i) 20.0, ii) 49.0, iii) 120.0? (The χ^2 table below may be of help.)
- (iv) If $M = 3$ and $N = 20$ describe how you would calculate 95% confidence intervals in each parameter taken alone.
- (v) Describe how you would calculate 95% joint confidence ellipse for any two of the three parameters,

ν	$\chi^2(95\%)$	$\chi^2(50\%)$	$\chi^2(5\%)$
5	1.15	4.35	11.07
10	3.94	9.34	18.31
20	10.85	19.34	31.41
50	34.76	49.33	67.50
100	77.93	99.33	124.34

Table 1: Percentage points of the χ^2 distribution with ν degrees of freedom

Question 4

- (i) A nonlinear forward problem can be written in the form

$$d_i = g_i(\mathbf{m})$$

where d_i is the i th datum and $g_i(\mathbf{m})$ describes the prediction of the i th datum from a model \mathbf{m} . If the data have a covariance matrix C_d^{-1} write down the least squares data prediction error, $\phi(\mathbf{m})$, for this problem.

- (ii) How does the minimization of $\phi(\mathbf{m})$ help solve the inverse problem ?
- (iii) Write down the Taylor expansion of $g_i(\mathbf{m})$ about a reference model \mathbf{m}_o .
- (iv) Use this Taylor expansion to linearize the inverse problem above and explain each term in your equation.
- (v) Show how the linearized inverse problem leads to a quadratic approximation to $\phi(\mathbf{m})$.
- (vi) Derive an expression which gives an iterative least squares solution to this problem for model perturbations $\delta\mathbf{m}$.
- (vii) Explain the conditions under which this linearized iterative algorithm would be appropriate to use ?
- (viii) Now consider a linear inverse problem

$$\mathbf{d} = \mathbf{G}\mathbf{m}.$$

If a solution to this problem is written in the form

$$\mathbf{m} = \mathbf{G}^{-g}\mathbf{d}$$

derive an expression for the model covariance matrix in terms of \mathbf{G}^{-g} and explain what this matrix means.

- (ix) For the same problem derive an expression for the model resolution matrix and describe what it means.
- (x) Discuss the relationship between the Model covariance and Model resolution using an example to illustrate your answer.

Homework 1: Solutions

1(i). Non-Linear.

Fails superposition test, but passes scaling test. Although re-defining the integrand as “slowness” [$S(r) = 1/V(r)$] gives it the appearance of linearity, in reality, the path along which slowness needs to be integrated to obtain travel times depends on the model parameter, $S(r)$ or $V(r)$, as a consequence of Fermat’s theorem!

1(ii). Linear.

Passes both scaling and superposition tests. Data,

$$d \equiv G(\bar{m}) = [1 \quad z] \begin{bmatrix} m_1 \\ m_2 \end{bmatrix} \equiv \Gamma \cdot \bar{m},$$

is a **linear** function of the model parameters, \mathbf{m} .

1(iii). Linear.

Passes both scaling and superposition tests. Data,

$$d \equiv \begin{bmatrix} M \\ I \end{bmatrix} = G(\rho) = \int_0^a \begin{bmatrix} 4\pi r^2 \\ \frac{8}{3}\pi r^2 \end{bmatrix} \rho(r) dr = \Gamma_r \cdot \rho(r),$$

where Γ_r is the linear integral operator, is a **linear** function of the model parameter, $\rho(r)$.

1(iv). “Conditionally” Linear.

If data,

$$d \equiv \tilde{U}(\bar{m}) \equiv X(T', \bar{m}) - T' - 0.5 = [C_0(T') \quad C_1(T') \quad C_2(T')] \begin{bmatrix} m_0 \\ m_1 \\ m_2 \end{bmatrix} \equiv \Gamma \cdot \bar{m},$$

then \tilde{U} passes both superposition and scaling tests. However, $X(\mathbf{m})$ is still a **linear** function of the model parameters, \mathbf{m} , irrespective of the rearrangement, because as we have seen above, it passes both tests once we subtract a constant (remember T' are data that we already know!).

2. Linearity of Forward Model, $G(\mathbf{m})$:

Let us assume that \mathbf{G} maps an M-vector in the model space into an N-vector in the data space, i.e., $\mathbf{G}_N: \mathcal{R}^M \rightarrow \mathcal{R}^N$. Expand the model vector in terms of the standard column basis:

$$\mathbf{e}_i = [0 \ 0 \dots 1(i^{th} term) \dots 0]^T, \text{ where } i = 1, 2, \dots, M.$$

So, $\bar{\mathbf{m}} = \sum_{i=1}^M m_i \bar{\mathbf{e}}_i$. The N data vectors can now be represented as,

$$\begin{aligned} \bar{\mathbf{d}} &= \bar{\mathbf{G}}(\bar{\mathbf{m}}) = \bar{\mathbf{G}}\left(\sum_{i=1}^M m_i \bar{\mathbf{e}}_i\right) \\ &= \sum_{i=1}^M \bar{\mathbf{G}}(m_i \bar{\mathbf{e}}_i), \quad (\text{Superposition}) \\ &= \sum_{i=1}^M \bar{\mathbf{G}}(\bar{\mathbf{e}}_i) m_i \quad (\text{Scaling}) \\ &= \begin{bmatrix} \bar{\mathbf{G}}(\bar{\mathbf{e}}_1) & \bar{\mathbf{G}}(\bar{\mathbf{e}}_2) & \dots & \bar{\mathbf{G}}(\bar{\mathbf{e}}_M) \end{bmatrix} \begin{bmatrix} m_1 \\ m_2 \\ \vdots \\ m_M \end{bmatrix} \\ &= \bar{\Gamma} \bar{\mathbf{m}} \end{aligned}$$

\mathbf{d} & $\mathbf{G}(\mathbf{e}_i)$ are column vectors of length N , and therefore, $\bar{\Gamma}$ is a matrix of dimension $N \times M$, whose elements depend on the problem parametrization and geometry. Each row of $\bar{\Gamma}$ determines how to weigh the model parameters in order to obtain the corresponding component of the data vector, \mathbf{d} .

3. For background information on this problem refer to §2.2 of Aster et al. (pre-print edition, 2003).

3(i) Goodness of fit is expressed in terms of the sum of squares of individual data errors (which are assumed to follow a Gaussian distribution). This sum, therefore, follows the χ^2 -distribution.

3(ii) (a) First, estimate the number of degrees of freedom (DoF) of the problem:

$$\nu = \text{#Data} - \text{#Model parameters} = N - M.$$

(b) Then estimate the p-value, the probability of obtaining a χ^2 value as large or larger than the observed value, for the above number of DoFs:

$$p(\chi^2 \geq \chi_{obs}^2) = \int_{\chi_{obs}^2}^{\infty} f_{\chi^2, \nu}(x) dx$$

(c) We want this number to be neither too close to 1 or too close to 0.

3(iii) #DoF, $\nu = N - M = 55 - 5 = 50$. NOTE: the %-values given in this problem are actually *p*-values.

- $\chi^2 = 20$: *p*-value is nearly one. There is a nearly 100% chance of that χ_{obs}^2 could be any worse – the model fits the data almost exactly! Either the data errors have been overestimated, or there is the potential of data-fraud.
- $\chi^2 = 49$: *p*-value is roughly 0.5. There is a 50% chance that χ_{obs}^2 could be any worse. So, this is an acceptable result.
- $\chi^2 = 120$: *p*-value is nearly zero. There is a *negligible* chance that χ_{obs}^2 could be any worse – we have the worst possible fit to the data. So, either the forward model is incorrect, or data errors have been underestimated (or do not follow a Gaussian).

3(iv) In a linear(-ized) inverse problem with Gaussian data errors, the model parameters can be expressed as a linear combination of the data (plus errors). Therefore, the model parameters themselves are normally distributed, with the mean (expected value) being given by the least squares solution, \mathbf{m}_{L2} . So, for a single parameter, the 95% confidence interval (i.e., interval for which the area under the Gaussian = 0.95) for model parameter *i* is given by $\pm 1.96\sigma_i$, where σ_i ($= \sqrt{C_{mii}}$) is the square-root of the diagonal term of the model covariance matrix, *C*, corresponding to that model parameter. So, $\mathbf{m}_i = \mathbf{m}_{L2,i} \pm 1.96\sigma_i \approx \mathbf{m}_{L2,i} \pm 2\sigma_i \equiv \mathbf{m}_{L2,i} \pm 2\sqrt{C_{ii}}$. The factor in front of the σ_i will be roughly 1.0 for the 68% confidence interval, and 3.0 for the 99% confidence interval.

3(v) In this case, we want to find the projections of the 3D error-ellipsoid on the planes defined by each pair of model parameters. Eq. 2.42 of Aster et al. (2003), can be re-written as:

$$\delta\mathbf{m}^T C_M^{-1} \delta\mathbf{m} \leq \Delta_{2DoF}^2$$

Substituting Eq 2.43 (Eigenvalue decomposition of $C_M^{-1} = P \Lambda P^T$) into Eq. 2.42, and considering only 2 model parameters at a time gives:

$$\frac{\delta m_1^2}{\left(\frac{\Delta_{2DoF}}{\sqrt{\lambda_1}}\right)^2} + \frac{\delta m_2^2}{\left(\frac{\Delta_{2DoF}}{\sqrt{\lambda_2}}\right)^2} \leq 1$$

where λ_i is the *i*th eigenvalue of the inverse of the model covariance matrix, and Δ_{2DoF} is the χ^2 distribution with $\nu = 2$. So, the above equation defines the region *inside* an ellipse with axes $\Delta_{\chi^2, 2DoF} / \sqrt{\lambda_i}$. So, the estimated values of the model parameters will be $\mathbf{m}_{L2,i} \pm \Delta_{\chi^2, 2DoF} / \sqrt{\lambda_i}$.

4(i). $\phi(\bar{m}) = (\bar{d} - \bar{g}(\bar{m}))^T C_d^{-1} (\bar{d} - \bar{g}(\bar{m}))$

- 4(ii).** Minimizing ϕ w.r.t. the model parameters, \mathbf{m} , gives us the model, \mathbf{m}_{L2} , that minimizes the residual between the forward model, $\mathbf{g}(\mathbf{m})$, and the data, \mathbf{d} . \mathbf{m}_{L2} is also the most likely model, given the data.

- 4(iii)** We want to linearize the forward problem in the neighborhood of a reference model, \mathbf{m}_0 :

$$\begin{aligned}\bar{g}(\bar{m}) &= \bar{g}(\bar{m}_0) + \frac{\partial \bar{g}}{\partial \bar{m}} \Big|_{\bar{m}=\bar{m}_0} (\bar{m} - \bar{m}_0) + \frac{\partial^2 \bar{g}}{\partial \bar{m}^2} \Big|_{\bar{m}=\bar{m}_0} (\bar{m} - \bar{m}_0)^2 + \dots \\ &\approx \bar{g}(\bar{m}_0) + \bar{\nabla} \bar{g}(\bar{m}_0)(\bar{m} - \bar{m}_0) \quad (\text{Ignoring Higher Order Terms, "HOT"}) \\ &= \bar{g}(\bar{m}_0) + G(\bar{m} - \bar{m}_0)\end{aligned}$$

where, G is a $N \times M$ matrix that gives the sensitivity of the forward problem to the model parameters at $\mathbf{m} = \mathbf{m}_0$:

$$G_{ij} = \frac{\partial g_j}{\partial m_i} \Big|_{\bar{m}=\bar{m}_0}$$

- 4(iv)**

$$\bar{d} = \bar{g}(\bar{m}) \approx \bar{g}(\bar{m}_0) + G(\bar{m} - \bar{m}_0), \text{ where } m_0 \text{ is some reference model.}$$

Let, $\delta \bar{d} = \bar{d} - \bar{g}(\bar{m}_0)$; $\delta \bar{m} = \bar{m} - \bar{m}_0$ (the perturbation)

$$\therefore \delta \bar{d} = G \cdot \delta \bar{m}$$

which is the **linearized inverse problem** for the perturbation of \mathbf{m} about $\mathbf{m} = \mathbf{m}_0$.

- 4(v)**

Using the same notation as above,

$$\bar{d} - \bar{g}(\bar{m}) \approx \bar{d} - \bar{g}(\bar{m}_0) - G \cdot \delta \bar{m} = \delta \bar{d} - G \cdot \delta \bar{m}$$

$$\text{Hence, } \phi(\bar{m}) = (\bar{d} - \bar{g}(\bar{m}))^T C_d^{-1} (\bar{d} - \bar{g}(\bar{m})) \approx (\delta \bar{d} - G \cdot \delta \bar{m})^T C_d^{-1} (\delta \bar{d} - G \cdot \delta \bar{m})$$

Here, we have ignored “HOT”. Also, since $\delta \mathbf{d}$, \mathbf{d} , & $G \delta \mathbf{m}$ are all $(N \times 1)$ vectors, and C_d^{-1} is a $(N \times N)$ matrix whose terms are independent of the model perturbations, $\delta \mathbf{m}$, the RHS of the above approximation is a quadratic expression in terms of the components of $\delta \mathbf{m}$.

- 4(vi).** In this case, minimizing ϕ w.r.t. the model parameter perturbations, $\delta\mathbf{m}$, gives us the model, $\delta\mathbf{m}_{L2}$, that minimizes the residual between the forward model perturbation, $\mathbf{G}\delta\mathbf{m}$, and the data perturbation, $\delta\mathbf{d}$: Assuming that the problem is over-determined, we can derive the least squares solution, by setting

$$\begin{aligned} \bar{\nabla}_{\bar{m}}\phi(\bar{m}) &= \bar{0} \\ \Rightarrow \bar{\nabla}_{\bar{m}}[(\delta\bar{d} - G.\delta\bar{m})^T C_d^{-1}(\delta\bar{d} - G.\delta\bar{m})] &= \bar{0} \\ \Rightarrow \bar{\nabla}_{\bar{m}}[\delta\bar{d}^T C_d^{-1}\delta\bar{d} - \delta\bar{d}^T C_d^{-1}G.\delta\bar{m} - \delta\bar{m}^T G^T.C_d^{-1}\delta\bar{d} + \delta\bar{m}^T G^T.C_d^{-1}G.\delta\bar{m})] &= \bar{0} \\ \Rightarrow -[\delta\bar{d}^T C_d^{-1}G]^T.I - I.G^T.C_d^{-1}\delta\bar{d} + I.G^T.C_d^{-1}G.\delta\bar{m} + [\delta\bar{m}^T G^T.C_d^{-1}G]^T.I &= \bar{0} \end{aligned}$$

where we have used the vector calculus relationships:

$$\bar{\nabla}_{\bar{x}}(A.\bar{x}) = A^T \bar{\nabla}_{\bar{x}}(\bar{x}) = A^T.I = A^T, \text{ and } \bar{\nabla}_{\bar{x}}(\bar{x}.B) = B\bar{\nabla}_{\bar{x}}(\bar{x}) = B.I = B.$$

Noting that C_d^{-1} is symmetric, we can simplify the above to get:

$$\begin{aligned} [\delta\bar{d}^T C_d^{-1}G]^T.I - I.G^T.C_d^{-1}\delta\bar{d} + I.G^T.C_d^{-1}G.\delta\bar{m} + [\delta\bar{m}^T G^T.C_d^{-1}G]^T.I &= \bar{0} \\ \Rightarrow -2.G^T.C_d^{-1}\delta\bar{d} + 2.G^T.C_d^{-1}G.\delta\bar{m} &= \bar{0} \\ \Rightarrow G^T.C_d^{-1}\delta\bar{d} &= G^T.C_d^{-1}G.\delta\bar{m}, \text{ or} \\ \delta\bar{m} &= (G^T.C_d^{-1}G)^{-1}(G^T.C_d^{-1})\delta\bar{d} \equiv \delta\bar{m}_{L_2} \end{aligned}$$

Which is the least squares solution. Now let,

$$\delta\bar{d}_0 = \bar{d} - \bar{g}(\bar{m}_0), \text{ and } G_0 = \left. \frac{\partial \bar{g}}{\partial \bar{m}} \right|_{\bar{m}=\bar{m}_0}, \text{ then}$$

$$\delta\bar{m}_1 \equiv \delta\bar{m}_{L2} = (G_0^T C_d^{-1} G_0)^{-1} G_0^T C_d^{-1} \delta\bar{d}_0,$$

$$\bar{m}_1 = \bar{m}_0 + \delta\bar{m}_1, \text{ and}$$

$$\delta\bar{d}_1 = \bar{d} - \bar{g}(\bar{m}_1), \text{ and } G_1 = \left. \frac{\partial \bar{g}}{\partial \bar{m}} \right|_{\bar{m}=\bar{m}_1} \dots \text{ and so on.}$$

So, we start with $\delta\mathbf{m}_I$ as the initial guess, and compute successive iterations of the perturbation:

$$\delta\bar{d}_n = \bar{d} - \bar{g}(\bar{m}_n), \text{ and } G_n = \left. \frac{\partial \bar{g}}{\partial \bar{m}} \right|_{\bar{m}=\bar{m}_n}$$

$$\delta\bar{m}_{n+1} = (G_n^T C_d^{-1} G_n)^{-1} G_n^T C_d^{-1} \delta\bar{d}_n,$$

$$\bar{m}_{n+1} = \bar{m}_n + \delta\bar{m}_{n+1}$$

- 4(vii).** Linearization works only when we can ignore the higher order terms (“HOT”, above). Thus, if the higher order derivatives are not negligible, as in the case of a very rough $\phi(\mathbf{m})$, this approximation fails. So, this approximation works well for “smooth” or weakly-nonlinear inverse problems. In addition, we also need a “good” first guess to the true model – that is, the reference model must be close enough to the true model for the iterations to converge to the global minimum.

4(viii). Let the covariance of the data vector, \mathbf{d} , be equal to C_d . We are given that $\mathbf{m} = G^g \mathbf{d}$. We want to find the covariance of the model parameters, \mathbf{m} . For simplicity, we write the above relationship as, $\mathbf{m} = A\mathbf{d}$. Now, each term of the model covariance matrix can be represented as:

$$\begin{aligned}
 C_{M,ij} &= Cov(m_i, m_j) = E[(m_i - E[m_i])(m_j - E[m_j])] \\
 &= E[m_i m_j] - E[m_i]E[m_j] \\
 &= E[(A_{ik} d_k)(A_{jm} d_m)] - E[A_{ik} d_k]E[A_{jm} d_m] \\
 &= E[(A_{ik} d_k d_m A_{mj}^T)] - A_{ik} E[d_k]E[d_m]A_{mj}^T \\
 &= A_{ik} E[d_k d_m]A_{mj}^T - A_{ik} E[d_k]E[d_m]A_{mj}^T \\
 &= A_{ik} (E[d_k d_m] - E[d_k]E[d_m])A_{mj}^T \\
 &= A_{ik} Cov(d_k, d_m)A_{mj}^T \\
 \therefore C_{M,ij} &= A_{ik} C_{d,km} A_{mj}^T
 \end{aligned}$$

or, $C_M = AC_d A^T$

Substituting the actual value of A into the last equation gives,

$$C_M = G^{-g} C_d G^{-g T}$$

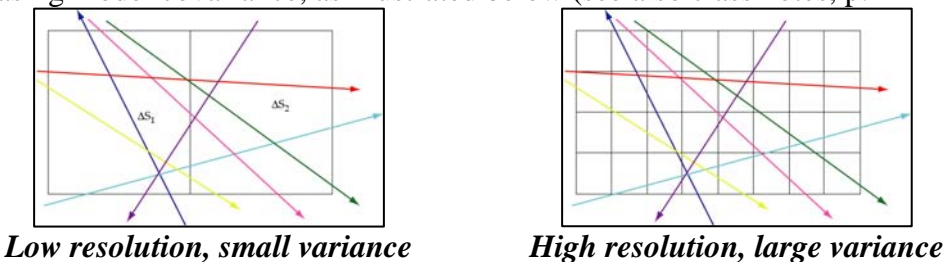
Like C_d , C_M is also a symmetric positive definite matrix. If we normalize the off-diagonal terms of each row of C_M , we obtain a dimensionless correlation matrix, ρ , which gives us the correlations among model parameters. If the off-diagonal terms of ρ are close to zero, then all model parameters can be independently estimated using the assumed forward model and the given data. If any of the off-diagonal terms are close to 1 (say ij^{th} term), then the corresponding model parameters (i^{th} and j^{th} parameters) are highly dependent on each other and cannot be independently estimated from the given data and our assumed model.

4(ix). The model resolution matrix, R , is defined from the following:

$$\bar{\mathbf{m}}_{\text{est}} = G^{-g} \bar{\mathbf{d}}_{\text{obs}} = G^{-g} G \bar{\mathbf{m}}_{\text{true}} = R \bar{\mathbf{m}}_{\text{true}}$$

For the least squares solution (over-determined problem), all model parameters are well resolved, i.e., they can be determined independent of each other, and $R = I$. Usually, R is a function of the inverse operator, G^g , and tends to have non-zero off-diagonal terms, indicating a statistical dependence between the elements of the model vector, \mathbf{m} . So, R determines what combinations of model parameters can be resolved by our assumed model, given the data.

4(x). For an underdetermined system (coarse parametrization), the model resolution has a broad scale length – that is, the individual model parameters are poorly resolved - but the model covariances are small. If we choose to increase the resolution (finer parametrization), it comes at the cost of increasing model covariance, as illustrated below (see also class notes, p.121-126).



Introduction to inverse problems

Practical sheet 1

Thursday 18th October 2007

Problem 1: Seismic profiling

A seismic profiling experiment is performed where the first arrival times of seismic energy from a mid-crustal refractor are made at distances (km) of

$$\mathbf{x} = \begin{bmatrix} 6.0000 \\ 10.1333 \\ 14.2667 \\ 18.4000 \\ 22.5333 \\ 26.6667 \end{bmatrix} \quad (1)$$

from the source, and are found to be (in seconds after the source origin time)

$$\mathbf{t} = \begin{bmatrix} 3.4935 \\ 4.2853 \\ 5.1374 \\ 5.8181 \\ 6.8632 \\ 8.1841 \end{bmatrix} \quad (2)$$

A two layer flat Earth structure gives the mathematical model

$$t_i = t_o + s_2 x_i$$

where the intercept time t_o depends on the thickness and slowness of the upper layer, and s_2 is the slowness of the lower layer. The estimated noise in first arrival time measurements is believed to be independent and normally distributed with expected value 0 and standard deviation $\sigma = 0.1\text{s}$.

- (a) Find the least squares solution for the two model parameters t_0 and s_2 . Plot the data the fitted model and the residuals.
- (b) Calculate and comment on the parameter correlation matrix. How will the correlation entries be reflected in the appearance of the error ellipsoid?
- (c) Plot the error ellipsoid in the (t_0, s_2) plane and calculate conservative 95% confidence intervals for t_0 and s_2 . Hint: The following MATLAB code will plot a 2-dimensional covariance ellipse, where `covm` is the covariance matrix and `m` is the 2-vector of model parameters.

```

%diagonalize the covariance matrix
[u, lam]=eig(inv(covm));
%generate a vector of angles from 0 to 2*pi
theta=(0:.01:2*pi);
%calculate the x component of the ellipsoid for all angles
r(:,1)=(delta/sqrt(lam(1,1)))*u(1,1)*cos(theta)+...
(delta/sqrt(lam(2,2)))*u(1,2)*sin(theta);
%calculate the y component of the ellipsoid for all angles
r(:,2)=(delta/sqrt(lam(1,1)))*u(2,1)*cos(theta)+...
(delta/sqrt(lam(2,2)))*u(2,2)*sin(theta);
%plot(x,y), adding in the model parameters
plot(m(1)+r(:,1),m(2)+r(:,2))

```

- (d) Evaluate the p value for this model (you may find the MATLAB Statistics Toolbox function `chi2cdf` to be useful here).
- (e) Evaluate the p value of χ^2 for 1000 Monte Carlo simulations using the data prediction from your model perturbed by noise that is consistent with the data assumptions. Compare a histogram of these χ^2 values with the theoretical χ^2 distribution for the correct number of degrees of freedom (you may find the MATLAB statistical toolbox function `chi2cdf` to be useful here).
- (f) Are your p value and Monte Carlo χ^2 distribution consistent with the theoretical modeling and the data set? If not, explain what is wrong.
- (g) Use IRLS to evaluate 1norm estimates for t_0 and s_2 . Plot the data predictions from your model relative to the true data and compare with (a).
- (h) Use Monte Carlo error propagation and IRLS to estimate symmetric 95% confidence intervals on the 1norm solution for t_0 and s_2 .
- (i) Examining the contributions from each of the data points to the 1 norm misfit measure, can you make a case that any of the data points are statistical outliers?

Problem 2: Earthquake location

An earthquake is often approximated as a point source and described by four hypocenter parameters, (x, y, z, t) , origin time and spatial location. The waves generated by an earthquake are registered at seismic stations. An earthquake can be located using the arrival times of the first arriving wave, the P-wave, at several seismic stations. In this exercise we will invert P-wave arrival times for the location and origin time of an earthquake. Methods for locating whales or foreign submarines in the ocean are similar.

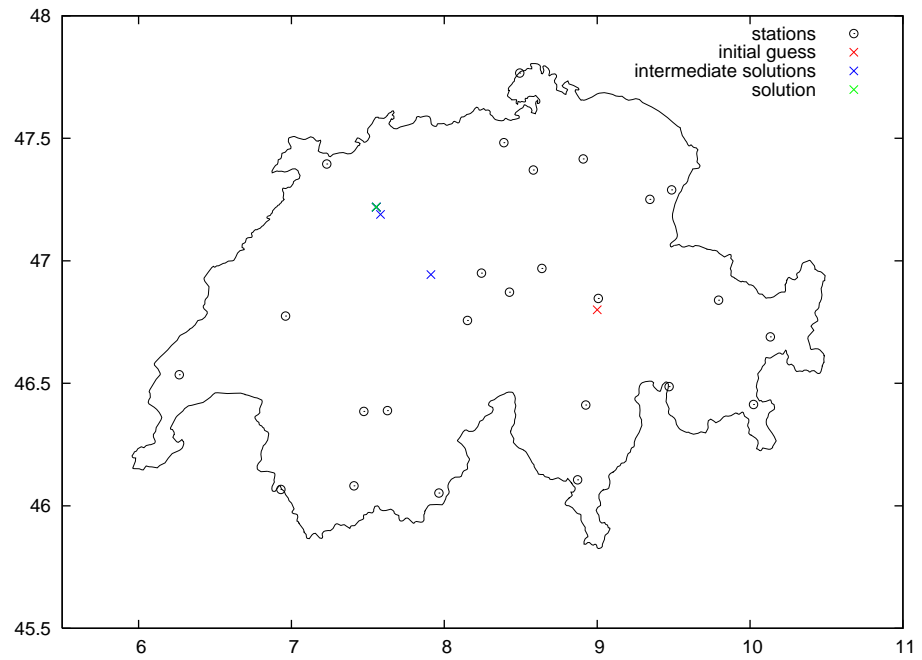
- (a) We will locate an earthquake using P-wave arrival times at stations of the Swiss national seismic network. Assume that the P waves travel with a constant known velocity v_p along straight wave paths. Although a seismologist would not consider these to be valid assumptions we will see that they are quite reasonable for obtaining a good idea of where and when the earthquake occurred. Define t_e as the origin time of the earthquake and (x_e, y_e, z_e) as the spatial location. Set up the system of equations describing the relation between the observed P-wave arrival times and the unknown earthquake parameters. Use the notation (x_i, y_i, z_i) for the location of the i-th station of the network.
- (b) Is retrieving the hypocenter from P wave arrival times a linear or a non-linear inverse problem? why ?
- (c) Earthquake depth is often poorly constrained. In this exercise we fix the depth to be $z_e = 10$ km. For t_e and epicenter (x_e, y_e) we have to make an initial guess that we will improve through inversion. Let's use the notation t_0 and (x_0, y_0) for the initial guess. Now make a first order Taylor expansion of the earthquake-station distance $D(x_e, y_e)$ around (x_0, y_0) . Here we approximate the epicenter by $x_e = x_0 + \delta x$ and $y_e = y_0 + \delta y$. Insert the Taylor expansion in your expression for the arrival time and obtain a linear relationship between arrival times and hypocentre perturbations.
- (d) Define the data d_i at station i as the difference between the original P wave arrival time t_i and the predicted arrival time determined from the initial guess original time t_0 and epicentre (x_0, y_0) . Define the model as $(m_1, m_2, m_3)^T = (\delta t, \delta x, \delta y)^T$. Does this pose a linear or non-linear inverse problem?
- (e) Write out an arbitrary row of matrix G of the earthquake location problem $d_i = G_{i,j} m_j$.
- (f) Now use MATLAB to locate the earthquake. The station coordinates and P wave arrival times are stored in the data file *loctim.txt*. Start MATLAB and store the columns of the data file in separate vectors. The first column contains latitude (in degrees), the second longitude (in degrees), the third elevation (in km), and the fourth P wave arrival time (in s after reference time 16:30) for 25 stations.
- (g) To compute distances we need to know how many km correspond to degree in latitude and longitude. For Switzerland one degree in latitude is approximately 111.19 km and one degree in longitude is about 75.82 km. Store these values and the constant value assumed for $v_p = 5.8$ km/s in separate MATLAB parameters.
- (h) Now make a first guess at the origin time and epicenter (t_0, x_0, y_0) . It might help to first draw the station locations on a "map", using the commands `plot(lon,lat,'*')` hold on Then

guess t_0 by dividing the estimated distance from guessed epicenter to a station by the P wave velocity. Enter the guesses in MATLAB variables and plot the location on the "map". The file *border.xy* contains the boundary for Switzerland.

- (i) Let MATLAB compute the vector $D_0 = D(x_0, y_0)$ with distances to all stations, the data vector with arrival time corrected for the arrival times predicted from the first guess, and the matrix G as defined in (8). (Make sure that the data vector is vertical.)
- (j) Let MATLAB compute the generalized inverse matrix G^{-g} for the least squares solution $m_j = G_{j,i}^{-g} d_i$ to the problem $d_i = G_{i,j} m_j$.
- (k) Using G^{-g} let MATLAB compute the model vector \mathbf{m} , which represents deviations to the initial guess. Then update the initial guess with the values for vector \mathbf{m} and plot the new epicenter on the "map".
- (l) Redefine the initial guess as the updated epicenter and origin time and repeat procedure 10 through 12 until the solution has converged. In this way we solve a non-linear inverse problem by iteratively solving a linearized version of the inverse problem.
- (m) Using 1s estimated standard deviation in the data. Calculate the data prediction error of your solution. Then apply the goodness of fit test. What significance level (p value or %) do you get for the solution. Interpret the result.
- (n) Finally let MATLAB compute the covariance matrix for model vector \mathbf{m} and estimate the standard deviation in origin time and epicentral coordinates, presuming for simplicity that the arrival time data have a standard deviation of 1 s.
- (o) Compare your solution for this earthquake, which occurred on Nov 13, 2000, with the SED (Swiss Seismological Service) solution. Is it consistent ?

D a t e T i m e (U T C) L o c a t i o n D e p M a g n i . T A G Y R e g i o n H H M M
 13Nov2000 16:30:40.1 47.2N 7.6E 10 ML=3.4 M*SED Balsthal / Switzerland

Do you get something like this ?



Introduction to inverse problems

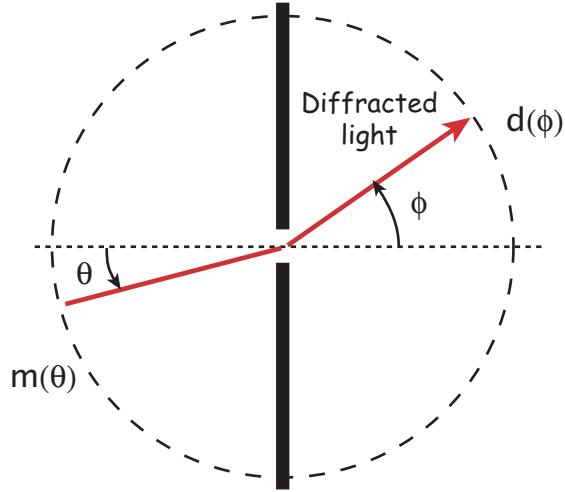
Practical sheet 2

Thursday 8th November 2007

Singular value decomposition

When light passes through a thin slit it is diffracted. The distribution of light intensity as a function of incidence angle θ is represented by $m(\theta)$. After passing through the slit it becomes $d(\phi)$, where ϕ is the angle as defined in the figure. $m(\theta)$ and $d(\phi)$ are related by the expression

$$d(\phi) = \int_{-\pi/2}^{\pi/2} (\cos(\phi) + \cos(\theta))^2 \left(\frac{\sin(\pi(\sin(\phi) + \sin(\theta))))}{\pi(\sin(\phi) + \sin(\theta))} \right)^2 m(\theta) d\theta \quad (1)$$



Here the data are measured intensity $d(\phi)$ at N equal intervals, $d(\phi_i) = d_i$, ($i = 1, \dots, N$) where $-\frac{\pi}{2} \leq \phi_i \leq \frac{\pi}{2}$, and the model is the incident intensity $m(\theta)$ discretized over the same angular intervals, $m(\theta_j) = m_j$, ($j = 1, \dots, N$), which leads to a discrete linear system of $N \times N$ equations, $\mathbf{d} = \mathbf{Gm}$, where

$$G_{i,j} = \Delta\phi (\cos(\phi_i) + \cos(\theta_j))^2 \left(\frac{\sin(\pi(\sin(\phi_i) + \sin(\theta_j))))}{\pi(\sin(\phi_i) + \sin(\theta_j))} \right)^2 \quad (2)$$

This results in a severely ill-posed inverse problem. MATLAB routine `[G, m, d] = shaw(20)` computes the G matrix along with a sample model and data for this problem with $N = 20$.

1. Calculate the singular values of the G matrix. Plot singular values s_i as a function of index i on a semi-log plot. What do you notice about the shape?

[You may find routine `svd` helpful here `[U, S, V] = svd(G)`. Note that eigenvalues are along the diagonal of matrix S (`diag(S)`). and a semilog plot is achieved with routine `semilogy`.]

2. Use MATLAB commands to get the rank and condition number of G . What do these terms mean ? Can you see how they are affect in the eigenvalue spectrum ?
3. Plot the eigenvector corresponding to the smallest non zero eigenvalue (i.e. s_p , where $p=\text{rank of } G$). What do you notice about its shape ?

For all of these plots a script like this might help

```
figure(2);
clf;
bookfonts
plotconst(V(:,p),-pi/2,pi/2);
ylabel('Intensity')
xlabel('\theta (radians)')
```

4. Plot the eigenvector corresponding to the the largest and 5th largest eigenvalue. Look at these together with your previous plot. How does the shape changes with eigenvalue ?
5. Generate an input spike model \mathbf{m} with zeros everywhere and the 10th element equal to 1. Plot this model, calculate the corresponding data using $\mathbf{d} = \mathbf{G}\mathbf{m}$ and plot this.

[You may find routine `zeros(20,1)` useful here.]

6. Apply the generalized inverse $\mathbf{G}^\dagger \mathbf{d} = \mathbf{V}_p \mathbf{S}_p^{-1} \mathbf{U}_p^T \mathbf{d}$ to obtain solutions for different values of p . Choose the highest p and lowest p and compare the models. How good is the recovery ?

[Note that `p=10; Up=U(:,1:p);` will set U_p to the matrix containing the first p columns of U .]

7. Now add 20 realizations of normal random noise with zero mean and standard deviation $\sigma = 10^{-6}$ to the data vector. Plot the noisy data and the no noise data on the same figure. Do you see much difference ?

[You may find a command of this form useful here

```
dn=spikedata+1.0e-6*randn(size(spikedata));
```

8. Calculate the solution for the noisy data, using the full rank of the generalized inverse, i.e. `p=rank(G)`. Plot the solution. How does it compare to the true solution ? What has happened ?

9. Calculate a solution by truncating the SVD to a smaller number of singular values and find a value for p which you think best recovers the true spike model. By reducing p what have you managed to do to the inverse problem ? What has been sacrificed to achieve this.

10. Repeat the exercise for the case with 100 data at equal intervals and with the model discretized at 100 intervals ($N=100$).

[i.e. use `[G100,m100,d100]=shaw(100); [U100,S100,V100]=svd(G100);`] Look at the eigenvalue spectrum, for this case. What do you notice about its shape ? Can you use this

to choose an optimal p value ? Generate a spike model ($m_j = 0; j = 1, \dots, 100; m_{50} = 1$) with noisy data as before and use you p value to generate a model. What is the recovery like now ?

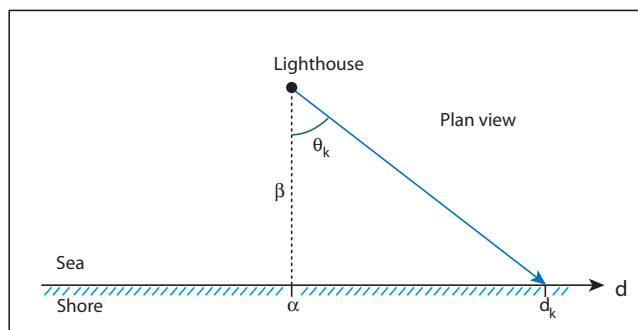
11. Repeat the exercise with only 6 data and 6 unknowns. How does the best solution change bewteen the N=6 and N=100 case and why ?

Introduction to inverse problems: Practical sheet 3

Wednesday 28th November 2007

Bayesian inference: The lighthouse problem

A lighthouse is somewhere off of a straight coastline at position α along the shore and a distance β out at sea¹. It emits a series of short highly collimated flashes at random intervals and hence random azimuths. These pulses are intercepted on the coast by photo-detectors that record only the fact that a flash has occurred, but not the angle from which it came. N flashes have been recorded at positions d_k , ($k = 1, \dots, N$). The problem is to find the lighthouse using the data.

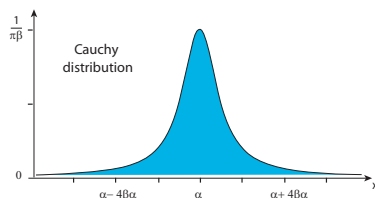


1. If θ_k is the rotation angle of the k -th flash ($-\pi/2 \leq \theta_k \leq \pi/2$). What is the relationship between θ_k and d_k ?
2. What is the probability density function (PDF) of the angles $p(\theta_k|\alpha, \beta)$?
3. Using the rule of transformation of variables,

$$p(x)dx = p(\theta)d\theta$$

what is the PDF of the observations $p(d_k|\alpha, \beta)$?

4. If random flashes are independent, then what is the likelihood function of the data given the model parameters (α, β) ? [Note that this can be written as $p(\mathbf{d}|\alpha, \beta)$.]
5. The answer to the previous question should be a symmetric Cauchy distribution.



¹The lighthouse problem was originally devised by Gull (1988) as an instructive problem for Cambridge undergraduates.

If the distance out to sea of the lighthouse, β , is known, what statistic of the data would you choose as an estimate of α ?

6. Lets generate some data for the case $\beta = \alpha = 1\text{km}$. With $N = 1, 2, 3, 8, 64, 512, 1024$ calculate random angles of the lighthouse flashes θ_k , ($k = 1, \dots, N$) and transform these to the measured data d_k , ($k = 1, \dots, N$).
7. Let's choose the mean of the data as an estimator of the lighthouse position [Was that your choice in 5 above ?] For each set of data calculate the mean of the d_k and compare to the true value of the lighthouse position ($\alpha = 1$). What do you notice as the number of data increases ?
8. Now we take a Bayesian approach to this problem. You already have the likelihood function $p(\mathbf{d}|\alpha, \beta)$. Lets choose a suitable prior for α to be uniform in the interval $\alpha_{\min} \leq \alpha \leq \alpha_{\max}$.

$$p(\alpha|\beta) = \begin{cases} A & \alpha_{\min} \leq \alpha \leq \alpha_{\max} \\ 0 & \text{otherwise} \end{cases}$$

where $A = [\alpha_{\max} - \alpha_{\min}]^{-1}$. Using Bayes' rule write down an expression for the log of the a posteriori density function $L = \ln[p(\alpha|\mathbf{d}, \beta)]$.

9. In generating the data sets above we used $\alpha = 1\text{ km}$, this is the true value of the lighthouse position. Now we see how the shape of the a posteriori PDF as a function of α compares to the true value. Plot $p(\alpha|\mathbf{d}, \beta)$ against α for each of the data sets and see how it changes as a function of the number of data collected N .

[Note: in plotting we only require the shape of the a posteriori PDF, $p(\mathbf{d}|\alpha, \beta)$, the absolute value is not needed. To avoid potential numerical underflows do the following: Calculate L for a uniform grid of α values between $\alpha_{\max} = 5\text{km}$ and $\alpha_{\min} = -5\text{km}$. Calculate L_{\max} ; subtract it from each L and then take exponentials to get $p(\alpha|\mathbf{d}, \beta)$. This will scale the maximum value to one, and allow $p(\alpha|\mathbf{d}, \beta)$ to be plotted against α .]

10. Mark on each plot the true position of the lighthouse and estimated value using the mean of the data. How does the Bayesian approach compare to the statistical approach in estimating α from the data ?
11. Has the central limit theorem been violated here ?

Interpretation of Inaccurate, Insufficient and Inconsistent Data

D. D. Jackson

(Received 1972 January 27)*

Summary

Many problems in physical science involve the estimation of a number of unknown parameters which bear a linear or quasi-linear relationship to a set of experimental data. The data may be contaminated by random errors, insufficient to determine the unknowns, redundant, or all of the above. This paper presents a method of optimizing the conclusions from such a data set. The problem is formulated as an ill-posed matrix equation, and general criteria are established for constructing an ‘inverse’ matrix. The ‘solution’ to the problem is defined in terms of a set of generalized eigenvectors of the matrix, and may be chosen to optimize the resolution provided by the data, the expected error in the solution, the fit to the data, the proximity of the solution to an arbitrary function, or any combination of the above. The classical ‘least-squares’ solution is discussed as a special case.

1. Formulation of the problem

Suppose that we wish to determine a set of unknown parameters $x_j, j = 1, \dots, m$ from a set of data $y_i, i = 1, \dots, n$ where y_i are each functionally related to the x_j in a known way. That is

$$\begin{aligned} y_1 &= A_1(x_1, \dots, x_m) \\ \vdots & \\ y_n &= A_n(x_1, \dots, x_m). \end{aligned}$$

Such a set of equations may arise by approximation of a continuous relationship $y(\eta) = A[\eta, x(\xi)]$ by a discrete representation, letting $y_i = y(\eta_i)$, $x_j = x(\xi_j)$; or by expansion of the continuous functions $y(\eta)$ and $x(\xi)$ in terms of appropriate sets of orthogonal functions, in which case y_i and x_j represent expansion coefficients (See Table 1 for notation conventions.)

If the functions $A_i(x_j)$ are linear in x_j , we may write the problem in matrix form

$$y_i = A_{ij} x_j \quad (1a)$$

or

$$\mathbf{y} = \mathbf{Ax}. \quad (1b)$$

* Received in original form 1971 October 29.

Table 1*Notation Conventions*

1. Repeated indices imply summation unless otherwise noted.
2. A bold-face block capital letter represents matrix of coefficients (e.g. $\mathbf{A} = (A_{ij})$).
3. A bold-face lower case letter represents a column vector (e.g. $\mathbf{x} = (x_i)$).
4. $\text{var}(x_k)$ represents the variance of x_k .

If the functions $A_i(x_j)$ are not strictly linear, but vary smoothly enough, they may be expanded in a Taylor series about some set of initial values of the x_j , say x_j^0

$$y_i = A_i(x_j^0) + \frac{\partial A_i}{\partial x_j} \Big|_{x_j^0} \Delta x_j + \dots \quad (2)$$

Defining $y_i \equiv A_i(x_j^0) + \Delta y_i$ and ignoring second and higher order terms in (2), we have

$$\Delta y_i = \frac{\partial A_i}{\partial x_j} \Big|_{x_j^0} \Delta x_j.$$

This is the same form as equation (1a), with the substitution of Δy_i for y_i ; Δx_j for x_j , and

$$\frac{\partial A_i}{\partial x_j} \Big|_{x_j^0} = A_{ij}.$$

For simplicity, we shall proceed using the notation of equation (1), with the understanding that the above substitution can be made at any stage of the calculations for a system which results from the perturbation of a quasi-linear problem.

Problem (1) may be approached by operating on both sides with an $(m \times n)$ ‘inverse’ matrix \mathbf{H} and letting the ‘solution’, or *model*, be

$$\hat{\mathbf{x}} \equiv \mathbf{H}\mathbf{Ax} = \mathbf{Hy}. \quad (3)$$

The operator \mathbf{H} will be a good inverse if it satisfies the following criteria.

(a) $\mathbf{AH} \approx \mathbf{I}_n$, the $n \times n$ identity matrix. This is a measure of how well the model fits the data, since $\mathbf{Ax} = \mathbf{y}$ if $\mathbf{AH} = \mathbf{I}_n$.

(b) $\mathbf{HA} \approx \mathbf{I}_m$. This is a measure of the uniqueness of the solution, since there may exist only one solution if $\mathbf{HA} = \mathbf{I}_m$.

(c) the uncertainties in $\hat{\mathbf{x}}$ are not too large, i.e. $\text{var}(\hat{\mathbf{x}})$ is small. For statistically independent data,

$$\text{var}(\hat{x}_k) = \sum_{i=1}^n H_{ki}^2 \text{var}(y_i). \quad (4)$$

Backus & Gilbert (1968) pointed out that, for under-determined systems, the product matrix \mathbf{HA} has a physical meaning related to the establishment of ‘unique’ properties of the solutions to equation (1). That is,

$$\hat{\mathbf{x}} = \mathbf{Rx}, \quad (5)$$

where $\mathbf{R} \equiv \mathbf{HA}$.

The matrix \mathbf{R} maps the entire set of solutions \mathbf{x} into a single vector $\hat{\mathbf{x}}$. Any element of $\hat{\mathbf{x}}$, say \hat{x}_k , may be interpreted as the result of convolving the k^{th} row of \mathbf{R} with any vector which satisfies (1). Thus, \mathbf{R} is a matrix whose rows are ‘windows’ through which we may view the general solution \mathbf{x} and obtain a unique result. If \mathbf{R} is an

identity matrix, the solution $\hat{\mathbf{x}}$ is unique, and each element is perfectly resolved. If \mathbf{R} is a near diagonal matrix, each element \hat{x}_k is in fact a weighted sum of nearby values x_j , j near k , for *any* solution to (1). Thus, the degree to which \mathbf{R} approximates the identity matrix is a measure of the resolution obtainable from the data. The rows of \mathbf{R} are thus called ‘resolving kernels’.

In a similar way, Wiggins (1972) showed that, for over-constrained systems, the product $\mathbf{S} \equiv \mathbf{A}\mathbf{H}$ is a measure of the independence of the data. The ‘theoretical’ data $\hat{\mathbf{y}} \equiv \mathbf{A}\hat{\mathbf{x}} = \mathbf{A}\mathbf{H}\mathbf{y}$ are a convolution of the matrix \mathbf{S} with the actual data \mathbf{y} . The matrix \mathbf{S} is referred to as the information density matrix.

The criteria (a), (b) and (c) are not equally important in all cases, and may be weighted for specific problems. Additional physical constraints may apply in some cases. The procedure below allows these to be incorporated easily.

2. The well-posed case

Consider as an example the case where \mathbf{A} is a square, symmetric, non-singular matrix. Elementary matrix theory (e.g. Hildebrand 1965) tells us that there exists a unique inverse \mathbf{A}^{-1} such that $\mathbf{A}\mathbf{A}^{-1} = \mathbf{A}^{-1}\mathbf{A} = \mathbf{I}_n$, the $n \times n$ identity matrix. Thus, criteria (a) and (b) are satisfied exactly and there is a unique solution, $\hat{\mathbf{x}} = \mathbf{A}^{-1}\mathbf{y}$, which satisfies the data exactly. The variance of the model will depend upon how non-singular the matrix \mathbf{A} really is.

The nature of the singularity is best understood in terms of the eigenvalues of the matrix \mathbf{A} . The eigenvectors \mathbf{v}_i and eigenvalues λ_i are defined by the equations

$$\mathbf{A}\mathbf{v}_i = \lambda_i \mathbf{v}_i \quad (\text{no summation})$$

where the \mathbf{v}_i are orthonormal, i.e.

$$\mathbf{v}_i^T \mathbf{v}_j = \delta_{ij}.$$

The matrix \mathbf{A} may be factored into the product

$$\mathbf{A} = \mathbf{V}\Lambda\mathbf{V}^T$$

where \mathbf{V} is an $n \times n$ matrix called an ‘orthonormal modal matrix’, whose columns are the eigenvectors \mathbf{v}_i , and Λ is an $n \times n$ diagonal matrix whose elements are the eigenvalues λ_i . It may be assumed without loss of generality that the eigenvalues are written in decreasing order of their absolute value, and that the eigenvectors are ordered correspondingly in the matrix \mathbf{V} . The matrix \mathbf{V} has the convenient properties

$$\mathbf{V}^T \mathbf{V} = \mathbf{V}\mathbf{V}^T = \mathbf{I}_n.$$

The inverse matrix \mathbf{A}^{-1} may then be written

$$\mathbf{A}^{-1} = \mathbf{V}\Lambda^{-1}\mathbf{V}^T \quad (6)$$

where Λ^{-1} is a diagonal matrix whose elements are λ_i^{-1} . Thus, the inverse matrix will cease to exist if any of the eigenvalues λ_i is zero. If λ_i is non-zero but very small, the operator \mathbf{A}^{-1} exists but does not satisfy criterion (c); that is, for statistically independent data,

$$\text{var } \hat{x}_k = \sum_{i=1}^n \left\{ \sum_{j=1}^n V_{kj} \lambda_j^{-1} V_{ij} \right\}^2 \text{var}(y_i)$$

will be very large because of the reciprocal eigenvalue in the bracket.

3. Generalized eigenvector analysis

Eigenvector analysis can be extended to the general real $n \times m$ case as discussed by Lanczos (1961). Two sets of eigenvectors \mathbf{u}_i and \mathbf{v}_j may be found such that

$$\mathbf{A} \mathbf{v}_j = \lambda_j \mathbf{u}_j \quad (\text{no summation}) \quad (7a)$$

$$\mathbf{A}^T \mathbf{u}_i = \lambda_i \mathbf{v}_i \quad (\text{no summation}) \quad (7b)$$

or

$$\mathbf{A}^T \mathbf{A} \mathbf{v}_j = \lambda_j^2 \mathbf{v}_j \quad j = 1, \dots, m \quad (\text{no summation}) \quad (8a)$$

$$\mathbf{A} \mathbf{A}^T \mathbf{u}_i = \lambda_i^2 \mathbf{u}_i \quad i = 1, \dots, n \quad (\text{no summation}) \quad (8b)$$

We shall again assume that the eigenvalues are ranked in decreasing order of magnitude. It can then be shown that

$$\lambda_i = \lambda_j \quad \text{if} \quad i = j, \quad i \leq p$$

$$\lambda_i = 0 \quad i > p$$

$$\lambda_j = 0 \quad j > p$$

for some integer p less than or equal to the minimum of m and n . That is, there are p non-zero eigenvalues common to (8a) and (8b), and all other eigenvalues are zero. The integer p may be interpreted as the potential number of degrees of freedom in the data.

The matrix \mathbf{A} can be factored into the product

$$\mathbf{A} = \mathbf{U} \mathbf{A} \mathbf{V}^T \quad (9)$$

where \mathbf{U} is an $n \times p$ matrix whose columns are the eigenvectors $\mathbf{u}_i, i = 1, \dots, p$; \mathbf{V} is the $m \times p$ matrix whose columns are the eigenvectors $\mathbf{v}_i, i = 1, \dots, p$ and Λ is the diagonal matrix of eigenvalues. After \mathbf{U} and \mathbf{V} are formed from the eigenvectors corresponding to the p non-zero eigenvalues, there remain $(n-p)$ eigenvectors \mathbf{u}_i , and $(m-p)$ eigenvectors \mathbf{v}_j , corresponding to zero eigenvalues. It is convenient to assemble these into the columns of matrices also, and to denote these matrices as \mathbf{U}_0 [an n by $(n-p)$ matrix] and \mathbf{V}_0 [an m by $(m-p)$ matrix]. By the orthonormality of the eigenvectors \mathbf{u}_i , we may obtain the following relationships

$$\mathbf{U}^T \mathbf{U} = \mathbf{I}_p \quad (10a)$$

$$\mathbf{U}_0^T \mathbf{U}_0 = \mathbf{I}_{n-p} \quad (10b)$$

$$\mathbf{U}^T \mathbf{U}_0 = \mathbf{0} \quad p \times (n-p) \quad (10c)$$

$$\mathbf{U}_0^T \mathbf{U} = \mathbf{0} \quad (n-p) \times p. \quad (10d)$$

If $p = n$, then \mathbf{U} contains the complete set of eigenvectors of the symmetric matrix $[\mathbf{A} \mathbf{A}^T]$, and is therefore an orthonormal modal matrix. It then satisfies

$$\mathbf{U} \mathbf{U}^T = \mathbf{I}_n \quad (10)$$

I shall demonstrate below that the condition $p = n$ guarantees the existence of a solution.

The eigenvectors $\mathbf{v}_i, i = 1, \dots, m$ are similarly a complete set of orthonormal vectors in the ‘model’ space. We have separated them into two groups: those to

which the model is sensitive (i.e. those in \mathbf{V}), and those which are annihilated by \mathbf{A} (i.e. those in \mathbf{V}_0). The matrices \mathbf{V} and \mathbf{V}_0 obey the same type of relationship as \mathbf{U} and \mathbf{U}_0

$$\mathbf{V}^T \mathbf{V} = \mathbf{I}_p \quad (11a)$$

$$\mathbf{V}_0^T \mathbf{V}_0 = \mathbf{I}_{m-p} \quad (11b)$$

$$\mathbf{V}^T \mathbf{V}_0 = \mathbf{0} \quad px(m-p) \quad (11c)$$

$$\mathbf{V}_0^T \mathbf{V} = \mathbf{0} \quad (m-p) \times p. \quad (11d)$$

If $p = m$, then \mathbf{V} contains the complete set of eigenvectors of the symmetric matrix $[\mathbf{A}^T \mathbf{A}]$, and is therefore an orthonormal modal matrix. It then satisfies

$$\mathbf{V}\mathbf{V}^T = \mathbf{I}_m. \quad (11)$$

The condition $p = m$ guarantees that, if a solution to equation (1) exists, it will be unique.

Before proceeding, it may be worthwhile to give a simple interpretation to equation (9). In an equation such as $\mathbf{B}\mathbf{f} = \mathbf{g}$ the column vector \mathbf{g} may be looked upon as a weighted sum of the columns of \mathbf{B} with the weighting factors given by the elements of the column vector \mathbf{f} . The matrix product $\mathbf{BF} = \mathbf{G}$ may be considered column by column: the first column of the matrix \mathbf{G} is a weighted sum of the columns of \mathbf{B} , with weighting factors $\mathbf{F}_{11}, \mathbf{F}_{21}$, etc., and similarly for the rest of the columns. A similar argument holds for row vectors: in the equation $\mathbf{f}^T \mathbf{B}^T = \mathbf{g}^T$, the row vector \mathbf{g}^T is a sum of the rows of \mathbf{B}^T with the same weighting factors as above. In the product $\mathbf{F}^T \mathbf{B}^T = \mathbf{G}^T$, each row of \mathbf{G}^T is a weighted sum of the rows of \mathbf{B}^T , with the weighting factors given in the appropriate rows of \mathbf{F}^T . Thus, in a long string of matrix multiplications, each column of the product matrix is a weighted sum of the columns of the *first* matrix in the string, and each row of the product is a sum of the rows of the *last* column in the string. Thus, from equation (9), each column of the matrix \mathbf{A} is a weighted sum of the columns of \mathbf{U} ; that is, the eigenvectors $\mathbf{u}_i, i = 1, \dots, p$. Each row of \mathbf{A} is a sum of the eigenvectors $\mathbf{v}_i, i = 1, \dots, p$.

Because the n eigenvectors $\mathbf{u}_i, i = 1, \dots, n$ form a complete set, we may express the data vector \mathbf{y} as a sum of the \mathbf{u}_i ; that is,

$$\mathbf{y} = \sum_{i=1}^n \beta_i \mathbf{u}_i = \sum_{i=1}^p \beta_i \mathbf{u}_i + \sum_{i=p+1}^n \beta_i \mathbf{u}_i = \mathbf{U}\beta + \mathbf{U}_0 \beta_0 \quad (12)$$

where the vector β has the p components β_1, \dots, β_p , and β_0 has the $(n-p)$ components $\beta_{p+1}, \dots, \beta_n$. By (10a) and (10b), $\beta = \mathbf{U}^T \mathbf{y}$, and $\beta_0 = \mathbf{U}_0^T \mathbf{y}$. In a similar way, we may express the ‘unknown’ vector $\boldsymbol{\epsilon}$ in terms of the $\mathbf{v}_i, i = 1, \dots, m$.

$$\mathbf{x} = \mathbf{V}\alpha + \mathbf{V}_0\alpha_0 \quad (13)$$

where $\alpha = \mathbf{V}^T \mathbf{x}$ is a vector with p components and $\alpha_0 = \mathbf{V}_0^T \mathbf{x}$ is a vector with $m-p$ components.

If we then replace all the quantities in equation (1) with the equivalent expressions in (9), (12) and (13), the ‘transformed’ equation becomes

$$\mathbf{UAV}^T [\mathbf{V}\alpha + \mathbf{V}_0\alpha_0] = \mathbf{U}\beta + \mathbf{U}_0\beta_0 \quad (14)$$

and the problem is now to find the unknown vectors α and α_0 . The existence of a solution is equivalent to the vanishing of the ‘residual’ vector, $\boldsymbol{\epsilon} \equiv \mathbf{Ax} - \mathbf{y}$. In the transformed notation

$$|\boldsymbol{\epsilon}|^2 = |\boldsymbol{\epsilon}^T \boldsymbol{\epsilon}| = |\Lambda\alpha - \beta|^2 + |\beta_0|^2. \quad (15)$$

The ‘least squares’ solution is that which minimizes $|\boldsymbol{\epsilon}|^2$, and requires that

$$\alpha = \Lambda^{-1} \beta \quad (16)$$

leaving the ‘least square error’ $|\beta_0|^2 = |\mathbf{U}_0^T \mathbf{y}|^2$. There will exist an exact solution only if $\mathbf{U}_0^T \mathbf{y} = \mathbf{0}$. For $p = n$, this condition must hold, since $\mathbf{U}_0 = \mathbf{0}$. For $p < n$, there may be an exact solution only if the data contain no contribution from the eigenvectors in \mathbf{U}_0 ; this leads to the $n-p$ constraints, $\mathbf{u}_i \cdot \mathbf{y} = 0$, $i = p+1, \dots, n$. When $p < n$, the system is said to be overconstrained.

The vector α_0 does not appear in (15), and thus the α_i may be chosen arbitrarily for $i = p+1, \dots, m$. The least squares solution will be unique only if $p = m$. When $p < m$, the system (1) is said to be underdetermined.

Notice that, if $p < m$ and $p < n$, the system (1) is both overconstrained and underdetermined. In this case, an exact solution may not exist. However, there will exist an infinite number of solutions satisfying the least-squares criterion.

4. The Lanczos inverse

To handle linear systems with the problems discussed above, Lanczos (1961) introduced the ‘natural’ inverse, which is equivalent to the ‘generalized inverse’ of Penrose (1955),

$$\mathbf{H}_L = \mathbf{V}\Lambda^{-1}\mathbf{U}^T. \quad (17)$$

This has a form reminiscent of equation (6). The corresponding model will be

$$\hat{\mathbf{x}}_L = \mathbf{H}_L \mathbf{y} = \mathbf{V}\Lambda^{-1}\mathbf{U}^T \mathbf{y}. \quad (18)$$

Expressing \mathbf{x}_L and \mathbf{y} in terms of their ‘transform’ variables as above,

$$\alpha = \mathbf{V}^T \hat{\mathbf{x}}_L = \Lambda^{-1} \beta \quad (19a)$$

and

$$\alpha_0 = \mathbf{V}_0^T \hat{\mathbf{x}}_L = \mathbf{0}. \quad (19b)$$

The Lanczos inverse has the following desirable properties. (a) It always exists! (b) Comparing (19a) with (16), it is evident that the Lanczos inverse is a ‘least squares’ inverse, and is thus an exact solution, if any exists. (c) Further, $\hat{\mathbf{x}}_L$ is that least squares solution which minimizes $|\mathbf{x}|^2$ since, for a least squares solution,

$$|\mathbf{x}|^2 = \Lambda^{-1} \beta|^2 + |\alpha_0|^2.$$

The first term is fixed, and the second term is minimized by $\alpha_0 = \mathbf{0}$. The property $|\mathbf{x}|^2 = \min$ is a useful one if \mathbf{x} represents a perturbation to some starting model in a quasi-linear problem. (d) The resolution matrix for the Lanczos inverse is given by

$$\mathbf{R} = \mathbf{H}\mathbf{A} = \mathbf{V}\Lambda^{-1}\mathbf{U}^T \cdot \mathbf{U}\Lambda\mathbf{V}^T = \mathbf{V}\mathbf{V}^T. \quad (20)$$

This is the optimum resolving matrix in the sense that it minimizes

$$r_k = \sum_{j=1}^m (H_{kj} A_{ij} - \delta_{kj})^2 \quad (21)$$

for each value of k . Equation (21) may be interpreted thus: each row of \mathbf{R} is the best fit to the corresponding row of the identity matrix, in the least squares sense, which may be formed from the rows of A , and (e) The Lanczos inverse similarity provides the best information density matrix

$$\mathbf{S} = \mathbf{AH} = \mathbf{UU}^T \quad (22)$$

in the sense that it minimizes

$$s_k = \sum_{j=1}^n (A_{kj} H_{ij} - \delta_{kj})^2 \quad (23)$$

I have claimed above that the Lanczos inverse is a least squares inverse, and thus for a purely overconstrained system, it must be identical to the inverse provided

by the standard least squares procedure. This procedure may be stated as follows: find the vector \mathbf{x} which minimizes $|\boldsymbol{\epsilon}|^2 = |\mathbf{Ax} - \mathbf{y}|^2$. We have

$$|\boldsymbol{\epsilon}|^2 = (\mathbf{Ax} - \mathbf{y})^T (\mathbf{Ax} - \mathbf{y}) = \mathbf{x}^T \mathbf{A}^T \mathbf{Ax} - \mathbf{x}^T \mathbf{A}^T \mathbf{y} - \mathbf{y}^T \mathbf{Ax} + \mathbf{y}^T \mathbf{y}.$$

Differentiating with respect to \mathbf{x}^T , and, setting the result equal to 0, we get

$$[\mathbf{A}^T \mathbf{A}] \mathbf{x} = \mathbf{A}^T \mathbf{y}. \quad (24)$$

If the matrix product in brackets is non-singular,

$$\hat{\mathbf{x}} = [\mathbf{A}^T \mathbf{A}]^{-1} \mathbf{A}^T \mathbf{y}. \quad (25)$$

Expressing \mathbf{A} in terms of equation (9),

$$\hat{\mathbf{x}} = [\mathbf{V} \Lambda^2 \mathbf{V}^T]^{-1} \mathbf{V} \Lambda \mathbf{U}^T \mathbf{y}. \quad (26)$$

As long as $p = m$, (that is, the system is not underdetermined) the inverse of the bracketed quantity is

$$\mathbf{V} \Lambda^{-2} \mathbf{V}^T,$$

and we have

$$\hat{\mathbf{x}} = \mathbf{V} \Lambda^{-1} \mathbf{U}^T \mathbf{y} = \mathbf{H}_L \mathbf{y}$$

as advertized.

It is interesting to observe what happens when $p < m$, that is the system is underdetermined as well as overconstrained. Then $\mathbf{A}^T \mathbf{A}$ will be singular, and the standard least squares procedure will fail. However, direct substitution will demonstrate that $\hat{\mathbf{x}} = \mathbf{H}_L \mathbf{y}$ satisfies equation (24) regardless of the singularity of $\mathbf{A}^T \mathbf{A}$. Thus, the standard least squares procedure is a short-cut to the Lanczos inverse for the strictly overconstrained case, but will not guarantee stability for the underdetermined case.

An analogous procedure to 'least squares' applies to the strictly underdetermined case (Smith & Franklin 1969). Here

$$\hat{\mathbf{x}} = \mathbf{A}^T [\mathbf{A} \mathbf{A}^T]^{-1} \mathbf{y} \quad (27)$$

which again is identical to the Lanczos inverse, provided that $\mathbf{A} \mathbf{A}^T$ is non-singular. This requires that $p = n$, that is, that the system not be overconstrained.

5. Modifications of the Lanczos inverse

Until this point, we have assumed that the data were dimensionless and statistically independent, and we have ignored criterion (c), the variance of the model. In this Section, I shall discuss modifications of the Lanczos inversion procedure which address these considerations.

First consider an overconstrained system for which the data are statistically independent, but have different units. One might then wish to generalize the least squares error criterion to minimize

$$\boldsymbol{\epsilon}^T \mathbf{D} \boldsymbol{\epsilon}$$

where \mathbf{D} is a diagonal matrix whose elements are

$$D_i = 1/\text{var}(y_i).$$

In this way, the residual for each data point is compared with its expected error. When the data are not statistically independent, it is logical to choose for D the inverse of the covariance matrix for the data (Kaula 1966). The problem may be handled with the same formulation used in the last section, provided that \mathbf{D} is a symmetric, positive definite matrix (a reasonable assumption for an inverse covariance matrix). I shall show below that there will exist a matrix \mathbf{E} such that $\mathbf{E}^T \mathbf{E} = \mathbf{D}$. We have already solved the problem $\boldsymbol{\epsilon}^T \boldsymbol{\epsilon} = \min$, where $\boldsymbol{\epsilon} = \mathbf{A} \hat{\mathbf{x}} - \mathbf{y}$. Now consider the equation

$$\mathbf{E} \boldsymbol{\epsilon} = \mathbf{E} \mathbf{A} \hat{\mathbf{x}} - \mathbf{E} \mathbf{y} \quad (28)$$

and let $\mathbf{E}\boldsymbol{\varepsilon} = \boldsymbol{\varepsilon}'$, $\mathbf{EA} = \mathbf{A}'$, and $\mathbf{Ey} = \mathbf{y}'$. We now have a problem of the form of equation (1), and we may use the standard least squares procedure or the Lanczos procedure to find $\hat{\mathbf{x}}$ which minimizes

$$\boldsymbol{\varepsilon}'^T \boldsymbol{\varepsilon}' = \boldsymbol{\varepsilon}^T \mathbf{D} \boldsymbol{\varepsilon}.$$

Thus, the problem is solved once \mathbf{E} is found. This may always be accomplished, because the symmetric, positive definite matrix \mathbf{D} may be decomposed into its eigenvectors and eigenvalues (which will be positive)

$$\mathbf{D} = \mathbf{V}_D \Lambda_D \mathbf{V}_D^T \quad (29)$$

and we may set

$$\mathbf{E} = \Lambda_D^{-\frac{1}{2}} \mathbf{V}_D^T \quad (30)$$

This weighting matrix \mathbf{E} puts the data in a dimensionless, statistically independent form. Where the data were already statistically independent, the weighting by \mathbf{E} is equivalent to dividing each equation in the system (1) by the standard deviation of the corresponding data point.

A similar transformation allows the use of the Lanczos procedure to find that solution of an underdetermined problem which minimizes

$$\mathbf{x}^T \mathbf{F} \mathbf{x}$$

where again \mathbf{F} is assumed to be a symmetric positive definite matrix. Where we are able to guess something about the statistics of the unknown parameters (cf. Jordan & Franklin 1971), the matrix \mathbf{F} may be chosen to be the inverse covariance matrix of the model parameters. We then let $\mathbf{x}' = \mathbf{Gx}$ and $\mathbf{A}' = \mathbf{AG}^{-1}$, where \mathbf{G} is selected such that $\mathbf{G}^T \mathbf{G} = \mathbf{F}$. We may then use the Lanczos procedure to find that $\hat{\mathbf{x}}'$ which minimizes $|\mathbf{x}'|^2$, and our desired solution is $\hat{\mathbf{x}} = \mathbf{G}^{-1} \hat{\mathbf{x}}'$.

The above transformations may be combined for the general solution, to find that $\hat{\mathbf{x}}$ which simultaneously minimizes $\boldsymbol{\varepsilon}^T \mathbf{D} \boldsymbol{\varepsilon}$ and $\mathbf{x}^T \mathbf{F} \mathbf{x}$. This is accomplished by letting $\hat{\mathbf{x}} = \mathbf{G}^{-1} \mathbf{H}_L' \mathbf{y}'$ where \mathbf{H}_L' is the Lanczos inverse for the matrix $\mathbf{A}' = \mathbf{EAG}^{-1}$, and $\mathbf{y}' = \mathbf{Ey}$. The effect of these transformations on the resolution and information density matrices is expressed by

$$\mathbf{R} = \mathbf{G}^{-1} \mathbf{R} \mathbf{G} \quad (31)$$

$$\mathbf{S} = \mathbf{E}^{-1} \mathbf{S}' \mathbf{F}. \quad (32)$$

Let us now address the problem of the variance of the model parameters. I have shown that we may assume the data to be statistically independent and to have unit variance, if the appropriate transformations are made in advance. By equation (4), we shall then have

$$\text{var } \hat{x}_k = \sum_{j=1}^p \left(\frac{V_{kj}}{\lambda_j} \right)^2. \quad (33)$$

This will be finite, but because the smallest non-zero eigenvalue may be pretty small, the variance could be unacceptably large. A sensible way to control the variance (Wiggins 1971) is to construct the inverse \mathbf{H} out of only those eigenvectors corresponding to the q largest eigenvalues, where $q \leq p$. This is equivalent to considering an eigenvalue to be zero if it is less than some modest threshold (i.e. assuming p less than it really is). The threshold may be set such that

$$\sum_{j=1}^q \left(\frac{V_{kj}}{\lambda_j} \right)^2 < t_k \quad (34)$$

for all k , where t_k is the maximum allowable variance of \hat{x}_k . The effect of reducing q is to reduce the number of eigenvectors belonging to \mathbf{U} and \mathbf{V} , while increasing by the same amount those belonging to \mathbf{U}_0 and \mathbf{V}_0 . This degrades the resolution and information density, so that we have a tradeoff as indicated symbolically in Fig. 1.

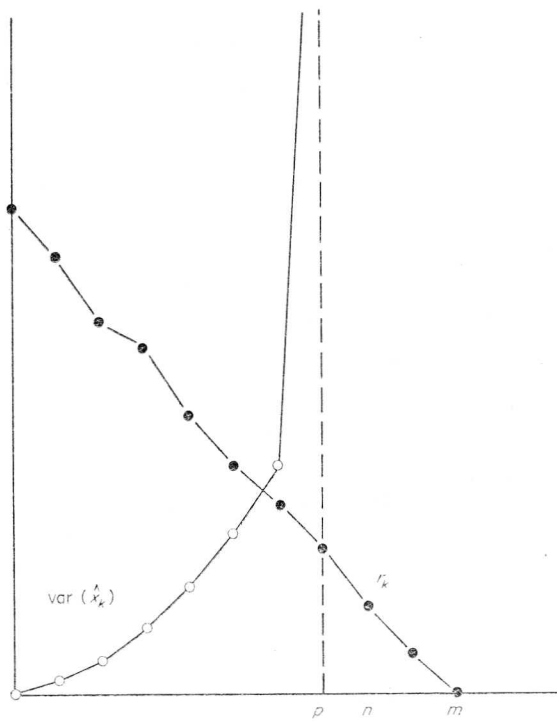


FIG. 1 Schematic diagram showing tradeoff between resolution and variance in the estimation of the k^{th} unknown parameter for a simultaneously underdetermined and overconstrained problem. The effective number of degrees of freedom, q , may be taken to be any integer less than or equal to p . Use of the 'generalized inverse' procedure, which requires that $p = n$, would lead to numerical instabilities for this case.

The integer q is the effective number of degrees of freedom in the data, and depends on the uncertainties in the data as well as on our need for certainty in the model. A great deal of care should be exercised in choosing the appropriate value of q . For systems which are fundamentally underdetermined, the ability to make any reliable interpretation from the model \hat{x} may be limited either by lack of resolution, or by large variance in \hat{x} . Surprisingly, the most important conclusions may often be made on the basis of a model which fits the data very poorly, even though exact solutions exist. This is because the exact solutions are not unique, and because the inverse operators which generate them may rely heavily upon poorly determined features of the data.

Similar arguments hold for systems which are basically overconstrained. If care is not exercised in choosing q , the model may be subject to unnecessarily large variance in an effort to satisfy poorly determined features of the data.

6. Special inverses for underdetermined systems

Let us examine in more detail the case of the strongly underdetermined system. This case will include those problems in which equation (1) is the result of discretizing a continuous relationship between a known function and an unknown function, because we may only handle finite amounts of data, yet we would in principle like to know an infinitude of details about the unknown function. A wise procedure is to use more parameters to describe the unknowns than are likely to be uniquely determined

by the data. One may then form a family of inverses, compare the tradeoff between resolution and variance for this family, and select that inverse which is most appropriate for interpreting the solution. This procedure simultaneously formulates intelligent questions (what is the effective number of degrees of freedom in the data, and which unknowns may be independently determined), while providing an answer with an acceptable variance. In this section, I shall describe some alternate techniques for optimizing the resolving kernels; describe a technique for finding the closest solution to some preassigned function, and discuss the wisdom of taking more data to obtain better resolution.

I have stated above that the Lanczos inverse provides the closest resolution matrix available, in a least squares sense, to the identity matrix. It is instructive to show that, in addition, it provides the most deltalike matrix which may be constructed from the incomplete set of p eigenvectors $\mathbf{v}_1, \mathbf{v}_2, \dots, \mathbf{v}_p$. That is, assume the resolution matrix to be of the form

$$\mathbf{R} = \mathbf{BV}^T. \quad (35)$$

Each row of \mathbf{R} will be some linear combination of the eigenvectors of \mathbf{V} . Let us denote by \mathbf{b}_k^T the k^{th} row of \mathbf{B} , and by δ_k^T the k^{th} row of the identity matrix (i.e. the j^{th} element of this vector is zero for $j \neq k$, 1 for $j = k$). We now determine \mathbf{b}_k^T as the least squares solution to

$$\mathbf{b}_k^T \mathbf{V}^T = \delta_k^T \quad (36)$$

or, transposing,

$$\mathbf{V}\mathbf{b}_k = \delta_k. \quad (37)$$

By (25), the least squares solution is

$$\hat{\mathbf{b}}_k = [\mathbf{V}^T \mathbf{V}]^{-1} \mathbf{V}^T \delta_k = \mathbf{V}^T \delta_k \quad (38)$$

and, transposing back, we have

$$\hat{\mathbf{b}}_k^T = \delta_k^T \mathbf{V}. \quad (39)$$

Performing this operation for every row, we have

$$\mathbf{B} = \mathbf{V} \quad (40)$$

and the most deltalike resolution matrix is

$$\mathbf{R} = \mathbf{VV}^T \quad (41)$$

identical to the Lanczos inverse.

The modified Lanczos inverse discussed in the last section controls the variance of the model by using only q of the possible p eigenvectors in the inverse. As phrased above, the same q eigenvectors are used in constructing each row of \mathbf{H} . However, it is useful to note in equation (4) that the variance of the k^{th} model parameter depends only on the parameters of the k^{th} row of \mathbf{H} . We may construct an inverse row by row, getting a different tradeoff curve of resolution *vs* variance for each row. That is

$$r_k = \sum_{i=1}^n \left(\sum_{j=1}^q V_{kj} V_{ij} - \delta_{ki} \right)^2 \quad (42)$$

$$\text{var}(\hat{x}_k) = \sum_{j=1}^q \left(\frac{V_{kj}}{\lambda_j} \right)^2 \quad (43)$$

where the integer q may now be a function of k . This allows us to examine each model parameter \hat{x}_k individually. In so doing, we implicitly ignore criterion (a), and the fit of the model $\hat{\mathbf{x}}$ to the data. If we form a model by independently estimating each value \hat{x}_k by this scheme, it is very likely that the model will not fit the data. This is

not a serious concern, if indeed the separate values \hat{x}_k have an intrinsic meaning which is useful in the eventual interpretation of this problem. On the other hand, if a true solution (1) is desired, one may increase the values of $q(k)$ at the expense of increased variance for the values \hat{x}_k .

There are some cases where it may be desirable to have a particular resolution kernel resemble some function other than the delta-function. For example, attempting to create a delta-like kernel may result in having a sharply peaked kernel with positive and negative 'side lobes', which could be avoided by letting the kernel have a somewhat broader peak. Or, it may be desirable to form an averaging kernel with a 'dipole' behaviour, that is, a sharp negative peak adjacent to a sharp positive peak, to obtain an estimate of the derivatives of the general solution \mathbf{x} . Such a problem may be very easily handled by substituting the desired optimum kernel function for δ_k in equation (39). The corresponding inverse matrix may be constructed by setting

$$\mathbf{H} = \mathbf{B}\Lambda^{-1}\mathbf{U}^T. \quad (44)$$

In other cases, it may be desirable to have the resolution kernel resemble a delta function, but proximity to a delta function may be more important for some elements than for others. For example, suppose one wants to estimate \hat{x}_k , and has evidence that x_j is very large for some particular value $j \neq k$. Then one would want to assure that the element R_{kj} is very small, at the expense of allowing other off-diagonal elements of \mathbf{R} to be somewhat larger. This may be accomplished by applying a weighting factor matrix to both sides of (25). If the weighting matrix is \mathbf{W} , and we let $\mathbf{W}^T\mathbf{W} = \mathbf{W}^2$, then

$$\mathbf{B} = [\mathbf{V}^T \mathbf{W}^2 \mathbf{V}]^{-1} \mathbf{V}^T \mathbf{W}^2. \quad (45)$$

Thus, the weighted resolution kernel, and its corresponding inverse \mathbf{H} , may be easily computed from the eigenvectors of the original matrix \mathbf{A} , avoiding the need to compute eigenvectors of a new, weighted matrix.

To summarize the above discussion, we may use the fact that each row of the resolution matrix must be composed of the eigenvectors \mathbf{v}_i , $i = 1, \dots, p$, and the standard least squares procedure (equation 25) to find that resolution kernel nearest to some desired function. The same trick may be used to find that solution of equation (1) which is nearest to some favourite function. The favourite function might be a hypothetical solution to (1), which would have special importance for interpretation. We know that the form of the general solution is

$$\mathbf{x} = \mathbf{V}\alpha + \mathbf{V}_0\alpha_0 \quad (46)$$

where α is determined by equation (1), while α_0 is arbitrary. We then seek the least squares solution to

$$\mathbf{V}\alpha + \mathbf{V}_0\alpha_0 = \mathbf{f} \quad (47)$$

where \mathbf{f} is the favourite function. By equation (25), we have

$$\alpha_0 = \mathbf{V}_0^T[\mathbf{f} - \mathbf{V}\alpha] = \mathbf{V}_0^T\mathbf{f} \quad (48)$$

so that the solution which best approximates \mathbf{f} is

$$\mathbf{x}_f = \mathbf{V}\alpha + \mathbf{V}_0\mathbf{V}_0^T\mathbf{f} = \hat{\mathbf{x}}_L + \mathbf{V}_0\mathbf{V}_0^T\mathbf{f}. \quad (49)$$

Let us now consider the problem of 'marginal utility of data'. Suppose we have analysed a large linear system according to the above procedures, and have found that the resolution provided by the data is insufficient. We wish to consider the improvement which would result from adding an $(n+1)^{st}$ measurement. Generally, the values of $A_{n+1,1}, \dots, A_{n+1,m}$ may be calculated in advance, and the variance of the $(n+1)^{st}$ measurement may be at least estimated in advance. We could, of course, add a new row to the matrix \mathbf{A} and start from scratch, finding a new set of eigenvalues

and eigenvectors, etc. However, a first order perturbation to the existing eigenvalues will probably be sufficient to answer the question at hand. Let us denote by \mathbf{a} the $m \times 1$ column vector whose values are $A_{n+1,1}, \dots, A_{n+1,m}$; then the new $(n+1)$ st row of \mathbf{A} is \mathbf{a}^T . Before adding the $(n+1)$ st row, we had from equation (8a) that

$$\mathbf{A}^T \mathbf{AV} = \mathbf{V}\Lambda^2. \quad (50)$$

If we denote by \mathbf{A}' the new matrix with the $(n+1)$ st row added.

$$\mathbf{A}' = \begin{pmatrix} \mathbf{A} \\ \mathbf{a}^T \end{pmatrix} \quad (n+1) \times m \quad (51)$$

the problem becomes that of finding \mathbf{V}' and Λ' such that

$$\mathbf{A}'^T \mathbf{A}' \mathbf{V}' = \mathbf{V}' \Lambda'^2. \quad (52)$$

First, we note that

$$\mathbf{A}'^T \mathbf{A}' = [\mathbf{A}^T \mathbf{A} + \mathbf{a} \mathbf{a}^T]. \quad (53)$$

Then, to first order, we assume that the eigenvectors are unchanged, that is $\mathbf{V}' = \mathbf{V}$. We then have

$$[\mathbf{A}^T \mathbf{A} + \mathbf{a} \mathbf{a}^T] \mathbf{V} = \mathbf{V} \Lambda'^2 \quad (54)$$

or

$$\Lambda'^2 = \mathbf{V}^T [\mathbf{A}^T \mathbf{A} + \mathbf{a} \mathbf{a}^T] \mathbf{V} = \Lambda^2 + \delta \Lambda^2. \quad (55)$$

Because the matrix \mathbf{V} is only approximately the matrix of eigenvectors for the problem (52), Λ'^2 will not be a truly diagonal matrix, but for large systems the off-diagonal elements will be small compared with the diagonal elements. (If they are not, first order perturbation theory is insufficient.) Ignoring off-diagonal elements, we have

$$\delta \lambda_j^2 = (\mathbf{V}_j^T \mathbf{a})^2.$$

We may now estimate the possible improvement in resolution and variance by recomputing the tradeoff curve, using the same eigenvectors \mathbf{v}_j but augmented eigenvalues

$$\lambda_j' = \sqrt{\lambda_j^2 + \delta \lambda_j^2}.$$

The direct effect of augmenting the λ_j will be to decrease the variance in \hat{x} , which in turn may allow more eigenvectors \mathbf{V} to be used in the inverse without violating the preset variance limit.

7. Special inverses for overconstrained systems

By now, it should be clear that each feature of the underdetermined system has its analog in the overconstrained system. For the underdetermined system, we were primarily interested in the tradeoff between resolution and variance and the completeness of the set of eigenvectors in \mathbf{V} . Here, we are most interested in the tradeoff between information density and variance, and the completeness of \mathbf{U} . Using the essentials of the least squares technique, we may design an inverse \mathbf{H} which will provide an information density \mathbf{S} closest in the least squares sense to any desired matrix of the proper dimensionality. If we design \mathbf{S} to approximate the unit matrix, we find which data act independently and which are seen through a hazy window. Designing \mathbf{S} to approximate a family of somewhat broader peaks may eliminate side lobes. Where the data represent successive values read from a continuous curve, designing the \mathbf{S} matrix to approximate a series of 'dipoles' will help reveal to what extent the derivative of the data curve represents independent information.

For the underdetermined system, the free eigenvectors in \mathbf{V}_0 could be used to search for a solution closest to some hypothetical function with special physical meaning. For overconstrained systems, the same principle may be used to test the

residual vector for components with special physical meaning (e.g. predictable errors with known properties but unknown magnitude). Removal of these components is equivalent to 'filtering' the data.

We may also consider the value of creating an additional unknown to help fit the data. This results in adding a new column to the matrix \mathbf{A} . First order perturbation theory may tell us quite easily the improvement this would allow in the information density matrix, and thus in the fit to the data.

8. Summary

The matrix equations which occur in real life situations do not need to be well conditioned. They may be simultaneously overconstrained and underdetermined. Even when the matrix relating the unknowns to the data appears non-singular, random errors in the data may reduce the effective number of degrees of freedom in a linear system. However, even the most ill-conditioned system may contain useful information. The matrix equation $\mathbf{Ax} = \mathbf{y}$ may be solved in terms of a linear operator on the data, $\hat{\mathbf{x}} = \mathbf{Hy}$. Useful criteria for constructing H are (a) $\mathbf{R} \equiv \mathbf{HA} \sim \mathbf{I}_m$; (b) $\mathbf{S} \equiv \mathbf{AH} \sim \mathbf{I}_n$; and (c) $\text{var}(\hat{x}_k) = \sum H_{ki}^2 \text{var}(y_i)$ is small.

For underconstrained systems, the matrix \mathbf{R} has a physical interpretation: the rows of \mathbf{R} represent windows through which the general solution (and thus, the 'real' solution) may be observed. For overconstrained systems, the model $\hat{\mathbf{x}}$ will in fact fit certain combinations of the data, determined by passing the real data through the windows represented by the rows of \mathbf{S} . In general, the performance of the inverse under (a) and (b) will be inversely related to performance under (c).

Decomposing the matrix \mathbf{A} into its eigenvalues and eigenvectors, $\mathbf{A} = \mathbf{UAV}^T$, allows the investigator to construct easily inverse operators which optimize any combination of the three criteria above, if (a) and (b) are taken in the least squares sense. Furthermore, special inverses may be easily constructed to test hypothetical features of solutions. Moreover, simple perturbation theory allows one to calculate easily the improvement in resolution and information density provided by taking more data or increasing the number of unknown parameters.

References

- Backus, George & Gilbert, F., 1968. The resolving power of gross earth data, *Geophys. J. R. astr. Soc.*, **16**, 169–205.
- Backus, George & Gilbert, F., 1970. Uniqueness in the inversion of inaccurate gross earth data, *Phil. Trans. R. Soc. Lond.*, **266A**, 123–192.
- Hildebrand, F., 1965. *Methods of applied mathematics*, Prentice-Hall, Englewood Cliffs, New Jersey.
- Jordan, T. H. & Franklin, J. N., 1971. Optimal solutions to a linear inverse problem in geophysics, *Proc. Nat. Acad. Sci.*, **68**, 291–293.
- Kaula, W., 1966. *Theory of satellite geodesy*, Blaisdell, Waltham, Mass.
- Lanczos, C., 1961. *Linear differential operators*, D. Van Nostrand Co., Lond.
- Penrose, R., 1955. A generalized inverse for matrices, *Proc. Camb. Phil. Soc.*, **51**, 406–413.
- Smith, M. L. & Franklin, J. N., Geophysical application of generalized inverse theory, *J. geophys. Res.*, **74**, 2783–2785.
- Wiggins, Ralph, 1972. The general linear inverse problem: implications of surface waves and free oscillations on earth structure, *Rev. Geophys. Space Phys.*, **10**, in press.

Monte Carlo sampling of solutions to inverse problems

Klaus Mosegaard

Niels Bohr Institute for Astronomy, Physics and Geophysics, Copenhagen

Albert Tarantola

Institut de Physique du Globe, Paris

Abstract. Probabilistic formulation of inverse problems leads to the definition of a probability distribution in the model space. This probability distribution combines a priori information with new information obtained by measuring some observable parameters (data). As, in the general case, the theory linking data with model parameters is nonlinear, the a posteriori probability in the model space may not be easy to describe (it may be multimodal, some moments may not be defined, etc.). When analysing an inverse problem, obtaining a maximum likelihood model is usually not sufficient, as we normally also wish to have information on the resolution power of the data. In the general case we may have a large number of model parameters, and an inspection of the marginal probability densities of interest may be impractical, or even useless. But it is possible to pseudorandomly generate a large collection of models according to the posterior probability distribution and to analyse and display the models in such a way that information on the relative likelihoods of model properties is conveyed to the spectator. This can be accomplished by means of an efficient Monte Carlo method, even in cases where no explicit formula for the a priori distribution is available. The most well known importance sampling method, the Metropolis algorithm, can be generalized, and this gives a method that allows analysis of (possibly highly nonlinear) inverse problems with complex a priori information and data with an arbitrary noise distribution.

Introduction

Inverse problem theory is the mathematical theory describing how information about a parameterized physical system can be derived from observational data, theoretical relationships between model parameters and data, and prior information. Inverse problem theory is largely developed in geophysics, where the inquiry is how to infer information about the Earth's interior from physical measurements at the surface. Examples are estimation of subsurface rock density, magnetization, and conductivity from surface measurements of gravity or electromagnetic fields. An important class of complex inverse problems is found in seismology, where recorded seismic waves at the Earth's surface or in boreholes are used to compute estimates of mechanical subsurface parameters.

In what follows, any given set of values representing a physical system, we call a model. Every model \mathbf{m} can be considered as a point in the model space \mathcal{M} . We will define different probability densities over \mathcal{M} . For instance, a probability density $\rho(\mathbf{m})$ will repre-

sent our a priori information on models, and another probability density, $\sigma(\mathbf{m})$ will represent our a posteriori information, deduced from $\rho(\mathbf{m})$ and from the degree of fit between data predicted from models and actually observed data. In fact, we will use the expression $\sigma(\mathbf{m}) = k \rho(\mathbf{m}) L(\mathbf{m})$ [see Tarantola, 1987], where $L(\mathbf{m})$, the likelihood function, is a measure of the degree of fit between data predicted from the model \mathbf{m} and the observed data (k is an appropriate normalization constant). Typically, this is done through the introduction of a misfit function $S(\mathbf{m})$, connected to $L(\mathbf{m})$ through an expression like $L(\mathbf{m}) = k \exp(-S(\mathbf{m}))$.

In seismology, the misfit function usually measures the degree of misfit between observed and computed seismograms as a function of the subsurface model parameters. It usually has many secondary minima. In terms of the probability density in the model space, we deal typically with a (possibly degenerate) global maximum, representing the most likely solution, and a large number of secondary maxima, representing other possible solutions. In such cases, a local search for the maximum likelihood solution using, for instance, a gradient method, is very likely to get trapped in secondary maxima. This problem is avoided when using a global search method. A global search is not confined to uphill (or downhill) moves in the model space and is therefore less influenced by the presence of local optima. Some global methods are not influenced at all.

The simplest of the global search methods is the exhaustive search. A systematic exploration of the (discretized) model space is performed, and all models within the considered model subspace are visited. Although this method may be ideal for problems with low dimensionality (i.e., with few parameters), the task is computationally unfeasible when problems with many model parameters are considered.

When analyzing highly nonlinear inverse problems of high dimensionality, it is therefore necessary to severely restrict the number of misfit calculations, as compared to the exhaustive search. One way to do this is to use a Monte Carlo search, which consists of a (possibly guided) random walk in the model space. A Monte Carlo search extensively samples the model space, avoids entrapment in local likelihood maxima, and therefore provides a useful way to attack such highly nonlinear inverse problems.

In resolution studies, the advantages of Monte Carlo methods become even more significant. Resolution analysis carried out by means of local methods gives erroneous results due to the inherent assumption that only one minimum for the misfit function exists. However, a Monte Carlo method can take advantage of the fact that all local likelihood maxima will be sampled, provided a sufficient number of iterations are performed.

Early geophysical examples of solution of inverse problems by means of Monte Carlo methods, are given by *Keilis-Borok and Yanovskaya* [1967] and *Press* [1968, 1971]. Press made the first attempts at randomly exploring the space of possible Earth models consistent with seismological data. More recent examples are given by *Rothman* [1985, 1986], who nicely solved a strongly nonlinear optimization problem arising in seismic reflection surveys, and *Landa et al.* [1989], *Mosegaard and Vestergaard* [1991], *Koren et al.*, [1991], and *Cary and Chapman* [1988], who all used Monte Carlo methods within the difficult context of seismic waveform fitting. Cary and Chapman and Koren et al. described the potential of Monte Carlo methods, not only for solving a model optimization problem but also for performing an analysis of resolution in the inverse problem.

The idea behind the Monte Carlo method is old, but its actual application to the solution of scientific problems is closely connected to the advent of modern electronic computers. J. von Neumann, S. Ulam and E. Fermi used the method in nuclear reaction studies, and the name "the Monte Carlo method" (an allusion to the famous casino) was first used by *Metropolis and Ulam* [1949]. Four years later, *Metropolis et al.* [1953] introduced an algorithm, now known as the Metropolis algorithm, that was able to (asymptotically) sample a space according to a Gibbs-Boltzmann distribution. This algorithm was a biased random walk whose individual steps (iterations) were based on very simple probabilistic rules.

It is not difficult to design random walks that sample the posterior probability density $\sigma(\mathbf{m})$. However, in cases where $\sigma(\mathbf{m})$ has narrow maxima, these maxima

(which are the most interesting features of $\sigma(\mathbf{m})$) will be very sparsely sampled (if sampled at all). In such cases, sampling of the model space can be improved by importance sampling, that is, by sampling the model space with a probability density as close to $\sigma(\mathbf{m})$ as possible. *Cary and Chapman* [1988] used the Monte Carlo method to determine $\sigma(\mathbf{m})$ for the refraction seismic waveform inversion problem, where the travel times were used as data, as well as waveforms, and the model parameters were the depths as a function of velocity. They improved the sampling of the model space by using a method described by *Wiggins* [1969, 1972] in which the model space was sampled according to the prior distribution $\rho(\mathbf{m})$. This approach is superior to a uniform sampling by crude Monte Carlo. However, the peaks of the prior distribution are typically much less pronounced than the peaks of the posterior distribution. Moreover, the peaks of the two distributions may not even coincide. It would therefore be preferable to draw sample models from the model space according to a probability distribution which is close to the posterior distribution $\sigma(\mathbf{m})$, the idea being to use a probability distribution that tends to $\sigma(\mathbf{m})$ as iterations proceed.

Geman and Geman [1984] discussed an application of simulated annealing to Bayesian image restoration. For their particular inverse problem, a two-dimensional deconvolution problem, they derived an expression for the posterior distribution from (1) the prior distribution, (2) a model of the convolutional two-dimensional image blurring mechanism, and (3) the parameters of the Gaussian noise model. By identifying this posterior distribution with a Gibbs-Boltzmann distribution, they performed a maximum a posteriori estimation in the model space, using a simulated annealing algorithm. In their paper, they mention the possibility of using the simulated annealing algorithm, not only for maximum a posteriori estimation but also to sample the model space according to the posterior distribution. However, they did not pursue this possibility further, nor did they describe how to extend this idea to inverse problems in general.

Marroquin et al. [1987] adopted an approach similar to that of Geman and Geman. However, they used the Metropolis algorithm to generate the posterior distribution, from which they computed model estimates. One of the problems raised by these authors was that their Bayesian approach requires an explicit formula for the a priori distribution.

Recent examples of using Bayes theorem and the Metropolis algorithm for generating a posteriori probabilities for an inverse problem are given by *Pedersen and Knudsen* [1990] and *Koren et al.* [1991].

In the present paper we will describe a method for random sampling of solutions to an inverse problem. The solutions are sampled at a rate proportional to their a posteriori probabilities, that is, models consistent with a priori information as well as observations are picked most often, whereas models that are in incompatible with either a priori information or observations (or both) are rarely sampled.

In brief, our sampling algorithm can be described as

consisting of two components. The first component generates a priori models, that is, models sampled with a frequency distribution equal to the a priori probability distribution in the model space. This is accomplished by means of a random walk, a kind of “Brownian motion” in the model space. The second component accepts or rejects attempted moves of the a priori random walk with probabilities that depend on the models ability to reproduce observations. Output from the combined algorithm consists of a collection of models that passed the test performed in the second component. This collection of models is shown to have a frequency distribution that is (asymptotically) proportional to the a posteriori probability distribution in the model space.

It is an important property of our method that in contrast to usual Bayesian inverse calculations, the a priori distribution need not be given by an explicit formula. In fact, the first component of our algorithm may consist of a large number of mutually dependent subprocesses, each of which generates part of the a priori models.

The definition of which models are accessible from a given model is an essential ingredient of the method, from a practical point of view. We will “jump” from a model to a neighboring model. But, what is a neighbor? The theory to be developed below is independent of the particular choice of model perturbations to be considered, but, as illustrated below, a bad definition of model neighborhood may lead to extremely inefficient algorithms.

Probabilistic Formulation of Inverse Problems

Parameters Taking Continuous Values

The “forward problem” is the problem of predicting (calculating) the “data values” $\mathbf{d}_{\text{cal}} = \{d_{\text{cal}}^1, d_{\text{cal}}^2, \dots\}$ that we should observe when making measurements on a certain system. Let the system be described (parameterized) by a parameter set $\mathbf{m} = \{m^1, m^2, \dots\}$. One generally writes as

$$\mathbf{d}_{\text{cal}} = \mathbf{g}(\mathbf{m}) \quad (1)$$

the, generally nonlinear, mapping from the model space \mathcal{M} into the data space \mathcal{D} that solves the forward problem.

In its crudest formulation, the “inverse problem” consists of the following question: An actual measurement of the data vector \mathbf{d} gave the value $\mathbf{d}_{\text{obs}} = \{d_{\text{obs}}^1, d_{\text{obs}}^2, \dots\}$. Which is the actual value of the model parameter vector \mathbf{m} ?

This problem may well be underdetermined, due to lack of significant data or due to experimental uncertainties. It can also be overdetermined, if we repeat similar measurements. Usually, it is both. A better question would have been: What information can we infer on the actual value of the model parameter vector \mathbf{m} ?

The “Bayesian approach” to inverse problems, describes the “a priori information” we may have on the

model vector by a probability density $\rho(\mathbf{m})$. Then, it combines this information with the information provided by the measurement of the data vector and with the information provided by the physical theory, as described for instance by equation (2), in order to define a probability density $\sigma(\mathbf{m})$ representing the “a posteriori information”. This a posteriori probability density describes all the information we have. It may well be multimodal, not have a mathematical expectation, have infinite variances, or some other pathologies, but it constitutes the complete solution to the inverse problem.

Whatever the particular approach to the problem may be [e.g., *Backus*, 1970a,b,c; *Tarantola and Valette*, 1982a; *Tarantola*, 1987], we end up with a solution of the form

$$\sigma(\mathbf{m}) = k \rho(\mathbf{m}) L(\mathbf{m}), \quad (2)$$

where k is an appropriate normalization constant. The a posteriori probability density $\sigma(\mathbf{m})$ equals the a priori probability density $\rho(\mathbf{m})$ times a “likelihood function” $L(\mathbf{m})$ which, crudely speaking, measures the fit between observed data and data predicted from the model \mathbf{m} (see an example below).

As an example, when we describe experimental results by a vector of observed values \mathbf{d}_{obs} with Gaussian experimental uncertainties described by a covariance matrix \mathbf{C} , then

$$L(\mathbf{m}) = k \exp \left[-\frac{1}{2} (\mathbf{g}(\mathbf{m}) - \mathbf{d}_{\text{obs}})^t \mathbf{C}^{-1} (\mathbf{g}(\mathbf{m}) - \mathbf{d}_{\text{obs}}) \right]. \quad (3)$$

If, instead, we describe experimental uncertainties using a Laplacian function, where d_{obs}^i are the “observed values” and σ^i are the estimated uncertainties, then

$$L(\mathbf{m}) = k \exp \left[- \sum_i \frac{|g^i(\mathbf{m}) - d_{\text{obs}}^i|}{\sigma^i} \right]. \quad (4)$$

As a last example (to be used below), if the measured data values d_{obs}^i are contaminated by statistically independent, random errors ε_i given by a double Gaussian probability density function,

$$f(\varepsilon) = k \left[a \exp \left(-\frac{\varepsilon^2}{2\sigma_1^2} \right) + b \exp \left(-\frac{\varepsilon^2}{2\sigma_2^2} \right) \right], \quad (5)$$

then

$$\begin{aligned} L(\mathbf{m}) &= k \prod_i \left[a \exp \left(-\frac{(g^i(\mathbf{m}) - d_{\text{obs}}^i)^2}{2\sigma_1^2} \right) \right. \\ &\quad \left. + b \exp \left(-\frac{(g^i(\mathbf{m}) - d_{\text{obs}}^i)^2}{2\sigma_2^2} \right) \right]. \end{aligned} \quad (6)$$

These three examples are very simplistic. While in this paper we show the way to introduce realistic a priori information in the model space, we do not attempt to advance in the difficult topic of realistically describing data uncertainties.

Discretization of Parameters

So far, the theory has been developed for parameters that, although finite in number, may take continuous

values. Then, at any point \mathbf{m}_i we can define a probability density $f(\mathbf{m}_i)$, but not a probability, which can only be defined for a region of the space:

$$P(\mathbf{m} \in \mathcal{A}) = \underbrace{\int dm^1 \int dm^2 \dots}_{\mathcal{A}} f(\mathbf{m}). \quad (7)$$

Here, m^1, m^2, \dots denote the different components of the vector \mathbf{m} .

For numerical computations, we discretize the space by defining a grid of points, where each point represents a surrounding region $\Delta m^1 \Delta m^2 \dots$, small enough for the probability densities under consideration to be almost constant inside it. Then, when we say "the probability of the point \mathbf{m}_i " we mean "the probability of the region $\Delta m^1 \Delta m^2 \dots$ surrounding the point \mathbf{m}_i ". In the limit of an infinitely dense grid and assuming a continuous $f(\mathbf{m})$, "the probability of the point \mathbf{m}_i " tends to

$$f_i = f(\mathbf{m}_i) \Delta m^1 \Delta m^2 \dots \quad (8)$$

The discrete version of equation (2) is then

$$\sigma_i = \frac{\rho_i L(\mathbf{m}_i)}{\sum_j \rho_j L(\mathbf{m}_j)}, \quad (9)$$

where

$$\sigma_i = \sigma(\mathbf{m}_i) \Delta m^1 \Delta m^2 \dots, \quad (10)$$

and

$$\rho_i = \rho(\mathbf{m}_i) \Delta m^1 \Delta m^2 \dots. \quad (11)$$

For simplicity, we will rather write

$$\sigma_i = \frac{\rho_i L_i}{\sum_j \rho_j L_j}, \quad (12)$$

where we use the notation

$$L_i = L(\mathbf{m}_i) \quad (13)$$

(note that $\Delta m^1 \Delta m^2 \dots$ does not enter into the definition of L_i).

Once the probability (12) has been defined, we could design a method to sample directly the posterior probability σ_i (and, in fact, the methods below could be used that way). But any efficient method will proceed by first sampling the prior probability ρ_i . It will then modify this sampling procedure in such a way that the probability σ_i is eventually sampled. This, after all, only corresponds to the Bayesian viewpoint on probabilities: one never creates a probability ex nihilo but rather modifies some prior into a posterior.

Monte Carlo Sampling of Probabilities

Essentially, the sampling problem can be stated as follows: given a set of points in a space, with a probability p_i attached to every point i , how can we define random rules to select points such that the probability of selecting point i is p_i ?

Terminology

Consider a random process that selects points in the model space. If the probability of selecting point i is p_i , then the points selected by the process are called "samples" of the probability distribution $\{p_i\}$. Depending on the random process, successive samples i, j, k, \dots may be dependent or independent, in the sense that the probability of sampling k may or may not depend on the fact that i and j have just been sampled.

An important class of efficient Monte Carlo (i.e., random) sampling methods is the random walks. The possible paths of a random walk define a graph in the model space (see Figure 1). All models in the discrete model space are nodes of the graph, and the edges of the graph define the possible steps of the random walk. The graph defines the "neighborhood" of a model as the set of all models directly connected to it. Sampling is then made by defining a random walk on the graph: one defines the probability P_{ij} for the random walker to go to point i if it currently is at the neighboring point j . P_{ij} is called the "transition probability". (As, at each step, the random walker must go somewhere, including the possibility of staying at the same point, P_{ij} satisfies $\sum_i P_{ij} = 1$.) For the sake of mathematical simplicity, we shall always assume that a graph connects any point with itself: staying at the point is considered as a "transition" (a "step"), and the current point, having been reselected, contributes with one more sample.

Consider a random walk, defined by the transition probabilities $\{P_{ij}\}$, and assume that the model where it is initiated is only known probabilistically: there is a probability q_i that the random walk is initiated at point i . Then, when the number of steps tends to infinity, the probability that the random walker is at point i will converge to some other probability p_i [Feller, 1970]. We say that $\{p_i\}$ is an "equilibrium

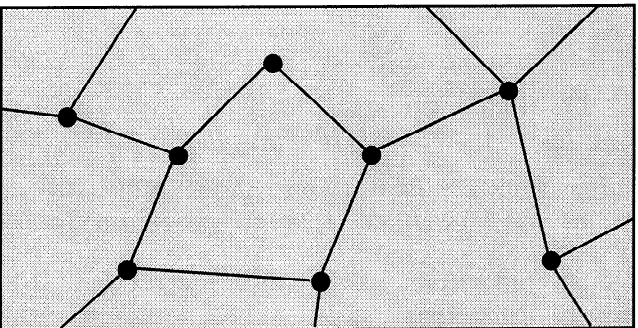


Figure 1. Part of a graph in the model space. The graph defines the possible steps of a random walk in the space. The random walk obeys some probabilistic rules that allow it to jump from one model to a connected model in each step. The random walker will, asymptotically, have some probability, say p_i , to be at point i at a given step. The neighborhood of given model is defined as the models to which a random walker can go in one step, if it starts at the given model. Thus a neighborhood is defined solely through the graph and does not need to be a metric concept.

probability distribution" of $\{P_{ij}\}$. (Then, $\{p_i\}$ is an eigenvector with eigenvalue 1 of $\{P_{ij}\}$: $\sum_j P_{ij}p_j = p_i$.) If the random walk always equilibrates at the same probability $\{p_i\}$, independent of the initial probability $\{q_i\}$, then there is only one equilibrium probability $\{p_i\}$. (Then, $\{p_i\}$ is a unique eigenvector of $\{P_{ij}\}$.) This is the case if the graph is "connected", that is, if it is possible to go from any point to any other point in the graph (in a sufficient number of steps) [Feller, 1970].

Many random walks can be defined that have a given probability distribution $\{p_i\}$ as their equilibrium probability. Some random walks converge more rapidly than others to their equilibrium probability. Successive models i, j, k, \dots obtained with a random walk will, of course, not be independent unless we only consider models separated by a sufficient number of steps. Instead of letting p_i represent the probability that a (single) random walker is at point i (in which case $\sum_i p_i = 1$), we can let p_i be the number of "particles" at point i . Then, $\sum_i p_i$ represents the total number of particles. None of the results presented below will depend on the way $\{p_i\}$ is normalized.

If, at some moment, the probability for the random walker to be at a point j is p_j and the transition probabilities are P_{ij} , then $f_{ij} = P_{ij}p_j$ represents the probability that the next transition will be from j to i : while P_{ij} is the conditional probability of going to point i if the random walker is at j , f_{ij} is the unconditional probability that the next step will be a transition to i from j .

When p_i is interpreted as the number of particles at point i , f_{ij} is called the "flow", as it can be interpreted as the number of particles going to point i from point j in a single step. (The flow corresponding to an equilibrated random walk has the property that the number of particles p_i at point i is constant in time. Thus that a random walk has equilibrated at a distribution $\{p_i\}$ means that in each step, the total flow into a given point is equal to the total flow out from the point. Since each of the p_i particles at point i must move in each step (possibly to point i itself), the flow has the property that the total flow out from point i and hence the total flow into the point must equal p_i : $\sum_j f_{ij} = \sum_k f_{ki} = p_i$.) The concept of flow is important for designing rules that sample probabilities (see Appendix A).

Naïve Walks

Consider an arbitrary (connected) graph, as the one suggested in Figure 1, and denote by n_i the number of neighbors of point i (including the point i itself). Consider also a random walker that performs a "naive random walk". That is, when he is at some point j , he moves to one of j 's neighbors, say neighbor i , chosen uniformly at random (with equal probability). It is easy to prove (see Appendix B) that the random walk so defined equilibrates at the probability distribution given by $p_i = n_i / \sum_j n_j$, i.e., with all points having a probability proportional to their number of neighbors.

Uniform Walks

Consider now a random walker that when he is at some point j , first chooses, uniformly at random, one of j 's neighbors, say neighbor i , and then uses the following rule to decide if he moves to i or if he stays at j :

1. If $n_i \leq n_j$ (i.e., if the "new" point has less neighbors than the "old" point (or the same number), then always move to i .

2. If $n_i > n_j$ (i.e., if the "new" point has more neighbors than the "old" point), then make a random decision to move to i , or to stay at j , with the probability n_j/n_i of moving to i .

It is easy to prove (see Appendix B) that the random walk so defined equilibrates at the uniform probability, i.e., with all points having the same probability. This method of uniform sampling was first derived by Wiggins [1969].

The theory developed so far is valid for general, discrete (and finite) spaces, where the notion of metric is not necessarily introduced. In the special case of metric, Euclidean spaces, it is possible to choose Cartesian coordinates, and to define the points in the space, where the random walk will be made, as a standard Cartesian grid of points. Let us, for instance, choose a graph as the one indicated in Figure 2. Then, away from the boundaries, the rule above degenerates into a (uniform) random choice of one of the $2N+1$ neighbors that any point has (including itself) in a space of dimension N . It can be shown (see Appendix B) that the walks so defined produce symmetric flows.

Modification of Random Walks

Assume that some random rules are given that define a random walk having $\{\rho_i\}$ as its equilibrium probability (uniform or not). How can the rules be modified so that the new random walk equilibrates at the probability

$$\sigma_i = \frac{\rho_i L_i}{\sum_j \rho_j L_j} ? \quad (14)$$

Consider the following situation. Some random rules define a random walk that samples the prior probability $\{\rho_i\}$. At each step, the random walker is at point j ,

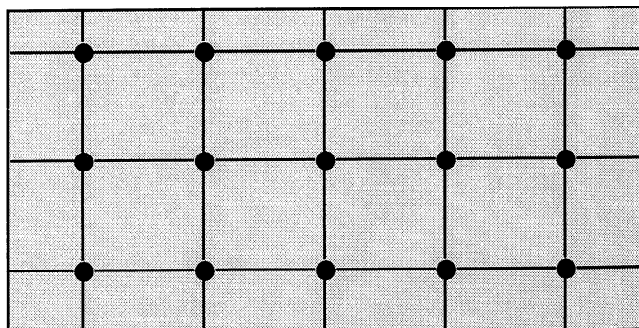


Figure 2. Part of a Cartesian graph in an Euclidean space. In this case, the definition of rules that sample points with the uniform probability is trivial.

and an application of the rules would lead to a transition to point i . If that “proposed transition” $i \leftarrow j$ was always accepted, then the random walker would sample the prior probability $\{\rho_i\}$. Let us, however, instead of always accepting the proposed transition $i \leftarrow j$, sometimes thwart it by using the following rule to decide if he is allowed to move to i or if he is forced to stay at j :

1. If $L_i \geq L_j$ (i.e., if the “new” point has higher (or equal) likelihood than the “old” point), then accept the proposed transition to i .

2. If $L_i < L_j$ (i.e., if the “new” point has lower likelihood than the “old” point), then make a random decision to move to i , or to stay at j , with the probability L_i/L_j of moving to i .

Then it can be proved (see Appendix C) that the random walker will sample the posterior probability σ_i defined by equation (14). This modification rule, reminiscent of the Metropolis algorithm, is not the only one possible (see Appendix C).

To see that our algorithm degenerates into the Metropolis algorithm [Metropolis *et al.*, 1953] when used to sample the Gibbs-Boltzmann distribution, put $q_j = \exp(-E_j/T) / \sum_i \exp(-E_i/T)$, where E_j is an “energy” associated to the j -th point in the space and T is a “temperature”. The summation in the denominator is over the entire space. In this way, our acceptance rule becomes the classical Metropolis rule: point i is always accepted if $E_i \leq E_j$, but if $E_i > E_j$, it is only accepted with probability $p_{ij}^{\text{acc}} = \exp(-(E_i - E_j)/T)$. Accordingly, we will refer to the above acceptance rule as the “Metropolis rule”.

As an example, let us consider the case of independent, identically distributed Gaussian uncertainties. Then the likelihood function describing the experimental uncertainties (equation (3)) degenerates into

$$L(\mathbf{m}) = k \exp\left(-\frac{S(\mathbf{m})}{s^2}\right), \quad (15)$$

where

$$S(\mathbf{m}) = \frac{1}{2} \sum_{i=1}^N (g^i(\mathbf{m}) - d_{\text{obs}}^i)^2 \quad (16)$$

is the misfit function, \mathbf{m} is a model vector, \mathbf{d} is a data vector, $g(\mathbf{m})$ is the forward modeling function, and s^2 is the total “noise” variance. In this example, s^2 is the same for all N data values. The acceptance probability for a perturbed model becomes in this case

$$P_{\text{accept}} = \begin{cases} 1 & \text{if } S(\mathbf{m}_{\text{new}}) \leq S(\mathbf{m}_{\text{old}}) \\ \exp\left(-\frac{\Delta S}{s^2}\right) & \text{if } S(\mathbf{m}_{\text{new}}) > S(\mathbf{m}_{\text{old}}) \end{cases}, \quad (17)$$

where

$$\Delta S = S(\mathbf{m}_{\text{new}}) - S(\mathbf{m}_{\text{old}}). \quad (18)$$

This means that the perturbation is accepted if the perturbed model improves the data fit, and has a probability of being accepted of $P_{\text{accept}} = \exp(-\Delta S/s^2)$ if it degrades the data fit. From (17) we see that in the case of uniform a priori distribution, our algorithm be-

comes identical to the traditional Metropolis algorithm by identifying the misfit function S with the thermodynamic energy E and by identifying the noise variance s^2 with (k times) the thermodynamic temperature T .

Starting a Random Walk

We have just shown how a random walk sampling some prior probability $\{\rho_i\}$ can be modified by the Metropolis rule to sample the posterior probability $\{\sigma_i\}$. This procedure is very suitable for solution of inverse problems. Usually, we will define some probabilistic rules that, when applied directly, would generate models $\mathbf{m}_1, \mathbf{m}_2, \dots$ that, by definition, would be samples of the prior probability $\{\rho_i\}$. The application of the Metropolis rule defined above will modify this random walk in the model space so that it produces samples of the posterior probability $\{\sigma_i\}$ instead.

The fact that we have a random walk that samples the prior does not imply that we have an expression that allows us to calculate the value of the prior probability ρ_i of any model \mathbf{m}_i . The numerical example below gives an example of this. Of course, using the random walk that samples the prior and making the histograms of the models selected would be a numerical way of obtaining the value of the prior probability ρ_i for every model \mathbf{m}_i , but this is not a question that normally arises.

Using random rules that, if unmodified, generate samples of the prior and using the Metropolis rule to modify this random walk in order to sample the posterior corresponds to the Bayesian way of modifying a prior probability into a posterior. This approach will usually lead to efficient random walks, since the algorithm only explores the (usually) very limited subset of models that are consistent with our a priori information.

It often happens that we have data of different nature, as for instance in geophysics, when we have gravity, magnetic, or seismic data. Then, typically, data uncertainties are independent, and the total likelihood of a model, $L(\mathbf{m})$, can be expressed as a product of partial likelihoods: $L(\mathbf{m}) = L_1(\mathbf{m}) L_2(\mathbf{m}) \dots$, one for each data type. Using the Metropolis rule directly to the total likelihood $L(\mathbf{m})$ would force us to solve the full forward problem (usually the most time-consuming part of the algorithm) to every model proposed by the prior random walk. Instead, we can use the Metropolis rule in cascade: If the random walk sampling the prior is modified first by considering the partial likelihood $L_1(\mathbf{m})$, then we define a random walk that samples the product of the prior probability density $\rho(\mathbf{m})$ and $L_1(\mathbf{m})$. In turn, this random walk can be modified by considering the partial likelihood $L_2(\mathbf{m})$, and so on, until the posterior probability density that takes into account the total data set is sampled. Practically this means that, once a model is proposed by the rules sampling the prior, the forward problem is solved for the first data subset. The proposed model may then be accepted or rejected. If it is rejected by the Metropolis rule (typically when there is a large misfit between the synthetic data and the observed data for this first data

subset), then there is no need to solve the forward problem for the other data subsets, and the rules sampling the prior have to propose a new model. More generally: Each time the Metropolis rule rejects a model at some stage of the algorithm, we go back to the lower level and propose a new model. When the solution of the forward modeling is inexpensive for certain data subsets, using this "cascade rule" may render the algorithm much more efficient than using the Metropolis rule to the total data set.

If, for some reason, we are not able to directly design a random walk that samples the prior, but we have an expression that gives the value of the prior probability ρ_i for any model \mathbf{m}_i (an example is given by expression (19) below), we can, for instance, start a random walk that samples the model space with uniform probability (see the section on uniform walks). Using the Metropolis rules given above but replacing the likelihood values L_i by the prior probabilities ρ_i , we will obviously produce a random walk that samples the prior (the product of a constant times ρ_i equals ρ_i). Then, in cascade, we can use the Metropolis rule, with the likelihood values L_i , to modify this random walk into a random walk that samples the posterior probability $\sigma_i = \text{const } \rho_i L_i$.

A second option is to modify directly a uniform random walk (using the Metropolis rule above but with the product $\rho_i L_i$ instead of L_i) into a walk that directly samples the posterior, but this results, generally, in an inefficient random walk.

Multistep Iterations

An algorithm will converge to a unique equilibrium distribution if the graph that describes the move of a random walker in a single iteration is connected [Feller, 1970]. Often, it is convenient to split up an iteration in a number of steps, having its own graph and its own transition probabilities. A typical example is a random walk on a set of discrete points in an N -dimensional Euclidean space, as the one suggested in Figure 2. In this case the points are located in a regular grid having N mutually perpendicular axes, and one is typically interested in dividing an iteration of the random walk into N steps, where the n th move of the random walker is in a direction parallel to the n th axis.

The question is now: if we want to form an iteration consisting of a series of steps, can we give a sufficient condition to be satisfied by each step such that the complete iteration has the desired convergence properties? It is easy to see that if the individual steps in an iteration all have the same distribution $\{p_i\}$ as an equilibrium distribution (not necessarily unique), then the complete iteration also has $\{p_i\}$ as an equilibrium distribution. (The transition probability matrix for a complete iteration is equal to the product of the transition probability matrices for the individual steps. Since the vector of equilibrium probabilities is an eigenvector with eigenvalue 1 for each of the step transition probability matrices, it is also an eigenvector with eigenvalue 1, and hence the equilibrium distribution, for the tran-

sition probability matrix for the complete iteration.) If this distribution is to be the unique equilibrium distribution for the complete iteration, then the graph of the complete iteration must be connected. That is, it must be possible to go from any point to any other point by performing iterations consisting of the specified steps.

If the steps of an iteration satisfy these sufficient conditions, there is also another way of defining an iteration with the desired, unique equilibrium distribution. Instead of performing an iteration as a series of steps, it is possible to define the iteration as consisting of one of the steps, chosen randomly (with any distribution having nonzero probabilities) among the possible steps (see Appendix D). Of course, a step of an iteration can, in the same way, be built from substeps and in this way acquire the same (not necessarily unique) equilibrium distribution as the substeps.

Sampling the a Priori Probability Density

We have previously assumed that we were able to sample the a priori probability density $\rho(\mathbf{m})$. Let us see how this can be achieved.

There are two ways of defining the a priori probability distribution:

1. By defining a (pseudo) random process (i.e., a set of pseudo random rules) whose output is models assumed to represent pseudo random realizations of $\rho(\mathbf{m})$
2. By explicitly giving a formula for the a priori probability density $\rho(\mathbf{m})$.

Let us see an example of each.

First Example

From nearby wells we may have found that in a certain area of locally horizontal stratification, the distribution of layer thicknesses is approximately an exponential distribution, and the mass densities in the layers follow a log-normal distribution. Hence we can decide to generate one dimensional Earth models for mass density by the following random walk in the model space:

In each iteration:

1. Select a layer uniformly at random.
2. Choose a new value for the layer thickness according to the exponential distribution.
3. Choose a value for the mass density inside the layer, according to the log-normal distribution.

If we decide to discretize the model at constant Δz intervals, $\mathbf{m} = \{\rho(z_1), \rho(z_2), \dots\}$ will have some probability distribution (representing our a priori knowledge) for the parameters $\{\rho(z_1), \rho(z_2), \dots\}$ which we may not need to characterize explicitly.

In this example, the pseudo random procedure produces, by its very definition, samples $\mathbf{m}_1, \mathbf{m}_2, \dots$ of the a priori probability density $\rho(\mathbf{m})$. These samples will be the input to the Metropolis decision rule. We recommend in particular this way of handling the a priori information, as it allows arbitrarily complex a priori information to enter the solution to an inverse problem.

For an example of this procedure, see the section on numerical example.

Second Example

We may choose the probability density

$$\rho(\mathbf{m}) = k \exp \left(- \sum_{\alpha} \frac{|m^{\alpha} - m_{prior}^{\alpha}|}{\sigma^{\alpha}} \right), \quad (19)$$

where m^{α} represent components of the vector \mathbf{m} .

In this example, where we only have an expression for $\rho(\mathbf{m})$, we have to generate samples from this distribution. This can be done in many different ways. One way is to start with a naïve walk, as described above, and then use the Metropolis rule to modify it, in order to sample $\rho(\mathbf{m})$.

Sampling the a Posteriori Probability Density

In the previous section we described how to perform a random walk in the model space producing samples $\mathbf{m}_1, \mathbf{m}_2, \mathbf{m}_3, \dots$ of the a priori probability $\rho(\mathbf{m})$. In order to obtain samples of the a posteriori probability $\sigma(\mathbf{m}) = k \rho(\mathbf{m}) L(\mathbf{m})$ we simply need to use the results given in the section on modification of random walks: if \mathbf{m}_j is the “current point” and if the random walk sampling the prior would move from point \mathbf{m}_j to point \mathbf{m}_i (and whatever the used rules may be), accept the move if $L(\mathbf{m}_i) \geq L(\mathbf{m}_j)$, and decide randomly to accept or reject the move if $L(\mathbf{m}_i) < L(\mathbf{m}_j)$, with a probability $P = L(\mathbf{m}_i)/L(\mathbf{m}_j)$ of accepting the move.

Numerical Example

We now illustrate the theory developed in this paper with the inversion of gravity data. This is a classical example for testing any theory of inversion, and similar examples are given by *Dorman* [1975], *Parker* [1977] and *Jackson* [1979].

As the relationship between mass density and gravity data is strictly linear, one may wonder why we should illustrate a Monte Carlo method, with its inherent ability to solve nonlinear problems, with the gravity inversion example. The reason is that our major concern is not the possibility of solving nonlinear problems, but the possibility of using, in standard geophysical inverse problems, realistic a priori information in the model space and realistic description of data uncertainties. This is what forces us to leave the comfortable realm of least squares and related methods and to develop the notions described here. It should be noted that the complex a priori knowledge used in this example renders the a posteriori distribution non-Gaussian.

The Problem

We consider a subsurface with a vertical fault, extending from the surface to infinite depth, as depicted in Figure 3. At the left of the fault the medium is ho-

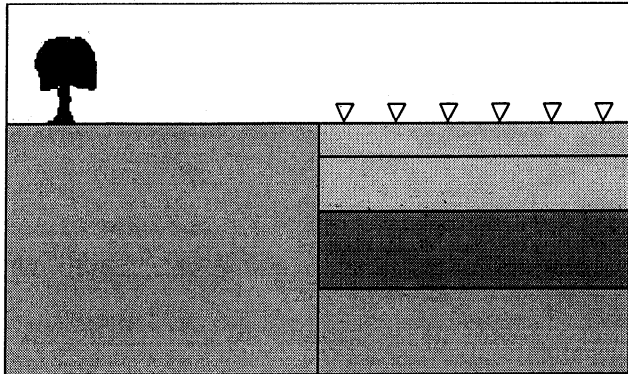


Figure 3. The geological model considered in our numerical example.

mogeneous, while at the right of the fault the medium is depth dependent and characterized by a vertical profile of mass density $\rho(z)$.

The contrasts of mass density across the vertical fault produce a gravity anomaly at the surface. Let us assume that we have observed the horizontal gradient of the vertical component of the gravity at 20 equispaced points to the right of the fault, the first point being located 2 km from the fault, and the last point being located 40 km from the fault. The forward problem of computing the data values $d_i = d(x_i)$ from the density contrast function is solved by

$$d(x) = \frac{\partial g}{\partial x}(x) = 2G \int_0^{\infty} dz \frac{z \Delta \rho(z)}{z^2 + x^2}, \quad (20)$$

where x is the horizontal distance from the fault, z is the depth, $g(x)$ is the vertical component of the gravity, $\Delta \rho(z)$ is the horizontal density contrast across the fault at depth z , and G is the gravitational constant.

The a Priori Information

Let us assume that in addition to the “hard” model constraints described above, we have the following a priori knowledge about the subsurface structure: The density of the rock to the left of the vertical fault is known to be 2570 kg/m³. To the right of the fault is a stack of (half) layers, and we have the a priori information that the thicknesses ℓ_i of the layers are distributed according to the exponential probability density

$$f(\ell) = \frac{1}{\ell_0} \exp \left(-\frac{\ell}{\ell_0} \right), \quad (21)$$

where ℓ_0 , the mean layer thickness, has the value $\ell_0 = 4$ km.

Independently of the thickness of the layers, the mass density for each layer follows an empirical probability density, displayed in Figure 4. To simplify the calculation, the stack of layers is assumed to have a total thickness of 100 km, resting on a homogeneous basement having the same mass density as the half space at the left of the fault (2570 kg/m³), and the top layer is truncated (eroded) at the surface.

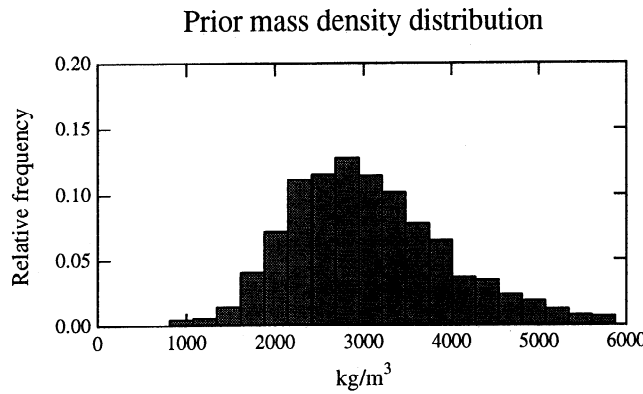


Figure 4. The a priori probability density function for the mass density inside each layer. The a priori probability density function for the thickness of each layer is an exponential function.

True Model, Experimental Uncertainties, and Observed Data Values

The measured data is assumed to be the response of a “true model” (Figure 5). The exact data corresponding to the true model are shown in Figure 6. The measured data values are assumed to be contaminated by statistically independent, random errors ε_i modeled by the sum of two Gaussian probability density functions,

$$f(\varepsilon) = \frac{a}{\sqrt{2\pi}\sigma_1} \exp\left(-\frac{\varepsilon^2}{2\sigma_1^2}\right) + \frac{(1-a)}{\sqrt{2\pi}\sigma_2} \exp\left(-\frac{\varepsilon^2}{2\sigma_2^2}\right), \quad (22)$$

where we have chosen the constants $\sigma_1 = 0.25 10^{-9} \text{s}^{-2}$, $\sigma_2 = 1.25 10^{-9} \text{s}^{-2}$, and $a = 0.25$ (see Figure 7).

The simulated observations, which are formed by summing the “true” data and the simulated noise, are displayed in Figure 6. Then, the likelihood function $L(\mathbf{m})$, measuring the degree of fit between synthetic and observed data is the one given by equation (6).

The Sampling Algorithm

The prior random walk. Let us now describe how our algorithm works. First, we define the graph in the model space that will guide our random walk.

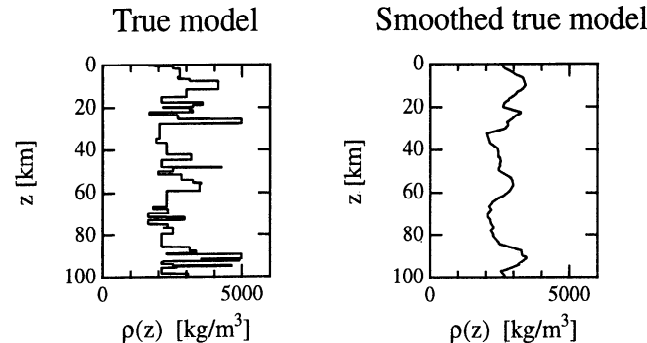


Figure 5. The true model used to generate synthetic data.

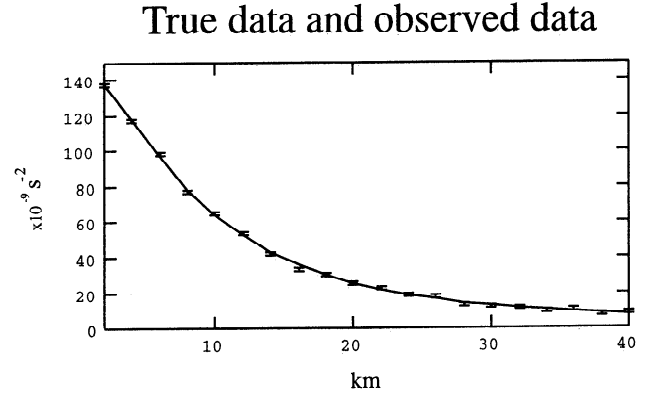


Figure 6. Synthetic data (solid line) used for the inversion, generated from the “true model” of Figure 5, and the “observed data” (points with error bars), equal to the “true data” plus some noise.

To ensure efficiency of the algorithm, it is important that very few of the possible steps in the model space lead to a radical change in the synthetic data generated from these models.

A simple way of sampling the a priori probability in the model space would be to use a random walk that generates successive models totally independently. To generate a new model, we could, for instance, pseudorandomly generate layer thicknesses $\ell_1, \ell_2 \dots$ from bottom to top, according to the exponential distribution given by equation (21), until they add up to the 100 km of total thickness (“eroding”, if necessary, the top layer). Then we could pseudorandomly generate, inside each layer, the corresponding value for the mass density, according to the empirical distribution displayed in Figure 4. However this would produce a radical change in the synthetic data in each step of the random walk, and therefore it would be a very inefficient algorithm. The reason is that if the current model is one having a high posterior probability, a radical change would most likely lead to one of the very abundant models having a low posterior probability and would therefore be rejected by the algorithm.

Another way to produce samples of the a priori probability in the model space could be the following: Given a sample of the prior (i.e., given a model), we could produce another sample by, for instance, randomly choos-

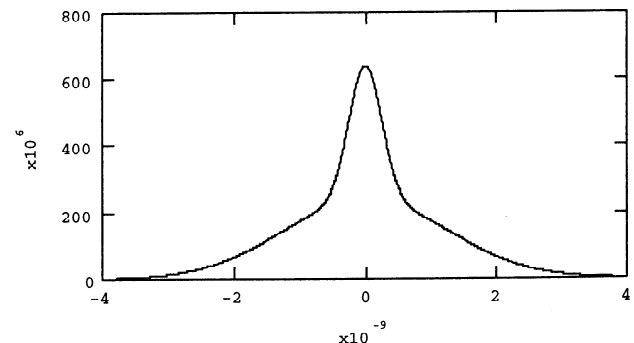


Figure 7. The arbitrary function used to model data uncertainties, as a sum of two Gaussians.

ing a layer and replacing its thickness by a new thickness drawn from the exponential distribution given by equation (21) or by replacing its mass density by a new mass density drawn from the empirical distribution displayed in Figure 4.

It is obvious that iterating this procedure, we would always produce models whose layer thicknesses and mass densities are distributed properly; i.e., we would produce samples of the prior probability in the model space. Successive models will be "close" in some sense, but our numerical experimentation has shown that they are still too far apart: when testing models produced by this prior random walk by the likelihood function $L(\mathbf{m})$ (see below), the probability of being accepted as samples of the a posteriori probability is extremely low. The reason is that when perturbing one layer thickness, all the layers above are shifted (remember that we go from bottom to top), and this strongly changes the synthetic data.

Therefore we decided to define the neighbors of a model as the models we can get, not by changing the thickness of a layer but by creating or destroying a new interface in the model (in a way described below). Then, all the other layers remain intact, and we only make a small perturbation in the synthetic data.

More precisely, the neighbors of a model are the models we can get by performing one of the following three perturbations: (1) changing the mass density in one layer, (2) adding a new layer boundary and assigning mass densities to the layers above and below it, or (3) removing one layer boundary and assigning a mass density to the new compound layer. To complete the description of our algorithm, we will now specify the random rules used by the random walk on the graph.

In each iteration it is first decided which kind of model perturbation step should be performed next. Performing a "pure" layer density perturbation has the same probability (0.5) as performing a layer boundary perturbation (removing or adding a boundary).

In case of a step involving a pure layer mass density perturbation, a layer is selected uniformly at random and a (new) density is chosen for that layer according to the density histogram of Figure 4.

In case of a layer boundary perturbation step we face the problem of adding or removing layer boundaries in such a way that if the step was iterated alone, it would leave the (a priori) distribution of models unchanged. In particular, the exponential layer thickness distribution $(1/\ell_0) \exp(-\ell/\ell_0)$ should be maintained. There is a simple solution to this problem: we exploit the fact that (approximately) exponentially distributed layer thicknesses can be obtained by assuming that the probability that a layer interface is present at a given depth (sample point) is equal to $(40 \text{ m} / \ell_0) = 0.01$ and independent of the presence of other layer interfaces.

A layer boundary perturbation step therefore works as follows. First, we select one of the 2500 discrete points of the current mass density function, uniformly at random. We then randomly decide if there should exist a layer boundary at that point or not. The probability for the point to be a layer boundary is 0.01.

In case this operation creates a new layer boundary, we generate a mass density for the layers above and below the new layer boundary according to the a priori probability distribution shown in Figure 4.

In case this operation removes a layer boundary, we generate a mass density for the new compound layer (consisting of the layers above and below the removed layer boundary) according to the a priori probability distribution.

This exactly corresponds to the a priori information we wanted to input to our problem: the random walk in the model space so defined is sampling the probability density describing our a priori information.

The posterior random walk. Let us now describe how the above prior random walk is modified into a new random walk, sampling the posterior distribution.

Every time a model perturbation is attempted by the prior random walk, the gravity response is computed from the perturbed layer sequence \mathbf{m}_{pert} by summing up the contributions from the layers in the interval between 0 km depth and 100 km depth. The contribution from a homogeneous half layer is given by

$$G\Delta\rho \log\left(\frac{D^2 + x^2}{d^2 + x^2}\right) \quad (23)$$

where d is the depth to the top of the homogenous half layer, D is the depth to the bottom of the half layer, $\Delta\rho$ is the layer density, and x is the horizontal distance to the edge of the half layer.

From the computed gravity response $\mathbf{g}(\mathbf{m}_{\text{pert}})$ and the observed gravity response \mathbf{d}_{obs} the value of the likelihood function $L(\mathbf{m}_{\text{pert}})$ is computed using equation (6). The attempted perturbation is now accepted or rejected according to the Metropolis rule, using the likelihoods $L(\mathbf{m}_{\text{cur}})$ and $L(\mathbf{m}_{\text{pert}})$ of the current and perturbed models, respectively (see the section on sampling the a posteriori probability density).

This completes the description of the algorithm used in our numerical example. There are, however, a few remaining issues concerning the use of its output models. Most importantly, we want independent samples from the a posteriori distribution.

If independent sample models are required, one has to wait some time between saving the samples. In practice, a single test run of, say, 1000 iterations is performed, and the value of the likelihood function is recorded for the current model of each iteration. After some iterations the likelihood has risen from the usually very low value of the initial model to a rather stable "equilibrium level", around which it fluctuates during the remaining iterations. By calculating the autocorrelation function for the equilibrium part of this series of likelihood values, it is possible to estimate the waiting time (in iterations) between statistically independent likelihood values. This waiting time is a very rough measure of the minimum waiting time between statistically independent model samples from $\sigma(\mathbf{m})$. The waiting time between saving model samples in our computations is 100 iterations. A discussion of the validity of the above measure is beyond the scope of this paper. It shall,

however, be noted that the described method is only approximate and that the crucial problem of estimating how many iterations are needed to yield a sufficient number of samples (to characterize a given inverse problem) is still unsolved.

Making of a Movie

First, the comparison between computed and observed data is “turned off”, so as to generate a sample of models representing the a priori probability. This has two purposes. First, it allows us to make statistics and to verify that the algorithm is working correctly. More importantly, it allows us to really understand which sort of a priori information we are inputting to the problem. Figure 8, for instance, shows 30 of the models representing the a priori probability distribution, of the many tens of thousands generated. We call this figure a “movie”, as this is the way the whole set of generated models is displayed on a computer screen. These 30 models give an approximate idea of the sort of a priori information used. Of course, more models are needed if we want a more accurate representation of the a priori probability.

We may not be interested in the models per se but only in smooth Earth models (for instance, if we know that only smooth properties are resolved by the data). The movie of Figure 8, then easily becomes the smooth movie displayed in Figure 9 (where the density at each point is arbitrarily chosen to be a simple average over 250 points surrounding it).

“Turning on” the comparison between computed and observed data, i.e., using the Metropolis rule, the ran-

dom walk sampling the prior distribution is modified and starts sampling the posterior distribution. Figure 10 shows a movie with some samples of the posterior distribution, and Figure 11 shows the smoothed samples.

Let us first concentrate on the a posteriori movie of Figure 10. It is obvious that many different models are possible. This is no surprise, as gravity data do not constrain strongly the Earth model. But it is important to look at Figure 12. We display the a priori and the a posteriori data movie, i.e., the synthetic data corresponding to models of the a priori random walk in the model space and the synthetic data corresponding to models of the a posteriori random walk in the model space, when the Metropolis rule is biasing the prior random walk towards the posterior. Even though the models in the posterior movie of Figure 10 are quite different, all of them predict data that, within experimental uncertainties, are models with high likelihood: gravity data alone can not have a preferred model.

Let us now analyze the smoothed models of Figure 11. They do not look as “random” as the models without smoothing: they all have a zone of high-density contrast centered around 10 km depth, which is a “structure” resolved by the data.

Answering Questions

From the viewpoint defended here, there are no well-posed questions or ill-posed questions, but just questions that have a probabilistic answer.

Making histograms. We may be interested in the value of the mass density at some depth, say z_0 . Each

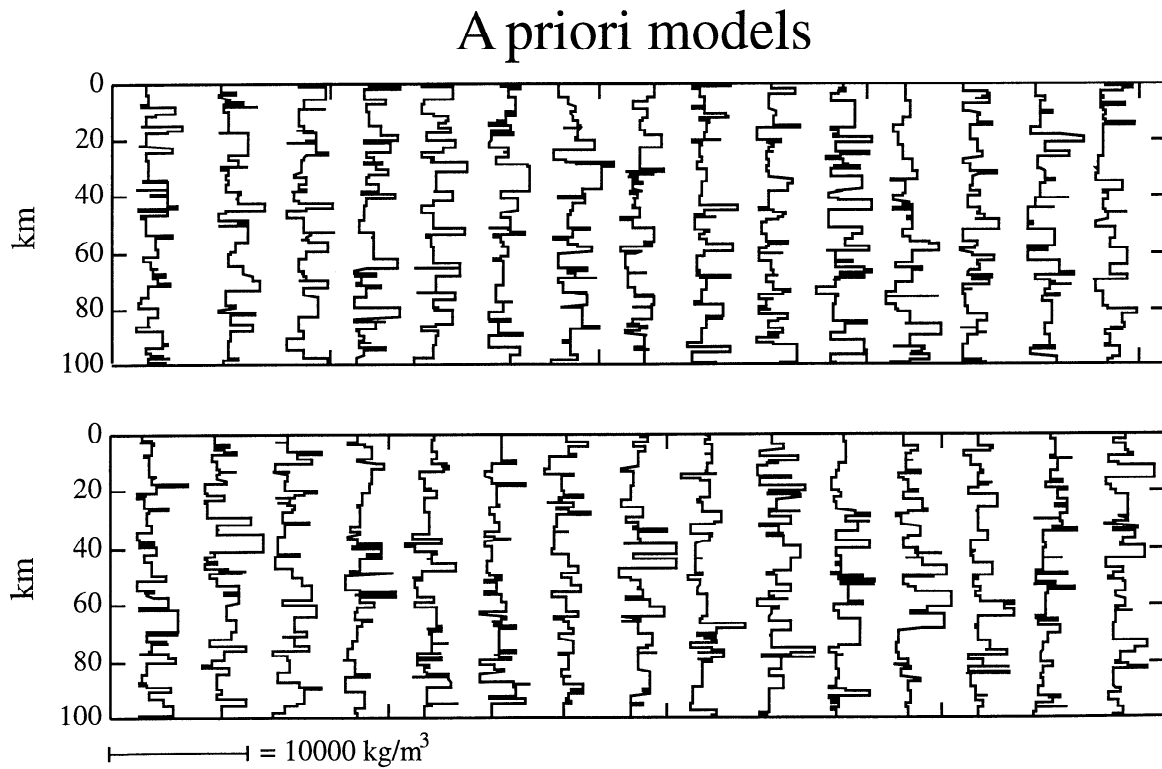


Figure 8. Some images of a movie representing the a priori probability density.

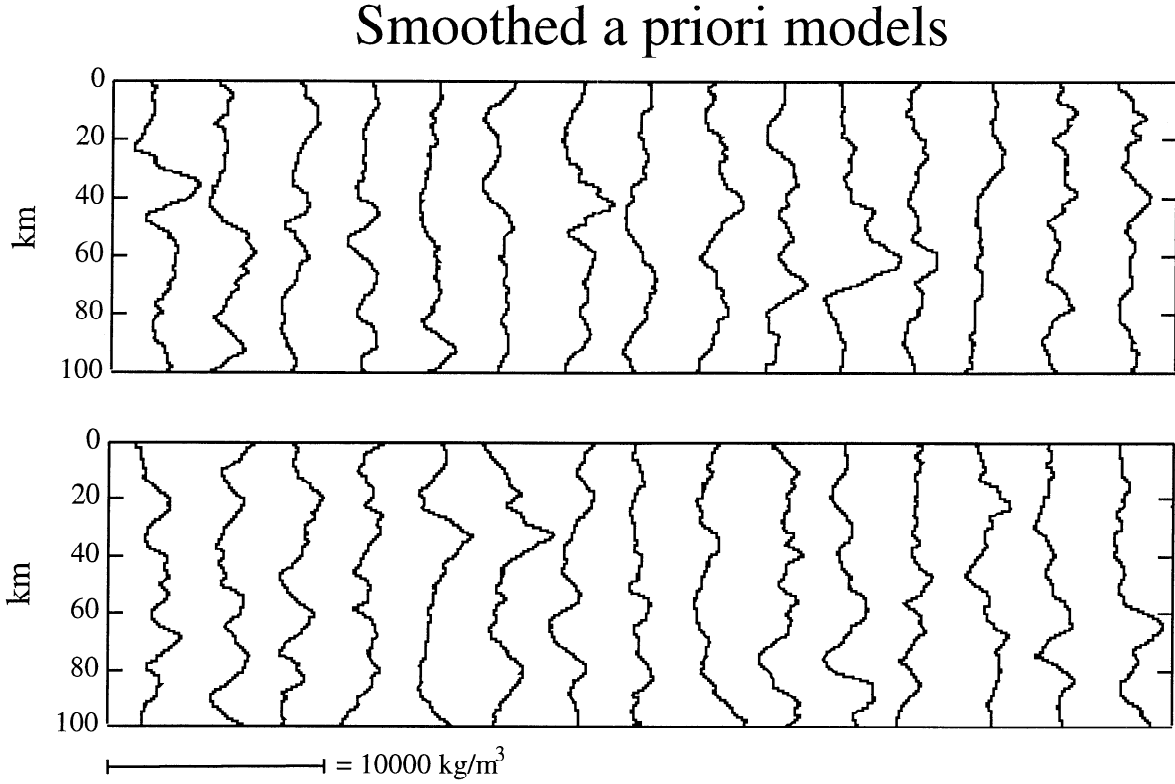


Figure 9. Same as Figure 8 but with the models smoothed.

of our many samples (of both the a priori and the a posteriori probability in the model space) has a particular value of the mass density at z_0 . The histogram of these values clearly represents the marginal probability distribution for the mass density at that point.

Figures 13 and 14 show both the prior and posterior histograms for the mass density at 2 km, 10 km and 80 km depth, respectively. In particular, we see, when comparing the prior and posterior histograms at 2 km depth, that the mass density to some extent has been

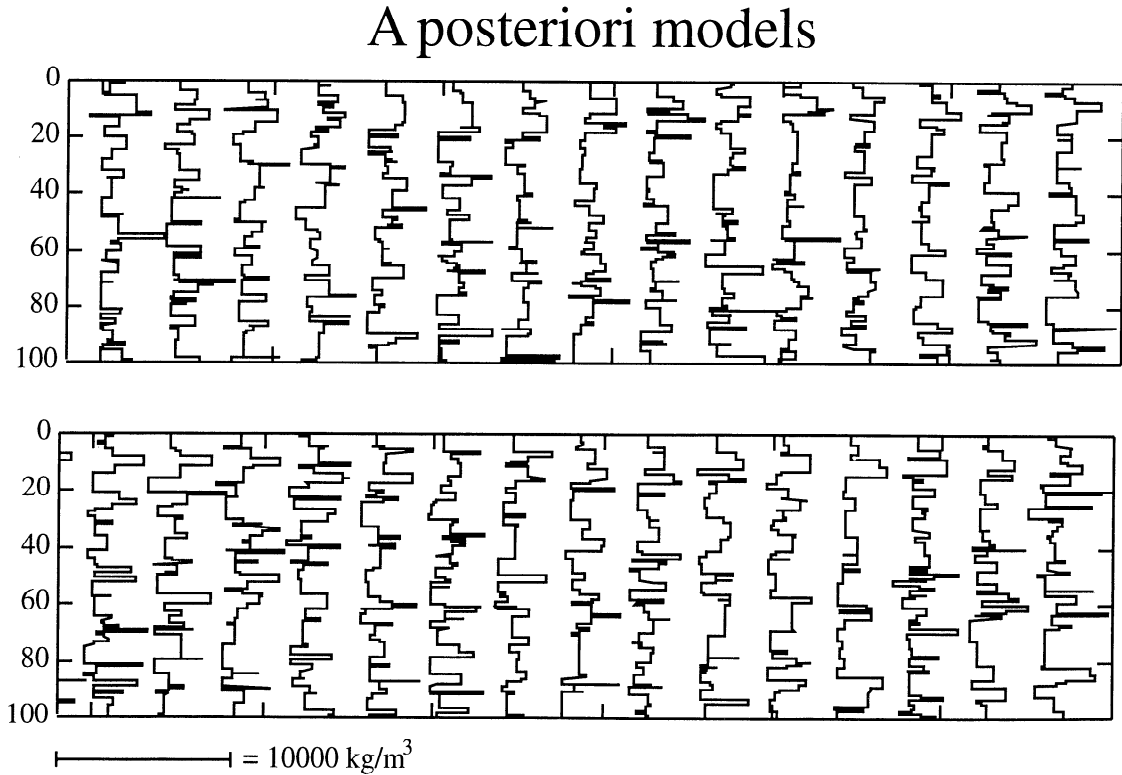


Figure 10. Some images of a movie representing the a posteriori probability density.

Smoothed a posteriori models

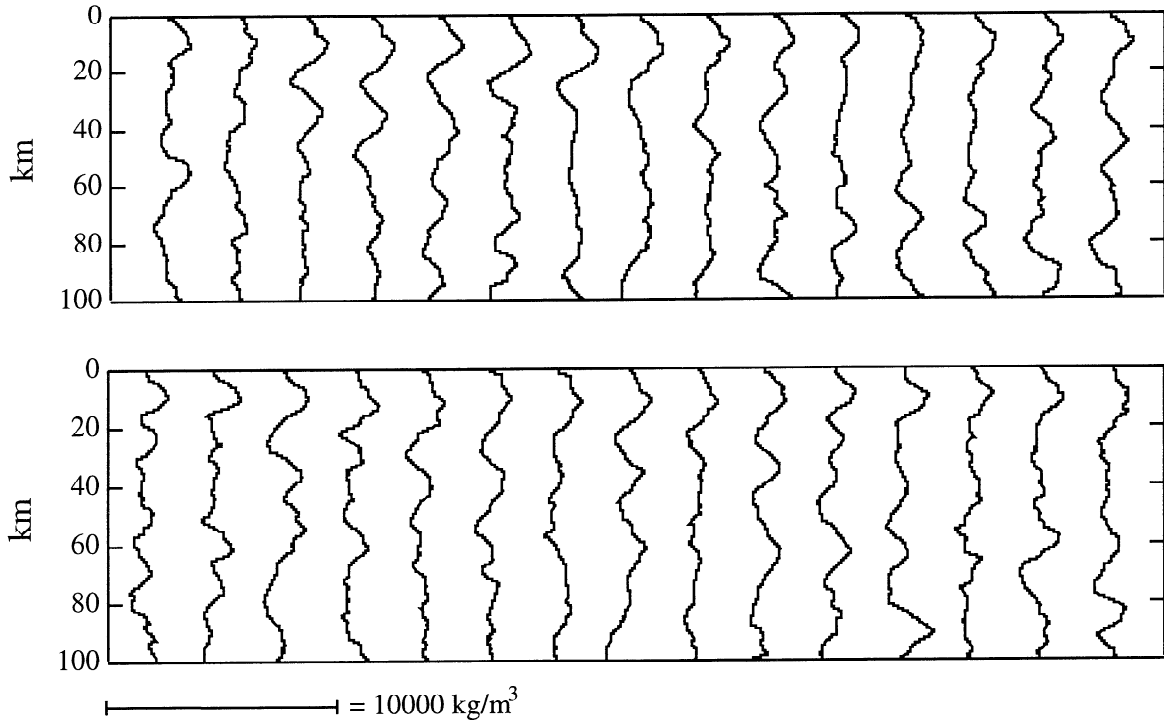


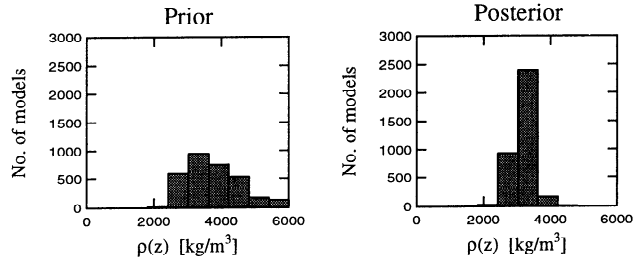
Figure 11. Same as Figure 10, smoothed. The smoothed models do not look as “random” as the models without smoothing (Figure 10): they all have “bump” at about 10 km depth, which is a “structure” resolved by the data.

resolved there: the histogram has been slightly “narrowed”. This is not the case at 80 km depth. Instead of the value of the mass density at some particular depth, we may be interested in the average mass density between, say, z_1 and z_2 . Taking this average for all our samples gives the histogram shown at the bottom of Figure 14.

Computing central estimators, or estimators of dispersion. Central estimators and estimators of dispersion are traditional parameters used to characterize simple probability distributions. It is well known that while mean values and standard deviations are

good measures for Gaussian functions, median values and mean deviations are better adapted to Laplacian (double exponential) functions. We can compute both estimators (or any other), as we are not dependent on any particular assumption.

Marginal distribution at $z = 2$ km



Marginal distribution at $z = 10$ km

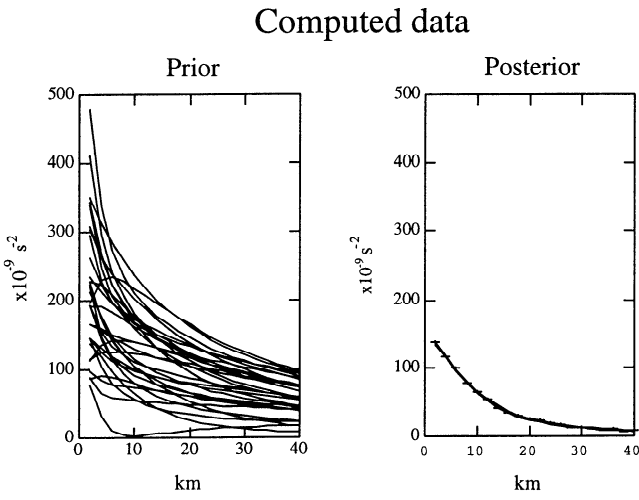
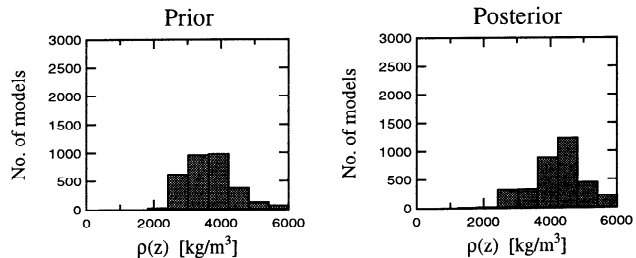


Figure 12. The a priori and a posteriori data movie.

Figure 13. Prior and posterior histograms for the mass density respectively at 2 km and 10 km. When comparing the prior and posterior histograms at 2 km depth, we see that the mass density has been quite well resolved there: the histogram has been considerably “narrowed”.

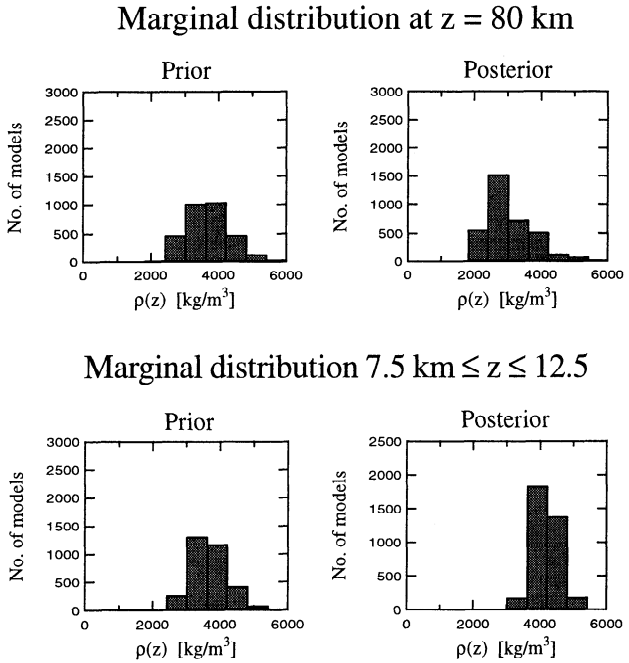


Figure 14. Prior and posterior histograms for the mass density at 80 km depth, and average mass density between 7.5 km and 12.5 km. The mass density at 80 km depth has been less well “resolved” than at 2 km depth (see Figure 13).

Figure 15 shows the mean value for the mass density, plus and minus the standard deviation, and the median, plus and minus the mean deviation for both the a priori and the a posteriori movie. Again, these plots represent the mean and median (and corresponding deviations) of the a priori and a posteriori probability distributions in the model space. Notice that the mean and the median a posteriori models both show the zone of high density contrast centered around 10 km depth, characteristic of the true model of Figure 5, a feature well resolved by our data.

Computing correlations. We may also ask how correlated are the mass density values at different depth locations. From our movies, we can, for instance, easily compute the covariance function $C(z, z')$. The correlation function is given by $c(z, z') = C(z, z') / (\sigma(z)\sigma(z'))$, where $\sigma(z)$ is the standard deviation at point z (just estimated). The correlation function, taking its values in the interval $(-1, +1)$, has a simpler interpretation than the covariance function.

We have chosen to compute the correlation between a point arbitrarily chosen at $z_0 = 10$ km and all other points, i.e., the function $c(z_0, z)$. The result is displayed in Figure 16.

Notice that correlations in the a priori probability distribution decay approximately exponentially, and that they are all positive. In the a posteriori probability distribution, anticorrelations appear. This means, roughly speaking, that if the mass density of any particular realization is in error at 10 km depth, it is likely that it will also be in error, but with opposite sign, in the layers just above and below 10 km.

The approximate exponential decay of the correlation in the prior probability results from the exponential probability chosen for the layer thicknesses. The anticorrelations appearing in the posterior probability describe the uncertainty in our posterior models due to the type of information brought by the gravity data.

Discussion

All the results presented in Figures 8 and 9, and the left parts of Figures 13 to 16 concern the a priori movie (i.e., they correspond to the sampling of the model space according to the a priori probability density). Should we at this point decide that we are not representing well enough our a priori information or that we are inputting a priori information that we do not actually have, it would be time to change the way we generate pseudorandom models. If the a priori movie is acceptable, we can “switch on” the synthetic data calculation, and the filter described above, to generate samples of the a posteriori probability distribution, i.e., to produce the a posteriori movie.

It should be properly understood in which way the feature at 10 km depth is “resolved” by the data. None of the models of the a posteriori movie shows a clear density bump at 10 km depth, as the considered inverse problem has a highly nonunique solution (i.e., many different models fit the data and are in accordance with

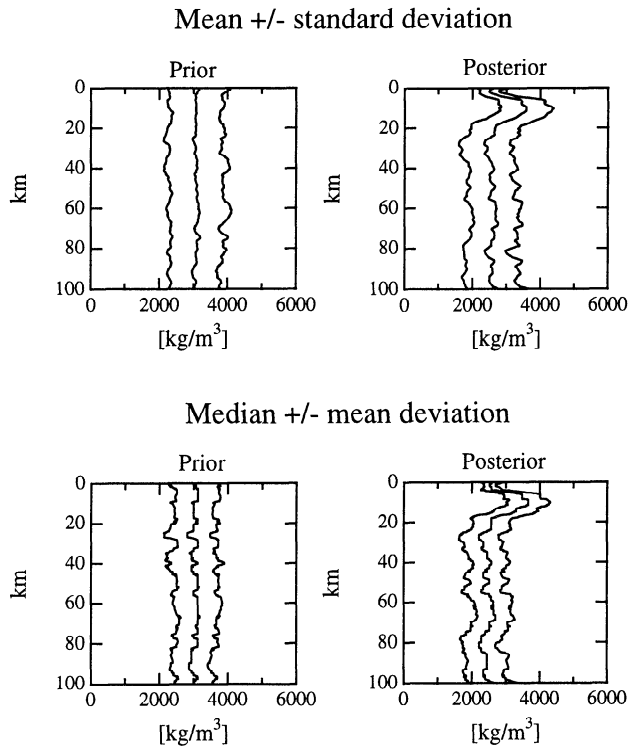


Figure 15. Mean value for the mass density, plus and minus the standard deviation, and the median, plus and minus the mean deviation for both, the a priori and the a posteriori movie. These represent the mean and median (and corresponding deviations) of the a priori and a posteriori probability distributions in the model space.

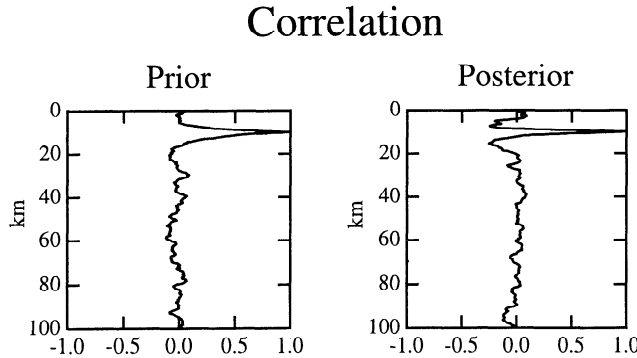


Figure 16. The (left) a priori and (right) a posteriori correlation functions $c(z_0, z)$ for $z_0 = 10$ km. Notice the anticorrelations appearing in the posterior correlation function.

the a priori information). From the a posteriori movie we can not conclude that the true model does have the bump, as many models without it are acceptable. Simply, models with the bump, and arbitrary “high frequencies” superimposed have a greater chance of being accepted.

General Considerations

There are two major differences between our Metropolis rule (for solving inverse problems) and the original Metropolis algorithm. First, it allows an introduction of non-uniform a priori probabilities. Moreover, an explicit expression for the a priori probabilities is unnecessary: an algorithm that samples the model space according to the prior is sufficient. Second, our Metropolis rule is valid for an arbitrary probability (i.e., it is not linked to the Gibbs-Boltzmann distribution).

Our algorithm has been developed for sampling of discrete spaces according to given probabilities. However, it can be used for optimization. The Metropolis algorithm is already used in simulated annealing [Kirkpatrick et al., 1983], where the desired distribution is changed during the process, starting with a uniform distribution and ending with a near-delta distribution, centered at the optimal solution. We could also find the “best model” by artificially using in the equations values for the experimental uncertainties that tend to zero. However, we do not recommend paying any interest to this concept of “best model”.

The method developed above is independent of the way probabilities have been normalized. This is important, as many interesting properties of a probability distribution can be inferred from a random walk, even before the walk has been so extensive that it allows an effective estimation of the denominator of equation (14).

Although we have designed a sampling algorithm (and given proof of its convergence to the desired distribution), we have only addressed heuristically the difficult problem of designing efficient algorithms. It can be shown that the Metropolis rule is the most efficient acceptance rule of the kind we consider (see Appendix C), but the acceptance rule is only part of the efficiency

problem: defining the graph (i.e., how the models can be perturbed) is a nontrivial task, and we have only shown an example of it, having no general theory to propose.

Conclusion

We have described a near-neighbor sampling algorithm (random walk) that combines prior information with information from measurements and from the theoretical relationship between data and model parameters. The input to the algorithm consists of random models generated according to the prior distribution $\rho(\mathbf{m})$ and the corresponding values of the likelihood function that carries information from measurements and the theoretical data/model relationship. Output from the algorithm are pseudo-random realizations of the posterior distribution $\sigma(\mathbf{m})$. We applied the algorithm to a highly nonunique, linear inverse problem, to show the method’s ability to extract information from noisy data.

The a posteriori distribution contains all the information about the parameterized physical system that can be derived from the available sources. Unfortunately, this distribution is multidimensional and is therefore impossible to display directly.

It is important to direct future efforts toward the development of methods for analyzing and displaying key properties of a posteriori distributions of highly nonlinear inverse problems. For this class of inverse problems, the a posteriori distributions are typically multimodal, and traditional techniques for analyzing error and resolution properties of unimodal a posteriori distributions break down. There is no known way of understanding uncertainties in the result of a highly nonlinear inverse problem. Here, we have defined the a posteriori probability density $\sigma(\mathbf{m})$, which contains all the information, but how to extract it? Clearly, computing standard deviations or covariances may be meaningless, if the posterior probability density is far from Gaussian, which is always the case for highly nonlinear problems. Also, an extensive exploration of the model space cannot be made if the space is of high dimension, as, for instance, in the problem of interpretation of seismic reflection data.

In that problem, each model is usually represented by an image. Using the methods described above, we should start by generating pseudo random models with the prior distribution $\rho(\mathbf{m})$. The movie should show models that, on the grounds of our prior information, are more or less likely. In geophysics, this is the right time for a geologist to tell us if he agrees with the movie or if, on the contrary, he sees too many unlikely or too few likely models. When the geologist is satisfied, we now can turn to look at the data, and to run the Metropolis rule, using data misfits, to converge to the posterior probability distribution $\sigma(\mathbf{m})$. The movie is now showing only models which are likely after examination of prior evidence and of geophysical data.

It must be understood that this point of view is much

more general than the usual one. For instance, imagine a problem where certain parameters can be resolved deterministically and other parameters can only be resolved statistically. This is the case, for instance, when inverting seismograms to obtain earth models. The major impedance contrasts, for instance, can be deterministically resolved from reflected energy. However, imagine that our space of admissible models contains models with very fine layering, much finer than the seismic wavelength. The position of these very fine layers can not be resolved deterministically, but, as some properties of the seismograms (coda amplitude decay, etc.) do contain information on the average density of fine layers, models (with fine layering) compatible with this information should be generated. Those fine layers could of course not be located individually, but if the data, say, perfectly resolve the average density of a series of layers, all the selected models should display the same average density of these layers. A simple illustration of this possibility has been made here with the “bump” in our mass density models.

From the final collection of models we can start posing questions. Ask for instance for any particular property of the model, for instance, the depth of a particular layer, the smoothed matter density distribution, etc. We have now many examples of that property. It may happen that all the models give the same value for it: the property is well constrained by the data. Some, using old terminology, would say that asking for that property is a “well-posed question”. On the contrary it may happen that all the models give absolutely different answers to the question.

In general, we are able to estimate statistics on that property and give answers with a clear probabilistic meaning. In almost all the interesting cases, those statistics will not follow the nice bell-shaped Gaussian distribution, but this should not be an obstacle to a proper analysis of uncertainties. We are well aware of the often tremendous computational task imposed by this approach to inversion. However, the alternative may be an uncertain estimation of uncertainties.

Appendix A: Design of Random Walk With a Desired Equilibrium Distribution

The design of a random walk that equilibrates at a desired distribution $\{p_i\}$ can be formulated as the design of an equilibrium flow having a throughput of p_i particles at point i . The simplest equilibrium flows are symmetric, that is, they satisfy $f_{ij} = f_{ji}$: the transition $i \leftarrow j$ is as likely as the transition $i \rightarrow j$. It is easy to define a symmetric flow on any graph, but it will in general not have the required throughput of p_j particles at point j . This requirement can be satisfied if the following adjustment of the flow is made: first, multiply all the flows f_{ij} with the same positive constant c . This constant must be small enough to assure that the throughput of the resulting flows cf_{ij}

at every point j is smaller than its desired probability p_j . Finally, at every point j , add a flow f_{jj} , going from the point to itself, such that the throughput at j gets the right size p_j . Neither the flow scaling nor the addition of f_{jj} will destroy the equilibrium property of the flow. In practice, it is unnecessary to add a flow f_{jj} explicitly, since it is implicit in our algorithms that if no move away from the current point takes place, the move goes from the current point to itself. This rule automatically adjusts the throughput at j to the right size p_j .

Appendix B: Naïve and Uniform Random Walks

Naïve Walks

Consider two arbitrary neighbors, i and j , having n_i and n_j neighbors, respectively, and a random walk with the simple transition probabilities $p_{ji} = 1/n_i$ and $p_{ij} = 1/n_j$ (choosing one of the neighbors, as the next point, uniformly at random). If we want the equilibrium flow to be symmetric, $p_{ji}q_i = p_{ij}q_j$, which is satisfied if $q_i = n_i$. Furthermore, the above probabilities make all the flows $f_{ji} = p_{ji}q_i$ equal to unity. So, the total throughput through point i is $\sum_k f_{ik} = \sum_j f_{ji} = n_i = q_i$. Hence $q_i = n_i$ must be the equilibrium distribution for the random walk.

Uniform Walks

The rules for the uniform walk follows now directly from applying the Metropolis rule (see later) to the above random walk. The Metropolis acceptance probabilities are $p_{ji}^{\text{acc}} = \min(v_j, v_i)/v_i$, where $v_i = 1/q_i$ and $v_j = 1/q_j$ are the “modification probabilities”.

Appendix C: Modifying a Random Walk by Introduction of an Acceptance Rule

Consider a random walk P_{ij} with equilibrium distribution ρ_j and equilibrium flow f_{ij} . We can multiply f_{ij} with any symmetric flow ψ_{ij} , where $\psi_{ij} \leq L_j$, for all i and j , and the resulting flow $\varphi_{ij} = f_{ij}\psi_{ij}$ will also be symmetric and hence an equilibrium flow. The transition probabilities of a “modified” algorithm with flow φ_{ij} and equilibrium probability σ_j is obtained by dividing φ_{ij} with the product probability $\sigma_j = \rho_j L_j$. This gives the transition probability: $P_{ij}^{\text{modified}} = f_{ij}\psi_{ij}/\rho_j L_j = P_{ij}\psi_{ij}/L_j$, which is equal to the product of two factors: the initial transition probability, and a new probability: the acceptance probability $P_{ij}^{\text{acc}} = \psi_{ij}/L_j$. If we choose to multiply f_{ij} with the symmetric flow $\psi_{ij} = \min(L_i, L_j)$, we obtain the Metropolis acceptance probability $P_{ij}^{\text{metrop}} = \min(L_i, L_j)/L_j$, which is one for $L_i \geq L_j$, and equals L_i/L_j when $L_i < L_j$. Choosing, instead, $\psi_{ij} = L_i L_j/(L_i + L_j)$, we get the “logistic rule” with acceptance probability $P_{ij}^{\log} = L_i/(L_i + L_j)$. The simplest algorithm can be derived from $\psi_{ij} = \min_i(L_i)$, giving the acceptance probability $P_{ij}^{\text{evap}} = \min_i(L_i)/L_j$.

The acceptance rule for this constant flow we call the "evaporation rule", as the move by a random walker away from the current point depends only on the desired probability at that point and that this recalls the behavior of a water molecule trying to evaporate from a hot point. A last example appears by choosing $\psi_{ij} = L_i L_j$, which gives the acceptance probability $P_{ij}^{\text{cond}} = L_i$. We refer to this acceptance rule as the "condensation rule", as it recalls the behavior of a water molecule trying to condensate at a cold point. The efficiency of an acceptance rule can be defined as the sum of acceptance probabilities for all possible transitions. The acceptance rule with maximum efficiency is obtained by simultaneously maximizing ψ_{ij} for all pairs of points j and i . Since the only constraint on ψ_{ij} (except for positivity) is that ψ_{ij} is symmetric and $\psi_{kl} \leq L_l$, for all k and l , we have $\psi_{ij} \leq L_j$ and $\psi_{ij} \leq L_i$. This means that the acceptance rule with maximum efficiency is the Metropolis rule, where $\psi_{ij} = \min(L_i, L_j)$.

Appendix D: An Iteration Consisting of a Randomly Chosen Step

In this case, the transition probability matrix for the iteration is equal to a linear combination of the transition probability matrices for the individual steps. The coefficient of the transition probability matrix for a given step is the probability that this step is selected. Since the vector of desired probabilities is an equilibrium distribution (eigenvector with eigenvalue 1) for each of the step transition probability matrices, and since the sum of all the coefficients in the linear combination is equal to 1, it is also an equilibrium distribution for the transition probability matrix for the complete iteration. This equilibrium distribution is unique, since it is possible, following the given steps, to go from any point to any other point in the space.

Acknowledgments. We thank Zvi Koren and Miguel Bosch for helpful discussions on different aspects of Monte Carlo optimization. This research has been supported in part by the Danish Energy Ministry, the Danish Natural Science Research Council (SNF), the French Ministry of National Education (MEN), the French National Research Center (CNRS, INSU) and the sponsors of the Groupe de Tomographie Géophysique (Amoco, CGG, DIA, Elf, IFP, Schlumberger, Shell, Statoil).

References

- Backus, G., Inference from inadequate and inaccurate data, I, *Proc. Natl. Acad. Sci. U.S.A.*, 65 (1), 1–105, 1970a.
 Backus, G., Inference from inadequate and inaccurate data, II, *Proc. Natl. Acad. Sci. U.S.A.*, 65 (2), 281–287, 1970b.
 Backus, G., Inference from inadequate and inaccurate data, III, *Proc. Natl. Acad. Sci. U.S.A.*, 67 (1), 282–289, 1970c.
 Cary, P.W., and C.H. Chapman, Automatic 1-D waveform inversion of marine seismic refraction data, *Geophys. J. R. Astron. Soc.*, 93, 527–546, 1988.
 Dorman, L.M., The gravitational edge effect, *J. Geophys. Res.*, 80, 2949–2950, 1975.
 Feller, W., *An Introduction to Probability Theory and Its Applications*, John Wiley, New York, 1970.
 Geman, S., and D. Geman, Stochastic relaxation, Gibbs distributions, and the Bayesian restoration of images, *IEEE Trans. Pattern Anal. Mach. Intel.*, PAMI-6, 721–741, 1984.
 Jackson, D.D., The use of a priori data to resolve non-uniqueness in linear inversion, *Geophys. J. R. Astron. Soc.*, 57, 137–157, 1979.
 Keilis-Borok, V.J., and T.B. Yanovskaya, Inverse problems in seismology (structural review), *Geophys. J. R. Astron. Soc.*, 13, 223–234, 1967.
 Kirkpatrick, S., C.D. Gelatt, Jr., and M.P. Vecchi, Optimization by simulated annealing, *Science*, 220, 671–680, 1983.
 Koren, Z., K. Mosegaard, E. Landa, P. Thore, and A. Tarantola, Monte Carlo estimation and resolution analysis of seismic background velocities, *J. Geophys. Res.*, 96, 20289–20299, 1991.
 Landa, E., W. Beydoun, and A. Tarantola, Reference velocity model estimation from prestack waveforms: Coherence optimization by simulated annealing, *Geophysics*, 54, 984–990, 1989.
 Marroquin, J., S. Mitter, and T. Poggio, Probabilistic solution of ill-posed problems in computational vision, *J. Am. Stat. Assoc.*, 82, 76–89, 1987.
 Metropolis, N., and S.M. Ulam, The Monte Carlo method, *J. Am. Stat. Assoc.*, 44, 335–341, 1949.
 Metropolis, N., A.W. Rosenbluth, M.N. Rosenbluth, A.H. Teller, and E. Teller, Equation of state calculations by fast computing machines, *J. Chem. Phys.*, 1, (6), 1087–1092, 1953.
 Mosegaard, K., and P.D. Vestergaard, A simulated annealing approach to seismic model optimization with sparse prior information, *Geophys. Prospect.*, 39, 599–611, 1991.
 Parker, R.L., Understanding Inverse Theory, *Annu. Rev. Earth Planet. Sci.*, 5, 35–64, 1977.
 Pedersen, J.B., and O. Knudsen, Variability of estimated binding parameters, *Biophys. Chem.*, 36, 167–176, 1990.
 Press, F., Earth models obtained by Monte Carlo inversion, *J. Geophys. Res.*, 73, 5223–5234, 1968.
 Press, F., An introduction to Earth structure and seismotectonics, *Proc. of the Int. Sch. Phys. Enrico Fermi*, 209–241, 1971.
 Rothman, D.H., Nonlinear inversion, statistical mechanics, and residual statics estimation, *Geophysics*, 50, 2797–2807, 1985.
 Rothman, D.H., Automatic estimation of large residual statics corrections, *Geophysics*, 51, 332–346, 1986.
 Tarantola, A., *Inverse Problem Theory: Methods for Data Fitting and Model Parameter Estimation*, Elsevier, New York, 1987.
 Tarantola, A., and B. Valette, Inverse problems = Quest for information, *J. Geophys.*, 50, 159–170, 1982a.
 Tarantola, A., and B. Valette, Generalized nonlinear inverse problems solved using the least squares criterion, *Rev. Geophys.*, 20, 219–232, 1982b.
 Wiggins, R.A., Monte Carlo inversion of body wave observations, *J. Geophys. Res.*, 74, 3171–3181, 1969.
 Wiggins, R.A., The general linear inverse problem: Implication of surface waves and free oscillations for Earth structure, *Rev. Geophys.*, 10, 251–285, 1972.
-
- K. Mosegaard, Niels Bohr Institute for Astronomy, Physics and Geophysics, Dept. of Geophysics, Haraldsgade 6, DK-2200 Copenhagen N, Denmark (klaus@osiris.gfy.ku.dk).
 A. Tarantola, Institut de Physique du Globe, 4 Place Jussieu, F-75252 Paris Cedex 05, France (tarantola@ipgj.jussieu.fr).

(Received June 1, 1994; revised November 11, 1994; accepted November 29, 1994.)

UNDERSTANDING INVERSE THEORY

*10066

Robert L. Parker

Institute of Geophysics and Planetary Physics, Scripps Institution of Oceanography,
University of California, San Diego, La Jolla, California 92093

INTRODUCTION

Much of our knowledge of the Earth's interior is perforce based on the interpretation of measurements made at the surface, rather than direct sampling of the material in the interior. In the past few years there have been great advances in the mathematical aspects of this problem, and the topic has come to be called geophysical inverse theory. To apply these ideas, there must be a valid mathematical model of the physics of the system under study, so that one would be able to calculate the values of observations made on an exactly known structure: the calculation of the behavior of a specified system is the solution of the "forward" or "direct" problem. Frequently it is the forward problem that presents a difficult challenge to the theoretical geophysicist. Illustrations include the mechanism of earthquake rupture or the generation of the Earth's magnetic field; in problems like these, inverse theory is normally quite inappropriate. When the forward problem has been completely solved, there are of course unknown parameters in the mathematical model representing physical properties of the Earth such as Lamé parameters, density or electrical conductivity. The goal of inverse theory is to determine the parameters from the observations or, in the face of the inevitable limitations of actual measurement, to find out as much as possible about them. The quality that distinguishes inverse theory from the parameter estimation problem of statistics (Bard 1974, Rao 1973) is that the unknowns are *functions*, not merely a handful of real numbers. This means that the solution contains in principle an infinite number of variables, and therefore with real data the problem is as underdetermined as it can be. Naturally, there are geophysical problems containing a relatively small number of free parameters: for example, in describing the relative instantaneous motion of N lithospheric plates, we find that the assumption of internal rigidity reduces the number of unknowns to $3N - 3$ for the $N - 1$ relative angular velocity vectors (McKenzie & Parker 1974). Sometimes, however, unknown structures are conceived in terms of small numbers of homogeneous layers for reasons of computational simplicity rather than on any convincing geophysical or

geological grounds. Such simplification may lead to false confidence in the solution because the true amount of freedom has not been allowed in the parameters.

The theory falls into two distinct parts. One deals with the ideal case in which the data are supposed to be known exactly and as densely as desired, and is of course mainly the province of the applied mathematician. The other treats the practical problems that are created by incomplete and imprecise data. It might be thought that an exact solution to an inverse problem with perfect data would prove extremely useful for the practical case. Actually, this often turns out to be untrue because geophysical inverse problems are almost always unstable in a sense to be defined more precisely later; when this is so, the solution obtained by the analytic technique is very sensitive to the way in which the data set is completed and to the errors in it. In my view analytical studies are more valuable for their results concerning uniqueness and conditions for existence and stability.

The advances mentioned earlier arise primarily from a recognition that practical inverse problems never possess unique solutions and that an honest attempt to interpret the data must appraise the variety of compatible solutions. In the class of linear problems there is now a very satisfactory body of theory for achieving this end, but work on the larger and more prevalent class of nonlinear problems is still in a relatively primitive state and perhaps always will be.

The plan of this article is as follows. In the next section I outline and discuss some mathematical questions in the analysis of idealized data. Although many of the points raised by the geophysical problems are fascinating to the mathematician, I have tried to keep in mind that the aim of our science is to learn about the Earth and therefore I attempt to restrict discussion to matters of practical consequence. After this, I deal directly with the problem of using actual measurements. First, there is a fairly extended account of the linear theory in which I permit myself occasionally to give some of the mathematical details. Here the principles of the celebrated Backus-Gilbert method are described and a particular formulation is given of the spectral expansion method which has made possible the solution of so many practical problems. Finally, there is a section on the analysis of nonlinear systems, consisting of a discussion of the linearization approximation and a brief sketch of some of the commendable efforts to do without approximation.

ANALYSIS OF PERFECT DATA

The task of retrieving model parameters from a complete and precise set of data is clearly a mathematical undertaking. There is no single simple method of attacking the various aspects of inverse theory, but instead methods are drawn from almost every branch of applied mathematics. Therefore, I make no attempt to give any derivations in this section, but rather to highlight the fundamental concepts and the way that they impinge upon the more empirical side of geophysics. I consider the questions of existence, uniqueness, construction, and stability, which are some of the concerns that must be dealt with in a complete solution of an inverse problem. Sabatier (1971) has given a more extended account of these topics in a wide-ranging comparative review.

Mathematicians take the view, logically enough, that before attempting to calculate parameters, one ought to define the class of possible data that are associated with the model.

This is the question of *existence* and, although it receives little attention in the geophysical literature, it is of great importance in testing the assumptions behind any mathematical model. Every model contains simplifications and approximations, some of which may be hard to justify initially; for example, in many inverse problems the idealization of horizontal (or radial) stratification is introduced at the outset. To give a concrete instance, consider the problem of electrical conductivity sounding with the magneto-telluric method (Cagniard 1953). Here recordings are made in one place of orthogonal components of the horizontal electric and magnetic field (E_x and B_y , say, with z vertical). The ratio of the Fourier transforms of the two signals is related to the electrical conductivity profile of a horizontally layered medium beneath the observing station. If the medium is truly layered, the orientation of the x and y axes will not affect the results, i.e. the magneto-telluric ratio is isotropic. Mathematically this is a statement of a *necessary condition* for the existence of a solution to the inverse problem of finding $\sigma(z)$ from the ratio. When the data are not isotropic we know that there is no solution to the problem as posed and that one of our model assumptions is false. Under these circumstances it would be foolish to continue with an interpretation based on the original model. Suppose now that an isotropic ratio was indeed observed; does this in itself guarantee a solution of the kind proposed? This is equivalent to asking whether isotropy is a *sufficient condition* for existence. In fact, isotropy is by no means enough to insure a corresponding layered solution: a particularly thorough exploration of the various restraints imposed upon the data by the layering assumption has been given by Weidelt (1972). All of these are further necessary conditions; a sufficient condition for their problem has never been derived to my knowledge. Another geophysical inverse problem which has been considered from this viewpoint is that of body-wave travel times; Gerver & Markusevitch (1966) give a detailed account.

A different mathematical matter of great geophysical importance is the question of *uniqueness*: if it is granted that there is a solution for a given set of data, is there only one such solution? Profound consequences follow if the answer is no, for it is then established that even perfect data (complete and exact) do not contain enough information to recover the Earth's structure. Several courses are then open: one can explore what further assumptions can be plausibly made about the Earth to narrow the class of solutions (perhaps down to uniqueness); alternatively, additional kinds of measurements might be introduced; or finally, one may be willing to tolerate the ambiguity if the class of admissible solutions still contains decisive information about the Earth. The last course is indeed the one that must be followed when actual observations are to be analyzed.

Uniqueness is often rather difficult to prove and, in the absence of a proof, practising geophysicists naturally proceed without one. This has sometimes led to surprises. Consider the problem of modelling the geomagnetic field. For technical reasons the intensity of a magnetic field is far easier to measure accurately than its

three components; these reasons become even more compelling when the instruments are in orbit about the Earth. Therefore our knowledge of the global field depends heavily upon intensity values. The question arises whether one can uniquely¹ recover a harmonic vector field when only its intensity is known. To simplify the problem assume $|\mathbf{B}|$ is known everywhere on the surface of a sphere and that the field has an internal source. Here the forward problem is trivial: calculation of $|\mathbf{B}|$ from \mathbf{B} . Backus (1970) was able to devise a doubly infinite family of pairs of vector fields, in which the members of each pair generate identical intensities on a sphere: this counter-example demonstrates the impossibility of a general uniqueness proof. Backus (1968) also proved a series of uniqueness results, however, one being that the vector acceleration of gravity, \mathbf{g} , can be determined uniquely from $|\mathbf{g}|$ alone. Models of the geomagnetic field largely based on the intensity observations had of course been constructed, but a problematic inaccuracy in predicting the components was soon discovered (Cain 1971), and the poor performance of models based upon intensity became a major worry (Stern & Bredekamp 1975). It is now widely agreed that lack of uniqueness in the analytic problem is a major factor (called the Backus Ambiguity). In this case the only way to improve the solution appears to be measurement of the component values themselves.

An example of nonuniqueness, known for three centuries, is one that arises in the interpretation of gravitational fields: whereas a knowledge of the density structure of a system completely specifies its external gravitational field, a complete knowledge of the external field does not specify the density structure uniquely. In this case further information can be supplied by our knowledge of geology: for example, in exploration work and crustal studies it may often be assumed that the buried systems consist of relatively homogeneous units, perhaps with known densities; then the problem is to determine the shapes of these units. With several more assumptions about the buried body (e.g. that it is finite in extent and that a vertical line never intersects the body more than once) Smith (1961) was able to prove a uniqueness theorem stating that there is only one uniform body responsible for a given gravity anomaly, when the density is specified.

Uniqueness has been established for a number of geophysical inverse problems, e.g. the body-wave travel-time problem (Gerver & Markusevitch 1966) and the magneto-telluric problem mentioned earlier (Bailey 1970). Perhaps the most important exception is in the normal-mode inverse problem: the frequencies of free oscillation of the Earth have in the past five years yielded a precise, detailed picture of the mechanical structure of the deep interior (e.g. Gilbert & Dziewonski 1975), but there is no proof that the totality of such frequencies actually defines only one Earth model. Progress has been made on some analogous systems, however (Barcilon 1976).

We come next to the matter of *construction*, which, as Sabatier (1971) has remarked, receives an undue degree of attention. The uniqueness and existence of a solution are granted; what is now required is a procedure that will, in a finite number of steps, produce the solution with any specified finite precision. If iterative

¹ There is of course a trivial ambiguity of sign since both $+\mathbf{B}$ and $-\mathbf{B}$ give rise to the same $|\mathbf{B}|$. A single additional measurement of \mathbf{B} serves to resolve this ambiguity.

methods are involved, a global convergence proof is required, and on this point most purely numerical schemes founder.

The classical solution of a geophysical inverse problem is the renowned Herglotz-Wiechert formula for obtaining the velocity-depth function from travel-time distance measurements in seismology (Bullen 1965). The idealized problem is as follows. A surface source emits signals travelling as seismic body waves through a spherically symmetric Earth, in which the continuous velocity v increases monotonically with depth. The time, T , taken for the earliest impulse to travel from the source to an observer at a range Δ (measured as an angle at the center of the Earth) is assumed known everywhere in some finite range, including $\Delta = 0$. If the rate of increase of v with depth is great enough but not too great, T is a monotonically increasing, differentiable function of Δ , and from the ray geometry we have

$$\frac{r_\Delta}{v_\Delta} = \frac{dT}{d\Delta},$$

where r_Δ is the radius of greatest penetration of a ray arriving at range Δ and v_Δ is the velocity at that radius. Then r_Δ can be found from the integral

$$\ln(a/r_\Delta) = \frac{1}{\pi} \int_0^\Delta \cosh^{-1} \left[\frac{dT/dT}{d\Delta'/d\Delta} \right] d\Delta',$$

where a is the Earth's radius. This formula combined with the first gives a means for constructing v at a radius of r . A similar formula can be developed for a flat Earth model. If the velocity fails to increase quickly enough with depth or there is a decreasing velocity, the derivative $dT/d\Delta$ ceases to exist and the method fails. Indeed there is no longer only one solution in the latter case, and then arrival-time functions of buried sources are needed to find the velocity (Gerver & Markusevitch 1966). This classical method is one that has been used with actual measurements, and it is the basis of a novel technique devised to account for data inadequacy, as we shall see later.

The geophysical inverse problem that seems to have collected the largest number of distinct methods of construction is the magneto-telluric problem, or its close relative, the problem of electromagnetic induction where only magnetic fields are recorded. The method of Siebert (1964) relies on the behavior of the data as the frequency tends to infinity and constructs a power series for the solution. Bailey's approach (Bailey 1970) uses the response data over the whole frequency range to develop a nonlinear integro-differential equation based upon the principle of causality (i.e. that the currents in the Earth must flow after the forcing field has been applied, never before). Weidelt (1972) employs a modification of the Gel'fand-Levitan method (1955). This method has the advantage of a degree of generality, for inverse problems where unknown parameters appear as coefficients in a Sturm-Liouville differential equation can usually be cast into the required form. A Fredholm integral equation is derived from the spectrum of the differential operator. Weston (1972) uses the Gel'fand-Levitan approach, but on data recorded in the time domain, rather than using the frequency-domain Fourier transform.

Having applied some of these methods to field observations, Bailey (1973) concluded that they were not particularly successful. The reason for this, in simple terms, is that the relevant equations describe magnetic and electric fields diffusing into the Earth, and that the information about deep structures is returned to the surface by strongly attenuated fields. Thus, unless the measurements are of astronomical precision, that information is lost. The analytic solutions seem to rely heavily upon the infinite density and precision of the idealized data and are therefore unsuitable for application to actual measurements.

There is a way to predict whether, in a particular problem, the solution depends upon the data in this rather unsatisfactory way: it is by deciding the question of *stability* of the problem. Mathematically, a problem is said to be stable if the solution depends continuously on the data and unstable if it does not. In simple terms this means that for all data sets lying close² to a particular set the solutions fall close to each other. This concept was introduced by Hadamard (1902) in connection with the study of boundary-value problems and he designated unstable problems "ill-posed." Very many inverse problems in geophysics are unstable in this sense. The best known example is that of downward continuation of harmonic fields (Bullard & Cooper 1948). Here the data are measurements of a harmonic function (typically a gravity or magnetic anomaly) taken on a particular level: the field values are then required at a deeper level that is nearer the sources. It is easy to show that two fields may differ by an arbitrarily small amount at the upper level, yet be quite different at the lower one, if the difference between the two original signals is confined to short enough wavelengths. This indicates the instability of downward continuation, which has long been recognized. One consequence of this instability is the corresponding lack of stability in any procedure to construct the source structure from potential field observations because downward continuation is implicit in all such processes.

Almost no work has been done on stability in the Western literature on analytical geophysical inverse problems, but the Russian school of applied mathematicians has made some important contributions here (e.g. see Lavrentiev 1967). Numerical methods for mitigating the undesirable effects of instability are discussed when we consider linear inverse problems in the next section.

ANALYSIS OF EXPERIMENTAL DATA: LINEAR PROBLEMS

Introduction

The class of linear inverse problems is particularly simple and it is the class about which the most is known; indeed, nonlinear problems are often treated by making approximations that reduce them locally to linear ones. A linear inverse problem is defined as one in which the data are linear functionals³ of the model. Fortunately

² The concept of closeness requires the introduction of a metric onto the space of functions defining the model and the observations. Usually a measure based on a norm is meant, like the two-norm: then the distance between f_1 and f_2 is $\|f_1 - f_2\|_2$.

³ Mathematically, a functional is a mapping that maps a set of functions into the real numbers.

we can be more specific, since in geophysics it is almost always true that the model is related to the data via an integral transform:

$$e(x) = \int_I G(x, y)m(y) dy, \quad (1)$$

where m is the unknown function we are seeking, e a function representing the observations, and G a kernel derived from theory (for definiteness the independent variables may be thought of as one-dimensional and I as a real interval). Viewed as an equation for m , (1) is a Fredholm integral equation of the first kind. The two analytical questions of greatest importance for practical situations are those of uniqueness and stability.

The problem of uniqueness of solutions to equation (1) can be boiled down to the question: are there any nontrivial solutions $a(y)$ to the equation

$$0 = \int_I G(x, y)a(y) dy?$$

If the answer is no, then $m(y)$ is unique. If it is yes, then the class,⁴ A , of all such solutions (so that $a \in A$) is called the annihilator of $G(x, y)$. Our knowledge of $e(x)$ can tell us nothing whatsoever about those parts of m that belong to A , and therefore these parts must be deduced from information other than that contained in e . For the complex kernels G of physical processes it is relatively rare that uniqueness can be established; in those cases that can be handled, a common procedure is to transform (1) into one of the well-studied integral transforms, for example:

$$\text{Laplace: } G(x, y) = e^{-xy}, \quad 0 \leq y < \infty,$$

$$\text{Fourier: } G(x, y) = e^{2\pi i xy}, \quad -\infty < y < \infty,$$

$$\text{Hankel: } G(x, y) = J_v(xy)(xy)^{1/2}, \quad 0 \leq y < \infty.$$

All of these have unique solutions for a sufficiently well-behaved class of model functions. Furthermore, many Volterra equations [which contain the Heaviside function $H(x - y)$] can be shown to possess unique solutions, e.g. the Abel equation with

$$G(x, y) = H(x - y)(x - y)^{-v}, \quad 0 < v < 1.$$

Suppose an annihilator exists for a particular $G(x, y)$; its presence will not necessarily be revealed by numerical solutions of (1) because the (necessarily finite-dimensional) representation of $G(x, y)$ may not be singular, even though the true kernel is.

The matter of stability is also of great importance from a practical viewpoint. As we have seen in the previous section, the construction of solutions to an unstable problem is difficult: the smallest error in e may result in a wild excursion of m that bears no relation to the true solution. The numerical inversion of the Fourier and Laplace transforms is a good illustration of the influence of stability. Both

⁴ A is actually a linear vector space; it is also sometimes called the null space of $G(x, y)$.

transforms possess unique inverses and analytic methods for their construction. However, the inversion of the Fourier transform is stable (in the two-norm) while the inversion of the Laplace transform is not (in any conventional norm); this fact accounts for the relative ease with which numerical inversion can be performed on the Fourier transform, while the Laplace transform is notoriously difficult to invert.

For linear problems the study of stability is not difficult. Roughly speaking, if the kernel G tends to "smooth" m , the inversion is unstable. A fairly widely applicable result is that, if I is finite and G is continuous, inversion for m is not stable.

In addition to downward continuation, some other unstable linear problems of geophysics are inversion of surface strain for fault displacement (Weertman 1965) and calculation of density contrasts arising from isostatic compensation (Dorman & Lewis 1972). Actually, differentiation of a data series is an unstable process also, and since differentiation enters some nonlinear construction methods (e.g. the Gel'sfand-Levitan method) they may be unstable also.

Limitations of Experimental Data

The first limitation of actual observations that comes to mind is their imprecision: everyone knows that experimentally determined numbers are inexact. From a mathematical viewpoint, an equally important property is availability of only a finite number of measurements; indeed we shall maintain that it is *always* realistic to replace (1) with

$$e(x_i) = \int_I G(x_i, y)m(y) dy, \quad i = 1, 2 \dots N,$$

or

$$e_i = \int_I G_i(y)m(y) dy, \quad i = 1, 2 \dots N. \quad (2)$$

This manifestation of observational inadequacy is immediately obvious in some measurements, such as digital samples in the time domain or the determination of free periods of vibration of the Earth. When continuous records are considered, such as seismograms, it is still possible to reduce the continuous curves to a finite list of numbers. One way of achieving this is to construct a Fourier series⁵ for the record; we may discard coefficients corresponding to frequencies higher than some finite limit because the sensing and recording instruments cannot respond to arbitrarily high frequency inputs.

The inadequacy of real measurements as expressed by the finiteness of N in (2) is in principle independent of their inaccuracy, and it is useful initially to study the idealized situation where the numbers e_i are perfectly accurate. This enables us to deal at once with the question of uniqueness and existence in regard to $m(y)$ determined from (2). It is easy to show that there are infinitely many different

⁵ All actual records are finite in duration and of bounded variation—these conditions guarantee the existence of the Fourier series.

solutions $a(y)$ to

$$\int_I G_i(y) a(y) dy = 0, \quad i = 1, 2, \dots, N;$$

in fact the annihilator here is infinite-dimensional for any finite collection of $G_i(y)$ whatever. Therefore models constructed from actual measurements can never be unique. Furthermore, if the kernels G_i are linearly independent (as they usually are in practical problems), solutions to (2) always exist.

Experimental error contributes additional indeterminacy to that caused by incompleteness of the data. In the following discussions of various methods, we assume that the statistical errors in e_i can be adequately described by a Gaussian distribution with known parameters. Although this may frequently be a poor approximation, there are two reasons for retaining it: first, the analysis can be carried out exactly under this assumption; second, knowledge of the true statistical distribution in a set of measurements is usually very poor so that an elaborate treatment based on a perfectly general error law seems hardly justified. Here we shall consider only statistically independent data, but there is no great difficulty in generalizing to the case of a joint-normal distribution over the N -data set (Gilbert 1971).

Since the actual solution $m(y)$ cannot be recovered from our measurements, there are in fact two courses open to us: (a) we can derive properties of $m(y)$ that all solutions share, which then must be properties of the true solution; (b) we can introduce assumptions about m to restrict the class of admissible solutions. In our development we begin by following the first course and this leads us naturally to suggestions of what useful yet plausible assumptions might be made.

Backus-Gilbert Formulation

Backus & Gilbert (1968) suggested that a very simple type of model-property be calculated, namely linear functions of m . By taking linear combinations of the data we can compute all functionals of the form

$$l = \int_I F(y)m(y) dy, \quad (3)$$

where l is calculated from the data (assumed error-free for the moment). Thus we have

$$l = \sum_{i=1}^N \alpha_i e_i, \quad (4)$$

and $F(y)$ is given by

$$F(y) = \sum_{i=1}^N \alpha_i G_i(y). \quad (5)$$

The weights α_i are of course entirely arbitrary. If these weights could be chosen so that $F(y)$ approached the Dirac function $\delta(y - y_0)$, the value of l would become $m(y_0)$. This is usually not feasible but Backus & Gilbert showed how to construct

functions $F(y)$ that are concentrated as much as possible on a chosen y_0 and are small elsewhere. One way of doing this is to define a delta-function quality measure such as

$$S[\delta] = 12 \int_I [\delta(y, y_0)(y - y_0)]^2 dy, \quad (6)$$

with $\int_I \delta(y, y_0) dy = 1$.

Here the approximation $\delta(y, y_0)$ is intended to focus upon the position y_0 . The measure S has dimensions of length and is indeed a rough estimator of the width of peak in δ around y_0 ; the smaller S can be made, the more closely $\delta(y, y_0)$ resembles the improper function $\delta(y - y_0)$. We now identify δ with F in (5) and choose α_i so as to minimize S for a particular point y_0 . Then the model property l in (4) gives us a smoothed estimate of the true $m(y_0)$, the degree of smoothing depending on the shape of $\delta(y, y_0)$. Further, we can loosely identify the length S with the averaging width associated with our estimate l of $m(y_0)$; when S is large we obtain only a blurred picture of m at y_0 , whereas small S indicates good resolution. Recall that these averages are universal properties of any solution to (2) and that such averages of any member of the annihilator would always vanish.

It should also be understood that (6) is only one of a variety of ways to define deviation of δ from a delta function. One important reason for choosing this particular definition is that it leads to *linear* equations for the coefficients α_i when the smallest S is sought. It shares this almost essential property with several other definitions of "deltaness," for example,

$$W = 12 \left[\int_I \left[\int_I^y \delta(y', y_0) dy' - H(y - y_0) \right]^2 dy \right]$$

where $H(y)$ is the Heaviside function. A general, unifying theory of the criteria for "deltaness" appears in a rather difficult paper by Backus (1970b). He considered different operations for mapping the linear space of functionals containing distributions into a "smoother" Hilbert space and thereby generated a very wide (but not exhaustive) class of quality measures. Sometimes an appropriate choice of criterion can result in substantial reduction in numerical work; for example, by using the W -measure above, Oldenburg (1976) was able to arrive at equations for α_i that were particularly simple to solve.

Before discussion of the role of experimental error in the Backus-Gilbert formulation, it is worthwhile asking how l is related to the true value of $m(y_0)$. In fact, $m(y_0)$ can be arbitrarily far from l . The only circumstance in which the two numbers will be close is that when the model $m(y)$ is itself smooth in some sense. If we are willing to assume a certain degree of smoothness for all admissible models, we can calculate the greatest deviation between our estimator and the true value. These ideas are made precise by Backus (1970a,b) who gives a very general treatment of the problem. Actually this approach has enjoyed almost no practical application, perhaps because of the difficulty in estimating the numbers that quantify smoothness.

When statistical uncertainty is included, we find that the number l in equation (4) has an error that is easily computed when Gaussian statistics describe the random-

ness in e_i . This error is given by

$$\sigma^2 = \text{var}[l] = \sum \alpha_i^2 \text{var}[e_i], \quad (7)$$

when the e_i are uncorrelated. We should like to make σ^2 in (7) and S in (6) simultaneously as small as possible because they both quantify deficiencies in l as an estimator of $m(y_0)$. Backus & Gilbert (1970) showed how to obtain the best possible values of α_i , but a unique set is not possible: there is a single degree of freedom in the choice, and this leads us to the concept of a trade-off diagram.

Consider the plane defined by the variables σ^2 and S (Figure 1). It is possible to show that, for an arbitrary set of α_i (subject only to the condition $\int \delta dy = 1$), there is a region \mathcal{R} inside of which all associated pairs (S, σ^2) must lie. Clearly, to do the best job we should like to be on the lower-left edge of the region, because then, for a given value of σ^2 , there would be no way to obtain a smaller (i.e. better) value of S . The curve on the lower left side of the region \mathcal{R} is called the *trade-off curve*. Backus & Gilbert proved that decreasing S always increased σ^2 on this part of the boundary of \mathcal{R} , so that improved resolution can only be obtained at the price of degraded statistical reliability. There is no "best" point on the curve. In some applications a poor resolution may be acceptable if good statistical precision is thereby guaranteed: for example, when the solution is very flat, one may be content

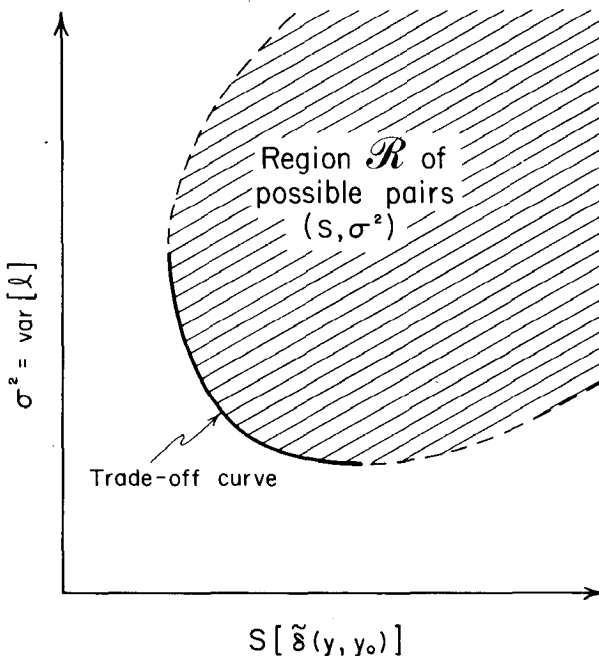


Figure 1 Region of feasible pairs (S, σ^2) shown shaded. The trade-off curve on which the best σ^2 is found for a given S is on the extreme left-lower edge of the region.

to average over a fairly broad interval to obtain precise estimates of the model value, while with rapidly varying solutions one might wish to obtain high resolution, even with relatively poor precision.

The Backus-Gilbert approach is not really a method for finding solutions $m(y)$ to (1); indeed, considered as a function of y_0 , l in (4) does not usually satisfy the original data, even when they are error-free. Rather, it is a technique for assessing the significance of a solution. One may judge whether a particular feature (like a jump or spike) is really resolved by the data (Dorman & Lewis 1972; Hobbs 1973); one can compute how much detail is available in principle from a given distribution of observations. To calculate solutions $m(y)$ [especially when (1) is a linearization of a nonlinear problem] a different method has been found that offers distinct advantages, mainly with regard to numerical stability: this is the spectral expansion method.

A Spectral Expansion

The procedure to be described is a particular formulation of the numerical solution to practical linear inverse problems advocated by many authors (Gilbert 1971; Jackson 1972; Wiggins 1972; Jupp & Vozoff 1975), all of whom based the solution ultimately upon the philosophy of Lanczos (1961). Most workers have dealt with finite-dimensional models because this allows a direct description in terms of matrices and makes possible a limited form of the Backus-Gilbert interpretation of the results. The approach developed here, following Gilbert (1971), is in greater harmony with the cardinal factor distinguishing inverse theory from conventional parameter estimation, namely, that the space of unknowns is infinite-dimensional.

Analytic instability appears as extremely poor conditioning in the matrices encountered in a numerical solution, even if nonuniqueness is evaded by reducing the number of unknowns sought. The spectral expansion explicitly isolates those parts of the solution that are well determined by the data and those that are not; furthermore, the statistically reliable component of m (as derived from the known error estimates in the data) are also those with the highest numerical reliability in actual, finite-accuracy computations. These features of the method make it the most suitable when very large data sets are handled, even though it is up to ten times slower computationally than simple matrix inversion.

We treat noisy data from the beginning: consider (2) weighted by the inverse of the standard error of each measurement (recall that statistically independent e_i are assumed with individual Gaussian error distributions of zero mean and standard error σ_i)

$$\frac{e_i}{\sigma_i} = \int_I \frac{G_i(y)}{\sigma_i} m(y) dy, \quad i = 1, 2 \dots N,$$

which we shall write as

$$e'_i = \int_I G'_i(y)m(y) dy, \quad i = 1, 2 \dots N. \quad (6)$$

Thus e'_i is dimensionless with unit variance. Define the matrix Γ with elements Γ_{ij}

thus:

$$\Gamma_{ij} = \int_I G'_i(y) G'_j(y) dy.$$

Γ is easily shown to be positive-definite and symmetric, so that it may be diagonalized with an orthogonal matrix \mathbf{O} thus:

$$\mathbf{O}^T \boldsymbol{\Gamma} \mathbf{O} = \boldsymbol{\Lambda},$$

where

$$\boldsymbol{\Lambda} = \text{diag } \{\lambda_1, \lambda_2 \dots \lambda_N\},$$

and

$$\lambda_1 \geq \lambda_2 \geq \lambda_3 \geq \dots \lambda_N > 0.$$

Some of the eigenvalues of Γ may be zero if the $G_i(y)$ are linearly dependent, but we shall ignore this case for the moment. The set of eigenvalues will be called the spectrum of the problem defined by (6). This spectrum is not the same as that of the analytic problem (1), since the values λ_i depend critically upon the estimated errors in the data and the distribution of the observations. Now consider the functions $\psi_i(y)$ defined by

$$\psi_i(y) = \lambda_i^{-1/2} \sum_j O_{ji} G'_j(y).$$

It can easily be verified that $\psi_i(y)$ are an orthonormal set, i.e.

$$\int_I \psi_i \psi_j dy = \delta_{ij}.$$

Therefore we may consider an expansion of m in terms of these orthogonal functions

$$m = \sum_{i=1}^N a_i \psi_i + \psi_*, \quad (7)$$

where $\psi_* \in A$ (the annihilator)⁶ and $\int \psi_* \psi_i dy = 0$. The coefficients of this expansion are obviously

$$\begin{aligned} a_i &= \int_I \psi_i m dy \\ &= \lambda_i^{-1/2} \sum_j O_{ji} e'_j \end{aligned} \quad (8)$$

and are common properties of all solutions satisfying the data. It requires a little algebra to show that the standard error of each coefficient a_i is $\lambda_i^{-1/2}$ and that the a_i are statistically independent. Thus the expansion of m is in terms of functions whose coefficients increase in uncertainty; after ψ_N we reach ψ_* , whose uncertainty is total.

⁶ If any zero eigenvalues occur their (associated) functions should be assimilated into ψ_* , not normalized by the factor $\lambda^{-1/2}$.

When analytically unstable problems are treated in this way, it is almost invariably the case that the functions $\psi_i(y)$ become more oscillatory as i increases; i.e. the largest eigenvalues are associated with the smoothest functions. Then the smoothest parts of m are most accurately determined because their coefficients are most precise. However, such behavior is not universal, because examples can be constructed with the opposite pattern,⁷ but these exceptions are so rare in practice that we shall proceed on the assumption that the expansion (7) is in order of decreasing smoothness. What can we say about ψ_* , the part of m quite undetermined by the data? It is possible to verify that this too is an oscillatory function by asking for the smoothest possible member of A : we might define this function to be the one with the least value of $\int (d^2f/dy^2)^2 dy$ and calculate its shape with the usual calculus of variations. No one has ever done this to my knowledge. A geophysical example with relatively smooth members in the annihilator is given by Parker & Huestis (1974), where the annihilator contains all the components that do not average to zero.

Another common property of the spectra obtained in practical problems is the condensation of the eigenvalues towards zero; this means that the spacing between eigenvalues gets smaller as their magnitude decreases. When many of the eigenvalues are small (i.e. a small fraction of λ_1) this indicates a numerically (and physically) very poorly posed problem, since now many of the coefficients exhibit large uncertainties.

Let us now return to (7) and regard it as an expansion in the natural "modes" of the data. Perhaps we should like to "filter out" the noisy components of the series and thus gain some statistical stability in our estimate of m . Clearly we should then discard those functions ψ_i where coefficients exhibit unacceptably large variance; if at the same time this means throwing out high frequency components, our solution will also be a smoothed version of the true m (provided ψ_* is not a smooth function). This is of course exactly analogous to the Backus-Gilbert formulation. The more reliable, truncated version of (7) can be accurately represented as that part of m expandable with the smoother functions ψ_i . We may further say either (a) that the high frequency parts are less interesting, or perhaps (b) that they can be assumed to be of small amplitude anyway.

The precise number of components to be accepted in the expansion is still largely a matter of judgement. One factor that should be taken into account is that the truncated series (7) no longer fits the original data precisely. Because of the random component in e_i , we should not expect or demand exact agreement. If we define χ^2 to be the squared two-norm misfit to the data thus:

$$\chi^2 = \sum_{i=1}^N (\tilde{e}_i - e_i^*)^2,$$

where \tilde{e}_i is the value obtained by substituting the truncated series into the right side of (6), we find after a little algebra that

⁷ For example, consider the set of kernels $G'_n(y) = n \sin \pi ny$, $n = 1, 2, \dots, N$ with $0 \leq y \leq 1$; here we have $\lambda_n = n^2/2$ and $\psi_n(y) = 2^{-1/2} \sin \pi ny$.

$$\chi^2 = \sum_{j=L+1}^N \lambda_j a_j^2;$$

here L terms have been accepted in (7). This equation shows that those coefficients a_i associated with small eigenvalues contribute relatively little to the misfit compared with their contributions to the solution or its uncertainty.

Now χ^2 is the standard statistic, since e'_i has unit variance. It is possible to pick L so as to make χ^2 equal to its expected value; the difficulty here is in selecting the number of degrees of freedom, because the underlying model m has in principle an infinite number of parameters. If one regards the truncated series as the "model," one has $v = N - L$, and L can be picked to make $P(\chi^2) = 0.5$. In fact v so defined is regarded by many (see Richards 1975) to be the number of independent data in the original set: often v is only 10% of N .

Other methods of stabilizing (7) have been suggested; for example one can choose m with the smallest norm, $\|m\|_2$ (here $\sqrt{\sum a_i^2}$), subject to its not exceeding a certain misfit level (Jackson 1973). This has the effect of replacing λ_i by $\lambda_i + C$ in (8), the equation for a_i , where C is a positive constant determined by a nonlinear equation. Evidently this has the same effect of reducing the influence of the functions associated with small eigenvalues. The method of Twomey (1963), which seeks the smoothest model in another sense, has the same sort of properties, as does the method of Franklin (1970).

An Illustration

The following example is based upon a solution to a geophysical inverse problem given by Dorman (1975). The objective is to determine the density structure within the Earth from gravity observations but, as noted earlier, further restrictions of some kind are always required to reduce the large degree of ambiguity in the general problem. Here very strong geometric constraints are imposed: the two-dimensional system (Figure 2) consists of two quarter-spaces, each horizontally layered; gravity anomaly gradients $\partial \Delta g / \partial x$ are measured on the surface $y = 0$. This is a model for a vertical fault with vertical displacement or the figuration that may be encountered across an oceanic fracture zone where two lithospheric plates of different ages meet. Gravity gradients are no longer commonly measured, but this type of data is assumed here for mathematical convenience. The solution to the

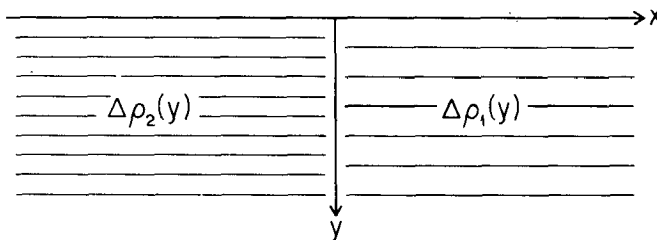


Figure 2 Geometry of gravitational edge effect problem. Each quarter-space is horizontally stratified and they meet along the plane $x = 0$.

forward problem is found to depend only upon the difference in density $\Delta\rho$ between the layers on each side at a given level:

$$\Delta g'(x) = \int_0^\infty \frac{2\mathcal{G}y}{y^2 + x^2} \Delta\rho(y) dy, \quad (9)$$

where \mathcal{G} is Newton's gravitation constant and $\Delta g'$ is written for $\partial\Delta g/\partial x$. Our aim is to recover $\Delta\rho$ from $\Delta g'$.

In order to justify some later steps, it is useful to restrict $\Delta\rho$ to a particular class: $\Delta\rho \in L^1(0, \infty)$. This means that the integral of the magnitude of $\Delta\rho$ is assumed to be bounded. We could reasonably assume also that $\Delta\rho$ itself is everywhere bounded, then $\Delta\rho \in L^2(0, \infty)$ also, but this additional restriction is not particularly valuable in the analysis.

Let us first observe some of the conditions for existence of a solution. From (9) it is obvious that $\Delta g'(x) = \Delta g'(-x)$, i.e. Δg is an even function and this is a necessary condition for existence. Indeed, the approximate symmetry of the measured anomalies over a transform fault is a reason for proposing a model of this kind for that system. Consider now complex values of x ; we must of course keep y real, but (9) allows us to calculate $\Delta g'$ for any x real or complex. It is easy to show that $\Delta g'$ is an analytic function of a complex variable whose only singularities are on the imaginary x axis. This implies that $\Delta g'$ is infinitely differentiable on the real axis (which is accessible to observation!) except possibly at the origin, $x = 0$. The analyticity conditions on $\Delta g'$ are clearly necessary from (9). A little strengthening of these restrictions concerning the decay of $\Delta g'$ at large $|x|$ results in a sufficient condition but the details will not detain us.

Dorman's development proceeds as follows. The Fourier transform of $\Delta g'$ is taken:

$$\begin{aligned} \overline{\Delta g'}(k) &= \int_{-\infty}^{\infty} \Delta g'(x) e^{ikx} dx \\ &= \int_{-\infty}^{\infty} dx e^{ikx} \int_0^\infty \frac{2\mathcal{G}y\Delta\rho(y)}{x^2 + y^2} dy \\ &= \int_0^\infty 2\pi\mathcal{G}\Delta\rho(y) e^{-|k|y} dy \end{aligned} \quad (10)$$

The validity of interchanging the integrations and the existence of the transform follow from Fubini's theorem and the fact that $\Delta\rho \in L^1$. Restricting ourselves to positive k , we note that (10) is simply a Laplace transform so that it may formally be inverted:

$$\Delta\rho(y) = \mathcal{L}^{-1}[\overline{\Delta g'}(k)]/2\pi\mathcal{G}.$$

This is Dorman's solution. Uniqueness of $\Delta\rho$ is a direct consequence of Lerch's lemma which states that two functions with the same Laplace transform are identical up to a set with measure zero. The analytical machinery for finding $\Delta\rho$ from $\Delta g'$ is an integral in the complex k plane on the Bromwich contour. This procedure is of little account practically because of its inherent instability.

This brings us to the question of stability. Rather than appealing to the well-known instability of the inverse Laplace transform, let us deal directly with (9). We construct an example of noncontinuous dependence of $\Delta\rho$ on $\Delta g'$. First we need a distance measure for the space of data and density functions. In the latter case, a natural choice is based upon the one-norm:

$$\|\Delta\rho\|_1 = \int_0^\infty |\Delta\rho(y)| dy;$$

this is because $\Delta\rho \in L^1(0, \infty)$ and therefore all $\Delta\rho$'s of interest possess bounded one-norms. We shall use a one-norm on the space of analytic functions containing $\Delta g'$ just for symmetry. Now a density function $\delta\rho \in L^1$ must be found for which the corresponding $\|\Delta g'\|_1$ can be made as small as desired, while $\|\delta\rho\|_1$ remains bounded away from zero. The smoothing action of the kernel in (9) suggests that an oscillating function might be suitable, and after some experimentation I discovered the function

$$\delta\rho(y) = \frac{\rho_0 a^2 \sin \mu y}{(a^2 + y^2)}$$

with $\rho_0, a, \mu > 0$. Since $|\sin \mu y| \geq \sin^2 \mu y$, it is easily shown that

$$\|\delta\rho\|_1 \geq \pi \rho_0 a (1 - e^{-2\mu a})/4.$$

The form of $\delta\rho$ makes it easy to find $\Delta g'$ from (9) with the calculus of residues: the expression is not important, only the fact that $0 \leq g'(x)$ for all x . Obviously then we have

$$\begin{aligned} \|\Delta g'\|_1 &= \int_0^\infty \Delta g'(x) dx \\ &= \pi \mathcal{G} \int_0^\infty \delta\rho(y) dy; \end{aligned}$$

this last result comes from (10) with $k = 0$. Thus we have

$$\|\Delta g'\|_1 = \pi \mathcal{G} \rho_0 a^2 \int_0^\infty \frac{\sin \mu y}{a^2 + y^2} dy.$$

By the Riemann-Lebesgue theorem, $\|\Delta g'\|_1$ can be made as small as we please by choosing a large enough μ , but from the earlier inequality, $\|\delta\rho\|_1$ does not decrease below some fixed value. Because of the linearity of the problem, this $\delta\rho$ perturbation can be added to any other $\Delta\rho$, and it will be seen that arbitrarily close functions $\Delta g'$ are associated with functions $\Delta\rho$ that never come closer together than some fixed separation. The same test function also serves to demonstrate instability with the two-norm or the uniform norm.

One final analytic point I cannot resist including is the equivalence of (9) to the equation of Weertman (1965) which relates fault displacement to surface strain in a simple system. Weertman found a different way of constructing solutions. His results show that, if $\Delta g'$ is regarded as the real-axis realization of a complex function of

complex x , the corresponding density is simply

$$\Delta\rho(y) = -\text{Im } \Delta g'(iy)/\pi G,$$

that is, $\Delta\rho$ can be obtained by analytic continuation of $\Delta g'$ onto the imaginary x axis. Analytic continuation in the complex plane can be cast into a form that requires the solution of Laplace's equation with over-determined boundary conditions, the unstable problem that Hadamard (1902) first used to illustrate the concept.

We come now to a demonstration of the spectral expansion method. Gravity gradients were computed for a density difference model of 100 kg m^{-3} between 5 and 15 km, zero elsewhere; then zero-mean, normally distributed random errors were added to the 20 exact values. The values are plotted in Figure 3. Note that gradients have been provided on only one side of the density interface; this avoids certain difficulties of exact linear dependence in the Backus-Gilbert analysis, and it would be natural with real observations to average the two half-profiles together to get the best estimate of the symmetric function. The range of these "observations" is from 0 – $15 \mu\text{m s}^{-2} \text{ km}^{-1}$, and the standard error of the noise is $0.1 \mu\text{m s}^{-2} \text{ km}^{-1}$ (there appears to be no definitive statement about gravity units in the SI system; therefore I have picked these. Note $1 \mu\text{m s}^{-2} \text{ km}^{-1} \equiv 0.1 \text{ mgal km}^{-1}$). The scaled data and their kernels are calculated next in order to find the orthogonal kernels, ψ_i . The matrix Γ is easily shown to be

$$\Gamma_{ij} = 2\pi G^2/(x_i + x_j)\sigma^2,$$

where x_i is the coordinate of the i th measurement and σ^2 the variance of each datum. The eigenvalues of Γ cover an enormous range, as can be seen from Table 1; the number of very small values indicates the very poor conditioning of the matrix. Some of the corresponding orthogonal functions are shown in Figure 4 where the standard pattern, increasingly oscillatory functions with decreasing eigenvalue, is

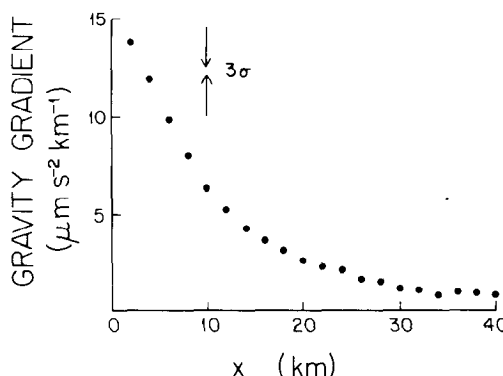


Figure 3 Artificial data values used in numerical examples. There are twenty gravity gradients computed at 2 km intervals from $x = 0$; the value at $x = 0$ is not included because the associated data kernel is singular.

Table 1 Selected values of parameters derived in the numerical solution of the gravitational edge-effect problem: λ_i stands for eigenvalues of matrix Γ ; a_i , spectral expansion coefficient in (7); $\lambda_i^{-1/2}$, standard error of a_i ; $\chi^2(i)$, normalized squared misfit of expansion when all terms up to and including the i th have been summed in (7).

i	λ_i ($\text{m}^6 \text{ kg}^{-2} \text{ km}^{-1}$)	a_i ($\text{kg m}^{-3} \text{ km}^{1/2}$)	$\lambda_i^{-1/2}$ ($\text{kg m}^{-3} \text{ km}^{1/2}$)	$\chi^2(i)$
1	2.090	166.7	0.692	4441.0
2	0.3721	89.3	1.64	1474.0
3	4.683×10^{-2}	-175.1	4.62	37.8
4	4.855×10^{-3}	-63.1	14.3	18.5
5	4.253×10^{-4}	47.1	48.5	17.6
6	3.179×10^{-5}	302.0	177.4	14.6
7	2.037×10^{-6}	491.0	700.7	14.2
8	1.122×10^{-7}	-4186.0	2986.0	12.2
9	5.312×10^{-9}	-1022.0	13720.0	12.2
10	2.158×10^{-10}	36972.0	68075.0	11.9
20	1.930×10^{-29}	2.976×10^{14}	2.276×10^{14}	0

evident. In Table 1 the column headed $\chi^2(i)$ gives the value of the misfit when all terms in (7) up to i have been included. Since there are 20 data, a value of about 20 is to be expected, a smaller value indicating over-fitting. Thus an expansion with only four functions would seem appropriate; we are led to the same conclusion by examining $\lambda_i^{-1/2}$, the errors in the coefficients, since after $i = 4$ there is a rapid deterioration in the accuracy of a_i . Figure 5 shows the result of taking four terms in (7).

If we had ignored the problems of error and instability and tried to fit the data exactly (recall there are infinitely many such solutions), we would find that the rather small errors in the data are magnified grotesquely in the solution. For example the $\Delta\rho$ with the smallest two-norm is found by summing (7) all the way up to N : this yields a density contrast function with oscillations exceeding $\pm 5 \times 10^{14} \text{ kg m}^{-3}$ and because that solution minimizes $\|\Delta\rho\|_2$ it represents one of the smallest possible functions that fits the data precisely.

The Backus-Gilbert analysis tells the same story as the spectral expansion. Ignoring the noise in the data, I constructed two delta-function approximations, one for a depth of 15 km, the other for 50 km (Figure 6). There is a little trouble with (6) over the infinite interval, because the integral is divergent for general linear contributions of G_i . This can be remedied in several ways, some more elegant (Backus 1970b) than others; I chose the crudest device of restricting the depth to 100 km, equivalent to the assumption that there are no density variations below that level. As can be seen from the figures, the distribution of observations is capable in principle of resolving rather fine details around 15 km, and the resolution is not too bad even at 50 km. However, when the standard error of the linear estimate is calculated we find that it exceeds $10^{12} \text{ kg m}^{-3}$ for both cases. Clearly it is desirable to sacrifice resolving ability for improved statistical properties. Figure 7

is the trade-off diagram for the two depths. This shows that to obtain a standard error of $\pm 20 \text{ kg m}^{-3}$ (recall from Figure 5 typical values are around 50 kg m^{-3} at 15 km) we need a resolving width of about 11 km, which is perhaps geophysically interesting. The curve for $y_0 = 50 \text{ km}$ leads to the discouraging conclusion that little useful information is contained in the data about densities so deep in the Earth.

ANALYSIS OF EXPERIMENTAL DATA: NONLINEAR PROBLEMS

Linearization and the Fréchet Derivative

Many of the most important geophysical problems are nonlinear, which means that the solution to the forward problem cannot be expressed with linear functionals

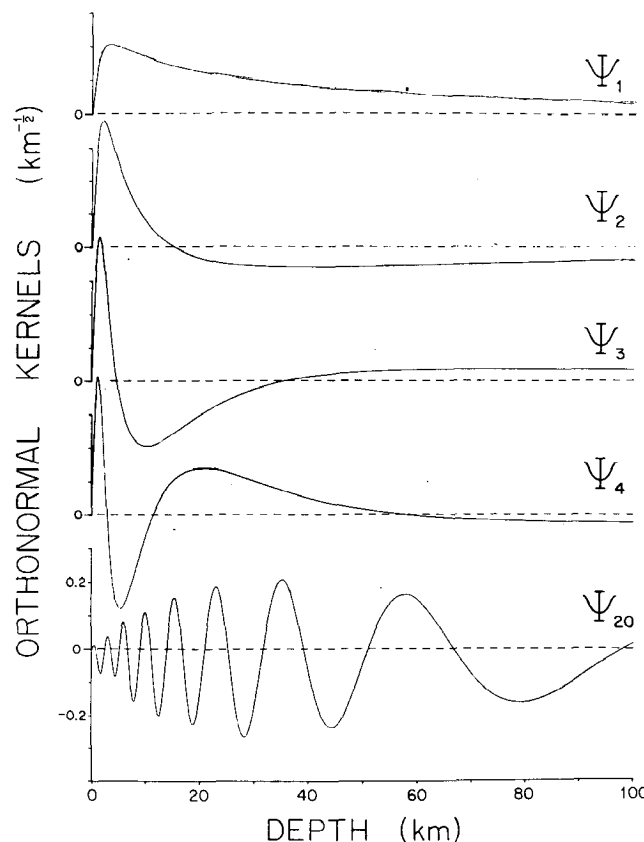


Figure 4 Orthonormal kernels found by diagonalization of Γ . The function ψ_i exhibits i zero-crossings (counting the one at $y = 0$). Thus ψ_{20} has three more zero-crossings than are shown in the figure, all deeper than 100 km.

over the model space. However, the powerful tools of linear theory are so attractive that geophysicists are often willing to make approximations allowing their use. One difficulty is that of establishing the validity of the approximation; cautionary comments (e.g. Anderssen 1975) and examples of the failure of linearization (Wiggins

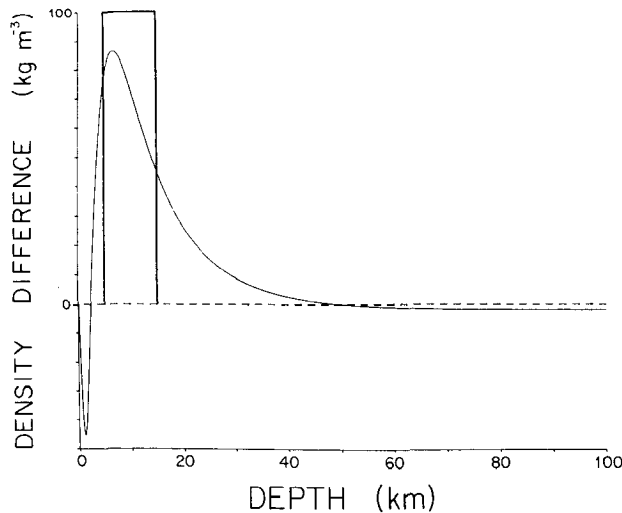


Figure 5 Original density function (box-car) and solution derived from four orthonormal kernels (smooth curve).

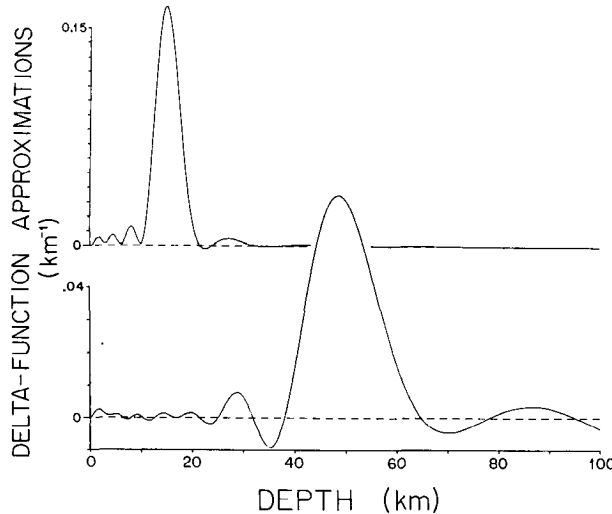


Figure 6 Best delta-function approximations according to the *S*-criterion for target depths of 15 km and 50 km.

et al 1973, Sabatier 1974) have appeared in the literature warning of the misleading results that can sometimes occur. In some cases, unfortunately, there appears to be no satisfactory alternative for the construction of a solution from real observations or assessment of its significance.

The approximation to which we have been alluding is *linearization*. Suppose the *i*th observation e_i is related to the model via a (nonlinear) functional F_i , formally:

$$e_i = F_i[m] \quad i = 1, 2, \dots, N. \quad (11)$$

This deceptively simple equation may hide such complex calculations as the solution of many coupled, ordinary differential equations, as in the case of the inverse problem for the mechanical structure of the Earth from free oscillation data (Backus & Gilbert 1967); it represents the fact that the forward problem is completely solved and that when a particular m is given we can, somehow, find all the appropriate data associated with it. Next, consider a second model $m + \delta m$

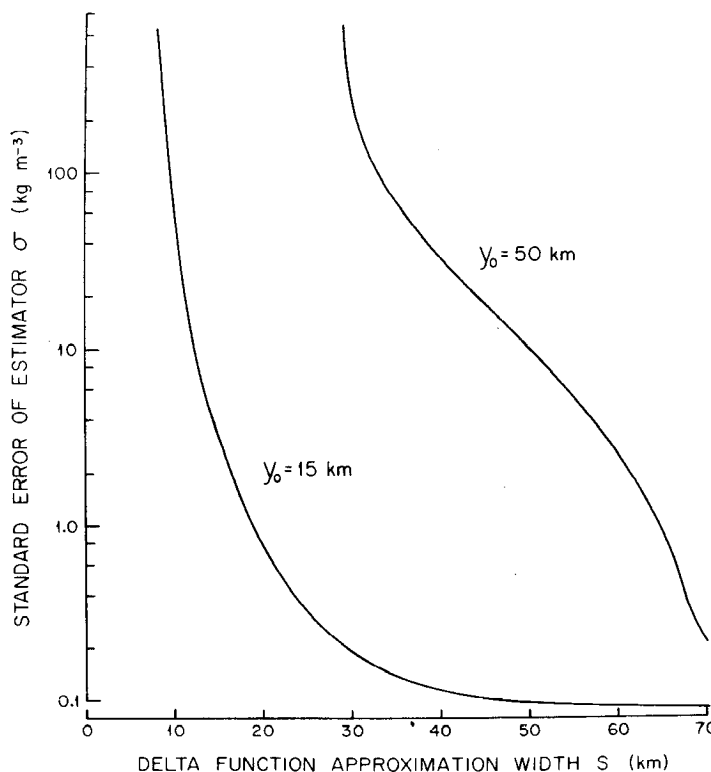


Figure 7 Part of the trade-off curves of standard error σ , and resolution width S according to the S -criterion for target depths of 15 km and 50 km. The complete diagram extends to $10^{14} \text{ kg m}^{-3}$ in σ and 200 km in S but such extreme values are meaningless.

close⁸ to m and with associated data $e_i + \delta e_i$. To find the new data we might solve a perturbation problem, since m is in a certain sense small; it will be assumed that the solution of this perturbation problem can be written

$$\delta e_i = \int_I D_i(m; y) \delta m(y) dy + O \int_I [\delta m(y)]^2 dy \quad (12)$$

(once more, a simple single-parameter, one-dimensional problem has been chosen for simplicity). Then F_i is said to be *Fréchet differentiable* at m and the function D_i is the *Fréchet derivative* of F_i at m . Another name for D_i , sometimes used in the applied mathematical literature, is the “sensitivity function.” Equation (12) can be compared with the more familiar expression obtained when there are a finite number of parameters, μ_j , governing e_i :

$$\delta e_i = \sum_j \frac{\partial F_i}{\partial \mu_j} \delta \mu_j + O \left(\sum_j \delta \mu_j^2 \right). \quad (13)$$

This reveals a correspondence between the partial derivatives $\partial F_i / \partial \mu_j$ and the Fréchet derivative $D_i(m; y)$ if the parameter μ_j is the value of the model m in the j th layer.

Quite surprisingly, perhaps, the solution to perturbations of almost all forward problems in geophysics can be written as (12), and therefore these problems are Fréchet differentiable. One way of arriving at a perturbed solution in the required form is of course through standard perturbation analysis (e.g. Parker 1970 or Johnson & Gilbert 1972); another powerful technique particularly useful in certain seismic problems utilizes the variational formulation of the equations (e.g. Backus & Gilbert 1967 or Gilbert 1976), but there is insufficient space here to deal with these ideas as they deserve.

Having obtained (12) we can see that, if the term $O \int \delta m^2 dy$ is dropped, it is identical with (2), where $D_i(m; y)$ plays the role of $G_i(y)$. Thus we treat the system as if it were locally linear. Using (12) and the spectral expansion method we could attempt to discover the perturbation δm that would bring an initial guess model into satisfactory agreement with the real observations. If the guess solution and a satisfactory one are not sufficiently close, the neglected term in (12) may not be truly negligible and the new solution will not be satisfactory when substituted into the full nonlinear equation (11). Then the process should be repeated, linearizing about the most recent estimate of m , until improvement ceases or a satisfactory solution is obtained. There is of course no guarantee that this procedure will work at all: it may be that no solution exists matching the observations to an adequate degree, and then it is obvious that the iterative process must fail (recall, however, that in a *linear* problem there are always an infinite number of “good” models, each fitting the observations arbitrarily well, provided the $G_i(y)$ are linearly independent); the other alternative is that, even though satisfactory solutions exist, the initial guess is so far from any of them that divergence ensues. The reader will perhaps recognize this iterative procedure as analogous to Newton’s solution of nonlinear equations in several unknowns (Ortega & Rheinboldt 1970).

⁸ See footnote 2.

Consider now the situation in which a satisfactory solution has been arrived at; to assess its significance one can simply apply the Backus-Gilbert method to the problem linearized about the best-fitting solution, in the hope that the neglected nonlinear terms do not make an important contribution. One serious problem is that there might be several satisfactory solutions widely separated in the model space, but the linearization affords approximate description of the neighborhood of only one of them. Nothing can be done about this except to attempt a more exhaustive search of the model space for other possible solutions.

There is one final remark I wish to make concerning the use of the Fréchet derivative (12) rather than the corresponding approximate representation (13). Some authors prefer to parameterize their models through layers or cells so that (13) seems a very natural way to express the solution to the perturbation problem. It is apparently not well appreciated that the Fréchet derivative D_i is often far easier to find both algebraically and computationally than the corresponding partial differential coefficients. Even if a finite representation is chosen, there are still great advantages to finding $\partial F_i / \partial \mu_j$ from D_i . A case in point is the following: consider the inverse problem of discovering the shape of crystalline basement that is everywhere buried under sediments. The data are the gravity anomalies caused by the (known) density contrast between the two materials, $\Delta\rho$. If we let $h(\mathbf{x})$ be the depth at a horizontal position $\mathbf{x} = (x, y)$, then the solution to the forward problem is

$$\Delta g(\mathbf{x}_i) = \int_S \frac{\mathcal{G}\Delta\rho \, dS}{[|\mathbf{x}_i - \mathbf{x}|^2 + h(\mathbf{x})^2]^{1/2}}, \quad i = 1, 2, \dots, N,$$

where $\Delta g(\mathbf{x}_i)$ is the anomaly observer at \mathbf{x}_i on a horizontal level and \mathcal{G} is Newton's gravitational constant. Clearly this is a nonlinear problem for h . It is easy to show that

$$D_i(h; \mathbf{x}) = -\frac{\mathcal{G}\Delta\rho h(\mathbf{x})}{[|\mathbf{x}_i - \mathbf{x}|^2 + h(\mathbf{x})^2]^{3/2}}, \quad i = 1, 2, \dots, N$$

and that these Fréchet derivatives exist for all h with $h(\mathbf{x}) > 0$ for all $\mathbf{x} \in S$. In contrast, the formula for $\partial \Delta g(\mathbf{x}_i) / \partial h_j$, when the plane is divided into square cells and h is then forced to be constant within each cell, apparently extends over many lines (Burkhard & Jackson 1976). It would be very simple to derive an approximation for $\partial \Delta g(\mathbf{x}_i) / \partial h_j$ by rough numerical quadrature of D_i .

Fully Nonlinear Treatment

Linearization is very successful at discovering an acceptable solution to a nonlinear inverse problem, but a finite number of data do not specify a unique solution (except in certain pathological cases). It is not enough to possess one adequate solution, because, in order to draw valid conclusions about the Earth, we need in principle to consider every possible solution, not just one of them. Linearization provides only a partial answer to this question by giving an approximate description of the neighborhood near the preferred model. The difficulty of describing the complete class of viable solutions makes it convenient to consider a simpler problem whose solution is geophysically just as important: the derivation of properties that

all solutions have in common. The Backus-Gilbert local averages are an example of a shared property in the linear case. The properties that seem to be most amenable to mathematical analysis in nonlinear systems are upper and lower bounds of various parameters, and these are extremely important geophysical quantities. In the next few paragraphs we discuss three different approaches to the practical calculation of the limits placed by the data on geophysical models.

The method of widest applicability is Monte Carlo modelling (Keilis-Borok & Yanovskaja 1967; Anderssen et al 1972). The principle is simple; one parameterizes the model space with a large but finite number of unknowns and then generates a sequence of structures at random, testing each one against the observations. While most structures will fail the test, some will pass and these form a family of solutions whose common properties are chosen to represent those of the complete class. Normally the structures investigated are profiles of a single parameter, e.g. seismic velocity or density as a function of depth; the property invariably investigated is the "corridor" of upper and lower limits varying with depth within which all solutions are hypothesized to lie. There is unfortunately an objection to the use of a corridor that is seldom mentioned. Consider for example a layer 1 mm thick with density 10^6 kg m^{-3} ; should such a layer exist within the Earth it would be undetectable by seismic or gravimetric means because it is so thin. Therefore the addition of such a layer to an acceptable solution would not upset agreement with the observations. Since the layer could be placed at any depth, the upper bound in density cannot be lower than 10^6 kg m^{-3} anywhere, a geophysically uninformative value. There are of course ways of eliminating improbable extreme cases like this. One way is suggested by the Backus-Gilbert trade-off diagram: the corridor is defined to concern the average value of density in a succession of layers with specified thicknesses. Alternatively, gradients larger than a certain amount can be rejected a priori as "geophysically unreasonable." Whatever method is chosen, the fact remains that the corridor is sensitive to additional information not present in the original observations. Practical applications of the Monte Carlo approach usually impose other restrictions as well, such as an a priori corridor of reasonable maximum and minimum parameter values; these assumptions are made to reduce the Herculean effort of conducting a complete search, since they decrease the size of the parameter space. The possibly strong dependence on seemingly unimportant computational details must be kept in mind when one wishes to interpret the results of these studies.

The method has been applied notably to seismic problems, for example the determination of the interior mechanical structure using the dispersion of surface waves (e.g. Jackson 1973, who uses a refinement based upon local linearization to ease the computational labor) or from the frequencies of free oscillation of the Earth (e.g. Press 1968), but the great number and precision of recent observations precludes any further direct application in the latter problem.

The next nonlinear treatment is in some respects the antithesis of the Monte Carlo method: it is an elegant treatment of a specific problem and is based on an analytic construction algorithm. The problem is that of inverting travel-time distance data for seismic velocity, and the underlying analysis is of course the

Herglotz-Wiechert solution discussed earlier. There are different variations (McMechan & Wiggins 1972; Bessonova et al 1974) depending upon what type of data are assumed (array studies can give direct estimates of $dT/d\Delta$, for example), but the objective is again to discover a corridor within which all permissible velocities must fall. The principle of the method is to use the Herglotz-Wiechert formula (in spherical or flat-Earth form) to give the greatest or least depths at which a specified velocity can occur. Considerable complications ensue when the possibility of low-velocity zones is permitted, but only then is the method useful practically, for such layers are commonly encountered in crustal and upper mantle studies. When the velocity decreases (or fails to increase rapidly enough with depth in the sphere), a unique solution no longer is possible even with perfect data. To cope with this difficulty a limit is placed a priori on the permissible magnitude of any velocity reversals, which has the gratifying effect of automatically eliminating troublesome thin layers with high velocities. The size of the bound can be fairly well estimated from a knowledge of the materials likely to be encountered. Unlike Monte Carlo searching the method is cheap computationally, so that different assumed values can be tried if necessary. Clear comparative reviews of this extremal technique and the corresponding linearization have been given by Wiggins et al (1973) and Kennett (1976).

The last approach is one I have personally been working on for several years, and I believe it is the one with the greatest potential. The principle is to choose a scalar property of the model and then to maximize or minimize its value subject to the constraints that the solution fit the data and that any other necessary restrictions be taken into account. If we return briefly to a linear inverse problem and choose a *linear* functional of the model, we discover that there is no upper or lower limit to this value of the functional unless it happens to be made up of a linear combination of data kernels (leading to Backus-Gilbert theory). But when a nonlinear functional of m is used, bounds can often be discovered. This remark suggests that property extremization is a process that must contain some nonlinear element to succeed. The most satisfying application of the method so far has been to the inverse problem of determining the shape of a buried body of known density from the gravity anomalies it produces, a nonlinear problem mentioned several times already. My solution (Parker 1975) depends upon discovering the body with the smallest possible maximum density fitting the observations, which is a nonlinear functional of the model in a linear problem. An additional constraint is frequently needed, namely, the density contrast should be positive. It turns out that the body of least density is uniform and its shape is unique, i.e. there is only one body with that density fitting the data.⁹ These two properties enable us to find restrictions on the shape of a uniform body if we now assume the density is known but the shape is not. For example, one can give a level, above which any buried uniform body with the specified density must protrude or another level which it must penetrate from above. Similarly, constraints on lateral extent can be obtained. Very

⁹ Here is an example of an inverse problem where a finite number of data are compatible with only one solution, but of course this happens only when the buried body has a very special shape and the density is a very special value.

recently, Sabatier (1976) has shown that my approach, which seemed very specific to this one problem, is in fact an example of a problem that can be dealt with by means of convex analysis and linear programming theory.

The foregoing theory centered upon finding the minimum of a nonlinear functional in a linear forward problem. In principle there is no reason why nonlinear forward problems cannot be treated directly, as I have shown (Parker 1972). Now the Fréchet derivatives D_i enter in place of the linear kernels G_i ; when this happened during linearization an approximation was involved, but here none is made. Unfortunately, as with nearly all nonlinear analysis, the resultant equations are difficult to solve even numerically and it is often almost impossible to show rigorously that a global extremum has been found, not merely a local one. Both of these troubles diminish if only a very small number of observations are available.

The place where parameter extremization may make the greatest impact in future is in the testing of hypotheses. Often a physical model of a geological system is arrived at by extrapolation or the synthesis of circumstantial evidence; sometimes (but not as often as one would wish perhaps) the model can be tested against geophysical data. Naturally the test cannot prove the correctness of the model, but it may be able to reject it or choose between two competing hypotheses. One powerful way of making a test is to use the physical model to predict, say, a lower limit on a property such as the mean seismic velocity in a certain depth range or the maximum value of S -wave attenuation. Then the solution to the appropriate inverse problem is found to maximize the chosen parameter; if the greatest value is smaller than that predicted, the model must be rejected; if it is within the predicted range there is no conflict with the geophysical data.

A recent unusual example of this approach has been given by Gubbins (1975), who, using the spherical harmonics of the geomagnetic field, derives a lower limit on the energy requirements of the geomagnetic dynamo to test a mechanism invoking earthquakes to maintain the field. He then compares this with the available energy. Unfortunately the test was inconclusive because of the uncertainty in that figure, but a stronger test involving gravity anomalies (but not using parameter extremization) was more decisive in ruling against the model.

Another ingenious application is that of Jordan (1975): he uses the observed travel-time differences of shear waves between continent and ocean and the Love wave dispersion data over corresponding pure oceanic and continental paths to argue for continental influences as deep as 400 km into the mantle. In this case the parameter minimized is the depth to which velocity differences are permitted between the two regimes. Jordan finds that with limits on only two data (the mean travel time difference in the heterogeneous region and the difference in Love wave dispersion at about 180 s) the smallest allowed layer thickness is 310 km. Additional data force even larger values.

CONCLUSIONS

Indirect measurements will continue to be the major source of information about the Earth's deep interior and about much shallower regions also. The problem of

providing some model consistent with the data has for practical purposes been solved by the use of the spectral expansion (or its finite-dimensional equivalents) and linearization if the equations are nonlinear. However, most geophysicists are now conscious of their obligation to assess the range covered by all satisfactory solutions. In the linear case the elegant concept of resolution and its inverse relation with statistical error has made the Backus-Gilbert analysis a most appealing treatment. With nonlinear equations the two general techniques, linearization and the Monte Carlo search, suffer from drawbacks that, to me at least, make them somewhat unattractive.

One of the most promising alternative strategies is to use the data directly to test a hypothesis. This requires the construction of only one solution, the one violating the hypothesis the least, yet still satisfying the demands of observation. As yet few geophysicists have tried the idea, but it offers a means of bypassing the difficult problem of completely characterizing an infinite set of models.

Literature Cited

- Anderssen, R. S., Worthington, M. H., Cleary, J. R. 1972. Density modelling by Monte Carlo inversion—I Methodology. *Geophys. J. R. Astron. Soc.* 29: 433–44
- Anderssen, R. S. 1975. On the inversion of global electromagnetic induction data. *Phys. Earth Planet. Inter.* 10: 292–98
- Backus, G. E. 1968. Application of a nonlinear boundary-value problem for Laplace's equation to gravity and geomagnetic intensity surveys. *Q. J. Mech. Appl. Math.* 21: 195–221
- Backus, G. E. 1970. Non-uniqueness of the external geomagnetic field determined by surface intensity measurements. *J. Geophys. Res.* 75: 6339–341
- Backus, G. E. 1970a. Interference from inadequate and inaccurate data, I. *Proc. Nat. Acad. Sci. USA* 65: 1–7
- Backus, G. E. 1970b. Interference from inadequate and inaccurate data, II. *Proc. Nat. Acad. Sci. USA* 65: 281–87
- Backus, G. E., Gilbert, F. 1967. Numerical application of a formalism for geophysical inverse problems. *Geophys. J. R. Astron. Soc.* 13: 247–76
- Backus, G. E., Gilbert, F. 1968. The resolving power of gross Earth data. *Geophys. J. R. Astron. Soc.* 16: 169–205
- Backus, G. E., Gilbert, F. 1970. Uniqueness in the inversion of inaccurate gross Earth data. *Phil. Trans. R. Soc. London Ser. A* 266: 123–92
- Bailey, R. C. 1970. Inversion of the geomagnetic induction problem. *Proc. R. Soc. London* 315: 185–94
- Bailey, R. C. 1973. Global geomagnetic sounding—methods and results. *Phys. Earth Planet. Inter.* 7: 234–44
- Barcilon, V. 1976. A discrete model of the inverse Love wave problem. *Geophys. J. R. Astron. Soc.* 44: 61–76
- Bard, Y. 1974. *Nonlinear Parameter Estimation*. New York: Academic. 341 pp.
- Bessonova, E. N., Fishman, V. M., Ryaboyi, V. Z., Sitnikova, G. A. 1974. The tau method for the inversion of travel times—I Deep seismic sounding data. *Geophys. J. R. Astron. Soc.* 36: 377–98
- Bullard, E. C., Cooper, R. I. B. 1948. The determination of the masses necessary to produce a given gravitational field. *Proc. R. Soc. London A* 194: 332–47
- Bullen, K. E. 1965. *An Introduction to the Theory of Seismology*. Cambridge Univ. Press. 381 pp.
- Burkhard, N., Jackson, D. D. 1976. Application of stabilized linear inverse theory to gravity data. *J. Geophys. Res.* 81: 1513–32
- Cagniard, L. 1953. Basic theory of the magneto-telluric method of geophysical prospecting. *Geophysics* 18: 605–35
- Cain, J. C. 1971. Geomagnetic models from satellite surveys. *Rev. Geophys. Space Phys.* 9: 259–73
- Dorman, L. M. 1975. The gravitational edge effect. *J. Geophys. Res.* 80: 2949–50
- Dorman, L. M., Lewis, B. T. R. 1972. Experimental isostasy (3). *J. Geophys. Res.* 77: 3068–77
- Franklin, J. N. 1970. Well-posed stochastic extension of ill-posed problems. *J. Math. Anal. Appl.* 31: 682–716
- Gel'fand, I. M., Levitan, R. M. 1955. On the determination of a differential equation

- by its spectral function. *Am. Math. Soc. Transl. Ser. 2*, 1: 253–304.
- Gerver, M., Markusevitch, V. 1966. Determination of seismic wave velocity from the travel-time curve. *Geophys. J. R. Astron. Soc.* 11: 165–73.
- Gilbert, F. 1971. Ranking and winnowing gross Earth data for inversion and resolution. *Geophys. J. R. Astron. Soc.* 23: 125–28.
- Gilbert, F. 1976. Differential kernels for group velocity. *Geophys. J. R. Astron. Soc.* 44: 649–60.
- Gilbert, F., Dziewonski, A. M. 1975. An application of normal mode theory to the retrieval of structural parameters and source mechanisms from seismic spectra. *Phil. Trans. R. Soc. London A* 278: 187–269.
- Gubbins, D. 1975. Can the Earth's magnetic field be sustained by core oscillations? *Geophys. Res. Lett.* 2: 409–12.
- Hadamard, J. 1902. Sur les problèmes aux dérivées partielles et leur significations physiques. *Bull. Univ. Princeton* 13: 1–20.
- Hobbs, B. A. 1973. The inverse problem of the moon's electrical conductivity. *Earth Planet. Sci. Lett.* 17: 380–84.
- Jackson, D. D. 1972. Interpretation of inaccurate, insufficient and inconsistent data. *Geophys. J. R. Astron. Soc.* 28: 97–110.
- Jackson, D. D. 1973. Marginal solutions of quasi-linear inverse problems in geophysics: the edgehog method. *Geophys. J. R. Astron. Soc.* 35: 121–36.
- Johnson, L. E., Gilbert, F. 1972. Inversion and inference for teleseismic ray data. *Methods of Computational Physics*, 12: 231–66. New York: Academic.
- Jordan, T. H. 1975. The continental tectosphere. *Rev. Geophys. Space Phys.* 13: 1–12.
- Jupp, D., Vozoff, K. 1975. Stable iterative methods for the inversion of geophysical data. *Geophys. J. R. Astron. Soc.* 42: 957–76.
- Keilis-Borok, V. I., Yanovskaja, T. B. 1967. Inverse problems of seismology (structural review). *Geophys. J. R. Astron. Soc.* 13: 223–34.
- Kennett, B. L. N. 1976. A comparison of travel-time inversions. *Geophys. J. R. Astron. Soc.* 44: 517–36.
- Lanczos, C. 1961. *Linear Differential Operators*. London: van Nostrand. 564 pp.
- Lavrentiev, M. M. 1967. *Some Improperly Posed Problems of Mathematical Physics*. Heidelberg: Springer. 72 pp.
- McKenzie, D., Parker, R. L. 1974. Plate tectonics in ω -space. *Earth Planet. Sci. Lett.* 22: 285–93.
- McMechan, G. A., Wiggins, R. A. 1972. Depth limits in body wave inversions. *Geophys. J. R. Astron. Soc.* 36: 239–43.
- Oldenburg, D. W. 1976. Calculations of Fourier transforms by the Backus-Gilbert method. *Geophys. J. R. Astron. Soc.* 44: 413–31.
- Ortega, J. M., Rheinboldt, W. C. 1970. *Iterative Solution of Nonlinear Equations in Several Variables*. New York: Academic. 572 pp.
- Parker, R. L. 1970. The inverse problem of electrical conductivity in the mantle. *Geophys. J. R. Astron. Soc.* 22: 121–38.
- Parker, R. L. 1972. Inverse theory with grossly inadequate data. *Geophys. J. R. Astron. Soc.* 29: 123–38.
- Parker, R. L. 1975. The theory of ideal bodies for gravity interpretation. *Geophys. J. R. Astron. Soc.* 42: 315–34.
- Parker, R. L., Huestis, S. P. 1974. The inversion of magnetic anomalies in the presence of topography. *J. Geophys. Res.* 79: 1587–93.
- Press, F. 1968. Earth models obtained by Monte Carlo inversion. *J. Geophys. Res.* 73: 5223–34.
- Rao, C. R. 1973. *Linear Statistical Inference and its Applications*. New York: Wiley. 625 pp.
- Richards, P. G. 1975. Theoretical seismology. *Rev. Geophys. Space Phys.* 13: 295–98.
- Sabatier, P. C. 1971. Comparative evolution of inverse problems. *NASA Tech. Memo. X-62, 150*.
- Sabatier, P. C. 1974. Remarks on approximate methods in geophysical inverse problems. *Proc. R. Soc. London A* 337: 49–71.
- Sabatier, P. C. 1976. Positivity constraints in linear inverse problems. *Geophys. J. R. Astron. Soc.* In press.
- Siebert, M. 1964. Ein Verfahren zur unmittelbaren Bestimmung der vertikalen Leitfähigkeitsverteilung im Rahmen der Erdmagnetischen Tiefenonderung. *Nachr. Akad. Wiss. Göttingen Math. Phys. Kl. 2*.
- Smith, R. A. 1961. A uniqueness theorem concerning gravity fields. *Proc. Cambridge Phil. Soc.* 57: 865–70.
- Stern, D. P., Bredekamp, J. H. 1975. Error enhancement in geomagnetic models derived from scalar data. *J. Geophys. Res.* 80: 1776–82.
- Twomey, S. 1963. On the numerical solution of Fredholm integral equations of the first kind by the inversion of the linear system produced by quadrature. *J. Assoc. Comput. Mach.* 10: 97–101.

- Weidelt, P. 1972. The inverse problem of geomagnetic induction. *Z. Geophys.* 38: 257–89
- Weertman, J. 1965. Relationship between displacements on a free surface and the stress on a fault. *Bull. Seismol. Soc. Am.* 55: 945–53
- Weston, V. H. 1972. On the inverse problem for a hyperbolic dispersive partial differential equation. *J. Math. Phys.* 12: 1952–56
- Wiggins, R. A. 1972. The general linear inverse problem: implication of surface waves and free oscillations for Earth structure. *Rev. Geophys. Space Phys.* 10: 251–85
- Wiggins, R. A., McMechan, G. A., Toksöz, M. N. 1973. Range of Earth-structure non-uniqueness implied by body wave observations. *Rev. Geophys. Space Phys.* 11: 87–113

CONTENTS

AMERICAN GEOLOGY SINCE 1910—A PERSONAL APPRAISAL, <i>James Gilluly</i>	1
BIOSTRATIGRAPHY OF THE CAMBRIAN SYSTEM—A PROGRESS REPORT, <i>Allison R. Palmer</i>	13
UNDERSTANDING INVERSE THEORY, <i>Robert L. Parker</i>	35
A REVIEW OF HYDROGEN, CARBON, NITROGEN, OXYGEN, SULPHUR, AND CHLORINE STABLE ISOTOPE FRACTIONATION AMONG GASEOUS MOLECULES, <i>P. Richet, Y. Bottinga, and M. Javoy</i>	65
DISCRIMINATION BETWEEN EARTHQUAKES AND UNDERGROUND EXPLOSIONS, <i>Robert Blandford</i>	111
QUATERNARY VEGETATION HISTORY—SOME COMPARISONS BETWEEN EUROPE AND AMERICA, <i>H. E. Wright, Jr.</i>	123
PALEOECOLOGICAL TRANSFER FUNCTIONS, <i>Harvey Maurice Sachs, T. Webb III, and D. R. Clark</i>	159
COMPOSITION OF THE MANTLE AND CORE, <i>Don L. Anderson</i>	179
TRANSMISSION ELECTRON MICROSCOPY IN EARTH SCIENCE, <i>P. E. Champness</i>	203
GEOCHEMISTRY OF ATMOSPHERIC RADON AND RADON PRODUCTS, <i>Karl Y. Turekian, Y. Nozaki, and Larry K. Benninger</i>	227
GEOCHRONOLOGY OF SOME ALKALIC ROCK PROVINCES IN EASTERN AND CENTRAL UNITED STATES, <i>Robert E. Zartman</i>	257
TRANSPORT PHENOMENA IN CHEMICAL RATE PROCESSES IN SEDIMENTS, <i>Patrick A. Domenico</i>	287
THE HISTORY OF THE EARTH'S SURFACE TEMPERATURE DURING THE PAST 100 MILLION YEARS, <i>Samuel M. Savin</i>	319
LASER-DISTANCE MEASURING TECHNIQUES, <i>Judah Levine</i>	357
AULACOGENS AND CONTINENTAL BREAKUP, <i>Kevin Burke</i>	371
METAMORPHISM OF ALPINE PERIDOTITE AND SERPENTINITE, <i>Bernard W. Evans</i>	397
THE EVOLUTION OF THE LUNAR REGOLITH, <i>Yves Langevin and James R. Arnold</i>	449
THEORETICAL FOUNDATIONS OF EQUATIONS OF STATE FOR THE TERRESTRIAL PLANETS, <i>Leon Thomsen</i>	491
CRATERING AND OBLITERATION HISTORY OF MARS, <i>Clark R. Chapman and Kenneth L. Jones</i>	515
INDEXES	
AUTHOR INDEX	541
CUMULATIVE INDEX OF CONTRIBUTING AUTHORS, VOLUMES 1–5	554
CUMULATIVE INDEX OF CHAPTER TITLES, VOLUMES 1–5	555

SEISMIC TRAVELTIME TOMOGRAPHY OF THE CRUST AND LITHOSPHERE

N. Rawlinson and M. Sambridge

*Research School of Earth Sciences, Australian National University,
Canberra ACT 0200, Australia*

1 Introduction

1.1 Motivation

Seismic data represent one of the most valuable resources for investigating the internal structure and composition of the earth. One of the first people to deduce earth structure from seismic records was Mohorovičić, a Serbian seismologist who, in 1909, observed two distinct traveltimes from a regional earthquake. He determined that one curve corresponded to a direct crustal phase and the other to a wave refracted by a discontinuity in elastic properties between crust and upper mantle. This world-wide discontinuity is now known as the Mohorovičić discontinuity or Moho for short. On a larger scale, the method of Herglotz and Wiechart (see, for example, Gubbins, 1992) was first implemented in 1910 to construct a 1-D whole earth model. The method uses the relationship between angular distance and ray parameter to determine velocity as a function of radius within the earth.

Today, an abundance of methods exist for determining earth structure from seismic waves. Different components of the seismic record may be used, including traveltimes, amplitudes, waveform spectra, full waveforms or the entire wavefield. Source-receiver configurations also differ - receiver arrays may be in-line or 3-D, sources may be close or distant to the receiver array, sources may be natural or artificial, and the scale of the study may be from tens of meters to the whole earth. Finally, there are a multitude of ways of translating the data extracted from the seismogram into a representation of seismic structure.

The purpose of this article is to review a particular class of methods for imaging earth structure called seismic traveltome tomography. This is a form of seismic traveltome inversion that is used to constrain 2-D and 3-D models of the Earth represented by a significant number of parameters. The word *tomography* literally means *slice picture* (from the Greek word *tomos* meaning *slice*) and was first used in medical imaging to describe the process of mapping the internal density distribution of the human body using x-rays (Lee & Pereyra, 1993). The term was later appropriated by the seismological community to describe a similar process using seismic waves to map earth structure. Seismologists now routinely use *tomography* to refer to 3-D structural imaging even though, strictly speaking, the word was originally designed to describe the imaging of 2-D slices only.

Inversion of source-receiver traveltimes of seismic waves is undoubtedly the most popular technique for imaging subsurface structure at all scales. However, comprehensive up-to-date reviews of the methodology and their application are rarely found in the literature (some useful reference works include Nolet, 1987b; Iyer & Hirahara, 1993; Kennett, 1998). We hope to at least partially address this problem. Here, we restrict ourselves to traveltome tomography used in studies of the crust and lithosphere. These local scale studies typically involve the deployment of seismometer arrays with a spatial coverage of several hundred km or less in any dimension. The class of data that may be

recorded in such experiments include normal incidence reflection, refraction and wide-angle reflection, teleseismic and local earthquake arrival times. Although the inversion methods used in these studies are often common to a wide range of other seismic tomography applications, the point here is that they are presented in the context of traveltimes inversion for local-scale structure.

The widespread use of body wave traveltimes in seismic tomography is undoubtedly related to the relative ease with which they may be extracted from a seismogram and the simple relationship that exists between traveltimes and wavespeed. However, much more information is contained in a seismic waveform than simply the arrival time of a particular phase. Surface wave tomography, which utilizes the surface waveform component of an arriving wavetrain to build 3-D images of shear wavespeed, is the most commonly used type of waveform tomography. It is generally carried out at regional or global scales and has been particularly important in mapping beneath oceans (Nolet, 1987a); oceanic upper mantle is rarely probed by body wave tomography since few seismic recorders are placed in an ocean setting. The methodology and application of surface wave tomography falls outside the scope of this review, so we refer the interested reader to the texts of Iyer & Hirahara (1993) and Kennett (2002) and the journal papers of Cara & Lévêque (1987), Nolet (1990), Zielhuis & van der Hilst (1996) and Debayle & Kennett (2000) for more information on the subject.

This paper sets out to review commonly used methods of traveltimes inversion for crustal and lithospheric imaging from the mid 1970s, when seismic tomography was first used, until recently, and provide a comprehensive list of references. However, we would like the paper to be more than just a concatenation of method descriptions and a discussion of their relative merits. This is achieved in several ways. First, we impart a tutorial flavor to the paper by being instructive as well as informative; this will be of particular benefit to readers who are not very familiar with seismic tomography. For example, many schematic diagrams and technical drawings are included to try and illustrate basic concepts, or clarify important ideas. Second, recent techniques that have seen little or no application in seismic tomography but show significant potential are also explained (e.g. the fast marching method of traveltimes determination and global optimization techniques). Third, to help understand how the various methods are used in real data applications, and how different classes of data influence the formulation of the inverse problem, we present a number of case studies in detail. Generally, these examples are very recent, although we also discuss earlier applications to emphasize how the methodology has evolved. Lastly, we discuss in some detail the future of seismic traveltimes tomography as a tool for subsurface imaging, and in particular the frontier areas of research that remain to be explored.

In the remainder of this section, the basic concepts underlying seismic traveltimes tomography are introduced, and the four types of data for analyzing crustal and lithospheric structure are described (i.e. coincident reflection, refraction and wide-angle reflection, local earthquake and teleseismic). In Section 2, we review methods of seismic traveltimes tomography, and in particular focus on model parameterization, techniques for determining traveltimes, inversion schemes and practical methods for analyzing solution robustness. Application of these methods to each of the four data types are then presented and compared in Section 3, with most examples taken from the existing literature. In Section 4, we conclude with a discussion on possible future developments in seismic traveltimes tomography.

1.2 Seismic Traveltimes Tomography: Formulation

If we represent some elastic property of the subsurface (e.g. velocity) by a set of model parameters \mathbf{m} , then a set of data (e.g. traveltimes) \mathbf{d} can be predicted for a given source-receiver array by line

integration through the model. The relationship between data and model parameters, $\mathbf{d} = \mathbf{g}(\mathbf{m})$, forms the basis of any tomographic method. For an observed dataset \mathbf{d}_{obs} and an initial model \mathbf{m}_0 , the difference $\mathbf{d}_{obs} - \mathbf{g}(\mathbf{m}_0)$ gives an indication of how well the current model predictions satisfy the data. The inverse problem in tomography is then to manipulate \mathbf{m} in order to minimize the difference between observed and predicted data subject to any regularization that may be imposed. The end result will be a mathematical representation of the true structure whose accuracy will depend on a number of factors including: i) how well the observed data are satisfied by the model predictions, ii) assumptions made in parameterizing the model, iii) errors in the observed data, iv) accuracy of the method for determining model predictions $\mathbf{g}(\mathbf{m})$, and v) the extent to which the data constrain the model parameters. The tomographic method therefore depends implicitly on the general principles of inverse theory (Tarantola, 1987; Menke, 1989; Parker, 1994).

The steps required to produce a tomographic image from seismic data can thus be defined as follows:

1. **Model parameterization:** The seismic structure of the region being mapped is defined in terms of a set of unknown model parameters. Tomographic methods generally require an initial estimate of model parameter values to be specified.
2. **Forward calculation:** A procedure is defined for the calculation of model data (e.g. traveltimes) given a set of values for the model parameters.
3. **Inversion:** Automated adjustment of the model parameter values with the object of better matching the model data to the observed data subject to any regularization that may be imposed.
4. **Analysis of solution robustness:** May be based on estimates of covariance and resolution from linear theory or on the reconstruction of test models using synthetic datasets.

In seismic travelttime tomography the model data are traveltimes and the model parameters define velocity variations. The travelttime of a ray in a continuous velocity medium $v(\mathbf{x})$ is:

$$t = \int_{L(v)} \frac{1}{v(\mathbf{x})} dl \quad (1)$$

where L is the ray path and $v(\mathbf{x})$ is the velocity field. Eq. 1 is non-linear since the integration path depends on the velocity. This inherent non-linearity means that the inverse problem can be very difficult to solve. There are three basic approaches that are used, which we define as (i) linear tomography, (ii) iterative non-linear tomography, and (iii) fully non-linear tomography. In linear tomography, the relationship between travelttime residual and velocity perturbation is linearized about a reference model and corrections to the velocity field are made under this assumption. Thus, ray paths are determined only once (through the initial or reference model) and are not re-traced. Iterative non-linear tomography also ignores the path dependence of the velocity correction in the inversion step, but accounts for the non-linearity of the problem by iteratively applying corrections and re-tracing rays (i.e. repeating steps 2 and 3 in the above formulation) until, for example, the data are satisfied, or the rate of data fit improvement per iteration satisfies a given tolerance. Fully non-linear tomography locates a solution without relying on linearization in any way, but is rarely done in practice.

The linearization assumption commonly adopted in travelttime tomography is reasonable provided it can be shown that the source-receiver path is not significantly perturbed by the adjustments

made to the model parameter values in the inverse step. If we now consider a perturbation $\delta v(\mathbf{x})$ to a reference velocity field $v_0(\mathbf{x})$, so that $v(\mathbf{x}) = v_0(\mathbf{x}) + \delta v(\mathbf{x})$, then both the ray path and source-receiver traveltimes must also be perturbed in the new velocity field $v(\mathbf{x})$ relative to $v_0(\mathbf{x})$. If the new path is $L(v) = L_0 + \delta L$ where L_0 is the path in $v_0(\mathbf{x})$ and $t = t_0 + \delta t$ where t_0 is the traveltimes along L_0 in $v_0(\mathbf{x})$, then the traveltimes in $v(\mathbf{x})$ can be written:

$$t = \int_{L_0 + \delta L} \frac{1}{v_0 + \delta v} dl \quad (2)$$

The integrand in Eq. 2 may be expanded using the geometric series:

$$\frac{1}{v_0 + \delta v} = \frac{1/v_0}{1 - (-\delta v/v_0)} = \frac{1}{v_0} - \frac{\delta v}{v_0^2} + \frac{\delta v^2}{v_0^3} - \dots \quad (3)$$

Substitution of this expression into Eq. 2 and ignoring second-order terms yields:

$$t = \int_{L_0 + \delta L} \frac{1}{v_0} - \frac{\delta v}{v_0^2} dl + O(\delta v^2) \quad (4)$$

which to first order may be separated as:

$$t = \int_{L_0} \frac{1}{v_0} - \frac{\delta v}{v_0^2} dl + \int_{\delta L} \frac{1}{v_0} - \frac{\delta v}{v_0^2} dl + O(\delta v^2) \quad (5)$$

The second integral on the RHS can be set to zero since Fermat's Principle states that, for fixed endpoints, the traveltimes along a ray path is stationary with respect to perturbations in the path ($\partial t / \partial L = 0$). Since $t = t_0 + \delta t$, then the perturbation in traveltimes resulting from a perturbation to the velocity field is given by:

$$\delta t = - \int_{L_0} \frac{\delta v}{v_0^2} dl + O(\delta v^2) \quad (6)$$

The implication of Eq. 6 is that if the velocity along the path is perturbed, then the corresponding traveltime perturbation calculated along the original path will be accurate to first order (see Snieder & Sambridge, 1993, for a discussion of the case in which ray end points are perturbed). It is interesting to note that if the above calculation is performed in terms of a perturbation in slowness $s(\mathbf{x}) = 1/v(\mathbf{x})$ rather than velocity, then the resulting expression for a perturbation in traveltime is given by:

$$\delta t = \int_{L_0} \delta s dl + O(\delta s^2) \quad (7)$$

which is linearly dependent on δs .

Studies that use linear tomography may deal with tens to hundreds of thousands of model parameters (e.g. Inoue et al., 1990; Spakman, 1991; van der Hilst et al., 1997; Bijwaard et al., 1998), making an iterative non-linear approach computationally expensive, or have data geometries (such as teleseismic) that make a linear assumption more valid (e.g. Achauer 1994). It is worth noting, however, that a number of recent regional and global scale travelttime tomography studies involving hundreds of thousands to millions of ray paths and hundreds of thousands of model parameters have used iterative non-linear inversion schemes (Bijwaard & Spakman, 2000; Gorbatov et al., 2000,

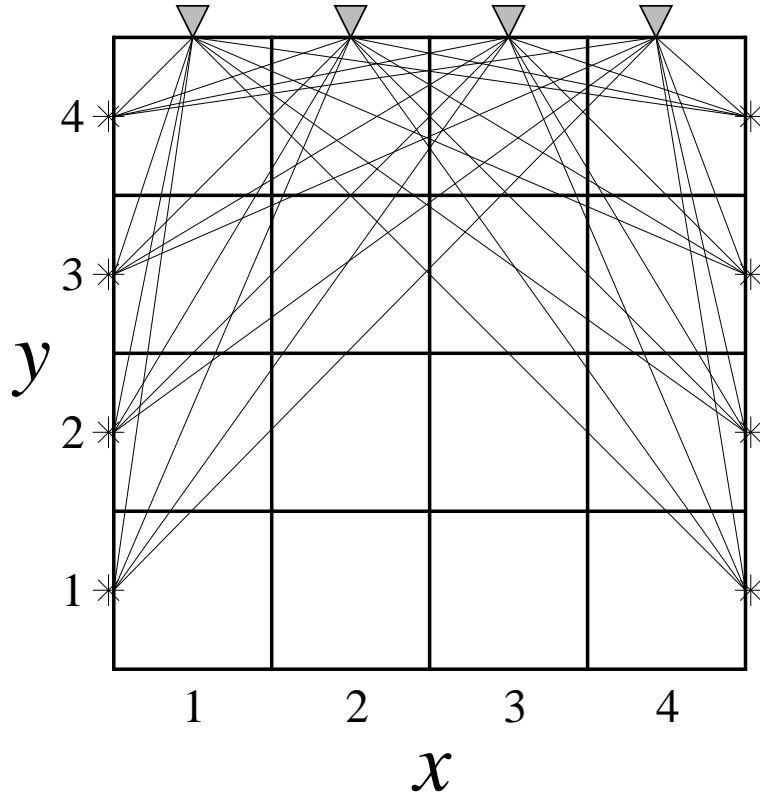


Figure 1: Schematic representation of a source-receiver array (sources denoted by asterisks, receivers by triangles) that bounds a model volume represented by a set of 16 constant velocity blocks labeled using (x, y) coordinates. Ray paths connect sources and receivers and demonstrate why the inverse problem often requires regularization. Blocks (2,1) and (3,1) are not constrained by the data, blocks (1,1), (2,2), (3,2) and (4,1) are relatively poorly constrained by the data while blocks like (2,4) and (3,4) are relatively well constrained by the data.

2001). Local earthquake and wide-angle tomography, for which ray paths depend strongly on velocity structure, generally use an iterative non-linear approach (e.g. Hole, 1992; Graeber & Asch, 1999).

Common model parameterizations include constant velocity (or slowness) blocks, a grid of velocity nodes with a specified interpolant like trilinear or cubic splines, and to a lesser extent, spectral parameterizations like truncated Fourier series. Interface parameterizations use similar schemes except those appropriate to a surface rather than a volume. The forward problem of finding source-receiver ray paths and traveltimes is often solved using ray tracing techniques like shooting and bending, first-arrival wavefront tracking on a grid (e.g. eikonal solvers) and network methods, also known as Shortest Path Raytracing (SPR). The inverse step of adjusting model parameters to satisfy observed data subject to regularization constraints is frequently solved using gradient methods (e.g. Gauss-Newton, subspace inversion) and backprojection methods like ART or SIRT. Global optimization methods like genetic algorithms (Goldberg, 1989) have been used but only rarely. Regularization (i.e. applying other constraints to the model in addition to those supplied by the data) is an important consideration in the inverse step due to the often under-determined or mixed-determined nature of the problem (see Fig. 1). A means of analyzing solution robustness is a critical step in a meaningful interpretation of an inversion result. Estimates of *a posteriori* model resolution and covariance from linear theory have been used, as have synthetic reconstructions (e.g. the checkerboard

test) that use the same source-receiver geometry as the original experiment. All the above methods are discussed in more detail in Section 2.

Due to its origins in radiology and early seismic imaging, the term tomography is generally only applied to methods that invert for a property (e.g. velocity) that is described throughout the model volume. If only interface structure is inverted for (e.g. Hole, 1992; Rawlinson & Houseman, 1998), then the term tomography is generally not applied, even though the method conforms to the procedures described above. However, in this paper we assume that the term tomography may be used for any method that generally follows the four steps listed above and results in 2-D or 3-D representations of subsurface structure.

1.3 Traveltime Data used in Studies of the Crust and Lithosphere

The four classes of data we consider for the tomographic determination of crustal and lithospheric structure are normal incidence reflection, refraction and wide-angle reflection, local earthquake and teleseismic. Normal incidence reflection surveys and refraction and wide-angle reflection surveys use controlled or artificial sources (e.g. airgun shots, explosions, vibroseis) to generate seismic energy. The benefits of controlled sources include precise identification of source location and origin time, control over data coverage, and knowledge of source waveform. However, compared to experiments that use earthquake sources, surveys of this nature tend to be more expensive and cannot be used to probe deep structure (air-gun shots tend not to penetrate very far beyond the base of the crust) unless powerful sources such as nuclear explosions are used. PNEs (Peaceful Nuclear Explosions) can be detected thousands of kilometers away and have occasionally been recorded by long in-line receiver arrays (Priestley et al., 1994; Ryberg et al., 1996; Nielsen et al., 1999). Due to the advent of the Comprehensive Test Ban Treaty, PNEs are unlikely to be used in the future.

Normal incidence reflection seismic surveys use in-line arrays of sources and receivers to image crustal structure on depth scales of tens of meters to tens of kilometers. This seismic method is referred to as *normal incidence* (or *coincident*) because the aim is to map reflections from sub-horizontal interfaces using near-vertically propagating P -waves (see Fig. 2a). The most common way of analyzing this data is to plot traces from adjacent sources or receivers next to each other on a horizontal distance versus two-way traveltimes axis to produce a reflection section. Variations in the earth's impulse response can then be linked to variations in earth structure. To produce a usable reflection section, significant processing is required (Yilmaz, 1987; Telford et al., 1990) to remove or reduce effects caused by the source wavetrain, multiples, normal moveout, near-surface complexities, diffraction and data noise. The entire seismic wavefield is used and is mapped directly to the model space. For this reason, reflection seismic sections are unequaled in terms of detail and resolution. The method is most effective when used to image discontinuous changes in seismic structure (i.e. reflectors).

As shown in Fig. 2a, the paths taken by the seismic energy in a seismic reflection experiment are not strictly vertical, as the shot is recorded by an array of receivers at varying offsets (usually small compared to the maximum depth of the recorded energy) from the source. The multiplicity of data permits stacking to boost signal-to-noise ratio and the variation of ray trajectories also makes it possible to explicitly image elastic properties using traveltimes in a process known as reflection tomography (Bishop et al., 1985; Farra & Madariaga, 1988; Williamson, 1990; Blundell, 1993; Carroll & Beresford, 1996; Kosloff et al., 1996). Structure is commonly represented by a series of sub-horizontal layers separated by continuous interfaces. Usually, both interface geometry and layer velocity are varied by the inversion to satisfy the observed traveltimes.

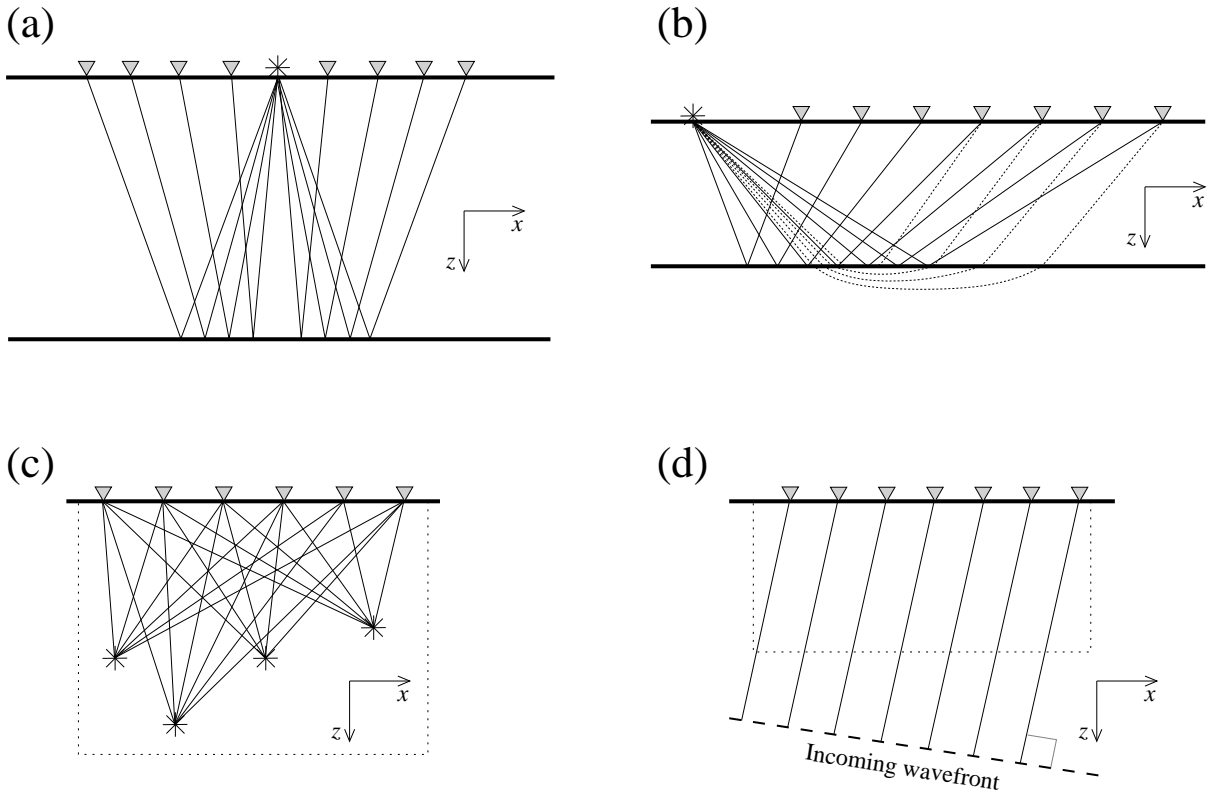


Figure 2: Schematic source-receiver geometries for various seismic surveys (sources are denoted by asterisks, receivers by triangles): (a) Normal incidence reflection array (common source), (b) wide-angle seismic array; thin black lines denote reflected rays, dotted lines denote refracted rays, (c) local earthquake array - sources lie within modeled region (dotted line), and (d) teleseismic array - sources lie outside modeled region (dotted line).

Although it is sometimes possible for coincident reflection data to resolve the trade-off that exists between lateral variation of velocity within a layer and interface depth (Blundell, 1993), the often small offsets between source and receiver make it difficult. Refraction and wide-angle reflection surveys use arrays with large offsets between sources and receivers (see Fig. 2b). In this case, traces from adjacent receivers recorded from a single shot, or from adjacent shots recorded at a single receiver, may be plotted on a time versus offset plot to reveal the presence of coherent traveltimes. The term *wide-angle data* normally implies the presence of both refraction and reflection information (e.g. Riahi & Lund, 1994; Zelt et al., 1996). Wide-angle tomography shares many similarities with reflection tomography. Model structure is commonly represented by layers with both interface geometry and layer velocity constrained by the inversion procedure. Reflected rays tend to be more sensitive to variations in interface structure, while refracted rays tend to be more sensitive to variations in layer velocity.

Recently, interpretation of wide-angle seismic data has been carried out in 3-D using multiple in-line arrays of sources and large receiver arrays. Inversion methods for 3-D wide-angle data have been presented by a number of authors including Hole (1992), Hole et al. (1992), Riahi et al. (1997), Zelt & Barton (1998), Zelt et al. (1999) and Rawlinson et al. (2001a). Interpretation methods for such datasets have developed rapidly in recent years, although many still cannot deal with the level of structural detail commonly obtained from 2-D datasets (e.g. Kodaira et al., 1998).

One of the first papers to be published on seismic tomography was that of Aki & Lee (1976), who

inverted first-arrival P -wave traveltimes from local earthquakes for velocity structure and hypocenter location in Bear Valley, California. The source-receiver geometry for this type of study is shown schematically in Fig. 2c - the earthquake sources lie beneath the receiver array within the model volume. The hypocenter coordinates, which are not accurately known, must be included in the inversion. Although Fig. 2c shows a 2-D experiment, most local earthquake studies are 3-D. Since the publication of the Aki & Lee (1976) paper, this branch of tomography has come into common usage and is now popularly known as Local Earthquake Tomography or LET (Thurber, 1993).

LET has been used to image the lithosphere and upper asthenosphere to depths of up to 200 km in subduction zone settings (Abers, 1994; Graeber & Asch, 1999). High resolution images of the crust have also been obtained using shallow earthquakes (Thurber, 1983; Chiarabba et al., 1997). In such cases, the results of LET can be usefully compared with wide-angle studies of the same region (Eberhart-Phillips, 1990). Advantages of LET over wide-angle tomography include greater depth of penetration and the added structural information provided by the relocated hypocenters, e.g. the existence of double seismic zones (Hasegawa et al., 1978; Kawakatsu, 1985; Kao & Rau, 1999). On the other hand, the relocation of hypocenters adds to the non-uniqueness of the solution and phases other than first-arrival P and S can be difficult to incorporate. For this reason, LET models rarely include interfaces, although Zhao et al. (1992) included interfaces in their LET model of NE Japan by using observed SP waves converted at the Moho and PS/SP waves converted at the upper boundary of the subducted Pacific Plate.

A significant difference between LET and teleseismic tomography is source location; in a teleseismic study, earthquakes are generally thousands of km away from the receiver array. The target region of the crust and upper mantle lies beneath the receiver array. A key assumption of teleseismic tomography is that only the region beneath the receiver array contains significant lateral variations in velocity. Elsewhere, a 1-D earth model is adequate to predict the geometry and inclination of the wavefront before it strikes the target region. Therefore, it is possible to trace the rays through a 1-D reference model of the earth until they penetrate the teleseismic model. Normally, relative traveltimes rather than absolute traveltimes are used in the inversion; this helps to account for errors in hypocenter location and large scale mantle heterogeneities. Fig. 2d shows a schematic diagram of a wavefront from a distant earthquake incident on a teleseismic receiver array. As in LET, teleseismic tomography is usually carried out in 3-D.

A seminal paper by Aki et al. (1977) used teleseismic data recorded at the Norsar array to invert for velocity anomalies to a depth of 126 km. The final solution was produced by linear inversion. The assumption of linearity is more accurate in teleseismic tomography than in LET or wide-angle inversion. This occurs because the ray paths tend to be near-vertical as they transmit through the model volume and hence are less affected by the dominant variations of velocity with depth. Consequently, many teleseismic tomography images, even those published recently, are the result of linear inversions (Humphreys & Clayton, 1990; Glahn & Granet, 1993; Seber et al., 1996; Saltzer & Humphreys, 1997). If the traveltimes residuals are suggestive of significant lateral structure, then an iterative non-linear approach may be required (Weiland et al., 1995; McQueen & Lambeck, 1996; Rawlinson & Houseman, 1998; Frederiksen et al., 1998; Steck et al., 1998; Graeber et al., 2002).

The main difficulties in teleseismic tomography arise because of the irregular and unpredictable nature of earthquakes. Earthquakes tend to occur at plate boundaries, so it is common to have a very uneven distribution (in terms of azimuth and inclination) of ray paths through the target volume. Another factor is that relative traveltimes residuals only provide good constraints on lateral variations in velocity relative to an *a priori* lateral average. Vertical variations in the velocity field of the

solution model are poorly constrained and therefore must be interpreted with caution (Lévêque & Masson, 1999).

The depth extent of teleseismic investigations may range from crustal (e.g. Lambeck et al., 1988; Rawlinson & Houseman, 1998) to many hundreds of kilometers (e.g. Humphreys & Clayton, 1990). The horizontal extent of the receiver array and the source distribution determines the depth to which features may be resolved. The vertical dimension of the model volume is often chosen on this basis, but it is always possible that structure outside the solution region causes some of the variation between traveltimes residuals (e.g. Benz et al., 1992).

2 Methods of Traveltimes Inversion

2.1 Representation of Structure

The traveltimes of a seismic wave between source and receiver is solely dependent on the velocity structure of the medium through which the wave propagates. Therefore, subsurface structure in a seismic traveltimes inversion is represented by variations in P or S wave velocity (or slowness). As mentioned in Section 1.2, velocity variations may be defined by a set of interfaces whose geometry is varied to satisfy the data, a set of constant velocity blocks or nodes with a specified interpolation function, or a combination of velocity and interface parameters. The most appropriate choice will depend on the *a priori* information (e.g. known faults or other interfaces), whether or not the data indicates the presence of interfaces (e.g. reflections, mode conversions), whether data coverage is adequate to resolve the trade-off between interface position and velocity, and finally, the capabilities of the inversion routine.

2.1.1 Velocity Parameterization

Constant velocity blocks (Fig. 3a) are simple to define and result in linear ray paths within each block. On the other hand, they are not a natural choice for representing smooth variations in subsurface structure due to the velocity discontinuities that exist between adjacent blocks. These artificial discontinuities may also cause unwarranted ray shadow zones and triplications. However, if a large number of blocks are used and restrictions are placed on the size of the velocity changes between adjacent blocks, then a reasonable approximation to a continuously varying velocity field is possible. In teleseismic tomography, constant velocity blocks have been used by many authors including Aki et al. (1977), Oncescu et al. (1984), Humphreys & Clayton (1988), Humphreys & Clayton (1990), Benz et al. (1992), Achauer (1994) and Saltzer & Humphreys (1997). In wide-angle traveltimes inversions, the use of constant velocity blocks is not as common. Zhu & Ebel (1994) and Hildebrand et al. (1989) use constant velocity blocks in the inversion of 3-D refraction traveltimes while Williamson (1990) and Blundell (1993) use them in an inversion of reflection traveltimes. Similarly, constant velocity blocks are only rarely used in local earthquake tomography (Aki & Lee, 1976; Nakanishi, 1985). This scheme for representing structure is often avoided when strong ray curvature is expected.

An alternative to a block parameterization is to define velocities at the vertices of a rectangular grid (see Fig. 3b) together with a specified interpolation function. One of the first examples of this approach was by Thurber (1983) in the context of local earthquake tomography. To describe the velocity at any point (x, y, z) within a rectangular grid of nodes, he used a trilinear interpolation

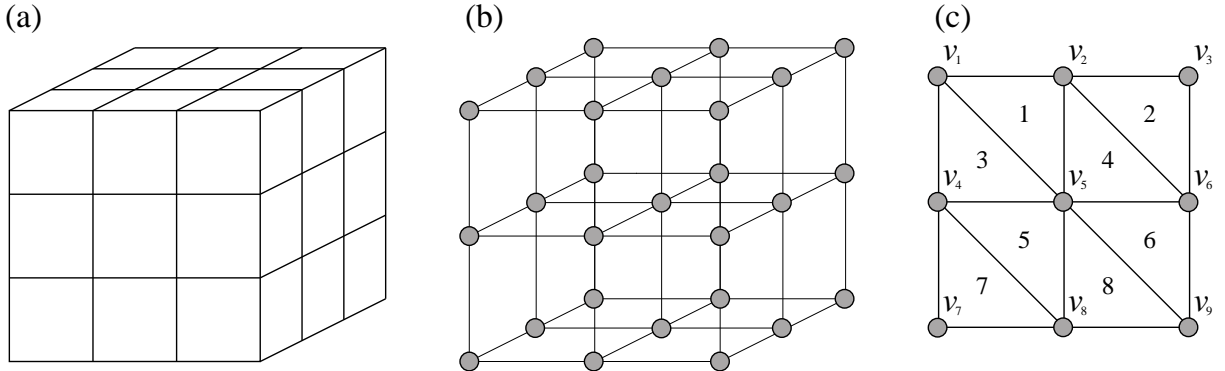


Figure 3: Different types of velocity parameterization: (a) constant velocity blocks, (b) a grid of velocity nodes, and (c) triangulated velocity grid designed for constant velocity gradient cells (after White, 1989).

function:

$$v(x, y, z) = \sum_{i=1}^2 \sum_{j=1}^2 \sum_{k=1}^2 V(x_i, y_j, z_k) \left(1 - \left|\frac{x - x_i}{x_2 - x_1}\right|\right) \left(1 - \left|\frac{y - y_j}{y_2 - y_1}\right|\right) \left(1 - \left|\frac{z - z_k}{z_2 - z_1}\right|\right) \quad (8)$$

where $V(x_i, y_j, z_k)$ are the velocity values at the eight grid points surrounding (x, y, z) . The use of Eq. 8 ensures that the velocity field will be continuous throughout the model volume, although the velocity gradient will be discontinuous from cell to cell. This model parameterization is now commonly used in local earthquake tomography (Eberhart-Phillips, 1986, 1990; Zhao et al., 1992; Eberhart-Phillips & Michael, 1993; Scott et al., 1994; Haslinger et al., 1999), presumably because most of these inversions are based on the SIMULPS code devised by Thurber (1983). Zhao et al. (1994) and Steck et al. (1998) have used this parameterization in teleseismic tomography, although Zhao et al. (1994) use a modified form of Eq. 8 for spherical coordinates.

Higher order interpolation functions must be used if the velocity field is to have continuous first and second derivatives, which are required for some ray tracing methods (Thomson & Gubbins, 1982). Cubic spline interpolation results in continuous first and second derivatives and has been used by a number of authors. Thomson & Gubbins (1982), in a NORSAR teleseismic study, use the following cubic spline function to describe the slowness field within a regular 3-D spherical grid of nodes:

$$s(r, \theta, \phi) = \sum_{i=1}^4 \sum_{j=1}^4 \sum_{k=1}^4 S_{ijk} C_i(R) C_j(\Theta) C_k(\Phi) \quad (9)$$

where S_{ijk} are the slowness values at the nodes of the $4 \times 4 \times 4$ grid surrounding the point (r, θ, ϕ) . $C_i(R)$, $C_j(\Theta)$ and $C_k(\Phi)$ are known as the cardinal splines (modified by Thomson & Gubbins, 1982, for local support) and R , Θ and Φ are the local coordinates of r , θ and ϕ . Nodal values do not necessarily equal the spline values at the node points. Sambridge (1990) uses a similar parameterization in Cartesian coordinates to describe a 3-D model constrained by traveltimes from local earthquakes and explosions.

Cubic B-splines are similar to the cardinal splines described above in that they are locally supported and do not necessarily pass through the node values. Conventional cubic spline interpolation forces the spline to pass through node values and is not locally supported. Undesirable effects of non-local support include poorly resolved portions of the model having a global influence and unrealistic velocity fluctuations between nodes (Shalev, 1993). In 2-D wide-angle travelttime tomography, cubic

spline interpolation has been employed by Lutter et al. (1990), while Farra & Madariaga (1988) and McCaughey & Singh (1997) have used cubic B-spline bases.

An interpolation method which features inherent flexibility is splines under tension (Smith & Wessel, 1990). Here, a tension factor is used to control the mode of interpolation, which, in the case of Neele et al. (1993), can vary between near trilinear interpolation and cubic spline interpolation. The scheme features continuous first and second derivatives. Usually, one will choose a tension factor that results in a smooth model but minimizes unrealistic oscillations and maximizes local control. Neele et al. (1993), VanDecar et al. (1995) and Ritsema et al. (1998) all use this approach in the inversion of teleseismic traveltimes.

A method of parameterization that goes some way towards bridging the gap between a block approach and a grid approach is one which uses cells with a constant velocity gradient. White (1989) describes a method of 2-D refraction tomography in which a rectangular grid of nodes is used to define triangular regions of constant velocity gradient (see Fig. 3c). The velocity within each cell is given by:

$$v(x, y) = v_o + (x - x_o)\nabla_x v + (z - z_o)\nabla_z v \quad (10)$$

where v_o , $\nabla_x v$ and $\nabla_z v$ are determined using the velocities at the vertices of the triangle (e.g. $v_o = v_1$, $\nabla_x v = (v_2 - v_1)/\Delta x$, $\nabla_z v = (v_5 - v_2)/\Delta z$ in cell 1 of Fig. 3c). The attributes of this method are that velocity varies continuously throughout the medium and rays can be traced analytically within each cell. However, the velocity gradient is discontinuous at each cell boundary which, in conjunction with their triangular shape, can result in difficulties in finding the source-receiver ray path. A similar method was used by Chapman & Drummond (1982) for refracted rays. Another interpolation function that can be used with the triangular cell geometry which also allows analytic ray tracing is the constant gradient of quadratic slowness $1/v^2$ (Červený, 1987). The extension of these procedures to 3-D involves the use of tetrahedral cells, with the linear interpolation functions described in terms of the velocity nodes at the four vertices of the tetrahedron. It is important to note that these methods of parameterization are used primarily because they facilitate analytic ray tracing and only secondly because they provide an adequate approximation to actual subsurface velocity distribution, which is inevitably more complex.

Rather than use a block or grid-based parameterization, one could use a scheme in which velocity is discretized in the wavenumber domain rather than the spatial domain. Spectral parameterizations that use some form of truncated Fourier series fall into this category. In their inversion of reflection amplitudes and traveltimes, Wang & Pratt (1997) describe a 2-D slowness distribution using the Fourier series:

$$\begin{aligned} s(\mathbf{r}) = & a_{00} + \sum_{m=1}^N [a_{m0} \cos(\mathbf{k} \cdot \mathbf{r}) + b_{m0} \sin(\mathbf{k} \cdot \mathbf{r})] \\ & + \sum_{m=-N}^N \sum_{n=1}^N [a_{mn} \cos(\mathbf{k} \cdot \mathbf{r}) + b_{mn} \sin(\mathbf{k} \cdot \mathbf{r})] \end{aligned} \quad (11)$$

where $\mathbf{r} = xi + zj$ and $\mathbf{k} = m\pi k_0 i + n\pi k_0 j$ are the position and wavenumber vector respectively, and a_{mn} and b_{mn} are the amplitude coefficients of the $(m, n)^{th}$ harmonic term, which become the unknowns in the inversion step. The advantage of this type of parameterization is that it defines a velocity field which is infinitely differentiable and whose smoothness can be controlled through the choice of the number of harmonic terms N that are used. Eq. 11 defines a non-local parameterization, however, so poorly resolved portions of a solution model may have a detrimental effect on other

regions of the model. Spectral parameterizations have been used in wide-angle traveltimes inversion by Hildebrand et al. (1989), Hammer et al. (1994) and Wiggins et al. (1996) to study crustal structure beneath deep oceans.

2.1.2 Including Interfaces

Velocity discontinuities are most commonly included in velocity models when the subsurface is represented by sub horizontal layers (see Fig. 4). In 2-D and 3-D traveltimes inversion, the use of layered parameterizations has almost exclusively been the domain of reflection and refraction tomography. Reflection sections only image reflectors and refraction sections usually contain obvious later-arriving traveltimes curves associated with velocity discontinuities. The issues related to choosing an appropriate interface parameterization are similar to those for choosing an appropriate velocity parameterization - representation of the geological structure and suitability for use in the forward and inverse solution steps.

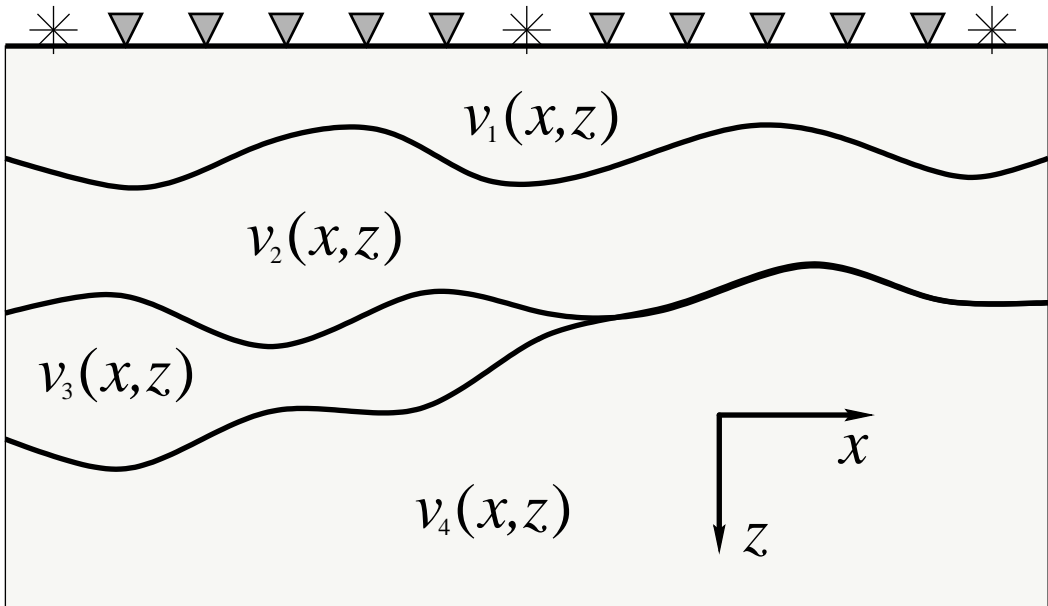


Figure 4: Schematic representation of the kind of layered velocity structure that can be imaged in reflection and wide-angle traveltimes inversion. The velocity functions $v_i(x, z)$ describe the velocity variation within a layer.

In 2-D, piecewise linear segments (see Fig. 5a) are probably the simplest means of representing interface geometry. The wide-angle method of Zelt & Smith (1992) and the reflection method of Williamson (1990) employ this type of interface parameterization. One obvious problem with using piecewise linear segments is that the gradient of the interface is discontinuous at the joins between segments. Such discontinuity may not be geologically realistic and will create artificial shadow zones because incident rays with very similar paths may depart from the interface along very different paths if they intersect the interface on either side of a point of gradient discontinuity. Zelt & Smith (1992) avoid this problem by using an averaging filter to smooth the interface so that the departing ray has a trajectory consistent with the smooth interface, but the point of projection is still given by the intersection point of the incident ray with the piecewise linear interface.

The logical extension of piecewise linear segments to a 3-D model with interface surfaces is

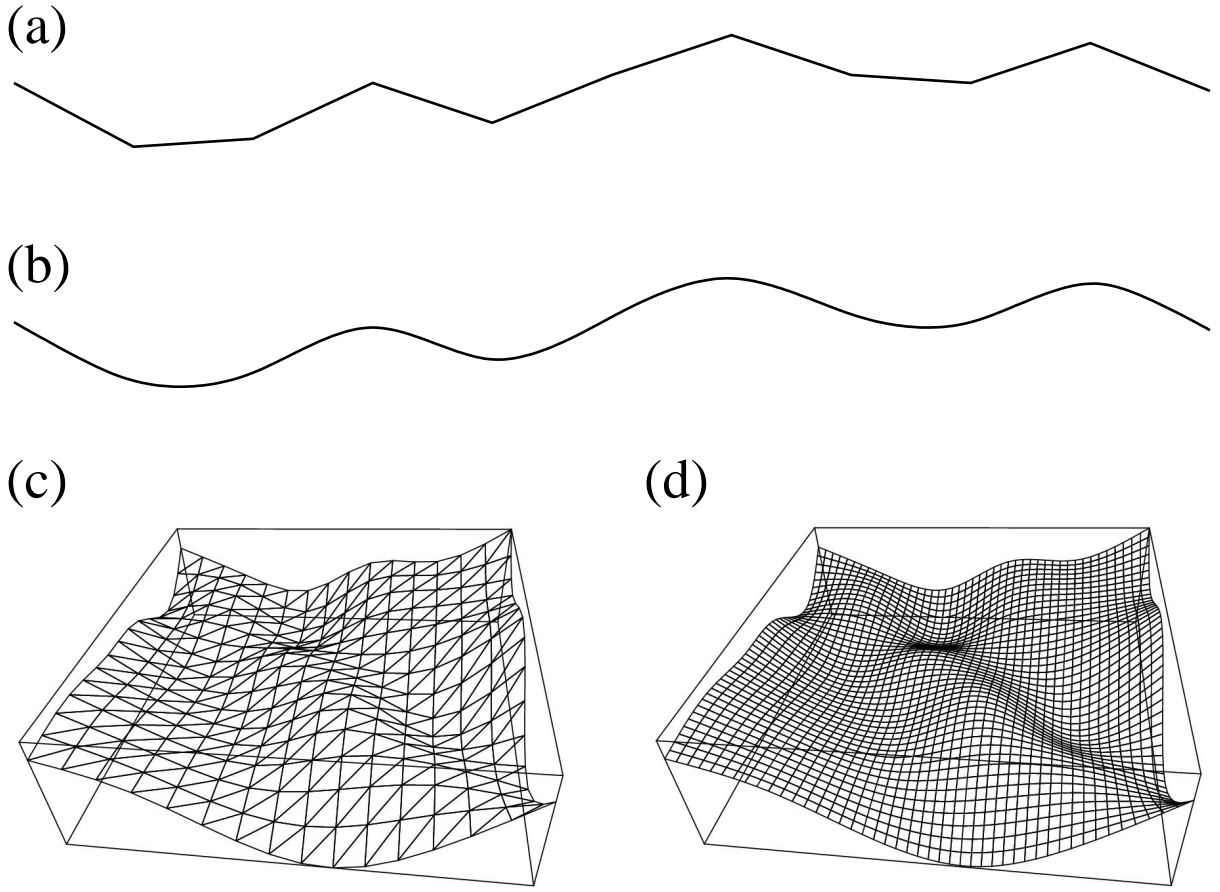


Figure 5: Types of interface parameterization for 2-D (a-b) and 3-D (c-d) models. (a) Piecewise linear segments, (b) piecewise cubic B-spline interpolation, (c) surface defined by mosaic of triangular patches, (d) surface defined by mosaic of bicubic B-spline patches - note that the surface is visualized here by orthogonal sets of lines.

to use piecewise triangular area segments (see Fig. 5c). Cambridge (1990) has used this approach in the inversion of local earthquake and quarry blast traveltimes. Guizou et al. (1996) also used a triangulated interface structure in the tomographic inversion of reflection traveltimes in order to work with geological models created in GOCAD (a computer aided design tool for modeling geological objects). One advantage of triangulation is that multi-valued surfaces are easily described.

Analogous to defining velocity on a grid of nodes, an interface may be described by a grid of depth nodes with a specified interpolation function (piecewise linear segments can be viewed as a special case of this). Piecewise cubic spline functions with C_2 continuity (see Fig. 5b) are commonly used in wide-angle inversions. Conventional cubic splines have been used in a number of 2-D schemes including those by White (1989), Lutter & Nowack (1990) and Rawlinson & Houseman (1998). Červený et al. (1984) parameterize a layered model with splines under tension for both interfaces and layer velocity fields. Cubic B-splines, which feature local control of interface geometry, have been used by Farra & Madariaga (1988) and McCaughey & Singh (1997). In 3-D, the use of smooth interfaces (see Fig. 5d) is less common, mainly because methods for the inversion of 3-D layered structures are less wide spread. The ray tracing method of Gjøystdal et al. (1984) parameterizes interfaces in terms of bicubic splines, and the reflection tomography method of Chiu et al. (1986) describes interfaces using n^{th} order polynomials (in practice, they use $n \leq 3$). Like con-

tinuous velocity variations, interfaces are also amenable to spectral parameterization. For example, Wang & Houseman (1994) describe interfaces using a truncated Fourier series where the number of harmonic terms controls the allowable flexibility of the interface. The problems associated with the use of a global parameterization outlined above for velocity also apply to interface structure.

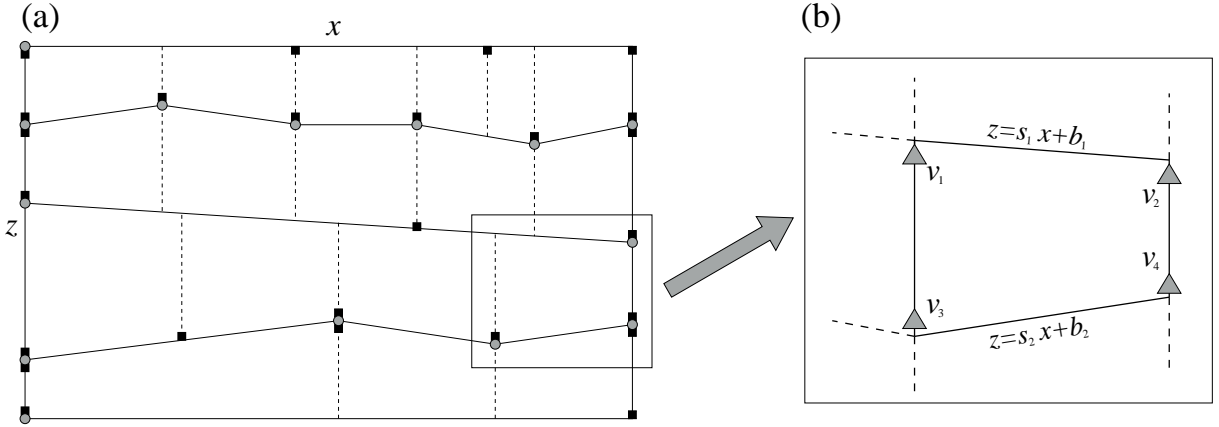


Figure 6: Example of a layered structure parameterized using the method of Zelt & Smith (1992). (a) Structure composed of four layers with layer velocity defined by 25 velocity nodes (black squares) and interface structure defined by 14 boundary nodes (grey circles). There is no velocity discontinuity between the second and third layers and dashed lines indicate the lateral boundaries of trapezoids. (b) The velocity field within a trapezoid is defined by interpolating between four corner values (grey triangles). If no velocity node lies at a corner, then the required value is obtained by linear interpolation from adjacent nodes.

Irregular parameterizations are not very commonly used in traveltome tomography. However, irregular shaped elements can be adapted to suit variations in subsurface data coverage. The frequently used 2-D wide-angle inversion method of Zelt & Smith (1992) uses such a method. Layer boundaries are described by a set of one or more arbitrarily spaced nodes interpolated linearly. Within each layer, velocity nodes are specified on the upper and lower boundaries, the number and spacing of which may vary (Fig. 6a). To facilitate velocity interpolation, each layer is divided laterally into trapezoidal blocks separated by vertical boundaries, which occur at each upper and lower boundary node and velocity node. The velocity within each trapezoid is interpolated using the velocity values at the four corners (obtained by linear interpolation if a velocity node does not occupy a corner) such that the velocity within each layer varies linearly between the upper and lower boundaries in the vertical direction, and linearly along the upper and lower boundaries between nodes. Layer boundaries may or may not represent velocity discontinuities. Fig. 6b shows the design of a trapezoid in more detail. The velocity within a trapezoid is given by (Zelt & Smith, 1992):

$$v(x, z) = \frac{c_1x + c_2x^2 + c_3z + c_4xz + c_5}{c_6x + c_7} \quad (12)$$

where $\{c_i\}$ are linear combinations of the corner velocities. The inherent flexibility of this technique means that a velocity structure with or without layering can be represented. If layers are present, then it is possible for the velocity within the layers to vary arbitrarily.

Another example of irregular parameterization is given by Rawlinson et al. (2001a) in their method of wide-angle traveltome inversion for 3-D layered crustal structure. They make use of bicubic B-splines in parametric form to describe interface geometry. For a set of control vertices

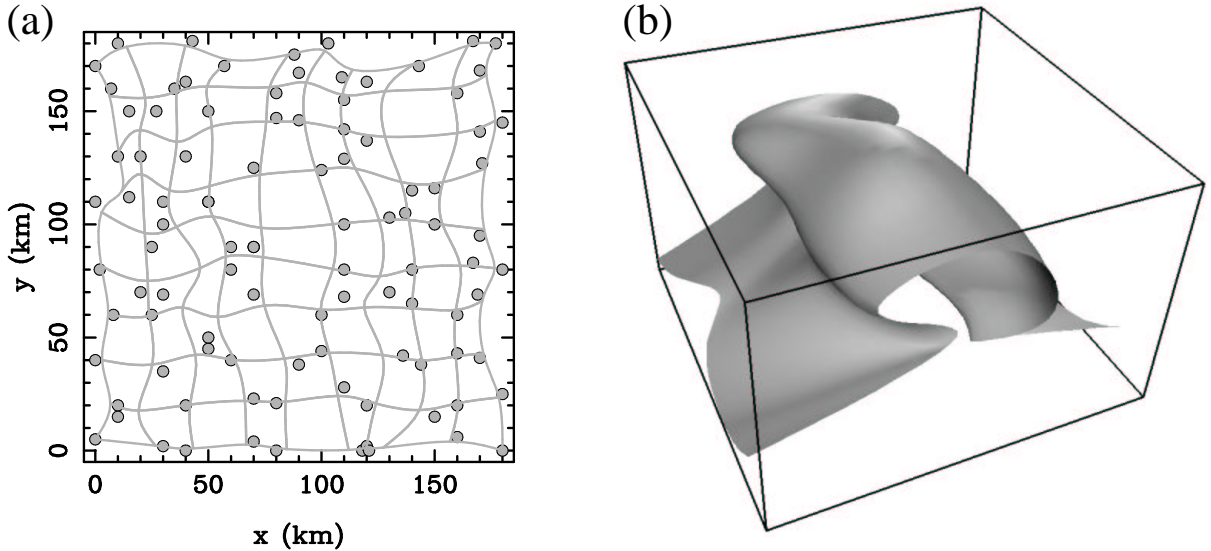


Figure 7: Flexibility of a cubic B-spline parameterization in parametric form. (a) Irregular grid of nodes describing a surface. Grey lines indicate surface patch boundaries. (b) Multivalued surface described by cubic B-splines.

$\mathbf{p}_{i,j} = (x_{i,j}, y_{i,j}, z_{i,j})$ where $i = 1, \dots, m$ and $j = 1, \dots, n$, the B-spline for the ij^{th} surface patch is:

$$\mathbf{B}_{i,j}(u, v) = \sum_{k=-1}^2 \sum_{l=-1}^2 b_k(u) b_l(v) \mathbf{p}_{i+k, j+l} \quad (13)$$

so that any point on a surface patch is a function of two independent parameters u ($0 \leq u \leq 1$) and v ($0 \leq v \leq 1$). The weighting factors $\{b_i\}$ are the uniform cubic B-spline basis functions (Bartels et al., 1987). Properties of a surface constructed using a mosaic of B-spline patches defined by Eq. 13 include C_2 continuity and local control. Fig. 5d shows a bicubic B-spline surface described by a regular grid of 16×16 vertices. In addition to inherent smoothness and local control, vertices may lie on an irregular grid (Fig. 7a) and the surface may also be multivalued (Fig. 7b), although Rawlinson et al. (2001a) did not make use of the latter property in their inversions. Control vertices may be widely spaced in regions of poor data coverage and closely spaced in regions of good data coverage.

Fault surfaces are another common feature of earth structure that may need to be represented in a model. Explicit representation of faults is not common in seismic methods. Faults are often near-vertical and cause discontinuities in the interfaces and velocity fields of sub-horizontal layers offset by the fault. Ray-tracing through such a medium may be difficult and the inverse problem is likely to be highly non-linear. Lambeck et al. (1988) and Lambeck & Burgess (1992) computed teleseismic traveltimes residuals for a 2-D model in which constant velocity layers bounded by piecewise linear interfaces were not required to be laterally continuous across the model, thus allowing faults to be defined. Inversion of traveltimes residuals was not attempted in either study, however. Wide-angle inversion methods that allow for complex lateral structure (e.g. Zelt & Smith, 1992) are usually not designed to represent faults. Laterally discontinuous structures like those found at subduction zones (Zelt, 1999) can be represented because interfaces tend to have a shallow dip and layer dislocation is not usually needed. Wang & Braile (1996), using a method based on that of Zelt & Smith (1992), represent faults implicitly by sharp near-vertical jumps in sub-horizontal interface structure in adj-

cent interfaces. However, these structures were constrained manually during the inversion process.

When interfaces are used in conjunction with layer velocities specified by blocks or a grid of nodes, then it is usually necessary to extrapolate the velocity field of each layer beyond the surrounding interfaces. These velocity parameters are redundant unless changes in interface geometry made by the inversion step cause the relevant nodes to lie within the layer. The velocity within each layer is usually defined to be independent of velocities in other layers, so any spatial overlap of velocity nodes from adjacent layers is of no consequence. In a 3-D wide-angle inversion study, Zelt et al. (1999) describe velocity structure using a continuous velocity parameterization but include “floating” reflectors. These floating reflectors allow reflections to be used to constrain interface structure and velocity but simplify traveltime determination by associating the reflectors with sharp gradients in velocity rather than with velocity discontinuities.

As mentioned earlier, the use of interfaces in teleseismic travelttime tomography is rare. Zhao et al. (1994) employ fixed interfaces described either by a power series or piecewise linear interpolation in their simultaneous inversion of local, regional and teleseismic traveltimes for velocity variation. Davis (1991) uses backprojection to invert teleseismic travelttime residuals for the structure of the lithosphere-asthenosphere boundary in East Africa, defining interface geometry in terms of a polynomial expansion. Kohler & Davis (1997) use a similar procedure to determine 2-D crustal thickness variations in California from teleseismic travelttime residuals.

2.2 Travelttime Determination

The calculation of ray traveltimes between known end points through a given velocity structure is often called the forward problem. When more than one ray path exists between a given source and receiver, the path with minimum travelttime is the one usually required because first-arrivals are always easier to identify on a seismogram. Often, other quantities such as Fréchet derivatives are calculated together with travelttime, but these parameters and their methods of computation are described in the next section in the context of the relevant inversion method.

The travelttime of a seismic wave between source S and receiver R is given by the integral:

$$t = \int_S^R \frac{1}{v(\mathbf{x})} dl \quad (14)$$

where dl is differential path length, \mathbf{x} is the position vector and v is velocity. The difficulty in performing this integration, as pointed out in Section 1.2, is that the path taken by the seismic energy depends on the velocity structure, and the path needs to be known in order to evaluate the integral. For an elastic medium, the propagation of seismic wavefronts can be described by the eikonal equation:

$$(\nabla_{\mathbf{x}} T)^2 = \frac{1}{[v(\mathbf{x})]^2} \quad (15)$$

where T is the travelttime of the wavefront. This description of wave propagation is subject to the so-called high frequency assumption: the wavelength of a seismic wave should be much less than the length scale of the velocity variations of the medium through which it passes. If travelttime is described by the equation $T = T(\mathbf{x})$ and time is held constant, then $T_A = T(\mathbf{x})$ is an implicit equation for the wavefront at time T_A (Aki & Richards, 1980). If T_A is increased to, say, T_B , then the equation $T_B = T(\mathbf{x})$ will describe the new geometry and position of the wavefront at a time $T_B - T_A$ later. If instead a point of constant phase on the wave is described as $\mathbf{x} = \mathbf{x}(T)$ then,

rather than implicitly describing a wavefront (i.e. a surface), we explicitly describe a ray path (i.e. a curve). Ray paths are by definition everywhere normal to wavefronts. The equation that governs the geometry of ray paths can be derived from the eikonal equation by considering how a small change in time dt effects a point \mathbf{x} on a wavefront (see Aki & Richards, 1980). The resultant *ray equation*:

$$\frac{d}{dl} \left(\frac{1}{v(\mathbf{x})} \frac{d\mathbf{x}}{dl} \right) = \nabla \left(\frac{1}{v(\mathbf{x})} \right) \quad (16)$$

can be used to describe ray path geometry for any given velocity field $v(\mathbf{x})$. A consequence of Eq. 16 is Fermat's principle - that of all the paths that join two points A and B in a velocity medium, the true ray path(s) will be stationary in time. In other words, the path along which the integral in Eq. 14 is performed is one which extremizes t . This property was used to derive Eq. 6.

In traveltime tomography, the traditional means of determining source-receiver traveltimes is ray tracing (Červený, 1987, 2001). More recently, wavefront tracking schemes such as finite difference solutions of the eikonal equation have been employed (Vidale, 1988, 1990; Qin et al., 1992). Another method that has seen recent application is network/graph theory, which makes direct use of Fermat's principle (Nakanishi & Yamaguchi, 1986; Moser, 1991). Each of these methods of traveltime determination is described below.

2.2.1 Ray Tracing

The problem of finding a ray path between a source and receiver is a two point boundary value problem, for which there are two basic methods of solution: shooting and bending.

2.2.1.1 Shooting method Shooting methods of ray tracing rely on formulating the ray equation (Eq. 16) as an initial value problem, where a complete ray path can be determined provided the source coordinates and initial ray direction are known. The boundary value problem is then solved by shooting rays through the medium from the source and using information from the computed paths to update the initial ray trajectories so that they more accurately target the receivers (see Fig. 8). Rays may also be shot from receiver to source as the principle of reciprocity applies.

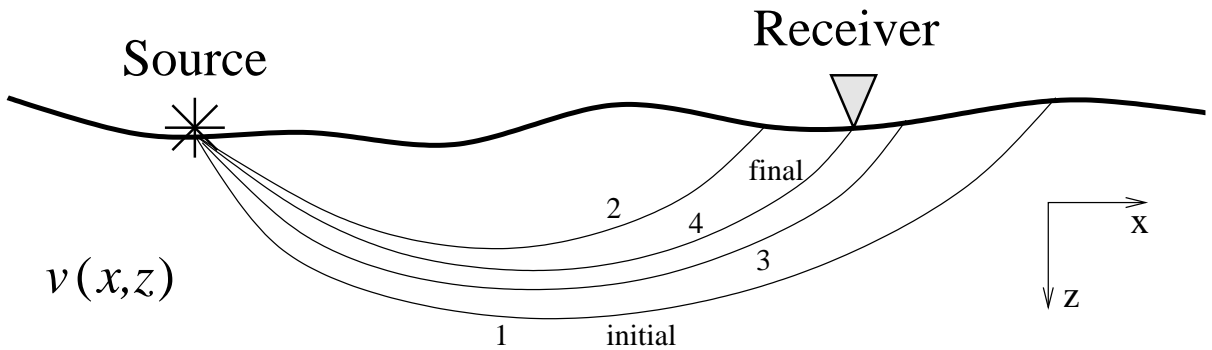


Figure 8: Principle of the shooting method. The initial projection angle of ray 1 is iteratively adjusted until the final ray (4) passes sufficiently close to the receiver.

The ease with which the initial value problem can be solved depends on how the velocity distribution is parameterized. For constant velocity (or slowness) block models, the path within a block

is simply a straight line with traveltimes varying linearly with distance. At cell boundaries, new trajectories are calculated using Snell's Law:

$$\frac{\sin \theta_i}{v_i} = \frac{\sin \theta_r}{v_r} \quad (17)$$

where θ_i and θ_r are the angles of incident and refracted rays relative to the normal vector to the interface, and v_i and v_r are the velocities of the media containing the incident and refracted rays respectively.

Analytic ray tracing is also possible for media with a constant velocity gradient. Telford et al. (1976) derive parametric equations for ray path geometry and traveltimes when velocity varies linearly with depth z :

$$\left. \begin{aligned} x &= \frac{1}{pk}(\cos i_o - \cos i) \\ z &= \frac{1}{pk}(\sin i - \sin i_o) \\ t &= \frac{1}{k} \ln \left(\frac{\tan \frac{i}{2}}{\tan \frac{i_o}{2}} \right) \end{aligned} \right\} \quad (18)$$

where i is the inclination of the ray (from the downgoing vertical), i_o is the initial inclination, k is the velocity gradient and p is the ray parameter. When the velocity gradient is arbitrarily oriented, such as when a grid of constant velocity gradient triangles or tetrahedra are used (see Section 2.1), then these expressions are modified by rotation of the coordinate system (White, 1989). Simple analytic solutions are also possible when there is a constant gradient of quadratic slowness (see Červený, 1987).

Only a few simple velocity functions allow for analytic solutions of the initial value problem. For the case of an arbitrary differentiable velocity function $v(\mathbf{x})$, numerical solution of an initial value formulation of the ray equation is required. For example, Zelt & Smith (1992), as part of their 2-D wide-angle traveltime inversion method, solve two pairs of first-order differential equations:

$$\frac{dz}{dx} = \cot \theta \quad \frac{d\theta}{dx} = \frac{v_z - v_x \cot \theta}{v} \quad (19)$$

or

$$\frac{dx}{dz} = \tan \theta \quad \frac{d\theta}{dz} = \frac{v_z \tan \theta - v_x}{v} \quad (20)$$

with initial conditions provided by source location (x_o, z_o) and ray take-off angle θ_o . θ is the angle of incidence (relative to the z -axis), $v_z = \partial v / \partial z$ and $v_x = \partial v / \partial x$. Eq. 19 is used for near horizontal rays and Eq. 20 is used for near vertical rays. Both systems of equations are solved using a Runge-Kutta method with error control. Traveltimes are determined by numerical integration of Eq. 14 using the trapezoidal rule. Sambridge & Kennett (1990) use the following set of equations to solve the

initial value problem in 3-D:

$$\left. \begin{aligned} \frac{\partial x}{\partial t} &= v \sin i \cos j \\ \frac{\partial y}{\partial t} &= v \sin i \sin j \\ \frac{\partial z}{\partial t} &= v \cos i \\ \frac{\partial i}{\partial t} &= -\cos i \left(\frac{\partial v}{\partial x} \cos j + \frac{\partial v}{\partial y} \sin j \right) + \frac{\partial v}{\partial z} \sin i \\ \frac{\partial j}{\partial t} &= \frac{1}{\sin i} \left(\frac{\partial v}{\partial x} \sin j - \frac{\partial v}{\partial y} \cos j \right) \end{aligned} \right\} \quad (21)$$

where i and j represent the incidence angle and azimuth respectively of the ray. They also use a Runge-Kutta method to solve the system with the ray travelttime t as the integration variable. The accuracy of the ray path and associated travelttime determined via numerical ray tracing depends on the accuracy of the solution scheme (4th order accurate in this case) and the length of the integration step.

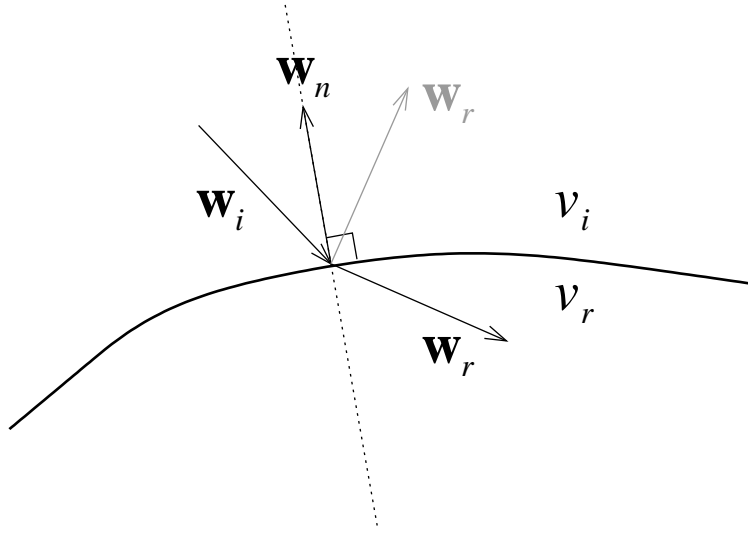


Figure 9: At an interface, rays may refract and/or reflect. \mathbf{w}_i is tangent to the incident path, \mathbf{w}_r is tangent to the refracted (or reflected) path and \mathbf{w}_n is normal to the interface.

When interfaces are included in a discontinuous velocity model, the reflection and transmission laws for a ray path at an interface can be described in terms of Snell's Law (Eq. 17). The geometrical consequence of Snell's Law is that the angle of reflection equals the angle of incidence, and that the reflected/transmitted ray lies in the same plane as the incident ray and the vector normal to the interface at the intersection point. Formulating these constraints into a procedure for determining the new ray direction is relatively straightforward once the ray-interface intersection point is located. For example, if \mathbf{w}_i is a vector tangent to the incident ray path at the intersection point, and \mathbf{w}_r is a vector tangent to the refracted ray path at the intersection point (see Fig. 9), then the relation between these

two vectors is given by (see Červený, 1987):

$$\mathbf{w}_r = \mathbf{w}_i + \left\{ \kappa \left[\frac{1}{v_r^2} - \frac{1}{v_i^2} + (\mathbf{w}_i \cdot \mathbf{w}_n)^2 \right]^{1/2} - \mathbf{w}_i \cdot \mathbf{w}_n \right\} \mathbf{w}_n \quad (22)$$

where \mathbf{w}_n is a normal vector to the interface at the intersection point and v_i and v_r are the velocities of the incident and refracted rays respectively at the intersection point. $\kappa = \text{sign}(\mathbf{w}_i \cdot \mathbf{w}_n)$ and equals +1 if \mathbf{w}_i makes an acute angle with \mathbf{w}_n and -1 otherwise. When reflected rays are required, then $v_i = v_r$ and Eq. 22 reduces to:

$$\mathbf{w}_r = \mathbf{w}_i - 2(\mathbf{w}_i \cdot \mathbf{w}_n)\mathbf{w}_n \quad (23)$$

where \mathbf{w}_r now points in the direction of the reflected ray. When analytic ray tracing is used, the ray-interface intersection point can often be found by solving a system of equations which equate a point on the ray with a point on the surface (e.g. Rawlinson et al., 2001a). In numerical ray tracing, the step length of the integration may be iteratively updated in order to obtain a point on the ray path sufficiently close to the interface (e.g. Sambridge & Kennett, 1990).

Solution of the initial value problem is the first step in finding a ray path from source to receiver. The next and generally more difficult step is to solve the two-point boundary value problem. Julian & Gubbins (1977) suggest two iterative methods of solution. The first of these is Newton's method which can be written for the 3-D problem as:

$$\begin{bmatrix} \frac{\partial h}{\partial i_o} & \frac{\partial h}{\partial j_o} \\ \frac{\partial g}{\partial i_o} & \frac{\partial g}{\partial j_o} \end{bmatrix}_n \begin{bmatrix} i_o^{n+1} - i_o^n \\ j_o^{n+1} - j_o^n \end{bmatrix} = \begin{bmatrix} H - h(i_o^n, j_o^n) \\ G - g(i_o^n, j_o^n) \end{bmatrix} \quad (24)$$

where (h, g) are the calculated horizontal coordinates of the ray endpoint, (H, G) are the desired coordinates and (i_o, j_o) are respectively the inclination and azimuth of the ray at the source. Solution of this system gives the updated projection coordinates (i_o^{n+1}, j_o^{n+1}) , and the process is iterated until an appropriate tolerance criterion is met. The difficulty with this scheme is the accurate determination of the partial derivative matrix. The second method is that of false position, which involves fitting a plane to the $h(i_o, j_o)$ and $g(i_o, j_o)$ of three known rays. The improved estimate (i_o^{n+1}, j_o^{n+1}) corresponds to where (H, G) lies on the plane. The method of false position is quicker at each iteration than Newton's method but converges more slowly. Sambridge & Kennett (1990) use Eq. 24 to solve the two point problem and determine accurate values for the partial derivatives by solving, in conjunction with the initial value problem, two systems of first-order differential equations that describe the geometrical spreading of the wavefront. A perturbation is applied to the initial ray projection angle if the ray gets trapped in a local minimum. In an application of the method (Sambridge, 1990), the initial trajectory of the first-guess ray path is provided by solving the two point problem for a laterally averaged version of the model, as suggested by Thurber & Ellsworth (1980).

The method used by Sambridge (1990) to calculate the partial derivatives in Eq. 24 is a specific application of paraxial ray approximation (Červený & Pšenčík, 1983; Červený et al., 1984; Červený, 1987; Farra & Madariaga, 1988; Červený, 2001), a method that is commonly used to solve the two-point problem in reflection and refraction ray tracing. The method is based on using a ray-centered coordinate system, where a particular ray Ω is taken to define one of the three coordinate axes. The wavefield in the vicinity of the central ray can be determined from quantities that are integrated along

the central ray using dynamic ray tracing. Geometric spreading and wavefront curvature parameters along the initial ray Ω can be used to rapidly locate the two-point ray path from an initial ray that is not too far from the target (see Červený et al., 1984).

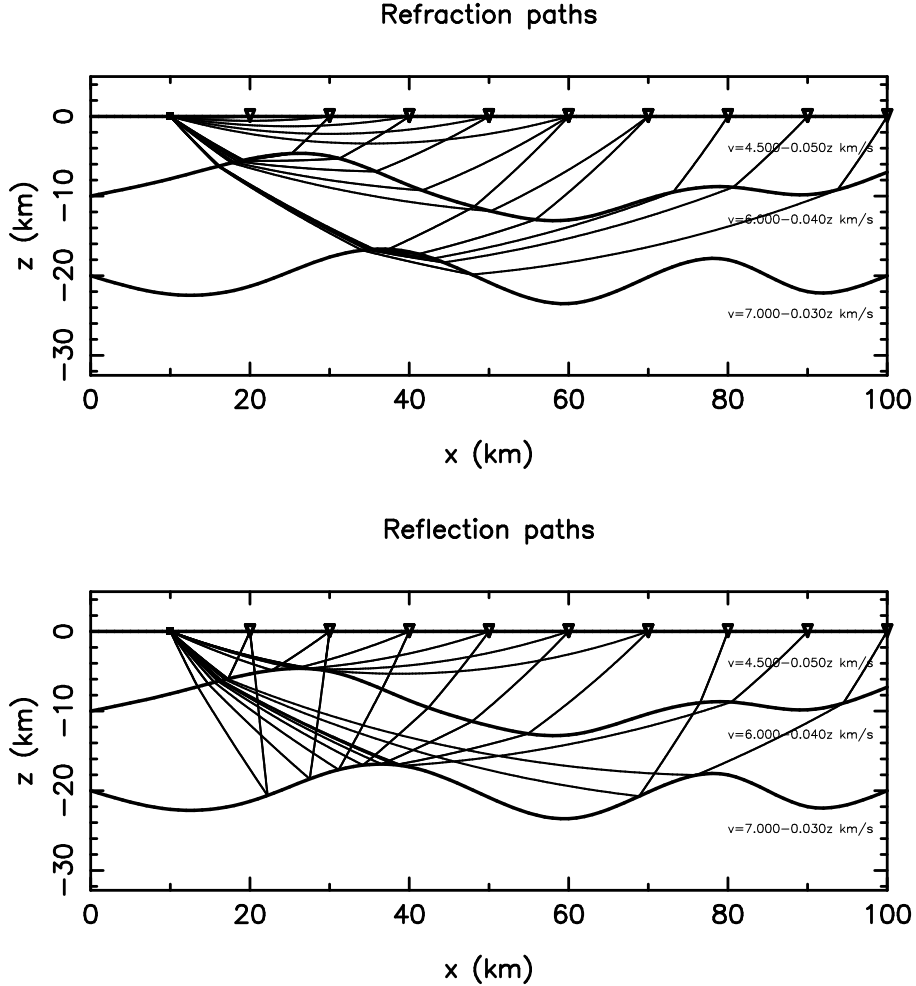


Figure 10: Shooting method of Rawlinson et al. (2001a) used to find source-receiver refraction and reflection ray paths.

In 2-D problems, a shooting approach is often used because the source-receiver array lies on a single vertical plane, making the shooting of a single fan of rays an effective way of obtaining nearby rays to all targets. Zelt & Smith (1992) use a bisection method to find rays that bound each required phase (e.g. a set of rays that all reflect back to the surface from a particular interface). The boundary value problem is approximately solved by shooting a fan of rays into each defined region and linearly interpolating the required quantities between the two closest rays that bracket a receiver. Blundell (1993) uses a similar approach of shooting a fan of rays from the source to find 2-D reflection arrivals. The two-point problem is then solved using a secant algorithm or a bisection algorithm with a pair of rays that bracket the receiver. Similar methods were used by Cassell (1982) and Langan et al. (1985). Other applications of shooting methods in 2-D reflection and/or refraction travelttime inversion include those by Farra & Madariaga (1988), White (1989), Lutter et al. (1990), Williamson (1990), Zelt & Smith (1992) and McCaughey & Singh (1997). Examples of its use in 3-D reflection

and/or refraction traveltimes are harder to find although several 3-D tomographic studies that combined refraction and local earthquake data (Benz & Smith, 1984; Ankeny et al., 1986; Sambridge, 1990) and some teleseismic tomography studies (Neele et al., 1993; VanDecar et al., 1995) have used shooting methods of ray tracing. Recently, Rawlinson et al. (2001a) developed a shooting method for finding refraction and reflection arrivals in 3-D layered media. Layer velocity varies linearly with depth in their model, so they were able to analytically trace rays within layers using equations similar to Eq. 18. The boundary value problem was solved using the Newton scheme of Eq. 24. Fig. 10 shows two-point paths through a 2-D layered model found using this method.

2.2.1.2 Bending method The bending method of ray tracing operates by adjusting the geometry of an initial arbitrary path that joins the source and receiver (Fig. 11) until it becomes a true ray path (i.e. it satisfies Fermat's principle). The bending method proposed by Julian & Gubbins (1977) is designed for a continuous 3-D velocity medium and locates a two-point ray path by solving a system of first-order differential equations. If the ray path is described parametrically as $\mathbf{x} = \mathbf{x}(q)$ where the

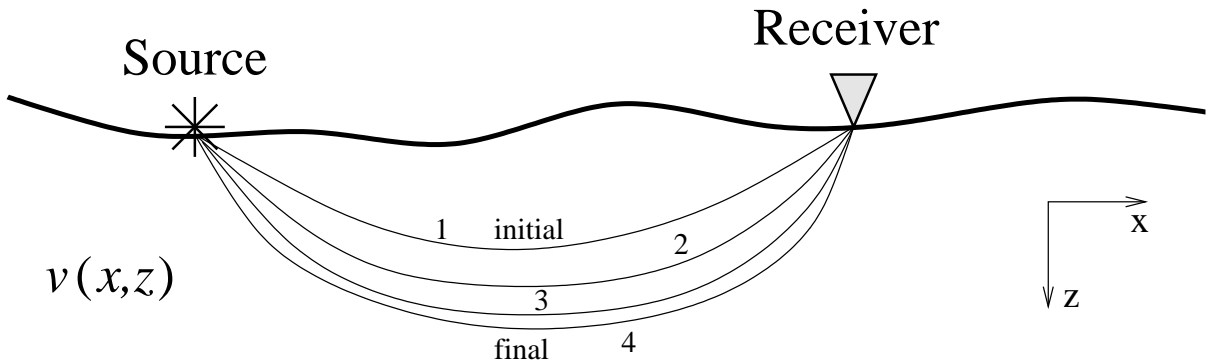


Figure 11: Principle of the bending method. The geometry of the initial path (ray 1) is adjusted until it satisfies Fermat's principle (ray 4).

choice for q can be made later, then Eq. 14 can be written:

$$t = \int_{q_S}^{q_R} s F dq \quad (25)$$

where s is slowness and:

$$F = \frac{dl}{dq} = \sqrt{\dot{x}^2 + \dot{y}^2 + \dot{z}^2} \quad (26)$$

with the differentials \dot{x} , \dot{y} and \dot{z} being taken with respect to q . The calculus of variations can be employed to describe the path which extremizes t . The Euler-Lagrange equations are (Julian & Gubbins, 1977):

$$\left. \begin{aligned} \frac{d}{dq} \frac{\partial}{\partial \dot{x}} (sF) &= \frac{\partial}{\partial x} (sF) \\ \frac{d}{dq} \frac{\partial}{\partial \dot{y}} (sF) &= \frac{\partial}{\partial y} (sF) \\ \frac{\partial F}{\partial q} &= 0 \end{aligned} \right\} \quad (27)$$

where $q = l/L$; L is the total length of the source-receiver ray path and $0 \leq l \leq L$. This choice for q results in a single-valued representation of the ray. The boundary conditions are then $\mathbf{x}(0) = \mathbf{x}_S$ and

$\mathbf{x}(1) = \mathbf{x}_R$ where \mathbf{x}_S and \mathbf{x}_R are the source and receiver coordinates respectively. These equations are non-linear and cannot be solved directly. If some initial path $\mathbf{x}^0(q)$ is chosen that passes through S and R , then an improved estimate may be given by:

$$\mathbf{x}^1(q) = \mathbf{x}^0(q) + \boldsymbol{\xi}^0(q) \quad (28)$$

where $\boldsymbol{\xi}^0(q)$ represents a perturbation to the initial path. If Eq. 28 is substituted into Eq. 27, then the resulting equations for $\boldsymbol{\xi}^0$ can be linearized and solved (see Julian & Gubbins, 1977), thus giving the improved estimate \mathbf{x}^1 . This process can be repeated until the solutions converge.

Pereyra et al. (1980) use a similar approach to locate two-point paths in arbitrary continuous media. They also extend their method to allow for the presence of interfaces. For a medium with an arbitrary number of interfaces that separate regions of smooth velocity variation, the bending problem can be treated by considering a separate system of non-linear differential equations in each smooth region. It is then possible to use the known discontinuity condition at each interface that is traversed by the ray to couple the separate systems. The disadvantage here is that the order in which the interfaces are traversed needs to be known in advance.

Um & Thurber (1987) develop a pseudo-bending technique for solving the two-point problem in continuous 3-D media. Their method is based on a perturbation scheme in which the integration step size is progressively halved. The initial guess path is defined by three points which are linearly interpolated. The center point is then iteratively perturbed using a geometric interpretation of the ray equation until the traveltimes extremum converges within a specified limit, at which point the ray equation will be approximately satisfied. The number of path segments is then doubled and the three-point perturbation scheme is repeated working from both endpoints to the middle (a total of three times for this step). The number of segments is doubled again and the procedure is repeated iteratively (see Fig. 12), until the change in traveltime between successive iterations satisfies some convergence criterion.

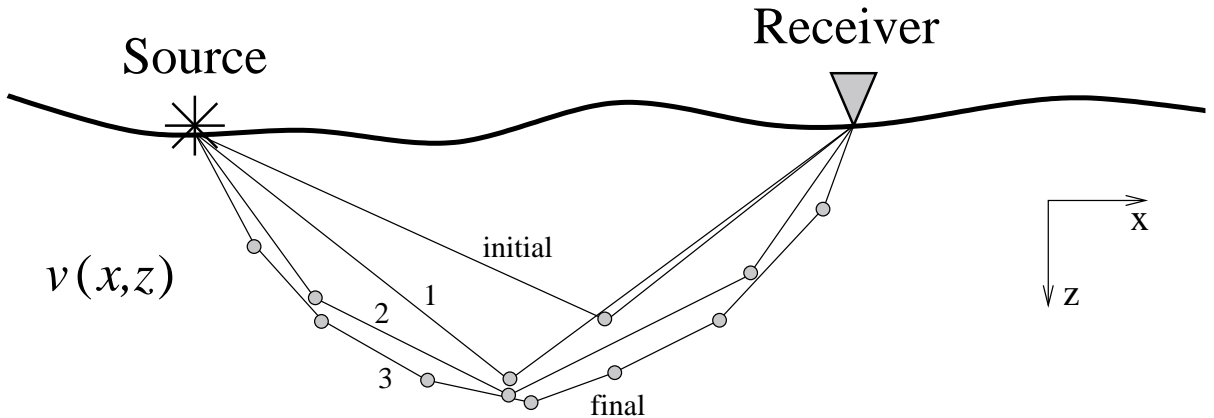


Figure 12: Principle of the pseudo-bending method of Um & Thurber (1987). An initial guess ray defined by three points is provided. The center point is perturbed to best satisfy the ray equation. Then the number of segments is doubled and the process is repeated. This figure schematically represents three such iterations.

Compared to earlier bending methods, the pseudo-bending technique is much faster (Um & Thurber, 1987). Zhao et al. (1992) modify this technique to cope with interfaces as follows. Consider two points A and B close to but on either side of an interface. Straight lines connect A and B separately to a point C on the interface. The correct ray-interface intersection point is obtained by adjusting the point C using a bisection method until Snell's Law is satisfied.

Prothero et al. (1988) develop a 3-D bending method based on the simplex method of function minimization. The first stage of the method is to locate the minimum-time circular path between source and receiver using an exhaustive search method. Perturbations to this path, described by a sum of sine wave harmonics, are then made using the simplex method which searches for the amplitude coefficients that produce the path of least time. The method is more robust than the pseudo-bending method of Um & Thurber (1987) but is significantly slower (Prothero et al., 1988).

Bending methods of ray tracing have been used by a number of authors in studies that invert teleseismic data (Thomson & Gubbins, 1982; Zhao et al., 1994, 1996; Steck et al., 1998), but not by many in the inversion of reflection or refraction data. Chiu et al. (1986) use a bending method in the inversion of 3-D reflection traveltimes and Zhao et al. (1997) use the pseudo-bending method in the inversion of refraction traveltimes for 2-D crustal structure. In local earthquake tomography, bending methods are probably most commonly used to find source-receiver paths and traveltimes (Eberhart-Phillips, 1990; Zhao et al., 1992; Scott et al., 1994; Eberhart-Phillips & Reyners, 1997; Graeber & Asch, 1999). In comparing their bending and shooting methods, Julian & Gubbins (1977) found that bending is computationally faster than shooting by a factor of 10 or more in media with continuous velocity variations. When discontinuities are present, however, the formulation of the bending problem becomes much more complex. In general, for smooth velocity structures that do not cause complex ray geometries, bending methods are more efficient, but when interfaces or strong velocity gradients are present, shooting methods tend to be more robust and therefore preferable (Červený, 1987; Sambridge & Kennett, 1990).

The only other type of ray tracing scheme that is mentioned here is approximate ray tracing (Thurber & Ellsworth, 1980). Here, the velocity in a region local to the source and receiver is laterally averaged, and a 1-D ray tracer is used to find the minimum time-path through this laterally invariant structure. The resultant traveltimes and path approximate the true first-arrival traveltimes and path through the 3-D model. If more accuracy is required, the ray path estimate can be used as a starting path in a bending routine (Thurber & Ellsworth, 1980). A variant of this technique was introduced by Thurber (1983), in which a large number of circular arcs with differing curvature and dip are joined between source and receiver. The traveltimes along each arc are then computed using the 3-D velocity model. An approximation to the first-arrival ray is then selected by choosing the arc with minimum traveltimes. Thurber (1983) and Eberhart-Phillips (1986) have used this style of approximate ray tracing in local earthquake tomography.

2.2.2 Wavefront Tracking

Rather than tracing rays from point to point through a medium to determine source-receiver traveltimes, an alternative is to track the propagation path of the entire wavefront. The traveltimes from the source to all points in the medium is found using this approach. The most common means of wavefront tracking employs finite-difference solutions of the eikonal equation on a regular grid to calculate the first-arrival traveltimes field.

2.2.2.1 Finite difference schemes Vidale (1988) proposed a finite difference scheme that involves progressively integrating the traveltimes along an expanding square in 2-D. Strictly speaking, this method doesn't track wavefronts to determine the traveltime field, but it represents a precursor

to the class of schemes that do, and is still widely used. The eikonal equation (Eq. 15) in 2-D is:

$$\left(\frac{\partial T}{\partial x}\right)^2 + \left(\frac{\partial T}{\partial z}\right)^2 = [s(x, z)]^2 \quad (29)$$

where $s(x, z)$ is the slowness field and $T(x, z)$ is the traveltime of a propagating wave. Vidale's method is formulated for a structure defined by a square grid of velocity nodes. Consider the grid points surrounding some local source point A in Fig. 13. If the traveltime to point A is T_0 then the traveltimes to the points B_i are given by:

$$T_{B_i} = T_0 + \frac{h}{2}(s_{B_i} + s_A) \quad (30)$$

where h is the node separation and s_{B_i} and s_A are the slowness at the nodes B_i and A respectively. The next step is to find the traveltimes to the corner points T_{C_i} . If the top right hand group of nodes in Fig. 13 with known traveltimes to $A(T_0)$, $B_1(T_1)$ and $B_2(T_2)$ are considered, then the traveltime to the point $C_1(T_3)$ can be determined from the eikonal equation. The two differential terms in Eq. 29 can be approximated with finite differences:

$$\left. \begin{aligned} \frac{\partial T}{\partial x} &= \frac{1}{2h}(T_1 + T_3 - T_0 - T_2) \\ \frac{\partial T}{\partial z} &= \frac{1}{2h}(T_2 + T_3 - T_0 - T_1) \end{aligned} \right\} \quad (31)$$

which, when substituted into Eq. 29, gives:

$$T_3 = T_0 + \sqrt{2(h\bar{s})^2 - (T_2 - T_1)^2} \quad (32)$$

where \bar{s} is the average slowness of all four points under consideration.

The resulting scheme can be used to calculate the traveltimes to all the C_i . The traveltimes to the next set of grid points can then be determined as the scheme progresses by solving along squares of increasing size around the source point (see Fig. 14). Solving for the traveltime to node points along a new square cannot be done in an arbitrary order; a scheme (e.g. Vidale, 1988) is required to determine the order of solution that will result in the least traveltime to each new node. Only these times will be valid seismic traveltimes. Vidale (1988) also gives another formulation that assumes locally circular wavefronts. The locally circular wavefront approximation is most accurate for strongly curved wavefronts and the locally plane wavefront approximation is most accurate for wavefronts with low curvature. Vidale (1990) extends the method to 3-D.

The problem with using an expanding square to progressively determine the traveltime field is that its geometry does not, in general, resemble the shape of the first-arrival wavefront. Consequently, the computed traveltimes may not represent first-arrivals, especially if the structure contains large velocity contrasts. Fig. 15 shows a schematic example in which the traveltime from A to B is determined for path 1 by the expanding square method, but path 2 has the least traveltime by virtue of the high velocity zone. Qin et al. (1992) propose a scheme that calculates the traveltime field using an expanding wavefront method. They use the same propagator equations (Equations 30 and 32) and start by calculating the traveltimes to the eight grid points (in 2-D) about the source. Thereafter, the point of global minimum traveltime along the perimeter of the points processed so far is used as the next source to locally expand the solution region. Using this approach, the traveltime field

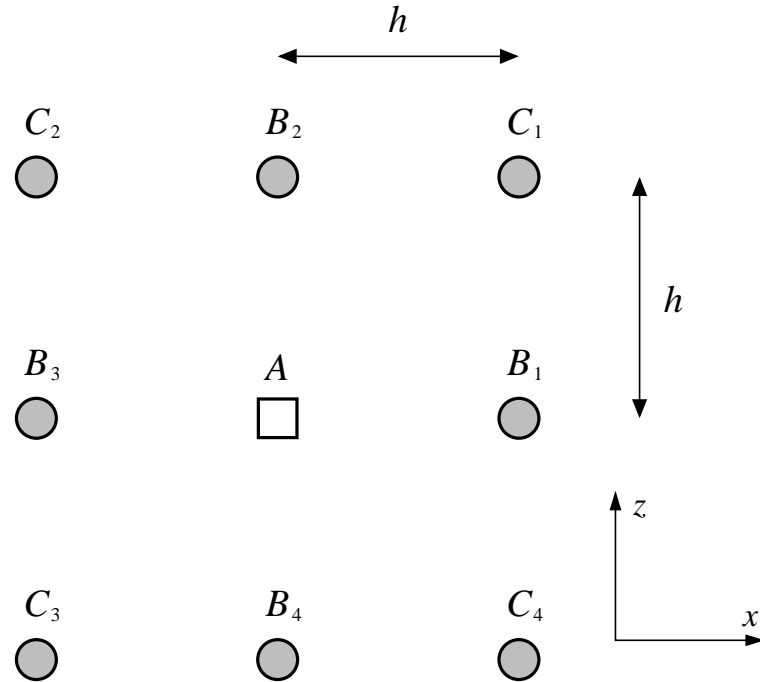


Figure 13: Method used by Vidale (1988) to find the first-arrival traveltime field for a continuous velocity medium. See text for details.

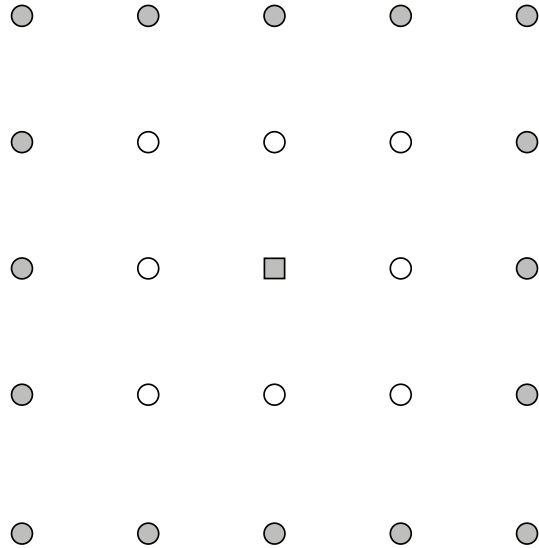


Figure 14: The expanding square method for determining the traveltime field. Traveltimes to the filled circles are determined from the open circles. The filled square is the source.

is determined using an expanding geometry that closely resembles the true shape of the wavefront and the possibility of computing arrivals other than first-arrivals is minimized. Where steep velocity gradients or discontinuities are encountered, however, problems can still occur as only outward propagating rays are considered.

Cao & Greenhalgh (1994) also solve the eikonal equation using a finite difference scheme and a solution region defined by an expanding wavefront. They consider two different model discretization schemes; one in which each node is placed at the center of a cell (i.e. same as the Vidale scheme),

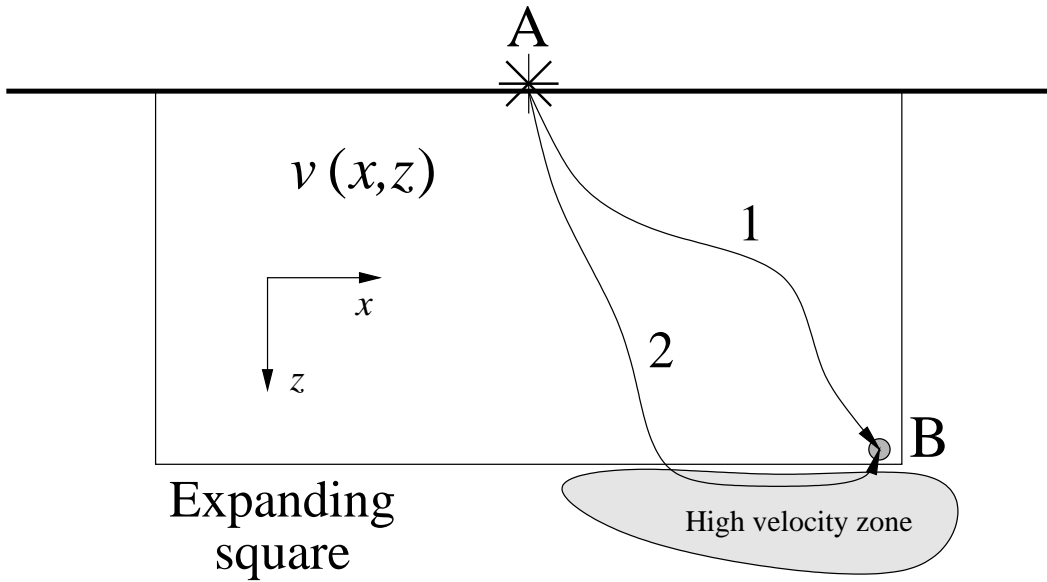


Figure 15: Schematic illustration showing how the expanding square method can fail. The traveltimes along path 1 is determined by the expanding square but path 2 has a shorter traveltimes due to the high velocity zone.

and one in which the nodes are placed at the corner of a cell with uniform slowness. They found that the corner node discretization provided superior solutions.

The presence of discontinuities such as interfaces between layers can be simulated by assigning the appropriate velocity values to the grid points that lie on either side of the interface. This means that accurate first-arrival times can be determined without separately parameterized interfaces forming a part of the model for the forward step. However, the expanding square formalism of Vidale (1988) may fail for head-waves traveling along an interface with a large velocity contrast as causality may be violated in a similar way as suggested in Fig. 15. Hole & Zelt (1995) and Afnimar & Koketsu (2000) address this problem by introducing special head-wave operators.

If reflection traveltimes are sought, the finite difference method needs to be modified. Riahi & Juhlin (1994) and Hole & Zelt (1995) both develop schemes for calculating reflection traveltimes by modifying the Vidale (1990) method. Riahi & Juhlin (1994) solve the eikonal equation starting from both source and receiver and tracking first-arrivals through the grid to the interface. The correct reflection point will then be the one which minimizes source-receiver traveltimes. The drawback of this approach is the need to track traveltimes through the grid from all sources and all receivers. Hole & Zelt (1995) overcome this problem by assuming that the incoming wavefront from the source and the interface are sufficiently smooth to validate a local planar approximation. Thus, the reflected traveltimes to nodes that are adjacent to the interface can be determined using only the depth to the reflector, the normal vector to the reflector, and the direction vectors of the incident ray and reflected ray (from Snell's law). If the wavefront incident on the reflector contains gradient discontinuities or strong curvature, the accuracy of this scheme will be reduced.

Unlike ray tracing methods of traveltime determination, wavefront tracking approaches do not explicitly find ray paths. If they are used as part of a tomographic-style inversion scheme, then some way of locating ray paths is required. One way of doing this is to start at the receiver and follow the traveltime gradient ∇T back through the computed traveltime field to the source. ∇T will always be oriented perpendicular to the first-arrival wavefront and will therefore trace out the first-arrival

ray path. In practice, this could be done on a cell by cell basis using the average traveltimes gradient within each cell to orientate a local line segment approximation to the path. Thus, the complete ray path will be described in terms of piecewise linear segments. For example, if we consider a 2-D cell surrounded by grid points $T_{i,j}$, $T_{i+1,j}$, $T_{i,j-1}$ and $T_{i+1,j-1}$, then the average traveltimes gradient is approximately:

$$\nabla T = \left(\frac{T_{i+1,j} - T_{i,j} - T_{i,j-1} + T_{i+1,j-1}}{2\delta x}, \frac{T_{i,j} - T_{i,j-1} - T_{i+1,j-1} + T_{i+1,j}}{2\delta z} \right) \quad (33)$$

A number of authors have developed schemes that draw on the basic idea of Vidale (1988); van Trier & Symes (1991) determine traveltimes on a regular grid using an upwind finite-difference method which solves a hyperbolic conservation law that describes changes in the gradient components of the traveltimes field. Podvin & Lecomte (1991) employ a method that uses Huygen's principle in the finite difference approximation; Faria & Stoffa (1994) propose a scheme that explicitly uses Fermat's Principle to determine first-arrivals on a gridded traveltimes field. These three methods are more suited to solution by massively parallel or vector computation than the methods of Vidale (1988) and Qin et al. (1992).

2.2.2.2 Fast marching method A problem with many of the eikonal grid-based methods (e.g. Vidale, 1988, 1990; Qin et al., 1992) is that they have numerical difficulties when the true wavefront is not differentiable. In other words, the first-arriving wavefront may contain kinks (discontinuities in gradient); this is particularly the case in complex velocity media where multi-pathing (the wavefront crosses itself) can occur. One way of addressing this problem is to search for “weak solutions” of Eq. 15. A weak solution to a differential equation is an entropy satisfying approximate solution that is not differentiable everywhere but satisfies an integral formulation of the equation. The key advantage of such a formulation is that more general solutions are permitted, in particular ones that don't necessarily satisfy the differentiability demands of the original equation.

The Fast Marching Method (FMM) of Sethian & Popovici (1999) for solving the eikonal equation on a 3-D grid uses this approach. In its simplest form, the FMM uses the first-order upwind difference scheme:

$$\begin{bmatrix} \max(D_{ijk}^{-x}T, -D_{ijk}^{+x}T, 0)^2 + \\ \max(D_{ijk}^{-y}T, -D_{ijk}^{+y}T, 0)^2 + \\ \max(D_{ijk}^{-z}T, -D_{ijk}^{+z}T, 0)^2 \end{bmatrix}^{\frac{1}{2}} = s_{ijk} \quad (34)$$

where the following finite difference operator notation is used:

$$D^{+x}T = \frac{T(x + \delta x) - T(x)}{\delta x} \quad (35)$$

$$D^{-x}T = \frac{T(x) - T(x - \delta x)}{\delta x} \quad (36)$$

and s_{ijk} is slowness at the grid point (i, j, k) . Eq. 34 is a non-linear equation (quadratic) for the traveltimes T_{ijk} . Of the two possible solutions, the larger value is always the correct value. The FMM of Sethian & Popovici (1999) systematically constructs traveltimes T in a downwind fashion from known values upwind using a narrow band method. The narrow band basically represents the propagating wavefront, and grid points are tagged as either *alive*, *close* or *far*, depending on whether

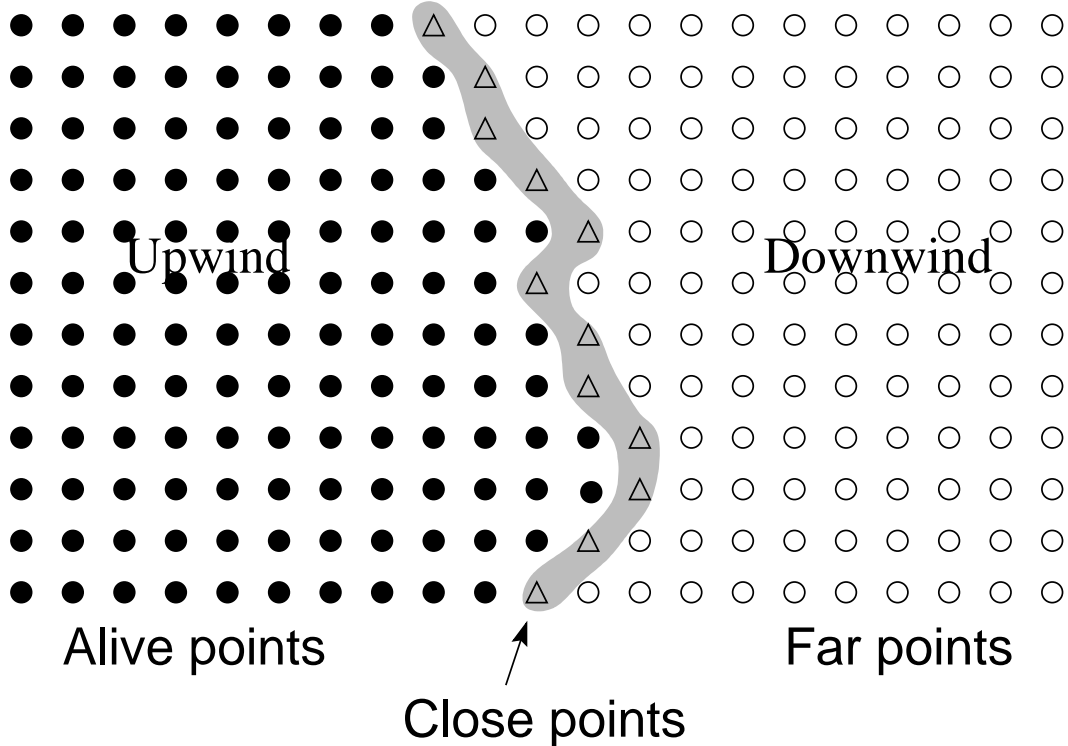


Figure 16: Principle of the narrow band method. *Alive* points have their traveltimes correctly calculated. *Close* points form a band about the *alive* points and have trial values. *Far* points have no values calculated. *Alive* points lie upwind of the narrow band while *far* points lie downwind.

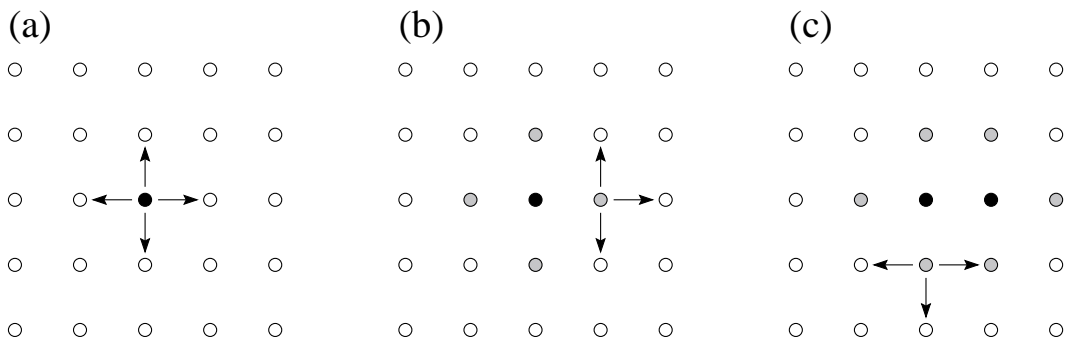


Figure 17: Principal of the FMM in 2-D. (a) Starting from the source point (black dot) in the center of a grid, traveltimes to the four neighboring grid points are determined using Eq. 34. (b) The smallest of these four values (grey dots) must be correct, so all *close* neighbors to this point that are not *alive* (white dots) have their values computed, and added to the narrow band defined by the grey dots. (c) The smallest of these six *close* points again must be correct, and all neighboring points have their values computed (or recomputed).

they have had the band pass through them, they are inside the band, or are yet to be touched by the band, respectively (see Fig. 16).

The FMM begins from a source point (or wavefront), and calculates the traveltimes at neighboring grid points using Eq. 34 (for example) to form the first stage of the narrow band. The point with minimum traveltime is then accepted as *alive* (i.e. it is a true first-arrival traveltime), and all neighboring points to this *alive* point are updated (if *close*) or calculated for the first time (if *far*), in

which case they become *close* and the narrow band progresses downwind (see Fig. 17). Choosing the *close* point with minimum traveltimes means that causality is satisfied. The key to an efficient implementation of the narrow band scheme is to be able to rapidly locate the *close* point with minimum traveltimes. Heap sorting of traveltimes using a binary tree (Sethian & Popovici, 1999) means that the FMM will have an efficiency of $O(N \log N)$ where N is the number of grid points. Fig. 18 shows a wavefront calculated using the FMM propagating through a complex 2-D velocity model. Source-receiver ray paths, calculated by following the steepest descent direction (using Eq. 33) through the computed traveltimes field from each receiver, are also shown. The velocity variations have been made extremely large to illustrate the robustness of the scheme, which remains stable despite the propagating wavefront exhibiting significant discontinuities in gradient.

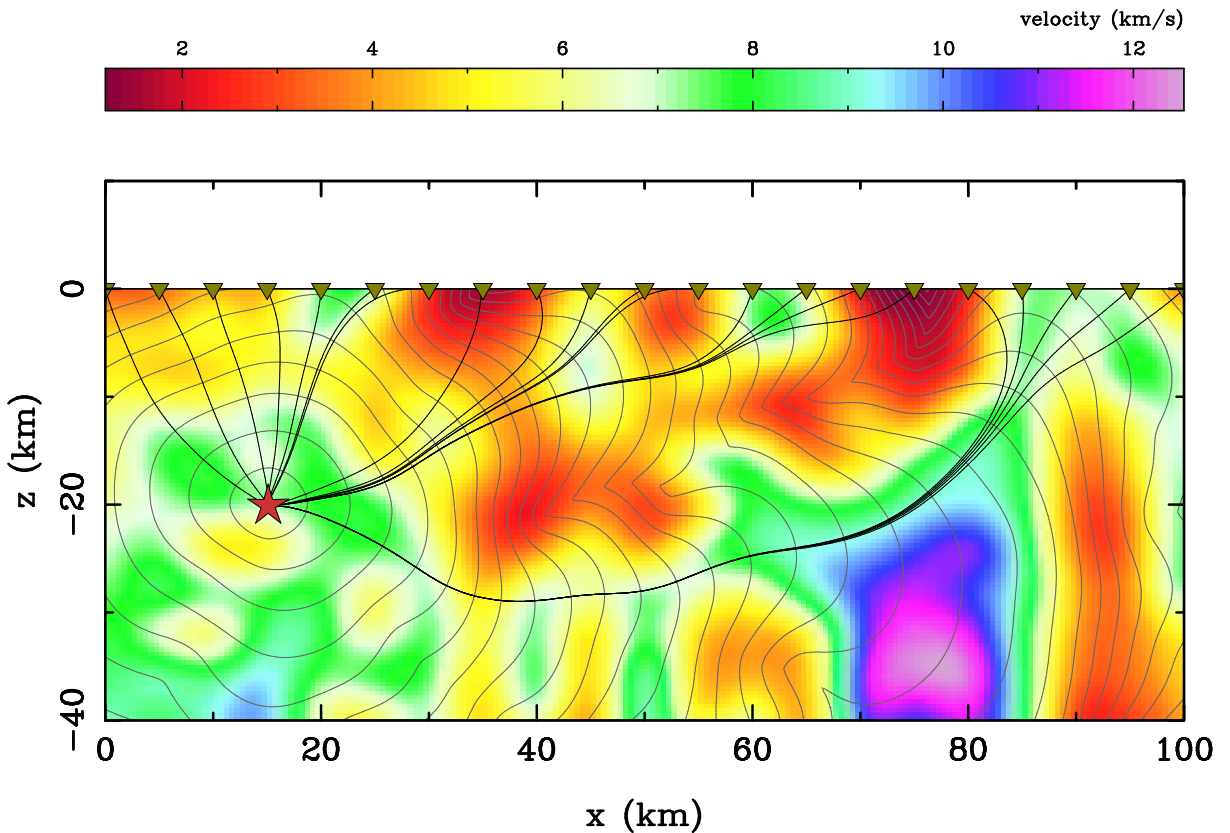


Figure 18: Example of the FMM in a complex 2-D velocity medium. The grid on which the eikonal equation is solved has a spacing of 200 m in both x and z ; the total number of points is 100,701. Wavefronts are shown by thin grey lines and are visualized at 0.5 s intervals; rays are denoted by black lines and are always perpendicular to the wavefronts.

To increase the accuracy of the FMM scheme without increasing the number of grid points, higher order differences may be used to approximate the traveltimes gradient (Popovici & Sethian, 2002). However, since causality must be respected, they cannot simply replace the first-order differences in all cases (Sethian, 1999). Kim (2001) advocates using the average normal slowness \hat{s}_{ijk} in place of s_{ijk} to increase accuracy since velocities specified at grid points don't account for the true variation across a cell. For point sources, Alkhalifah & Fomel (2001) suggest using a spherical rather than Cartesian grid since the latter tends to under-sample the wavefront near the source where curvature is high, and hence introduces traveltimes errors. This source of error occurs for any Car-

sian grid-based method that determines the traveltimes from a point source. Although the FMM scheme is yet to be applied to tomographic problems, we have described it in some detail because it is the first unconditionally stable eikonal scheme and will probably come into more common use in the near future.

Finite difference grid methods that solve the eikonal equation are generally much quicker (Vidale, 1988; Sethian & Popovici, 1999) than the ray tracing methods described in Section 2.2.1, especially for problems involving relatively few receivers and many sources or vice versa. They are designed to calculate first-arrival traveltimes, they find diffraction paths in shadow zones, and they can often work in regions of complex velocity (e.g. Sethian & Popovici, 1999). Ray methods do not necessarily find the first-arrival path and often fail in shadow zones. The grid-based methods can also determine the arrivals of head-waves and diffractions that cannot be found by conventional geometric ray tracing.

Finite-difference schemes do have their disadvantages, one of the principal being algorithm stability, although the FMM scheme recently introduced by Sethian & Popovici (1999) overcomes this problem. They also only locate first-arrivals, unless explicit conditions, such as reflections from an interface, are specified. While this is desirable in many cases, later arrivals can be of interest, such as in the generation of synthetic seismograms. Another disadvantage of grid methods is that the medium needs to be densely sampled by velocity nodes in order to achieve accurate traveltimes, with consequent demands on processing power and memory. For a 3-D problem, computation time will increase at least in proportion to M^3 where M is the number of nodes in one dimension. The increase in computation time for ray-tracing methods is generally not as dramatic. Regional and global studies, which often use a large number of model parameters, do not usually employ grid-based methods to find traveltimes and ray paths. Apart from computation time, specific phases (e.g. PcP , PP , PcS) which are not first-arrivals are sometimes used, which would also complicate the implementation of a grid method. Grid methods are also not common in teleseismic tomography, possibly because of the need to find ray paths from the source point to the model region through a global 1-D velocity model, a task easily accomplished by ray tracing. Similarly, examples of applications in local earthquake tomography are hard to find, although there doesn't seem to be any particular reason why grid methods are unsuited to this class of problem.

In contrast, finite difference solutions of the eikonal equation have been used frequently in the forward step of wide-angle traveltime inversions, especially in 3-D. Hole (1992) presents a method for the inversion of first-arrival traveltimes for 3-D velocity variation using a finite-difference approach. Hole et al. (1992) use a similar forward scheme in the inversion for interface structure using broadside refractions from the Queen Charlotte Basin, Canada. Also using finite-difference techniques, Riahi et al. (1997) invert wide-angle reflections for Moho structure beneath the Gulf of Bothnia and Zelt et al. (1996) invert both reflection and refraction traveltimes for velocity and interface structure beneath the southwestern Canadian Cordillera. Other studies to use finite difference solutions of the eikonal equation in 3-D wide-angle traveltime inversions include Zelt & Barton (1998), Zelt et al. (1999, 2001) and Day et al. (2001). Parsons et al. (1996) use a finite difference approach in the inversion of wide-angle traveltimes for the 2-D crustal structure of the Colorado Plateau.

2.2.3 Shortest Path Ray Tracing (SPR)

The shortest path or network method uses Fermat's principle directly to find the path of the first-arrival ray between source and receiver. To do this, a grid of nodes is specified within the velocity

medium and a network or graph is formed by connecting neighboring nodes with traveltime path segments. The first-arrival ray path between source and receiver will then correspond to the path through the network which has the least traveltime.

In a seminal paper by Nakanishi & Yamaguchi (1986), the velocity field is defined by a set of constant velocity blocks with network nodes placed on the interface between the blocks. Connection paths between adjacent nodes do not cross any cell boundaries (see Fig. 19a), so the traveltime t between two nodes is simply $t = ds$ where d is the distance between the two nodes and s is cell slowness. A similar approach is used by Fischer & Lees (1993). Moser (1991) uses a rectangular grid with the network nodes coinciding with the velocity nodes (see Fig. 19b). The traveltime between two connected nodes is estimated by $t = d(s_1 + s_2)/2$ where s_1 and s_2 are the slowness at the two nodes.

Once the network structure and method of traveltime determination between two nodes has been chosen, the next step is to use a shortest path algorithm to locate the ray path. Essentially, the problem is to locate the path of minimum traveltime from all the possible paths between source and receiver through the given network. An algorithm that is often used in network theory is that of Dijkstra (1959) for which computation time is proportional to the number of nodes squared.

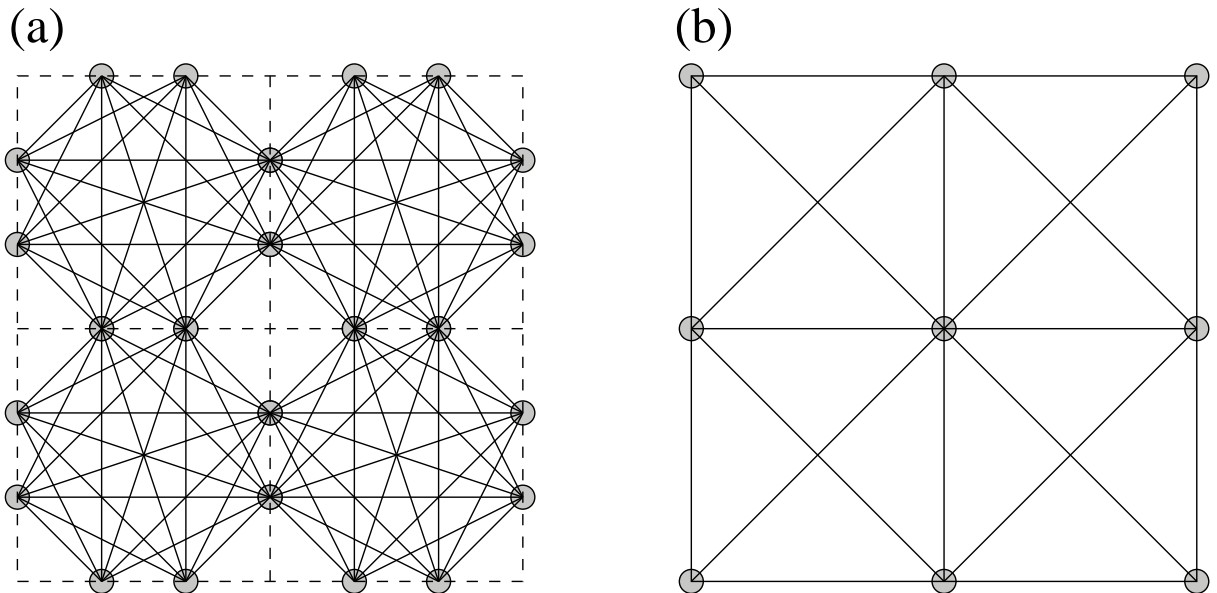


Figure 19: Two types of node arrangements for an SPR network (after Moser, 1991). Connectors are indicated by solid lines in both cases. (a) Network nodes along constant slowness cell boundaries (dashed). (b) Network nodes that coincide with velocity nodes.

Errors in SPR are due to the finite node spacing and angular distribution of node connectors (Moser, 1991). A coarse grid of nodes may poorly approximate the velocity variations while a limited range of angles between adjacent connectors may result in a poor approximation to the true path. Obviously, increasing the number of nodes and connectors will result in superior solutions but may come at a significant computational cost. Much work has been done to increase the computational speed of the shortest path algorithm, with particular attention given to the use of efficient sorting algorithms (Moser, 1991; Klimeš & Kvasnička, 1994; Cheng & House, 1996; Zhang & Toksöz, 1998).

SPR will by definition find the first-arrival traveltime between any given source and receiver.

However, it is possible to impose constraints on the path so that some other arrivals such as reflections or multiples can be determined. Moser (1991) demonstrated a method for reflections which requires the shortest path to visit a specified set of nodes that lie on the interface.

In their original implementation of SPR, Nakanishi & Yamaguchi (1986) inverted traveltimes from local earthquakes, while Zhang & Toksöz (1998) used it in the inversion of refraction traveltimes. Toomey et al. (1994) inverted first-arrival refraction traveltimes for 3-D crustal velocity structure using a scheme similar to that of Moser (1991) to solve the forward problem. Apart from these examples, the use of SPR in tomographic inversions is not common. SPR shows similar advantages to finite differences (see Section 2.2.2) relative to conventional ray tracing methods. It can correctly locate diffraction paths and head waves and always finds first-arrivals. The main advantage SPR has over most finite difference methods is robustness; it is capable of working in highly complex media. Cheng & House (1996) claim it to be the most robust numerical scheme for traveltime calculations, although the introduction of the FMM challenges this claim. SPR methods also tend to be slower than eikonal methods.

2.3 Solving the Inverse Step

The inversion step, which involves the adjustment of the model parameters \mathbf{m} to better satisfy the observed data \mathbf{d}_{obs} through the known relationship $\mathbf{d} = \mathbf{g}(\mathbf{m})$, can be performed in a number of ways. In traveltime tomography, the functional \mathbf{g} is non-linear because the ray path depends on the velocity structure. Ideally, an inversion scheme should account for this non-linearity. The three approaches to solving the inversion step that will be considered below are backprojection, gradient methods and global optimization techniques.

2.3.1 Backprojection

In Section 1.2, we showed that the perturbation of a ray path only has a second order effect on traveltime. In terms of slowness, this was written (see Eq. 7):

$$\delta t = \int_{L_0} \delta s(\mathbf{x}) dl + O(\delta s(\mathbf{x})^2) \quad (37)$$

If a continuum is described by M constant slowness blocks, then the discrete form of Eq. 37 for N rays can be written:

$$\mathbf{d} = \mathbf{G}\mathbf{m} \quad (38)$$

where \mathbf{d} are the traveltime residuals, \mathbf{m} the slowness perturbations and \mathbf{G} an $N \times M$ matrix of ray lengths l_{ij} corresponding to the distance traversed by each ray in each block. Note that for the general case \mathbf{m} (e.g. velocity nodes, interface depths etc.) in Eq. 38, $\mathbf{G} = \partial\mathbf{g}/\partial\mathbf{m}$ where $\mathbf{g}(\mathbf{m})$ is the model prediction. Many of the elements of \mathbf{G} will be zero since each ray path will usually only traverse a small subset of the M blocks. Backprojection methods can be used to solve Eq. 38 for the slowness perturbations \mathbf{m} by iteratively mapping traveltime anomalies into slowness perturbations along the ray paths until the data are satisfied. Backprojection methods generally use constant slowness (or velocity) blocks. Two well known backprojection techniques for solving Eq. 38 are the Algebraic Reconstruction Technique (ART) and the Simultaneous Iterative Reconstruction Technique (SIRT), both of which originate from medical imaging.

In ART, the model is updated on a ray by ray basis. The residual d_n for the n^{th} ray path is distributed along the path by adjusting each component of \mathbf{m} in proportion to the length l_{nj} of the ray segment in the j^{th} cell:

$$m_j^{k+1} = m_j^k + \frac{t_n^{k+1} l_{nj}}{\sum_{m=1}^M l_{nm}^2} \quad (39)$$

where $t_n^{k+1} = d_n - t_n^k$ is the difference between the residuals at the 0^{th} and k^{th} iteration, m_j^k is the approximation to the j^{th} model parameter at the k^{th} iteration, $m_j^1 = 0$ and $t_n^1 = 0$. The residual along the $(n+1)^{th}$ ray is then determined for the updated velocity field \mathbf{m} using the original path and is backprojected in the same manner. A single iteration of the method consists of performing this backprojection for the N ray paths. Rays are then retraced and the backprojection repeated until the data are satisfied to within tolerance, or the solution converges. The main problem with ART is that it suffers from poor convergence properties (Blundell, 1993). It has been used by McMechan (1983) in cross-hole tomography and Nakanishi & Yamaguchi (1986) in local earthquake tomography.

SIRT addresses some of the convergence problems associated with ART by averaging the perturbations applied to each parameter from all the rays that are influenced by the parameter. Thus, the SIRT algorithm may be written (Blundell, 1993):

$$m_j^{k+1} = m_j^k + \frac{1}{R_j^k} \sum_{n=1}^{R_j^k} \left[\frac{t_n^{k+1} l_{nj}}{\sum_{m=1}^M l_{nm}^2} \right] \quad (40)$$

where R_j^k is the number of rays that the j^{th} model parameter influences for the k^{th} iteration. The SIRT method has been used in the inversion of teleseismic traveltimes by Dueker et al. (1993), Granet & Trampert (1989) and McQueen & Lambeck (1996). Blundell (1993) used SIRT (as well as other methods) in the inversion of reflection traveltimes for both velocity structure and interface depth.

Authors who have used variants of these backprojection schemes include Humphreys & Clayton (1990), Hole (1992) and Zelt & Barton (1998). Humphreys & Clayton (1990) used block subbinning, filtering and spatial averaging in the backprojected inversion of teleseismic traveltimes. Block subbinning reduces the weight of rays that come from dominant directions, and thus reduces blurring of the image along these paths. Filtering is done using point spread functions to reduce the natural tendency of backprojection to blur an image if resolution is not perfect, and spatial averaging is used to smooth the solution. Hole (1992) also uses smoothing in the backprojected inversion of wide-angle traveltimes. Zelt & Barton (1998), in their 3-D wide-angle seismic inversion method, implement several other modifications aimed at improving the convergence and accuracy of backprojection.

Inversion using backprojection tends to be computationally more rapid at each iteration compared to other techniques, but often converges more slowly and with less stability. This is at least partly due to the use of more *ad hoc* regularization (like spatial averaging) compared to, for example, the formal inclusion of such constraints in the inversion permitted by gradient methods.

2.3.2 Gradient Methods

The inverse problem in seismic tomography can be formulated as one of minimizing an objective function consisting of a data residual term and one or more regularization terms. As before, let \mathbf{d} denote a data vector of length N which is dependent on a model vector \mathbf{m} of length M as $\mathbf{d} = \mathbf{g}(\mathbf{m})$. For an initial estimate \mathbf{m}_0 of the model parameters, comparing $\mathbf{d} = \mathbf{g}(\mathbf{m}_0)$ with the observed traveltimes \mathbf{d}_{obs} gives an indication of the accuracy of the model. The misfit can be quantified by constructing an objective function $S(\mathbf{m})$, consisting of a weighted sum of data misfit and regularization terms, that is to be minimized.

An essential component of the objective function is a term $\Psi(\mathbf{m})$ which measures the difference between the observed and predicted data. If it is assumed that the error in the relationship $\mathbf{d}_{obs} \approx \mathbf{g}(\mathbf{m}_{true})$ is Gaussian, then a least squares or L_2 measure of this difference is suitable:

$$\Psi(\mathbf{m}) = \|\mathbf{g}(\mathbf{m}) - \mathbf{d}_{obs}\|^2 \quad (41)$$

If uncertainty estimates have been made for the observed data (usually based on picking error), then more accurate data are given a greater weight in the objective function by writing $\Psi(\mathbf{m})$ as:

$$\Psi(\mathbf{m}) = (\mathbf{g}(\mathbf{m}) - \mathbf{d}_{obs})^T \mathbf{C}_d^{-1} (\mathbf{g}(\mathbf{m}) - \mathbf{d}_{obs}) \quad (42)$$

where \mathbf{C}_d is a data covariance matrix. If the errors are assumed to be uncorrelated, then $\mathbf{C}_d = [\delta_{ij}(\sigma_d^j)^2]$ where σ_d^j is the uncertainty of the j^{th} traveltime. Strictly speaking, \mathbf{C}_d is best referred to as a data weighting matrix rather than a data covariance matrix unless it truly reflects the uncertainty associated with the data. A major weakness in this definition of data misfit is that the L_2 -norm is sensitive to outliers. This means that if only a few data have spurious values (e.g. from incorrect phase identification), then they will have a significant influence on the size of $\Psi(\mathbf{m})$ since each residual is squared; the L_2 -norm is a non-robust measure. A solution produced by the minimization of $\Psi(\mathbf{m})$ is then likely to be less reliable than one produced using, for example, an L_1 norm (Menke, 1989). Despite this weakness, most inversion methods appeal to Gaussian statistics and adopt an L_2 norm. See Claerbout & Muir (1973) for a discussion of robustness in error distribution.

A common problem with tomographic inversion is that not all model parameters will be well constrained by the data alone (i.e. the problem may be under-determined or mixed-determined). A regularization term $\Phi(\mathbf{m})$ is often included in the objective function to provide additional constraints on the model parameters, thereby reducing the non-uniqueness of the solution. The regularization term is typically defined as:

$$\Phi(\mathbf{m}) = (\mathbf{m} - \mathbf{m}_0)^T \mathbf{C}_m^{-1} (\mathbf{m} - \mathbf{m}_0) \quad (43)$$

where \mathbf{C}_m is an *a priori* model covariance matrix. If uncertainties in the initial model are assumed to be uncorrelated, then $\mathbf{C}_m = [\delta_{ij}(\sigma_m^j)^2]$ where σ_m^j is the uncertainty associated with the j^{th} model parameter of the initial model. Again, this should really be referred to as a model weighting matrix unless its entries reflect the true statistical uncertainties of the initial model. The effect of $\Phi(\mathbf{m})$ is to encourage solution models \mathbf{m} that are near a reference model \mathbf{m}_0 . The values used in \mathbf{C}_m are usually based on prior information.

Another approach to regularization is the minimum structure solution (Constable et al., 1987) which attempts to find an acceptable trade-off between satisfying the data and finding a model with the minimum amount of structural variation. One way of including this requirement in the objective function is to use the term (Sambridge, 1990):

$$\Omega(\mathbf{m}) = \mathbf{m}^T \mathbf{D}^T \mathbf{D} \mathbf{m} \quad (44)$$

where \mathbf{Dm} is a finite difference estimate of a specified spatial derivative. For example, if m_1, m_2, \dots, m_M represent contiguous depth nodes of an interface in 2-D space, then the gradient of the interface could be regulated using:

$$\mathbf{Dm} = \begin{bmatrix} -1 & 1 & 0 & \dots & \dots & 0 \\ 0 & -1 & 1 & 0 & \dots & 0 \\ \dots & 0 & \dots & \dots & \dots & \dots \\ \dots & \dots & \dots & \dots & \dots & \dots \\ \dots & \dots & \dots & 0 & -1 & 1 \\ \dots & \dots & \dots & 0 & 0 & 0 \end{bmatrix} \begin{bmatrix} m_1 \\ m_2 \\ m_3 \\ \dots \\ m_{M-1} \\ m_M \end{bmatrix} \quad (45)$$

Alternatively, the curvature of the interface could be regulated using:

$$\mathbf{Dm} = \begin{bmatrix} 0 & 0 & 0 & 0 & \dots & 0 \\ 1 & -2 & 1 & 0 & \dots & 0 \\ 0 & 1 & -2 & 1 & \dots & \dots \\ \dots & \dots & \dots & \dots & \dots & \dots \\ \dots & \dots & \dots & 1 & -2 & 1 \\ \dots & \dots & \dots & 0 & 0 & 0 \end{bmatrix} \begin{bmatrix} m_1 \\ m_2 \\ m_3 \\ \dots \\ m_{M-1} \\ m_M \end{bmatrix} \quad (46)$$

An explicit smoothing term such as Eq. 46 in the objective function may be necessary if crude parameterizations such as constant velocity blocks are used to simulate a continuously varying velocity field. However, if an implicitly smooth parameterization like cubic splines is used, then an explicit smoothing term may be unnecessary. In other words, the same smooth result could be achieved by reducing the number of parameters and hence the size of the inverse problem. The appropriate number of parameters required to represent the model for a given dataset could be chosen on a statistical basis, such as employing the F test (Menke, 1989).

Using the L_2 terms described above in Equations 42 - 44, the objective function $S(\mathbf{m})$ can be written in full as:

$$S(\mathbf{m}) = \frac{1}{2} [\Psi(\mathbf{m}) + \epsilon\Phi(\mathbf{m}) + \eta\Omega(\mathbf{m})] \quad (47)$$

where ϵ is referred to as the *damping factor* and η as the *smoothing factor* (when \mathbf{D} is the second derivative operator, which is usually the case). Multiplication of all terms by 1/2 is done simply to prevent the expressions for the first and second derivatives of S having all elements multiplied by 2 (see Eq. 49 and Eq. 50). ϵ and η govern the trade-off between how well the solution \mathbf{m}_{est} will satisfy the data, how closely \mathbf{m}_{est} is to \mathbf{m}_0 , and the smoothness of \mathbf{m}_{est} . There are several means for choosing appropriate values for ϵ and η . One way is to use the largest values of ϵ and η for which the data are still satisfied, but there will be a trade-off between ϵ and η . When only damping or smoothing is invoked, then this approach is simpler to implement. However, it may be that the relationship between the data fit and the model perturbation or model roughness is highly non-linear, in which case this criterion may not be robust. A better approach is to inspect the trade-off curves between data fit and model roughness (or perturbation) for different values of η (or ϵ), as shown schematically in Fig. 20. If both η and ϵ are non-zero, then a contour plot which shows traveltimes fit contoured on a plot of model roughness vs. model perturbation (Fig. 21) could be used, but the main drawback here is the considerable computational effort required. An alternative approach is to perform a synthetic reconstruction using the same source-receiver geometry as the real experiment. The appropriate amount of damping and smoothing would then be given by the values of η and ϵ which resulted in the most accurate reconstruction of the synthetic model.

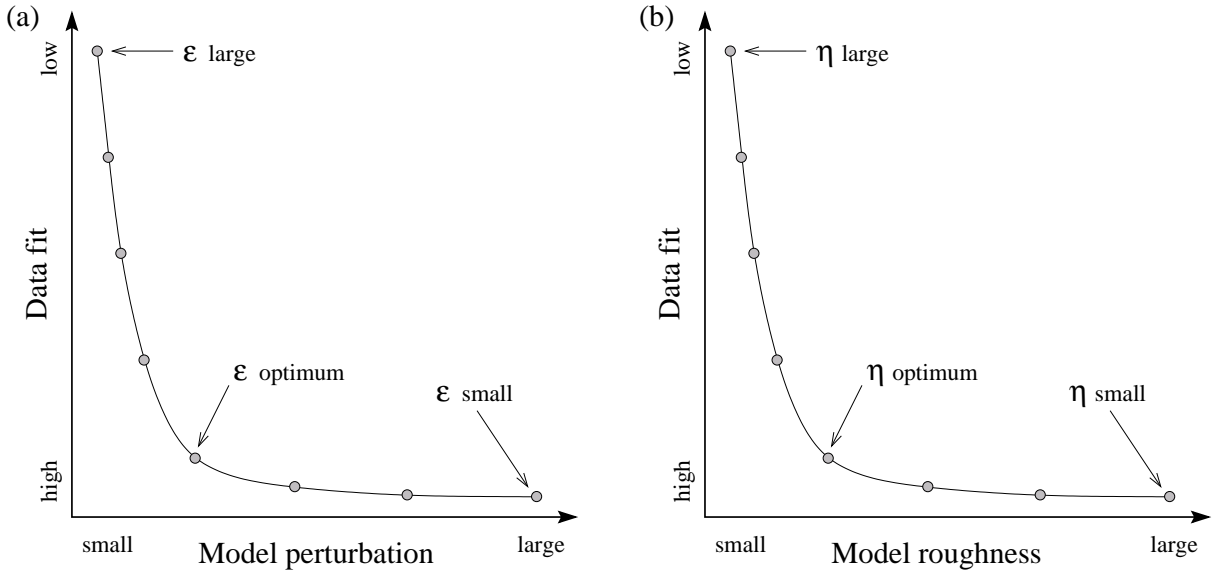


Figure 20: Schematic illustration of trade-off curves that could be used to choose appropriate damping or smoothing parameters for an inversion. A number of separate (eight in these examples) inversions with different values of ϵ or η are required in order to construct these curves. (a) Data fit vs. model perturbation for different values of ϵ . (b) Data fit vs. model roughness for different values of η .

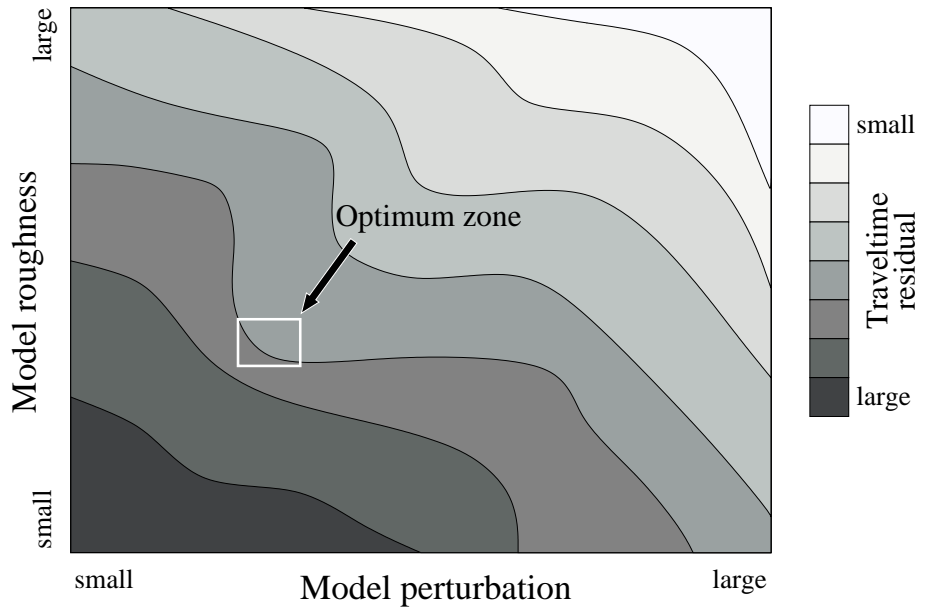


Figure 21: Possible scheme for choosing ϵ and η simultaneously. Contours of traveltme misfit for a set of solution models are plotted on a graph of model perturbation vs. model roughness. The optimum region has low roughness and model perturbation but adequately satisfies the data. Computational effort is the main drawback of this approach.

Many studies involving the tomographic inversion of real data use a semi-quantitative approach to choosing η and/or ϵ (or other trade-off parameters) like those outlined above (e.g. Oncescu et al., 1984; White, 1989; Neele et al., 1993; Steck et al., 1998; Graeber & Asch, 1999; Rawlinson et al., 2001a). At this stage, it is important to point out that the objective function expressed in Eq. 47 in a sense juxtaposes two different regularization frameworks: Bayesian and Occam's. In a Bayesian-

style inversion, knowledge of *a priori* information is of paramount importance. To properly honor this approach, smoothing would be ignored (i.e. set $\eta=0$), the data covariance matrix would reflect the known statistical properties of the data and the initial model estimate would be based on *a priori* model information. In addition, we would set $\epsilon = 1$ since the *a priori* model covariance matrix would reflect the uncertainties associated with the *a priori* information. Minimization of the objective function then results in a solution that assimilates the information contained in the data with the *a priori* information, resulting in an *a posteriori* model distribution. The posterior model uncertainties should then be less than the prior uncertainties, which is the desired outcome (how much less depends on how good the data are). The principal difficulty with this approach is that meaningful *a priori* information concerning model and data errors is difficult to obtain in practice. Nevertheless, this Bayesian approach has been adopted by a number of authors (e.g. Aki et al., 1977; Lutter & Nowack, 1990). Scales & Snieder (1997) discuss the merits and difficulties of adopting a Bayesian framework for inversion.

The other regularization framework is suggested by Occam's principle of seeking a solution with the least structure necessary to fit the data (Constable et al., 1987). In this case $\epsilon = 0$ since we don't want the initial model, whose accuracy is poorly known, to unduly influence the solution model. This type of scheme is also popular (e.g. Sambridge, 1990; Zelt & Barton, 1998; Day et al., 2001). Often, however, a mixture of both frameworks is used, in which case one seeks a physically reasonable model that contains no unnecessary structure, is not highly perturbed from the initial model and satisfies the data. This explains to some extent why the choice of ϵ and η is often subjective.

Gradient-based inversion methods make use of the derivatives of $S(\mathbf{m})$ at a specified point in model space. A basic assumption that is shared by all practical gradient methods is that $S(\mathbf{m})$ is sufficiently smooth to allow a local quadratic approximation about some current model:

$$S(\mathbf{m} + \delta\mathbf{m}) \approx S(\mathbf{m}) + \hat{\boldsymbol{\gamma}}\delta\mathbf{m} + \frac{1}{2}\delta\mathbf{m}^T \hat{\mathbf{H}}\delta\mathbf{m} \quad (48)$$

where $\delta\mathbf{m}$ is a perturbation to the current model and $\hat{\boldsymbol{\gamma}} = \partial S / \partial \mathbf{m}$ and $\hat{\mathbf{H}} = \partial^2 S / \partial \mathbf{m}^2$ are the gradient vector and Hessian matrix respectively. Evaluating these partial derivatives for Eq. 47 gives:

$$\hat{\boldsymbol{\gamma}} = \mathbf{G}^T \mathbf{C}_d^{-1} [\mathbf{g}(\mathbf{m}) - \mathbf{d}_{obs}] + \epsilon \mathbf{C}_m^{-1} (\mathbf{m} - \mathbf{m}_0) + \eta \mathbf{D}^T \mathbf{D} \mathbf{m} \quad (49)$$

$$\hat{\mathbf{H}} = \mathbf{G}^T \mathbf{C}_d^{-1} \mathbf{G} + \nabla_{\mathbf{m}} \mathbf{G}^T \mathbf{C}_d^{-1} [\mathbf{g}(\mathbf{m}) - \mathbf{d}_{obs}] + \epsilon \mathbf{C}_m^{-1} + \eta \mathbf{D}^T \mathbf{D} \quad (50)$$

where $\mathbf{G} = \partial \mathbf{g} / \partial \mathbf{m}$ is the Fréchet matrix of partial derivatives calculated during the solution of the forward problem. As mentioned earlier, for the case of constant slowness blocks, $\mathbf{G} = [l_{ij}]$ where l_{ij} is the ray segment length of the i^{th} ray in the j^{th} block. Usually, the second derivative term in $\hat{\mathbf{H}}$ is neglected since it is time consuming to evaluate, and its effect is small if $\mathbf{g}(\mathbf{m}) - \mathbf{d}_{obs}$ is small, or if the forward problem is quasi-linear ($\nabla_{\mathbf{m}} \mathbf{G} \approx 0$). Both $\hat{\boldsymbol{\gamma}}$ and $\hat{\mathbf{H}}$ do not lie in model space, but in the dual of model space (Tarantola, 1987). If $\boldsymbol{\gamma}$ is the steepest ascent vector in model space then $\boldsymbol{\gamma} = \mathbf{C}_m \hat{\boldsymbol{\gamma}}$ and \mathbf{H} , the curvature operator in model space, is $\mathbf{H} = \mathbf{C}_m \hat{\mathbf{H}}$.

Since \mathbf{g} is generally non-linear, the minimization of Eq. 47 requires an iterative approach:

$$\mathbf{m}_{n+1} = \mathbf{m}_n + \delta\mathbf{m}_n \quad (51)$$

where \mathbf{m}_0 is the initial model. The objective function is minimized for the current ray path estimate at each step to produce \mathbf{m}_{n+1} , after which new ray paths are computed for the next iteration. The iterations cease either when the observed traveltimes are satisfied or when the change in $S(\mathbf{m})$ with

iteration gets sufficiently small. A useful measure of data fit is provided by the normalized χ^2 misfit function defined by:

$$\chi^2 = \frac{1}{N} \sum_{i=1}^N \left(\frac{d_m^i - d_{obs}^i}{\sigma_d^i} \right)^2 \quad (52)$$

where $\{d_m^i\} = \mathbf{g}(\mathbf{m})$, $\{d_{obs}^i\}$ is the set of observed data and $\{\sigma_d^i\}$ are the traveltimes uncertainties (or weights). An inversion solution fits the data to the level of the noise when $\chi^2 = 1$. Once this value is achieved, there is little point in continuing with the iterative inversion process. However, Eq. 52 measures the data fit in an average sense, and it is still possible to have $\chi^2 < 1$ while one or more model traveltimes residuals are larger than their respective error estimates. If the data misfit does not fall below $\chi^2 = 1$, then statistical hypothesis testing (e.g. Kreyszig, 1993) can be used to stop the iterative process. For example, if the data misfit has a normal distribution, we can test whether the data variance at iteration n is significantly different from the variance at iteration $n + 1$ (usually referred to as an F -test). The F -test has been used by numerous authors (e.g. Thurber, 1983; Eberhart-Phillips, 1986; Steck et al., 1998; Graeber & Asch, 1999).

The following gradient-based inversion methods can be used to determine $\delta\mathbf{m}_n$ in Eq. 51.

2.3.2.1 Gauss-Newton method and damped-least squares The Gauss-Newton method locates the updated point \mathbf{m}_{n+1} by finding the minimum of the tangent paraboloid to $S(\mathbf{m})$ at \mathbf{m}_n . At the minimum of S , the gradient will vanish, so \mathbf{m} is required such that:

$$\mathbf{F}(\mathbf{m}) = \mathbf{G}^T \mathbf{C}_d^{-1} (\mathbf{g}(\mathbf{m}) - \mathbf{d}_{obs}) + \epsilon \mathbf{C}_m^{-1} (\mathbf{m} - \mathbf{m}_0) + \eta \mathbf{D}^T \mathbf{D} \mathbf{m} = 0 \quad (53)$$

where $\mathbf{F}(\mathbf{m}) = \hat{\gamma}$. If we are at some point \mathbf{m}_n , then a more accurate estimate \mathbf{m}_{n+1} can be obtained using a Taylor series expansion of Eq. 53 and ignoring second order terms:

$$F_i(m_{n+1}^1, \dots, m_{n+1}^M) = F_i(m_n^1, \dots, m_n^M) + \sum_{j=1}^M (m_{n+1}^j - m_n^j) \left. \frac{\partial F_i}{\partial m^j} \right|_{\mathbf{m}_n} = 0 \quad (54)$$

which may be rewritten as:

$$\mathbf{m}_{n+1} = \mathbf{m}_n - \left[\frac{\partial \mathbf{F}}{\partial \mathbf{m}} \right]_n^{-1} [\mathbf{F}_n] = \mathbf{m}_n - \left[\frac{\partial^2 S}{\partial \mathbf{m}^2} \right]_n^{-1} \left[\frac{\partial S}{\partial \mathbf{m}} \right]_n \quad (55)$$

where $(\partial S / \partial \mathbf{m})_n$ is the gradient vector and $(\partial^2 S / \partial \mathbf{m}^2)_n$ is the Hessian matrix. Substituting Eq. 49 and Eq. 50 into Eq. 55 gives the Gauss-Newton solution:

$$\begin{aligned} \delta\mathbf{m}_n = & -[\mathbf{G}_n^T \mathbf{C}_d^{-1} \mathbf{G}_n + \nabla_{\mathbf{m}} \mathbf{G}_n^T \mathbf{C}_d^{-1} (\mathbf{g}(\mathbf{m}_n) - \mathbf{d}_{obs}) + \epsilon \mathbf{C}_m^{-1} + \eta \mathbf{D}^T \mathbf{D}]^{-1} \\ & \times [\mathbf{G}_n^T \mathbf{C}_d^{-1} [\mathbf{g}(\mathbf{m}_n) - \mathbf{d}_{obs}] + \epsilon \mathbf{C}_m^{-1} (\mathbf{m}_n - \mathbf{m}_0) + \eta \mathbf{D}^T \mathbf{D} \mathbf{m}_n] \end{aligned} \quad (56)$$

As mentioned earlier, the second derivative term in the Hessian matrix is usually ignored, which gives the quasi-Newton solution:

$$\begin{aligned} \delta\mathbf{m}_n = & -[\mathbf{G}_n^T \mathbf{C}_d^{-1} \mathbf{G}_n + \epsilon \mathbf{C}_m^{-1} + \eta \mathbf{D}^T \mathbf{D}]^{-1} [\mathbf{G}_n^T \mathbf{C}_d^{-1} [\mathbf{g}(\mathbf{m}_n) - \mathbf{d}_{obs}] \\ & + \epsilon \mathbf{C}_m^{-1} (\mathbf{m}_n - \mathbf{m}_0) + \eta \mathbf{D}^T \mathbf{D} \mathbf{m}_n] \end{aligned} \quad (57)$$

Straightforward implementation of this method requires an $M \times M$ matrix equation to be solved. If the number of model parameters is large, the solution will be computationally expensive, and if data coverage is poor, the problem may well be ill-conditioned.

If instead we assume that the relationship $\mathbf{d} = \mathbf{g}(\mathbf{m})$ is linearizable then (c.f. Eq. 38):

$$\mathbf{d}_{obs} \approx \mathbf{g}(\mathbf{m}_0) + \mathbf{G}(\mathbf{m} - \mathbf{m}_0) \quad (58)$$

or $\delta\mathbf{d} = \mathbf{G}\delta\mathbf{m}$ with $\delta\mathbf{d} = \mathbf{d}_{obs} - \mathbf{g}(\mathbf{m}_0)$ and $\delta\mathbf{m} = \mathbf{m} - \mathbf{m}_0$ (i.e. Eq. 38 with $\mathbf{G} = \partial\mathbf{g}/\partial\mathbf{m}$). If Eq. 58 is exactly linear, then the Newton and quasi-Newton solutions are the same because the second derivative terms in the Hessian matrix are zero. Because a one-step solution is possible in the linear case, the objective function is sometimes written:

$$S(\mathbf{m}) = \frac{1}{2} \left[(\mathbf{G}\delta\mathbf{m} - \delta\mathbf{d})^T \mathbf{C}_d^{-1} (\mathbf{G}\delta\mathbf{m} - \delta\mathbf{d}) + \epsilon \delta\mathbf{m}^T \mathbf{C}_m^{-1} \delta\mathbf{m} + \eta \delta\mathbf{m}^T \mathbf{D}^T \mathbf{D} \delta\mathbf{m} \right] \quad (59)$$

where last term on the RHS smooths the perturbations to the prior model. The functional in this case is:

$$\mathbf{F}(\mathbf{m}) = \mathbf{G}^T \mathbf{C}_d^{-1} (\mathbf{G}\delta\mathbf{m} - \delta\mathbf{d}) + \epsilon \mathbf{C}_m^{-1} \delta\mathbf{m} + \eta \mathbf{D}^T \mathbf{D} \delta\mathbf{m} = 0 \quad (60)$$

and the solution can be written as:

$$\delta\mathbf{m} = [\mathbf{G}^T \mathbf{C}_d^{-1} \mathbf{G} + \epsilon \mathbf{C}_m^{-1} + \eta \mathbf{D}^T \mathbf{D}]^{-1} \mathbf{G}^T \mathbf{C}_d^{-1} \delta\mathbf{d} \quad (61)$$

When no smoothing is used ($\eta = 0$) and the matrices \mathbf{C}_d and \mathbf{C}_m represent the known *a priori* error statistics, then Eq. 61 becomes:

$$\delta\mathbf{m} = [\mathbf{G}^T \mathbf{C}_d^{-1} \mathbf{G} + \mathbf{C}_m^{-1}]^{-1} \mathbf{G}^T \mathbf{C}_d^{-1} \delta\mathbf{d} \quad (62)$$

which is the maximum likelihood solution to the inverse problem or the *stochastic inverse* (Aki et al., 1977). The expressions for $\delta\mathbf{m}$ in Eq. 57, Eq. 61 or Eq. 62 are often referred to as Damped Least Squares (DLS) solutions to the inverse problem (particularly when $\eta = 0$).

It is interesting to note the differences between the solution given by Eq. 57 and Eq. 61. First, the smoothing term in Eq. 61 smoothes the perturbations to the model, not the model itself. Second, if Eq. 61 is applied iteratively, then the damping regularization is not necessarily the same as that imposed by the iterative implementation of Eq. 57. In the latter, the term \mathbf{m}_0 usually represents the initial or starting model and the effect of the regularization is to favor a solution near the initial model (how “near” will depend on the value of ϵ). If, however, $\mathbf{m}_0 = \mathbf{m}_{prior}$, where \mathbf{m}_{prior} is the solution at the previous iteration, then the damping in Eq. 57 will be the same as that for Eq. 61, in which the misfit of the current model compared to the previous model is regulated. In damping, the use of \mathbf{m}_0 is often referred to as “jumping” while using \mathbf{m}_{prior} is often referred to as “creeping” (Shaw & Orcutt, 1985). Similarly, smoothing the perturbation to the model is “creeping” while smoothing the model is “jumping”. The DLS-type solution scheme is the technique most commonly used to solve the inverse step in seismic tomography. Many other variants to those discussed above have also been used - Spakman (1993) describes and compares several of them.

Studies that have used a DLS-type solution to the inverse problem in teleseismic tomography include those by Aki et al. (1977), Zhao et al. (1994), Weiland et al. (1995), Wiggins et al. (1996) and Steck et al. (1998). Authors who have used DLS solutions to invert wide-angle traveltimes include Kanasewich & Chiu (1985), Chiu et al. (1986), Farra & Madariaga (1988), White (1989), Lutter &

Nowack (1990), Lutter et al. (1990), Zelt & Smith (1992), Lutter et al. (1994), Kosloff et al. (1996), Wang & Braile (1996), McCaughey & Singh (1997) and Zelt & Barton (1998). Similarly, DLS is also popular in local earthquake tomography (Aki & Lee, 1976; Thurber, 1983; Eberhart-Phillips, 1986; Zhao et al., 1992; Graeber & Asch, 1999).

The most computationally expensive part of the DLS solution is to solve a matrix equation of dimension M . If the number of parameters is not large, then the solution may be found using methods like LU decomposition (Press et al., 1992) or Cholesky decomposition (Tarantola, 1987). A particularly useful solution technique for small to mid-size problems is Singular Value Decomposition (Press et al., 1992) or SVD. It is capable of robustly dealing with matrices that are singular or nearly singular, which is often the case in tomographic problems. In addition, SVD can be used to diagnose problems with the system of equations, such as the presence of equations that do not help constrain the solution. Another attractive feature of SVD is that covariance and resolution estimates associated with the solution model may be obtained at virtually no extra cost (e.g. White, 1989).

For models defined by large numbers of parameters, direct solution methods are cumbersome and iterative techniques are more practical. One such method is the conjugate gradient method of Hestenes & Stiefel (1952), which is able to take advantage of the sparse nature of linear systems commonly associated with seismic tomography problems (Scales, 1987). Conjugate gradients and LSQR, a variant of the conjugate gradient algorithm, are probably the most commonly used methods for solving linear systems of the form of Eq. 61 with a large number (e.g. 1000's - 100,000's) of unknowns (Nolet, 1985; Scales, 1987; VanDecar & Snieder, 1994).

The DLS-type solution to the inverse problem need not be formulated as a set of normal equations, such as Eq. 57 or Eq. 62. For example, Eq. 59 may be minimized by finding the least squares solution of the system:

$$\begin{bmatrix} \mathbf{C}_d^{-1/2} \mathbf{G} \\ \sqrt{\epsilon} \mathbf{C}_m^{-1/2} \\ \sqrt{\eta} \mathbf{D} \end{bmatrix} \delta \mathbf{m} = \begin{bmatrix} \mathbf{C}_d^{-1/2} \delta \mathbf{d} \\ 0 \\ 0 \end{bmatrix} \quad (63)$$

which is equivalent to solving Eq. 61. SVD or iterative solvers like LSQR can be used to solve Eq. 63 since they can equally well be applied to non-square systems and will solve the equations in the least-squares sense.

2.3.2.2 Steepest descent The method of steepest descent is probably the simplest gradient-based method for iterative minimization of an objective function. It is based on the idea that the objective function S may be minimized by successive searches along local directions of steepest descent. If $\boldsymbol{\gamma}_n$ is the direction of steepest ascent in model space at a point \mathbf{m}_n , the model correction is given by:

$$\delta \mathbf{m}_n = -\mu_n \boldsymbol{\gamma}_n \quad (64)$$

where the scalar μ_n is a positive real number whose value locates the minimum in the direction specified by $\boldsymbol{\gamma}_n$. The parameter μ_n can be found by line minimization as follows. By assuming that $\mathbf{g}(\mathbf{m})$ is locally linear, so that $\mathbf{g}(\mathbf{m}_{n+1}) = \mathbf{g}(\mathbf{m}_n) + \mathbf{G}_n(\mathbf{m}_{n+1} - \mathbf{m}_n)$, then $S(\mathbf{m})$ is quadratic so $\partial S(\mathbf{m})/\partial \mu_n = 0$ will give the value of μ_n . Substituting Eq. 64 into Eq. 48 gives:

$$S(\mathbf{m}_n - \mu_n \boldsymbol{\gamma}_n) = S(\mathbf{m}_n) - \mu_n \hat{\boldsymbol{\gamma}}_n^T \boldsymbol{\gamma}_n + \frac{1}{2} \mu_n^2 \boldsymbol{\gamma}_n^T \hat{\mathbf{H}}_n \boldsymbol{\gamma}_n \quad (65)$$

The partial derivative of Eq. 65 is:

$$\frac{\partial S(\mathbf{m}_n - \mu_n \boldsymbol{\gamma}_n)}{\partial \mu_n} = -\hat{\boldsymbol{\gamma}}_n^T \boldsymbol{\gamma}_n + \mu_n \boldsymbol{\gamma}_n^T \hat{\mathbf{H}}_n \boldsymbol{\gamma}_n = 0 \quad (66)$$

which can be rearranged to give:

$$\mu_n = \frac{\hat{\gamma}_n^T \gamma_n}{\gamma_n^T \hat{\mathbf{H}}_n \gamma_n} \quad (67)$$

An iterative line search could also be implemented to determine μ_n , but this may require numerous calculations of the forward step. The efficiency of the steepest descent method depends on the character of $S(\mathbf{m})$, but usually it is slow because the local direction of steepest descent may differ greatly from the direction in which the minimum is to be found. Fig. 22 schematically illustrates how the steepest descent method may be inefficient. Blundell (1993) investigates the properties of the steepest descent method in the context of inverting reflection traveltimes for velocity and interface depth but the method has not been widely used in seismic tomography.

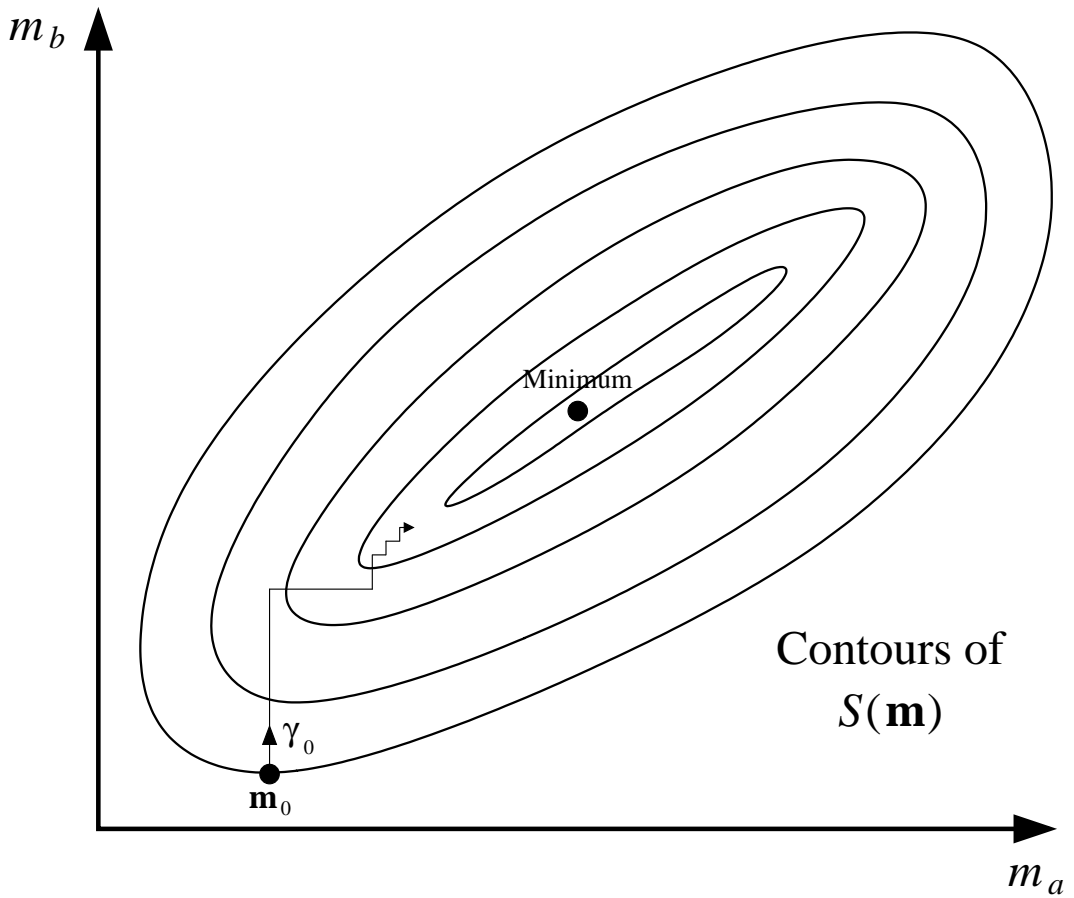


Figure 22: Illustration of the method of steepest descent in 2-D model space. The method can be inefficient in locating the solution if the local direction of steepest descent is oblique to the direction in which the minimum is to be found.

2.3.2.3 Conjugate gradients Hestenes & Stiefel (1952) first suggested the idea of conjugate gradient methods in regard to solving systems of linear equations. Fletcher & Reeves (1964) subsequently applied it to unconstrained optimization. At each iteration, the conjugate gradient method uses a new search direction that is conjugate to all the previous ones. In other words, the n^{th} iteration of the conjugate gradient method locates the minimum in an n -dimensional subspace spanned by the

current search direction and the $n - 1$ previous search directions. The algorithm may be defined by (see Tarantola, 1987):

$$\boldsymbol{\phi}_n = \boldsymbol{\gamma}_n + \alpha_n \boldsymbol{\phi}_{n-1} \quad (68)$$

$$\delta\mathbf{m}_n = -\mu_n \boldsymbol{\phi}_n \quad (69)$$

where $\{\boldsymbol{\phi}_n\}$ is a set of conjugate directions and $\boldsymbol{\phi}_0 = \boldsymbol{\gamma}_0$. The scalar μ_n can be determined by Eq. 67 (using $\boldsymbol{\phi}_n$ in place of $\boldsymbol{\gamma}_n$) and α_n is defined so that the new search direction is conjugate to the previous search directions (see Press et al., 1992):

$$\alpha_n = \frac{\boldsymbol{\gamma}_n^T \hat{\boldsymbol{\gamma}}_n}{\boldsymbol{\gamma}_{n-1}^T \hat{\boldsymbol{\gamma}}_{n-1}} \quad (70)$$

or

$$\alpha_n = \frac{\boldsymbol{\gamma}_n^T \hat{\boldsymbol{\gamma}}_n - \boldsymbol{\gamma}_n^T \hat{\boldsymbol{\gamma}}_{n-1}}{\boldsymbol{\gamma}_{n-1}^T \hat{\boldsymbol{\gamma}}_{n-1}} \quad (71)$$

Eq. 70 is the Fletcher-Reeves variant and Eq. 71 is the Polak-Ribiere variant. The latter formulation sometimes gives superior results when $S(\mathbf{m})$ is non-quadratic (Tarantola, 1987). In the context of seismic traveltimes inversion, the conjugate gradient method has been used infrequently for direct minimization of an objective function. Rawlinson & Houseman (1998) have used it to invert teleseismic traveltimes and Blundell (1993) has used it in the inversion of reflection traveltimes.

The principal advantage that both the steepest descent and conjugate gradient method have over the Newton and DLS methods is that a large system of linear equations does not need to be solved. Consequently, these methods are much more rapid at the inverse step. However, since they only minimize in one dimension at each iteration, they tend to converge more slowly. If the procedure for solving the forward step is fast compared to solving the $M \times M$ matrix equation, then steepest descent or conjugate gradients may be preferable. However, if the forward step is slow compared to solving the matrix inverse, then a Newton or DLS approach may be quicker.

2.3.2.4 Subspace method Both the steepest descent method and conjugate gradient method are examples of 1-D subspace methods in that they perform a line minimization at each iteration. In general, however, subspace methods may be constructed in which the minimization is carried out simultaneously along several search directions that together span a subspace of the model space. The basic theory for the general subspace inversion method is presented here; more details can be found in Kennett et al. (1988), Sambridge (1990) and Williamson (1990).

At each iteration, the subspace method restricts the minimization of the quadratic approximation of $S(\mathbf{m})$ to a p -dimensional subspace of model space, so that the perturbation $\delta\mathbf{m}$ (ignoring the iteration subscript n in $\delta\mathbf{m}_n$ for convenience) occurs in the space spanned by a set of p M -dimensional basis vectors $\{\mathbf{a}^j\}$:

$$\delta\mathbf{m} = \sum_{j=1}^p \mu_j \mathbf{a}^j = \mathbf{A}\boldsymbol{\mu} \quad (72)$$

where $\mathbf{A} = [\mathbf{a}^j]$ is the $M \times p$ projection matrix. The component μ_j determines the length of the corresponding vector \mathbf{a}^j that minimizes the quadratic form of $S(\mathbf{m})$ in the space spanned by \mathbf{a}^j . Hence, $\boldsymbol{\mu}$ is found by substituting Eq. 72 into Eq. 48, which gives in summation form:

$$S(\mathbf{m} + \delta\mathbf{m}) = S(\mathbf{m}) + \sum_{j=1}^p \mu_j \hat{\boldsymbol{\gamma}}^T \mathbf{a}^j + \frac{1}{2} \sum_{j=1}^p \sum_{k=1}^p \mu_j \mu_k [\mathbf{a}^k]^T \hat{\mathbf{H}} [\mathbf{a}^j] \quad (73)$$

and locating the minimum of S with respect to μ :

$$\frac{\partial S(\mathbf{m})}{\partial \mu_q} = \hat{\mathbf{y}}^T \mathbf{a}^q + \sum_{k=1}^p \mu_k [\mathbf{a}^k]^T \hat{\mathbf{H}}[\mathbf{a}^j] = 0 \quad (74)$$

for $q = 1, \dots, p$. Rearranging Eq. 74 for μ gives:

$$\mu = -[\mathbf{A}^T \hat{\mathbf{H}} \mathbf{A}]^{-1} \mathbf{A}^T \hat{\mathbf{y}} \quad (75)$$

and since $\delta \mathbf{m} = \mathbf{A} \mu$, the solution, taking $\hat{\mathbf{H}} = \mathbf{G}^T \mathbf{C}_d^{-1} \mathbf{G} + \epsilon \mathbf{C}_m^{-1} + \eta \mathbf{D}^T \mathbf{D}$, is:

$$\delta \mathbf{m} = -\mathbf{A}[\mathbf{A}^T (\mathbf{G}^T \mathbf{C}_d^{-1} \mathbf{G} + \epsilon \mathbf{C}_m^{-1} + \eta \mathbf{D}^T \mathbf{D}) \mathbf{A}]^{-1} \mathbf{A}^T \hat{\mathbf{y}} \quad (76)$$

which can be used iteratively in the manner specified by Eq. 51. The quantities \mathbf{A} , $\hat{\mathbf{y}}$ and \mathbf{G} are re-evaluated between successive iterations. Most implementations of the subspace method construct the basis vectors $\{\mathbf{a}^j\}$ in terms of the steepest ascent vector in model space \mathbf{y} and its rates of change (e.g. Kennett et al., 1988; Sambridge, 1990; Williamson, 1990; Blundell, 1993).

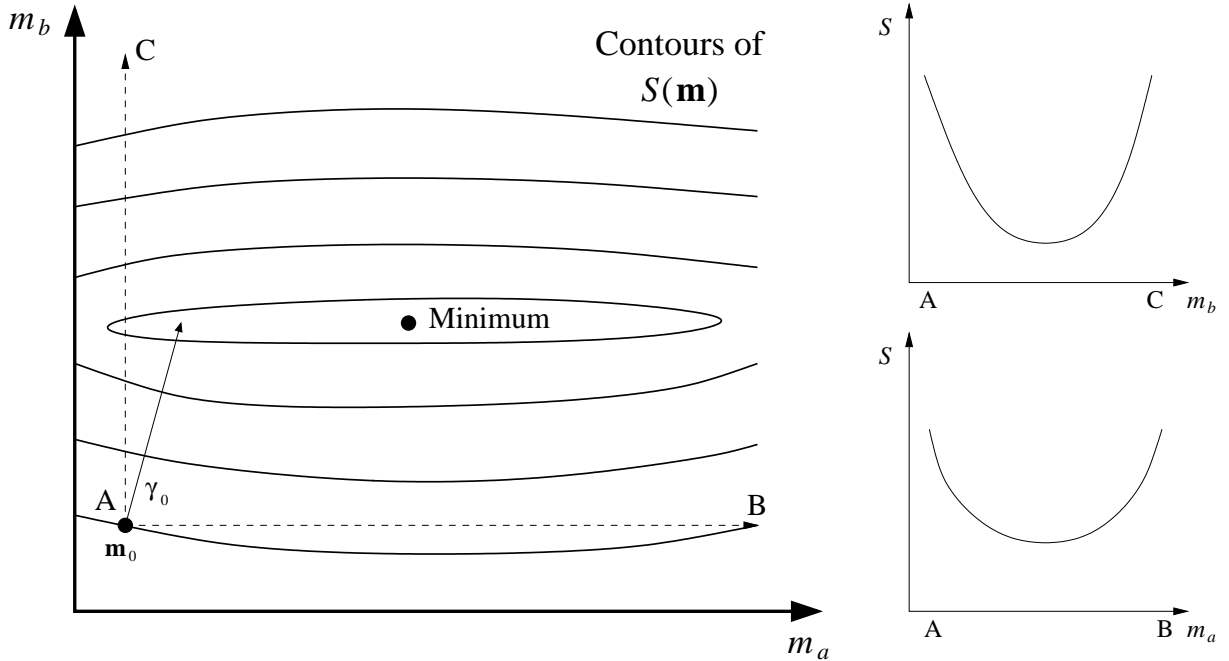


Figure 23: A contour plot of $S(\mathbf{m})$ which is a function of two parameters of different physical dimensions. $S(\mathbf{m})$ is much more sensitive to m_b than m_a , and a gradient method like steepest descents will converge slowly. Searching in directions specified by basis vectors (dotted lines) that only lie in space defined by a single parameter class eliminates these problems, since $S(\mathbf{m})$ is a function of only one parameter class in each of these directions.

The subspace method has several desirable characteristics. First, the determination of $\delta \mathbf{m}$ only requires the solution of a relatively small $p \times p$ system of linear equations - Williamson (1990) uses $p = 6$ and Blundell (1993) uses $p \leq 8$. Second, it offers a natural way of dealing with multiple parameter classes, such as velocity parameters and interface depth parameters, that are to be inverted for simultaneously. If the basis vectors $\{\mathbf{a}^j\}$ are chosen such that each vector only lies in the space spanned by a particular parameter class, then the minimization will account for the

different sensitivities of $S(\mathbf{m})$ with respect to the different parameter classes in a balanced way (see Fig. 23). Other gradient methods in which parameters of different physical dimensions are mixed can exhibit slow convergence and a strong dependence on relative scaling of the different parameter types (Kennett et al., 1988).

As an example of how one might choose a set of basis vectors, consider an inverse problem that has three different parameter classes that are to be constrained by the data. Three separate search directions can simply be obtained by partitioning the gradient vector in model space $\boldsymbol{\gamma} = \mathbf{C}_m \hat{\boldsymbol{\gamma}}$ on the basis of parameter class:

$$\boldsymbol{\gamma} = \mathbf{a}^1 + \mathbf{a}^2 + \mathbf{a}^3 = \begin{bmatrix} \boldsymbol{\gamma}^1 \\ 0 \\ 0 \end{bmatrix} + \begin{bmatrix} 0 \\ \boldsymbol{\gamma}^2 \\ 0 \end{bmatrix} + \begin{bmatrix} 0 \\ 0 \\ \boldsymbol{\gamma}^3 \end{bmatrix} \quad (77)$$

where \mathbf{a}^1 , \mathbf{a}^2 and \mathbf{a}^3 represent ascent vectors that lie in the space of only one parameter type. A further nine basis vectors can be obtained by pre-multiplying \mathbf{a}^1 , \mathbf{a}^2 and \mathbf{a}^3 by the model space Hessian $\mathbf{H} = \mathbf{C}_m \hat{\mathbf{H}}$ and partitioning the three vectors that result in the same way as Eq. 77. Additional basis vectors can be produced by repeating the process of pre-multiplication of the latest set of vectors by the partitioned model space Hessian. Once the required number of basis vectors is obtained, Gram-Schmidt orthogonalization should be applied to avoid interdependence:

$$\mathbf{a}_{orth}^i = \mathbf{a}^i - \sum_{j=1}^{i-1} \frac{\mathbf{a}^i \cdot \mathbf{a}^j}{\mathbf{a}^j \cdot \mathbf{a}^j} \mathbf{a}^j \quad (78)$$

for $i = 1, \dots, p$. The basis vectors $\{\mathbf{a}_{orth}^i\}$ are normalized and used in Eq. 76 via the projection matrix \mathbf{A} . If the subspace is large, then SVD may be more effective in finding the orthonormal set of subspace vectors due to the build-up of round-off error associated with the numerical implementation of Eq. 78 (Press et al., 1992). Choosing an appropriate number of basis vectors requires finding an acceptable balance between computational effort and rate of convergence.

Subspace methods have been applied to the inversion of reflection traveltimes for velocity and interface structure (Williamson, 1990; Blundell, 1993), to the inversion of local earthquake and artificial source traveltimes for velocity, interface structure and hypocenter location (Sambridge, 1990) and to the inversion of reflection amplitude data for interface structure (Wang & Houseman, 1994) and velocity (Wang & Houseman, 1995). Rawlinson et al. (2001a,b) use it in the inversion of refraction and wide-angle reflection traveltimes for the determination of layered crustal structure.

2.3.2.5 Fréchet matrix All gradient methods require the calculation of $\mathbf{G} = \partial \mathbf{g} / \partial \mathbf{m}$, which describes the rate of change of traveltimes with respect to model parameters. For such discrete models, \mathbf{G} defines the “Gateaux” derivative of \mathbf{g} ; the term “Fréchet” derivative should really only be used to describe the derivative of \mathbf{g} for a continuous model (Shaw & Orcutt, 1985). However, since \mathbf{G} is widely referred to as the Fréchet derivative/matrix even if the model is discrete, we will continue to do so here. The two basic parameter types that are normally encountered in traveltime inversion, especially of wide-angle data, are velocity (or slowness) and interface depth. First-order accurate expressions for the derivatives can be derived quite simply for both cases. They are usually calculated as part of the forward step of the tomographic problem. In local earthquake tomography, the source location is also an unknown, so derivatives of traveltime with respect to these parameters are required.

The linearized relationship between traveltime residual and velocity perturbation was given by Eq. 6:

$$\delta t = - \int_{L(v_0)} \frac{\delta v}{v_0^2} dl \quad (79)$$

where δv is the velocity perturbation and v_0 is the reference velocity field. If the velocity field is defined by a grid of velocity nodes, then to first-order the Fréchet derivatives are given by:

$$\frac{\partial t}{\partial v_n} = - \int_{L(v_0)} v_0^{-2} \frac{\partial v}{\partial v_n} dl \quad (80)$$

where v_n is the velocity of a particular node and $\partial v / \partial v_n$ is the change of velocity along the ray with respect to a change in v_n . This expression is usually straightforward to calculate if the velocity interpolation function $v = f(\mathbf{v}_{nodes})$ has a simple form (e.g. cubic B-splines). Fréchet derivatives have been calculated using Eq. 80 (or its equivalent for slowness) by most authors who use gradient methods and models parameterized by a grid of velocity nodes (e.g. White, 1989; Lutter et al., 1990; Sambridge, 1990).

First-order accurate analytic expressions can also be obtained for the Fréchet derivatives when the model parameters describe interface depths. The basic approach is to partition the problem:

$$\frac{\partial t}{\partial z_n} = \frac{\partial t}{\partial h_{int}} \frac{\partial h_{int}}{\partial z_{int}} \frac{\partial z_{int}}{\partial z_n} \quad (81)$$

where z_n is the depth coordinate of the interface node, h_{int} is displacement normal to the interface at the point of intersection by the ray and z_{int} is the depth coordinate of the intersection point. The first two derivatives on the RHS of Eq. 81 can be worked out analytically to first-order accuracy by assuming a locally linear wavefront and interface (e.g. Bishop et al., 1985; Nowack & Lyslo, 1989; White, 1989; Sambridge, 1990; Zelt & Smith, 1992; Blundell, 1993; Riahi & Juhlin, 1994). Consider Fig. 24 which shows a plane wave impinging on a planar interface that is perturbed by a distance Δh . Rays A and B show the path taken by the wave before and after the perturbation. It is easy to see that the difference in traveltime Δt between rays A and B from position 1 to position 2 is:

$$\Delta t = \frac{a}{v_j} - \frac{b}{v_{j+1}} \quad (82)$$

and since $a = -\mathbf{w}_j \cdot \mathbf{w}_n \Delta h$ and $b = -\mathbf{w}_{j+1} \cdot \mathbf{w}_n \Delta h$ (all vectors are unit vectors), substitution into Eq. 82 gives:

$$\Delta t = \left[\frac{\mathbf{w}_{j+1} \cdot \mathbf{w}_n}{v_{j+1}} - \frac{\mathbf{w}_j \cdot \mathbf{w}_n}{v_j} \right] \Delta h \quad (83)$$

and the approximation to the derivative is:

$$\frac{\partial t}{\partial h_{int}} \approx \frac{\mathbf{w}_{j+1} \cdot \mathbf{w}_n}{v_{j+1}} - \frac{\mathbf{w}_j \cdot \mathbf{w}_n}{v_j} \quad (84)$$

The second term in Eq. 81 can be derived from the fact that $\mathbf{w}_n \cdot \mathbf{w}_z = -\Delta h / \Delta z$ so the derivative is:

$$\frac{\partial h_{int}}{\partial z_{int}} \approx -\mathbf{w}_n \cdot \mathbf{w}_z \quad (85)$$

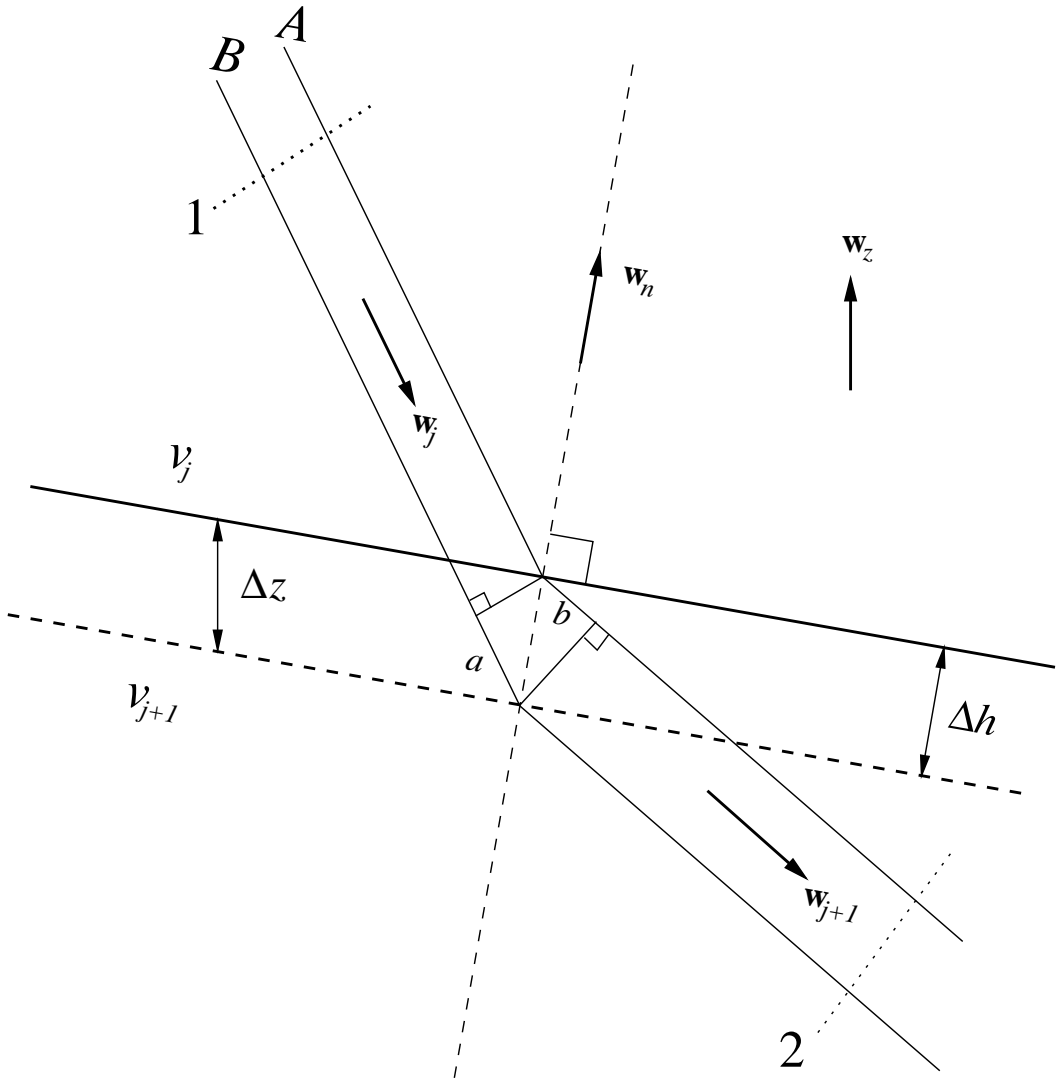


Figure 24: Plane wave incident on a perturbed planar interface for first-order approximation of interface Fréchet derivatives. \mathbf{w}_j is a unit vector parallel to rays A and B in layer j and \mathbf{w}_{j+1} is a unit vector parallel to rays A and B in layer $j + 1$. \mathbf{w}_n is the unit normal vector to the interface at the intersection point and $\mathbf{w}_z = [0, 0, 1]$.

Substitution of both partial derivatives into Eq. 81 gives:

$$\frac{\partial t}{\partial z_n} \approx \left[\frac{\mathbf{w}_j \cdot \mathbf{w}_n}{v_j} - \frac{\mathbf{w}_{j+1} \cdot \mathbf{w}_n}{v_{j+1}} \right] [\mathbf{w}_n \cdot \mathbf{w}_z] \frac{\partial z_{int}}{\partial z_n} \quad (86)$$

Note that Eq. 86 will work for any ray direction provided \mathbf{w}_j always points towards the interface and \mathbf{w}_{j+1} always points away from the interface, irrespective of whether the ray is upgoing or downgoing. For reflections, $\mathbf{w}_{j+1} \cdot \mathbf{w}_n = -\mathbf{w}_j \cdot \mathbf{w}_n$ and $v_{j+1} = v_j$. The term $\partial z_{int}/\partial z_n$ depends on the form of the interface depth interpolation function $z = f(\mathbf{z}_{nodes})$.

In 3-D space, four parameters describe the location of an earthquake hypocenter. The partial derivative of the traveltime t with respect to origin time t_o is simply:

$$\frac{\partial t}{\partial t_o} = -1 \quad (87)$$

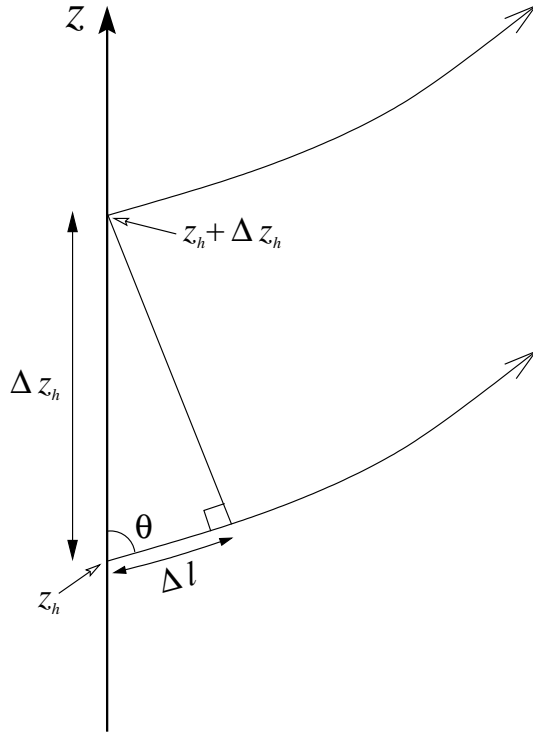


Figure 25: A change in depth Δz_h of the hypocenter results in a change in the path length Δl of the ray.

because $t = t_a - t_o$ where t_a is the arrival time. In Cartesian coordinates, the partial derivatives of traveltimes with respect to the three spatial coordinates are straightforward to derive. For example, consider a perturbation in depth Δz_h of the hypocenter (see Fig. 25). The corresponding change in path length Δl is given by:

$$\Delta l = -\Delta z_h \cos \theta_h \quad (88)$$

where θ_h is the angle between the ray and the z-axis at the hypocenter. Note that the change in path length is negative since the hypocenter is perturbed to a shallower depth. The change in traveltime is given by:

$$\Delta t = \frac{\Delta l}{v_h} = -\frac{\Delta z_h \cos \theta_h}{v_h} \quad (89)$$

where v_h is the velocity at the hypocenter. The first-order accurate expression for the partial derivative is thus given by:

$$\frac{\partial t}{\partial z_h} = -\frac{\cos \theta_h}{v_h} \quad (90)$$

Similarly, the partial derivatives for the remaining two parameters are:

$$\frac{\partial t}{\partial x_h} = -\frac{\cos \phi_h}{v_h} \quad (91)$$

$$\frac{\partial t}{\partial y_h} = -\frac{\cos \psi_h}{v_h} \quad (92)$$

where ϕ_h and ψ_h subtend the horizontal projection of the ray path and the x and y axes respectively at the hypocenter. Most local earthquake tomography schemes use this kind of hypocenter partial derivative (e.g. Thurber, 1983; Eberhart-Phillips, 1986; Sambridge, 1990).

2.3.3 Global Optimization

The inversion methods described in Section 2.3.1 and Section 2.3.2 are local in that they exploit information in regions of model space near an initial model estimate and thus avoid an extensive search of model space. Consequently, they cannot guarantee convergence to a global minimum solution. Local methods are prone to entrapment in local minima, especially if the subsurface velocity structure is complex and the starting model is not close to the true model. Fig. 26 illustrates these problems.

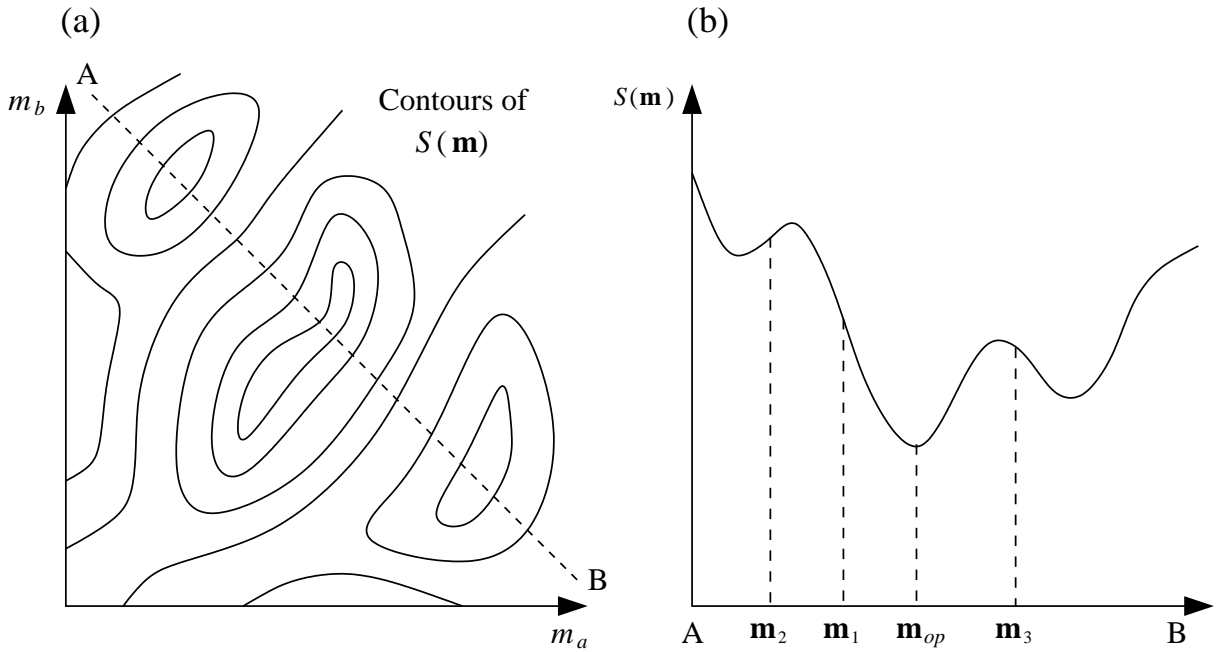


Figure 26: (a) Contours of $S(\mathbf{m})$ for a two parameter model. (b) Cross section through (a). Local methods are likely to locate the global optimum solution \mathbf{m}_{op} if initial model \mathbf{m}_1 is used, but are more likely to find local minima if initial models \mathbf{m}_2 or \mathbf{m}_3 are used.

In many realistic applications of traveltome tomography, particularly at regional and global scales, the need for global optimization techniques is hard to justify, because the *a priori* model information is relatively accurate and lateral heterogeneities are not very large (e.g. Widiyantoro & van der Hilst, 1997; Gorbatov et al., 2000). Therefore, the local minimum of the objective function in the vicinity of the initial model is also likely to be the global minimum of the objective function. However, the crust and lithosphere are generally less well constrained by *a priori* information and are also much more heterogeneous. This means that the initial model is likely to be more distant from the global minimum solution, and entrapment in a local minimum becomes more of a concern. A second motivation for using global methods is that they often produce an ensemble of solutions that satisfy the data to a similar level. This enables one to choose the model deemed most likely to represent the geology of the region (Pullammanappallil & Louie, 1993), and estimate posterior model uncertainties.

The computational burden of exploring large regions of model space is immense, especially for the large number of unknowns typically encountered in traveltome tomography. Recent interest in the use of global optimization techniques for solving geophysical inverse problems has been generated to a large degree by rapid advancements in computing power. Further advancements will continue to

make these techniques more practical and hence popular. Several types of global optimization that have been applied to seismic inversion use random processes to search model space and find better models. These Monte Carlo (MC) methods include genetic algorithms and simulated annealing. For recent reviews on the use of MC techniques for geophysical inverse problems, see Sambridge & Mosegaard (2001) and Mosegaard & Sambridge (2002).

The earliest Monte Carlo approach, defined simply as a uniform random search of model space, is the simplest of these global methods. The misfit function is evaluated at a set of points in model space that are randomly chosen between pairs of upper and lower bounds (chosen *a priori*). The selection of new points has no dependence on previous points. Each model generated by this process is tested for fitness and then accepted or rejected. The final set of accepted models can then be used for interpretation. If model space is not very large, say $M = 80$, and each m_i is discretized to assume only 10 possible values, the number of different models is 10^{80} . Of course, the uniform random search approach will not test every model, but it is likely to spend significant amounts of computation time exploring unfavorable regions of model space. Computation requirements will therefore become prohibitive if large numbers of model parameters are involved (Sambridge & Drikkoningen, 1992). Consequently, a basic Monte Carlo approach is not suited to most seismic traveltime inversion problems.

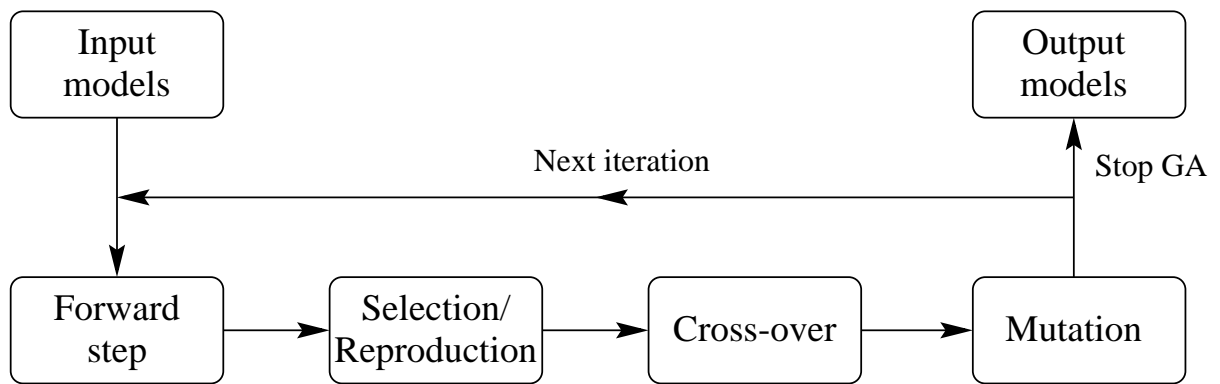


Figure 27: Flow chart for genetic algorithm solution of the inversion problem. Each step is carried out on a population of models and the process is terminated when the maximum fitness parameter of the population exceeds a given threshold.

Genetic algorithms use an analogue to biological evolution to develop new models from an initial pool of randomly picked models. The process of producing a new set of models from a pre-existing set involves four basic steps, summarized in the flowchart of Fig. 27. The first step is to solve the forward problem (i.e. determine traveltimes) for the set of input models. The next step, selection and reproduction, assigns a measure of fitness to each model in the pool based on the magnitude of the misfit function at the corresponding point in model space. Then a rule for selecting which models are to be used to create the next generation is applied. Two common choices for the selection operator are linear normalization selection and parent selection (Boschetti et al., 1996). Linear normalization selection ranks each model according to its fitness and then allows each model to generate a number of offspring proportional to its rank position. Parent selection causes pairs of models to be mated randomly so that each couple creates two offspring in the cross-over stage. The cross-over step creates a pool of offspring, each of which is a “mix” of its two parents. Sambridge & Drikkoningen (1992) represent models by binary strings and perform the cross-over by simply

cutting and transposing two segments at a randomly chosen point along the two strings.

Mutation involves randomly changing some parameter values (or bits if a binary string representation is used) in selected models. This ensures that some “freshness” remains in the model pool, although the mutation rate should be kept low (Boschetti et al., 1996, use a mutation rate of 1%) so that “good” models are not corrupted. The basic principle behind genetic algorithms is that models with a high fitness index will pass their characteristics to subsequent generations, while those aspects of the cycle that introduce random changes to the population permit new parts of the model space to be tested. For more detailed information on genetic algorithms, refer to Goldberg (1989) and Whitley (1994).

Simulated annealing is based on an analogy with physical annealing in thermodynamic systems to guide variations to the model parameters. The process of annealing in metallurgy involves the slow cooling of a metal, which allows the atoms to order themselves into stable, structurally strong, low energy configurations. In the analogue process, some starting model is represented by a collection of atoms (parameters) in equilibrium at a given temperature T . At each iteration, an atom is displaced (a parameter is varied) and the resultant change in the energy of the system ΔE (change in the objective function) is computed. If $\Delta E \leq 0$ the displacement is accepted and the new model is used as the starting point of the next iteration. If $\Delta E > 0$, then acceptance is probabilistic. Kirkpatrick et al. (1983) use the probability $P(\Delta E) = \exp(-\Delta E / K_B T)$ where T is analogous to temperature in controlling the probability of a randomly selected move and the constant K_B is analogous to Boltzmann’s constant. By repeating this step many times, the model evolves with the variation of parameters simulating the thermal motion of atoms held at a temperature T . The simulated annealing process consists of “melting” the system at a high T , then progressively lowering T until the system reaches an equilibrium state (it “freezes”). At each T , the simulation is iterated until a steady state is reached before moving to the next temperature level. More detailed explanations of this method can be found in Kirkpatrick et al. (1983) and Aarts & Korst (1989).

Global optimization using stochastic methods is a rapidly developing field of science. However, current applications to seismic traveltimes inversion problems have been limited due to computational expense. Genetic algorithms have been used in the 1-D inversion of marine refraction waveforms (Sambridge & Drikkonen, 1992; Drikkonen & White, 1995) and the 2-D inversion of refraction traveltimes (Boschetti et al., 1996). The latter paper inverts for 45 model parameters. While this number of parameters is insufficient to adequately parameterize many seismic datasets, it is possible to use such a coarse model as a starting point for subsequent refinement using local optimization techniques. The idea behind this two-stage inversion is that the globally optimized coarse model will be near enough the global minimum to allow the local method to locate the global solution. Boschetti et al. (1996) use genetic algorithms in this context. Simulated annealing has been used by Pullammanappallil & Louie (1993) in the inversion of reflection traveltimes for 2-D velocity structure and interface geometry. Asad et al. (1999) use simulated annealing to produce a coarse 3-D model from local earthquake traveltimes before refining it with the gradient method of Thurber (1983), in a scheme similar in principle to that of Boschetti et al. (1996). Global optimization techniques can find global minimum solutions to highly non-linear inverse problems, but the computational expense when large numbers of parameters are involved currently limits their use in seismic data inversion.

2.4 Analysis of Solution Quality

The process of producing a solution to an inverse problem using the above methods is not complete until some estimate of solution robustness or quality is made. Simply producing a single solution

that minimizes an objective function (i.e. best satisfies the data and *a priori* constraints) without knowledge of resolution or non-uniqueness is inadequate. Two approaches are commonly used to assess solution robustness in traveltome tomography. The first approach assumes local linearity to estimate model covariance and resolution; the second tests resolution by reconstructing a synthetic model using the same source-receiver geometry as the real experiment.

2.4.1 Resolution and Covariance Matrices

To derive expressions for posterior model covariance and resolution, we will assume that the objective function is of the form of Eq. 47 with $\eta = 0$. The reason this is done is because it is more straightforward and common to consider covariance and resolution matrices in a Bayesian framework. In other words, the error statistics associated with the *a priori* model information and data are well known, thus allowing the two sets of information to be objectively combined to produce a more accurate posterior model distribution. In such circumstances, $\epsilon = 1$ and \mathbf{C}_m represents the true *a priori* model covariance. In the following derivation, however, we will retain ϵ as a variable to examine its effect on covariance and resolution if it is used as a tuning parameter in the inversion. For an objective function of the form Eq. 47 with $\eta = 0$, the maximum likelihood solution is given by the \mathbf{m} that satisfies Eq. 53 with $\eta = 0$, which may be written as:

$$\epsilon \mathbf{C}_m^{-1}(\mathbf{m} - \mathbf{m}_0) = -\mathbf{G}^T \mathbf{C}_d^{-1}(\mathbf{g}(\mathbf{m}) - \mathbf{d}_{obs}) \quad (93)$$

Adding $\mathbf{G}^T \mathbf{C}_d^{-1} \mathbf{G}(\mathbf{m} - \mathbf{m}_0)$ to both sides gives:

$$\mathbf{m} - \mathbf{m}_o = [\mathbf{G}^T \mathbf{C}_d^{-1} \mathbf{G} + \epsilon \mathbf{C}_m^{-1}]^{-1} \mathbf{G}^T \mathbf{C}_d^{-1} [\mathbf{d}_{obs} - \mathbf{g}(\mathbf{m}) + \mathbf{G}(\mathbf{m} - \mathbf{m}_o)] \quad (94)$$

which is an implicit equation for \mathbf{m} . Following Tarantola (1987), let \mathbf{m}_{true} represent the true model, which is unknown. The observed data are related to \mathbf{m}_{true} by:

$$\mathbf{d}_{obs} = \mathbf{g}(\mathbf{m}_{true}) + \boldsymbol{\zeta} \quad (95)$$

where $\boldsymbol{\zeta}$ represents observational and model representation errors. The resolution operator \mathbf{r} defines the relationship between the calculated solution \mathbf{m} and the true solution:

$$\mathbf{m} = \mathbf{r}(\mathbf{m}_{true}) \quad (96)$$

If \mathbf{r} is linear, then $\mathbf{m} = \mathbf{r}(\mathbf{m}_0) + \mathbf{R}(\mathbf{m}_{true} - \mathbf{m}_0)$, where $\mathbf{R} = \partial \mathbf{r} / \partial \mathbf{m}$ and $\mathbf{m}_0 = \mathbf{r}(\mathbf{m}_0)$ so that:

$$\mathbf{m} - \mathbf{m}_0 = \mathbf{R}(\mathbf{m}_{true} - \mathbf{m}_0) \quad (97)$$

If we assume that $\boldsymbol{\zeta} = \{0\}$ in Eq. 95 and let $\mathbf{m} = \mathbf{m}_{true}$ on the RHS of Eq. 94, then Eq. 97 can be written in the form of Eq. 94 with the resolution matrix \mathbf{R} given by:

$$\mathbf{R} = [\mathbf{G}^T \mathbf{C}_d^{-1} \mathbf{G} + \epsilon \mathbf{C}_m^{-1}]^{-1} \mathbf{G}^T \mathbf{C}_d^{-1} \mathbf{G} \quad (98)$$

The diagonal elements of R range between zero and one. If $\mathbf{R} = \mathbf{I}$, then, according to Eq. 97, $\mathbf{m} = \mathbf{m}_{true}$ and the solution model is perfectly resolved. If $\mathbf{R} \neq \mathbf{I}$, then the model parameter estimates represent weighted averages of the true model parameters.

The matrix \mathbf{C}_m describes *a priori* model covariance, with the square root of the diagonal entries indicating the uncertainty associated with the initial model parameter values. The constraints supplied by the data will result in changes to these uncertainties. The *a posteriori* covariance matrix \mathbf{C}_M

describes the error in the solution parameters and is related to the resolution matrix by (Tarantola, 1987):

$$\mathbf{R} = \mathbf{I} - \mathbf{C}_M \mathbf{C}_m^{-1} \quad (99)$$

Substituting Eq. 98 for \mathbf{R} and solving for \mathbf{C}_M gives:

$$\mathbf{C}_M = \epsilon [\mathbf{G}^T \mathbf{C}_d^{-1} \mathbf{G} + \epsilon \mathbf{C}_m^{-1}]^{-1} \quad (100)$$

The diagonal elements of \mathbf{C}_M indicate the posterior uncertainty associated with each model parameter. The Fréchet matrix \mathbf{G} in Equations 98 and 100 is calculated at the solution point. Off-diagonal elements of the posterior covariance matrix are more conveniently interpreted in terms of correlations (Tarantola, 1987):

$$\rho^{ij} = \frac{C_M^{ij}}{(C_M^{ii})^{\frac{1}{2}} (C_M^{jj})^{\frac{1}{2}}} \quad (101)$$

where $-1 \leq \rho^{ij} \leq 1$ and $i, j = 1, \dots, M$. A strong correlation between uncertainties means that the two parameters have not been independently resolved by the dataset.

If ϵ is treated as a damping factor in the inversion (i.e. its value is varied to tune the solution), then \mathbf{C}_m no longer truly represents the *a priori* model covariance. In this case, the resolution and posterior covariance will have a dependence on the value chosen for ϵ . From the above definition of \mathbf{R} (Eq. 98), as $\epsilon \rightarrow 0$, then $\mathbf{R} \rightarrow \mathbf{I}$ and the solution approaches perfect resolution. As $\epsilon \rightarrow \infty$, then $\mathbf{R} \rightarrow \mathbf{0}$ and the model is not resolved by the data at all. If we rearrange Eq. 100 as:

$$\mathbf{C}_M^{-1} = \frac{\mathbf{G}^T \mathbf{C}_d^{-1} \mathbf{G}}{\epsilon} + \mathbf{C}_m^{-1} \quad (102)$$

we see that as $\epsilon \rightarrow 0$, the *a priori* covariance becomes increasingly irrelevant to the value of the posterior covariance, whereas when $\epsilon \rightarrow \infty$, $\mathbf{C}_M \rightarrow \mathbf{C}_m$. From a Bayesian viewpoint, having $\epsilon \rightarrow 0$ means that there is no *a priori* model information and the information contained in the data is totally responsible for the state of the posterior model information. In contrast, $\epsilon \rightarrow \infty$ means that there are no errors associated with the *a prior* model information, in which case the data are irrelevant. These two end member states are not possible in practice, and reflect the fact that the inclusion of a damping parameter is not consistent with a Bayesian paradigm. In short, the use of ϵ as a damping parameter to tune the solution makes the absolute values of resolution and posterior covariance rather meaningless. However, their relative values will still be useful indicators of the effect the data have had in constraining the solution model. For example, it is reasonable to interpret parameters associated with diagonal elements of the resolution matrix that are large as meaning that the data have been more effective in constraining them than those parameters with smaller resolution values.

The principal difficulties with \mathbf{R} and \mathbf{C}_M are that (i) they are derived from linear theory and are less meaningful as the non-linearity of the problem increases (Snieder, 1998, has considered perturbation theory as a means of extending these concepts to a non-linear regime), (ii) errors in model representation are not taken into account, and (iii) they require the inversion of an $M \times M$ matrix, $\mathbf{G}^T \mathbf{C}_d^{-1} \mathbf{G} + \epsilon \mathbf{C}_m^{-1}$, which may be impractical for large numbers of parameters. Nevertheless, they have been used in many teleseismic traveltimes inversions (e.g. Aki et al., 1977; Benz et al., 1992; Steck et al., 1998), wide-angle traveltimes inversions (e.g. White, 1989; Hole, 1992; Zelt & Smith, 1992; Riahi & Lund, 1994; Wang & Braile, 1996) and local earthquake tomography studies

(e.g. Eberhart-Phillips, 1990; Eberhart-Phillips & Michael, 1993; Abers, 1994; Protti et al., 1996; Graeber & Asch, 1999). McCaughey & Singh (1997) and Zhang & Toksöz (1998) also consider correlations (Eq. 101) as part of their interpretation of solution quality.

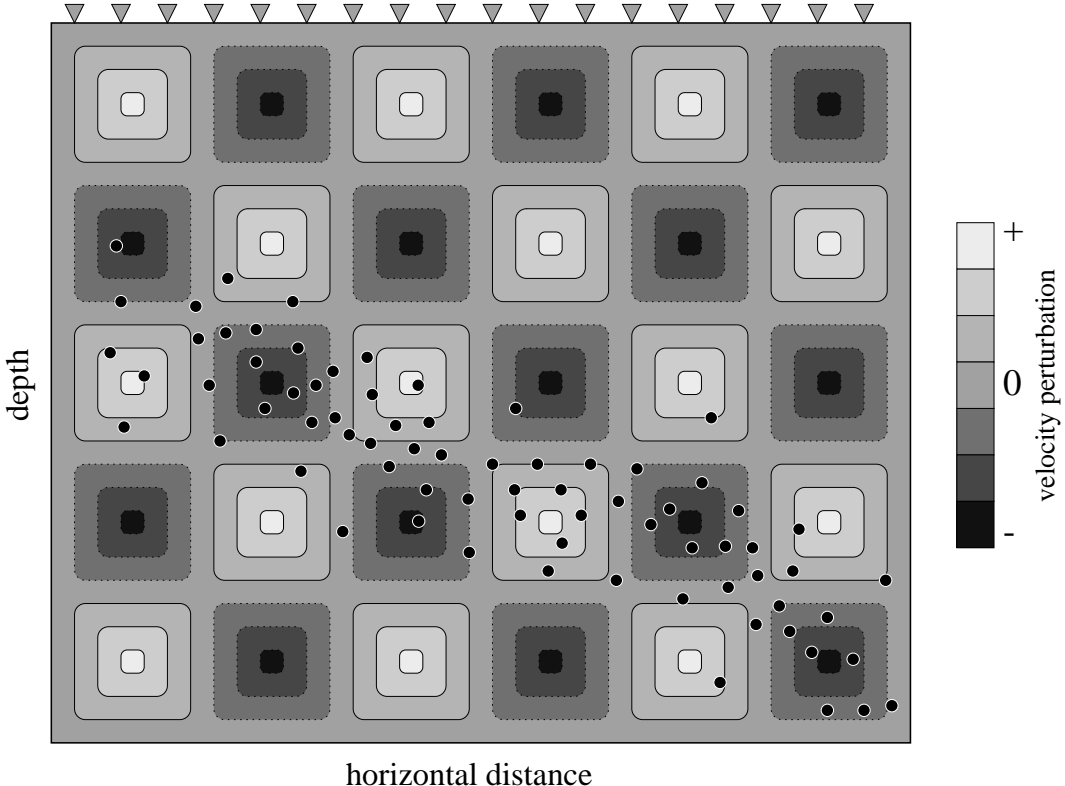


Figure 28: Schematic diagram showing a checkerboard test model for a local earthquake tomography scenario. Sources (black dots with white edges) and receivers (grey-filled triangles) are positioned identically to the real experiment and rays are traced through the synthetic structure. The synthetic traveltimes are then inverted, starting from some given initial model, in an attempt to recover the checkerboard pattern.

2.4.2 Synthetic Tests

Parameterizations that describe continuous velocity fields often opt for resolution tests that attempt to reconstruct a synthetic model using the same source-receiver geometry as the real experiment. The rationale behind this approach is that if a known structure with similar length scales to the solution model can be recovered using the same (for linearized solutions) or similar (for iterative non-linear solutions) ray paths, then the solution model should be reliable. The quality criterion is the similarity between the recovered model and the synthetic model. The so-called “checkerboard test” (Fig. 28), in which the synthetic model is divided into alternating regions of high and low velocity with a length scale equal (or greater) to the smallest wavelength structure recovered in the solution model, is a common test model. The initial model used for the test is the same as that used for the real inversion. Regions in which the checkerboard pattern is recovered clearly are those regions in which structure in the solution model can be considered to be well resolved. Lévêque et al. (1993) demonstrate that such an approach is not necessarily as reliable as it might seem. It is possible for the small scale structure of the checkerboard test to be well retrieved while larger-scale structure

is poorly retrieved. Furthermore, if the solution takes into account the non-linearity of the inverse problem, then the ray-path coverage will have a dependence on the velocity distribution. Thus, while a checkerboard reconstruction can account for the non-linearity of the traveltime dependence on the checkerboard structure, it cannot account for the non-linearity of the traveltime dependence on the true structure. Thus, rather than iteratively invert for the checkerboard structure, it may be better to simply use the ray-path geometry from the model produced by the inversion of the real data in a linear inversion. Alternatively, one could test a number of different synthetic models to investigate the effect of different structures (and hence ray geometries) on the resolution; this would be advisable especially if the solution model is complex.

Teleseismic traveltime tomography studies that have used checkerboard resolution tests include those by Glahn & Granet (1993), Achauer (1994) and Seber et al. (1996). Ritsema et al. (1998) used several different synthetic models rather than checkerboards and analyzed the accuracy of their recovery. This kind of analysis is not commonly used in wide-angle studies, although recently, Zelt (1998), Zelt et al. (1999, 2001) and Day et al. (2001) implemented checkerboard tests for analyzing the resolution of velocity structure (Zelt et al., 1999, also use it for interface structure) derived from wide-angle traveltime inversion. In local earthquake tomography, checkerboard tests have been implemented by Chiarabba et al. (1997) and Graeber & Asch (1999); Walck & Clayton (1987) and Walck (1988) used synthetic reconstructions with anomalies positioned in key localities (i.e. regions of high geological interest).

3 Applications to Observed Data

In this section, we review some applications of traveltime inversion methods to real data. Our aim is to give an idea of how the methods described above can be put together to solve a 2-D or 3-D inverse problem in practice. With this in mind, we tend to focus our attention on several selected case studies, rather than just briefly describe numerous examples. The choice of which methods to use is usually influenced by the class of data (reflection, wide-angle, local earthquake, teleseismic) that is available (see Section 1.3). For example, normal incidence reflection data, as its name suggests, predominantly contains reflected phases, so interfaces must be included in the parameterization. Teleseismic data, on the other hand, do not contain reflected phases, so structure in this case is generally represented by a continuous velocity variation. Thus, the different data types often resolve different aspects of structure, a feature that will also be discussed in some detail below.

3.1 Reflection Tomography

A number of 2-D schemes for the tomographic interpretation of reflection data have been presented over the years but not many of them have been extensively applied to real data (at least, there are not many examples in the literature). Bishop et al. (1985) presented one of the first methods for the simultaneous determination of velocity and depth in laterally varying media. In their method, the subsurface is represented by sub-horizontal layers separated by interfaces with a cubic spline parameterization. Within each layer, velocity is permitted to vary laterally and vertically by means of a grid of constant velocity gradient boxes. Within each box, a ray path segment will have the geometry of a circular arc, and therefore has an analytic expression. A shooting method of ray tracing determines source-receiver ray paths and traveltimes, and a Gauss-Newton method is used to iteratively minimize an objective function consisting of a data residual term and a model length

term (i.e. damping but no smoothing). The system of linear equations is solved using a Gauss-Seidel algorithm with successive over-relaxation. The method was applied to Common Depth Point (CDP) data from a pair of intersecting profiles in a region with permafrost. Significant shallow velocity variations due to the presence of the permafrost were imaged and the depth estimates to the interfaces at the intersection of the profiles agreed significantly better than those determined by conventional seismic processing. The maximum depth to which structure was imaged was ~ 5.5 km.

It has been recognized by a number of authors that reflection traveltimes poorly resolve vertical variations of velocity within a layer (Farra & Madariaga, 1988; Kosloff et al., 1996). In the method of Farra & Madariaga (1988), a layered parameterization is adopted in which interfaces and lateral velocity variations within layers are described by cubic B-splines. Velocity within a layer is vertically invariant. Source-receiver ray paths and traveltimes are found with a shooting method of ray tracing that uses elements of paraxial ray theory to iteratively correct the ray take-off angle. The objective function they minimize consists of a data residual term and a penalty function which restricts the model behavior in accordance with the available *a priori* model information. A DLS approach is applied to iteratively minimize the objective function, and SVD is used to solve the system of linear equations at each step. They also make use of a layer-stripping approach. In this scheme, reflection traveltimes from the top interface are initially used to constrain the top layer only. Once these data are satisfied, traveltimes for the second interface are also introduced and together they are used to constrain the first two layers. The scheme continues in this manner through each successive layer. Farra & Madariaga (1988) applied their scheme to a synthetic model that included a layer pinchout, and showed that it can be reconstructed using a model with 1-D structure as a starting model. Coupled oscillations of interfaces and velocity variations were found to occur in regions where the data were unable to resolve the trade-off between interface depth variation and lateral velocity variation within a layer. They then applied the scheme to data from the Paris Basin. The maximum offset between source and receiver was 1.68 km, and structure was imaged to a depth of 2 km. A total of 99 parameters (57 velocity, 42 interface) were used to describe the model. The initial model was described by four flat constant velocity layers. In the solution model, the interfaces remained nearly horizontal, but the layer velocities had significant lateral variations. The recovered interface geometries are consistent with the known structure of the region.

Imaging of 3-D structure by reflection tomography is not very common. Chiu et al. (1986) developed and applied a scheme to vibroseis data collected on Vancouver Island. Their method assumes that subsurface structure can be adequately represented by constant velocity layers that separate interfaces described by n^{th} -order polynomial surfaces. A ray bending scheme is used to solve the forward problem, and an iterative damped least squares approach is used to solve the inverse problem. As in the above methods the linear system of equations are solved with SVD. However, in their application to crooked line vibroseis data collected as part of PROJECT LITHOPROBE, only 110 traveltime picks were available to constrain the structure of a two-interface model, consisting of a decollement zone and an under-thrusting oceanic crust. They found that planar interfaces were adequate to satisfy the data, making this a rather limited example of 3-D tomography.

In general, coincident reflection traveltimes alone do not seem to be sufficient to resolve both interface depth variations and arbitrary velocity variations within a layer, despite the relatively dense ray coverage associated with most reflection experiments. Williamson (1990) confirms this limitation by using a multi-stage inversion scheme in which progressively shorter length scales are permitted in both velocity and interface geometry as the iterative process proceeds. Despite satisfying the data and finding that longer wavelength components may be adequately recovered, Williamson

(1990) also found that shorter wavelength velocity-depth trade-offs cannot be resolved without further information. This may take the form of *a priori* information to help constrain the problem, and/or simplifying assumptions made about the structure (e.g. constant velocity layers, layers in which velocity has no vertical variation). While this may be sufficient at shallow depths, a basic drawback of reflection tomography is that the resolving power of the data decreases with depth due to the geometry of the experiment. Thus, it is usually limited to near-surface applications.

3.2 Wide-Angle Tomography

Unlike coincident reflection tomography, inversion of wide-angle traveltimes for 2-D or 3-D crustal structure has been applied to many datasets from around the world. For example, numerous studies have been carried out in Canada (e.g., Hole et al., 1992; Kanasewich et al., 1994; Clowes et al., 1995; Zelt & White, 1995; Morozov et al., 1998; Zelt et al., 2001), the U.S. (e.g. Lutter & Nowack, 1990; Jarchow et al., 1994; Zhu & Ebel, 1994; Parsons et al., 1996; Wang & Braile, 1996; Lizarralde & Holbrook, 1997), Europe (e.g. Riahi & Lund, 1994; Staples et al., 1997; Darbyshire et al., 1998; Louden & Fan, 1998; Mjelde et al., 1998; Korenaga et al., 2000; Morgan et al., 2000) and in oceanic settings (e.g. Hildebrand et al., 1989; Wiggins et al., 1996; Kodaira et al., 1998; Recq et al., 1998; Day et al., 2001; Grevemeyer et al., 2001). Experiments involving marine air-gun sources and land based receivers or OBSs (Ocean Bottom Seismometers) are quite common since they can be coupled with coincident reflection studies. As discussed in Section 1.3, wide-angle data contain both refraction and wide-angle reflection phases. The traveltimes of rays that refract tend to constrain velocity variations better than wide-angle reflections, which in turn are better at constraining interface depth. Thus, with adequate data coverage, the simultaneous inversion of refraction and reflection traveltimes can result in a well constrained solution model that includes both variations in interface depth and layer velocity.

Wide-angle experiments are usually performed in 2-D (i.e. recorded by an in-line array of sources and receivers), although recent studies (Zelt & Barton, 1998; Zelt et al., 1999; Day et al., 2001; Rawlinson et al., 2001b; Zelt et al., 2001) indicate that 3-D wide-angle surveys are becoming more frequent. In 2-D experiments, data coverage is often quite dense, and tomographic-style interpretation techniques are usually designed to allow both interface structure and layer velocities to be constrained by the data. One of the most frequently used methods for the tomographic style inversion of 2-D wide-angle traveltimes was developed by Zelt & Smith (1992). In their method, the model is parameterized in terms of a layered network of irregular blocks (see Section 2.1), which allows velocity to vary both laterally and vertically within a layer. Layer pinchouts and isolated bodies can also be included by reducing layer thickness to zero. The advantage of this approach to structural representation is that velocity and interface node distribution can be adapted to suit the resolving power of the dataset. Refractions, reflections and head waves are traced through the model by numerically solving the initial value problem formulated in terms of a pair of first order ordinary differential equations (Eq. 19 and Eq. 20). Linear interpolation between rays that bracket a given receiver is used to estimate the corresponding traveltime and Fréchet derivatives. The inverse problem is solved using an iterative DLS method (damping but no smoothing), with rays re-traced after each iteration. LU decomposition is used to solve the system of linear equations.

A number of authors have adopted the approach of Zelt & Smith (1992) to invert wide-angle data, including Kanasewich et al. (1994), Riahi & Juhlin (1994), Staples et al. (1997), Ye et al. (1997), Darbyshire et al. (1998), Kodaira et al. (1998), Morozov et al. (1998) and Navin et al. (1998). Darbyshire et al. (1998) applied it to data from the ICEMELT refraction line to image crustal

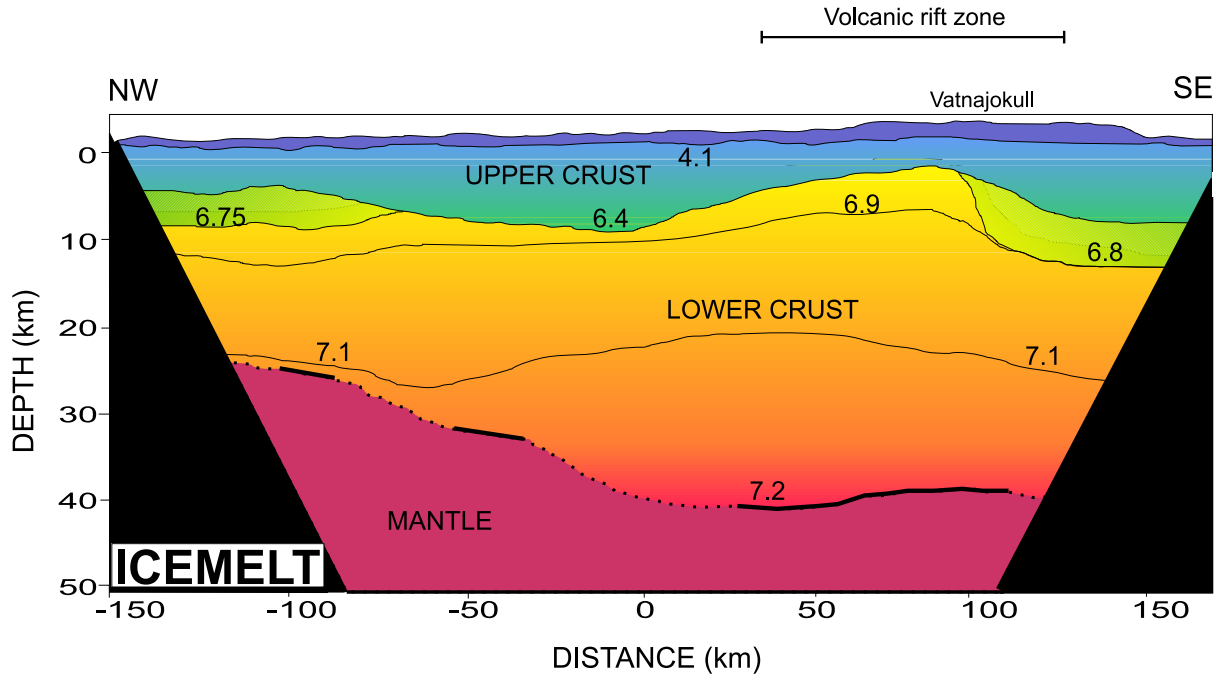


Figure 29: Crustal model obtained from the ICEMELT refraction line in Iceland using the wide-angle traveltimes inversion method of Zelt & Smith (1992). Solid lines on the Moho represent those parts of the interface constrained by the data. [From Darbyshire et al. (1998). Copyright 1998 Royal Astronomical Society. Reproduced by permission of Blackwell Science Ltd.]

structure above the Iceland mantle plume. In their study, up to 60 land-based recorders were used to record seismic energy from six explosive shots along a 310 km line traversing Iceland from north to south. A total of 181 traveltimes picks were used to constrain the crustal model, which included both interfaces and velocity variations within a layer. The inversion solution produced a normalized χ^2 misfit value of 1.31. Fig. 29 shows the ICEMELT crustal model produced by the inversion of refraction and wide-angle reflection traveltimes. The upper crust is characterized by high vertical velocity gradients ($>0.2 \text{ s}^{-1}$) and considerable lateral heterogeneity. By contrast, the lower crust is less complex and features much smaller vertical velocity gradients ($<0.03 \text{ s}^{-1}$). The crust thickens to nearly 40 km depth above the mantle plume, a feature interpreted to be caused by increased melt generation due to elevated mantle temperatures and active convection in the plume core. Two of the methods used by Darbyshire et al. (1998) to analyze the robustness of their solution model are ray coverage and estimates of resolution from linear theory. Fig. 30a shows all the ray paths used to constrain the ICEMELT model, and Fig. 30b shows a plot of the diagonal elements of the resolution matrix; values ≥ 0.5 are considered well resolved. Several regions in the upper and lower crust are poorly resolved while the mid crust is generally well resolved.

Darbyshire et al. (1998) did not use the inversion routine of Zelt & Smith (1992) in a completely automated fashion. Manual intervention (i.e. the user empirically tunes one or more parameter values instead of the inversion routine) was used to refine some of the upper crustal structure. In 2-D wide-angle modeling, it is sometimes necessary to intervene during the inversion process to prevent unrealistic model perturbations caused, for example, by insufficient data constraints or extreme non-linearity. In some studies (e.g. Iwasaki et al., 1990; Gürbüz & Evans, 1991; Grad et al., 1997; Iwasaki et al., 1998; Recq et al., 1998), the inversion is performed completely manually in a process called “forward modeling” (i.e. one tries to satisfy the data by adjusting model parameter values using trial

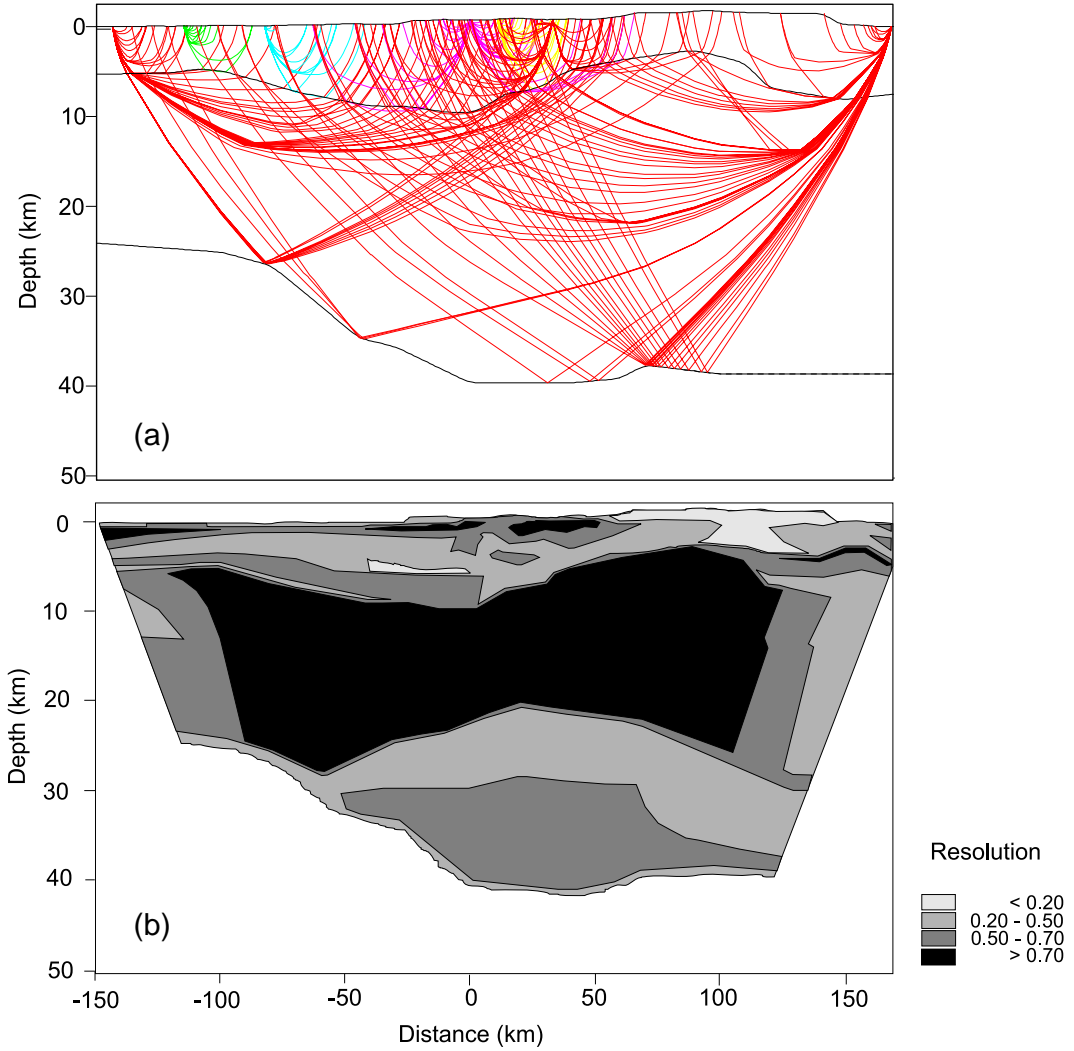


Figure 30: (a) All ray paths used to constrain the model in Fig. 29 and (b) diagonal elements of the resolution matrix obtained from linear theory. Regions that are considered well constrained have a value ≥ 0.5 . [From Darbyshire et al. (1998). Copyright 1998 Royal Astronomical Society. Reproduced by permission of Blackwell Science Ltd.]

and error). The advantage of this approach is that the user has complete control over the state of the model, and that hypothetical structures may be tested against the data. On the other hand, if there are a large number of model parameters, repeated forward modeling becomes very time consuming.

Wide-angle seismic studies that attempt to constrain structure in 3-D usually do not consider both interface structure and layer velocity variations. For example, Hole (1992), Hammer et al. (1994), Toomey et al. (1994), Zelt & Barton (1998), Day et al. (2001) and Zelt et al. (2001) inverted first arrivals for continuously varying velocity, and Hole et al. (1992) and Riahi & Juhlin (1994) inverted refraction and reflection traveltimes respectively for interface structure. Studies that have attempted to invert for both parameter types include Zelt et al. (1996), who use a layer stripping approach, and Zelt (1999), who use floating reflectors coupled with sharp velocity gradients to simulate discontinuities. Most of the above 3-D wide-angle studies use methods to solve the forward problem of traveltime and ray path determination based on the finite difference approach of Vidale (1990).

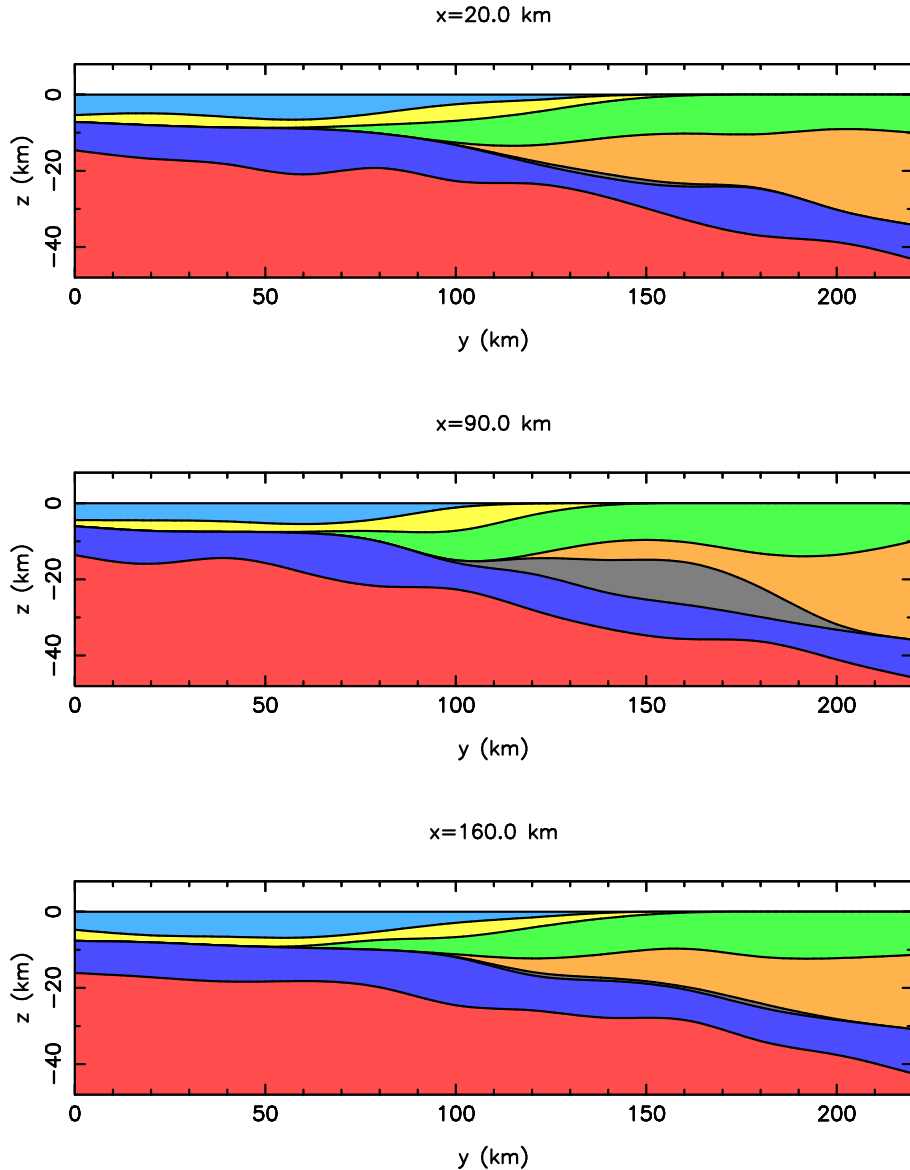


Figure 31: Three cross sections taken approximately perpendicular to the strike of the subducting slab of a synthetic subduction zone. Rawlinson (2000) showed that it was possible to reconstruct the underplated low velocity lens (grey) from an initial model with only 2-D structure using wide-angle refraction and reflection traveltimes. Land based receivers and marine sources were used in the synthetic test, which demonstrated the flexibility of the method developed by Rawlinson et al. (2001a). From top to bottom, the ocean layer is shown in light blue, the sediment layer in yellow, the upper crustal layer in green, the lower crustal layer in amber, the subducting ocean crust in dark blue, and the lithospheric mantle in red.

In fact, it is probably true to say that this is the only branch of seismic tomography in which this method predominates.

A method for the inversion of 3-D wide-angle seismic traveltimes that uses conventional ray tracing, rather than grid-based eikonal methods, was presented by Rawlinson et al. (2001a). In this scheme, crustal structure is represented by layers separated by smoothly varying interfaces with a cubic B-spline parameterization. Within each layer, the velocity varies linearly with depth. This restriction on the layer velocity field means that rays can be traced analytically within a layer, thus allowing rapid solution of the initial value problem. The two point problem is solved using a shooting

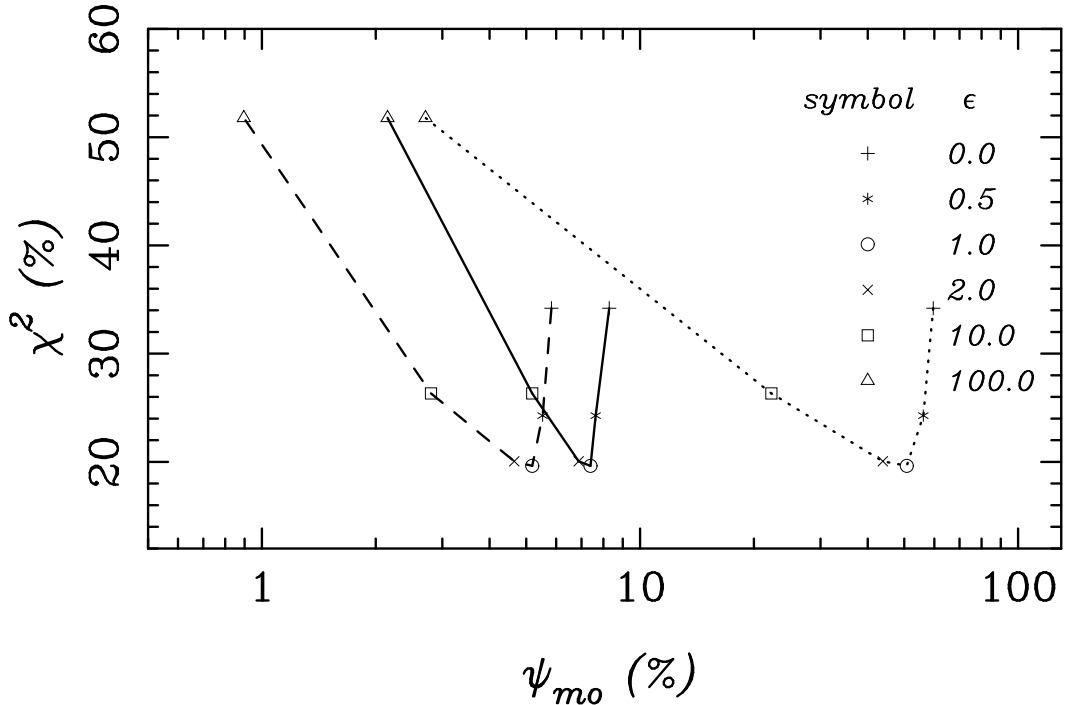


Figure 32: Traveltime inversion trade-off curves for various values of the damping factor ϵ after four iterations of the inversion performed by Rawlinson et al. (2001b) for the crustal structure of Tasmania. The ordinate axis plots the percentage improvement in χ^2 from the starting model, while the abscissa plots the percentage perturbation of the solution model from the initial model; this is plotted for each parameter type: interface node depth (solid line), layer velocity (dashed line) and layer velocity gradient (dotted line).

method which uses a Newton-type method to accurately locate the required two-point paths. A subspace inversion method is used to iteratively solve the inverse problem of minimizing an objective function consisting of a data residual term and a damping term. A smoothing term was not included because the smooth nature of the cubic B-spline parameterization facilitated implicit smoothing by varying the node density as required. An obvious drawback of the method is that the assumption of a crustal layer with laterally invariant velocity may not be applicable in some circumstances. However, if such a model is able to satisfy a given dataset, then it may be difficult to argue for a more complex model. Novel features of the method are that layers may pinch out and the horizontal distribution of the nodes may be varied to suite the resolving power of the dataset. Quite complex structure may therefore be represented. An example is provided by Rawlinson (2000) where a relatively complex synthetic subduction zone (see Fig. 31), which includes an underplated low velocity lens, was successfully reconstructed from a starting model with only 2-D structure.

Rawlinson et al. (2001b) applied the method of Rawlinson et al. (2001a) to wide-angle data collected as part of the TASGO project. In this study, an array of 44 land-based recorders was distributed throughout the island state of Tasmania, SE Australia, to record seismic energy from an encircling array of marine normal incidence reflection shot lines. The size of the dataset was reduced from its maximum potential by a number of recorder failures, low signal to noise ratios at several sites and the limited range of the airguns (usually <200 km). A total of 2590 P_n and $P_m P$ traveltimes from 13 shot lines to 21 receivers were used to constrain a two layer model of Tasmania. This consisted of the crust and the upper mantle separated by a Moho of variable depth. Lateral variations of velocity within the crust were not included because P_n and $P_m P$ arrivals poorly

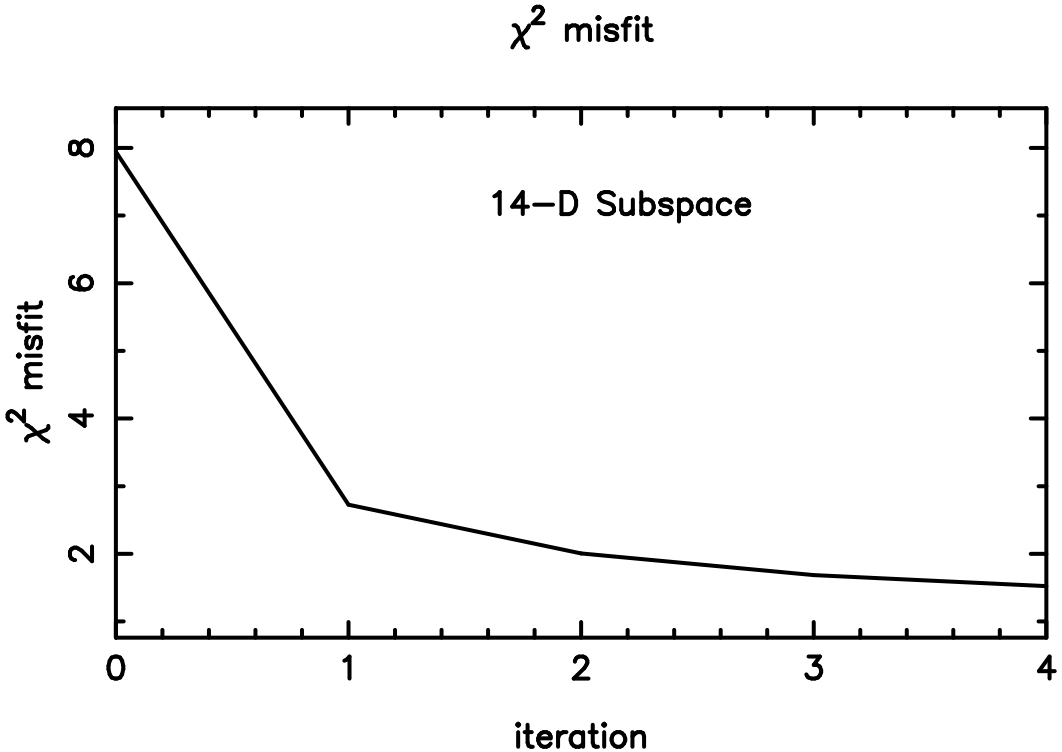


Figure 33: χ^2 misfit versus iteration number for the inversion (using $\epsilon = 1.0$) of P_n and $P_m P$ traveltimes done by Rawlinson et al. (2001b) for the Moho structure of Tasmania.

constrain such features, and the coverage of crustal arrivals was rather poor.

The Moho is represented by a rectangular grid of 600 nodes spaced 20 km apart. The total number of unknowns in the inverse problem is therefore 604 - only two parameters are required to describe the linear velocity gradients in each of the crust and mantle. A simple 1-D model with the Moho at 30 km depth was chosen as a starting model. The damping factor ϵ , that weights the relative importance of the data and the *a priori* model information, was selected by inspection of a trade-off curve (Fig. 32). Since there are three parameter classes in the inverse problem (interface node depth, layer velocity and layer velocity gradient), a trade-off curve is shown for each. From these diagrams, a value of $\epsilon = 1$ was taken. Note that $\epsilon = 2$ generates a near-identical model. A 14-D subspace inversion scheme was applied to minimize the objective function; after four iterations, the RMS travelttime fit was reduced to 176 ms from an initial value of 371 ms. The corresponding normalized χ^2 misfit versus iteration is shown in Fig. 33.

The Moho structure of the solution model is shown in Fig. 34 along with the diagonal elements of the resolution matrix. Outside the horizontal bounds of the source-receiver array, much of the Moho has not been perturbed from its initial value of 30 km due to a lack of ray path coverage. This is supported by the resolution map, which also indicates poor data coverage in central and NE Tasmania (Fig. 34b). A striking feature of the solution model is a major change in crustal thickness beneath the Arthur Lineament metamorphic belt in NW Tasmania (Fig. 34a). This has been interpreted to represent the NW limit of deformation in Tasmania during the Mid-Late Cambrian Tyennan Orogeny.

3-D wide-angle tomographic problems often involve large datasets and a large number of unknowns. For example, in their inversion for continuously varying velocity structure, Zelt & Barton (1998) use 53,479 first-arrival picks and separately invert for 315,000 unknowns using a backpro-

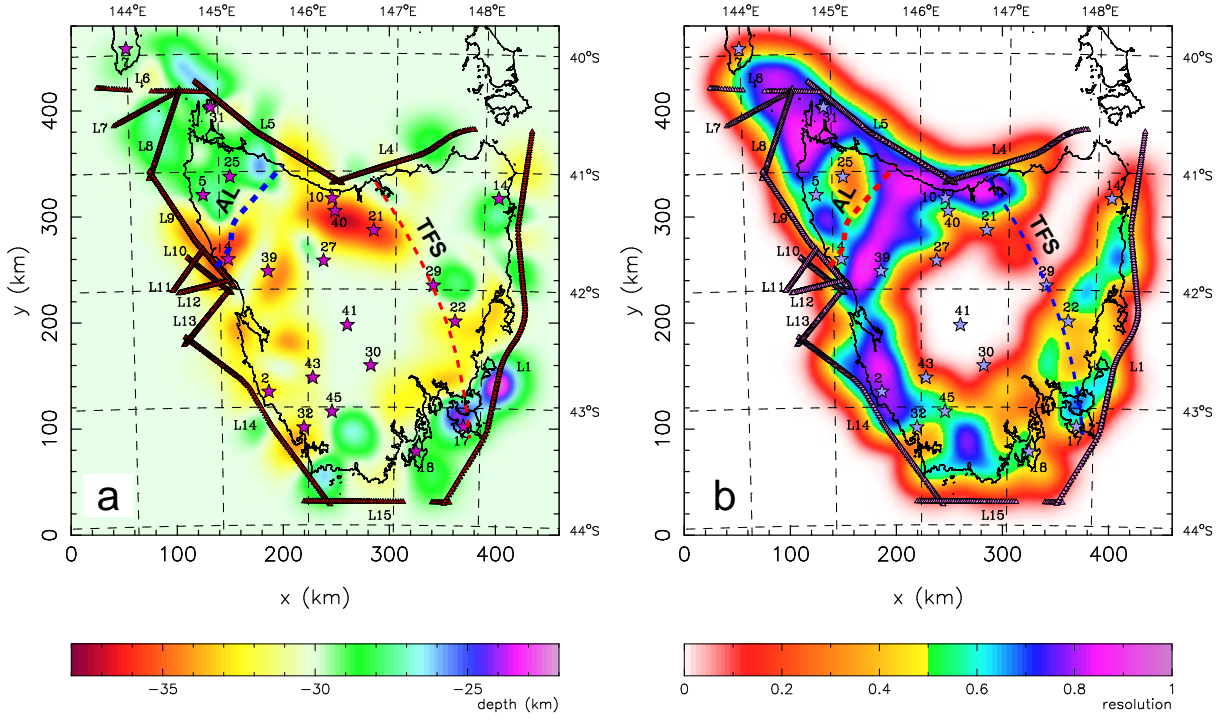


Figure 34: (a) Moho depth and (b) diagonal elements of the resolution matrix of the solution model for Tasmania produced from the TASGO wide-angle dataset. In both diagrams, stars indicate recorders and small triangles indicate shot points from which data were picked. Contiguous triangles form shot lines except where data gaps occur (e.g. lines 4 and 15). Thick dashed lines denote tectonic element boundaries: Arthur Lineament (AL) and Tamar Fracture System (TFS). [From Rawlinson et al. (2001b). Copyright 2001 American Geophysical Union. Reproduced by permission of American Geophysical Union]

jection method and 35,000 unknowns using a regularized least squares method. Studies of a similar magnitude were recently carried out by Day et al. (2001) and Zelt et al. (2001).

In summary, wide-angle tomography has proven to be a useful tool for revealing information about crustal structure. Its strength is its ability to resolve the trade-off between interface depth and lateral velocity variation within a layer given sufficient data coverage. This is in contrast to coincident reflection tomography. The main weaknesses of wide-angle tomography are the difficulty of picking reflection phases, which are always later arrivals, and the presence of extreme lateral variations in crustal structure, which can cause significant ray-path perturbations, and hence violate the local linearity assumption upon which iterative inversion methods are based.

3.3 Local Earthquake Tomography

Local earthquake tomography (LET) is a common tool for imaging subsurface structure in seismically active areas. Studies have been carried out in many different regions including California (Aki & Lee, 1976; Thurber, 1983; Eberhart-Phillips, 1986; Walck & Clayton, 1987; Walck, 1988; Zhao & Kanamori, 1992; Eberhart-Phillips & Michael, 1993; Scott et al., 1994), Taiwan (Kao & Rau, 1999), Japan (Nakanishi, 1985; Zhao et al., 1992), South America (Bosch, 1997; Graeber & Asch, 1999) and the Mediterranean (Chiarabba et al., 1997; Luca et al., 1997; Papazachos & Nolet, 1997; Haslinger et al., 1999). Apart from the source-receiver geometry, one of the distinguishing features of LET compared to the other types of tomography discussed here, is the need to relocate earthquake

hypocenters (spatial location and origin time) as part of the image reconstruction. This is because accurate hypocenter location requires an accurate knowledge of the velocity structure in the region occupied by the earthquakes and the recorders whose data are used in the location process. Adequate data are therefore required to resolve the trade-off between variations in structure and variations in hypocenter locations.

One of the original LET studies was carried out by Aki & Lee (1976). In their method, 3-D crustal structure is represented by constant slowness blocks. The initial model is completely homogeneous, and the inversion is linear, so rays consist of straight line paths between sources and receivers. Slowness perturbations for each block and hypocenter corrections are simultaneously inverted for using a DLS approach (damping but no smoothing). The method was applied to data collected at 60 stations in Bear Valley, California, from 32 local earthquakes. The $x \times y \times z$ block size was set at $3 \times 4 \times 5 \text{ km}^3$, with a total of 264 blocks used to span a volume of $24 \times 44 \times 15 \text{ km}^3$ which included all receivers and sources. 1218 first-arrival times were inverted for all unknowns. Estimates of covariance and resolution from linear theory were used to analyze the robustness of the velocity solution and relocated hypocenters. A feature of the solution model is a narrow low velocity band oriented along the San Andreas fault zone in the upper 5 km.

The conceptual basis of LET has not really altered since the study of Aki & Lee (1976). However, some refinements have been made. For example, Thurber (1983) used approximate 3-D ray tracing (which allows iterative improvement of the solution model) and a continuously varying velocity field via linear interpolation of a uniform grid of velocity nodes. Eberhart-Phillips (1990) introduced a pseudo bending scheme to find more accurate two-point paths starting from rays calculated using the approximate ray tracing method of Thurber (1983). These refinements are common to most implementations of LET in recent times and are encapsulated in the commonly used computer package SIMULPS12 (Evans et al., 1994).

A relatively recent application of LET was carried out by Graeber & Asch (1999) to image the subduction zone structure beneath the southern central Andes. In this study, local earthquakes were recorded by a network of 31 recorders deployed in northern Chile between the Coastal Cordillera and the Western Cordillera. A total of 16,488 P -arrivals from 764 events were inverted for P -velocity structure and hypocenter location using the SIMULPS12 algorithm. The initial model required by the inversion scheme was based upon a model produced by a separate inversion of the data for 1-D structure and hypocenter location only. The optimum damping factor for the DLS solution was obtained by visual inspection of the data variance vs. solution variance trade-off curve approximated by performing several single-iteration inversions with a range of damping values. Station delay terms were also included in the inversion as unknowns to help offset the effects of near surface structure. The solution model was obtained after 12 iterations of the DLS method, which reduced the data variance by 63% with respect to the optimum 1-D model. Fig. 35 shows a series of vertical slices through the resulting P -wave velocity model, which is described by a total of 2496 nodes. Relocated hypocenters are also shown in this figure. Only those parts of the velocity model that are relatively well resolved according to the diagonal elements of the resolution matrix are shown in Fig. 35. The solution model clearly suggests the presence of a subduction zone involving the easterly subduction of oceanic crust beneath continental crust, with the geometry of the subducted plate also indicated by the relocated hypocenters.

Apart from calculating the resolution matrix to investigate solution robustness, Graeber & Asch (1999) also performed several synthetic resolution tests, including a checkerboard test. The results of this test at two cross-sections are shown in Fig. 36. As expected, the reconstruction below the

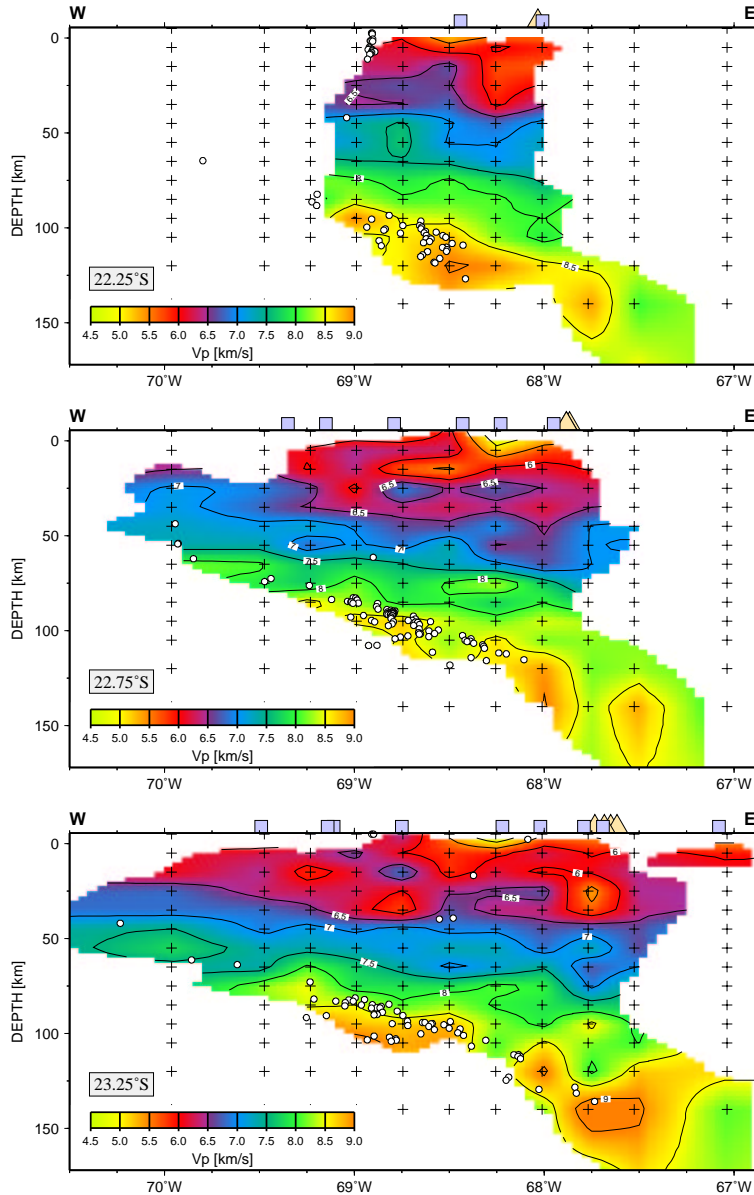


Figure 35: Cross-sections through a 3-D velocity model of the southern central Andes produced by inversion of local earthquake arrival times. Absolute velocities shown are a sum of initial velocities and calculated perturbations from an iterative non-linear inversion technique. Stations, recent volcanoes and hypocenters adjacent to the sections are denoted by squares, triangles and open circles respectively. Velocity grid nodes are denoted by crosses. [From Graeber & Asch (1999). Copyright 1999 American Geophysical Union. Reproduced by permission of American Geophysical Union]

hypocenters is generally poor, but in the region between the hypocenters and receivers the reconstruction is generally good.

In addition to using first-arrival P -wave data, it is also quite common in LET to utilize S -wave data. A particularly useful property to map is the P -to- S velocity ratio (V_p/V_s). For example, regions with high levels of hydration are likely to have elevated V_p/V_s since the shear modulus will be reduced compared to the bulk modulus. One way of determining V_p/V_s is to separately invert for P and S velocity structure and then compare the results (e.g. Eberhart-Phillips, 1990). One problem with this is that the S -wave dataset is often smaller and of poorer quality than the P -wave dataset,

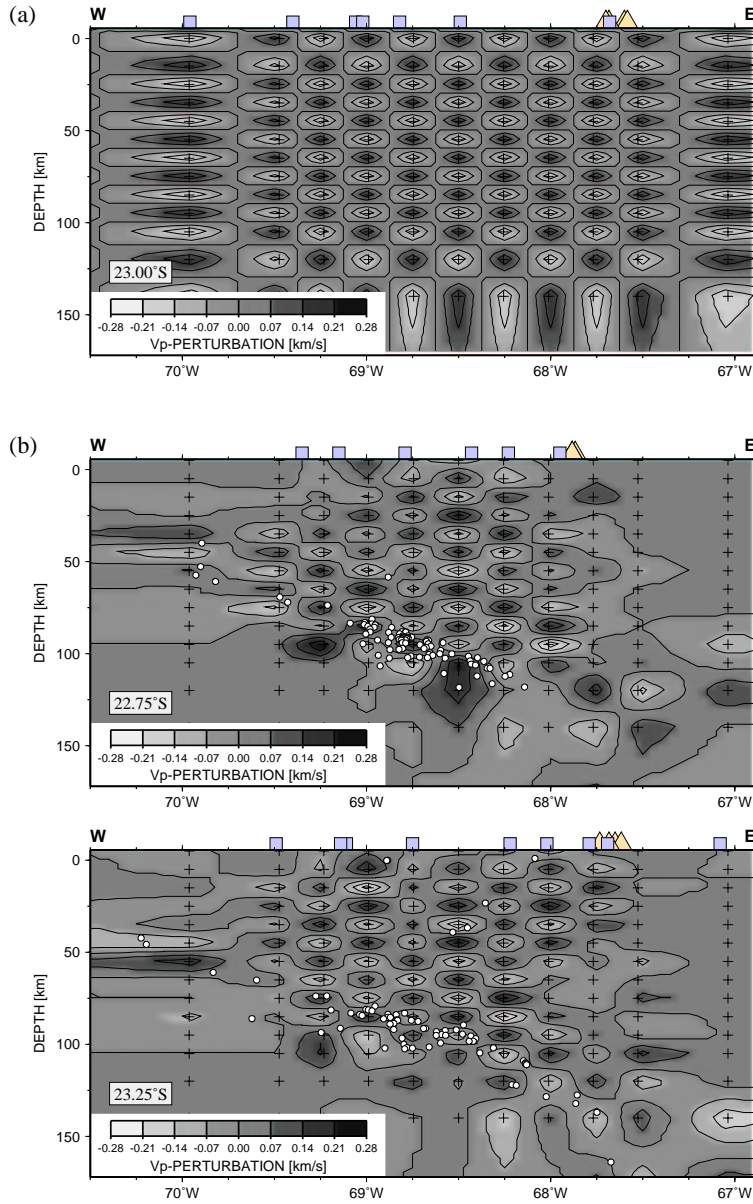


Figure 36: Checkerboard resolution test for the model shown in Fig. 35. (a) Synthetic checkerboard model, and (b) recovered checkerboard at two different latitudes. Symbols are defined as in Fig. 35. [From Graeber & Asch (1999). Copyright 1999 American Geophysical Union. Reproduced by permission of American Geophysical Union]

making detailed comparison of the two models difficult. An alternative is to directly invert the difference in P and S arrival times $T_s - T_p$ for V_p/V_s . Walck (1988) used this approach to construct a model of the 3-D variation in V_p/V_s in the Coso Region, California using backprojection. Graeber & Asch (1999) also construct an image of V_p/V_s by considering 8238 $T_s - T_p$ arrival time residuals. Their inversion for V_p/V_s was performed simultaneously with the inversion for V_p , hypocenter location and station delays. They found elevated V_p/V_s ratios in the zone above the subducting oceanic crust, suggesting the release of aqueous fluids from the oceanic crust into the overlying material.

Although restricted to regions of active seismicity, LET is a useful tool for mapping subsurface

structure at a variety of scales. Shallow earthquakes can be used to image the upper few kilometers of the crust (e.g. Walck, 1988; Chiarabba et al., 1997) while deep earthquakes from regions like subduction zones can be used to image lithospheric scale structure (e.g. Graeber & Asch, 1999). While relocation of earthquake hypocenters is a necessary part of the reconstruction of the velocity field from the data, their distribution provides valuable additional information on subsurface structure. Inclusion of S -wave data in the form of inversion of $T_s - T_p$ for V_p/V_s is not commonly considered in the other forms of tomography described in this paper, further distinguishing LET as a method worth considering provided local earthquake sources are available.

3.4 Teleseismic Tomography

Like wide-angle tomography and local earthquake tomography, teleseismic tomography has been used extensively to map the structure of the crust and lithosphere. Studies are often carried out on a variety of scales ranging from 10s of km (e.g. Rawlinson & Houseman, 1998; Steck et al., 1998) to 100s of km (e.g. Humphreys & Clayton, 1990; Dorbath & Paul, 1996). In the latter type of study, mantle beneath the lithosphere is also imaged. Usually, the horizontal extent of the receiver array and the source distribution determines the depth to which features may be resolved. Most teleseismic studies are carried out in 3-D (e.g. Aki et al., 1977; Oncescu et al., 1984; Humphreys & Clayton, 1990; Benz et al., 1992; Glahn & Granet, 1993; Achauer, 1994; Seber et al., 1996; Saltzer & Humphreys, 1997; Ritsema et al., 1998; Steck et al., 1998; Graeber et al., 2002), with relatively few 2-D studies (e.g. Evans, 1982; McQueen & Lambeck, 1996) probably because of the difficulty in lining up an array of recorders on roughly the same great circle as a set of teleseismic earthquakes with good angular coverage.

The data utilized by teleseismic tomography studies are the relative traveltimes residuals of identifiable phases (usually the direct P -phase). These are obtained by calculating the difference between predicted and observed traveltimes and subtracting the mean for each source-receiver set. Predicted traveltimes are usually obtained by ray tracing through a 1-D reference model of the Earth, such as IASP91 (Kennett & Engdahl, 1991). Removing the mean from each set of traveltime residuals means that they are relatively insensitive to errors in hypocenter location. However, they also become insensitive to vertical variations in structure. One consequence of this is that the horizontally averaged velocity structure of the solution model will simply reflect the horizontally averaged velocity structure of the initial model. Interpretation of the resulting models must therefore be done with care (see Lévêque & Masson, 1999, for more details).

One of the first papers to describe a method of seismic tomography was that of Aki et al. (1977), who developed a scheme in the context of application to teleseismic data. In their method, the lithosphere is represented by layers composed of constant velocity blocks. Incoming wavefronts from teleseismic events are assumed to be locally planar beneath the model region and the initial model has constant velocity layers. Thus, the task of ray tracing from the incident wavefront to the receiver array is straightforward. Linear inversion is performed using either a stochastic inverse or a generalized inverse approach. The stochastic solution is essentially a DLS solution with $\epsilon = 1$, while the generalized inverse solution has $\epsilon = 0$, but identifies a minimum length solution using SVD. The method was applied to data collected by the Norwegian Seismic Array (Norsar) to image lithospheric structure in southeastern Norway. A total of 1496 traveltime residuals from 93 events recorded at 22 sites (each consisting of six seismometers) were inverted for the slowness perturbation of 405 constant velocity blocks contained in a five-layer model of the lithosphere (9×9 blocks per layer). The model region has a horizontal coverage of 180×180 km and extends to a depth of 126

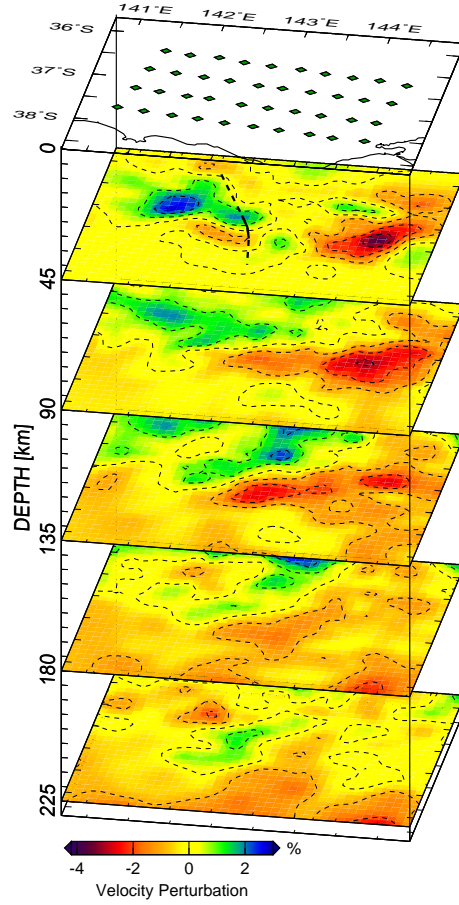


Figure 37: Horizontal sections taken through the 3-D solution model of western Victoria obtained by inversion of teleseismic traveltimes residuals. Receivers are denoted by green diamonds and the dashed line on the 45 km depth slice indicates the approximate location of the Moyston Fault Zone. [From Graeber et al. (2002). Copyright 2002 Royal Astronomical Society. Reproduced by permission of Blackwell Science Ltd.]

km. Estimates of *a posteriori* model covariance and resolution obtained from linear theory were used to analyze the solution models. The encouraging results produced by this study undoubtedly catalyzed the numerous seismic tomography studies of the crust and lithosphere that soon followed.

A recent example of teleseismic tomography, which reflects the way in which the method has evolved since the paper of Aki et al. (1977), is that of Graeber et al. (2002). In this study, an array of 40 short period recorders were distributed throughout an area of about $270 \times 150 \text{ km}^2$ in western Victoria, SE Australia. The tomographic scheme of VanDecar (1991) was used to invert 4067 teleseismic traveltimes residuals for the velocity structure of the crust and upper mantle to a depth of 405 km. In this scheme, velocity structure is represented by a spherical grid of slowness nodes (27,898 of them in this case) interpolated by splines under tension. A shooting method of ray-tracing based on the method of Creager & Jordan (1984) finds source-receiver traveltimes and ray paths through the 3-D model. To solve the inverse problem, a gradient-based iterative non-linear scheme is employed. The objective function consists of a data misfit term and a number of regularization terms including damping, flattening (first-derivative smoothing) and smoothing (second-derivative smoothing). In addition, station and hypocenter corrections are included as unknowns. Station corrections help

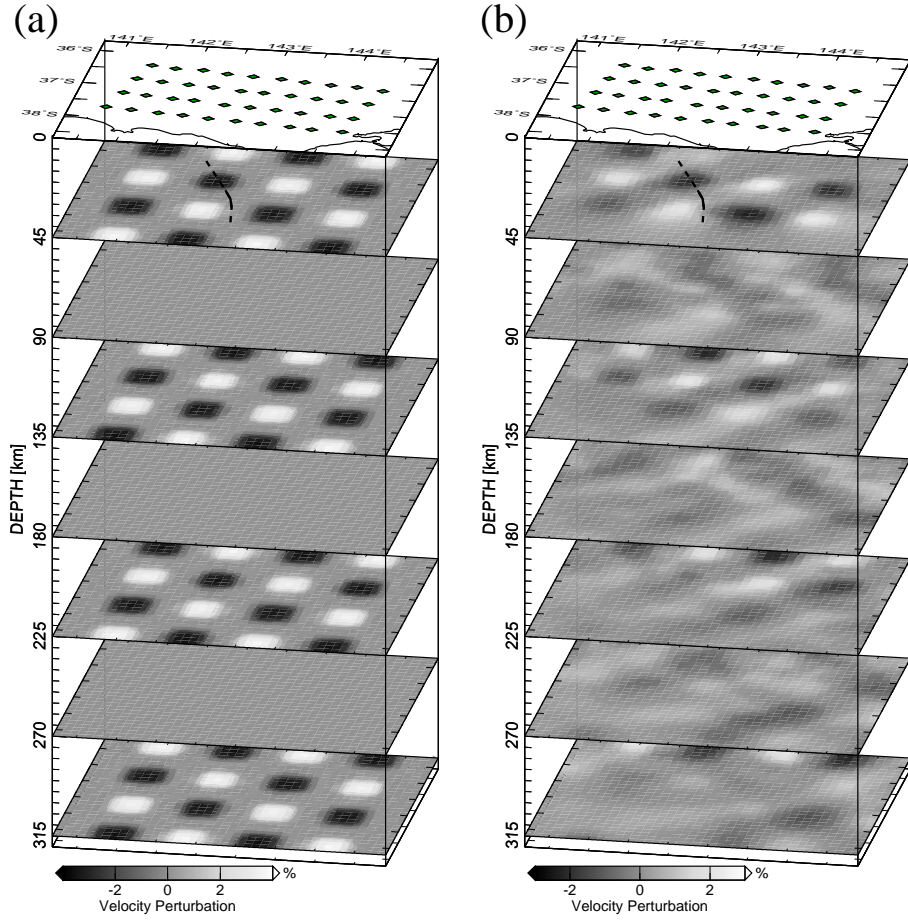


Figure 38: Synthetic checkerboard resolution test for the model shown in Fig. 37. (a) Original checkerboard model, and (b) reconstructed checkerboard. [From Graeber et al. (2002). Copyright 2002 Royal Astronomical Society. Reproduced by permission of Blackwell Science Ltd.]

reduce the mapping of near surface effects into deeper structure. Hypocenter adjustments are usually kept small because they are poorly constrained. The minimization of the objective function is achieved by assuming local linearization which allows the objective function to be written as a matrix equation (cf. Eq. 63). This matrix equation is then solved using a conjugate gradient method. The linear inversion and 3-D ray-tracing are performed iteratively to account for the non-linear nature of the inverse problem.

The solution model produced by Graeber et al. (2002) using this scheme is shown in Fig. 37 as a series of horizontal slices. One of the prominent features of the model is a relatively slow anomaly in the east which decreases in amplitude with depth. Graeber et al. (2002) interpret this feature, which lies beneath the Newer Volcanic Province, as a thermal anomaly related to Pliocene and Pleistocene hotspot-fueled volcanism. Synthetic tests were used to examine the robustness of the inversion solution. Fig. 38 shows the results of a checkerboard resolution test. In this version, alternating fast and slow anomalies are separated by zones of zero anomaly to permit smearing effects to be detected more easily (Fig. 38a). The reconstruction (Fig. 38b) recovers the checkerboard pattern more successfully nearer the surface. The amplitudes of the recovered checkerboard anomalies are generally less than the synthetic model, which is a typical feature of this type of test. The degraded structure of the recovered checkerboard is due partly to the source coverage - in this study, few

earthquakes from the south and west were detected.

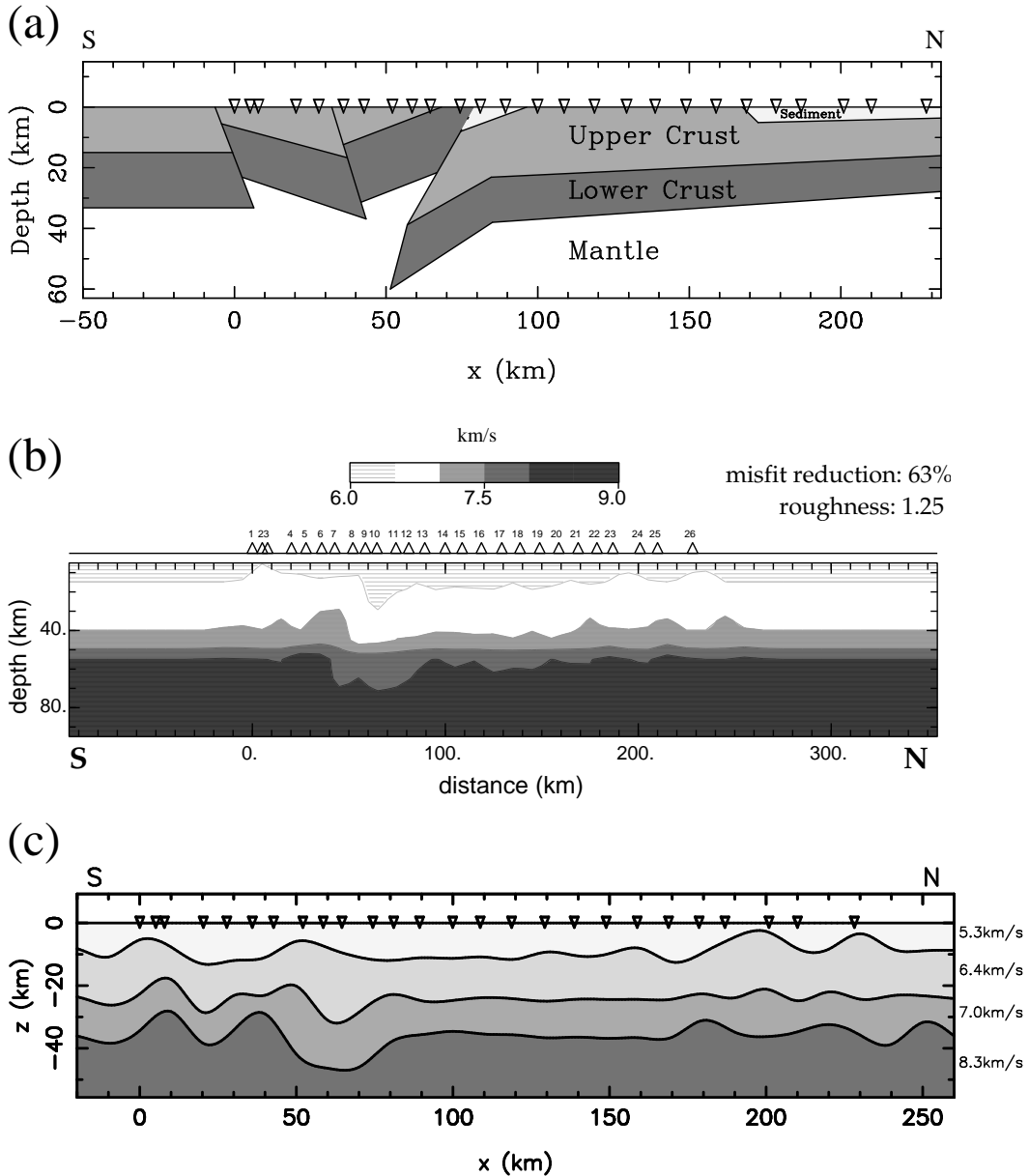


Figure 39: Three models derived from the Musgrave Line teleseismic dataset using different methods. (a) Crustal structure obtained by Lambeck & Burgess (1992) using forward modeling, (b) contours of velocity for the model obtained by inversion for slowness perturbation by McQueen & Lambeck (1996), and (c) crustal structure obtained by Rawlinson & Houseman (1998) using inversion for interface geometry. Note the differences in scale between (a), (b) and (c). [Modified from Rawlinson & Houseman (1998). Copyright 1998 Royal Astronomical Society. Reproduced by permission of Blackwell Science Ltd.]

In most teleseismic tomography studies, traveltimes residuals are matched by adjusting velocity (or slowness) parameters that describe a continuous velocity field; interfaces are rarely included. There are several reasons for this. First, teleseismic data do not contain obvious signs of an interface, such as the “reflectors” seen in normal-incidence seismic sections, or the later arriving, large amplitude reflection curves evident in refraction studies. Interfaces may cause mode conversions

in teleseismic arrivals, but these are not easy to detect, particularly if the analysis relies on single component data. Second, methods that invert for both interface structure and continuous velocity variation must be able to address the trade-off between velocity and interface position. In teleseismic tomography, only transmitted rays are available, so the prospect of producing a well resolved combination of velocity and interface parameters is low. Finally the number and approximate depths of interfaces needs to be known *a priori* as there is little information in the data on this aspect. To some extent, this problem also occurs when a continuous velocity field is assumed, in that it is not possible to derive an initial model from the data itself. In such circumstances, the starting model may be obtained from other sources, such as wide-angle studies, or even global 1-D velocity models such as IASP91 (see Graeber et al., 2002). Surface wave inversion and teleseismic receiver function results may also be useful in locating approximate interface positions. Since the Earth is characterized by both continuous and discontinuous changes in structure, it is reasonable to investigate the other end member model type (i.e. consisting only of variable interfaces) when inverting teleseismic traveltimes residuals for subsurface structure. This has been done by Davis (1991), Kohler (1997) and Rawlinson & Houseman (1998).

In the 2-D method of Rawlinson & Houseman (1998), structure is represented by sub-horizontal constant velocity layers. Interfaces are described by nodes interpolated by cubic splines. The depths of the nodes are the unknowns in the inversion. Rays are traced from a planar incident wavefront to the receiver array by means of a shooting method. A conjugate gradient method is used to minimize an objective function that consists only of a data residual term. The method is iterative, with ray-tracing applied after each application of the conjugate gradient method to account for the non-linear nature of the inverse problem. Synthetic tests showed that multiple interfaces may be reconstructed simultaneously in the presence of noise, and with relatively inaccurate initial models. For example, if the initial interfaces have an inaccurate average depth, their shape can still be recovered, but the average depth of the interface will not change. The method was applied to the Musgrave Line dataset collected in central Australia that traversed portions of the Musgrave Block and the Amadeus Basin. A three-interface crustal model was used to represent structure, and the data consisted of traveltimes from only five incoming wavefronts. The initial model was based on a 1-D refraction interpretation of wide-angle data collected nearby.

The Musgrave Line dataset was previously interpreted by Lambeck & Burgess (1992) and McQueen & Lambeck (1996) using different methods. Lambeck & Burgess (1992) used forward modeling to satisfy the data with structure represented in terms of constant velocity layers with piece-wise linear boundaries. McQueen & Lambeck (1996) used a SIRT backprojection method to invert the traveltimes residuals for perturbations in slowness on a rectangular grid of constant slowness cells. Lateral structure was permitted to a depth of over 90 km. Both methods used a 2.5 D approach (i.e. models are defined in 3-D space but are restricted to 2-D structure), allowing additional out-of-plane sources to be considered.

Fig. 39 compares all three models for the Musgrave Line that have been derived using different assumptions about structure and different approaches to satisfy the data. In terms of defining laterally slow and fast regions, all three models have a reasonable level of agreement. It is interesting to note that the two end member inversion models both satisfy the data to approximately the same level (63% misfit reduction for Fig. 39b and 62% misfit reduction for Fig. 39c), suggesting that inverting for interface structure and inverting for velocity variation are equally valid as far as the data are concerned. One advantage a tomographic inversion approach has over forward modeling is the ability to test the robustness of the solution. Fig. 40 shows two synthetic tests used to assess the

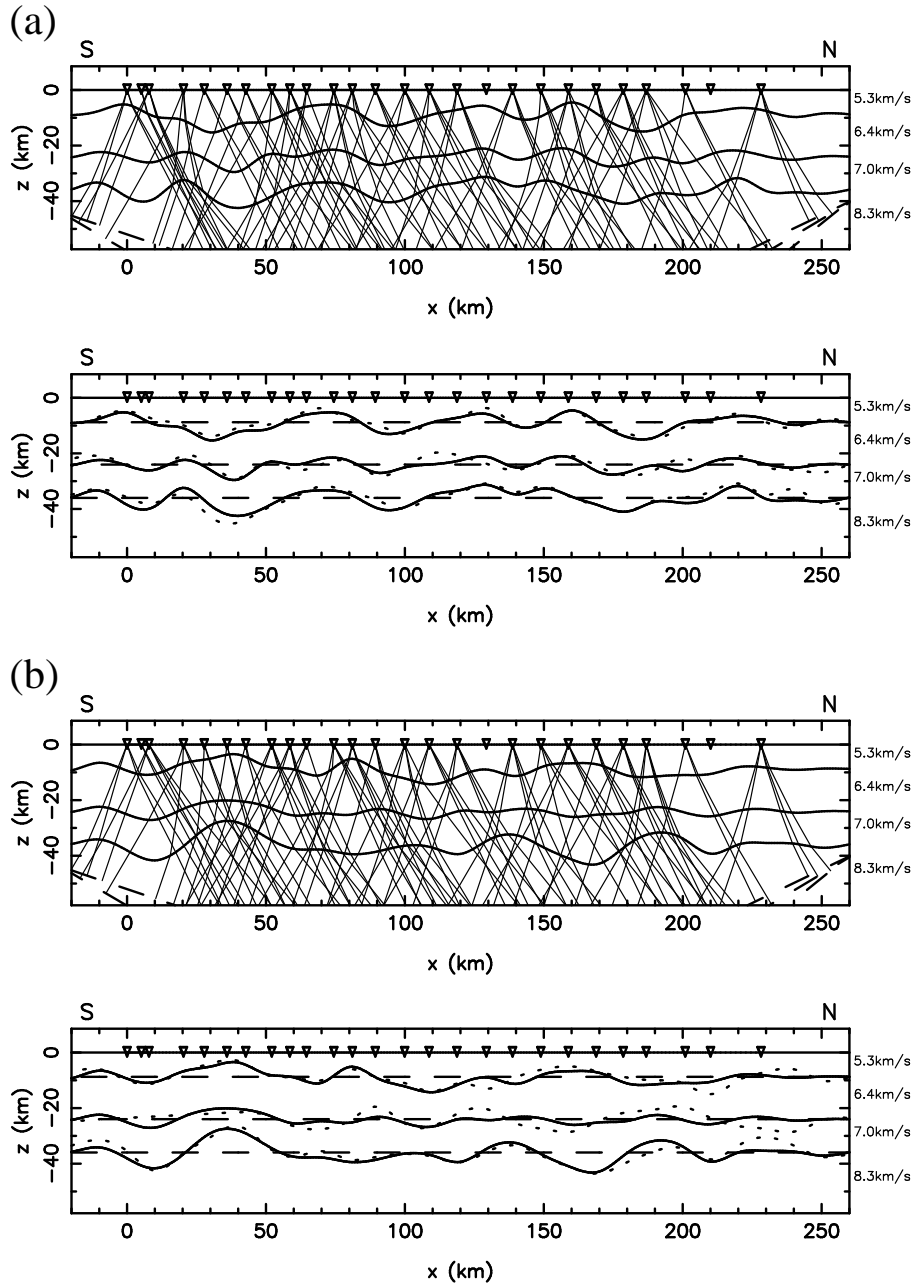


Figure 40: Two synthetic tests designed to analyze the robustness of the solution given in Fig. 39c. Ray diagrams show paths from the five wavefronts through the recovered structure. Dashed lines show the initial model, dotted lines the true model and solid lines the reconstruction. The synthetic models in (a) and (b) were chosen to be quite different in order to illustrate the effect of different ray geometries on the reconstruction.

quality of the solution shown in Fig. 39c. Both structures were chosen arbitrarily, and the tests use the same wavefront geometry and receiver array as the Musgrave Line experiment. The reconstruction of all three interfaces is generally quite accurate in both tests, suggesting that most of the significant structure contained in the solution model (Fig. 39c) is well constrained by the data.

Teleseismic tomography is a useful tool for investigating crust and upper mantle structure. Compared to local earthquake tomography, its main advantages are that it can be used to map structure

at greater depths, and that it is not restricted to regions of active seismicity. However, the fact that relative traveltimes residuals must be used means that only relative perturbations in lateral structure can be resolved. In addition, the assumption that the model region is completely responsible for the teleseismic traveltimes residuals will not always be valid. Also, the near-vertical incidence angle of ray-paths and the sometimes poor azimuthal source coverage may lead to significant smearing effects that in turn can lead to incorrect interpretations of results (see Keller et al., 2000). On the other hand, the interface structure shown in Fig. 39c demonstrates one advantage of the near-vertical transmission of rays: highly complex lateral structure may be resolved. Wide-angle tomography (for example) would have great difficulty imaging such structural complexity.

4 Future Developments

Traveltimes tomography still remains the most popular approach for imaging subsurface structure on crustal and lithospheric scales. A wide array of schemes and algorithms can be found to tackle these problems, and there is little doubt that traveltimes tomography will continue to play a role in the imaging of earth structure well into the future. Our aim here is to discuss, and to some degree speculate on, the possible directions in which seismic traveltimes tomography methods may develop, and whether it will continue to be the predominant interpretation technique for large datasets.

A current limitation of many traveltimes tomography techniques is that they only consider first-arrivals and ignore the potentially vast amount of information contained in later arriving phases. Exceptions include coincident reflection tomography and wide-angle tomography. In the case of reflection tomography, the number of phases picked usually corresponds to the number of interfaces contained in the model. Wide-angle tomography often includes later arriving reflection phases in a similar fashion. One of the principal difficulties in including traveltimes information from later-arriving phases is that they are often obscured by the wavetrain of earlier arriving phases. This can make identification difficult or impossible. Another difficulty is that even if coherent later arrivals can be picked, they need to be related to model structure in order to be useful. For first-arrivals picked from a seismogram, this is not required because we just need to search for the transmission paths through the structures that correspond to first arrivals. Of course, this task is not necessarily straight forward, but the point is that we don't need to know anything about the ray path *a priori*. For wide-angle reflection phases, for example, we do need to know which interface they reflect from. If a layered parameterization is used, with the number of interfaces defined by the number of reflection phases identified, then the problem of association may not arise. If the interfaces are defined *a priori*, then it may not be easy to relate later arrivals with structure. One approach is to constrain the initial model using only first-arrivals plus any other phases that can be confidently identified, and then use the updated model to predict the traveltimes of other phases that weren't picked but may be evident in the data. A direct comparison with the observed data may allow additional phases to be picked with more confidence (Zelt, 1999). Multiples and phase conversions may also be identified in this manner.

As well as the problems of detection and association of later arrivals described above, yet another difficulty is that current methods of traveltimes and ray path determination used in tomography are only capable of finding a small subset of all possible arrivals. Obvious examples are the grid-based methods (Section 2.2.2) and SPR (Section 2.2.3), both of which are limited to first-arrivals. Both methods can be made to find reflection arrivals but not later arrivals associated with caustics. Traditional ray tracing methods can find multiple arrivals - for example, by shooting an extremely dense

spread of rays, or by bending using a large variety of initial paths. However, in even moderately complex media, these approaches would be very computationally expensive. Recently, significant effort has been made in developing and implementing schemes for computing multivalued traveltimes maps. One approach, often referred to as *wavefront construction*, involves the discrete propagation of a wavefront through a medium by using local ray tracing from each wavefront surface. Rays are traced for a given time step, with the end points of the rays describing the geometry of the new wavefront. New rays are introduced by interpolation if diverging rays cause parts of the wavefront to be poorly sampled. Multiple arrivals can be found using this scheme, including caustics. This basic idea for locating multiple arrivals has been developed by a number of authors (e.g. Vinje et al., 1993; Ettrich & Gajewski, 1996; Lucio et al., 1996; Lambaré et al., 1996; Vinje et al., 1996, 1999). Other schemes for finding multi-valued traveltimes fields include Big Ray tracing (Benamou, 1996; Abgrall, 1999), which is a two-step procedure involving relatively coarse ray tracing followed by solution of the eikonal equation in spatial domains defined by adjacent ray paths, and Dynamic Surface Extension (Steinhoff et al., 2000), which shares similarities with wavefront construction.

The use of these schemes within a tomographic inversion may allow the traveltimes of more later arrivals to be utilized, thus resulting in a potentially better constrained and more detailed solution. With the advent of modern high fidelity broad band digital seismometers, much more information on the later arriving wavefield is being recorded, and new methodology such as wavefront construction is required to better exploit this type of data.

Another area in which traveltime tomography may see more development is in the combining of different datasets in a simultaneous inversion. Usually, tomographic studies constrain structure using just one type of data (reflection, wide-angle, local earthquake, teleseismic), but this need not be the case provided more than one overlapping dataset is available. For example, wide-angle or LET arrays are likely to detect teleseismic arrivals during their deployment, which could be exploited together with the principal dataset. Studies that combine different datasets have been carried out in the past. Thurber (1983) and Ankeny et al. (1986) included refraction traveltimes from several explosive sources in a LET study, Parsons & Zoback (1997) simultaneously inverted local earthquake, explosive source and airgun traveltimes for the crustal structure of the San Francisco Peninsula, and Sato et al. (1996) simultaneously inverted local earthquake and teleseismic traveltimes data to image structure beneath the northeastern Japan arc. Methods that combine coincident reflection and wide-angle data in a simultaneous inversion have been developed by Wang & Braile (1996) and McCaughey & Singh (1997).

An often important component of subsurface velocity structure (especially in regions exhibiting significant deformation) that is frequently ignored in traveltime tomography studies is anisotropy. If the effects of anisotropy are severe enough, reconstructions that assume isotropy may produce erroneous results (Watanabe et al., 1996). The principal reason for ignoring anisotropy is that the data can usually be satisfied adequately with an isotropic model. Introducing anisotropy effectively increases the number of unknowns considerably for the same spatial resolution, meaning that the inverse problem is likely to become under-determined for most realistic datasets. As a consequence, traveltime tomography studies that have considered anisotropy usually make several assumptions about structure to reduce the number of unknowns. For example, Hearn (1996) inverted P_n traveltimes for lateral variations in both velocity and anisotropy in the uppermost mantle. The Moho surface along which the ray paths propagate is assumed to be planar, and is parameterized in terms of cells. Each cell is associated with three unknowns: slowness and two coefficients of azimuthal anisotropy. Using multiple traveltime datasets and later arriving phases as suggested above may

make anisotropy tomography a more realistic proposition as data coverage will be greatly improved.

The traveltimes of seismic phases constitute just one of the components of the recorded waveform. Combining traveltimes with amplitude information or using the shape of the waveform itself is likely to yield much more information than traveltimes alone. Wang & Pratt (1997) combined traveltime and amplitude data in reflection tomography. They showed that using both datasets in an inversion for velocity or interface structure results in more accurate solutions compared to inversions that invert only one data type. Neele et al. (1993) combined amplitude and traveltimes from a teleseismic dataset in a joint inversion for upper mantle structure. Pratt et al. (1996) demonstrated via 2-D synthetic tests that wavefield inversion of wide-angle seismic data produces velocity models of significantly greater resolution than traveltime inversion. Combining traveltime data with non-seismic data is also likely to be further developed in the future. Using both gravity data and traveltime data from wide-angle surveys to constrain crustal models has been done in the past. For example, Vogt et al. (1998) used a forward modeling approach to reconcile the two data types and produce a structural model for the Hatton Basin and continental margin. Lees & VanDecar (1991) simultaneously inverted local earthquake traveltimes and Bouger gravity anomalies for crustal structure in Western Washington.

Like most other areas of science, increases in computing power will also influence the way in which traveltime tomography will be approached in the future. Indeed, many of the potential future developments described above are reliant to some extent on the availability of greater computing power. Computationally intensive methods for solving the inverse step of the problem like genetic algorithms or simulated annealing (Section 2.3.3) will become more feasible for larger scale problems. Currently, they are limited to perhaps several hundred unknowns at most. Also, the results from other studies could be used to improve model accuracy. For example, a teleseismic model could be embedded within a lower resolution global model to help prevent the mapping of aspherical mantle structure into the local region of interest. This has been done in the context of regional-scale traveltime inversion by Widjiantoro & van der Hilst (1997); in this study, global and regional traveltimes were inverted simultaneously for a regional model on a $1^\circ \times 1^\circ$ grid embedded within a global model with a $5^\circ \times 5^\circ$ cell size. However, the non-linearity of the problem was not accounted for in the inversion, probably due in part to the significant computational expense involved.

In conclusion, there are still many new ways in which seismic traveltimes can be exploited in tomographic-style problems. Most current methods use only a small subset of the recorded information, such as first arrivals. The new generation of methods are likely to be able to represent continuous and discontinuous structure, use a wide variety of data geometries (e.g. coincident reflection, wide-angle etc.), incorporate traveltimes from later phases, account for anisotropy, use other aspects of the waveform such as amplitudes, and perhaps be able to use other data types such as gravity. The optimum method would use all the information contained in the recorded waveform to constrain structure, but practical implementation of such an approach is a long way off. Seismic traveltimes have played an important role in helping us to understand the structure and composition of the crust and lithosphere via tomographic inversion, and will continue to do so well into the future.

ACKNOWLEDGMENTS

We thank Fiona Darbyshire for kindly supplying Fig. 29 and Fig. 30, and Frank Graeber for kindly supplying Fig. 35, Fig. 36, Fig. 37 and Fig. 38. Greg Houseman is thanked for useful discussions on an early version of this work, and an anonymous referee is thanked for constructive comments on the original manuscript.

References

- Aarts, E. & Korst, J., 1989. *Simulated Annealing and Boltzmann machines*, John Wiley & Sons, Chichester.
- Abers, G. A., 1994. Three-dimensional inversion of regional P and S arrival times in the East Aleutians and sources of subduction zone gravity highs, *J. Geophys. Res.*, **99**, 4395–4412.
- Abgrall, R., 1999. Big ray-tracing and eikonal solver on unstructured grids: Application to the computation of a multivalued travelttime field in the Marmousi model, *Geophysics*, **64**, 230–239.
- Achauer, U., 1994. New ideas on the Kenya rift based on the inversion of the combined dataset of the 1985 and 1989/90 seismic tomography experiments, *Tectonophysics*, **236**, 305–329.
- Afnimar & Koketsu, K., 2000. Finite difference travelttime calculation for head waves travelling along an irregular interface, *Geophys. J. Int.*, **143**, 729–734.
- Aki, K. & Lee, W. H. K., 1976. Determination of the three-dimensional velocity anomalies under a seismic array using first P arrival times from local earthquakes 1. A homogeneous intial model, *J. Geophys. Res.*, **81**, 4381–4399.
- Aki, K. & Richards, P. G., 1980. *Quantitative seismology: theory and methods*, W. H. Freeman, San Francisco.
- Aki, K., Christoffersson, A., & Husebye, E. S., 1977. Determination of the three-dimensional seismic structure of the lithosphere, *J. Geophys. Res.*, **82**, 277–296.
- Alkhalifah, T. & Fomel, S., 2001. Implementing the fast marching eikonal solver: Spherical versus Cartesian coordinates, *Geophysical Prospecting*, **49**, 165–178.
- Ankeny, L. A., Braile, L. W., & Olsen, K. H., 1986. Upper crustal structure beneath the Jemez Mountains volcanic field, New Mexico, determined by three-dimensional simultaneous inversion of seismic refraction and earthquake data, *J. Geophys. Res.*, **91**, 6188–6198.
- Asad, A. M., Pullammanappallil, S. K., Anooshehpoor, A., & Louie, J. N., 1999. Inversion of travelttime data for earthquake locations and three-dimensional velocity structure in the Eureka Valley area, eastern California, *Bull. Seism. Soc. Am.*, **89**, 796–810.
- Bartels, R. H., Beatty, J. C., & Barsky, B. A., 1987. *An introduction to splines for use in computer graphics and geometric modelling*, Morgan Kaufmann, Los Altos.
- Benamou, J. D., 1996. Big ray tracing: Multivalued travel time field computation using viscosity solutions of the Eikonal equation, *J. Comp. Phys.*, **128**, 463–474.
- Benz, H. M. & Smith, R. B., 1984. Simultaneous inversion for lateral velocity variations and hypocenters in the Yellowstone region using earthquake and refraction data, *J. Geophys. Res.*, **89**, 1208–1220.
- Benz, H. M., Zandt, G., & Oppenheimer, D. H., 1992. Lithospheric structure of northern California from teleseismic images of the upper mantle, *J. Geophys. Res.*, **97**, 4791–4807.

- Bijwaard, H. & Spakman, W., 2000. Non-linear global P -wave tomography by iterated linearized inversion, *Geophys. J. Int.*, **141**, 71–82.
- Bijwaard, H., Spakman, W., & Engdahl, E. R., 1998. Closing the gap between regional and global travel time tomography, *J. Geophys. Res.*, **103**, 30,055–30,078.
- Bishop, T. P., Bube, K. P., Cutler, R. T., Langan, R. T., Love, P. L., Resnick, J. R., Shuey, R. T., Spindler, D. A., & Wyld, H. W., 1985. Tomographic determination of velocity and depth in laterally varying media, *Geophysics*, **50**, 903–923.
- Blundell, C. A., 1993. *Resolution analysis of seismic P -wave velocity estimates using reflection tomographic inversion*, Ph.D. thesis, Monash University.
- Bosch, M., 1997. P wave velocity tomography of the Venezuelan region from local arrival times, *J. Geophys. Res.*, **102**, 5455–5472.
- Boschetti, F., Dentith, M. K., & List, R. D., 1996. Inversion of seismic refraction data using genetic algorithms, *Geophysics*, **61**, 1715–1727.
- Cao, S. & Greenhalgh, S., 1994. Finite-difference solution of the eikonal equation using an efficient, first-arrival, wavefront tracking scheme, *Geophysics*, **59**, 632–643.
- Cara, M. & Lévéque, J. J., 1987. Waveform inversion using secondary observables, *Geophys. Res. Lett.*, **14**, 1046–1049.
- Carroll, S. & Beresford, G., 1996. Combining reflection tomography with layer replacement for velocity analysis of near-surface reefs, *Geophysics*, **61**, 561–569.
- Cassell, B. R., 1982. A method for calculating synthetic seismograms in laterally varying media, *Geophys. J. Royal Astr. Soc.*, **69**, 339–354.
- Červený, V., 1987. Ray tracing algorithms in three-dimensional laterally varying layered structures, in *Seismic tomography: With applications in global seismology and exploration geophysics*, edited by G. Nolet, pp. 99–133, D. Reidel, Dordrecht.
- Červený, V., 2001. *Seismic Ray Theory*, Cambridge University Press, Cambridge.
- Červený, V. & Pšenčík, I., 1983. Gaussian beams and paraxial ray approximation in three-dimensional elastic inhomogeneous media, *J. Geophys.*, **53**, 1–15.
- Červený, V., Klimeš, L., & Pšenčík, I., 1984. Paraxial ray approximations in the computation of seismic wavefields in inhomogeneous media, *Geophys. J. Royal Astr. Soc.*, **79**, 89–104.
- Chapman, C. H. & Drummond, R., 1982. Body-wave seismograms in inhomogeneous media using Maslov asymptotic theory, *Bull. Seism. Soc. Am.*, **72**, S277–S317.
- Cheng, N. & House, L., 1996. Minimum traveltimes calculations in 3-D graph theory, *Geophysics*, **61**, 1895–1898.
- Chiabba, C., Amoto, A., & Meghraoui, M., 1997. Tomographic images of the El Asnam fault zone, *J. Geophys. Res.*, **102**, 24,485–24,498.

- Chiu, S. K. L., Kanasewich, E. R., & Phadke, S., 1986. Three-dimensional determination of structure and velocity by seismic tomography, *Geophysics*, **51**, 1559–1571.
- Claerbout, J. F. & Muir, F., 1973. Robust modelling with erratic data, *Geophysics*, **38**, 826–844.
- Clowes, R. M., Zelt, C. A., Amor, J. R., & Ellis, R. M., 1995. Lithospheric structure in the southern Canadian Cordillera from a network of seismic refraction lines, *Can. J. Earth Sci.*, **32**, 1485–1513.
- Constable, S. C., Parker, R. L., & Constable, C. G., 1987. Occam's inversion: A practical algorithm for generating smooth models from electromagnetic sounding data, *Geophysics*, **52**, 289–300.
- Creager, K. C. & Jordan, T. H., 1984. Slab penetration into the lower mantle, *J. Geophys. Res.*, **89**, 3031–3049.
- Darbyshire, F. A., Bjarnason, I. J., White, R. S., & Flórenz, O. G., 1998. Crustal structure above the Iceland mantle plume, imaged by the ICEMELT refraction profile, *Geophys. J. Int.*, **135**, 1131–1149.
- Davis, P. M., 1991. Continental rift structures and dynamics with reference to teleseismic studies of the Rio Grande and East African rifts, *Tectonophysics*, **197**, 309–325.
- Day, A. J., Peirce, C., & Sinha, M. C., 2001. Three-dimensional crustal structure and magma chamber geometry at the intermediate-spreading, back-arc Valu Fa Ridge, Lau Basin - results of a wide-angle seismic tomographic inversion, *Geophys. J. Int.*, **146**, 31–52.
- Debayle, E. & Kennett, B. L. N., 2000. The australian continental upper mantle: Structure and deformation inferred from surface waves, *J. Geophys. Res.*, **105**, 25,423–25,450.
- Dijkstra, E. W., 1959. A note on two problems in connection with graphs, *Numer. Math.*, **1**, 269–271.
- Dorbath, C. & Paul, A., 1996. Tomography of the Andean crust and mantle at 20°S: First results of the Lithoscope experiment, *Phys. Earth Planet. Inter.*, **97**, 133–144.
- Drijkoningen, G. G. & White, R. S., 1995. Seismic velocity structure of oceanic crust by inversion using genetic algorithms, *Geophys. J. Int.*, **123**, 653–664.
- Dueker, K., Humphreys, E., & Biasi, G., 1993. Teleseismic imaging of the western United States upper mantle structure using the simultaneous iterative reconstruction technique, in *Seismic tomography: theory and practice*, edited by H. M. Iyer & K. Hirahara, pp. 265–298, Chapman & Hall, London.
- Eberhart-Phillips, D., 1986. Three-dimensional velocity structure in northern California coast ranges from inversion of local earthquake arrival times, *Bull. Seism. Soc. Am.*, **76**, 1025–1052.
- Eberhart-Phillips, D., 1990. Three-dimensional *P* and *S* velocity structure in the Coalinga Region, California, *J. Geophys. Res.*, **95**, 15,343–15,363.
- Eberhart-Phillips, D. & Michael, A. J., 1993. Three-dimensional velocity structure, seismicity, and fault structure in the Parkfield Region, central California, *J. Geophys. Res.*, **98**, 15,737–15,758.

- Eberhart-Phillips, D. & Reyners, M., 1997. Continental subduction and three-dimensional crustal structure: The northern South Island, New Zealand, *J. Geophys. Res.*, **102**, 11,848–11,861.
- Ettrich, N. & Gajewski, D., 1996. Wave front construction in smooth media for prestack depth migration, *Pageoph.*, **148**, 481–502.
- Evans, J., Eberhart-Phillips, D., & Thurber, C., 1994. User's manual for *SIMULPS12* for imaging v_P and v_P/v_S : A derivative of the "Thurber" tomographic inversion *SIMUL3* for local earthquakes and explosions, Open file report 431, U.S. Geological Survey.
- Evans, J. R., 1982. Compressional wave velocity structure of the upper 350 km under the Eastern Snake River Plain near Rexburg, Idaho, *J. Geophys. Res.*, **87**, 2654–2670.
- Faria, E. L. & Stoffa, P. L., 1994. Traveltime computation in transversely isotropic media, *Geophysics*, **59**, 272–281.
- Farra, V. & Madariaga, R., 1988. Non-linear reflection tomography, *Geophys. J.*, **95**, 135–147.
- Fischer, R. & Lees, J. M., 1993. Shortest path ray tracing with sparse graphs, *Geophysics*, **58**, 987–996.
- Fletcher, R. & Reeves, C. M., 1964. Function minimization by conjugate gradients, *Comput. J.*, **7**, 149–154.
- Frederiksen, A. W., Bostock, M. G., VanDecar, J. C., & Cassidy, J. F., 1998. Seismic structure of the upper mantle beneath the northern Canadian Cordillera from teleseismic travel-time inversion, *Tectonophysics*, **294**, 43–55.
- Gjøystdal, H., Reinhardsen, J. E., & Ursin, B., 1984. Traveltime and wavefront curvature calculations in three-dimensional inhomogeneous layered media with curved interfaces, *Geophysics*, **49**, 1466–1494.
- Glahn, A. & Granet, M., 1993. Southern Rhine Graben: Small-wavelength tomographic study and implications for the dynamic evolution of the graben, *Geophys. J. Int.*, **113**, 399–418.
- Goldberg, D. E., 1989. *Genetic Algorithms in Search, Optimization, and Machine Learning*, Addison-Wesley, Reading.
- Gorbatov, A., Widjiantoro, S., Fukao, Y., & Gordeev, E., 2000. Signature of remnant slabs in the North Pacific from P -wave tomography, *Geophys. J. Int.*, **142**, 27–36.
- Gorbatov, A., Fukao, Y., Widjiantoro, S., & Gordeev, E., 2001. Seismic evidence for a mantle plume oceanwards of the Kamchatka-Aleutian trench junction, *Geophys. J. Int.*, **146**, 282–288.
- Grad, M., Shiobara, H., Janik, T., Guterch, A., & Shimamura, H., 1997. Crustal model of the Bransfield Rift, West Antarctica, from detailed OBS refraction experiments, *Geophys. J. Int.*, **130**, 506–518.
- Graeber, F. M. & Asch, G., 1999. Three-dimensional models of P wave velocity and P -to- S velocity ratio in the southern central Andes by simultaneous inversion of local earthquake data, *J. Geophys. Res.*, **104**, 20,237–20,256.

- Graeber, F. M., Houseman, G. A., & Greenhalgh, S. A., 2002. Regional teleseismic tomography of the western Lachlan Orogen and the Newer Volcanic Province, southeast Australia, *Geophys. J. Int.*, **149**, 249–266.
- Granet, M. & Trampert, J., 1989. Large-scale P -velocity structures in the Euro-Mediterranean area, *Geophys. J. Int.*, **99**, 583–594.
- Grevemeyer, I., Fleuh, E. R., Reichert, C., Biala, J., Kläschen, D., & Kopp, C., 2001. Crustal architecture and deep structure of the Ninetyeast Ridge hotspot trail from active-source ocean bottom seismology, *Geophys. J. Int.*, **144**, 414–431.
- Gubbins, D., 1992. *Seismology and plate tectonics*, Cambridge University Press, Cambridge.
- Guizou, J. L., Mallet, J. L., & Madariaga, R., 1996. 3-D seismic reflection tomography on top of the GOCAD depth modeler, *Geophysics*, **61**, 1499–1510.
- Gürbüz, C. & Evans, J. R., 1991. A seismic refraction study of the western Tuz Gölü basin, central Turkey, *Geophys. J. Int.*, **106**, 239–251.
- Hammer, P. T. C., Dorman, L. M., Hildebrand, J. A., & Cornuelle, B. D., 1994. Jasper Seamount structure: Seafloor seismic refraction tomography, *J. Geophys. Res.*, **99**, 6731–6752.
- Hasegawa, A., Umino, N., & Takagi, A., 1978. Double-planed deep seismic zone and upper-mantle structure in the northeastern Japan arc, *Geophys. J. Royal Astr. Soc.*, **54**, 281–296.
- Haslinger, F., Kissling, E., Ansorge, J., Hatzfeld, D., Papadimitriou, E., Karakostas, V., Makropoulos, K., Kahle, H. G., & Peter, Y., 1999. 3D crustal structure from local earthquake tomography around the Gulf of Arta (Ionian region, NW Greece), *Tectonophysics*, **304**, 201–218.
- Hearn, T. M., 1996. Anisotropic Pn tomography in the western United States, *J. Geophys. Res.*, **101**, 8403–8414.
- Hestenes, M. & Stiefel, E., 1952. Methods of conjugate gradients for solving linear systems, *Nat. Bur. Stand. J. Res.*, **49**, 409–436.
- Hildebrand, J. A., Dorman, L. M., Hammer, P. T. C., Schreiner, A. E., & Cornuelle, B. D., 1989. Seismic tomography of Jasper Seamount, *Geophys. Res. Lett.*, **16**, 1355–1358.
- Hole, J. A., 1992. Nonlinear high-resolution three-dimensional travel-time tomography, *J. Geophys. Res.*, **97**, 6553–6562.
- Hole, J. A. & Zelt, B. C., 1995. 3-D finite-difference reflection travel times, *Geophys. J. Int.*, **121**, 427–434.
- Hole, J. A., Clowes, R. M., & Ellis, R. M., 1992. Interface inversion using broadside seismic refraction data and three-dimensional traveltimes calculations, *J. Geophys. Res.*, **97**, 3417–3429.
- Humphreys, E. & Clayton, R. W., 1988. Adaption of back projection tomography to seismic travel time problems, *J. Geophys. Res.*, **93**, 1073–1085.

- Humphreys, E. D. & Clayton, R. W., 1990. Tomographic image of the Southern California Mantle, *J. Geophys. Res.*, **95**, 19,725–19,746.
- Inoue, H., Fukao, Y., Tanabe, K., & Ogata, Y., 1990. Whole mantle *P*-wave travel time tomography, *Phys. Earth Planet. Inter.*, **59**, 294–328.
- Iwasaki, T., Hirata, N., Kanazawa, T., Melles, J., Suyehiro, K., Urabe, T., Möller, L., Makris, J., & Shimamura, H., 1990. Crustal and upper mantle structure in the Ryukyu Island Arc deduced from deep seismic sounding, *Geophys. J. Int.*, **102**, 631–651.
- Iwasaki, T., Ozel, O., Moriya, T., Sakai, S., Suzuki, S., Aoki, G., Maeda, T., & Iidaka, T., 1998. Lateral structural variations across a collision zone in central Hokkaido, Japan, as revealed by wide-angle seismic experiments, *Geophys. J. Int.*, **132**, 435–457.
- Iyer, H. & Hirahara, K., 1993. *Seismic Tomography: Theory and Practice*, Chapman & Hall, London.
- Jarchow, C. M., Catchings, R. D., & Lutter, W. J., 1994. Large-explosive source, wide-recording aperture, seismic profiling on the Columbia Plateau, Washington, *Geophysics*, **59**, 259–271.
- Julian, B. R. & Gubbins, D., 1977. Three-dimensional seismic ray tracing, *J. Geophys.*, **43**, 95–113.
- Kanasewich, E., Burianyk, M. J. A., Ellis, R. M., Clowes, R. M., White, D. J., Lôté, T., Forsyth, D. A., Luetgert, J. A., & Spence, G. D., 1994. Crustal velocity structure of the Omineca Belt, southwestern Canadian Cordillera, *J. Geophys. Res.*, **99**, 2653–2670.
- Kanasewich, E. R. & Chiu, S. K. L., 1985. Least-squares inversion of spatial seismic refraction data, *Bull. Seism. Soc. Am.*, **75**, 865–880.
- Kao, H. & Rau, R. J., 1999. Detailed structures of the subducted Philippine Sea plate beneath northeast Taiwan: A new type of double seismic zone, *J. Geophys. Res.*, **104**, 1015–1033.
- Kawakatsu, H., 1985. Double seismic zone in Tonga, *Nature*, **316**, 53–55.
- Keller, W. R., Anderson, D. L., & Clayton, R. W., 2000. Resolution of tomographic models of the mantle beneath Iceland, *Geophys. Res. Lett.*, **27**, 3993–3996.
- Kennett, B. L. N., 1998. *Seismic wave propagation and seismic tomography*, Research School of Earth Sciences, Institute of Advanced Studies, The Australian National University, Canberra.
- Kennett, B. L. N., 2002. *The Seismic Wavefield, Volume 2: Interpretation of Seismograms on Regional and Global Scales*, Cambridge University Press, Cambridge.
- Kennett, B. L. N. & Engdahl, E. R., 1991. Traveltimes for global earthquake location and phase identification, *Geophys. J. Int.*, **105**, 429–465.
- Kennett, B. L. N., Sambridge, M. S., & Williamson, P. R., 1988. Subspace methods for large scale inverse problems involving multiple parameter classes, *Geophys. J.*, **94**, 237–247.
- Kim, S., 2001. An $O(N)$ level set method for eikonal equations, *SIAM J. Sci. Comput.*, **22**, 2178–2193.

- Kirkpatrick, S., Gelatt, Jr, C. D., & Vecchi, M. P., 1983. Optimization by simulated annealing, *Science*, **220**, 671–680.
- Klimeš, L. & Kvasnička, M., 1994. 3-D network ray tracing, *Geophys. J. Int.*, **116**, 726–738.
- Kodaira, S., Mjelde, R., Gunnarsson, K., Shiobara, H., & Shimamura, H., 1998. Structure of the Jan Mayen microcontinent and implications for its evolution, *Geophys. J. Int.*, **132**, 383–400.
- Kohler, M. D., 1997. Three-dimensional velocity structure and resolution of the core-mantle boundary region from whole-mantle inversions of body waves, *Phys. Earth Planet. Inter.*, **101**, 85–104.
- Kohler, M. D. & Davis, P. M., 1997. Crustal thickness variations in southern California from Los Angeles Region Seismic Experiment passive phase teleseismic travel times, *Bull. Seism. Soc. Am.*, **87**, 1330–1344.
- Korenaga, J., Holbrook, W. S., Kent, G. M., Kelemen, R. S., Detrick, R. S., Larsen, H. C., Hopper, J. R., & Dahl-Jensen, T., 2000. Crustal structure of the southeast Greenland margin from joint refraction and reflection tomography, *J. Geophys. Res.*, **105**, 21,591–21,614.
- Kosloff, D., Sherwood, J., Koren, Z., Machet, E., & Falkovitz, Y., 1996. Velocity and interface depth determination by tomography of depth migrated gathers, *Geophysics*, **61**, 1511–1523.
- Kreyszig, E., 1993. *Advanced engineering mathematics*, John Wiley & Sons, Inc., New York.
- Lambaré, G., Lucio, P. S., & Hanyga, A., 1996. Two-dimensional multivalued traveltimes and amplitude maps by uniform sampling of a ray field, *Geophys. J. Int.*, **125**, 584–598.
- Lambeck, K. & Burgess, G., 1992. Deep crustal structure of the Musgrave Block, central Australia: results from teleseismic traveltimes anomalies, *Australian Journal of Earth Sciences*, **39**, 1–19.
- Lambeck, K., Burgess, G., & Shaw, R. D., 1988. Teleseismic travel-time anomalies and deep crustal structure in central Australia, *Geophys. J.*, **94**, 105–124.
- Langan, R. T., Lerche, I., & Cutler, R. T., 1985. Tracing of rays through heterogeneous media: An accurate and efficient procedure, *Geophysics*, **50**, 1456–1465.
- Lee, W. H. K. & Pereyra, V., 1993. Mathematical introduction to seismic tomography, in *Seismic tomography: theory and practice*, edited by H. M. Iyer & K. Hirahara, pp. 9–22, Chapman & Hall, London.
- Lees, J. M. & VanDecar, J. C., 1991. Seismic tomography constrained by Bouguer gravity anomalies: Applications in western Washington, *Pageoph*, **135**, 31–52.
- Lévêque, J. J. & Masson, F., 1999. From ACH tomographic models to absolute velocity models, *Geophys. J. Int.*, **137**, 621–629.
- Lévêque, J. J., Rivern, L., & Wittlinger, G., 1993. On the use of the checker-board test to assess the resolution of tomographic inversions, *Geophys. J. Int.*, **115**, 313–318.
- Lizarralde, D. & Holbrook, W. S., 1997. U.S. mid-Atlantic margin structure and early thermal evolution, *J. Geophys. Res.*, **102**, 22,855–22,875.

- Louden, K. E. & Fan, J., 1998. Crustal structures of Grenville, Makkovik, and southern Nain provinces along the Lithoprobe ECSSOT Transect: Regional seismic refraction and gravity models and their tectonic implications, *Can. J. Earth Sci.*, **35**, 583–601.
- Luca, G. D., Filippi, L., Caccamo, D., Neri, G., & Scarpa, R., 1997. Crustal structure and seismicity of southern Tyrrhenian basin, *Phys. Earth Planet. Inter.*, **103**, 117–133.
- Lucio, P. S., Lambaré, G., & Hanyga, A., 1996. 3D multivalued travel time and amplitude maps, *Geophys.*, **148**, 449–479.
- Lutter, W. J. & Nowack, R. L., 1990. Inversion for crustal structure using reflections from the PASSCAL Ouachita experiment, *J. Geophys. Res.*, **95**, 4633–4646.
- Lutter, W. J., Nowack, R. L., & Braile, L., 1990. Seismic imaging of upper crustal structure using travel times from the PASSCAL Ouachita experiment, *J. Geophys. Res.*, **95**, 4621–4631.
- Lutter, W. J., Catchings, R. D., & Jarchow, C. M., 1994. An image of the Columbia Plateau from inversion of high-resolution seismic data, *Geophysics*, **59**, 1278–1289.
- McCaughey, M. & Singh, S. C., 1997. Simultaneous velocity and interface tomography of normal-incidence and wide-aperture seismic traveltimes, *Geophys. J. Int.*, **131**, 87–99.
- McMechan, G. A., 1983. Seismic tomography in boreholes, *Geophys. J. Royal Astr. Soc.*, **74**, 601–612.
- McQueen, H. W. S. & Lambeck, K., 1996. Determination of crustal structure in central Australia by inversion of traveltimes residuals, *Geophys. J. Int.*, **126**, 645–662.
- Menke, W., 1989. *Geophysical data analysis: Discrete inverse theory*, Academic Press, New York.
- Mjelde, R., Digranes, P., Shimamura, H., Shiobara, H., Kodaira, S., Brekke, H., Egebjerg, T., Sørensen, N., & Thorbjørnsen, S., 1998. Crustal structure of the northern part of the Vøring Basin, mid-Norway margin, from wide-angle seismic and gravity data, *Tectonophysics*, **293**, 175–205.
- Morgan, R. P. L., Barton, P. J., Warner, M., Morgan, J., Price, C., & Jones, K., 2000. Lithospheric structure north of Scotland - I. *P*-wave modelling, deep reflection profiles and gravity, *Geophys. J. Int.*, **142**, 716–736.
- Morozov, I. B., Smithson, S. B., Hollister, L. S., & Diebold, J. B., 1998. Wide-angle seismic imaging across accreted terranes, southeastern Alaska and western British Columbia, *Tectonophysics*, **299**, 281–296.
- Mosegaard, K. & Sambridge, M., 2002. Monte Carlo analysis of inverse problems, *Inverse Problems*, **18**, R29–R54.
- Moser, T. J., 1991. Shortest path calculation of seismic rays, *Geophysics*, **56**, 59–67.
- Nakanishi, I., 1985. Three-dimensional structure beneath the Hokkaido-Tohoku region as derived from a tomographic inversion of *P*-arrival times, *J. Phys. Earth*, **33**, 241–256.

- Nakanishi, I. & Yamaguchi, K., 1986. A numerical experiment on nonlinear image reconstruction from first-arrival times for two-dimensional island arc structure, *J. Phys. Earth*, **34**, 195–201.
- Navin, D. A., Peirce, C., & Sinha, M. C., 1998. The RAMESSES experiment -II. Evidence for accumulated melt beneath a slow spreading ridge from wide-angle refraction and multichannel reflection seismic profiles, *Geophys. J. Int.*, **135**, 746–772.
- Neele, F., VanDecar, J., & Snieder, R., 1993. The use of *P* wave amplitude data in a joint inversion with travel times for upper mantle velocity structure, *J. Geophys. Res.*, **98**, 12,033–12,054.
- Nielsen, L., Thybo, H., & Solodilov, L., 1999. Seismic tomographic inversion of Russian PNE data along profile Kraton, *Geophys. Res. Lett.*, **26**, 3413–3416.
- Nolet, G., 1985. Solving or resolving inadequate and noisy tomographic systems, *J. Comp. Phys.*, **61**, 463–482.
- Nolet, G., 1987. Waveform tomography, in *Seismic tomography: With applications in global seismology and exploration geophysics*, edited by G. Nolet, pp. 301–322, D. Reidel, Dordrecht.
- Nolet, G., 1987. *Seismic tomography: With applications in global seismology and exploration geophysics*, D. Reidel, Dordrecht.
- Nolet, G., 1990. Partitioned waveform inversion and two-dimensional structure under the network of autonomously recording seismographs, *J. Geophys. Res.*, **95**, 8499–8512.
- Nowack, R. L. & Lyslo, J. A., 1989. Fréchet derivatives for curved interfaces in the ray approximation, *Geophys. J.*, **97**, 497–509.
- Onescu, M. C., Burlacu, V., Anghel, M., & Smalberger, V., 1984. Three-dimensional *P*-wave velocity image under the Carpathian Arc, *Tectonophysics*, **106**, 305–319.
- Papazachos, C. & Nolet, G., 1997. *P* and *S* deep velocity structure of the Hellenic area obtained by robust nonlinear inversion of travel times, *J. Geophys. Res.*, **102**, 8349–8367.
- Parker, R. L., 1994. *Geophysical inverse theory*, Princeton University Press, Princeton.
- Parsons, T. & Zoback, M. L., 1997. Three-dimensional upper crustal velocity structure beneath San Francisco Peninsula, California, *J. Geophys. Res.*, **102**, 5473–5490.
- Parsons, T., McCarthy, J., Kohler, W. M., Ammon, C. J., Benz, H. M., Hole, J. A., & Criley, E. E., 1996. Crustal structure of the Colorado Plateau, Arizona: Application of new long-offset seismic data analysis techniques, *J. Geophys. Res.*, **101**, 11,173–11,194.
- Pereyra, V., Lee, W. H. K., & Keller, H. B., 1980. Solving two-point seismic-ray tracing problems in a heterogeneous medium, *Bull. Seism. Soc. Am.*, **70**, 79–99.
- Podvin, P. & Lecomte, I., 1991. Finite difference computation of traveltimes in very contrasted velocity models: a massively parallel approach and its associated tools, *Geophys. J. Int.*, **105**, 271–284.

- Popovici, A. M. & Sethian, J. A., 2002. 3-D imaging using higher order fast marching traveltimes, *Geophysics*, **67**, 604–609.
- Pratt, R. G., Song, Z. M., Williamson, P., & Warner, M., 1996. Two-dimensional velocity models from wide-angle seismic data by wavefield inversion, *Geophys. J. Int.*, **124**, 323–340.
- Press, W. H., Tuckolsky, S. A., Vetterling, W. T., & Flannery, B. P., 1992. *Numerical Recipes in FORTRAN*, Cambridge University Press, Cambridge.
- Priestley, K., Cipar, J., Egorkin, A., & Pavlenkova, N., 1994. Upper-mantle velocity structure beneath the Siberian platform, *Geophys. J. Int.*, **118**, 369–378.
- Prothero, W. A., Taylor, W. J., & Eickemeyer, J. A., 1988. A fast, two-point, three-dimensional raytracing algorithm using a simple step search method, *Bull. Seism. Soc. Am.*, **78**, 1190–1198.
- Protti, M., Schwartz, S. Y., & Zandt, G., 1996. Simultaneous inversion for earthquake location and velocity structure beneath central Costa Rica, *Bull. Seism. Soc. Am.*, **86**, 19–31.
- Pullammanappallil, S. K. & Louie, J. N., 1993. Inversion of seismic reflection traveltimes using a nonlinear optimization scheme, *Geophysics*, **58**, 1607–1620.
- Qin, F., Luo, Y., Olsen, K. B., Cai, W., & Schuster, G. T., 1992. Finite-difference solution of the eikonal equation along expanding wavefronts, *Geophysics*, **57**, 478–487.
- Rawlinson, N., 2000. *Inversion of Seismic Data for Layered Crustal Structure*, Ph.D. thesis, Monash University.
- Rawlinson, N. & Houseman, G. A., 1998. Inversion for interface structure using teleseismic traveltimes residuals, *Geophys. J. Int.*, **133**, 756–772.
- Rawlinson, N., Houseman, G. A., & Collins, C. D. N., 2001a. Inversion of seismic refraction and wide-angle reflection traveltimes for 3-D layered crustal structure, *Geophys. J. Int.*, **145**, 381–401.
- Rawlinson, N., Houseman, G. A., Collins, C. D. N., & Drummond, B. J., 2001b. New evidence of Tasmania's tectonic history from a novel seismic experiment, *Geophys. Res. Lett.*, **28**, 3337–3340.
- Recq, M., Goslin, J., Charvis, P., & Operto, S., 1998. Small-scale crustal variability within an intraplate structure: The Crozet Bank (southern Indian Ocean), *Geophys. J. Int.*, **134**, 145–156.
- Riahi, M. A. & Juhlin, C., 1994. 3-D interpretation of reflected arrival times by finite-difference techniques, *Geophysics*, **59**, 844–849.
- Riahi, M. A. & Lund, C. E., 1994. Two-dimensional modelling and interpretation of seismic wide-angle data from the western Gulf of Bothnia, *Tectonophysics*, **239**, 149–164.
- Riahi, M. A., Lund, C. E., & Pederson, L. B., 1997. Three-dimensional image of the Moho undulations beneath the Gulf of Bothnia using wide-angle seismic data, *Geophys. J. Int.*, **129**, 461–471.
- Ritsema, J., Nyblade, A. A., Owens, T. J., Langston, C. A., & VanDecar, J. C., 1998. Upper mantle seismic velocity structure beneath Tanzania, east Africa: Implications for the stability of cratonic lithosphere, *J. Geophys. Res.*, **103**, 21,201–21,213.

- Ryberg, T., Wenzel, F., Mechle, J., Egorkin, A., Fuchs, K., & Solodilov, L., 1996. Two-dimensional velocity structure beneath northern Eurasia derived from the super long-range seismic profile Quartz, *Bull. Seism. Soc. Am.*, **86**, 857–867.
- Saltzer, R. L. & Humphreys, E. D., 1997. Upper mantle P wave velocity structure of the eastern Snake River Plain and its relationship to geodynamic models of the region, *J. Geophys. Res.*, **102**, 11,829–11,841.
- Sambridge, M. & Mosegaard, K., 2001. Monte Carlo methods in geophysical inverse problems, *Rev. of Geophys.*, **submitted**.
- Sambridge, M. S., 1990. Non-linear arrival time inversion: Constraining velocity anomalies by seeking smooth models in 3-D, *Geophys. J. Int.*, **102**, 653–677.
- Sambridge, M. S. & Drijkoningen, G., 1992. Genetic algorithms in seismic waveform inversion, *Geophys. J. Int.*, **109**, 323–342.
- Sambridge, M. S. & Kennett, B. L. N., 1990. Boundary value ray tracing in a heterogeneous medium: A simple and versatile algorithm, *Geophys. J. Int.*, **101**, 157–168.
- Sato, T., Kosuga, M., & Tanaka, K., 1996. Tomographic inversion for P wave velocity structure beneath the northeastern Japan arc using local and teleseismic data, *J. Geophys. Res.*, **101**, 17,597–17,615.
- Scales, J. A., 1987. Tomographic inversion via the conjugate gradient method, *Geophysics*, **52**, 179–185.
- Scales, J. A. & Snieder, R., 1997. To Bayes or not to Bayes, *Geophysics*, **62**, 1045–1046.
- Scott, J. S., Masters, T. G., & Vernon, F. L., 1994. 3-D velocity structure of the San Jacinto fault zone near Anza, California-I. P waves, *Geophys. J. Int.*, **119**, 611–626.
- Seber, D., Barazangi, M., Tadili, B. A., Ramdani, M., Ibenbrahim, A., & Sari, D. B., 1996. Three-dimensional upper mantle structure beneath the intraplate Atlas and interplate Rif mountains of Morocco, *J. Geophys. Res.*, **101**, 3125–3138.
- Sethian, J. A., 1999. *Level Set Methods and Fast marching Methods*, Cambridge University Press, Cambridge.
- Sethian, J. A. & Popovici, A. M., 1999. 3-D traveltimes computation using the fast marching method, *Geophysics*, **64**, 516–523.
- Shalev, E., 1993. Cubic B-splines: Strategies of translating a simple structure to B-spline parameterization, *Bull. Seism. Soc. Am.*, **83**, 1617–1627.
- Shaw, P. R. & Orcutt, A., 1985. Waveform inversion of seismic refraction data and applications to young Pacific crust, *Geophys. J. Royal Astr. Soc.*, **82**, 375–414.
- Smith, W. H. F. & Wessel, P., 1990. Gridding with continuous curvature splines in tension, *Geophysics*, **55**, 293–305.

- Snieder, R., 1998. The role of nonlinearity in inverse problems, *Inverse Problems*, **14**, 387–404.
- Snieder, R. & Sambridge, M., 1993. The ambiguity in ray perturbation theory, *J. Geophys. Res.*, **98**, 22,021–22,034.
- Spakman, W., 1991. Delay-time tomography of the upper mantle below Europe, the Mediterranean and Asia Minor, *Geophys. J. Int.*, **107**, 309–332.
- Spakman, W., 1993. Iterative strategies for nonlinear travel-time tomography using global earthquake data, in *Seismic tomography: theory and practice*, edited by H. M. Iyer & K. Hirahara, pp. 190–226, Chapman & Hall, London.
- Staples, R. K., White, R. S., Brandsdóttir, Menke, W., Maguire, P. K. H., & McBride, J. H., 1997. Färöe-Iceland Ridge experiment 1. Crustal structure of northeastern Iceland, *J. Geophys. Res.*, **102**, 7849–7866.
- Steck, L. K., Thurber, C. H., Fehler, M., Lutter, W. J., Roberts, P. M., Baldridge, W. S., Stafford, D. G., & Sessions, R., 1998. Crust and upper mantle P wave velocity structure beneath Valles caldera, New Mexico: Results from the Jemez teleseismic tomography experiment, *J. Geophys. Res.*, **103**, 24,301–24,320.
- Steinhoff, J., Fan, M., & Wang, L., 2000. A new Eulerian method for the computation of propagating short acoustic and electromagnetic pulses, *J. Comp. Phys.*, **157**, 683–706.
- Tarantola, A., 1987. *Inverse problem theory*, Elsevier, Amsterdam.
- Telford, W. M., Geldart, L. P., Sheriff, R. E., & Keys, D. A., 1976. *Applied Geophysics*, Cambridge University Press, Cambridge.
- Telford, W. M., Geldart, L. P., & Sheriff, R. E., 1990. *Applied Geophysics*, Cambridge University Press, Cambridge.
- Thomson, C. J. & Gubbins, D., 1982. Three-dimensional lithospheric modelling at NORSAR: linearity of the method and amplitude variations from the anomalies, *Geophys. J. Royal Astr. Soc.*, **71**, 1–36.
- Thurber, C. H., 1983. Earthquake locations and three-dimensional crustal structure in the Coyote Lake area, central California, *J. Geophys. Res.*, **88**, 8226–8236.
- Thurber, C. H., 1993. Local earthquake tomography: Velocities and V_p/V_s - theory, in *Seismic tomography: theory and practice*, edited by H. M. Iyer & K. Hirahara, pp. 563–583, Chapman & Hall, London.
- Thurber, C. H. & Ellsworth, W. L., 1980. Rapid solution of ray tracing problems in heterogeneous media, *Bull. Seism. Soc. Am.*, **70**, 1137–1148.
- Toomey, D. R., Solomon, S. C., & Purdy, G. M., 1994. Tomographic imaging of the shallow crustal structure of the East Pacific Rise at $9^{\circ}30'N$, *J. Geophys. Res.*, **99**, 24,135–24,157.
- Um, J. & Thurber, C., 1987. A fast algorithm for two-point seismic ray tracing, *Bull. Seism. Soc. Am.*, **77**, 972–986.

- van der Hilst, R. D., Widjiantoro, S., & Engdahl, E. R., 1997. Evidence for deep mantle circulation from global tomography, *Nature*, **386**, 578–584.
- van Trier, J. & Symes, W. W., 1991. Upwind finite-difference calculation of traveltimes, *Geophysics*, **56**, 812–821.
- VanDecar, J. C., 1991. *Upper-mantle structure of the Cascadia subduction zone from non-linear teleseismic travel-time inversion*, Ph.D. thesis, University of Washington.
- VanDecar, J. C. & Snieder, R., 1994. Obtaining smooth solutions to large, linear, inverse problems, *Geophysics*, **59**, 818–829.
- VanDecar, J. C., James, D. E., & Assumpção, M., 1995. Seismic evidence for a fossil mantle plume beneath South America and implications for plate driving forces, *Nature*, **378**, 25–31.
- Vidale, J. E., 1988. Finite-difference calculations of traveltimes, *Bull. Seism. Soc. Am.*, **78**, 2062–2076.
- Vidale, J. E., 1990. Finite-difference calculations of traveltimes in three dimensions, *Geophysics*, **55**, 521–526.
- Vinje, V., Iversen, E., & Gjøystdal, H., 1993. Traveltime and amplitude estimation using wavefront construction, *Geophysics*, **58**, 1157–1166.
- Vinje, V., Iversen, E., Åstebøl, K., & Gjøystdal, H., 1996. Estimation of multivalued arrivals in 3D models using wavefront construction - Part I, *Geophysical Prospecting*, **44**, 819–842.
- Vinje, V., Åstebøl, K., Iversen, E., & Gjøystdal, H., 1999. 3-D ray modelling by wavefront construction in open models, *Geophysical Prospecting*, **64**, 1912–1919.
- Vogt, U., Makris, J., O'Reilly, B., Hausser, F., Readman, P. W., Jacob, A. W. B., & Shannon, P. M., 1998. The Hatton Basin and continental margin: Crustal structure from wide-angle seismic and gravity data, *J. Geophys. Res.*, **103**, 12,545–12,566.
- Walck, M. C., 1988. Three-dimensional V_p/V_s variations for the Coso region, California, *J. Geophys. Res.*, **93**, 2047–2052.
- Walck, M. C. & Clayton, R. W., 1987. P wave velocity variations in the Coso region, California, derived from local earthquake travel times, *J. Geophys. Res.*, **92**, 393–405.
- Wang, B. & Braile, L. W., 1996. Simultaneous inversion of reflection and refraction seismic data and application to field data from the northern Rio Grande rift, *Geophys. J. Int.*, **125**, 443–458.
- Wang, W. & Houseman, G. A., 1994. Inversion of reflection seismic amplitude data for interface geometry, *Geophys. J. Int.*, **117**, 92–110.
- Wang, Y. & Houseman, G. A., 1995. Tomographic inversion of reflection seismic amplitude data for velocity variation, *Geophys. J. Int.*, **123**, 355–372.
- Wang, Y. & Pratt, R. G., 1997. Sensitivities of seismic traveltimes and amplitudes in reflection tomography, *Geophys. J. Int.*, **131**, 618–642.

- Watanabe, T., Hirai, t., & Sassa, K., 1996. Seismic traveltimes tomography in anisotropic heterogeneous media, *J. Appl. Geophys.*, **35**, 133–143.
- Weiland, C. M., Steck, L. K., Dawson, P. B., & Korneev, V. A., 1995. Nonlinear teleseismic tomography at Long Valley caldera, using three-dimensional minimum travel time ray tracing, *J. Geophys. Res.*, **100**, 20,379–20,390.
- White, D. J., 1989. Two-dimensional seismic refraction tomography, *Geophys. J.*, **97**, 223–245.
- Whitley, D. L., 1994. A genetic algorithm tutorial, *Stats. and Comput.*, **4**, 65–85.
- Widiyantoro, S. & van der Hilst, R., 1997. Mantle structure beneath Indonesia inferred from high-resolution tomographic imaging, *Geophys. J. Int.*, **130**, 167–182.
- Wiggins, S. M., Dorman, L. M., Cornuelle, B. D., & Hildebrand, J. A., 1996. Hess deep rift valley structure from seismic tomography, *J. Geophys. Res.*, **101**, 22,335–22,353.
- Williamson, P. R., 1990. Tomographic inversion in reflection seismology, *Geophys. J. Int.*, **100**, 255–274.
- Ye, S., Flueh, E. R., Klaeschen, D., & von Huene, R., 1997. Crustal structure along the EDGE transect beneath the Kodiak shelf off Alaska derived from OBH seismic refraction data, *Geophys. J. Int.*, **130**, 283–302.
- Yilmaz, O., 1987. *Seismic data processing*, Society of Exploration Geophysicists, Tulsa.
- Zelt, B. C., Ellis, R. M., Clowes, R. M., & Hole, J. A., 1996. Inversion of three-dimensional wide-angle seismic data from the southwestern Canada Cordillera, *J. Geophys. Res.*, **286**, 209–221.
- Zelt, B. C., Ellis, R. M., Zelt, C. A., Hyndman, R. D., Lowe, C., Spence, G. D., & Fisher, M. A., 2001. Three-dimensional crustal velocity structure beneath the Strait of Georgia, British Columbia, *Geophys. J. Int.*, **144**, 695–712.
- Zelt, C. A., 1998. Lateral velocity resolution from three-dimensional seismic refraction data, *Geophys. J. Int.*, **135**, 1101–1112.
- Zelt, C. A., 1999. Modelling strategies and model assessment for wide-angle seismic traveltimes data, *Geophys. J. Int.*, **139**, 183–204.
- Zelt, C. A. & Barton, P. J., 1998. Three-dimensional seismic refraction tomography: A comparison of two methods applied to data from the Faeroe Basin, *J. Geophys. Res.*, **103**, 7187–7210.
- Zelt, C. A. & Smith, R. B., 1992. Seismic traveltimes inversion for 2-D crustal velocity structure, *Geophys. J. Int.*, **108**, 16–34.
- Zelt, C. A. & White, D. J., 1995. Crustal structure and tectonics of the southeastern Canadian Cordillera, *J. Geophys. Res.*, **100**, 24,255–24,273.
- Zelt, C. A., Hojka, A. M., Flueh, E. R., & McIntosh, K. D., 1999. 3D simultaneous seismic refraction and reflection tomography of wide-angle data from the central Chilean margin, *Geophys. Res. Lett.*, **26**, 2577–2580.

- Zhang, J. & Toksöz, M. N., 1998. Nonlinear refraction traveltimes tomography, *Geophysics*, **63**, 1726–1737.
- Zhao, D. & Kanamori, H., 1992. *P*-wave image of the crust and uppermost mantle in southern California, *Geophys. Res. Lett.*, **23**, 2329–2332.
- Zhao, D., Hasegawa, A., & Horiuchi, S., 1992. Tomographic imaging of *P* and *S* wave velocity structure beneath Northeastern Japan, *J. Geophys. Res.*, **97**, 19,909–19,928.
- Zhao, D., Hasegawa, A., & Kanamori, H., 1994. Deep structure of Japan subduction zone as derived from local, regional, and teleseismic events, *J. Geophys. Res.*, **99**, 22,313–22,329.
- Zhao, D., Kanamori, H., & Humphreys, E., 1996. Simultaneous inversion of local and teleseismic data for the crust and mantle structure of southern California, *Phys. Earth Planet. Inter.*, **93**, 191–214.
- Zhao, Z., Kubota, R., Fumio, S., & Iizuka, S., 1997. Crustal structure in the southern Kanto-Tokai region derived from tomographic method for seismic explosion survey, *J. Geophys. Res.*, **45**, 433–453.
- Zhu, H. & Ebel, J. E., 1994. Tomographic inversion for the seismic velocity structure beneath northern New England using seismic refraction data, *J. Geophys. Res.*, **99**, 15,331–15,357.
- Zielhuis, A. & van der Hilst, R. D., 1996. Upper-mantle shear velocity beneath eastern Australia from inversion of waveforms from SKIPPY portable arrays, *Geophys. J. Int.*, **127**, 1–16.

MONTE CARLO METHODS IN GEOPHYSICAL INVERSE PROBLEMS

Malcolm Sambridge

*Research School of Earth Sciences
Institute of Advanced Studies
Australian National University
Canberra, ACT, Australia*

Klaus Mosegaard

*Niels Bohr Institute for Astronomy
Physics and Geophysics
University of Copenhagen
Copenhagen, Denmark*

Received 27 June 2000; revised 15 December 2001; accepted 9 September 2002; published 5 December 2002.

[1] Monte Carlo inversion techniques were first used by Earth scientists more than 30 years ago. Since that time they have been applied to a wide range of problems, from the inversion of free oscillation data for whole Earth seismic structure to studies at the meter-scale lengths encountered in exploration seismology. This paper traces the development and application of Monte Carlo methods for inverse problems in the Earth sciences and in particular geophysics. The major developments in theory and application are traced from the earliest work of the Russian school and the pioneering studies in the west by *Press* [1968] to modern importance sampling and ensemble inference methods. The paper is divided into two parts. The first is a literature review, and the second is a summary of Monte Carlo techniques that are currently popular in geophysics. These include

simulated annealing, genetic algorithms, and other importance sampling approaches. The objective is to act as both an introduction for newcomers to the field and a comprehensive reference source for researchers already familiar with Monte Carlo inversion. It is our hope that the paper will serve as a timely summary of an expanding and versatile methodology and also encourage applications to new areas of the Earth sciences. **INDEX TERMS:** 3260 Mathematical Geophysics: Inverse theory; 1794 History of Geophysics: Instruments and techniques; 0902 Exploration Geophysics: Computational methods, seismic; 7294 Seismology: Instruments and techniques; **KEYWORDS:** Monte Carlo nonlinear inversion numerical techniques **Citation:** Sambridge, M., and K. Mosegaard, Monte Carlo Methods in Geophysical Inverse Problems, *Rev. Geophys.*, 40(3), 1009, doi:10.1029/2000RG00089, 2002.

1. INTRODUCTION

[2] *Hammersley and Handscomb* [1964] define *Monte Carlo* methods as “the branch of experimental mathematics that is concerned with experiments on random numbers.” (A glossary is included to define some commonly used terms. The first occurrence of each is italicized in text.) Today, perhaps, we would modify this definition slightly to “experiments making use of random numbers to solve problems that are either probabilistic or deterministic in nature.” By this we mean either the simulation of actual random processes (a probabilistic problem) or the use of random numbers to solve problems that do not involve any random process (a deterministic problem). The origin of modern Monte Carlo methods stem from work on the atomic bomb during the Second World War, when they were mainly used for numerical simulation of neutron diffusion in fissile material, that is, a probabilistic problem. Later it was realized that Monte Carlo methods could also be used for deterministic problems, for example, evaluating multidimensional integrals. Early successes came in the fields of operations research: *Thomson* [1957] describes a Monte

Carlo simulation of the fluctuations of traffic in the British telephone system.

[3] In the 50 years since the modern development of Monte Carlo methods by Ulam, von Neumann, Fermi, and Metropolis, they have been applied to a large array of problems in the physical, mathematical, biological, and chemical sciences (see *Hammersley and Handscomb* [1964] for an early but still very readable account of their origins and uses). Although the phrase “Monte Carlo method” was first used by *Metropolis and Ulam* [1949], there are documented examples of essentially the same principles being applied much earlier. *Kelvin* [1901] had described the use of “astonishingly modern Monte Carlo techniques” (as noted by *Hammersley and Handscomb* [1964]) in a discussion of the Boltzmann equation. Earlier still, *Hall* [1873] recounts numerical experiments to determine the value of π by injured officers during the American Civil War. This procedure consisted of throwing a needle onto a board containing parallel straight lines. The statistics of number of times the needle intersected each line could be used to estimate π . The usefulness of Monte Carlo type of numerical experiments was therefore known well before the beginning of the

century; however, their systematic development and widespread use had to wait for the arrival of the electronic computer.

[4] The direct simulation of probability distributions is at the basis of all Monte Carlo methods. The early work of *Metropolis et al.* [1953] was the first to show how to sample a space according to a Gibbs-Boltzmann distribution, using simple probabilistic rules. Today the development of Monte Carlo techniques and the underlying statistical theory is a large and active area of research [*Flournay and Tsutakawa*, 1989]. Earth scientists have embraced the use of Monte Carlo methods for more than 30 years. This paper traces some of those developments and, in particular, the use of Monte Carlo methods in *inverse problems*, where information is to be inferred from indirect data, for example, estimating the variations of seismic wave speed at depth in the Earth from observations at the surface. Real geophysical observations are often noisy and incomplete and always imperfectly constrain the quantities of interest. Monte Carlo techniques are one of a number of approaches that have been applied with success to geophysical inverse problems. Over the past 15 years the range of problems to which they have been applied has grown steadily. The purpose of this review paper is to summarize the role played by Monte Carlo methods in (mainly) geophysical *inversion* and also to provide a starting point for newcomers to the field.

[5] This paper consists of two parts. The first is a literature review, which describes the origins and major developments in the use of Monte Carlo methods for geophysical inverse problems. It is hoped that this will give an overview of the field to the newcomer and act as a source of references for further study. The second part of the paper is intended as more of a tutorial. Here we describe some of the details of how to use modern Monte Carlo methods for inversion, parameter estimation, optimization, uncertainty analysis, and *ensemble inference*. We have tried to emphasize the limitations as well as the usefulness of Monte Carlo-based methods and also to highlight some of the trends in current research. In addition to an extensive bibliography and glossary of common terms we have also included a list of world wide web addresses where (at the time of writing) further material, computer code, and other information can be found. It is hoped that this will serve as a starting point for the interested reader to explore this active interdisciplinary research field for themselves.

2. A BRIEF HISTORY OF MONTE CARLO INVERSION IN GEOPHYSICS

2.1. Beginnings of Monte Carlo Inversion

[6] In the summer of 1966 the third international symposium on Geophysical Theory and Computers was held at Cambridge, United Kingdom. The subsequent proceedings were published a year later as a special issue

of the *Geophysical Journal of the Royal Astronomical Society* and contain some classic papers. One of these is the now famous article by *Backus and Gilbert* [1967], which, along with several others by the same authors [*Backus and Gilbert*, 1968, 1970], established the foundations of geophysical inverse theory. In this paper it was shown that nonuniqueness was a fundamental property of geophysical inverse problems; that is, if any *Earth model* could be found to satisfy “gross Earth data,” then an infinite number of them would exist. In the same paper it was shown how this nonuniqueness could be exploited to generate unique models with special properties as an aid to interpretation. In the same volume is a paper by *Keilis-Borok and Yanovskaya* [1967] (describing earlier work in the USSR), which was the first to introduce Monte Carlo inversion methods into geophysics. From that date the use of Monte Carlo inversion techniques has become widespread in geophysics, but interestingly enough their initial appeal was that they offered a way of dealing with the nonuniqueness problem.

[7] At this time *Monte Carlo inversion (MCI)* meant generating discrete Earth models in a uniform random fashion between pairs of upper and lower bounds, which were chosen *a priori*. Each generated Earth model was tested for its fit to the available data and then accepted or rejected. The final set of accepted Earth models were used for interpretation [*Press*, 1970b]. As the computational power became available in the latter part of the 1960s, Monte Carlo inversion became feasible for some important problems in seismology. The first applications were to the inversion of seismic body-wave travel times (compressional and shear) and 97 eigenperiods of the Earth’s free oscillations for variations in the Earth’s compressional (α), shear (β) wave velocities, and density (ρ) as a function of depth [*Press*, 1968; *Wiggins*, 1969; *Press*, 1970a, 1970b].

[8] The main appeal of MCI was that it avoided all assumptions of linearity between the observables and the unknowns representing the Earth model upon which most previous techniques relied. In addition, it was thought that a measure of uniqueness of the solutions would be obtained by examining the degree to which the successful models agreed or disagreed [*Press*, 1968]. The original Monte Carlo paper by *Keilis-Borok and Yanovskaya* [1967] introduced the “hedgehog” inversion (attributed to V. Valius and later published by *Valius* [1968]), which sought to map out a region of *acceptable models* in *parameter space*. This was done by deterministically sampling all models in the vicinity of an acceptable model, which had previously been determined by MCI. The whole process could then be repeated many times over. This approach was later used in the estimation of upper mantle Q structure from Rayleigh wave attenuation [*Burton and Kennett*, 1972; *Burton*, 1977] and in other surface-wave dispersion studies [*Biswas and Knopoff*, 1974].

[9] Shortly after its introduction, criticisms of Monte

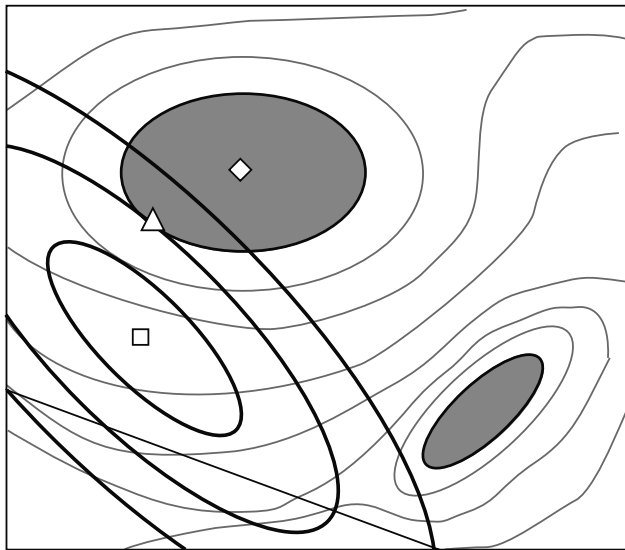


Figure 1. Contours of a data misfit function, $\phi(\mathbf{m})$, (shaded) in the parameter space of a nonlinear problem. The two shaded areas represent the regions of acceptable data fit, while the darker elliptical lines are contours of some regularization function, $\psi(\mathbf{m})$. The diamond represents the model with the best data fit and is distinct from the triangle, which is the data-acceptable model with least ψ . The square is the model with minimum ψ , but it does not satisfy the data.

Carlo inversion followed. One problem was that it is never known whether sufficient number of models had been tested. It was always possible that acceptable models may exist that bear no resemblance to the satisfactory models that had been obtained; hence the real Earth may lay outside of the estimated “nonuniqueness bounds.” An uncomfortable possibility was that the acceptable models might form multiple unconnected “islands” in parameter space (see Figure 1). An MCI approach might miss some of these islands altogether. (In the work of Press [1968], 5 million Earth models were tested, and just 6 were found that passed all data tests. See Figures 2 and 3). In practice, this meant that sets of upper and lower bounds estimated by MCI could not be literally interpreted as “hard” bounds on, say, velocity or density as a function of depth. For this reason Press [1970b] refers to his estimated envelope of acceptable Earth models as “a guide to hypotheses rather than firm conclusions.”

[10] An approach developed by Anderssen and Senata [1971, 1972] went some way to answering these criticisms. They developed a statistical procedure for estimating the reliability of a given set of nonuniqueness bounds. Their method was subsequently applied to the inversion of seismic and density profiles by a number of authors [Worthington *et al.*, 1972, 1974; Goncz and Cleary, 1976].

[11] Another criticism of MCI, argued by Haddon and Bullen [1969], was that the successful models generated were likely to contain unnecessary complexity (e.g., the typical small-scale oscillations that had been obtained in

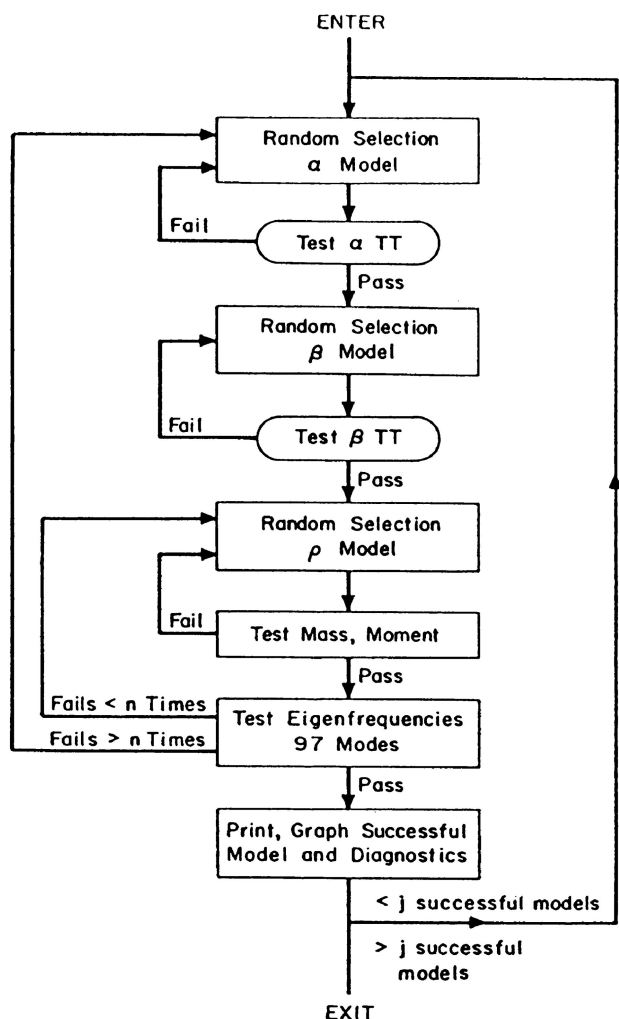


Figure 2. The flow chart of the early Monte Carlo algorithm used by Press [1968]. Note that the 1-D Earth model had to satisfy data constraints on travel times, eigenfrequencies, and mass and moment of inertia of the Earth before passing into the output population (see Figure 3). (From Press [1968].)

velocity or density depth profiles). This was because the likelihood of generating a parametrically simple model was very small, and hence MCI results were biased toward physically unrealistic Earth models. One way this difficulty was addressed was by seeking families of “uncomplicated” Earth models, with acceptable fit to data. Wiggins [1969] devised a parameterization for 1-D velocity profiles that allowed one to impose velocity, velocity gradient with depth, and velocity curvature bounds simultaneously. This technique has been used in a number of areas since [e.g., Cary and Chapman, 1988; Kennett, 1998]. Anderssen *et al.* [1972] extended the earlier work of Anderssen and Senata [1972] to include constraints on the form of the Earth models generated by MCI. They noted that the resulting set of parameter bounds obtained by MCI would be affected by the constraints imposed on the Earth model. For example, if the gradient of a density profile were constrained tightly over a

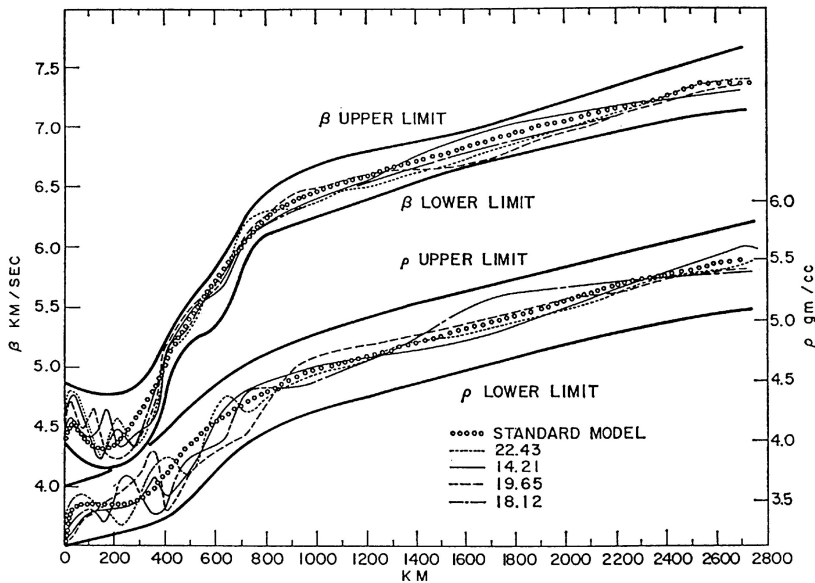


Figure 3. The six seismic and density Earth models that passed all tests shown in Figure 2 from the 5 million generated (from Press [1968]).

particular depth range, then this would result in relatively narrow bounds on the density, giving the false impression that the average density over the depth range was well determined. Clearly, care had to be used when interpreting MCI results obtained under smoothness constraints.

2.2. Monte Carlo Techniques Fall Out of Favor

[12] During the 1970s, attention moved away from Monte Carlo inversion and toward linear inverse problems and the use of prior information to resolve non-uniqueness (often referred to as ill posedness in linear problems) [Wiggins, 1972; Jackson, 1972; 1979]. Linear inversion techniques became popular and were applied widely (for a recent summary see Snieder and Trampert [1999]). Uniform Monte Carlo searching of parameter spaces was thought to be too inefficient and too inaccurate for problems involving large numbers of unknowns, for example, 50–100. (Note that in the earlier work of Press [1968] and Wiggins [1969] it was possible to increase efficiency, by testing “partial models” against subsets of the data, and thereby reject many unacceptable models early on. Figure 2 shows an outline of Press’s original MCI algorithm where this is employed.) Nevertheless, uniform random search methods still found applications. In addition to the regional and global travel time studies, other applications of MCI have included electromagnetic induction [Anderssen, 1970], Rayleigh wave attenuation [Mills and Fitch, 1977; Mills and Hales, 1978], regional magnetotelluric studies [Hermance and Grillot, 1974; Jones and Hutton, 1979], estimation of mantle viscosities [Ricard et al., 1989], and estimation of plate rotation vectors [Jestin et al., 1994].

[13] An attractive feature of discrete linear inversion schemes was that estimates of resolution and model

covariance could be obtained [Franklin, 1970; Jordan and Franklin, 1971; Wiggins, 1972]. In this case, resolution measures the degree by which model parameters can be independently determined (from each other), while model covariance measures the degree by which errors in the data propagate into uncertainty in the model parameters. Together they allow assessment of confidence bounds and trade-offs between parameters, which can be very useful in analyzing inversion results.

[14] A difficulty with linearized estimates of resolution and covariance is that they are based on local derivative approximations, evaluated about the best data fitting model, and as such can become less accurate, as the data-model relationship becomes more nonlinear. This can often lead to an underestimate of uncertainty and hence overconfidence in results. Around the same time as applications of discrete inverse theory were becoming widespread, it was shown how Monte Carlo sampling techniques could also be used to determine resolution estimates but without the need for invoking derivative approximations [Wiggins, 1972; Kennett and Nolet, 1978].

[15] The influence of nonlinearity can vary considerably between problems. For example, earthquake hypocenter location using travel times of seismic phases is often described as weakly nonlinear [see Buland, 1976] (although examples exist of the failure of linearization even in this case [e.g., Billings et al., 1994; Lomax et al., 2000]). In contrast, the estimation of seismic velocity structure from high-frequency seismic (body) wave forms can be highly nonlinear [see Mellman, 1980; Cary and Chapman, 1988]. In the latter case, subtle changes in velocity structure can significantly influence the details of the observed seismograms.

[16] Once nonlinearity is taken into account, it can be

useful to view the process of inversion in terms of optimization in a high-dimensional parameter space. Usually, some *objective function* is devised that measures the discrepancy between observables and theoretical predictions from a model. The precise nature of the optimization problem to be solved can vary considerably. For example, one might seek to minimize an objective function based solely on a measure of fit to data [e.g., Cary and Chapman, 1988] or one based on a linear combination of data fit and model regularization (for a discussion see Menke [1989]). A constrained optimization problem can be produced with the addition of (explicit) constraints on the unknowns [e.g., Sabatier, 1977a, 1977b, 1977c; Parker, 1994], or the data itself might enter only in these constraints, while the objective function represents regularization on the model. (This is often called extremal inversion; for examples, see Jackson [1976], Parker [1977], Constable *et al.* [1987] and Parker [1994]). In some cases these formulations are equivalent, and, in general, the most appropriate one will depend on the particular problem in hand and the questions being asked of the data.

[17] In linear problems it is common to use a quadratic criterion to measure data misfit. This leads to least squares techniques and an ellipsoidal objective function in parameter space (see Figure 4a). Most (discrete) linearized inversion techniques correspond to a gradient-based optimization algorithm, for example, steepest descent, conjugate gradients, Newton-Raphson (see Gill *et al.* [1981] and Press *et al.* [1992] for summaries). Linearized inversion techniques can be applied to weakly nonlinear problems and in some cases highly nonlinear ones, when a good enough guess at the solution is available in advance. As the nonlinearity of the data/model relationship increases, a data misfit objective function can become more complex, and hence optimization can become more difficult. Common descriptions involve terms like “narrow valleys,” “abrupt (non-smooth) gradient changes,” and multiple minima, although in truth not too many of these structures have been looked at in any detail. (See Scales *et al.* [1992] and Billings *et al.* [1994] for some rather nasty examples.)

[18] An example of a multimodal objective function arising from the residual statics problem is shown in Figure 4b [see Deng and Scales, 1999]. Here the data fit is measured by a *probability density function* (*PDF*) which reflects the alignment of phases. The global maximum of this function corresponds to the best data fit model, and locating it would be difficult with techniques based on gradients or matrix inversion, unless one started near the solution (in the “basin” of the global solution). In any case, for this type of objective function it might well be argued that the model corresponding to the globally maximum was of little use by itself, and inference should be based on the class of all acceptable models, if they could be found.

[19] From here on we will use the generic terms “misfit” and objective function to describe a combina-

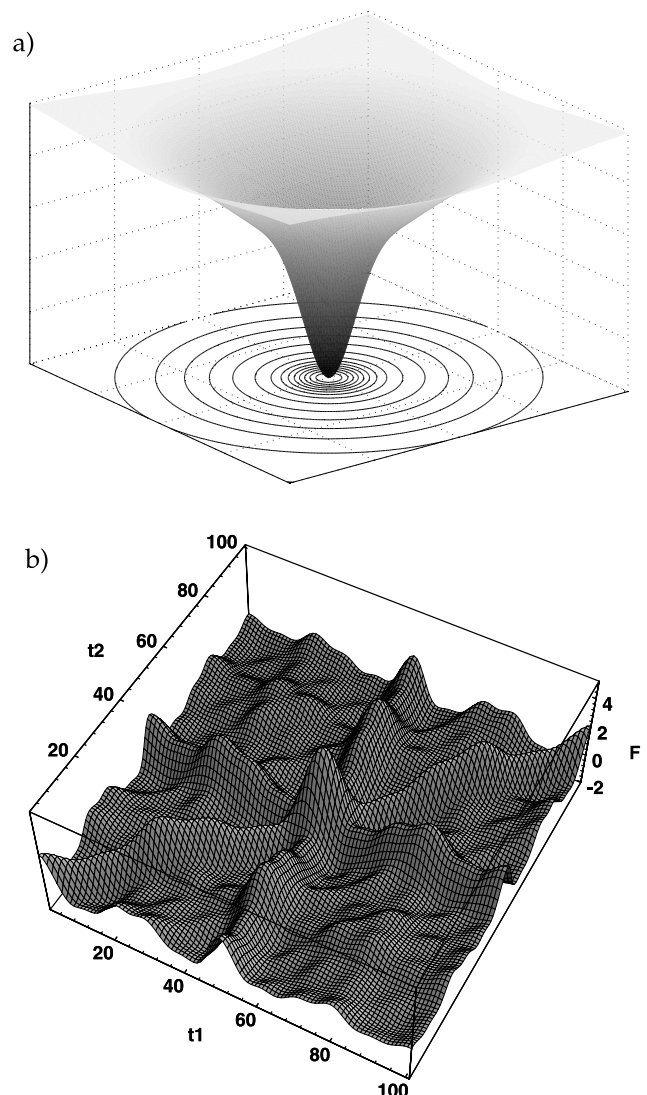


Figure 4. (a) Simple smoothly varying data misfit function with a single global minimum representing a best fit data model. Contours are projected onto the lower plane and are elliptical. (b) Probability density function for a two-dimensional residual statics problem after Deng and Scales, 1999. Here the global maximum represents the most likely model. Note that even in this “simple” problem, multiple maxima are observed with valleys and ridges inclined to the parameter axes.

tion of data misfit and perhaps a smoothing or regularization term, indeed any multidimensional function that might be optimized in an inversion procedure. Usually, one would minimize a *misfit function* (possibly under constraints), but as shown by Figure 4b we would seek to maximize a probability density function. (The latter arise in a probabilistic treatment of inversion problems discussed in section 3.3.)

2.3. Monte Carlo and Optimization

[20] Optimization procedures that depend on gradient approximations or matrix inversion can suffer from numerical instabilities caused by ill-conditioned matrices

or failure of convergence, etc. These situations usually arise when the objective function is highly irregular, multimodal, and nonsmooth or has discontinuities. Since Monte Carlo methods work by directly sampling a parameter space, they do not rely on the objective function being smooth in any sense, nor do they involve any potentially numerical unstable process, like matrix inversion. In this sense they are inherently stable. If the random search process is inefficient, then convergence to an optimum (or even local) solution may be slow, but it will, nevertheless, continue. With gradient based methods, there is the possibility that no solution will be found because of complete failure of the iterative procedure.

[21] As the available computational power grew in the 1980s and more sophisticated *direct search* methods became available, Monte Carlo techniques came back into vogue for geophysical inversion. At this stage our definition of a Monte Carlo technique needs an update. A more general definition (and the one we shall adopt) is a method that uses *pseudorandom* sampling to search a parameter space to retrieve Earth models or other information about the unknowns of interest. The important change is that the search no longer needs to be uniform. Random sampling from highly nonuniform multidimensional distributions is now included in our definition of a Monte Carlo method. This issue has led to some confusion in the literature. The point to remember is that Monte Carlo does not imply uniform sampling, just as random samples do not imply uniform random samples.

[22] The work of Rothman [1985, 1986] introduced into geophysics the technique of simulated annealing, which is a nonuniform Monte Carlo method for *global optimization*. This approach was originally developed to simulate the statistical mechanics of systems in equilibrium but quickly gained attention as a general purpose global optimization method. *Simulated annealing* was originally devised by Kirkpatrick *et al.* [1983] [see also Geman and Geman, 1984] and is based on the *Metropolis sampling algorithm* of Metropolis *et al.* [1953]. A reference work is that of Aarts and Korst [1989]. The tutorial section of this review paper deals with this topic in more detail.

[23] In the work of Rothman [1985, 1986], simulated annealing was applied to the large residual statics problem of exploration seismics. The impressive results stimulated many applications to other geophysical optimization problems. These include the estimation of Earth models from fitting of seismic body waveforms in exploration seismics reflection seismics and migration [Jakobsen *et al.*, 1988; Jervis *et al.*, 1993; Varela *et al.*, 1998; Landa *et al.*, 1989; Mosegaard and Vestergaard, 1991; Vestergaard and Mosegaard, 1991; Sen and Stoffa, 1991]; inversion of travel/arrival time data [Pullammanappallil and Louie, 1993, 1994]; earthquake location and rupture histories [Billings, 1994; Hartzell and Liu, 1996]; seismic source and ground motion studies [Scherbaum *et al.*,

1994; Courboulex *et al.*, 1996; Ihmle and Ruegg, 1997]; estimation of crustal structure [Steck, 1995; Zhao *et al.*, 1996]; deconvolution of seismograms [Courboulex *et al.*, 1996; Calderon *et al.*, 1997]; thermodynamic modeling [Bina, 1998]; groundwater management and remediation [Dougherty and Marryott, 1991; Kou *et al.*, 1992; Rizzo and Dougherty, 1996; Rogers *et al.*, 1998]; more residual statics estimation [Vasudevan and Wilson, 1991; Nørmark and Mosegaard, 1993]; waste disposal site selection [Muttiyah *et al.*, 1996]; geostatistics [Datta *et al.*, 1995; Goovaerts, 1996; Pardo, 1998]; seismic ray tracing [Velis and Ulych, 1996]; and electromagnetic, resistivity, and magnetotelluric imaging [Gilbert and Virieux, 1991; Dossa and Oldenburg, 1991; Dittmer and Szymanski, 1995]. This is only a subset of the many papers making use of this technique over the past 10 years.

[24] The power of simulated annealing (SA) was that it could be used in cases where the model-data relationship was highly nonlinear and produced multimodal data misfit functions (as in Figure 4b). Simulated annealing remains one of the few approaches specifically designed for global optimization problems that has been successfully applied across several disciplines [Aarts and Korst, 1989]. The price of this sophistication is that control parameters (an “annealing schedule”) are introduced that govern the characteristics of the sampling, and these had to be determined externally. Subsequent work by Nulton and Salamon [1988], Andresen *et al.* [1988], and Hajek [1988] showed that a theoretically optimal annealing schedule could be achieved by monitoring the progress of the algorithm and adjusting as necessary [see also Mosegaard and Vestergaard, 1991]. Other authors designed more simplistic but quite effective alternatives [Szu and Hartley, 1987; Ingber, 1989; Basu and Frazer, 1990]. Global optimization techniques were here to stay and over the following years became a popular addition to the geophysicist’s tool bag.

[25] Some time after the appearance of simulated annealing, another direct search method was introduced into geophysics and applied widely. *Genetic algorithms* (GA) were originally devised as a model of adaptation in an artificial system by Holland [1975]. An early reference work is by Goldberg [1989], and a more recent tutorial is given by Whitley [1994]. As was the case with simulated annealing, geophysicists borrowed this technique from another discipline and used it for global optimization. Genetic algorithms fall into the class of Monte Carlo techniques because they also use random numbers to control components of the search.

[26] Genetic algorithms were first used by geophysicists in the early 1990s. A number of papers appeared in quick succession [Stoffa and Sen, 1991; Gallagher *et al.*, 1991; Wilson and Vasudevan, 1991; Smith *et al.*, 1992; Sen and Stoffa, 1992; Sambridge and Drikonigen, 1992; Scales *et al.*, 1992], largely in the area of seismic waveform fitting. Interestingly enough, genetic algorithms were not originally designed as function optimizers, and the range of problems to which they have been applied

is quite broad. (For reviews, see *Davis* [1987], *Goldberg* [1989], and *Gallagher and Sambridge* [1994].) Nevertheless, their main role in geophysics (as in many other disciplines) has been as a global optimization tool. Like simulated annealing, the metaphor underlying genetic algorithms is a natural optimization process, in this case biological evolution. Many variants of genetic algorithms exist (even when applied to optimization). Indeed, they are probably best viewed as a class of methods rather than as a well-defined algorithm. As with simulated annealing, some asymptotic convergence results are known for particular versions [*Davis and Principe*, 1991]. However, all versions involve control parameters, which determine the characteristics of the direct search process, and tuning them for each problem can be non-trivial.

[27] Within a few years of their introduction, genetic algorithms became quite popular within the Earth sciences and were applied in a wide range of areas. Some examples include earthquake hypocenter location [*Kennett and Sambridge*, 1992; *Sambridge and Gallagher*, 1993; *Billings et al.*, 1994; *Wan et al.*, 1997; *Muramatsu and Nakanishi*, 1997]; estimation of focal mechanisms and seismic source characteristics [*Kobayashi and Nakanishi*, 1994; *Zhou et al.*, 1995a; *Sileny*, 1998; *Yu et al.*, 1998]; mantle viscosity estimation [*King*, 1995; *Cadek et al.*, 1998; *Kido et al.*, 1998]; groundwater monitoring and management problems [*McKinney and Lin*, 1994; *Ritzel et al.*, 1994; *Cieniawski et al.*, 1995; *Rogers et al.*, 1995; *Tang and Mays*, 1998]; meteorite classification [*Conway and Bland*, 1998]; seismic anisotropy estimation [*Horne and Macbeth*, 1994; *Levin and Park*, 1997]; near-source seismic structure [*Zhou et al.*, 1995b]; regional, crustal seismic structure and surface wave studies [*Lomax and Snieder*, 1994, 1995a, 1995b; *Drijkoningen and White*, 1995; *Yamanaka and Ishida*, 1996; *Neves et al.*, 1996]; design of microseismic networks [*Jones et al.*, 1994]; fission track dating [*Gallagher*, 1995]; seismic profiling and migration [*Jervis et al.*, 1993; *Jin and Madariaga*, 1993; *Nolte and Frazer*, 1994; *Horne and Macbeth*, 1994; *Boschetti et al.*, 1996; *Docherty et al.*, 1997]; seismic receiver functions studies [*Shibutani et al.*, 1996]; problems in geotectonics [*Simpson and Priest*, 1993]; magnetotelluric inversion [*Everett and Schultz*, 1993]; inversion of potential fields [*Boschetti et al.*, 1997]; conditioning of linear systems of equations [*Curtis and Snieder*, 1997]; seismic ray tracing [*Sadeghi et al.*, 1999]; there are many others. Some studies have involved devising variants of the basic approach and adapting them to the characteristics of individual problems [e.g., *Sambridge and Gallagher*, 1993; *Koper et al.*, 1999].

[28] The question as to whether simulated annealing or genetic algorithms perform better for a particular problem (i.e., more efficiently, more likely to find acceptable or even optimal models, etc.) has been addressed by a number of authors, both within the Earth sciences and elsewhere [see *Scales et al.*, 1992; *Ingber and Rosen*, 1992; *Sen and Stoffa*, 1995; *Horne and Macbeth*,

1998]. Most commonly, these studies compare performance on particular optimization problems, and from these it is difficult to draw general conclusions. Quite clearly, their relative performance varies between applications and also with the particular versions of each method that are being compared. For a recent, very readable, discussion of the types of optimization problem for which they are each suited, see *Gershenson* [1999].

[29] A few other global optimization techniques (again originating in other fields) have made fleeting appearances in the geophysical literature. Two notable examples are evolutionary programming [*Minster et al.*, 1995] and Tabu (or Taboo) search [*Cvijović and Klinowski*, 1995; *Vinther and Mosegaard*, 1996; *Zheng and Wang*, 1996]. The former is related to genetic algorithms but was developed quite independently [*Fogel*, 1962; *Fogel et al.*, 1966]. Again, the primary motivation was not optimization but the simulation of complex adaptive systems (see *Gell-Mann* [1994] for a popular discussion). Tabu search is not strictly speaking a Monte Carlo method since it does not make use of random numbers, but it is able to climb out of local minima in misfit functions [*Cvijović and Klinowski*, 1995; *Vinther and Mosegaard*, 1996]. Very recently, a new Monte Carlo direct search technique known as a neighbourhood algorithm (NA) has been proposed, this time developed specifically for sampling in geophysical inverse problems [*Sambridge*, 1999a]. The approach makes use of concepts from the growing field of computational geometry and bears little resemblance to either genetic algorithms or simulated annealing. It is difficult to say much about these approaches with any confidence as experience with geophysical problems is still rather limited.

2.4. Ensemble Inference Rather Than Optimization

[30] The renewed interest in Monte Carlo techniques for global optimization and exploration raised a familiar question, that is, how to make use of the sampling they produced to assess trade-offs, constraints and resolution, in multimodal nonlinear problems. Put another way, how can one use the collection of Earth models generated by a Monte Carlo procedure to do more than estimate a set of “best fitting” parameters. This was, in effect, a return to the questions posed by the first users of Monte Carlo; however, the response adopted by the second generation of practitioners was to take a Bayesian approach. This statistical treatment of inverse problems became well known to geophysicists through the work of *Tarantola and Valette* [1982a, 1982b; see also *Tarantola*, 1987] and had been applied extensively to linearized problems. Monte Carlo techniques allowed an extension of the Bayesian philosophy to nonlinear problems.

[31] Bayesian inference is named after *Bayes* [1763], who presented a method for combining prior information on a model with the information from new data. In this formulation of an inverse problem all information is

represented in probabilistic terms (i.e., degrees of belief). Bayesian inference is reasonably general in that it can be applied to linear or nonlinear problems. (It is dealt with in more detail in the tutorial section of this paper.) In short, it combines the prior information known on the model, with the observed data, and produces the *posterior probability density function* (PDF) on the model parameters, which is taken as the “complete solution” to the inverse problem. (Standard references are by *Box and Tiao* [1973], and useful recent books are by *Smith* [1991] and *Gelman et al.* [1995]. Summaries within a geophysical context are given by *Duijndam* [1988a, 1988b] and *Mosegaard and Tarantola* [1995].) The Bayesian approach is not without its criticisms. For example, implicit in its formulation is that one must know the statistical character of all error, or noise, processes in the problem, which can be very difficult in some cases, especially when the theoretical predictions from a model involve approximations. In addition, it is a controversial issue as to whether prior information can be adequately represented probabilistically (see *Scales and Snieder* [1997] and *Gouveia and Scales* [1998] for a discussion). (Note that probabilistic prior information is often called “soft” and differs from strict inequalities on the model parameters, which are referred to as “hard” prior information [see *Backus*, 1988; *Stark*, 1992].)

[32] In a Bayesian approach the *posterior PDF* spans the entire model space. The case where it is a Gaussian can be dealt with effectively using linearized inversion techniques [see *Tarantola*, 1987; *Menke*, 1989]. Linearized techniques use local curvature information on the PDF about its maximum to estimate resolution and trade-offs. If the PDF is a Gaussian, then the local curvature defines the complete structure of the PDF in parameter space. For highly nonlinear problems the posterior PDF can have a complex multimodal shape, arising from the nature of the data fit (*likelihood function*) or perhaps from the inclusion of complex prior information. In this case, global optimization techniques are needed to identify the maximum of the posterior probability density; however, as the complexity of the PDF increases, a single “most probable” model (if one exists) has little meaning (see Figure 4b). Even if one could be found, a linearized treatment of resolution problem would be of little value (essentially because the local information on the PDF’s curvature is not representative of the PDF as a whole). In these cases, information on the complete shape of the posterior is needed to produce Bayesian measures of uncertainty and resolution. It is here that Monte Carlo methods have major advantages over linearized (local) methods, since the sampling they produce can be used to calculate Bayesian integrals. Within a Bayesian context then, the emphasis is less on optimization and more on sampling the most probable regions of parameter space as determined by the posterior PDF, a process known as *importance sampling*. (Compare this to the early MCI work where the emphasis was on exploring the acceptable regions of

parameter space, as defined by data and prior constraints.)

[33] *Monte Carlo integration* of multidimensional probability distributions is an active area of research in computational statistics (for summaries see *Flournoy and Tsutakawa* [1989], *Smith* [1991], *Smith and Roberts* [1993], and *Gelman et al.* [1995]). Over the past 10 years, geophysicists have begun to use *Markov Chain Monte Carlo* (MCMC) methods, which directly simulate the posterior PDF, that is, draw random samples distributed according to the posterior PDF, and from these calculate Bayesian estimates of constraint and resolution [see *Koren et al.*, 1991; *Mosegaard and Tarantola*, 1995; *Gallagher et al.*, 1997; *Gouveia and Scales*, 1998]. It is not surprising that many of these studies arise in seismology and in particular the estimation of Earth structure from high-frequency body waveforms, especially in exploration studies. This is an area where complex multimodal and multidimensional PDFs can result from the discrepancies between observed and predicted seismograms. An example is shown in Figure 4b, which comes from the work of *Deng and Scales* [1999].

[34] At the end of the 1990s, Monte Carlo integration and importance sampling have become firmly established as the technique of choice for Bayesian inversions in nonlinear problems. Debate continues over whether the Bayesian paradigm is appropriate in many cases (see *Scales and Snieder* [1997] for a discussion). However, Monte Carlo (adaptive or nonuniform) sampling of parameter spaces has also remained popular in studies that do not invoke the Bayesian philosophy. (Many of the papers cited above fall into this category.) In these cases the issues of mapping out and characterizing the class of acceptable models remain just as relevant today as when the original hedgehog algorithm was proposed more than 30 years ago [*Keilis-Borok and Yanovskaya*, 1967; *Valius*, 1968]. Characterizing the properties of all acceptable models, or an obtained finite ensemble, has been a central issue for many authors, and a variety of algorithms have been proposed (see *Constable et al.* [1987], *Vasco et al.* [1993], *Lomax and Snieder* [1994, 1995b] *Douma et al.* [1996], and *Sambridge* [1999b] for examples). This is perhaps the factor that most clearly distinguishes a study of inverse problems from that of parameter estimation.

[35] With the growth and spread of high-performance computing, Monte Carlo inversion techniques are no longer restricted to the owners of supercomputers. As their use becomes more widespread, we can expect that direct sampling of a parameter space will become routine for nonlinear problems, and the need for linearization will diminish in many cases. (This is arguably already the case for problems with relatively few unknowns, e.g., earthquake hypocenter location.) Also, one might expect that larger scale problems (i.e., involving many more unknowns) will increasingly be tackled using Monte Carlo techniques, within either a Bayesian or non-Bayesian framework. For the foreseeable future

very large scale nonlinear problems, like 3-D mantle seismic tomography, are likely to remain beyond the range of Monte Carlo techniques; however, it is worth noting that a Monte Carlo technique has already been applied to a 2-D borehole tomography problem (involving fewer unknowns than mantle tomography, but often more nonlinear) [Vasco *et al.*, 1993]. As Monte Carlo sampling is better understood and becomes more accessible, it seems likely that it will become an increasingly useful tool for nonlinear inversion. It is hoped that this paper, and in particular the following tutorial section, will add to that awareness and encourage students and researchers to think about it themselves.

3. MONTE CARLO METHODS: THE TECHNOLOGY OF INFORMATION

[36] In the next section we outline some of the main Monte Carlo approaches that have been used to tackle geophysical inverse problems. We describe some of the basic concepts and provide a source of references for further reading. Some open questions are also highlighted. At all times we assume that we have some criterion, ϕ , which measures the discrepancy between observations and predictions and perhaps includes some other information. Its evaluation for any given model, x , constitutes a solution to the *forward problem*. In some cases we may be interested in optimizing this objective function; in others we may be more interested in sampling it adequately enough to either evaluate Bayesian information measures (as discussed in section 3.3), or estimate properties of the data acceptable models that fit within our chosen (usually finite dimensional) parameter space.

[37] Several of the approaches discussed here are commonly associated with a Bayesian approach to inversion. However, it is worth noting that they can also be employed independently of a Bayesian inversion, that is, simply to perform a direct search of a parameter space.

3.1. Preliminaries

3.1.1. Linearization or Monte Carlo?

[38] The first question one needs to address is whether a Monte Carlo technique (like SA, GA, NA, etc.) or a linearized approach (based on matrix inversion) would be most appropriate for a particular problem. The answer depends on the nature of the data-model relationship, the number of unknowns, and, to a lesser extent, the computational resources available.

[39] As the data-model relationship becomes more complex, the misfit function (or PDF) will also increase in complexity (e.g., multimodal, etc.), and Monte Carlo techniques will be favored over linearized techniques for two reasons. The first is that they are more numerically stable in the optimization/parameter search stage. This is because they do not rely on the convergence of se-

quence of model perturbations (like a linearized approach) and at the same time avoid the need for matrix inversion.

[40] The second reason for favoring Monte Carlo techniques is that they are usually more reliable in appraising the solution, that is, estimating uncertainty by means of model covariance and resolution matrices (see section 3.3). This is (again) because they avoid derivatives and hence the numerical approximations on which linearized estimates of model covariance and resolution are based [see Menke, 1989]. Linearized techniques are prone to underestimate uncertainty when nonlinearity is severe. Also, a direct search of the parameter space may indicate significant trade-offs and even multiple classes of solution, which would not be found using linearization.

[41] Unfortunately, it is not possible to know whether linearized estimates of model covariance and resolution are accurate until a fully nonlinear calculation has been performed. The same is true for the optimization process itself, that is, whether linearized techniques are likely to be unstable or require heavy damping to converge, problems that could well be alleviated using a direct search technique.

[42] In some cases, for example, in many waveform inversion studies encountered in seismic exploration, the data-model relationship can become so complex that fully nonlinear direct search techniques are the only viable approach. At the opposite end of the scale, with discrete linear, or linearized, problems with relatively few unknowns (e.g., 10–50), it is often overlooked that Monte Carlo techniques can be both very convenient and efficient.

[43] It is also worth pointing out that linearization is not always possible or practical in some cases. This is the case when the observables are not differentiable functions of the unknowns. An example is when the forward problem involves a complex calculation such as the numerical modeling of landscape evolution in response to tectonic and erosional processes [van der Beek and Braun, 1999; Braun, 2002]. In this case the unknowns are the rate of tectonic uplift and parameters that relate rate of surface processes to geometrical features like drainage area and surface slope, while the observables are geochronological constraints on exhumation rate and morphological properties of the landscape. In these problems, there is no analytical relationship between unknowns and observables, and hence linearized techniques are not appropriate. However, direct search techniques can still be applied because they only require the ability to solve the forward problem. Furthermore, all of the direct search algorithms presented in section 3.2 can take advantage of parallel computation because each forward solution can be performed independently. It seems likely that this is an area where Monte Carlo techniques will find more applications in the future.

[44] It is important to stress that Monte Carlo techniques are not a panacea for geophysical inversion. They

are only applicable to discretized problems, that is, ones where a finite parameterization has been chosen, and as with all discrete inversion approaches, the results will inevitably be dependent on the suitability of that choice. Also, it is clear that as the number of unknowns become large (say, greater than a few hundred) then direct search techniques become impractical because of the computation involved. The actual limiting dimension will vary considerably between applications because it depends on the computational cost of solving the forward problem. However, it is also clear that as computing power continues to grow, so will the range of problems that can be addressed with Monte Carlo techniques.

3.1.2. Which Monte Carlo Technique?

[45] The choice between the competing flavors of Monte Carlo technique is much less clear than whether one should be used in the first place. In general, there appears to be no preferred method of choice in all circumstances. In the next few sections we discuss the basic mechanics of different classes of Monte Carlo approach and make some comparisons. Here we make a few general observations which may help in deciding on which Monte Carlo technique to choose.

[46] In cases where the cost of the forward modeling is not excessive and the number of unknowns is small (say <10), a simple deterministic grid search [e.g., Sambridge and Kennett, 1986] may be practical (see section 3.2.2). This would have the attraction of being both reliable (guaranteeing a global minimum on the chosen grid) and useful for uncertainty analysis because the samples are uniformly distributed and hence produce an unbiased sample of the parameter space. With modern computing power this most simplistic of techniques can become surprisingly efficient for some problems. Of course, grid search techniques become impractical when either the number of unknowns or the computational cost of the forward problem is high, and one must turn to the more sophisticated irregular parameter space sampling methods.

[47] It is beyond the scope of this paper to enter the (perhaps never-ending) argument between Bayesian and non-Bayesian approaches to inversion [Scales and Snieder, 1997]. However, it should be noted that a Bayesian inversion is often implemented with a Markov chain Monte Carlo (MCMC) approach (section 3.2.3.1), for example, using the Metropolis algorithm. This, in turn, is closely related to the optimization technique simulated annealing (section 3.2.3), and so, in general, if a Bayesian approach were preferred, then these would be the natural algorithms of choice for both optimization and uncertainty estimation (see section 3.2.3.1 for a discussion).

[48] Several authors have argued for genetic algorithms (section 3.2.4) as a powerful *parameter space search* technique (see above), although the ensemble of parameter space samples produced by a genetic algo-

rithm does not (in general) follow any prescribed probability distribution and so cannot be used directly for a quantitative uncertainty analysis (within a Bayesian framework) (see section 3.4). The neighbourhood algorithm (section 3.2.5), which is both a search and appraisal technique, offers a potential solution to this problem. Ultimately, the choice between Monte Carlo direct search techniques will often depend as much on issues of practical convenience, like the availability of suitable computer software, as the precise details of the algorithms.

3.1.3. Generating Random Samples

3.1.3.1. Pseudorandom Deviates

[49] All Monte Carlo techniques make use of random number generators of some kind. This is the case even when the ultimate task is to generate multidimensional random deviates distributed according to complicated PDFs, for example, with the *Metropolis-Hastings algorithm* (see section 3.2.3.1). The common approach is to generate *pseudorandom numbers* using a linear or multiplicative congruent method. For a survey of theory and methods, see Park and Miller [1988], and for descriptions of “workhorse” techniques, see Press *et al.* [1992]. Figure 5a shows 1000 pairs of pseudorandom numbers plotted as points in the plane.

3.1.3.2. Quasi-Random Sequences

[50] It is a nonobvious point that not all random number generators are equally uniform. One way this can be measured is in how fast the error in a Monte Carlo integration decreases as a function of the number of samples. For example, if one were to calculate the average of the x or y values of the pseudorandom points in Figure 5a, then (assuming the sides of the box were 0 to 1) the rate at which the estimate approaches 0.5 would decrease linearly proportional to $1/\sqrt{N}$, where N is the number of points. However, it is possible to do much better by using quasi-random (or subrandom) sequences. Figure 5b shows an example of $N = 1000$ points generated from two quasi sequences. The quasi sequence generates a set of points that are (in a well-defined sense) “maximally self-avoiding.” To the eye this looks like a regular grid with the vertices randomly perturbed. It is clear from Figure 5b that in this case the *quasi random numbers* are more evenly distributed than the pseudorandom deviates. It can be shown that as a consequence they result in more rapid convergence of Monte Carlo integrals. For example, if we calculated the average of the x and y values from the points in Figure 5b, then the numerical error would decrease proportional to $1/N$, which is much faster than for the pseudorandom case. As we show in section 3.3, the evaluation of MC integrals is central to Bayesian inference.

[51] The Sobol-Antonov-Saleev approach [Sobol, 1967; Antonov and Saleev, 1979] is an efficient way to generate quasi-random sequences and has been imple-

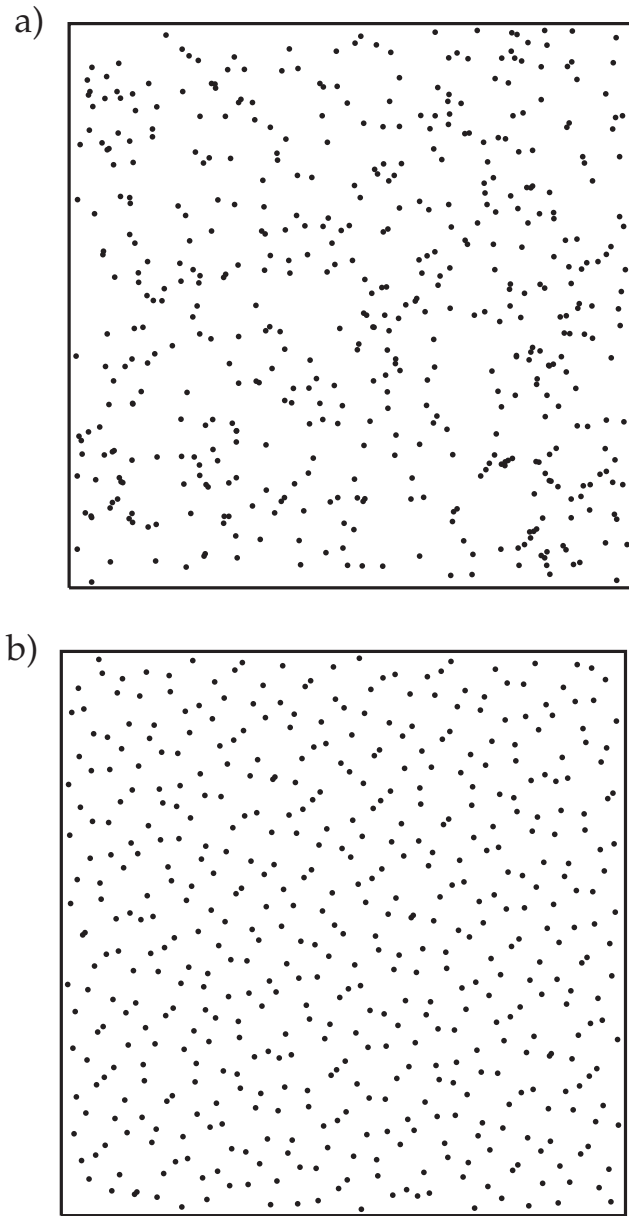


Figure 5. (a) The 1000 uniform points generated with a pseudorandom number generator, showing typical clustering and unevenness. (b) The 1000 uniform points generated with two sequences of quasi-random numbers. Note the considerably more uniform appearance and even density compared to Figure 5a.

mented in a convenient form by *Press et al.* [1992]. However, care must be taken in using quasi-random numbers, especially when they form the components of a vector (i.e., Earth model) in a multidimensional space. In this case each component in the (quasi-random) vector must be generated from an independent quasi sequence. The main problem is that some components of multidimensional quasi-random vectors can have a high degree of correlation. It is only when sufficiently many quasi vectors are generated that the correlation disappears. In dimensions as low as 10, it may require many thousands of samples before the overall correlation be-

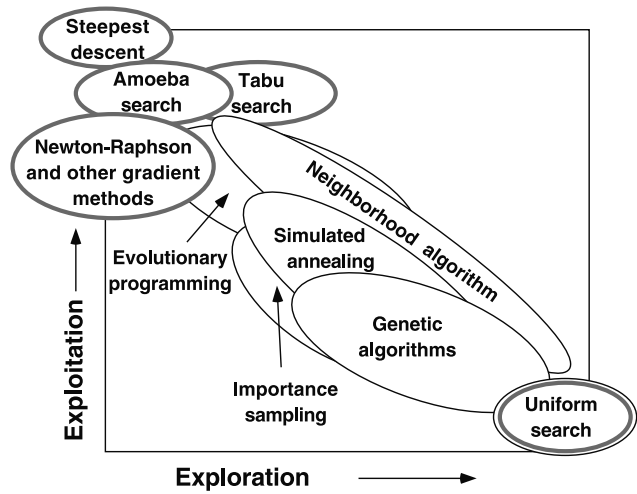


Figure 6. A schematic representation of various search/optimization algorithms in terms of the degrees to which they explore the parameter space and exploit information. Shaded borders indicate a deterministic (non-Monte Carlo) method. Uniform search includes the deterministic grid search.

tween all components is negligible, and hence the samples are usable. *Morokoff and Caflisch* [1994] describe these issues in detail. Quasi-random sequences are used in the neighbourhood algorithm of *Sambridge* [1999a] (see also section 3.2.5) and are finding increasing numbers of applications in multidimensional numerical integration [*Morokoff and Caflisch*, 1994].

3.2. Searching a Parameter Space With Monte Carlo Methods

3.2.1. Exploration Versus Exploitation

[52] A useful framework for comparing different search algorithms, random or not, is in terms of a trade-off between exploration and exploitation. By exploration we mean trying to improve the objective function by looking (randomly) in different regions of parameter space, without regard for what we have already learned from previous sampling. Exploitation is the opposite; we make decisions of where to sample next by only using the previous sampling and sometimes just the current best fit model. Most direct search Monte Carlo algorithms fall somewhere in between the extremes. Figure 6 shows our attempt to classify various techniques according to these definitions.

[53] From the point of view of optimization the rule of thumb is that the more explorative an algorithm is, the less likely it will fall into local minima, but the less efficient it will be at converging on a solution. Conversely, the exploitative algorithms will be more efficient at convergence but prone to entrapment, and hence the final result will depend on the starting point. Examples of methods that lie at the extremes would be a uniform random search, which is completely explorative, and a steepest descent algorithm [*Gill et al.*, 1981], which is

purely exploitative. Clearly, the most appropriate technique will depend on the nature of the problem. For smoothly varying near quadratic objective functions we would prefer an exploitative approach, which allows rapid converge, for example, a Newton-type descent method. For highly nonlinear problems with multiple minima/maxima in the objective function a combination of exploration and exploitation would probably suit best. However, controlling the trade-off between the two properties is often quite difficult, as is deciding in advance which approach is best suited to a particular problem.

3.2.2. Uniform Sampling

[54] The simplest form of randomized sampling of a parameter space is uniform sampling. For a problem with d distinct unknowns the i th random sample is the vector \mathbf{x}_i ,

$$\mathbf{x}_i = \sum_{i=1}^d r_i \mathbf{e}_i, \quad (1)$$

where r_i is a $(0,1)$ uniform random deviate and \mathbf{e}_i is the unit vector along the i th axis in parameter space. For each new sample some data fit, or other objective function, ϕ , must be evaluated, and hence forward modeling performed. As discussed above, this was the first fully nonlinear approach used by geophysicists more than 30 years ago. Note that, by definition, uniform sampling is not biased toward any particular region of parameter space, and there is hence no possibility of entrapment in local minima of ϕ . Equally, however, it does not concentrate sampling, and, even with modern supercomputers, it is usually inefficient once the number of unknowns becomes greater than ~ 10 . This is the so-called “curse of dimensionality.” For example, if we imagine the parameter space filled by a regular multidimensional Cartesian grid with $(n_k - 1)$ intervals per axis, then the number of distinct nodes (and hence models) in this grid is n_k^d , which can become enormous, even in relatively small dimensions.

[55] In practice, one always undersamples a parameter space. In many Monte Carlo studies the total number of samples generated is much smaller than the number of vertices of a single “unit cube” in a Cartesian grid, that is, 2^d , and in this sense one always tends to undersample parameter spaces in practice. For most problems the only viable approach is for the MC search algorithm to concentrate sampling in particular “promising” regions of parameter space, that is, adapt itself to the objective function ϕ . One area where uniform MC search has continued to be useful is in sampling under hard prior constraints on the unknowns. An example appears in the work of Wiggins [1972] [see also Cary and Chapman, 1998; Kennett, 1988].

3.2.3. Simulated Annealing

[56] The simulated annealing method exploits a statistical mechanical analogy to search for the global minimum of an objective function ϕ possessing a large number of secondary minima. The algorithm simulates the process of chemical annealing in which a melted crystalline material is cooled slowly through its freezing point, thereby approximately settling into its energy ground state. By identifying the objective function with the energy of the crystalline material and by appropriate definition of a temperature parameter for the simulations, it is possible to simulate a “cooling” of the system to be optimized. A sufficiently slow cooling of this system will, by analogy to the chemical annealing, result in convergence to a near-optimal configuration, characterized by a near-minimal value of the objective function.

[57] Simulated annealing is based on the Metropolis-Hastings algorithm or the Gibbs Sampler, and we shall therefore take a closer look at these algorithms here. Later, we shall also see why these algorithms are the workhorses in Bayesian Monte Carlo calculations.

3.2.3.1. Markov Chain Monte Carlo: Metropolis, Hastings, and Gibbs

[58] The idea behind the Metropolis-Hastings algorithm and the Gibbs Sampler is the same. They are both so-called Markov Chain Monte Carlo algorithms designed to generate samples of a probability distribution p over a high-dimensional space \mathcal{M} under the special difficulty that no explicit mathematical expression exists for p . Only an algorithm that allows us to calculate the values of p at a given point in the space is available. This is a typical situation in geophysics where p is a probability density derived from a misfit function ϕ through, for example,

$$p(\mathbf{m}_k) = A \cdot \exp(-B\phi(\mathbf{m}_k)), \quad (2)$$

where \mathbf{m}_k is a model and A and B are constants. Very often $p(\mathbf{m}_k)$ can only be evaluated for a particular Earth model through a very computer-intensive calculation.

[59] Let us consider the mechanics of the Metropolis-Hastings algorithm, for simplicity, we consider a situation where we wish to sample a probability distribution p in a discretized model space \mathcal{M} . Sampling from the distribution p means that the probability of visiting model \mathbf{m} is proportional to $p(\mathbf{m})$. To generate a simple algorithm that samples p , we can make the following assumptions:

1. The probability of visiting a point \mathbf{m}_i in model space, given that the algorithm currently is at point \mathbf{m}_j , depends only on \mathbf{m}_j and not on previously visited points. This is the so-called *Markov* property. This property means the algorithm is completely described by a transition probability matrix P_{ij} whose ij th component is the conditional probability of going to point \mathbf{m}_i , given the algorithm currently visits \mathbf{m}_j .

2. For all points \mathbf{m}_j in \mathcal{M} , there are exactly N points \mathbf{m}_i ,

including \mathbf{m}_j itself, for which P_{ij} is nonzero. If this property holds, we say that the algorithm is regular, and the set of N accessible points constitutes what we call the neighborhood \mathcal{N}_j of \mathbf{m}_j .

[60] It is possible for the algorithm to go from any point \mathbf{m}_j to any other point \mathbf{m}_i , given enough steps. An algorithm satisfying this property is called irreducible.

[61] The question now is, which transition probability matrix P_{ij} leads to an algorithm that samples the target distribution p ? The answer is that there exists infinitely many such transition probability matrices. We will choose one that is simple, namely, one that satisfies microscopic reversibility:

$$P_{ij}p(\mathbf{m}_j) = P_{ji}p(\mathbf{m}_i). \quad (3)$$

It is easy to see that any choice of P_{ij} satisfying microscopic reversibility will continue to sample p once it has already started doing so. This is a simple consequence of the fact that if the algorithm has probability $p(\mathbf{m}_j)$ of visiting \mathbf{m}_j , then the probability that a transition from \mathbf{m}_j to \mathbf{m}_i takes place in a given iteration is $P_{ij}p(\mathbf{m}_j)$. Similarly, the probability that a transition from \mathbf{m}_i to \mathbf{m}_j takes place in a given iteration is $P_{ji}p(\mathbf{m}_i)$. Microscopic reversibility means that the probability of these two transitions is the same at all times, and the fact that each pair of points in \mathcal{M} maintains mutual equilibrium in this way means that there is overall equilibrium sampling at the target distribution p . For more details see, for example, *Mosegaard and Tarantola [1995]* or *Mosegaard and Sambridge [2002]*.

[62] In the Metropolis-Hastings algorithm the transition probabilities P_{ij} are given by

$$P_{ij} = \frac{1}{N} \min \left(1, \frac{p(\mathbf{m}_i)}{p(\mathbf{m}_j)} \right), \quad (4)$$

and hence satisfy equation (3). This is, in practice, realized in the following way.

[63] Assume that the current point visited by the algorithm is \mathbf{m}_j . We now choose (or, rather, propose) one of its N neighbors \mathbf{m}_i with probability

$$P_{\text{proposal}} = 1/N. \quad (5)$$

Finally, we accept \mathbf{m}_i only with probability

$$P_{\text{accept}} = \min \left(1, \frac{p(\mathbf{m}_i)}{p(\mathbf{m}_j)} \right). \quad (6)$$

If \mathbf{m}_i is accepted, the algorithm goes to \mathbf{m}_i in this iteration, but if \mathbf{m}_i is rejected, the algorithm stays in \mathbf{m}_j (\mathbf{m}_j is visited once again). It is clear that the above algorithm has transition probabilities given by equation (4).

[64] The remaining question of how to make the algorithm sample p in the first place is more complicated, but fortunately it can be shown [see, e.g., *Tierney 1994*] that the distribution of samples produced by any algorithm satisfying our requirements will indeed converge toward p when the number of iterations goes to infinity.

The problem of estimating the speed of convergence is presently unresolved, but some practical advice on how to run this type of algorithm was found by *Hastings [1970]* and *Mosegaard [1998]*.

[65] According to the mechanics of the Gibbs Sampler in a typical implementation, operating in a K -dimensional model space, each iteration consists of K substeps, one for each parameter. The k th substep perturbs only the k th parameter, and it has its own transition probability matrix P_{ij}^k . The neighborhood \mathcal{N}_j^k of a point \mathbf{m}_j consists of all points \mathbf{m}_i that differ from \mathbf{m}_j in only the k th parameter. This means, in particular, that the neighborhoods of two points are either identical or disjoint.

[66] Assume again that the current point visited by the algorithm is \mathbf{m}_j . We now run K steps, and in each step, instead of proposing one of its N neighbors uniformly at random, we choose \mathbf{m}_i from the neighborhood \mathcal{N}_j^k according to the conditional probability distribution

$$p(\mathbf{m}_i | \mathcal{N}_j^k) = \frac{p(\mathbf{m}_i)}{\sum_{\mathbf{m}_k \in \mathcal{N}_j^k} p(\mathbf{m}_k)}, \quad (7)$$

without any accept/reject probability (i.e., the chosen \mathbf{m}_i is always accepted). In each step, only one parameter is perturbed (or is possibly left unchanged), so after completion of one iteration (consisting of all K steps), all parameters have been perturbed.

[67] That this algorithm samples p is easy to see. The transition probability matrix for each step is given by

$$P_{ij}^k = p(\mathbf{m}_i | \mathcal{N}_j^k), \quad (8)$$

which clearly satisfies microscopic reversibility, equation (3), so if $\mathbf{m}_i \in \mathcal{N}_j^k$, then

$$\begin{aligned} P_{ij}^k p(\mathbf{m}_j) &= p(\mathbf{m}_i | \mathcal{N}_j^k) p(\mathbf{m}_j) \\ &= \frac{p(\mathbf{m}_i)}{\sum_{\mathbf{m}_k \in \mathcal{N}_j^k} p(\mathbf{m}_k)} p(\mathbf{m}_j) \\ &= \frac{p(\mathbf{m}_j)}{\sum_{\mathbf{m}_k \in \mathcal{N}_i^k} p(\mathbf{m}_k)} p(\mathbf{m}_i) \\ &= p(\mathbf{m}_j | \mathcal{N}_i^k) p(\mathbf{m}_i) \\ &= P_{ji}^k p(\mathbf{m}_i), \end{aligned}$$

where we have used that the neighborhoods \mathcal{N}_j^k and \mathcal{N}_i^k are identical. Since each step of an iteration satisfies microscopic reversibility, so does the entire iteration, and the algorithm samples the target distribution p asymptotically.

[68] Whether the Metropolis-Hastings algorithm or the Gibbs Sampler is the most efficient depends on the problem at hand. The Gibbs Sampler takes much fewer iterations before it samples p correctly, but the many

steps needed to perform an iteration may render it inefficient for problems where evaluation of p is computer-intensive. Rothman [1986] gives an example of the use of a Gibbs Sampler in a case where p can be efficiently evaluated for all perturbations of a single model parameter.

3.2.3.2. Simulated Annealing Algorithm

[68] It is an empirical fact that the process of chemical annealing, where a crystalline material is slowly cooled through its melting point, results in formation of highly ordered, low-energy crystals. The slower the cooling, the more perfect is the crystal growth, and the lower is the lattice energy. This process can be viewed as a “physical optimization method” in which the objective function is the lattice energy E . The process can be simulated in large numerical systems by identifying the model parameters of the system with state space variables and the objective function of the optimization problem with the energy E . In each step of the algorithm, thermal fluctuations in the system are simulated by randomly perturbing model parameters, and the fluctuations are controlled by a temperature parameter T . The simulated annealing algorithm [Kirkpatrick *et al.*, 1983] runs as follows: In each step a random perturbation of the model parameters \mathbf{m}_j of the numerical system is attempted. The new set of model parameters \mathbf{m}_i are accepted if the value of the objective function E decreases. However, if E increases, the new parameters may be accepted with probability

$$P_{\text{accept}} = \exp\left(-\frac{\Delta E}{T}\right), \quad (9)$$

where ΔE is the change in the objective function and T is the temperature parameter. If the new model is rejected, a new perturbation is attempted in the next move, and the above process of decision is repeated.

[69] A close inspection of the above algorithm reveals that for constant temperature parameter T it is actually a Metropolis-Hastings algorithm designed to sample the probability distribution [Metropolis *et al.*, 1953],

$$P_B(\mathbf{m}) = \frac{\exp\left(-\frac{E(\mathbf{m})}{T}\right)}{Z(T)}, \quad (10)$$

which is known in statistical physics as the Gibbs-Boltzmann distribution. Here $1/Z(T)$ is a normalization constant. In simulated annealing, however, the temperature parameter is gradually decreased from a high value, allowing large “thermal” fluctuations, down to zero, where only decreasing values of the objective function are allowed. For decreasing temperature T the Gibbs-Boltzmann distribution converges toward a distribution having all its probability mass in the global minimum for E . In other words, as the temperature gradually approaches zero, the probability that our system is close to

the global minimum for its objective function approaches 1.

[70] In simulated annealing the Gibbs-Boltzmann distribution can also be sampled by means of a Gibbs sampler. Rothman [1986] gives an example where the residual statics problem of reflection seismology is solved in this way.

3.2.3.3. Nulton-Salamon Annealing Schedule

[71] In practice, one has to face the fact that the above theory is only true for an infinitely slow “cooling.” The problem is therefore to find a way to decrease the temperature in a finite number of steps, such that the probability that the system is close to the global minimum for E after the annealing simulation is maximum.

[72] Nulton and Salamon [1988] devised a near-optimal annealing method that keeps the numerical system close to “thermal equilibrium” at all times. The actual mean value $\langle E \rangle$ of the objective function is kept at a constant distance

$$v = \frac{\langle E \rangle - \langle E \rangle_{eq}}{\sigma_E(T)} \quad (11)$$

from the never realized equilibrium mean value $\langle E \rangle_{eq}$. Here $\sigma_E(T)$ is the standard deviation of the fluctuating objective function, and the distance v is known as the “thermodynamic speed.” The authors arrive at the following differential equation for the annealing temperature schedule $T(t)$:

$$\frac{dT}{dt} = -\frac{vT}{\epsilon(T) \sqrt{C(T)}}, \quad (12)$$

where $C(T)$ and $\epsilon(T)$ are the heat capacity and the relaxation time of the system, respectively. Estimation of $C(T)$ and $\epsilon(T)$ from statistical information about the system, collected during the annealing process, is described by Andresen *et al.* [1988]. An approximate, temperature-dependent transition probability matrix $P_E(T)$ for transitions between “energy levels” is formed during the annealing process. For each temperature the heat capacity can be evaluated from the eigenvector of $P_E(T \rightarrow \infty)$ with eigenvalue 1, and the relaxation time can be calculated from the second largest eigenvalue of $P_E(T)$.

[73] In practice, the thermodynamic speed v in equation (12) is adjusted such that the annealing temperature is close to zero after a predetermined number of iterations, given by the computer resources available to the optimization.

[74] Figure 7 shows an example where a reflection seismic data set was inverted through simulated annealing optimization. A common-depth-point gather from the data set was transformed into the $\tau - p$ domain (essentially a plane-wave decomposition), and two traces, representing ray parameters $p = 0.000025 \text{ s/m}$ and $p = 0.000185 \text{ s/m}$, respectively, were inverted to obtain a horizontally stratified nine-layer model. Each

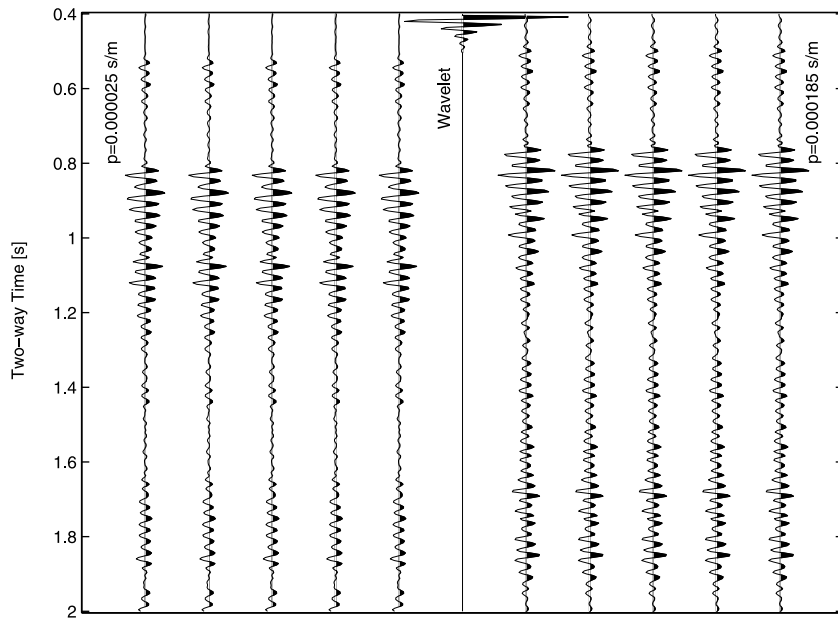


Figure 7. The two seismic $\tau-p$ data traces inverted by a simulated annealing procedure (each trace is repeated 5 times to facilitate inspection). A nine-layer, horizontally stratified P wave and density model was fitted to this data set using waveform modeling and the wavelet displayed in the middle of Figure 7.

layer was characterized by a P velocity, a density, and an attenuation. Figure 7 shows the two traces, each repeated 5 times, and the wavelet. Misfit (“energy” in simulated annealing terminology) was calculated by generating full waveform acoustic $\tau-p$ seismograms from the subsurface model and computing the L_2 -norm of the difference between computed and observed ($\tau-p$ transformed) data.

[75] Figure 8 shows the “thermodynamic portrait” of the problem, generated by the method described by Andresen *et al.* [1988]. The top left graph displays the approximate “density of states” for the problem, showing the fraction of models having misfit (energy) between E and $E + dE$. There are several reasons for the small values of the density of states at small energies. First of all, the fractional volume of the model space with near-optimal models is extremely small, a typical property of inverse problems with high-dimensional model spaces. Second, the fact that noise is present in the data means that zero energy cannot be obtained (unless we overparameterize the problem). A third reason is that the method used to estimate density of states is imperfect. Thermodynamic properties of the problem are estimated through an initial exploratory sampling of the model space, and this sampling visits very few low-energy models.

[76] From the density of states the temperature-dependent “heat capacity” for the problem can be calculated (top right graph of Figure 8). The heat capacity for this problem has two distinct peaks, and these two peaks indicate where annealing must “slow down” if the system is to remain close to equilibrium.

[77] The temperature-dependent relaxation time

(bottom left graph) shows a typical high value at low temperatures. This is the result of slow movement in an “energy landscape” with many secondary minima.

[78] The bottom right graph shows the resulting temperature schedule satisfying approximate constant thermodynamic speed. Practical experience shows that this kind of temperature schedule is far superior to ad hoc schedules not reflecting the thermodynamic properties of the problem [Jakobsen *et al.*, 1988; Andresen *et al.*, 1988; Koren *et al.*, 1991; Mosegaard and Vestergaard, 1991].

3.2.4. Genetic Algorithms

[79] It has long been observed that biological evolution is a form of optimization. In the natural world, fauna compete for survival and adapt to their surroundings. A natural system evolves by using a large population to explore many options in parallel rather than concentrating on trying many changes around a simple design [Gershenfeld, 1999]. Genetic algorithms, or GAs, as they have become known, are the class of numerical method that try to do the same thing. As noted above, GAs largely grew out of the work of Holland [1975], although independent earlier work of Fogel *et al.* [1966] first established the concept of evolutionary computation.

[80] In contrast to the basic form of simulated annealing, which keeps one set of parameters that are continually updated, GAs work on an ensemble of sets of parameters, with less emphasis placed on any particular member. (Note that there also exist more complex forms of simulated annealing where an ensemble of *random walkers* share or exchange statistical information about

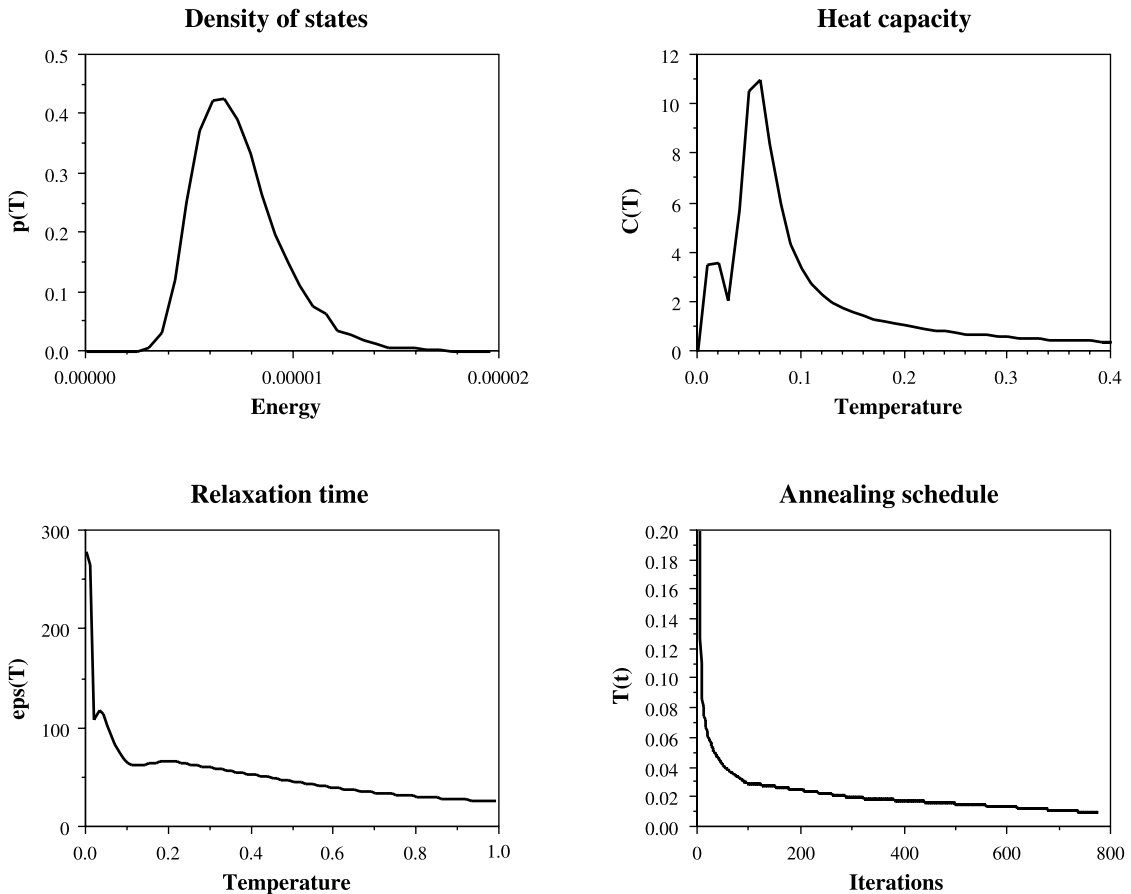


Figure 8. The “thermodynamic portrait” of the simulated annealing problem arising from inversion of the seismic data. The heat capacity can be calculated from the density of states. Combined with the relaxation time, it allows calculation of an annealing temperature schedule satisfying constant thermodynamic speed.

the misfit surface. See, for example, *Harland and Salamon* [1988], *Hoffmann et al.* [1990], *Mosegaard and Vestergaard* [1991], and *Ruppeiner et al.*, [1991]). The early history of GAs in the Earth sciences has been traced above. Here we provide a brief description of how they can be used to search a parameter space. For more information the reader is referred to the comprehensive summaries that have appeared [Davis, 1987; Goldberg, 1989; Rawlins, 1991; Whitley, 1994; Gallagher and Sambridge, 1994; Winter et al., 1995] and also to the web resources in Table 1.

[81] A key aspect of a genetic algorithm is the representation of complicated models with a simple encoding. The most common is that used by *Holland* [1975], and it consists of a simple bit string. For example, in a problem involving d unknowns, each could be allowed to take 2^n values and be represented by a bit string of length $d \times n$. This is, in effect, a parameterization of the problem. The overall effectiveness of a GA can depend crucially on how it is encoded. There are many other possibilities besides the simple bit string, some of which do not even involve direct representation of parameter values [e.g., *Mathias and Whitley*, 1992]. There is no doubt the most suitable will depend on the particular problem in hand.

[82] The genetic algorithm works with a population of Q models simultaneously. Usually, the population is initially generated randomly, but at each iteration it is altered by the action of three operators. The fitness (objective function) for each model in the starting population is evaluated by solving the forward problem for each of the Q models. The purpose of the GA is then to seek out fitter models in parameter space. The three operators are known as selection, crossover, and mutation, and they are illustrated for the simple bit string encoding in Figure 9.

3.2.4.1. Selection

[83] From the initial population of Q bit-strings an interim population of Q parents is generated by selecting models from the original group with the probability of selection determined by the fitness value. For example,

$$P(\mathbf{m}_k) = A \exp [-B\phi(\mathbf{m}_k)], \quad (13)$$

where A and B are problem specific constants. (Note the similarity with probability function used in the Metropolis-Hastings method, equation (2).) The higher the fitness of each model, the more likely that it will pass

Table 1. World Wide Web Addresses Where Papers, Tutorials, and Software on Monte Carlo and Global Optimization Methods Can Be Found.^a

Subject	Title	Address
Genetic algorithms	IlliGAL home page genitor group (Colorado state) genetic algorithm group genetic algorithms archive genetic programming notebook ensemble-based simulated annealing Optimization Technology Center adaptive simulated annealing global optimization survey global optimization archive MCMC reprint service neighbourhood algorithm page MCMC and SA in inverse problems BUGS website quasi Monte Carlo a website containing material and links from this article	www-illigal.ge.uiuc.edu www.cs.colostate.edu/~em genitor www.cs.gmu.edu/research/gag www.aic.nrl.navy.mil/galist www.geneticprogramming.com www-rohan.sdsu.edu/~frostr/Ebsa www.ece.nwu.edu/OTC www.ingber.com www.cs.sandia.gov/opt/survey www.mat.univie.ac.at/~neum/glopt.html www.statslab.cam.ac.uk/~mcmc rses.anu.edu.au/~malcolm/na www.gfy.ku.dk/~klaus/mcinversion www.mrc-bsu.cam.ac.uk/bugs www.mcqmc.org rses.anu.edu.au/~malcolm/mcgi
Simulated annealing and global optimisation		
Markov chain Monte Carlo and other		
Monte Carlo in geophysical inversion		

^aAll links were active at the time of writing.

into the next population. Since the population size does not change, multiple copies of the fitter models will survive at the expense of the less fit models, which may be extinguished completely. This operator introduces the element of survival of the fittest into the algorithm.

3.2.4.2. Crossover

[84] This operator cuts and mixes pairs of randomly chosen bit strings together. All Q parent strings are randomly paired to produce $Q/2$ couples. A crossover probability P_c is assigned, and if a random number

between 0 and 1 is less than P_c , parts of the two strings are interchanged (see Figure 9). If a crossover is selected, the location at which the strings are cut is determined randomly, otherwise the two parent strings are passed unscathed to the next generation (see Figure 9). In this way it is hoped that information is passed on to subsequent generations.

3.2.4.3. Mutation

[85] The purpose of the mutation operator is to maintain a degree of diversity in the population. Note that the

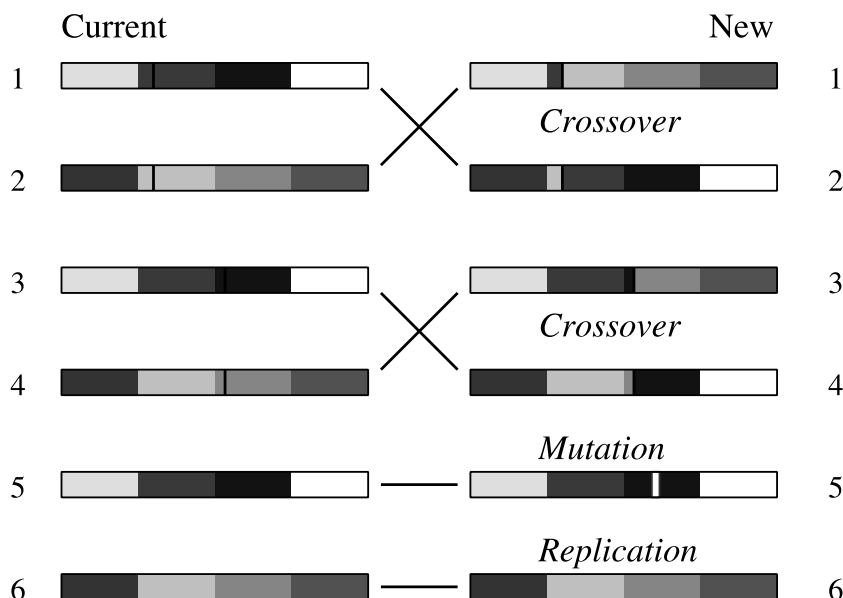


Figure 9. The effect of the three bit string operators in a genetic algorithm. In cases 1–4, the crossover operator cuts, swaps, and rejoins pairs of strings. In case 5, mutation changes a single bit. In case 6 a whole string is replicated. These operators act sequentially on a population of strings. The shading represents the values of four different variables encoded into the bit string.

selection operator acts to remove diversity of bit patterns from the population. In mutation any bit in an individual string is allowed to flip between 0 and 1. This is usually performed with a relatively low probability P_m .

[86] Overall, the action of the three operators is to produce a new population of models for which the forward problem must be solved and the fitness evaluated. After many iterations the population has the potential to evolve toward a fitter on-average state. Each stage involves randomized decisions which are influenced by the “control” parameters. Even in this basic description, we have five control parameters (Q , P_c , P_m , A , and B), which usually must be chosen (tuned) for each application. Although a GA is often thought of as a direct search method of global optimization (i.e., one not using gradient information), it can still become trapped in local minima or be stalled by complicated fitness landscapes. (The same is true of almost all other search and optimization methods.) Careful tuning of the control parameters may be required in these circumstances, and there is never any guarantee of convergence to a global minimum. Many variants of the basic genetic algorithm have been developed, several of them in geoscience applications (for discussions see *Gallagher and Sambridge [1994]*, *Sen and Stoffa [1995]*, *Koper et al. [1999]*, and the references above).

[87] The field of research into genetic algorithms has grown significantly over the past 10 years. A large literature has now developed, much of which can be found either through the papers cited above or the web resources in Table 1. Outside of the Earth sciences genetic algorithms have found applications in a range of areas and not just in function or combinatorial optimization problems. For example, in the original book by *Holland [1975]* the idea that GAs could be used to train neural networks is presented. As a Monte Carlo inversion method, GAs are perhaps best thought of as a direct search method in a parameter space. The result is an ensemble of models that are geared toward the better/fitter regions of parameter space. Information still needs to be extracted from the resulting ensemble, which is a focus of current research and is discussed further in section 3.4.

3.2.5. Other Approaches

[88] A major field within computational statistics is the development of techniques for Monte Carlo integration. Essentially, this means numerically evaluating multidimensional integrals of the form

$$I = \int_{\mathcal{M}} f(\mathbf{x}) d\mathbf{x}. \quad (14)$$

This type of integral occurs repeatedly in Bayesian inference studies. The main issue is to sample the multi-dimensional function $f(\mathbf{x})$ in some efficient manner so that numerical estimates of the integral can be made. A

large literature exists on the subject [see *Flournay and Tsutakawa, 1989*, and references therein]. The Metropolis-Hastings algorithm and Gibbs Sampler (discussed above) are examples of statistical importance sampling techniques that can be used for this task. Hence there is a direct connection between Monte Carlo integration and Monte Carlo (adaptive) sampling of a parameter space. In principle then, other types of importance sampling methods specifically designed for multidimensional integration might be useful to adaptively sample a parameter space.

[89] One such technique, widely used in the field of particle physics, is the Adaptive Monte Carlo algorithm of *Lepage [1978]*. This procedure iteratively generates its own sampling density function, which approximates the integrand in equation (14). The sampling density is chosen to be separable, that is, a function of M variables that is a product of M 1-D functions, one for each axis in parameter space. By drawing random samples according to this density function the algorithm samples in the significant regions of $f(\mathbf{x})$. If $f(\mathbf{x})$ were taken as the data misfit/objective function, then the algorithm could be used to successively concentrate sampling where the function was high and hence act as an MC search algorithm. For further details see *Lepage [1978]* and *Press et al. [1992]*. Given the wide use of this approach for multidimensional integration, it is surprising that to date it does not seem to have been used in geophysical inversion. One potential problem is that a separable sampling density may poorly represent multidimensional distributions when variables are highly correlated, which is likely in many inverse problems. In this case, narrow valleys can occur in the multidimensional fitness function, which is inclined with all of the parameter axes (A. Lomax personal communication, 1996).

[90] Another recent technique is the neighbourhood algorithm [*Sambridge, 1998, 1999a, 1999b*]. In this case the main idea is to generate a set of samples, at each generation, whose sampling density function is constructed from all previous models using the neighbourhood approximation. This is a partition of parameter space into Voronoi (nearest-neighbor) cells about each of the previous models. In this way the information in the previous samples drives the search for new models. At regular intervals the approximation is updated, and sampling can concentrate in multiple regions.

[91] As *Sambridge [1999a]* points out, the number of vertices of Voronoi cells grows exponentially as the dimension of the parameter space increases, because of the curse of dimensionality. However, the NA sampling algorithm does not require their explicit calculation and hence remains practical in problems with hundreds of unknowns. Figure 10 shows an example of the neighbourhood sampling algorithm on a simple test problem from *Sambridge [1998]*. At each iteration a choice must be made on how to sample from the current approximate fitness function. *Sambridge [1998]* used a Gibbs Sampler, while *Sambridge [1999a]* resampled particular

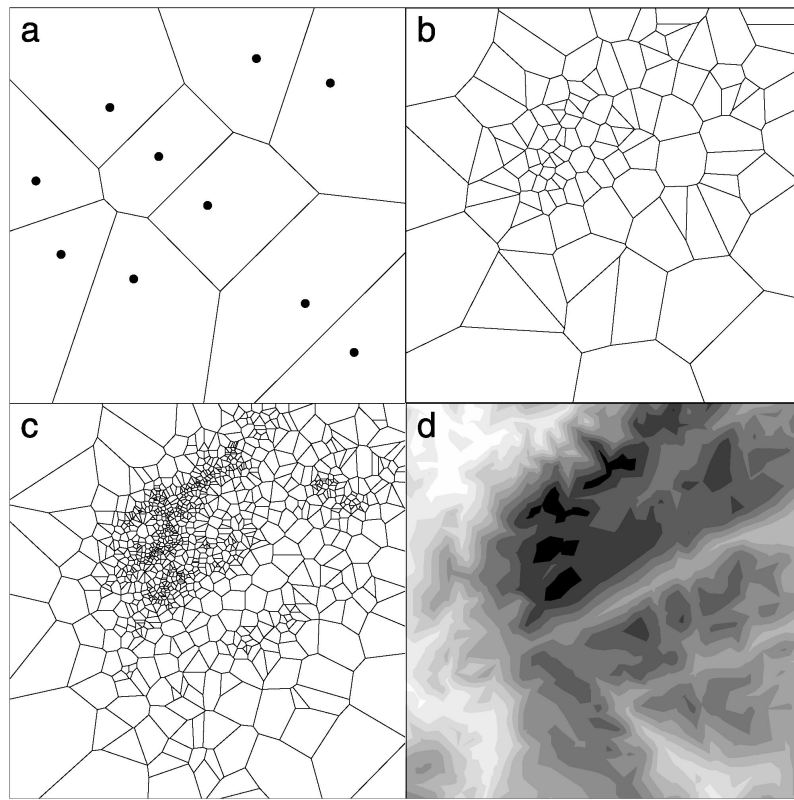


Figure 10. Voronoi cells drawn around the sampling produced by a neighbourhood algorithm [Sambridge, 1999a] for a simple 2-D problem. (a–c) Voronoi cells of about 10, 100, and 1000 generated samples, respectively. Figure 10c shows the true fitness surface. As the algorithm proceeds, each Voronoi diagram is used to guide the sampling. Note how the Voronoi cells are more concentrated in the darker regions where the fit is high. (From Sambridge [1999a].)

subsets of Voronoi cells. Like a genetic algorithm, the neighbourhood approach updates a population of models at each iteration but does so using the Voronoi cell concept to identify “promising regions” of parameter space. Initial results with this technique are quite promising, but more experience is required.

3.3. Bayesian Inference

[92] In a Bayesian formulation the solution to an inverse problem is given by the so-called posterior probability distribution $\sigma(\mathbf{m})$ over the model space \mathcal{M} . $\sigma(\mathbf{m})$ carries all information available on models originating from two sources:

1. The data are one source. This information is given by a likelihood function $L(\mathbf{m})$, measuring the likelihood of a given model \mathbf{m} through its misfit $\phi(\mathbf{m})$. A typical likelihood function can be expressed as

$$L(\mathbf{m}) = \text{const} \cdot \exp(-\phi(\mathbf{m})). \quad (15)$$

2. Data-independent prior information, expressed through a *prior probability density* $\rho(\mathbf{m})$, is another source. *Prior probability densities* may be simple Gaussian PDFs [see, e.g., Mosegaard, 1998; Mosegaard and Rygård-Hjalsted, 1999], or they may be more complicated

PDFs carrying information from earlier observations or measurements [see, e.g., Mosegaard *et al.*, 1997].

[93] The posterior PDF is related to data and prior information through the relation

$$\sigma(\mathbf{m}) = \text{const} \cdot L(\mathbf{m})\rho(\mathbf{m}). \quad (16)$$

In cases where no explicit mathematical expression for $L(\mathbf{m})$ and/or $\rho(\mathbf{m})$ is available, Monte Carlo sampling is the only efficient way to explore $\sigma(\mathbf{m})$. In Bayesian analysis the Metropolis-Hastings algorithm or the Gibbs Sampler is used to generate samples from $\sigma(\mathbf{m})$, thereby allowing us to estimate averages over the model space. The algorithm will sample a large number of models $\mathbf{m}_1, \dots, \mathbf{m}_N$, according to $\sigma(\mathbf{m})$, after which any average of a function $f(\mathbf{m})$ over the model space \mathcal{M} (e.g., a covariance or an expectation) can be approximated by the simple average:

$$E_f = \int_{\mathcal{M}} \sigma(\mathbf{m})f(\mathbf{m})d\mathbf{m} \approx \frac{1}{N} \sum_{n=1}^N f(\mathbf{m}_n). \quad (17)$$

The probability of an event $\in \subseteq \mathcal{M}$, containing all models in model space with a given feature, is found by putting $f(\mathbf{m})$ equal to the indicator function

$$f(\mathbf{m}) = \begin{cases} 1 & \text{if } \mathbf{m} \in \varepsilon \\ 0 & \text{otherwise.} \end{cases} \quad (18)$$

ε may, for instance, contain all Earth models that are “approximately” constant in a given area of the subsurface (appropriately defined) or models containing a sharp boundary (again appropriately defined) in a certain depth interval. In the special case when $\varepsilon = \mathcal{M}$ and $f(\mathbf{m}) = m_i$, the integral E_f is simply the mean $\langle m_i \rangle$ of the i th model parameter m_i . If $f(\mathbf{m}) = (m_i - \langle m_i \rangle)(m_j - \langle m_j \rangle)$, E_f becomes the posterior covariance between the i th and j th model parameters.

[94] In the general inverse problem, direct evaluation of E_f may be impossible because no analytical expression for $\sigma(\mathbf{m})$ is available. Even for a linear inverse problem with known $\sigma(\mathbf{m})$, we may not be able to evaluate E_f directly because of the complexity of f support ε . In all these cases the Metropolis-Hastings algorithm or the Gibbs Sampler allows us to perform an approximate, numerical evaluation of E_f .

[95] A large collection of samples from $\sigma(\mathbf{m})$ also allows us to compute approximate marginal distributions. For instance, samples from the 1-D marginal $\sigma(m_k)$ are obtained simply by collecting values of m_k from samples $\mathbf{m} = (m_1, \dots, m_k, \dots, m_M)$ of the posterior $\sigma(\mathbf{m})$.

[96] It is often very difficult to obtain good estimates of the averages E_f because the posterior $\sigma(\mathbf{m})$ may be multimodal and typically undersampled. The 1-D marginals, however, are usually quite well sampled because all the samples from the high-dimensional model space contribute to the 1-D histogram of m_k . For this reason, posterior 1-D marginals play an important role in applications.

[97] Although the above procedure looks very general and simple, the practical problem is often how to discover which features of the model have a high probability (in traditional non-Bayesian terminology: which features of the model are “well resolved”). It turns out that inspection of the output from the Monte Carlo sampling algorithm is often the most efficient way to discover well-resolved structure. An example of this is seen in Figures 11 and 12, taken from Mosegaard *et al.* [1997]. Seismic vertical-incidence reflection data d_{obs} from the base of the crust (Figure 11) were analyzed using a Metropolis-Hastings algorithm, generating posterior acoustic impedance models \mathbf{m}_n of the subsurface. A wavelet was estimated, and a full waveform forward algorithm was used to generate synthetic data $d(\mathbf{m})$ in the two-way time interval between 8.0 and 10.0 s. A likelihood function

$$L(\mathbf{m}) = \exp\left(\frac{\|d_{\text{obs}} - d(\mathbf{m})\|^2}{\sigma^2}\right)$$

measured the degree of fit between observed and computed data, where σ is the estimated standard deviation of the noise in the data. The prior probability density $\rho(\mathbf{m})$ for the acoustic impedance models was derived

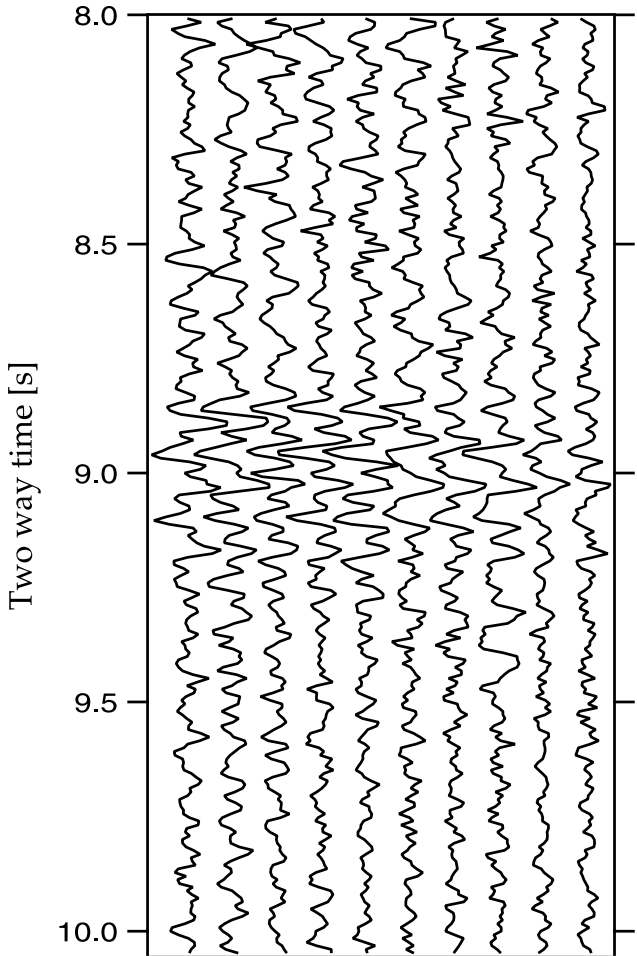


Figure 11. The seismic data used for Bayesian inversion, covering the time range of 8–10 s that contains the Moho reflection at ~8.9 s. (From Mosegaard *et al.* [1997].)

from histograms of reflection coefficients and layer thicknesses (Figure 13), obtained from laboratory measurements on near-surface rocks similar to those expected at the base of the crust (and corrected for pressure differences between surface and Moho). Samples from the posterior distribution $\sigma(\mathbf{m})$ are shown in Figure 12. Well-resolved structure is seen as structure that is persistent (occurs very often) in the output. In this case the simplest way to discover persistent structure is to plot all output models side by side or on top of each other. Figure 12 shows that impedance structure between 4.4 and 4.7 s two-way time is persistent and therefore well resolved. In contrast to this the main trend of the impedance and impedance fluctuations below 4.7 s are transient (nonpersistent) and therefore are poorly resolved.

[98] However, the above method is not useful for models which are more naturally plotted as a function of two or three spatial dimensions. A more generally valid method is to display all output models sequentially as pictures in a movie [Mosegaard and Tarantola, 1995]. Often, the human eye will be able to discover which

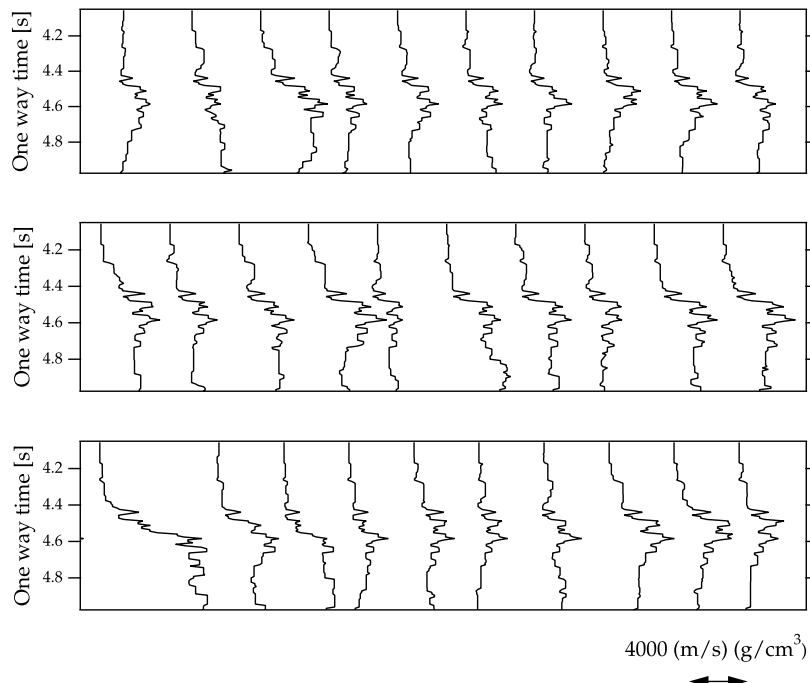


Figure 12. The results of the inversion on the seismic data set. A selection of a posterior models are plotted side by side to facilitate the discovery of well-resolved structure. Such structure is characterized by its presence in most (or all) of the posterior models. (From Mosegaard *et al.* [1997].)

structure is well resolved by the data and the prior information. This method can often be facilitated by viewing movies of models with different degrees of smoothing.

3.4. Ensemble Inference

[99] All of the Monte Carlo direct search algorithms discussed above require the solving of the forward problem many times. In each case the result is an ensemble of models, and the task is to try and use their collective sampling to extract some meaningful information about the Earth. In most cases the distribution of the complete ensemble (i.e., all models for which the forward problem has been solved) is arbitrary and follows no prescribed distribution. However, as discussed above, when Monte Carlo sampling is applied within a Bayesian context, the aim is to generate samples that follow a particular statistical distribution, usually the posterior PDF. In that case, “Bayesian information measures” (e.g., model covariance estimates, etc.) can be derived from a subset of the complete distribution. For the case when one has an arbitrary ensemble of models with a range of fits to the data, the question remains of how to draw inferences.

[100] A simple answer would be to examine the features present in only the best data fitting model. However, as discussed above, in almost all cases this is insufficient because of nonuniqueness in the problem and noise in the data. A useful thing to do may be to filter the complete ensemble into only those which have acceptable fit to the data (given a prior understanding of noise processes, etc.), as done by Press [1968, 1970a].

One could also include other criteria like prior constraints on the form of acceptable solutions, for example, the velocity gradient constraints used by Wiggins [1969, 1972]. The task then would be to try and determine properties that all of these acceptable models share in the hope that the real Earth shares it also.

[101] Several authors have proposed methods for characterizing an ensemble of data acceptable models. A summary is given by Sen and Stoffa [1995]. The earliest approach was simply to compare the models directly, usually by plotting them on top of one another [e.g., Press, 1968]. As more modern search algorithms were used, and many more acceptable models produced, more quantitative analyses were performed. Figure 14 shows an example from Lomax and Sneider [1995a] where upper mantle seismic S velocity models are sought that satisfy synthetic Rayleigh wave group-velocity dispersion data contaminated by noise. Figure 14a shows the ensemble of data-acceptable velocity models, and Figure 14b shows the ± 1 and $\pm 2\sigma$ spread, calculated for each depth. Although strictly speaking these intervals are not formal confidence limits on the velocity at each depth, they do provide an effective means at characterizing the ensemble. Note that in this synthetic problem the true solution is the IASP91 Earth model [Kennett and Engdahl, 1991], which plots neatly within the $\pm 1\sigma$ bounds. Other authors have made similar attempts at a graphical representation of the acceptable ensemble. Variations include plots of the density of acceptable models or all models weighted by data fit. For examples,

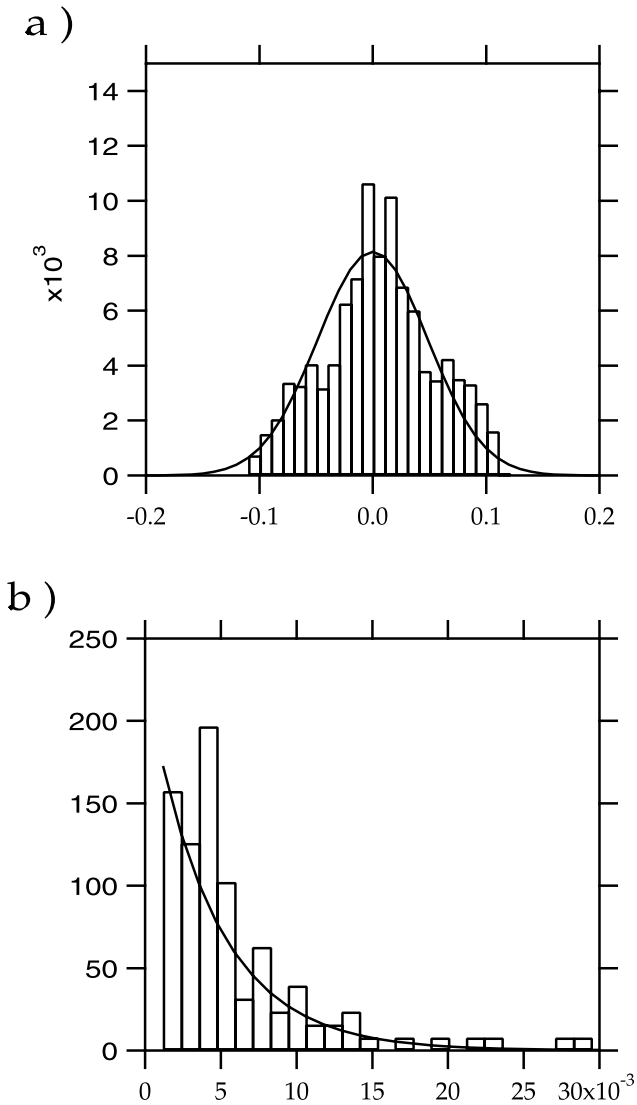


Figure 13. A priori information used in the Bayesian inversion scheme. (a) Reflection coefficients distribution obtained from studies of the igneous intrusions of Rum, Scotland, and the Great Dyke, Zimbabwe. The solid curve is a Gaussian distribution with standard deviation $\sigma = 0.047$. (b) Layer thickness distribution as a function of one-way travel time derived from observations of the Rum and Great Dyke intrusions. The solid curve is an exponential distribution with $\lambda = 225.0 \text{ s}^{-1}$. (From Mosegaard *et al.* [1997].)

see Basu and Frazer [1990], Nolte and Frazer [1994], Shibutani *et al.* [1996], and Kennett [1998].

[102] An alternative to graphical methods is the cluster analysis method proposed by Vasco *et al.* [1993]. They used statistical techniques to characterize the acceptable ensemble and make inferences about properties that all models shared. They illustrated their approach with some impressive applications to gravity inversion and cross-borehole seismic imaging. A related approach is that proposed by Douma *et al.* 1996. In their method the ensemble of acceptable models is projected onto a set of orthogonal functions. In this way they hope to determine

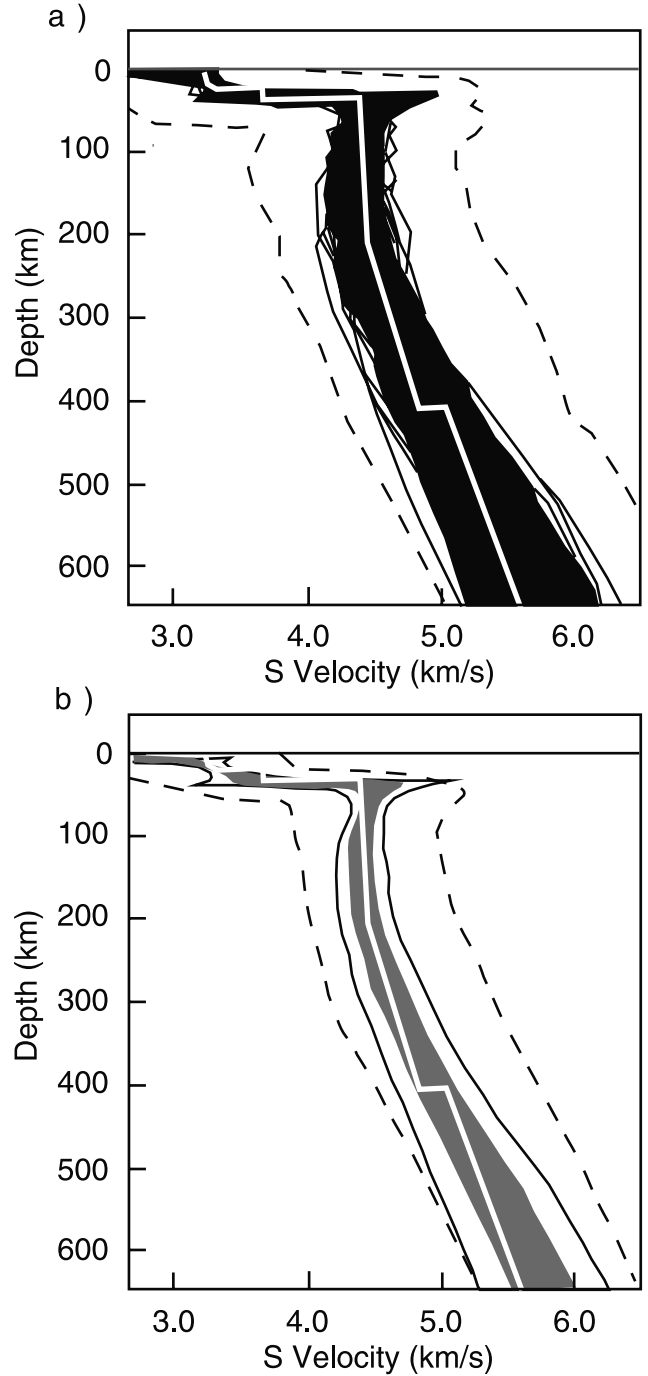


Figure 14. (a) Ensemble of upper mantle S velocity models generated by Lomax and Snieder [1995a], which have an acceptable level of data fit. The data are synthetically generated Rayleigh wave group velocity dispersion measurements. The dashed lines show the boundaries of the parameter space. (b) The $\pm 1\sigma$ (gray shaded region) and $\pm 2\sigma$ (solid line) in the distribution of the acceptable models, calculated at each depth. The outer dashed lines are the $\pm 2\sigma$ spread of a uniform distribution of models. Note how the spread measures are smooth, even though the individual acceptable models are not. The true model (thick white line) lies, for the most part, in the center of the $\pm 1\sigma$ region. (After Lomax and Snieder [1995a].)

the well constrained information hidden in the ensemble. As with the method of *Vasco et al.* [1993] the technique is appropriate if the ensemble forms a single cluster and not multiple disjointed clusters, as depicted in Figure 1. If multiple clusters exist, then they must be identified, and the approach applied separately to each.

[103] Recently, *Sambridge* [1999b] has proposed an approach to estimate Bayesian information measures from an arbitrarily distributed ensemble. In this case the neighborhood approximation (mentioned above in connection with a search algorithm) is applied to the complete ensemble, that is, all models for which the forward model has been solved. A standard MCMC integration procedure is then used to resample according to the neighborhood approximation and to produce unbiased estimates of Bayesian integrals. The advantage of this approach is that it can, in principle, extract Bayesian estimates from ensembles generated by any method, for example, a genetic algorithm. A caveat, which applies to all of these techniques, is that at best they can only extract what information exists in a given ensemble of models. If the available ensemble does not adequately represent (or sample) the acceptable region in parameter space, then the result will be biased.

[104] In the past few years, geophysicists have begun to develop techniques for ensemble inference. The underlying idea is that basing inferences on an ensemble of potential solutions is more useful than considering just one (usually best fit) model. The current range of approaches available are useful but by no means complete or applicable in all circumstances. It seems likely that this will be an area of further research in the next decade.

3.5. Resources on the Net

[105] It may be useful to the reader to have a list of web site addresses where more information can be found on various topics discussed in this paper. At some sites a computer code is also available. Table 1 shows a collection that we are aware of. Many other sites can be found by following the links on these pages.

4. CONCLUSIONS

[106] In this paper we have summarized the current state of the Monte Carlo methodology, as applied in geophysics. Some open questions and directions for future research have been discussed. The Earth sciences are a rich source of large and complicated inverse problems. Often they can be posed in a way suitable for attack with MC methods. In doing so, the Earth scientist must remember that the development of Monte Carlo techniques is a multidisciplinary effort, and it can be beneficial to look at what has been done elsewhere. It is hoped that this paper will facilitate that process by drawing the attention of geophysicists to relevant refer-

ence material in computational statistics and other fields.

[107] We have highlighted the connection between the computational approaches commonly used for data fitting and model appraisal with those in the fields of optimization and statistical inference. Techniques such as simulated annealing, genetic algorithms, and other statistical importance sampling methodologies have all started life elsewhere but become useful additions to the geophysicists tool bag. One issue that was prevalent at the outset (>30 years ago) was how to make robust inferences from an ensemble of data acceptable models. In recent times this question has come back into focus. Geophysicists are good at generating models, and even at finding some that fit data, but quantitative and reliable inferences are needed for drawing conclusions. The statistical and other approaches discussed in this paper have begun to answer these questions in a quantitative manner.

GLOSSARY

[108] Acceptable models: A set of Earth models (see definition) that are consistent with observations, taking into account the presence of noise and errors in the observables. Usually, the acceptable models are those for which the objective (or data misfit) function is less than, or equal to, a predetermined value.

[109] **Bayesian inference:** A (purely) probabilistic procedure for information updating. In the typical scenario prior information, represented by a prior probability distribution, is updated by information from experimental data, represented by a likelihood function. The resulting state of information is represented by the (normalized) product of the prior distribution and the likelihood function, the so-called posterior probability distribution. The terms “prior” and “posterior” refer to “before” and “after” data collection, respectively.

[110] **Direct search:** A parameter space search method (see definition) that does not use Fréchet derivatives or gradient information of the objective function. It only uses evaluations of the objective function at points in parameter space.

[111] **Earth model:** A representation of some physical properties of the Earth, usually in a discrete form where the earth property, for example, Earth’s density variation, is described by a finite number of parameters, for example, the average density of rocks in a series of depth intervals from the surface of the Earth.

[112] **Ensemble inference:** The procedure whereby information is extracted or conclusions are drawn from a collection of inputs, or Earth models, rather than a single model. Genetic Algorithms, Simulated Annealing, and the Neighbourhood algorithm are all examples of ensemble inference (direct search) techniques.

[113] **Forward problem:** The calculation of predictions from an Earth model, to be compared with the observa-

tions. The solution of the forward problem is a necessary step in determining the fit to the data. The degree of nonlinearity in the forward problem can be a major cause of difficulty in finding Earth models that fit data.

[114] **Genetic algorithm:** A computational method popular for global optimization problems. This is a fully nonlinear direct search method, which means that it avoids linearization and does not use derivatives of the objective function being optimized. The procedure is based on an analogy with principles of evolution and “survival of the fittest.” Originally developed as a model for adaptive behavior in an artificial system, it has been applied to complex optimization problems across the physical sciences.

[115] **Global optimization:** A numerical procedure where the values of some variables are sought that give an optimum value of some function, that is, maximum or minimum over all possibilities.

[116] **Importance sampling:** A Monte Carlo algorithm designed to sample a given function, or probability density, with a sampling density proportional to that function or probability density.

[117] **Inverse problem:** The term used to describe the situation where inversion is applied. (See definition of inversion).

[118] **Inversion:** The process by which information is obtained about a physical quantity from indirect information, for example, on Earth’s seismic structure from the travel times of elastic waves generated by earthquakes.

[119] **Likelihood function:** A function describing the probability that a given parameterized model is consistent with observed data. The likelihood function is a function of the model and measures the fit between model predictions and observations.

[120] **Markov Chain:** See random walk.

[121] **MCI (Monte Carlo Inversion):** The term used to describe the earliest forms of uniform random parameter space searching, as applied to seismological problems in the work of *Press* [1968, 1970a].

[122] **MCMC (Markov Chain Monte Carlo):** A multi-dimensional random sampling procedure where the next sample only depends on the location of the current sampling point.

[123] **Metropolis-Hastings algorithm:** A simple importance sampling algorithm (see definition of importance sampling) based on a random walk.

[124] **Misfit function:** The same as objective function, except that one always minimizes a misfit function.

[125] **Monte Carlo:** A prefix indicating that the method or approach makes use of repeated trials, or sampling, generated with the use of random numbers, named after the famous French city associated with casinos.

[126] **Monte Carlo integration:** A numerical integration procedure for functions, which is efficient in high-dimensional spaces. Instead of using functional values in a uniform grid to produce a numerical approximation of

an integral, they are evaluated at randomly selected points (often generated by an importance sampling algorithm (see above). The integral can then be approximated by an average of these values, and the chance of missing areas of high functional values is strongly reduced.

[127] **Objective function:** A function calculated from one or more variables which is usually the subject of an optimization process, that is, the variables are sought, which optimize the objective function. The objective function can be a measure of discrepancy with observed data (data misfit) or a combination of data misfit and other criteria.

[128] **Parameter space:** An abstract multidimensional region describing the set of all possible values that Earth models can take. Each point in the parameter space represents an Earth model.

[129] **Parameter space search:** The process of finding Earth models that have an acceptable or optimal value of the objective function.

[130] **Posterior PDF:** A probability density representing, in a Bayesian computation, the combination of prior information and data information.

[131] **Prior probability density:** A probability density representing, in a Bayesian computation, the information available before data is acquired (or considered).

[132] **Probability density function (PDF):** A statistical term used to describe the probability distribution associated with a random variable. For example, the well-known “bell-shaped” Gaussian distribution is a PDF of a one-dimensional normal random variable. The area under the curve between any two given values represents the probability that a realization of the variable will fall between these values. Multidimensional PDFs are used to describe the joint behavior of a random vector (whose components are all random variables).

[133] **Pseudorandom number:** The result of a numerical procedure (a generator), which has certain statistical properties. For example, the histogram of many pseudorandom numbers will tend toward a uniform distribution. Most computing systems provide pseudorandom number generators that use a linear congruent method [see *Park and Miller*, 1988].

[134] **Quasi-random number:** Sometimes called “sub-random” numbers, similar definition as for pseudorandom numbers. Often it is based on number theoretic techniques and usually converges much faster than pseudorandom numbers to a uniform distribution.

[135] **Random Walk:** A perturbative sequence of random changes to a point in a multidimensional space. A uniform random walk is one where the asymptotic convergence is to a uniform density of samples in parameter space. See also Markov Chain Monte Carlo (MCMC).

[136] **Simulated annealing:** A Metropolis-Hastings algorithm designed to simulate certain aspects of a statistical mechanical system. The simulated annealing (SA) algorithm samples a Gibbs-Boltzmann distribution in the model space, and a characteristic feature of this

distribution is its temperature parameter. When this parameter is gradually lowered, it is possible to simulate an annealing process in which the system is taken from a disordered high-temperature state to a well-ordered low temperature state.

[137] **ACKNOWLEDGMENTS.** We would like to acknowledge Steve Billings, Jean Braun, Kerry Gallagher, Brian Kennett, Anthony Lomax, John Scales, and Roel Snieder for their assistance with this manuscript and also these and many other colleagues who have contributed to our understanding of the subject. Thanks also go to Craig Bina, who suggested this paper in the first place. The constructive criticisms of two anonymous reviewers helped improve an earlier draft of this manuscript.

[138] Louise Kellogg was the Editor responsible for this paper. She thanks technical reviewer Anthony Lomax and another anonymous technical reviewer.

REFERENCES

- Aarts, E., and J. Korst, *Simulated Annealing and Boltzmann Machines*, John Wiley, New York, 1989.
- Anderssen, R. S., The character of non-uniqueness in the conductivity modelling problem for the Earth, *Pure Appl. Geophys.*, **80**, 238–259, 1970.
- Anderssen, R. S., and E. Senata, A simple statistical estimation procedure for Monte Carlo Inversion in geophysics, *Pure Appl. Geophys.*, **91**, 5–13, 1971.
- Anderssen, R. S., and E. Senata, A simple statistical estimation procedure for Monte Carlo inversion in geophysics: Efficiency and Hempel's paradox, *Pure Appl. Geophys.*, **96**, 5–14, 1972.
- Anderssen, R. S., M. H. Worthington, and J. R. Cleary, Density modelling by Monte Carlo Inversion, I, Methodology, *Geophys. J. R. Astron. Soc.*, **29**, 433–444, 1972.
- Andresen, B., K. H. Hoffman, K. Mosegaard, J. Nulton, J. M. Pedersen, and P. Salamon, *J. Phys.*, **49**, 1485, 1988.
- Antonov, I. A., and V. M. Saleev, *USSR Comput. Math. Math. Phys.*, **19**(1), 252–256, 1979.
- Backus, G. E., Bayesian inference in geomagnetism, *Geophys. J.*, **92**, 125–142, 1988.
- Backus, G. E., and J. F. Gilbert, Numerical applications of a formalism for geophysical inverse problems, *Geophys. J. R. Astron. Soc.*, **13**, 247–276, 1967.
- Backus, G. E., and J. F. Gilbert, The resolving power of gross Earth data, *Geophys. J. R. Astron. Soc.*, **16**, 169–205, 1968.
- Backus, G. E., and J. F. Gilbert, Uniqueness in the inversion of inaccurate gross Earth data, *Philos. Trans. R. Soc. London, Ser. A.*, **266**, 123–192, 1970.
- Basu, A., and L. N. Frazer, Rapid determination of critical temperature in simulated annealing inversion, *Science*, **249**, 1409–1412, 1990.
- Bayes, T., An essay towards solving a problem in the doctrine of chances, *Philos. Trans. R. Soc. London*, **53**, 370–418, 1763 (Reprinted, with biographical note by G. A. Barnard, in *Biometrika*, **45**, 293–315, 1958).
- Billings, S. D., Simulated annealing for earthquake location, *Geophys. J. Int.*, **118**, 680–692, 1994.
- Billings, S. D., B. L. N. Kennett, and M. S. Sambridge, Hypocentre location: Genetic algorithms incorporating problem specific information, *Geophys. J. R. Astron. Soc.*, **118**, 693–706, 1994.
- Bina, C. R., Free energy minimization by simulated annealing with applications to lithospheric slabs and mantle plumes, in *Geodynamics of Lithosphere and Earth's Mantle; Seismic Anisotropy as a Record of the Past and Present Dynamic Processes*, edited by J. Plomerova, R. C. Liebermann, and V. Babuska, *Pure Appl. Geophys.*, **151**, 605–618, 1998.
- Biswas, N. N., and L. Knopoff, The structure of the upper mantle under the United States from dispersion of Rayleigh waves, *Geophys. J. R. Astron. Soc.*, **36**, 515–539, 1974.
- Boschetti, F., M. C. Dentith, and R. D. List, Inversion of seismic refraction data using genetic algorithms, *Geophys.ics*, **61**, 1715–1727, 1996.
- Boschetti, F., M. C. Dentith, and R. D. List, Inversion of potential field data by genetic algorithms, *Geophys. Prospect.*, **45**(3), 461–478, 1997.
- Box, G. E. P., and G. C. Tiao, *Bayesian Inference in Statistical Analysis*, Addison-Wesley, Reading, Mass., 1973.
- Braun, J., Estimating exhumation rate and relief evolution by spectral analysis of age-elevation profiles, *Terra Nova*, **14**(3), 205–209, 2002.
- Buland, R., The mechanics of locating earthquakes, *Bull. Seismol. Soc. Am.*, **66**, 173–187, 1976.
- Burton, P. W., Inversions of high frequency $Q_\gamma^{-1}(f)$, *Geophys. J. R. Astron. Soc.*, **48**, 29–51, 1977.
- Burton, P. W., and B. L. N. Kennett, Upper Mantle Zone of low Q, *Nature*, **238**, 84, 87–90, 1972.
- Cadek, O., D. A. Yuen, and H. Cizkova, Mantle viscosity inferred from geoid and seismic tomography by genetic algorithms; results for layered mantle flow, in *Joint Inversion as a General Problem in Earth Sciences*, edited by L. Ballani, *Phys. Chem. Earth*, **23**, 9–10, 865–872, 1998.
- Calderon, M. C., M. K. Sen, and P. L. Stoffa, Hopfield neural networks, and mean field annealing for seismic deconvolution and multiple attenuation, *Geophysics*, **62**, 992–1002, 1997.
- Cary, P. W., and C. H. Chapman, Automatic 1-D waveform inversion of marine seismic refraction data, *Geophys. J.*, **93**, 527–546, 1988.
- Chunduru, R. K., M. K. Sen, and P. L. Stoffa, 2-D resistivity inversion using spline parameterization and simulated annealing, *Geophysics*, **61**, 151–161, 1996.
- Cieniawski, S. E., J. W. Eheart, and S. Ranjithan, Using genetic algorithms to solve a multiobjective groundwater monitoring problem, *Water Resour. Res.*, **31**(2), 399–409, 1995.
- Constable, S. C., R. L. Parker, and C. G. Constable, Occam's inversion: A practical algorithm for generating smooth models from electromagnetic sounding data, *Geophysics*, **52**, 289–300, 1987.
- Conway, A. J., and P. A. Bland, A genetic algorithm scheme for pairing meteorite finds, *Meteorol. Planet. Sci.*, **33**(3), 491–499, 1998.
- Courboulex, F., J. Virieux, and D. Gibert, On the use of simulated annealing method and cross-validation theory for deconvolution of seismograms, *Bull. Seismol. Soc. Am.*, **86**(4), 1187–1193, 1996a.
- Courboulex, F., J. Virieux, A. Deschamps, D. Gibert, and A. Zollo, Source investigation of a small event using empirical Green's functions and simulated annealing, *Geophys. J. Int.*, **125**, 768–780, 1996b.
- Curtis, A., and R. Snieder, Reconditioning inverse problems using the genetic algorithm and revised parameterization, *Geophysics*, **62**, 1524–1532, 1997.
- Cvijović, D., and J. Klinowski, Taboo Search: An Approach to the Multiple Minima Problem, *Science*, **267**, 664–666, 1995.
- Datta, G. A., L. W. Lake, and G. A. Pope, Stochastic simulation of categorical variables using a classification algorithm and simulated annealing, *Math. Geol.*, **27**(6), 763–787, 1995.
- Davis, L., *Genetic Algorithms and Simulated Annealing, Research Notes in Artificial Intelligence*, Pitman, London, 1987.
- Davis, T. E., and J. C. Principe, A simulated annealing like

- convergence theory for the simple genetic algorithm, in *Proc. of the Fourth International Conference on Genetic Algorithms*, Morgan Kaufmann, San Mateo, Calif., 1991.
- Deng, L. H., and J. A. Scales, Estimating the topography of multi-dimensional fitness functions, *Cent. for Wave Phenomena Tech. Rep.* 208, Colo. Sch. of Mines, Golden, 1999.
- Dittmer, J. K., and J. E. Szymanski, The stochastic inversion of magnetics and resistivity data using the simulated annealing algorithm, *Geophys. Prospect.*, 43(3), 397–416, 1995.
- Docherty, P., R. Silva, S. Singh, Z. M. Song, and M. Wood, Migration velocity analysis using a genetic algorithm, *Geophys. Prospect.*, 45(5), 865–878, 1997.
- Dosso, S. E., and D. W. Oldenburg, Magnetotelluric appraisal using simulated annealing, *Geophys. J. Int.*, 106, 370–385, 1991.
- Dougherty, D. E., and R. A. Marryott, Optimal groundwater management, 1, Simulated annealing, *Water Resour. Res.*, 27(10), 2493–2508, 1991.
- Douma, H., R. Snieder, and A. Lomax, Ensemble inference in terms of Empirical Orthogonal Functions, *Geophys. J. Int.*, 127, 363–378, 1996.
- Drijkoningen, G. G., and R. S. White, Seismic velocity structure of oceanic crust by inversion using genetic algorithms, *Geophys. J. Int.*, 123, 653–664, 1995.
- Duijndam, A. J. W., Bayesian estimation in seismic inversion part I: Principles, *Geophys. Prospect.*, 36, 878–898, 1988a.
- Duijndam, A. J. W., Bayesian estimation in seismic inversion part II: Uncertainty analysis, *Geophys. Prospect.*, 36, 899–918, 1988b.
- Everett, M. E., and A. Schultz, Two-dimensional nonlinear magneto-telluric inversion using a genetic algorithm, *J. Geomagn. Geoelectr.*, 45, 1013–1026, 1993.
- Flourney, N., and R. K. Tsutakawa (Eds.), Statistical Multiple Integration, in *Proceedings of the AMS-IMS-SIAM Summer Research Conference on Statistical Multiple Integration*, Am. Math. Soc., Providence, R. I., 1989.
- Fogel, L. J., Autonomous Automata, *Ind. Res.*, 4, 14–19, 1962.
- Fogel, L. J., A. J. Owens, and M. J. Walsh, *Artificial Intelligence Through Simulated Evolution*, John Wiley, New York, 1966.
- Franklin, J. N., Well posed stochastic extensions of ill posed linear problems, *J. Math. Anal. Appl.*, 31, 682–716, 1970.
- Gallagher, K., Evolving thermal histories from fission track data, *Earth Planet. Sci. Lett.*, 136, 421–435, 1995.
- Gallagher, K., and M. Sambridge, Genetic algorithms: A powerful tool for large-scale non-linear optimization problems, *Comput. Geosci.*, 20(7/8), 1229–1236, 1994.
- Gallagher, K., M. S. Sambridge, and G. G. Drijkoningen, Genetic algorithms: An evolution on Monte Carlo methods in strongly nonlinear geophysical optimization problems, *Geophys. Res. Lett.*, 18, 2177–2180, 1991.
- Gallagher, K., M. Ramsdale, L. Lonergan, and D. Morrow, The role of thermal conductivity measurements in modeling thermal histories in sedimentary basins, *Mar. Pet. Geol.*, 14, 201–214, 1997.
- Gelfand, A. E., and A. F. M. Smith, Sampling based approaches to calculating marginal densities, *J. Am. Stat. Assoc.*, 85, 398–409, 1990.
- Gell-Mann, M., *The Quark and the Jaguar: Adventures in the Simple and the Complex*, W. H. Freeman, New York, 1994.
- Gelman, A., J. B. Carlin, H. S. Stern, and D. B. Rubin, *Bayesian Data Analysis*, Chapman and Hall, New York, 1995.
- Geman, S., and D. Geman, Stochastic relaxation, Gibbs distributions and the Bayesian restoration of images, *IEEE Trans. Patt. Anal. Mach. Int.*, 6, 721–741, 1984.
- Gershensonfeld, N., *The Nature of Mathematical Modeling*, Cambridge Univ. Press, New York, 1999.
- Gilbert, D., and J. Virieux, Electromagnetic imaging and simulated annealing, *J. Geophys. Res.*, 96(5), 8057–8067, 1991.
- Gill, P. E., W. Murray, and M. H. Wright, *Practical Optimization*, Academic San Diego, Calif., 1981.
- Goldberg, D. E., *Genetic Algorithms in Search, Optimization, and Machine Learning*, Addison-Wesley, Reading, Mass., 1989.
- Goncz, J. H., and J. R. Cleary, Variations in the Structure of the Upper Mantle Beneath Australia, from Rayleigh Wave Observations, *Geophys. J. R. Astron. Soc.*, 44, 507–516, 1976.
- Goovaerts, P., Stochastic simulation of categorical variables using a classification algorithm and simulated annealing, *Math. Geol.*, 28(7), 909–921, 1996.
- Gouveia, W. P., and J. A. Scales, Bayesian seismic waveform inversion: Parameter estimation and uncertainty analysis, *J. Geophys. Res.*, 103(B2), 2759–2779, 1998.
- Haddon, R. A. W., and K. E. Bullen, An Earth model incorporating free Earth oscillation data, *Phys. Earth Planet. Inter.*, 2, 35–49, 1969.
- Hajek, B., Cooling schedules for optimal annealing, *Math. Oper. Res.*, 13, 311–329, 1988.
- Hall, A., On an experimental determination of π , *Messeng. Math.*, 2, 113–114, 1873.
- Hammersley, J. M., and D. C. Handscomb, *Monte Carlo Methods*, Chapman and Hall, New York, 1964.
- Harland, J. R., and P. Salamon, Simulated annealing: A review of the thermodynamic approach, *Proc. Suppl.*, 5A, 109–115, 1988.
- Hartzell, S., and P. Liu, Calculation of earthquake rupture histories using a hybrid global search algorithm; application to the 1992 Landers, California, earthquake, *Phys. Earth Planet. Inter.*, 95(1–2), 79–99, 1996.
- Hastings, W. K., Monte Carlo sampling methods using Markov Chain and their applications, *Biometrika*, 57, 97–109, 1970.
- Hermance, J. F., and L. R. Grillot, Constraints of temperatures beneath Iceland from magneto data, *Phys. Earth Planet. Inter.*, 8, 1–12, 1974.
- Hoffmann, K. H., P. Sibani, J. M. Pedersen, and P. Salamon, Optimal Ensemble Size for Parallel Implementations of Simulated Annealing, *Appl. Math. Lett.*, 3, 53–56, 1990.
- Holland, J. H., *Adaptation in Natural and Artificial Systems*, Univ. of Mich. Press, Ann Arbor, Mich., 1975.
- Horne, S., and C. Macbeth, Inversion for seismic anisotropy using genetic algorithms, *Geophys. Prospect.*, 42(8), 953–974, 1994.
- Horne, S., and C. Macbeth, A comparison of global optimisation methods for near-offset VSP inversion, *Comput. Geosci.*, 24(6), 563–572, 1998.
- Ihmle, P., and J. C. Ruegg, Source tomography by simulated annealing using broad-band surface waves and geodetic data; application to the $M_w = 8.1$ Chile 1995 event, *Geophys. J. Int.*, 131, 146–158, 1997.
- Ingber, L., Very fast simulated reannealing, *Math. Comput. Model.*, 12, 967–993, 1989.
- Ingber, L., and B. Rosen, Genetic algorithms and simulated reannealing: A comparison, *Math. Comput. Model.*, 16, 87–100, 1992.
- Jackson, D. D., Interpretation of inaccurate, insufficient and inconsistent data, *Geophys. J. R. Astron. Soc.*, 28, 97–110, 1972.
- Jackson, D. D., Marginal solutions to quasi-linear inverse problems in geophysics, *Geophys. J. R. Astron. Soc.*, 12, 165–180, 1973.
- Jackson, D. D., Most squares inversion, *J. Geophys. Res.*, 81, 1027–1030, 1976.
- Jackson, D. D., The use of a priori data to resolve nonuniqueness in linear inversion, *Geophys. J. R. Astron. Soc.*, 57, 137–157, 1979.
- Jackson, D. D., and M. Matsu'ura, A Bayesian approach to nonlinear inversion, *J. Geophys. Res.*, 90, 581–591, 1985.
- Jakobsen, M. O., M. Mosegaard, and J. M. Pedersen, Global

- model optimization in reflection seismology by simulated annealing, in *Model Optimization in Exploration Geophysics*, 2, *Proceedings of the 5th International Mathematical Geophysics Seminar*, vol. 2, edited by A. Vogel, Friedr. Vieweg and Sohn, pp 361–381, Braunschweig, Germany, 1988.
- Jervis, M., P. L. Stoffa, and M. K. Sen, 2-D migration velocity estimation using a genetic algorithm, *Geophys. Res. Lett.*, 20(14), 1495–1498, 1993.
- Jestin, F., P. Huchon, and J. M. Gaulier, The Somalia Plate and the East African rift system: Present-day kinematics, *Geophys. J. Int.*, 116, 637–654, 1994.
- Jin, S., and R. Madariaga, Background velocity inversion with a genetic algorithm, *Geophys. Res. Lett.*, 20(2), 93–96, 1993.
- Jin, S., and R. Madariaga, Nonlinear velocity inversion by a two-step Monte Carlo method, *Geophysics*, 59(4), 577–590, 1994.
- Jones, A. G., and R. Hutton, A multi-station magnetotelluric study in southern Scotland, II, Monte-Carlo inversion of the data and its geophysical and tectonic implications, *Geophys. J. R. Astron. Soc.*, 56, 351–368, 1979.
- Jones, R. H., C. M. Rayne, and U. Lindblom, The use of a genetic algorithm for the optimal design of microseismic monitoring networks, in *Rock Mechanics in Petroleum Engineering Proceedings*, A. A. Balkema, Brookfield, Vt., pp. 615–619, 1994.
- Jordan, T. H., and J. Franklin, Optimal solutions to a linear inverse problem in geophysics, *Proc. Natl. Acad. Sci.*, 70, 1410–1413, 1971.
- Keilis-Borok, V. I., and T. B. Yanovskaya, Inverse problems of seismology, *Geophys. J.*, 13, 223–234, 1967.
- Kelvin, Lord, Nineteenth century clouds over the dynamical theory of heat and light, *Philos. Mag.*, 2(6), 1–40, 1901.
- Kennett, B. L. N., Some aspects of non-linearity in inversion, *Geophys. J. R. Astron. Soc.*, 55, 373–391, 1978.
- Kennett, B. L. N., and G. Nolet, Resolution analysis for discrete systems, *Geophys. J. R. Astron. Soc.*, 53, 413–425, 1978.
- Kennett, B. L. N., On the density distribution within the Earth, *Geophysics. J. Int.*, 132, 374–382, 1998.
- Kennett, B. L. N., and E. R. Engdahl, Travel times for global earthquake location and phase identification, *Geophysics. J. Int.*, 105, 429–466, 1991.
- Kennett, B. L. N., and M. Sambridge, Earthquake location: Genetic algorithms for teleseisms, *Phys. Earth Planet. Inter.*, 75, 103–110, 1992.
- Kido, M., D. A. Yuen, O. Cadek, Mantle viscosity derived by genetic algorithm using oceanic geoid and seismic tomography for whole-mantle versus blocked-flow situations, *Phys. Earth Planet. Inter.*, 107, 307–326, 1998.
- King, S. D., Radial models of mantle viscosity: Results from a genetic algorithm, *Geophys. J. Int.*, 122, 725–734, 1995.
- Kirkpatrick, S. C., D. Gelatt, and M. P. Vecchi, Optimization by simulated annealing, *Science*, 220, 671–680, 1983.
- Kobayashi, R., and I. Nakanishi, Application of genetic algorithms to focal mechanism determination, *Geophys. Res. Lett.*, 21(8), 729–732, 1994.
- Koper, K. D., M. E. Wysession, and D. A. Wiens, Multimodal function optimization with a Niching genetic algorithm: A seismological example, *Bull. Seismol. Soc. Am.*, 89, 978–988, 1999.
- Koren, Z., K. Mosegaard, E. Landa, P. Thore, and A. Tarantola, Monte Carlo estimation and resolution analysis of seismic background velocities, *J. Geophys. Res.*, 96(B12), 20,289–20,299, 1991.
- Kuo, C. H., A. N. Michel, and W. G. Gray, Design of optimal pump-and-treat strategies for contaminated ground water remediation using the simulated annealing algorithm, *Adv. Water Resour.*, 15(2), 95–105, 1992.
- Landa, E., W. Beydoun, and A. Tarantola, Reference velocity model estimation from prestack waveforms: Coherency optimization by simulated annealing, *Geophys.*, 54(8), 984–990, 1989.
- Lepage, G. P., A new algorithm for adaptive multi-dimensional integration, *J. Comput. Phys.*, 27, 192–203, 1978.
- Levin, V., and J. Park, P-SH conversions in a flat-layered medium with anisotropy of arbitrary orientation, *Geophys. J. Int.*, 131, 253–266, 1997.
- Lomax, A., and R. Snieder, Finding sets of acceptable solutions with a genetic algorithm with application to surface wave group dispersion in Europe, *Geophys. Res. Lett.*, 21(24), 2617–2620, 1994.
- Lomax, A., and R. Snieder, Identifying sets of acceptable solutions to nonlinear geophysical inverse problems which have complicated misfit functions, *Nonlinear Proc. Geophys.*, 2, 222–227, 1995a.
- Lomax, A., and R. Snieder, The contrast in upper mantle shear-wave velocity between the East European Platform and tectonic Europe obtained with genetic algorithm inversion of Rayleigh-wave group dispersion, *Geophys. J. Int.*, 123, 169–182, 1995b.
- Lomax, A., J. Virieux, P. Volant, and C. Berge, Probabilistic earthquake location in 3D and layered models: Introduction of a Metropolis-Gibbs method and comparison with linear locations, in *Advances in Seismic Event Location*, edited by C. Thurber, and N. Rabinowitz, Kluwer, Acad. Norwell, Mass., 2000.
- Mathias, K., and D. L. Whitley, Genetic Operators, the Fitness Landscape and the Traveling Salesman Problem, in *Parallel Problem Solving from Nature-PPSN 2*, edited by R. Manner and B. Manderick, pp. 219–228, Elsevier Sci., New York, 1992.
- McKinney, D. C., and M. D. Lin, Genetic algorithm solution of groundwater management models, *Water Resour. Res.*, 30(6), 1897–1906, 1994.
- Mellman, G. R., A method of body-wave waveform inversion for determination of Earth structure, *Geophys. J. R. Astron. Soc.*, 62, 481–504, 1980.
- Menke, W., *Geophysical Data Analysis: Discrete Inverse Theory*, rev. ed., Academic, San Diego, Calif., 1989.
- Metropolis, N., and S. M. Ulam, The Monte Carlo method, *J. Am. Stat. Assoc.*, 44, 335–341, 1949.
- Metropolis, N., M. N. Rosenbluth, A. W. Rosenbluth, A. H. Teller, and E. Teller, Equation of state calculations by fast computing machines, *J. Chem. Phys.*, 21, 1087–1092, 1953.
- Mills, J. M., and T. J. Fitch, Thrust faulting and crust-upper mantle structure in East Australia, *Geophys. J. R. Astron. Soc.*, 48, 351–384, 1977.
- Mills, J. M., and A. L. Hales, Great-circle Rayleigh wave attenuation and group velocity, Part III, Inversion of global average group velocities and attenuation coefficients, *Phys. Earth Planet. Inter.*, 17(4), 307–322, 1978.
- Minster, J.-B. H., N. P. Williams, T. G. Masters, J. F. Gilbert, and J. S. Haase, Application of evolutionary programming to earthquake hypocenter determination, in *Proceedings of 4th Annual Conference of Evol. Prog.*, edited by J. R. McDonnell, R. C. Reynolds, and D. B. Fogel, pp. 3–17, MIT Press, 1995.
- Morokoff, W. J., and R. E. Caflisch, Quasi-random sequences and their discrepancies, *SIAM J. Sci. Comput.*, 15(6), 1251–1279, 1994.
- Morshed, J., and J. J. Kaluarachchi, Parameter estimation using artificial neural network and genetic algorithm for free-product migration and recovery, *Water Resour. Res.*, 34(5), 1101–1113, 1998.
- Mosegaard, K., Resolution analysis of general inverse problems through inverse Monte Carlo sampling, *Inverse Probl.*, 14, 405–426, 1998.

- Mosegaard, K., and C. Rygaard-Hjalsted, Bayesian analysis of implicit inverse problems, *Inverse Probl.*, 15, 573–583, 1999.
- Mosegaard, K., M. Sambridge, Monte Carlo analysis of inverse problems, *Inverse Probl.*, 18, R29–R54, 2002.
- Mosegaard, K., and A. Tarantola, Monte Carlo sampling of solutions to inverse problems, *J. Geophys. Res.*, 100(B7), 12,431–12,447, 1995.
- Mosegaard, K., and P. Vestergaard, A simulated annealing approach to seismic model optimization with sparse prior information, *Geophys. Prospect.*, 39(5), 599–611, 1991.
- Mosegaard, K., S. C. Singh, D. Snyder, and H. Wagner, Monte Carlo analysis of seismic reflections from Moho and the W-reflector, *J. Geophys. Res.*, 102, 2,969–2,981, 1997.
- Muramatsu, Y., and I. Nakanishi, Hypocenter determination using a genetic algorithm, *J. Natl. Disaster Sci.*, 19(1), 1–7, 1997.
- Muttiah, R. S., B. A. Engel, and D. D. Jones, Waste disposal site selection using GIS-based simulated annealing, in *Neural Network Applications in the Geosciences*, edited by B. G. Lees, *Comput. Geosci.*, 22(9), 1013–1017, 1996.
- Neves, F. A., S. C. Singh, and K. F. Priestley, Velocity structure of upper-mantle transition zones beneath central Eurasia from seismic inversion using genetic algorithms, *Geophys. J. Int.*, 125, 869–878, 1996.
- Nolte, B., and L. N. Frazer, Vertical seismic profile inversion with genetic algorithms, *Geophys. J. Int.*, 117, 162–179, 1994.
- Normark, E., and K. Mosegaard, Residual statics estimation: Scaling temperature schedules using simulated annealing, *Geophys. Prospect.*, 41(5), 565–578, 1993.
- Nulton, J. D., and P. Salamon, Statistical mechanics of combinatorial optimization, *Phys. Rev. A* 37, 1351–1356, 1988.
- Pardo, I. E., Optimal selection of number and location of rainfall gauges for areal rainfall estimation using geostatistics and simulated annealing, *J. Hydrol.*, 210, 206–220, 1998.
- Park, S. K., and K. W. Miller, Random number generators: Good ones are hard to find, *Commun. ACM*, 31, 1192–1201, 1988.
- Parker, R. L., Understanding inverse theory, *Annu. Rev. Earth Planet. Sci.*, 5, 35–64, 1977.
- Parker, R. L., *Geophysical Inverse Theory*, Princeton Univ. Press, Princeton, N. J., 1994.
- Press, F., Earth models obtained by Monte Carlo inversion, *J. Geophys. Res.*, 73, 5223–5234, 1968.
- Press, F., Earth models consistent with geophysical data, *Phys. Earth Planet. Inter.*, 3, 3–22, 1970a.
- Press, F., Regionalized Earth models, *J. Geophys. Res.*, 75, 6575–6581, 1970b.
- Press, W. H., B. P. Flannery, A. T. Saul, and W. T. Vetterling, *Numerical Recipes*, 2nd ed., Cambridge Univ. Press, New York, 1992.
- Pullammanappallil, S. K., and J. N. Louie, Inversion of seismic reflection traveltimes using a nonlinear optimization scheme, *Geophys.*, 58(11), 1607–1620, 1993.
- Pullammanappallil, S. K., and J. N. Louie, A generalized simulated-annealing optimization for inversion of first-arrival times, *Bull. Seismol. Soc. Am.*, 84(5), 1397–1409, 1994.
- Rawlins, G. J. E., (Ed.), *Foundations of Genetics Algorithms*, Morgan Kaufmann Burlington, Mass., 1991.
- Ricard, Y., C. Vigny, and C. Froidevaux, Mantle heterogeneities, geoid, and plate motion: A Monte Carlo inversion, *J. Geophys. Res.*, 94, 13,739–13,754, 1989.
- Ritzel, B. J., J. W. Eheart, and S. Ranjithan, Using genetic algorithms to solve a multiple objective groundwater pollution containment problem, *Water Resour. Res.*, 30(5), 1589–1603, 1994.
- Rizzo, D. M., and D. E. Dougherty, Design optimization for multiple management period groundwater remediation, *Water Resour. Res.*, 31(8), 2549–2561, 1995.
- Rogers, L. L., F. U. Dowla, and V. M. Johnson, Optimal field-scale groundwater remediation using neural networks and the genetic algorithm, *Environ. Sci. Tech.*, 29(5), 1145–1155, 1995.
- Rogers, L. L., V. M. Johnson, and R. B. Knapp, Remediation tradeoffs addressed with simulated annealing optimization, in *Computational Methods in Contamination and Remediation of Water Resources*, edited by V. N. Burganos, et al., *Comput. Methods Water Resour.*, 12(1), 59–66, Comput. Mech. Publ., Billerica, Mass., 1998.
- Rothman, D. H., Nonlinear inversion statistical mechanics, and residual statics corrections, *Geophysics*, 50, 2784–2796, 1985.
- Rothman, D. H., Automatic estimation of large residual statics corrections, *Geophysics*, 51, 332–346, 1986.
- Ruppeiner, G., J. M. Pedersen, and P. Salamon, Ensemble approach to simulated annealing, *J. Phys.*, 1(1), 455–470, 1991.
- Sabatier, P. C., On geophysical inverse problems and constraints, *J. Geophys.*, 43, 115–137, 1977a.
- Sabatier, P. C., Positivity constraints in linear inverse problems, I, General theory, *Geophys. J. R. Astron. Soc.*, 48, 415–441, 1977b.
- Sabatier, P. C., Positivity constraints in linear inverse problems, II, Applications, *Geophys. J. R. Astron. Soc.*, 48, 443–459, 1977c.
- Sadeghi, H., S. Suzuki, H. Takenaka, A two-point, three-dimensional seismic ray tracing using genetic algorithms, *Phys. Earth Planet. Inter.*, 113, 355–365, 1999.
- Sambridge, M., Exploring multi-dimensional landscapes without a map, *Inverse Probl.*, 14(3), 427–440, 1998.
- Sambridge, M., Geophysical inversion with a Neighbourhood algorithm, I, Searching a parameter space, *Geophys. J. Int.*, 138, 479–494, 1999a.
- Sambridge, M., Geophysical inversion with a neighbourhood algorithm, II, Appraising the ensemble, *Geophys. J. Int.*, 138, 727–746, 1999b.
- Sambridge, M., and G. G. Drijkoningen, Genetic algorithms in seismic waveform inversion, *Geophys. J. Int.*, 109, 323–342, 1992.
- Sambridge, M., and K. Gallagher, Hypocentre location using genetic algorithms, *Bull. Seismol. Soc. Am.*, 83(5), 1467–1491, 1993.
- Sambridge, M., and B. L. N. Kennett, A novel method of hypocentre location, *Geophys. J. R. Astron. Soc.*, 87, 679–697, 1986.
- Scales, J. A., and R. Snieder, To Bayes or not to Bayes, *Geophysics*, 62, 1045–1046, 1997.
- Scales, J. A., M. L. Smith, and T. L. Fischer, Global optimization methods for multimodal inverse problems, *J. Comput. Phys.*, 103(2), 258–268, 1992.
- Scherbaum, F., C. Palme, and H. Langer, Model parameter optimization for site-dependent simulation of ground motion by simulated annealing: Re-evaluation of the Ashigara Valley prediction experiment, *Nat. Hazards*, 10(3), 275–296, 1994.
- Sen, M. K., and P. L. Stoffa, Nonlinear one-dimensional seismic waveform inversion using simulated annealing, *Geophysics*, 56, 1624–1638, 1991.
- Sen, M. K., and P. L. Stoffa, Rapid sampling of model space using genetic algorithms, *Geophys. J. Int.*, 108, 281–292, 1992.
- Sen, M. K., and P. L. Stoffa, *Global Optimization Methods in Geophysical Inversion*, Adv. Explor. Geophys., vol. 4, Elsevier Sci., New York, 1995.
- Sharma, S. P., and P. Kaikkonen, Two-dimensional non-linear inversion of VLF-R data using simulated annealing, *Geophys. J. Int.*, 133, 649–668, 1998.
- Shibutani, T., M. Sambridge, and B. L. N. Kennett, Genetic algorithm inversion for receiver functions with application

- to crust and uppermost mantle structure beneath eastern Australia, *Geophys. Res. Lett.*, 23, 1829–1832, 1996.
- Sileny, J., Earthquake source parameters and their confidence regions by a genetic algorithm with a “memory,” *Geophys. J. Int.*, 134, 228–242, 1998.
- Simpson, A. R., and S. D. Priest, The application of genetic algorithms to optimisation problems in geotechnics, *Comput. Geotech.*, 15(1), 1–19, 1993.
- Smith, A. F. M., Bayesian computational methods, *Philos. Trans. R. Soc. London Ser. A*, 337, 369–386, 1991.
- Smith, A. F. M., and G. O. Roberts, Bayesian Computation via the Gibbs Sampler and Related Markov Chain Monte Carlo Methods, *J. R. Stat. Soc. Ser. B*, 55, 3–23, 1993.
- Smith, M. L., J. A. Scales, and T. L. Fischer, Global search and genetic algorithms, *Leading Edge*, 11, 22–26, 1992.
- Snieder, R., and J. Trampert, Inverse problems in geophysics, in *Wavefield Inversion*, edited by A. Virgin, pp. 119–190, Springer-Verlag, New York, 1999.
- Sobol, I. M., On the distribution of points in a cube and the approximate evaluation of integrals, *USSR Comput. Math. Math. Phys.*, 7(4), 86–112, 1967.
- Stark, P. B., Minimax confidence intervals in geomagnetism, *Geophys. J. Int.*, 108, 329–338, 1992.
- Steck, L. K., Simulated annealing inversion of teleseismic P-wave slowness and azimuth for crustal velocity structure at Long Valley Caldera, *Geophys. J. Int.*, 22, 497–500, 1995.
- Stoffa, P. L., and M. K. Sen, Nonlinear multiparameter optimization using genetic algorithms: Inversion of plane wave seismograms, *Geophys.*, 56, 1794–1810, 1991.
- Szu, H., and R. Hartley, Fast simulated annealing, *Phys. Lett. Ser. A*, 122, 157–162, 1987.
- Tang, A., and L. W. Mays, Genetic algorithms for optimal operation of soil aquifer treatment systems, *Water Resour. Manage.*, 12(5), 375–396, 1998.
- Tanner, M. A., *Tools for Statistical Inference: Methods for the Exploration of Posterior Distributions and Likelihood Functions*, 3rd ed., Springer-Verlag, New York, 1996.
- Tarantola, A., *Inverse Problem Theory*, Elsevier Sci., New York, 1987.
- Tarantola, A., and B. Valette, Inverse problems = quest for information, *J. Geophys.*, 50, 159–170, 1982a.
- Tarantola, A., and B. Valette, Generalized nonlinear inverse problems solved using the least squares criterion, *Rev. Geophys. Space Phys.*, 20(2), 219–232, 1982b.
- Thomson, W. E., Analogue computers for stochastic processes, in *Abbrev. Processes of the Oxford Math. Conference for Schoolteachers and Industrialists*, pp. 54–57, The Times Publ., London, 1957.
- Tierney, L., Markov chains for exploring posterior distributions, *Ann. Stat.*, 22, 1701–1762, 1994.
- Valius, V. P., Opredelenie seismicheskikh razrezov po sovokupnosti nabludennii, (Determination of seismological sections through ensemble control), *Vichislitelnaya Seismol.*, 4, 3–14, 1968.
- van der Beek, P., and J. Braun, Control on post-mid Cretaceous landscape evolution in the southeastern highlands of Australia: Insights from numerical surface process models, *J. Geophys. Res.*, 104, 4945–4966, 1999.
- Varela, C. L., P. L. Stoffa, and M. K. Sen, Background velocity estimation using non-linear optimization for reflection tomography and migration misfit, *Geophys. Prospect.*, 46(1), 51–78, 1998.
- Vasco, D. W., L. R. Johnson, and E. L. Majer, Ensemble inference in geophysical inverse problems, *Geophys. J. Int.*, 117, 711–728, 1993.
- Vasudevan, K., and W. G. Wilson, Simulated annealing statics computation using an order-based energy function, *Geophys.*, 56(11), 1831–1839, 1991.
- Velis, D. R., and T. J. Ulrych, Simulated annealing two-point ray tracing, *Geophys. Res. Lett.*, 32(2), 201–204, 1996.
- Vestergaard, P., and K. Mosegaard, Inversion of post-stack seismic data using simulated annealing, *Geophys. Prospect.*, 39(5), 613–624, 1991.
- Vinther, R., and K. Mosegaard, Seismic inversion through Tabu Search, *Geophys. Prospect.*, 44(4), 555–570, 1996.
- Wan, Y., R. Liu, and H. Li, The inversion of 3-D crustal structure and hypocenter location in the Beijing-Tianjin-Tangshan-Zhangjiakou area by genetic algorithm, *Acta Seismol. Sin.*, 10(6), 769–781, 1997.
- Whitley, D. L., A genetic algorithm tutorial, *Stat. Comput.*, 4, 65–85, 1994.
- Wiggins, R. A., Monte Carlo inversion of body wave observations, *J. Geophys. Res.*, 74, 3171–3181, 1969.
- Wiggins, R. A., The general inverse problem: Implication of surface waves and free oscillations for Earth Structure, *Rev. Geophys.*, 10, 251–285, 1972.
- Wilson, W. G., K. Vasudevan, Application of the genetic algorithm to residual statics estimation, *Geophys. Res. Lett.*, 18, 2181–2184, 1991.
- Winter, G., J. Periaux, M. Galan, and P. Cuesta, (Eds.), *Genetic Algorithms in Engineering and Computer Science*, John Wiley, New York, 1995.
- Worthington, M. H., J. R. Cleary, and R. S., Anderssen, Density modelling by Monte Carlo inversion, II, Comparison of recent Earth models, *Geophys. J. R. Astron. Soc.*, 29, 445–457, 1972.
- Worthington, M. H., J. R. Cleary, and R. S., Anderssen, Upper and lower mantle shear velocity modelling by Monte Carlo inversion, *Geophys. J. R. Astron. Soc.*, 36, 91–103, 1974.
- Yamanaka, H., and H. Ishida, Application of genetic algorithms to an inversion of surface-wave dispersion data, *Bull. Seismol. Soc. Am.*, 86(2), 436–444, 1996.
- Yu, T. T., J. Fernandez, and J. B. Rundle, Inverting the parameters of an earthquake-ruptured fault with a genetic algorithm, *Comput. and Geosci.*, 24(2), 173–182, 1998.
- Zhao, L. S., M. K. Sen, P. L. Stoffa, and C. Frohlich, Application of very fast simulated annealing to the determination of the crustal structure beneath Tibet, *Geophys. J. Int.*, 125, 355–370, 1996.
- Zheng, C., P. Wang, Parameter structure identification using tabu search and simulated annealing, *Adv. Water Resour.*, 19(4), 215–224, 1996.
- Zhou, R., F. Tajima, and P. L. Stoffa, Earthquake source parameter determination using genetic algorithms, *Geophys. Res. Lett.*, 22(4), 517–520, 1995a.
- Zhou, R., F. Tajima, and P. L. Stoffa, Application of genetic algorithms to constrain near-source velocity structure for the 1989 Sichuan earthquakes, *Bull. Seismol. Soc. Am.*, 85(2), 590–605, 1995b.

K. Mosegaard, Niels Bohr Institute for Astronomy, Physics, and Geophysics, Department of Geophysics, University of Copenhagen, Juliane Maries Vej 30, DK-2100 Copenhagen 0, Denmark. (Klaus@gfy.ku.dk)

M. Sambridge, Research School of Earth Sciences, Institute of Advanced Studies, Australian National University, Canberra ACT 0200, Australia. (malcolm@rses.anu.edu.au)